

AD-A274 054

AFIT/GE/ENG/93D-02



3



**DTIC**  
ELECTE  
DEC 23 1993  
**S A**

A STUDY OF TWO DIMENSIONAL TAPERED PERIODIC  
EDGE TREATMENTS TO REDUCE WIDEBAND EDGE  
DIFFRACTION

THESIS

Russell A. Burleson, First Lieutenant, USAF

AFIT/GE/ENG/93D-02



93-31064

226  
~~226~~

Approved for public release; distribution unlimited

93 12 22 177

**A STUDY OF TWO DIMENSIONAL TAPERED PERIODIC EDGE  
TREATMENTS TO REDUCE WIDEBAND EDGE DIFFRACTION**

**THESIS**

**Presented to the Faculty of the School of Engineering  
of the Air Force Institute of Technology**

**Air University**

**In Partial Fulfillment of the  
Requirements for the Degree of  
Master of Science in Electrical Engineering**

**Russell A. Burleson, B. S. E. E.  
Second Lieutenant, USAF**

**December 1993**

**DTIC QUALITY INSPECTED 3**

**Approved for public release; distribution unlimited**

Accession For	
NTIS ORASI	<input checked="" type="checkbox"/>
DTIC TAB	<input type="checkbox"/>
Unannounced	<input type="checkbox"/>
Justification	
By	
Distribution /	
Availability Codes	
Dist	Avail and/or Special
A-1	

The views expressed in this thesis are those of the author and do not reflect the official policy or position of the Department of Defense or the U. S. Government

## ***Preface and Acknowledgement***

The purpose of this study was to determine the effectiveness of tapered two dimensional periodic surfaces to reduce near grazing diffraction. Specific uses of this study are antenna design, radar cross section reduction, and radome diffraction reduction.

The tapers were developed for both principle polarizations using numerical methods. The designs were then built at Mission Research Corporation (MRC) and tested at the Ohio State University Electrosience Laboratory (OSU-ESL) compact range. The results for the taper designs showed success at reducing edge diffraction. The tapers were also modeled using several numerical methods. The results of these numerical methods supported the experimental results. One of the tapers especially was effective over a wide frequency range. This thesis has

Several people have contributed greatly to this thesis. I would like to thank Dr. Errol English of MRC and Dr. Lee Henderson of OSU-ESL, who were both instrumental in designing the tapers and interpreting the results. Prof. Raymond Luebbers and Chris Penney of Pennsylvania State University were very helpful with modeling the designs using the Finite Difference Time Domain technique for electromagnetics. I would also like to thank Drs Eric Walton, Robert Lee, and John Young of OSU-ESL for working to help develop the methodology for measuring the taper designs. Drs John Maloney, Larry Carin, Leopold Felsen, and Steve Miller were helpful in the design and manufacture of the tapers. I would also like to thank my thesis advisor Dr. Andrew Terzouli and my thesis committee Captain J. P. Skinner, Captain J. Sacchini, and Lt. Col. W. Baker for their help during the entire thesis process. I would also like to thank my sponsors Major Dennis Andersh of Wright Lab and Captain Raley Merek of Phillips Lab. Finally, I would like to thank my wife Heather for her help and understanding throughout the entire master's degree program.

**Russell A. Burleson**

## ***Table of Contents***

	<b>Page</b>
Preface	ii
List of Figures	v
Abstract	viii
I. Objectives of the Study	1
Introduction	1
Background	1
Problem Statement	4
Current Technologies	6
Assumptions	8
Methodology	10
Summary	11
II. Summary of Current Knowledge	12
Introduction	12
Inductive and Capacitive Periodic Structures	12
Parallel Wire Grids and Thin Strip Gratings	12
Meanderline Grids	17
Numerical Solutions for Capacitive and Inductive Tapers	21
Summary	25
III. Methodology	26
Introduction	26
Methodology in Design of Tapers	26
Experimentally Measure the Data	35
Numerically Validate the Data	37
Summary	45
IV. Results and Analysis	45
Introduction	46
PMM Output	46
Measured Results on the Impedance Taper Designs	59
MoM Results on First Taper Designs	66
FDTD Results on Second Capacitive Taper Design	68
Summary	71
V. Conclusions and Future Studies	72
Introduction	72
Success of the Taper Designs	72

	<b>Page</b>
Future Work	73
Overview	75
Appendix A: Results from PMM Output	76
Appendix B: First Measured Data	89
Appendix C: Second Measured Data	121
Appendix D: Method of Moments Data	202
Appendix E: FDTD Results	219
Bibliography	223
Vita	225

## ***List of Figures***

<b>Figure</b>	<b>Page</b>
1. Diffraction from a Conducting Strip	2
2. Possible Uses of Geometrical Tapers	4
3. Wait's Coordinate System for Parallel Wire Grids	15
4. PMM Coordinate System	16
5. Meanderlines Impedance as a Function of Polarization	18
6. Meanderline Grid	19
7. 2D Wedge Illuminated by an Infinite Line Source	21
8. MoM Basis Functions	23
9. Antenna Platform for Measurements	28
10. Transmission Coefficient vs Frequency for Inductive Design #1	29
11. Inductive Taper Design #1	30
12. Transmission Coefficient vs Frequency for Inductive Design #2	31
13. Inductive Taper Design #2	32
14. Capacitive Taper Designs #1 and #2	33
15. Reflection Coefficient vs Frequency for Capacitive Design #1	34
16. Reflection Coefficient vs Frequency for Capacitive Design #2	35
17. Compact Range Setup for Measuring the Bistatic Diffraction	37
18. MoM Model for Capacitive Design #1	39
19. Equivalent Thin Wire Approximations used in TMz MoM Code	39
20. MoM Model for Inductive Design #1	40
21. PMM Model for Inductive Design #1	41
22. PMM Model for Capacitive Design #1	42
23. PMM Model for Inductive Design #2	43

	<b>Page</b>
24. PMM Model for Capacitive Design #2	43
25. FDTD Model for Capacitive Design #2	44
26. Impedance vs Frequency for the Free Space Edge of Inductive Design #1	47
27. Impedance vs Frequency for the Free Space Edge of Inductive Design #2	48
28. Impedance vs Frequency for the Ground Plane Edge of Capacitive Design #1	49
29. Impedance vs Frequency for the Ground Plane Edge of Capacitive Design #2	50
30. Impedance vs Length for Inductive Design #1	52
31. Reflection Coefficient vs Length for Inductive Design #1	52
32. Impedance vs Length for Capacitive Design #1	53
33. Reflection coefficient vs Length for Capacitive Design #1	54
34. Impedance vs Length for Inductive Design #2	55
35. Reflection Coefficient vs Length of Inductive Design #2	55
36. Impedance vs Length for Capacitive Design #2	56
37. Reflection Coefficient vs Length of Capacitive Design #2	57
38. Impedance vs Frequency for Free Space Edge of Inductive Design #2 Without the Dielectric Substrate	58
39. Impedance vs Frequency for Ground Plane Edge of Capacitive Design #2 Without the Dielectric Substrate	58
40. Comparison of UTD and Measured Results From the Knife Edge	60
41. Azimuth Cut of Inductive Design #2 at 10 GHz	61
42. Frequency Sweep for Inductive Design #2 at 90° in the Shadow Region	61
43. Frequency Sweep for Inductive Design #2 at 120° in the Shadow Region	62
44. Frequency Sweep for Inductive Design #2 at 150° in the Shadow Region	62
45. Comparison of UTD and Measured Results From the Knife Edge	63
46. Azimuth Cut of Capacitive Design #2 at 10 GHz	64



	<b>Page</b>
47. Frequency Sweep for Capacitive Design #2 at 90° in the Shadow Region	64
48. Frequency Sweep for Capacitive Design #2 at 120° in the Shadow Region	65
49. Frequency Sweep for Inductive Design #2 at 150° in the Shadow Region	65
50. Comparison of MoM Results for Inductive Design #1	66
51. Comparison of MoM Results for Capacitive Design #1	68
52. Comparison of FDTD Results for Capacitive Design #2	70
53. Scattered Field from the Styrofoam Substrate Alone as a Function of Observation Angle	70
54. Scattered Field from the Styrofoam Substrate Alone as a Function of Frequency	71

### ***Abstract***

This is a brief summary of a study to reduce diffraction from an infinite two dimensional edge using tapered periodic surfaces. The concept is to use the impedance characteristics of a periodic surface to create a tapered impedance, much like a tapered resistance commonly used for diffraction reduction. This approach has several advantages over tapered resistive treatments to include ease of fabrication, better engineering control of the impedance and negligible loss absorbed by the taper. In this study, four periodic tapers were design, built and tested. These tapers were also modeled using a variety of numerical techniques. The results from this study were quite promising.

The tapers were designed using a periodic moment method (PMM) code. Assuming local periodicity the PMM code was used to determine the impedance of doubly-infinite structures. The taper was developed by determining the best taper response for a given bandwidth.

An antenna structure to simulate near grazing incidence of a plane wave on a two dimensional knife edge was used to test the taper designs. The tapers were then built and measured at the compact range at OSU-ESL over the frequency range 2-18 GHz.

The tapers were also modeled using several different numerical techniques. The first designs were modeled using method of moments (MoM) techniques. The second capacitive design was modeled using the finite difference time domain (FDTD) technique.

The results from the measurements were positive. The results from the numerical calculations supported the measurements and displayed the bandwidths indicated from earlier PMM calculations. The inductive designs developed were not very successful , but the capacitive taper proved to be quite effective over a wide frequency range.

# **A STUDY OF TWO DIMENSIONAL TAPERED PERIODIC EDGE TREATMENTS TO REDUCE WIDEBAND EDGE DIFFRACTION**

## ***Chapter 1: Objectives of the Study***

### ***Introduction***

***Overview.*** The purpose of this chapter is to describe a study of an edge diffraction reduction technique using a tapered periodic geometry. Many efforts have previously been made to reduce edge diffraction; however, these techniques did not use tapered periodic surfaces. Specifically, the purpose of this study is to examine the use of tapered periodic structures to reduce wideband edge diffraction near grazing incidence. These tapers will have specific application to antenna design for high power, time domain, and wideband antennas.

The first section of this chapter describes diffraction and the undesirable effects of diffraction in antenna design. The second section describes the general problem statement and explains the concepts proposed for reducing diffraction for both principle polarizations. The third section describes the current technologies to reduce diffraction. The last section describes the assumptions made in the study.

### ***Background***

***Purpose.*** The purpose of this section is to describe diffraction and the undesirable effects of diffraction in antenna design. This section defines terms associated with diffraction and antenna design used throughout this paper.

**Diffraction.** Diffraction is an important topic of study in electromagnetism. If an incident field illuminates a scatterer, then the total electric field in a region is defined as the incident plus the scattered fields (diffracted and reflected fields). In the far field region, the reflected field is present only at discrete angles for a flat scatterer (see Figure 1, Region 2). Diffraction, however, contributes scattered fields at all angles (see Figure 1, Regions 1-3), which makes diffraction the most prominent scattering mechanism for far field measurements. The shadowed region (see Figure 1, Region 3) fields consist of diffracted fields only. Edge diffraction is defined as diffraction coming from a sharp edge of the scatterer. Knife edges are edges which are made by an infinitesimally thin plates. This work will concern the study of reducing knife edge diffraction.

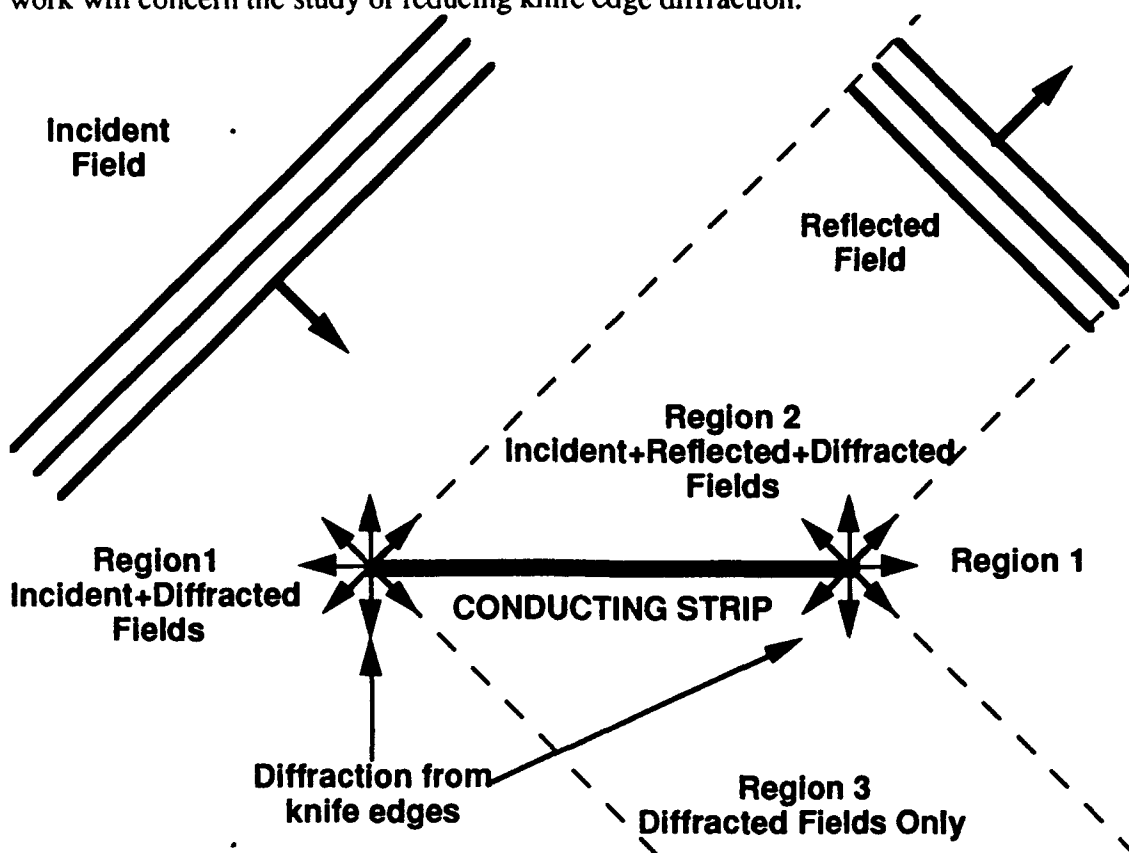
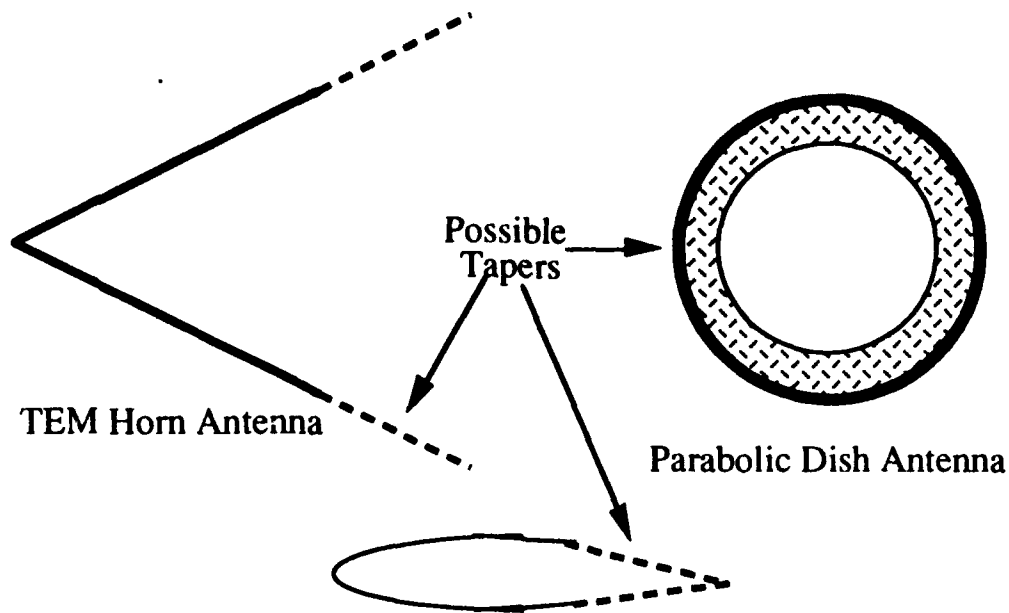


**Figure 1. Diffraction from a Conducting Strip.** This is a 2D conducting strip illuminated by an incident plane wave. The two scattering mechanisms are reflection and diffraction.

**Antenna Design.** A major use of the study of diffraction is to optimize antenna design. Several parameters determine the quality of an antenna. Some of these factors are directivity, gain, ringing, and pulse distortion [1]. Diffraction from the edges of an antenna adversely effects all of these factors. Therefore, reduction of diffraction from the edge of antennas has been a main source of study in electromagnetism. Directivity is a measure of how much of the energy of the signal is contained in the boresight view of the antenna. Diffraction causes sidelobes and reduces the directivity of the antenna. Gain is the measure of the boresight transmission of the antenna in relation to the input signal to the antenna. Diffraction spreads the energy out over all angles and therefore reduces the gain of the antenna. Ringing is an undesirable effect caused by the diffraction from the edge of an antenna radiating back into the antenna and causing periodic residual radiation. Ringing can give false signals for both transmitting and receiving transient antennas. Pulse distortion is any change in the radiated wave from the input pulse. Pulse distortion is caused by both geometry and materials having time dispersive and frequency dependent properties. Ringing and pulse distortion are of concern when working with time domain antennas. Reduction in diffraction from the edges of the antennas will have a positive affect on all of the mentioned parameters (see Figure 2 for applications).

**Radar Cross Section.** Another advantage of reducing diffraction is to reduce radar cross sections (RCS) of targets. Radar cross section is a measure used to quantify the magnitude of the returned signal of a target at given angles and frequencies. Since reflection only accounts for returns at discrete angles (assuming flat surfaces), reduction in diffraction is of high concern. Presently, materials are used with high magnetic loss to reduce diffracted fields. These materials are quite expensive and are generally effective on only a small frequency range. The tapers proposed here would also be of use to reduce traveling waves, which would be helpful when trying to make scattering measurements and measuring returns only from certain aspects of the structure (see Figure 2 for applications).



#### Trailing Edge Diffraction Reduction

**Figure 2. Possible Uses of Geometrical Tapers.** This diagram shows possible uses of the geometrical tapers proposed in this study. The tapers could possibly be used to reduce trailing edge diffraction or diffraction from the edge of antennas.

#### ***Problem Statement***

***Purpose.*** The purpose of this section is to define the problem to be studied in this paper. This section will first outline the objectives for understanding time domain edge diffraction. This section will then detail the concept of the periodic tapers to reduce diffraction.

***Determine Configurations For Edge Tapers.*** The first step in this study is to determine what configurations create the tapered effect desired. The concept is to create an impedance taper by varying the geometry of the periodic structures to impedance match the ground plane to free space. The work presented is directed at creating periodic surfaces which have total reactive impedance and no resistive impedance. Resistive impedance tapers absorb energy (through heat dissipation) and would not be useful for high powered

microwave applications. If the impedance is kept either capacitive (negative reactance) or inductive (positive reactance), then the phase shift will not result in time dispersion (only a time shift), because the entire scattered field would be shifted by the same phase shift ( $\pm\pi$ ). The first tapers were designed to not have a phase shift, but to increase bandwidth and performance this criteria was not used in the second design. The designs studied in this paper were determined by finding geometries which are completely reactive and could be tapered over a large frequency range. The designs were initially developed using a Periodic Moment Method (PMM) code [2]. This code was used to give information about the bandwidth and effectiveness of the design.

***Experimentally Verify the Effectiveness of the Tapered Surfaces.*** The designs developed from PMM were then tested. The designs were mounted on a platform with a long knife edge and then the diffracted fields were measured in the shadow region. If the tapers are effective, there should be a noticeable reduction in the shadow region fields. To match the idea of reduction of diffraction in antenna design, the diffraction from near grazing incidence was measured. The procedures and results from these measurements are presented in more detail in future chapters.

***Computationally Validate the Results*** After the tapers were measured, the next step was to see if computational tools exist to properly model this measurement. For the first designs, Method of Moments (MoM) codes existed to measure the reduction in diffraction. The MoM codes available could not model the second designs, since these structures involved dielectrics. A Finite Difference Time Domain (FDTD) code [3] was used to validate the measurements of the second capacitive design. No code was available that had accurate solutions for the second inductive taper.

## ***Current Technologies***

***Purpose.*** This section details some of the current technologies used to study and reduce diffraction. More detail on these technologies may be found in the next chapter.

***Resistive Loading for Time Domain Antennas.*** There have been several papers on resistively loading time domain antennas to reduce diffraction and thereby improve the performance of the antenna. Maloney et al [4] described a method for optimizing the resistive loading of a time domain antenna. Maloney's antenna was a biconical antenna which is analogous to a double wedge in 2D. This antenna was resistively loaded such that the impedance of the source was slowly matched to the impedance of free space. This antenna design was extremely effective for reduction in ringing and for reduction of sidelobes and edge diffraction for a transient (time domain) pulse. However, this antenna design, like all other resistively loaded antennas, was not efficient, over 14% of the energy was dissipated in the loading which causes severe problems when trying to use antennas for high power applications such as impulse radar or high powered microwave weapons. A resistively loaded antenna would melt from the heat of the dissipation for these applications. Clearly, methods other than resistive loading need to be developed for use in high powered systems.

***Thin Wire Measurements.*** Thin wire configurations have been studied extensively in the frequency domain. The frequency domain analysis has been mostly concerned with thin strip application to frequency selective surfaces (FSSs). These surfaces are useful for radomes and other structures where only a given frequency range is of interest and other frequencies would be a nuisance or even a threat. The study of these structures has principally focused on doubly-infinite arrays. The information that is most useful to this study is how FSSs can be truncated using edge treatments for a given frequency range.



Thin wire configurations were also studied as a singular subject. Analytical solutions were developed by Wait [5] and Yoder [6]. These techniques are quite simple to implement and give the scattering from an infinite array of infinitely long, thin, parallel wires. Others have studied, singly and doubly periodic structures both in free space and in the presence of a dielectric. Felsen and Carin [7][8][9] authored several papers where they demonstrated the use of Floquet mode analysis for the study of 2D thin strips. One important result of the research conducted by Felsen and Carin is that they developed a method for applying Floquet mode analysis, which is generally for infinite periodic structures, to finite non-periodic structures. This analysis does not lend itself very well to the study presented in this paper, because this technique does not handle dielectrics.

***Periodic Method of Moments.*** To study FSSs, researchers often use the PMM code mentioned earlier [2]. This PMM code can model doubly infinite periodic structures. This code can include dielectrics, networks, and work over a wide range of frequencies. Since each element in the doubly infinite array is identical, this PMM code cannot be used to model the periodic tapers. An in-depth discussion of the workings of PMM and the code developed by Henderson is presented in the next chapter.

***Method of Moments Numerical Modeling.*** One of the most accurate solutions for frequency domain electromagnetics is the MoM. MoM uses basis and testing functions to determine the equivalent scattering currents. These equivalent scattering currents can then be transformed into the scattered fields using the radiation integral. The MoM codes available can only handle perfect electrically conducting (PEC) materials or PEC loaded materials of finite extent, not lossless dielectrics. This numerical modeling technique was used to validate some of the impedance designs, but another technique was necessary for the designs which included dielectrics.

***Finite Difference Time Domain Numerical Modeling.*** There are several techniques used to model time domain electromagnetics. A popular numerical modeling approach is to solve Maxwell's equations directly in the time domain using FDTD. FDTD handled the complex structures involved in the two dimensional designs that involved dielectrics. The specifics of this technique are given in more detail in the following chapter.

### ***Assumptions***

***Purpose.*** The purpose of this section is to define the major assumptions made in this study. These assumptions are made for clearer understanding of the results. Some assumptions have different impacts on analytical, numerical and experimental accuracy. Each part of this section describes the assumptions made and the consequences of each assumption. In Chapter 4, the effects of these and other assumptions made will be explained in detail and contrasted to the results from the study.

***Plane Wave Incidence.*** The incident wave was assumed to be a plane wave. A plane wave is a wave which has the same field values for every point in a plane at a given time. Generally, if the incident source is far from the scatterer (more than 5 wavelengths), the plane wave approximation is accurate. This assumption is useful because plane waves are the easiest waves to numerically and analytically evaluate. The platform used in the measurements was sufficiently large enough that the source was several wavelengths from the long knife edge ( $5\lambda$  at the lowest frequency).

***PEC and Lossless Dielectrics Materials.*** In the initial study, the periodic structures were constructed completely out of PEC material. Beginning the study with PEC material had two major advantages: PEC material does not dissipate energy and PEC has the same infinite conductivity over all frequencies. The frequency independence prevented pulse distortion due to the materials and made the pulse distortion be a function of geometry only. Experimentally, materials with near infinite conductivities (copper,

aluminum) were readily available to build the structures. For FDTD and MoM numerical analysis, non-PEC material could be added easily in future studies. Unfortunately, when trying use particular resistive values in a taper design, materials may not be readily available which have the proper impedance value. This problem will make experimental validation of non-PEC materials and resistive tapers much more difficult. For the frequencies of interest, the dielectrics used in this study were nearly lossless.

**Structures Are Two-Dimensional (2D).** To study the 2D case, the entire configuration was considered to be infinite and constant in the  $\hat{z}$  direction. For both FDTD and MoM numerical techniques, 2D analysis was much faster and required less memory than three dimensional (3D) analysis. Therefore, the 2D assumption allowed local, inexpensive computational facilities to be used for the analysis. Experimentally, a 2D wire is impossible to realize, but if the wires are made at least 5 times longer than a wavelength at the lowest frequency, the 2D approximation is accurate within experimental error for predicted patterns in the transverse plane. Another problem experimentally is that the structures must be kept straight and constant in the  $\hat{z}$  direction. To solve this problem, the tapers were attached to styrofoam for stability and alignment. Styrofoam is an easy material to work with and has an index of refraction near unity. The 2D assumption is the one assumption that should present the most problems when trying to compare numerical data to experimental data. Further explanation of construction of the 2D configuration will be presented in Chapter 3.

**Local Periodicity.** Since the structures measured were almost periodic, methods of modeling for periodic structures were used in the design process. To use a completely periodic method for these tapered structures, local periodicity must be assumed. Local periodicity means that the changes in the immediate area of each scatterer are so small that

scattering can be approximated using periodic techniques. If the tapers are large enough, then the local changes will be small and the periodic techniques can be used to model the tapers accurately.

## ***Methodology***

***Purpose.*** The purpose of this section is to outline the methodology used in this study. Each subsection describes a different stage of the study. Also included in each subsection are important assumptions and considerations for error that must be taken into account.

***Design the Tapers Using PMM.*** The first step was to develop the taper designs. To do this, reflection and transmission coefficients were calculated from periodic designs using Henderson's PMM Code [2]. The ends of the taper designs were developed by trying to match the ground plane and the free space edges of the taper. The designs were then geometrically tapered in a linear fashion from one edge to another. The results from this part of the study were then transformed into equivalent impedances. These impedance tapers are displayed as impedance versus length or frequency in Chapter 4.

***Experimentally Confirm the Results in the Frequency Domain.*** After the designs were developed, the next stage was to experimentally confirm the numerical results. A platform was constructed to measure shadow region diffraction from a grazing incidence plane wave. This structure was measured both bare and with the periodic tapers at the Ohio State University Electrosience Laboratory (OSU-ESL) compact range. Because compact ranges use parabolic reflectors, the far field observation point approximation for a compact range was accurate. The measurements of most concern were comparisons of azimuth scans of the bare structure to tapered structures. The scans of the

bare structure were compared to the Uniform Theory of Diffraction (UTD) results for validation. Also frequency sweeps at discrete angles were taken to provide wideband frequency information.

***Numerically Validate the Results.*** The next step was to use numerical techniques to validate the experimental results. The analytical results were validated using two separate types of codes. The first type of code was a MoM code. Two separate MoM codes were used to model the first impedance taper designs. These two codes handled the two polarizations used in this study. The second type of code was a scattered field FDTD code by Dr. Ray Luebbers [3]. This code was purchased by the U. S. Air Force and has been experimentally validated for many different geometries. The Luebbers' code was run in a matter of a several hours on a Silicon Graphics machine.

## ***Summary***

***Overview.*** This chapter has outlined the study to be presented in this thesis. The first section gave a general overview to the background and reasons for reducing diffraction. The second section outlined the problem to be studied in this thesis. The third section described current technologies used to reduce diffraction. The next two sections gave the assumptions taken in this paper and the scope of the study. The last section gave a brief outline of the methodology to be taken in researching this topic. More detail on all of these topics is presented in the following chapters.

## ***Chapter 2: Summary of Current Knowledge***

### ***Introduction***

**Overview.** This chapter overviews current knowledge that pertains to the study. The first section covers current knowledge of an infinite parallel wire grids. The second section covers meanderline designs. The third section explains the abilities and limitations of numerical techniques to include the Uniform Theory of Diffraction (UTD), the Method of Moments (MoM), the Periodic Moment Method (PMM), and the Finite Difference Time Domain (FDTD). Each section covers how the knowledge obtained from each author can be used in the design and understanding of the tapers.

### ***Inductive and Capacitive Periodic Structures***

**Overview.** There are several different types of periodic structures that produce either capacitive or inductive impedance. In this study, the inductive properties of parallel wire grids and meanderlines are used for the E-field orthogonal to the plane of incidence. The capacitive properties of thin strips are used for the E-field parallel to the plane of incidence. To increase the continuity of the taper, the meanderline design was changed into an skewed slot array grid (by decreasing the spacing between elements). Analytical solutions did exist for the thin strip and thin wire grids, but numerical modeling of these structures was far more accurate and faster than analytical techniques.

### ***Parallel Wire Grids and Thin Strip Gratings***

**Overview.** Parallel wire grids have been studied for several years. Several analytical and numerical solutions for parallel wire grids have been developed. A parallel wire grid was used for the first inductive taper where the E-field is polarized parallel to the wires. Due to restrictions in manufacturing capability, a constant wire radius was assumed. To change the inductance, the spacing between the wires was changed. Wires

spaced close to each other displayed low inductance (ground plane side) and wires spaced far apart offered large inductance (free space side). Using the assumption of local periodicity, the inductive properties at any given point were determined on the tapered parallel wire grid using a infinite parallel wire grid model. On the free space edge, there was a limit to the spacing, due to grating lobes. Therefore, for near grazing incidence the spacing of wires was kept to less than  $\lambda/2$  for the highest frequency of interest.

**Wait's Solution for Parallel Wire Grids.** The first analytical solution was developed by Wait [5]. This solution is for arbitrary incidence on a parallel wire grid. In his paper, Wait described the scattered electric field as observed from a point (x,y,z) as

$$E_z^s = \frac{j\mu\omega I_0 \cos^2\theta}{4\pi} e^{j\beta y \cos\theta \sin\phi} e^{-j\beta z \sin\theta} \times \sum_{m=-\infty}^{\infty} \exp\left[\frac{j2\pi my}{d}\right] \frac{\exp\left[\frac{-2\pi|x|}{d} \sqrt{\left(\frac{m + d\cos\theta \sin\phi}{\lambda}\right)^2 - \left(\frac{d\cos\theta}{\lambda}\right)^2}\right]}{\sqrt{\left(\frac{m + d\cos\theta \sin\phi}{\lambda}\right)^2 - \left(\frac{d\cos\theta}{\lambda}\right)^2}}. \quad (2.1)$$

For a description of a, d,  $\theta$  and  $\phi$ , see Figure 3. If the observation point is in the far zone and assuming no grating lobes, only the  $m = 0$  term will be of consequence (the higher order terms will act as evanescent waves). This reduces the above equation into

$$E_z^s = \frac{\eta_0 I_0 \cos\theta}{2d \cos\phi} e^{j\beta q}, \quad (2.2)$$

where

$$q = -|x| \cos\phi \cos\theta + y \sin\phi \cos\theta - z \sin\theta.$$

In this particular study  $\theta = 0$ , and therefore  $E_x^s$  and  $E_y^s$  will be zero. This is reasonable as no cross polarization terms were expected when scanning wires about the orthogonal axis. In

the above equation,  $q$  represents the phase terms associated with propagation from the grid to the observation point. The current term  $I_0$  can be represented by

$$I_0 = \frac{-A_z d}{\frac{\eta_0 \cos \theta}{2 \cos \phi} + \frac{j \omega \mu d}{2 \pi} \cos^2 \theta \left[ \ln \left( \frac{d}{2 \pi a} \right) + F \left( \frac{d \cos \theta}{\lambda}, \phi \right) \right] + (\cos^2 \theta) Z_i d}, \quad (2.3a)$$

where

$$F \left( \frac{d \cos \theta}{\lambda}, \phi \right) = \frac{1}{2} \sum_{m=1}^{\infty} \left[ \frac{1}{\sqrt{\left( m + \frac{d \cos \theta \sin \phi}{\lambda} \right)^2 - \left( \frac{d \cos \theta}{\lambda} \right)^2}} + \frac{1}{\sqrt{\left( m - \frac{d \cos \theta \sin \phi}{\lambda} \right)^2 - \left( \frac{d \cos \theta}{\lambda} \right)^2}} - \frac{2}{m} \right] \quad (2.3b)$$

This solution is valid for wires spaced far apart ( $d > 5a$ ). This solution has been shown to match results from Henderson's PMM code.

**Yoder's Solution for Strip Gratings.** Yoder [6] developed another solution to parallel strip gratings in his master's thesis. This solution was based upon the Periodic Moment Method and showed excellent results compared to PMM calculations and Wait's solution. The coordinate axis used by Yoder was the same system as used in Henderson's PMM code (see Figure 4). This is the same coordinate system that is used throughout the rest of this thesis. The incident field will be described by two angles  $\alpha$  and  $\eta$ , where  $\alpha$  is the angle that the plane of incidence makes upon the  $xz$  plane (plane of the array) and  $\eta$  is the angle that the incident E-field makes from the  $-\hat{y}$  axis in the plane of incidence.



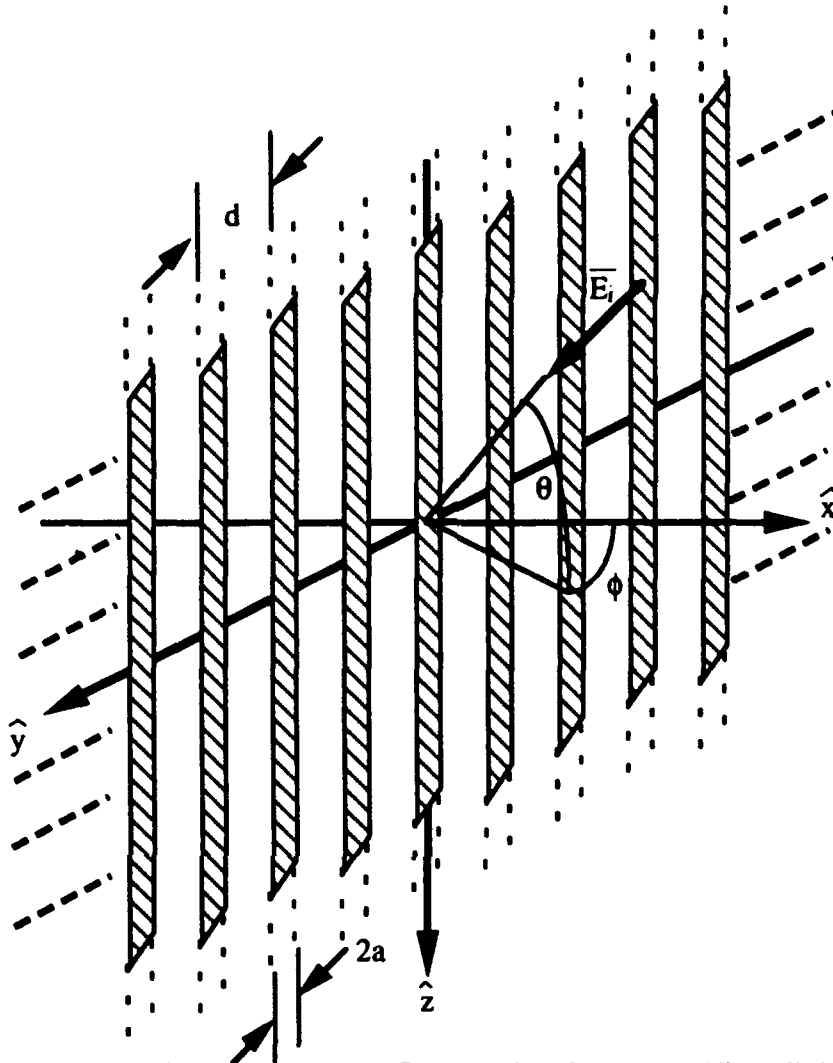


**Figure 3. Wait's Coordinate System for Parallel Wire Grids.** This is the coordinate system used by Wait [5].

Yoder then developed solutions for both parallel and orthogonal scans of the electric fields. The orthogonal scans are defined by  $\alpha = 0^\circ$  and parallel scans are defined by  $\alpha = 90^\circ$ . The two solutions developed by Yoder were

$$|E_{\perp}| = \left| \frac{\hat{z} \sec \eta}{\sum_{k=-\infty}^{\infty} \frac{\exp\left(-jba \sqrt{(\cos \eta)^2 - \left(\frac{k\lambda}{D_x}\right)^2} - 2\left(\frac{k\lambda}{D_x}\right) \sin \eta\right)}{\sqrt{(\cos \eta)^2 - \left(\frac{k\lambda}{D_x}\right)^2} - 2\left(\frac{k\lambda}{D_x}\right) \sin \eta}} \right|; \alpha = 0^\circ \quad (2.4)$$

and

$$|E_{||}| = \left| \frac{\sec \eta (\hat{y} \sin \eta - \hat{z} \cos \eta)}{\sum_{k=-\infty}^{\infty} \frac{\exp\left(-jba \sqrt{(\cos \eta)^2 - \left(\frac{k\lambda}{D_x}\right)^2}\right)}{\sqrt{(\cos \eta)^2 - \left(\frac{k\lambda}{D_x}\right)^2}}}\right| ; \alpha = 90^\circ \quad (2.5)$$

In this study, the orthogonal solution (Equation 2.4) is the only important result for the parallel wires. The parallel solution is important for the thin strip grid.

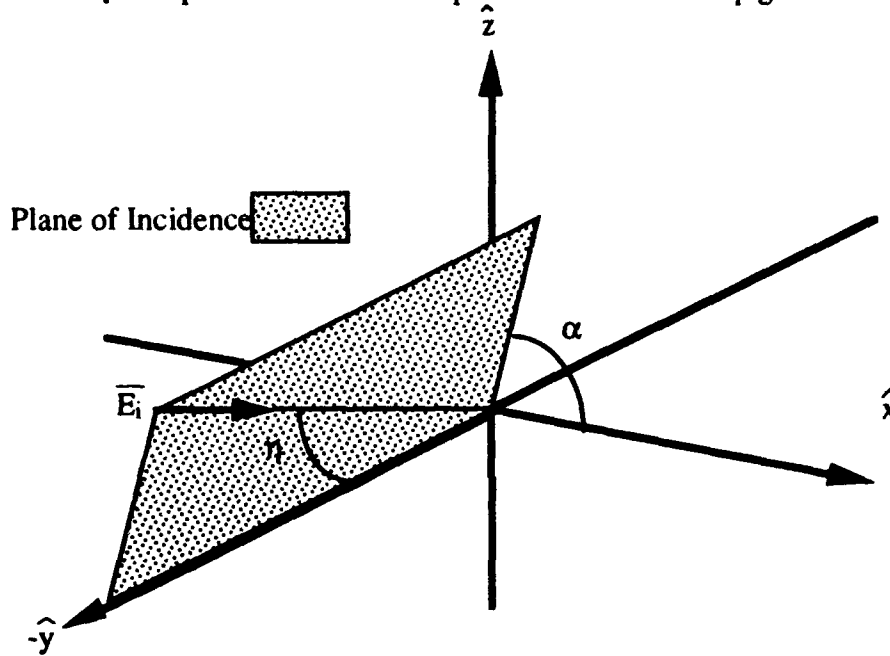


**Figure 4. PMM Coordinate System.** This is the coordinate system used by Henderson's PMM code and Yoder [2] [6]. This coordinate system will be used throughout this thesis.

***Primich's Solution for Multiple Thin Strip Gratings.*** Primich [10]

provided a solution for multiple thin strip gratings of equally spaced, identical strips in a non-skewed array. This solution works for strip gratings that are separated by free space with arbitrary incidence. Primich's solution works very well and compares favorably to experimental results. The first capacitive taper could be modeled using Primich's solution, but numerical techniques presented later will be much easier to implement. The second capacitive taper used multiple strip gratings, but the arrays were in skewed arrangement

(the second array was offset from the first array by half a center-to-center spacing). Also the second capacitive design had a thin dielectric slab in between the arrays.

***Felsen and Carin's Solution for Truncated Strip Gratings.*** Felsen and Carin [7][8][9] have authored several papers on Floquet mode adapted solutions to truncated periodic arrays in free space. Their solutions were based upon a saddle point technique of asymptotic solutions. These solutions were very accurate for both near and far field solutions. However, these solutions are more complicated than Wait or Yoder's solutions and were not used in this study.

***Solutions for Conductors on a Dielectric Slab.*** There are several solutions for scattering from periodic structures on a dielectric slab. Chen [11] and Lee [12] described scattering from periodic arrays of apertures. These solutions use MoM techniques to determine the scattered fields. These solutions also require that any dielectric placed on the array needs to be symmetrically placed. Montgomery [13] developed a solution for arbitrary placed dielectric media. Montgomery's solutions could model the second inductive design, but Henderson's PMM code provided a much easier numerical modeling of this design.

### ***Meanderline Grids.***

***Overview.*** Meanderline grids were first proposed by Lerner [14] as circular polarizers due to their special ability to advance or retard an electric field depending upon the polarization. Meanderlines have the property where the impedance is either inductive or capacitive depending upon the polarization of the E field (See Figure 5). If the E field is parallel polarized to the grid, the grid appears as a shunt inductance. If the E field is orthogonal polarized to the grid, the grid will appear as a shunt capacitance. This difference causes a linearly polarized wave, which is polarized at  $45^\circ$  to the grid, to become circularly polarized. The incident linearly polarized field has equal components parallel and orthogonal to the meanderline that are originally in phase with each other. The component

of the field orthogonal to the meanderline is advanced  $45^\circ$  and the component of the field parallel to the meanderline is retarded  $45^\circ$ . Since these components are now equal in magnitude and  $90^\circ$  out of phase, a circularly polarized wave is emitted. Several layers of meanderlines are sometimes used to make the circular polarizer have better wideband characteristics.

**Meanderlines Use in This Study.** Meanderlines have the advantage over parallel wires to be able increase the inductance, without having to increase spacing between elements. Terret et al [15] introduced a way of determining the susceptance using MoM techniques. Young et al [16] originally produced a method of finding analytically the loss mechanisms of meanderline designs. Chu and Lee [17] then developed a full analytical model of multi-layered meanderline with arbitrary incidence. Skewed slot arrays were used in this study in lieu of meanderlines for a more continuous taper design. (See Figure 6 and let  $S$  approach 0)

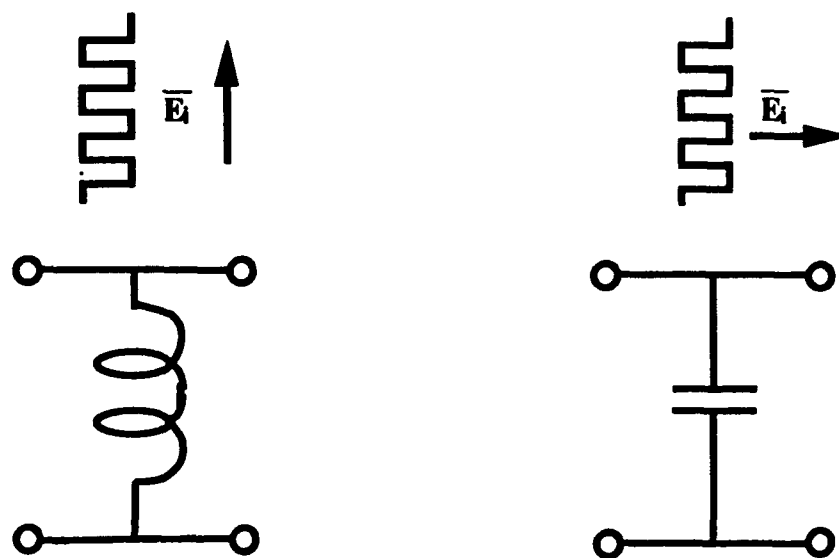


**Figure 5. Meanderlines Impedance as a Function of Polarization.** If the E-Field is polarized parallel to the meanderline, the meanderline design acts as an inductor. If the E-Field is polarized orthogonal to the meanderline, the meanderline design acts a capacitor.

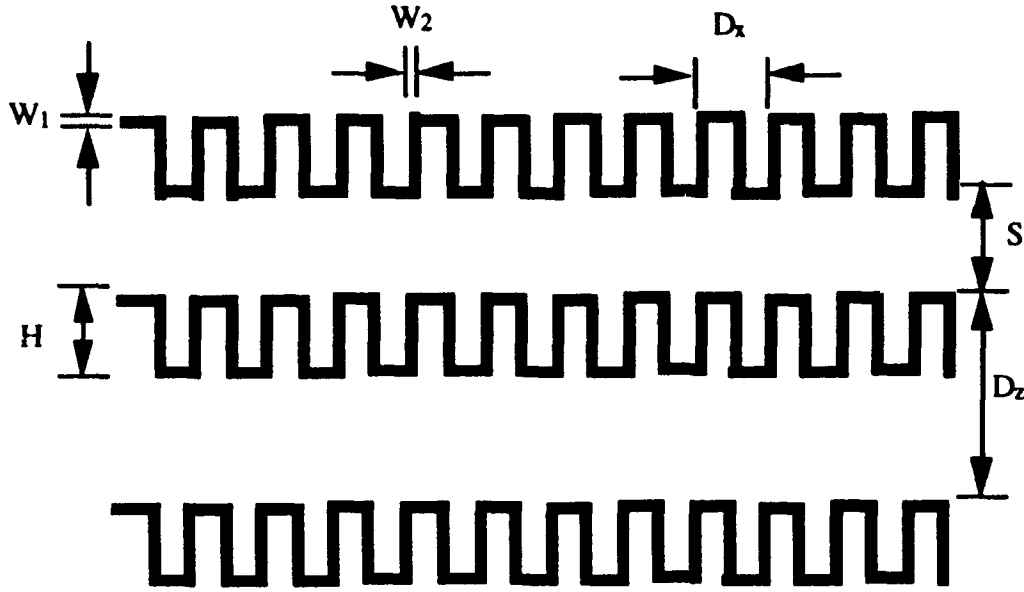


**Figure 6. Meanderline Grid.** The above figure defines the spacing of the meanderlines, the periodicity (pitch) of the design, the line widths and the alternating structure of the meanderlines to approximate slots. If  $S$  approaches 0, the above design becomes a skewed slot array.

**Young's Solution for Insertion Loss.** Young [16] identified the loss mechanisms in meanderline designs. He identified the meanderline loss, dielectric substrate loss and the loss of spacings between meanderline sheets. The loss term associated with the meanderlines is directly related to the  $Q$  of the inductive filter. The total loss of the meanderline design is

$$\Delta L_A \approx \frac{12.5}{w Q_{u,\text{total}}} \text{ dB}, \quad (2.6)$$

where  $Q_{u,\text{total}}$  is defined as

$$\frac{1}{Q_{u,\text{total}}} = \frac{1}{2} \left( \frac{1}{Q_{u,L}} + \frac{1}{Q_{u,C}} \right) + \frac{1}{Q_{u,\text{spacer}}} + \frac{1}{Q_{u,\text{dielectric}}}, \quad (2.7)$$

where  $Q_{u,L}$  is defined by

$$Q_{u,L} = \left( \frac{2500}{\rho \lambda} \right) \left( \frac{W_2(H - W_1)}{H - W_1 + D_x/2} \right) \log_{10} \left( \frac{D_x}{W_2} \right), \quad (2.8)$$

with

$\Delta L_A \equiv$  total insertion loss

$\delta \equiv$  skin depth

$\rho \equiv$  resistivity

$\lambda \equiv$  free space wavelength

In these calculations,  $Q_{u,C}$  is considered much larger than  $Q_{u,L}$  and therefore can be ignored. Also, the  $Q$  of the spacer and dielectric can be ignored if the thickness is less than 10 mils (which is true in this study). The variables used above are defined in Figure 6. If  $D_z$  was set to  $H$ , the meanderlines could be modeled as a skewed slot array, which will make the design have a more continuous taper and a larger bandwidth. This method was not used due to ease of computation of Henderson's PMM code.

**Terret's Solution for Scattering Using MoM.** Terret et al [15] developed a moment method solution for meanderlines. This solution broke the individual meanderlines into 6 modes. Terret's solution was not chosen in this study because the PMM code proved to be as accurate and computationally faster.

**Chu and Lee's Analytical Solution.** Chu and Lee [17] offered an analytical model for multi-layered meanderline designs. In Chu's solution, the effective sheet impedance of the meanderlines can be incorporated into a transmission line analogy for both orthogonal and parallel solutions. For the parallel polarized E-field (which is of interest in this study) the formula developed by Chu is

$$Z_{||} = \frac{j \eta D_x}{2\lambda \left[ 1 - \left( \frac{fH}{5.62} \right)^2 \right]} \left\{ K_4 \left[ -\frac{D_z}{D_x} \ln \left( \frac{\pi W_2}{2D_z} \right) \right] + K_5 \left[ \frac{2H}{D_x} \ln \left( \frac{4D_x}{\pi W_1} \right) - 0.492 \right] \right\} \quad (2.9)$$

where  $K_4$  and  $K_5$  are constants to be experimentally measured.

Since the constants  $K_4$  and  $K_5$  could not be determined, this method was not used.

## ***Numerical Solutions for Capacitive and Inductive Tapers***

**Overview.** This section details the numerical solutions used in this study. Due to the complexity of the designs, only Wait's and Yoder's methods may be of use to mathematically predict the inductance of parallel wire grids (the first inductive design). Therefore, numerical methods offer the best choice to model the impedance tapers. Each section will outline the workings of each method, the limitations of each method and the resources required for each method. Each one of these methods are well accepted methods to study electromagnetics. All the numerical codes used have been validated when compared to measured data.

**Uniform Theory of Diffraction (UTD).** Kouyoumjian and Pathak [18] developed the UTD in their classic paper in 1974. This solution used asymptotic methods to solve for diffraction from a wedge (see Figure 7), without the singularities at shadow boundaries from Keller's Geometrical Theory of Diffraction (GTD).

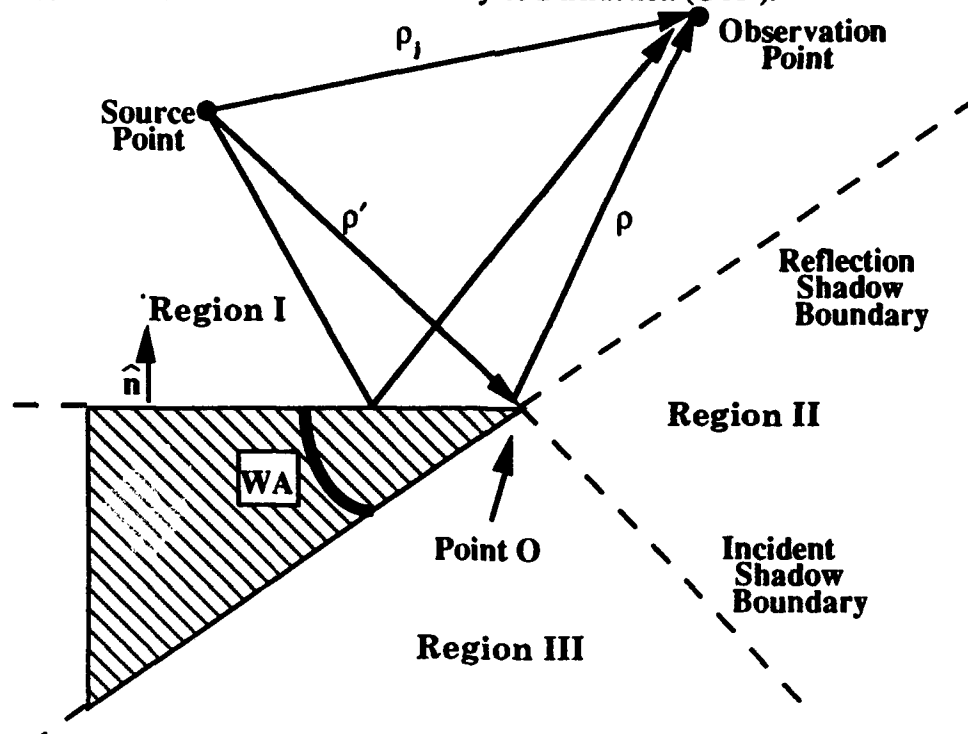


**Figure 7. 2D Wedge Illuminated by an Infinite Line Source.** This figure defines the values used in the UTD calculation. For this study,  $WA = 0$  and therefore  $n = 2$ .  $\rho' = 5$  to  $45 \lambda$  and  $\rho$  is very large for far field measurements.

The total field at an observation point is given by the incident field plus the reflected and diffracted fields. The incident and reflected fields are quite simple to find. Pathak's diffraction equation for both soft (orthogonal to the plane of incidence) and hard (parallel to the plane of incidence) polarizations is

$$u^{\text{diff}} = u^{\text{inc}} D_{s,h} \frac{e^{-jk\rho}}{\sqrt{\rho}}, \quad (2.10)$$

where  $u^{\text{inc}} = u(O)$  and

$$D_{h,s} = \frac{-e^{-j\pi/4}}{2\pi\sqrt{2\pi k}} \left[ \begin{array}{c} \left( \cot\left[\frac{\pi+(\phi-\phi')}{2n}\right] F[kL^i a^+(\phi-\phi')] + \right) \left( \cot\left[\frac{\pi+(\phi+\phi')}{2n}\right] F[kL^m a^+(\phi+\phi')] + \right) \\ \left( \cot\left[\frac{\pi-(\phi-\phi')}{2n}\right] F[kL^i a^-(\phi-\phi')] + \right) \left( \cot\left[\frac{\pi-(\phi+\phi')}{2n}\right] F[kL^m a^-(\phi+\phi')] + \right) \end{array} \right] \quad (2.11)$$

and where the transition function  $F(x)$  is defined as

$$F(x) = 2j\sqrt{x}e^{jx} \int_{\sqrt{x}}^{\infty} e^{-j\tau^2} d\tau, \quad (2.12)$$

$$a^{\pm}(\beta) = 2 \cos^2 \left[ \frac{2n\pi \pm \beta}{2} \right], \quad (2.13)$$

where  $N^{\pm}$  are integers which satisfy,

$$2\pi n N^{\pm} - \beta = \pm\pi, \quad (2.14)$$

where  $n$  describes the wedge angle in radians by

$$n = 2 - \frac{WA}{\pi}. \quad (2.15)$$

Because the wedge is made of flat plates

$$L^i = L^m = L^o = \frac{\rho\rho'}{\rho + \rho'}. \quad (2.16)$$



Two codes for UTD solutions were written for both hard and soft polarization. These codes are included in the Appendix C. Note that these two codes use two subroutine (WDC.FOR and FTF.FOR) to determine the wedge diffraction coefficient and the Fresnel transition function, which were developed at OSU. The exact values used in the UTD code are given in Chapter 3.

**Method of Moments (MoM).** MoM is one of the most widely used numerical methods in electromagnetics. MoM can be used to solve any linear operator equation by treating the equation as a system of linear equations. MoM determines the equivalent scattering currents and then uses the electric or magnetic field integral equations to determine the scattered fields. The currents can be found by using testing functions and basis functions. In this method, the equivalent scattering currents representing small wires or strips are found.

The two codes were used in this study for the TMz ( $H_z = 0$ ) and TEz ( $E_z = 0$ ) polarizations. The TMz polarization code was developed by myself and uses point testing functions (delta functions) and pulse basis functions (see Figure 8). For accuracy the length of the modes was kept beneath  $0.1\lambda$ . This code can handle PEC loaded scatterers as well. For this study, only PEC scatters were considered. The TEz code was a singly-periodic code for dipoles [19].

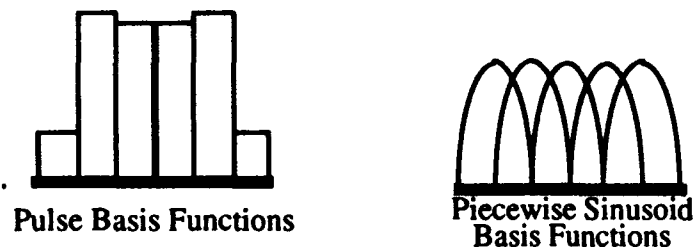


**Figure 8. MoM Basis Functions.** These are graphical representations of the two different basis functions on a thin strip used in this study.

This code handles singly periodic structures which are periodic and infinite in the  $\hat{z}$  direction. This code also can handle PEC and loaded structures as well as active elements.

This code used piece wise sinusoid functions for basis functions, therefore for accuracy the length of the modes must be kept beneath  $0.5\lambda$  (see Figure 8). These codes required only a Sun workstation to run and each run took around 10 minutes.

***Periodic Moment Method (PMM).*** The periodic moment method is a derivation of the moment method which finds the transmission and reflection coefficients for doubly-infinite arrays of scatterers using Floquet's theorem. The code used was version 3.1 by Henderson [2]. In this study the code was set up to use piece wise sinusoid basis functions. This code can handle arrays of slots and dipoles as well as slabs of dielectrics. To use this code, local periodicity was assumed. The code output was the plane wave reflection and transmission coefficients for orthogonal and parallel polarizations. This numerical method was used to determine the scattering from the periodic structures and the results were then used to design the tapers. The code has been mathematically and experimentally verified and was a very easy code to implement.

***Finite Difference Time Domain (FDTD).*** The conceptually simplest of all the numerical methods is FDTD. FDTD, first proposed by Yee [20], uses a central differencing technique to solve for Maxwell's equations directly in the time domain. The FDTD solutions were quite memory and time intensive on computational facilities (the runs required 50 MB of RAM and 5 hours of run time on a Silicon Graphics workstation). However, this method was able to handle inhomogenous media very easily and the output was inverse Fourier transformed to give frequency information from 0 to 70 GHz. The grid size was determined by the minimum time step and the smallest size of scatterers to be modeled. The number of time steps was determined by the amount of time required for the field to completely propagate through the medium [21]. The code used was TEARHTFI.FOR Version C developed by Luebbers [3] for the United States Air Force. This code used a second order Liao boundary condition [22] and standard near to far zone transform.

## ***Summary***

This chapter outlined the current knowledge on the subject of creating inductive or capacitive periodic surfaces. The analytic solutions presented were not used in this study due to the computational efficiency and ease of numerical analysis. The different numerical analyses used in this study were also outlined. The implementation of the numerical methods will be explained in more detail in Chapter 3.

## **Chapter 3: Methodology**

### **Introduction**

**Overview.** This chapter describes the methodology used in this study. In the first section, the taper design methodology is explained. The second section covers how the tapers were built. The third section covers how the measurements were made. The last section covers the numerical analysis of the tapers. Also any assumptions or possible sources of error are identified.

### **Methodology in Design of the Tapers**

**Overview.** This section describes how the tapers were designed. The tapers designed had capacitive or inductive properties. The desired properties of a taper design were the impedance match both ends of the taper (the ground plane edge and the free space edge) and the continuous tapering in the design (no discontinuities). These properties must occur over an appreciable bandwidth between 2-18 GHz. The difficulty with both capacitive and inductive designs was to create either a large enough capacitance or inductance. Henderson's PMM code [2] was used to study the frequency range 2-18 GHz for the crucial edge of the taper (free space edge for inductive taper and ground plane edge for capacitive taper). For each design, both a long and a short taper were developed. The long taper was  $2\lambda$  at the lowest frequency (30 cm) and the short taper was  $1\lambda$  at the lowest frequency (15 cm). From the first measurements, a second inductive and capacitive taper were developed.

**Test Platform.** Since the results from this study were to ultimately develop better tapering mechanisms for antennas, the tapers needed to be effective at near grazing incidence. To study the effectiveness of the taper designs, a platform was tried to simulate an semi-infinite thin ground plane ( a 2D wedge where  $n = 2$ ). The edge must be at least  $5\lambda$  (75 cm for 2 GHz) long to simulate a 2D edge. Also for a plane wave assumption, the

source must be at least  $5\lambda$  away from the edge. The AFIT Model Shop built the platform for the measurements. To minimize edge diffraction from the sides of the ground plane, the AEL horn was mounted at the apex of a triangular plate. The triangular plate was then mounted on a 2 inch styrofoam substrate for stability. The rear of the styrofoam substrate had the right angle edges cut off to form two  $45^\circ$  angle edges (this should reduce the small amount of scattering from the styrofoam substrate). The styrofoam extended 30 cm beyond the long edge of the triangle to support the impedance taper designs. The AEL horn antenna was then mounted by a wooden bracket to the apex of the triangle. The entire structure was then mounted a rotational platform by attaching a quarter-inch plywood plate under the styrofoam substrate. Since the distance from the antenna to the edge is more than  $5\lambda$ , the plane wave incidence on the edge was fairly valid. See Figure 9 for the setup for the antenna platform.

***Inductive Tapers.*** For the inductive tapers, the crucial edge was the free space edge (high impedance). Therefore, in the design of inductive tapers, it was important to develop the free space side so that the inductance was very high over the frequency band. To use Henderson's PMM code to develop the free space side of the inductive taper, the transmission coefficient was computed for the entire frequency range of interest (2-18 GHz). The design for the free space edge of the taper should have a high transmission coefficient (close to 0 dB) over the bandwidth. By determining the free space side of the taper, the rest of the taper was determined by linearly varying the taper variable (wire spacing in design #1 and slot length in design #2) to the ground plane edge. The first design was made by using the inductive properties of a parallel wire grid with tapered spacing. The second design used the inductive properties of thin slots by tapering slot length in a skewed slot array.

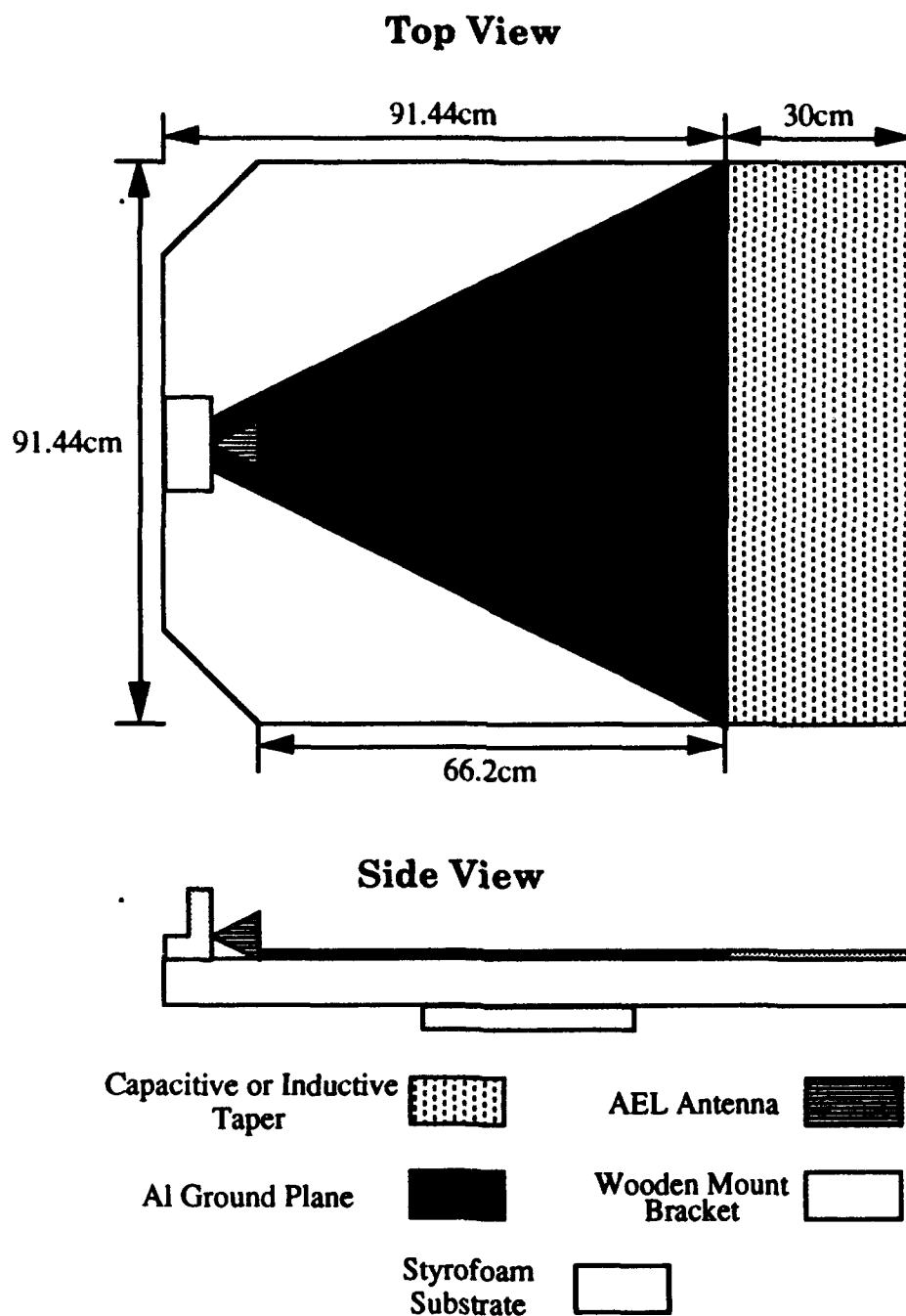


**Figure 9. Antenna Platform for Measurements.** This platform was designed to simulate a near grazing plane wave upon a 2D edge. The Aluminum ground plane should be illuminated only at the long edge (tapered edge). The entire structure was then mounted as an antenna and measured both with and without tapers for both polarizations. The styrofoam substrate was to provide stability for the tapers and the ground plane. The rear edges cut in the styrofoam were to reduce any small amount of scattering from the styrofoam substrate.

**Inductive Taper Design #1.** A parallel wire grid with constant radius wires with varying spacing was used as the first inductive taper. The largest spacing that had a high transmission coefficient over the frequency domain was 1 cm (see Figure 10). The wires were attached to a 2 mil poly-ethylene plastic sheet which was then attached to the styrofoam substrate. The wires that were available were made out of copper coated steel welding rods and were 91.44 cm long and had a 1/32 inch radius. These wires were then attached to the plastic with scotch tape. The spacing was linearly increased from 0 to 1 cm over the length of the taper (see Figure 11). A long (30 cm) and a short (15 cm) parallel wire taper were constructed and tested.

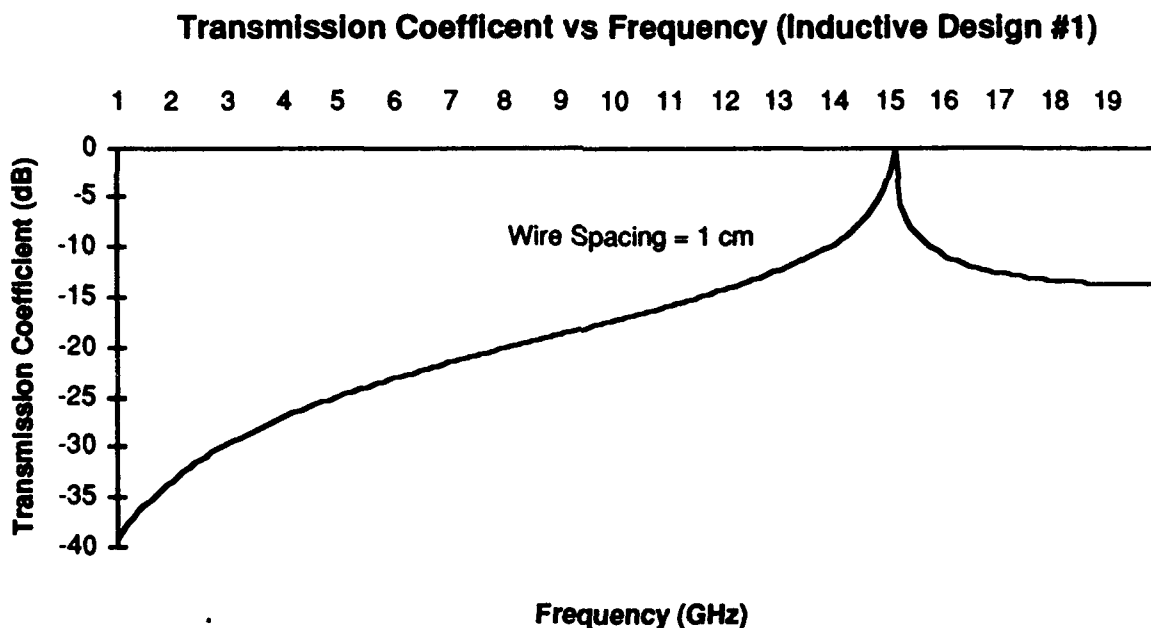


**Figure 10. Transmission Coefficient vs Frequency for Inductive Design #1.** This is the graph of the transmission coefficient for the free space edge of the first inductive taper computed using PMM at 10° off grazing incidence. This design is for an parallel wire grid of constant radius (1/32 inch) wires with 1 cm spacing.

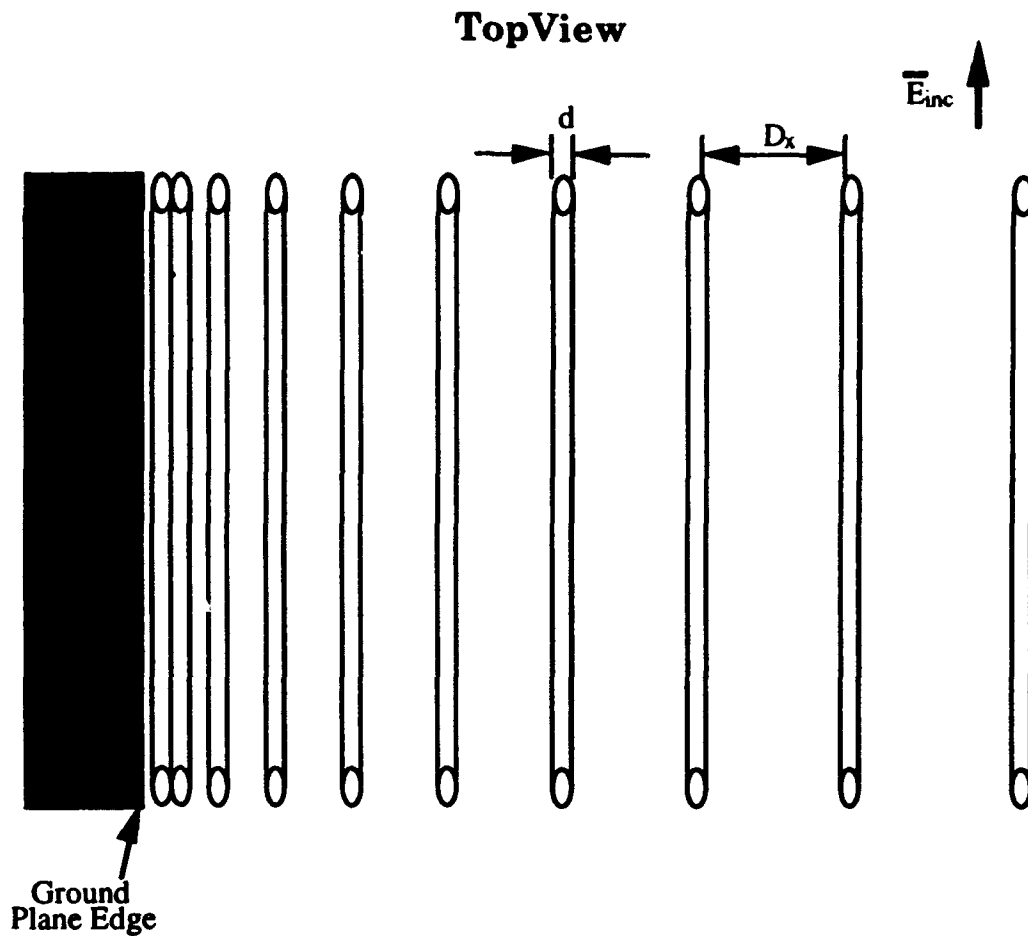


**Figure 11. Inductive Taper Design #1.** This was the first inductive taper design. Each wire had the same radius (1/32 inch). The spacing was linearly increased from 0 cm (ground plane edge) to 1 cm (free space end).

**Inductive Taper Design #2.** The second inductive taper was developed by using the inductive properties of thin slots. The impedance taper was made by increasing length of slots in a skewed array over the length of the taper (See Figure 13). The largest slot that had a high transmission coefficient over the frequency band was 350 mils (See Figure 12). This time the design was photo etched upon a 10 mil dielectric substrate ( $\epsilon_r = 4.5$ ). The minimum line width for the photo etch process was 5 mils; therefore, the length of the slots was linearly tapered from 5 mils to 350 mils. The slot width was held constant at 5 mils. Two inductive tapers were made using this design (15 and 30 cm long) and then tested.



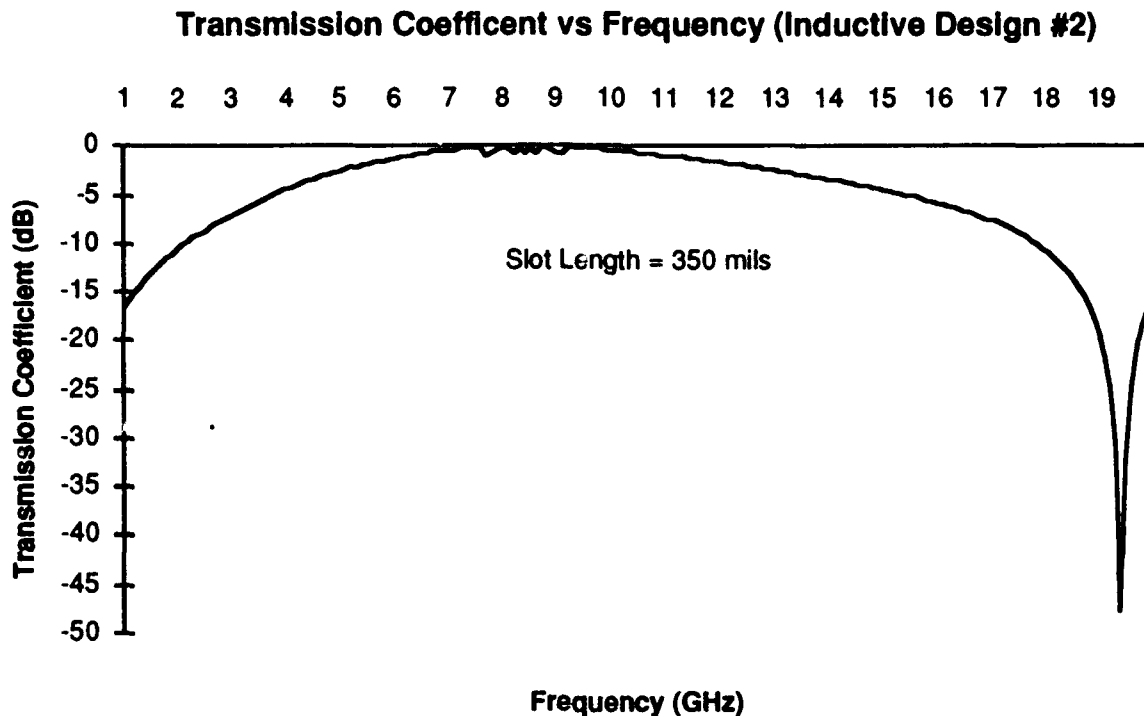


**Figure 12. Transmission Coefficient vs Frequency for Inductive Design #2.** This is the graph of the transmission coefficient for the free space edge of the second inductive taper computed using PMM at  $10^\circ$  off grazing incidence. This design was a skewed slot array of constant slot width (5 mils) wires with slot length 350 mils.

**Capacitive Tapers.** For the capacitive tapers, the edge that was difficult was the ground plane edge. The difficulty was to develop a design that had large capacitance (low impedance) over a large bandwidth. Using Henderson's PMM code, the reflection coefficient was measured over the bandwidth. The reflection coefficient for the ground plane side should be very close to unity (0 dB) over the bandwidth. Two separate capacitive tapers were designed. The first capacitive taper was developed by having thin strips of tapering lengths and constant center-to-center spacing. The second capacitive taper was made of two arrays of thin strips with tapered lengths and constant center-to-center spacing with a thin dielectric substrate slab in between them. The second array was offset from the first array by half of a center-to-center spacing.

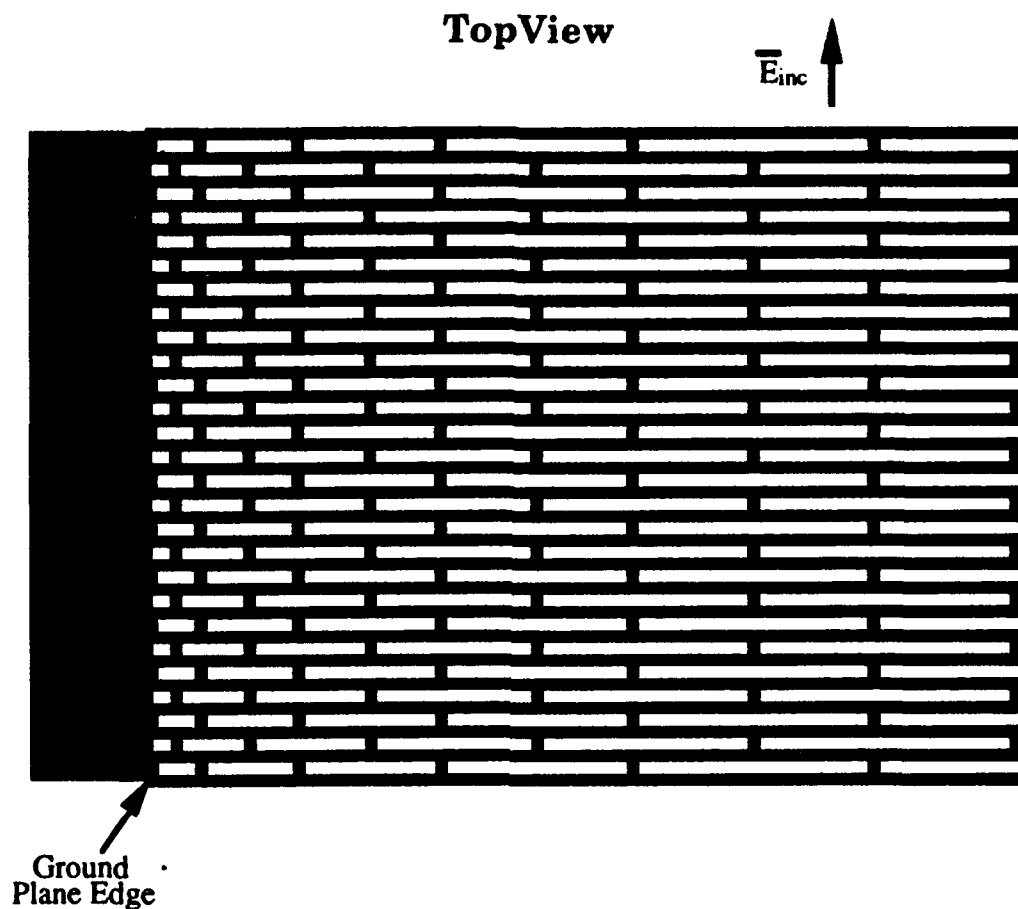


**Figure 13. Inductive Taper Design #2.** This was the second inductive taper design. Each slot had the same width (5 mils). The slot length was linearly increased from 5 mils (ground plane edge) to 350 mils (free space end).

**Capacitive Taper Design #1.** The first capacitive taper was made by spraying on thin strips using copper paint on a thin sheet of paper. The strips had a constant center to center spacing with a linearly decreasing strip width on a thin drafting paper with very near unity dielectric constant (See Figure 14). The strips had very high impedance due to difficulty in painting small straight strips over 90 cm long. Since these strips were hand painted, the smallest gap between strips was only 0.5 mm. From Henderson's code, the largest strip that had a high reflection coefficient was 5.5 mm (see Figure 15); therefore, the center to center spacing was 6 mm. The measured results from this first capacitive taper are very questionable due to the crude manufacturing. No short taper was made.

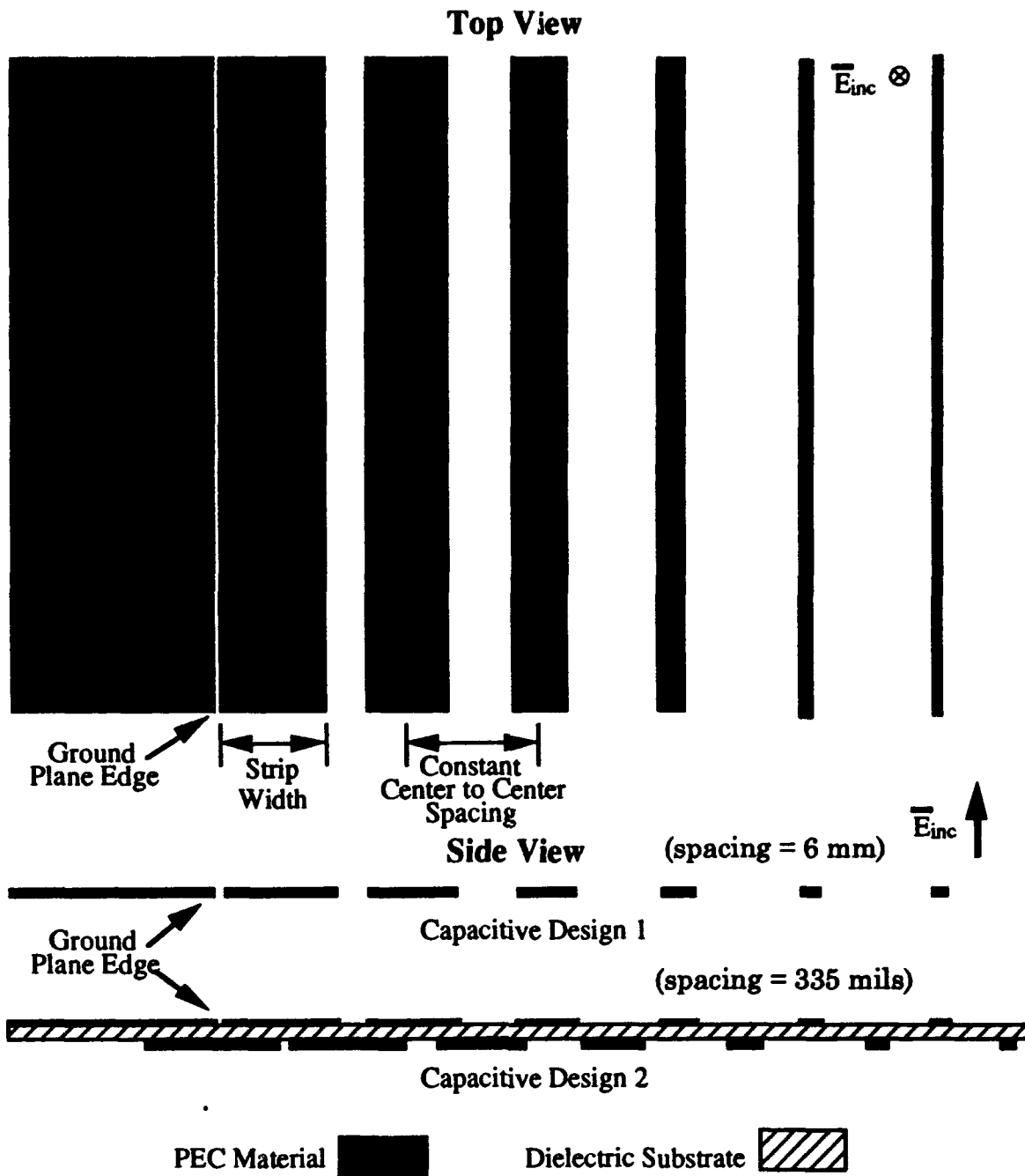


**Figure 14. Capacitive Taper Designs #1 and #2.** Both of the capacitive tapers had constant center-to-center spacing between the PEC strips. The strip widths were varied linearly from the ground plane edge to the free space edge. The first capacitive design strip width was tapered from 5.5 mm to 0.5 mm. The second capacitive design strip width was tapered from 330 mils to 5 mils. Also the second taper had another tapered array of strips on the bottom of the dielectric substrate that was offset by 167.5 mils.

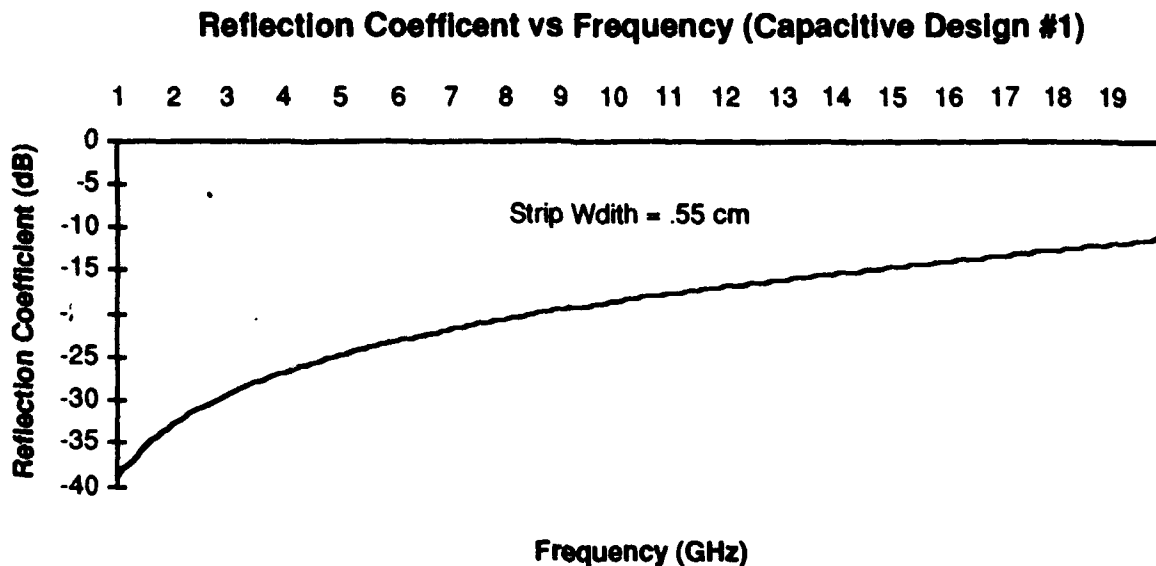


**Figure 15. Reflection Coefficient vs Frequency for Capacitive Design #1.** This is the graph of the reflection coefficient for the ground plane edge of the first capacitive taper computed using PMM at  $10^\circ$  off grazing incidence. This design was a thin strip array of constant center-to-center spacing (6 mm) with strip width 5.5 mm.

**Capacitive Taper Design #2.** The second taper was photo etched on a 10 mil dielectric substrate (with a 5 mil minimum line width). The dielectric substrate had a dielectric constant of 4.5 over 2-18 GHz. The second capacitive taper design had a constant center to center spacing design with varying strip widths. This design had a second array of thin strips on the bottom of the dielectric substrate (to increase the capacitance). The bottom array was the same as the top array except that it was offset by half of a center-to-center spacing (See Figure 14). The widest strip that had a 5 mil gap and a large reflection coefficient over the entire bandwidth was 330 mils wide (See Figure 16). The strip widths were therefore linearly tapered from 330 to 5 mils. Therefore, the center-to-center spacing for the second capacitive design was 335 mils. For the second capacitive design, two tapers were built (15 and 30 cm long) and tested at OSU-ESL compact range.

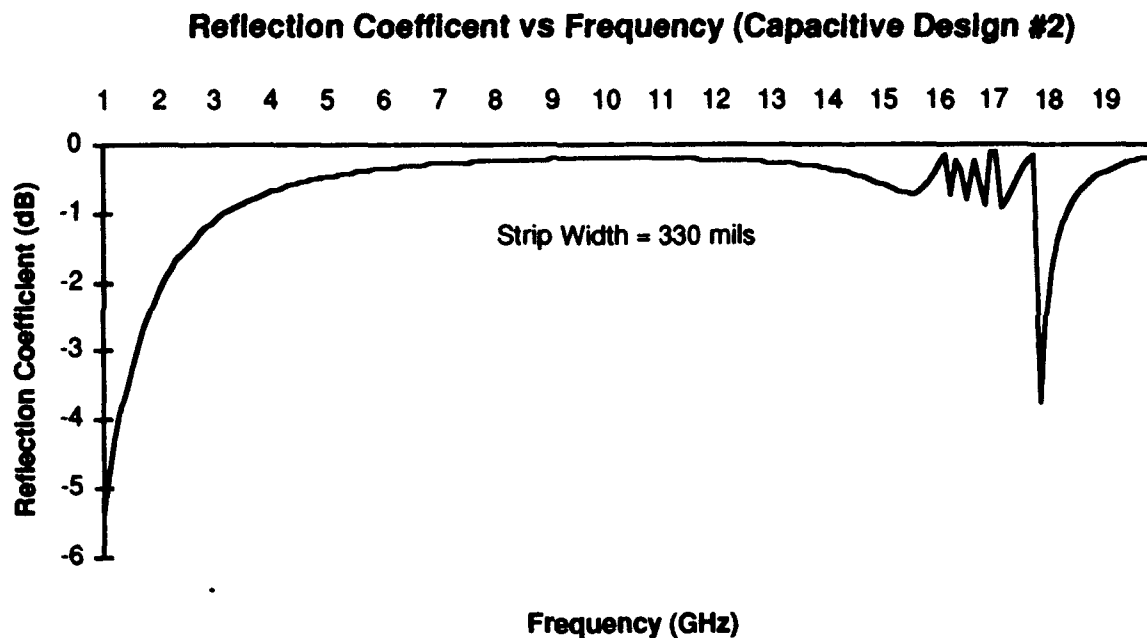


**Figure 16. Reflection Coefficient vs Frequency for Capacitive Design #2.** This is the graph of the reflection coefficient for the ground plane edge of the second capacitive taper computed using PMM at  $10^\circ$  off grazing incidence. This design was for two thin strip arrays of constant center-to-center spacing (335 mils), with strip width tapered from 330 mils to 5 mils.

### *Experimentally Measure the Data*

**Overview.** This section explains how the data was experimentally taken. The antenna platform and tapers were explained in the earlier section. In each experiment, the antenna platform without the edge taper was measured and then the platform with the tapers were measured. The measurements were made on two separate days. The first day the first inductive tapers and the first capacitive taper were measured. On the second day, the second inductive and capacitive tapers were measured. When determining the effectiveness of the tapers, the comparison between with taper and no taper measurements must be on the same day, because no calibration was done between each day's measurements.

**Compact Range.** The compact range used a parabolic reflector to create a far field observation point. There are two receive antennas at the focal point of the reflector, one for each principle polarization. In the center of the range, there is a platform with a rotator which supports the entire antenna platform. (See Figure 17).

**The Measured Data.** The total field was measured in dB for a variety of angles and frequencies. The angles recorded were the bistatic angles, because the source was fixed for all measurements (about  $4.7^\circ$  from grazing off the triangular ground plane). The first measurements were azimuth scans ( $90^\circ$ - $270^\circ$  in  $0.5^\circ$  increments) at discrete frequencies (2-18 GHz in 2 GHz increments). The second measurements were frequency scans (2-18 GHz in 20 MHz increments) at discrete azimuth angles ( $90^\circ$ ,  $120^\circ$ , and  $150^\circ$ ). For the inductive tapers, the American Electronics Laboratory (AEL) source horn was mounted to have soft polarization (E-field is parallel to the edge) on the long edge. For the capacitive tapers, the AEL source horn was rotated to have hard polarization (E-field is orthogonal to the edge) on the long edge. The horn was mounted on the apex of the ground plane by a small wooden bracket that was epoxied to the structure. The antenna was rotated to the proper polarization and then bolted into the wooden bracket. The taper was attached to the styrofoam substrate with masking tape. The interface between the taper and the ground plane was taped over using copper tape to reduce scattering from the discontinuity. To attach the first inductive design, the first wire of the taper was placed next to the ground plane. To attach the first capacitive taper, the first strip was taped to the ground plane using copper tape. To attach the second taper designs to the ground plane, a four inch thick copper strip was photo etched on the dielectric substrate before the taper began. The four inch thick copper strip was then taped using copper tape to the ground plane to reduce scattering from this interface.

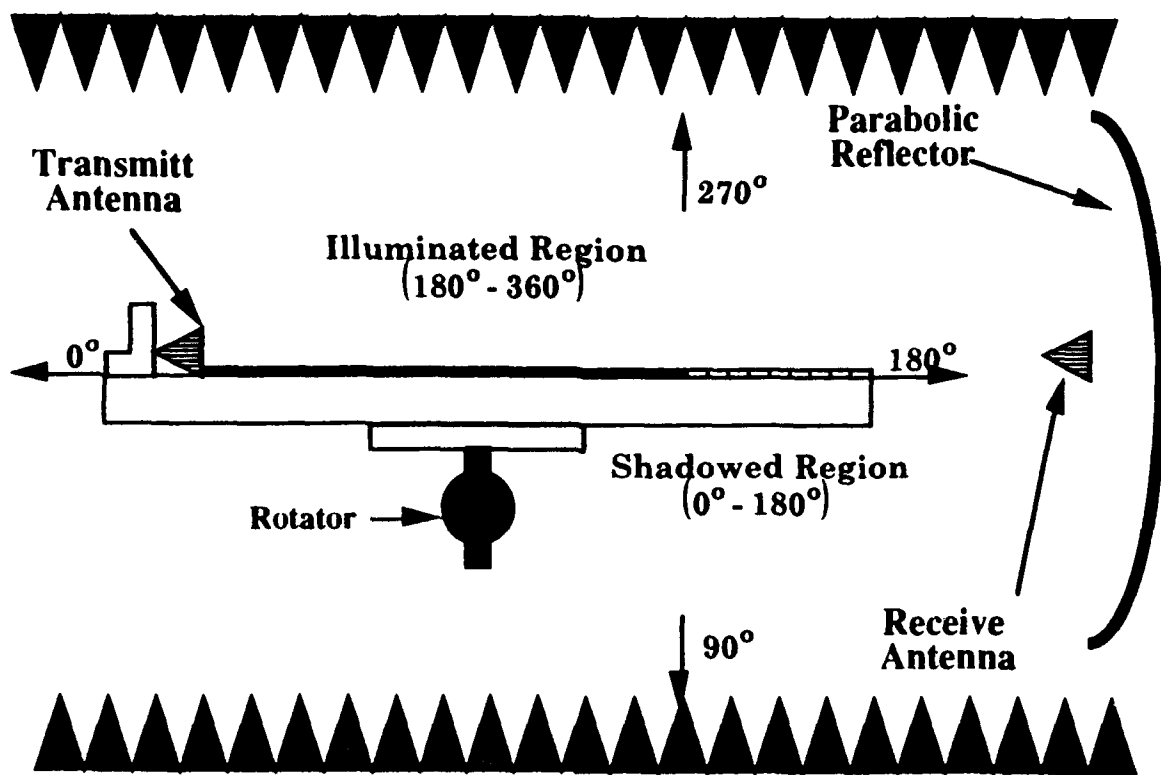


**Figure 17. Compact Range Setup for Measuring the Bistatic Diffraction Pattern.** This was the setup for measuring the bistatic diffraction. Note that the shadowed region was from  $0^\circ$  to  $180^\circ$  and the illuminated region was from  $180^\circ$  to  $360^\circ$ . The transmitting antenna should create an incident wave that is  $4.7^\circ$  off grazing incidence to the knife edge.

### *Numerically Validate the Data*

**Overview.** Numerical techniques were then used to validate the measurements. Each of the following sections describes the numerical techniques used to validate the measurements. The types of numerical techniques used were the Uniform Theory of Diffraction (UTD), the Method of Moments (MoM), the Periodic Moment Method (PMM), and the Finite Difference Time Domain (FDTD) technique. For information on the limitations of each numerical technique see Chapter 2.

**Uniform Theory of Diffraction (UTD).** To ensure that the results of the no taper measurements were valid, UTD calculations for a knife edge ( $n = 2$ ) were computed for comparison. The bistatic data was computed for both soft and hard polarizations for an infinite line source 30 inches ( $5$  to  $45 \lambda$  for 2-18 GHz) from the knife edge at an angle of  $4.7^\circ$  from the ground plane. The results were then compared to the measured data for the no taper measurements to ensure that the simulation of a knife edge is valid.

**Method of Moments (MoM).** Two 2D MoM codes were used to validate the results from the first set of tapers. The first capacitive design was tested using a code developed by Skinner [19]. This code used the periodic moment method for singly infinite arrays (infinite in the  $\hat{z}$  direction) for incident fields that are TE $_z$  polarized. To simulate the thin strips, thin dipoles (radius less than  $\lambda/10$ ) are placed 4 radii apart from each other in the  $\hat{z}$  direction, this simulated a continuous thin strip (See Figure 18). Capt. Skinner's code used piecewise sinusoid basis functions requiring each mode to be no longer than  $\lambda/2$ . The output of Skinner's code was the scattered field as a function of observation angle. The field was incident at an angle of  $170^\circ$ . The observed fields were measured from  $0$ - $360^\circ$  in  $0.5^\circ$  increments. The antenna platform was modeled as a large thin strip (1m long) with a taper on one side. The results from the tapered edge were compared to the results from the large thin strip alone.

The first inductive taper was tested using a code developed by myself for the TM $_z$  polarization. The TM $_z$  code used pulse basis functions and point testing functions. To model the large thin strip, each mode was less than  $\lambda/10$ . To model the thin wire taper, two separate thin wire approximations were used. The wires that were placed closer together than 5 wire radii ( $5r$ ) were represented by square wires with side length  $1.45r$  [1]. For the wires that were placed further apart than  $5r$ , the wires were represented by thin strips with length  $4r$  [1] (See Figure 19). This taper is described in Figure 20. For a listing of the FORTRAN code see Appendix D.



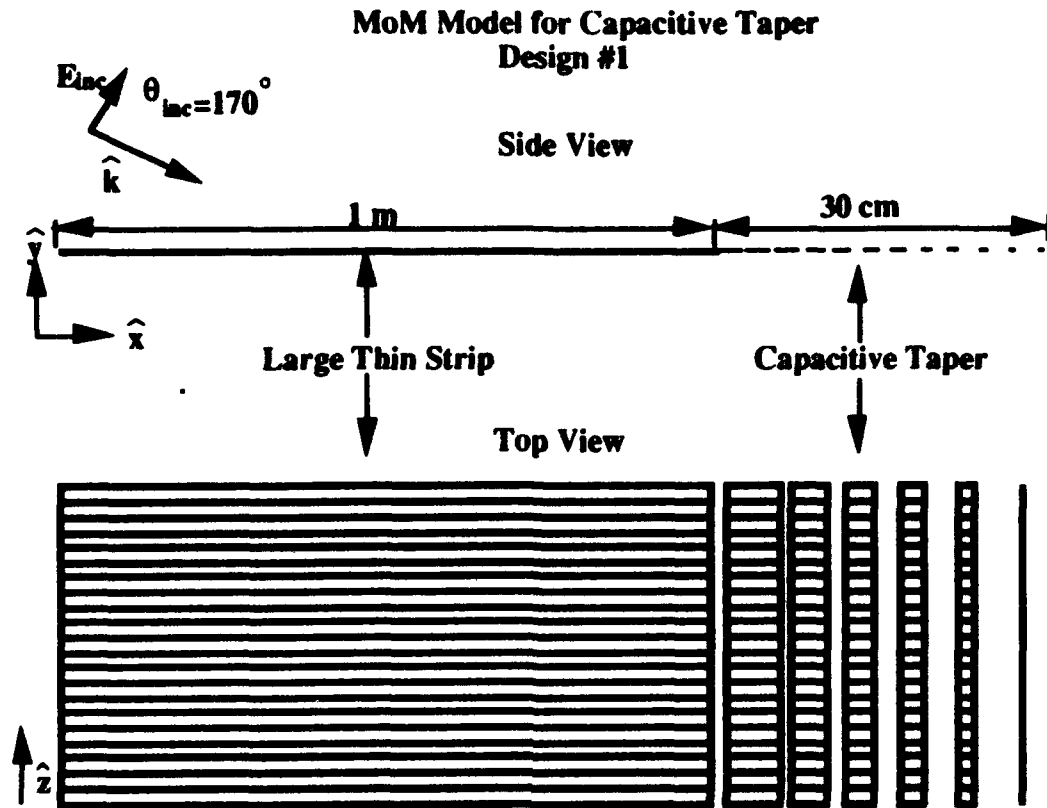


**Figure 18. MoM Model for Capacitive Design #1.** This was the MoM model used to study the first capacitive design. The results from the bistatic scattering with the taper were compared to the results from the bistatic scattering with no taper.

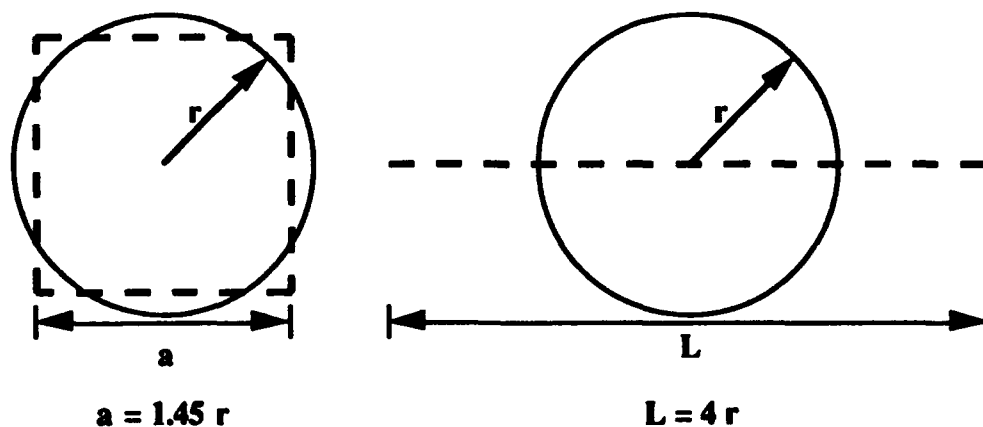


**Figure 19. Equivalent Thin Wire Approximations used in TMz MoM Code.** The thin wires used in the first inductive design were approximated as square wires and thin strips [1].

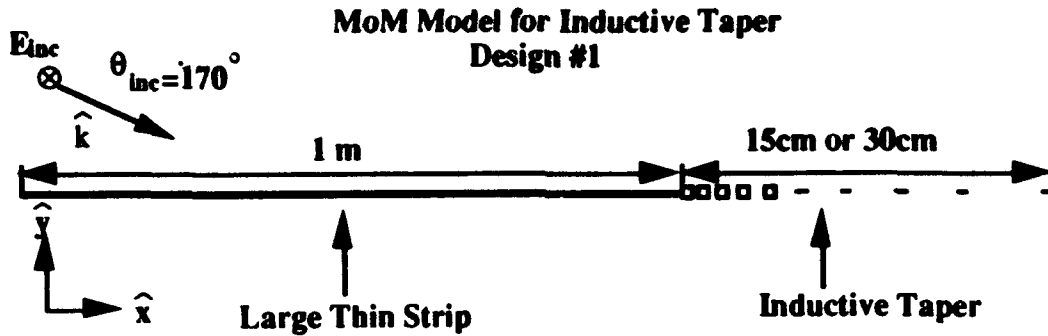


**Figure 20. MoM Model for Inductive Design #1.** This is the MoM model used to study the first inductive design. The results from the bistatic scattering with both long and short tapers were compared to the results from the bistatic scattering with no taper.

**Determine the Effective Impedance.** The next step was to determine the actual impedance taper by determining the impedance from the reflection coefficient. This solution translates the reflection coefficient to a thin sheet impedance. Because the taper designs are very thin (about 10 mils), this approximation was valid up to the first resonance, beyond that resonance another method would have to be used. The equation to determine the effective sheet impedance  $Z_s$  of the grid from the reflection coefficient,  $R$ , was

$$Z_s = \frac{-Z_c(1 + R)}{2R}, \text{ where.} \quad (3.1a)$$

$$Z_{||} = Z_o \cos \eta \quad (3.1b)$$

$$Z_{\perp} = \frac{Z_o}{\cos \eta} \quad (3.1c)$$

**Periodic Moment Method (PMM).** Henderson's PMM code was then used to determine the impedance as a function as length on the taper. By assuming local periodicity, the impedance at any point on the taper can be approximated by using the reflection coefficients from PMM. For PMM code listings see Appendix A.

For the first inductive design, the effective  $\epsilon_r$  of the array was set near zero so that the shape of the PWS approximate overlapping triangular functions. Overlapping triangular functions are better than the standard PWS for the parallel wires, because the

current on the wires should be constant in the  $\hat{z}$  direction for plane wave incidence.  $D_x$  was set to the spacing between wires (1 cm at the free space end).  $D_z$  was set to 0.25 cm and the wire radius was set to 1/32 inch. The length to width ratio was kept greater than 8:1 for accuracy of PMM. The incidence angle was defined by  $\alpha = 0$  and  $\eta = 80$ . (See Figure 21)

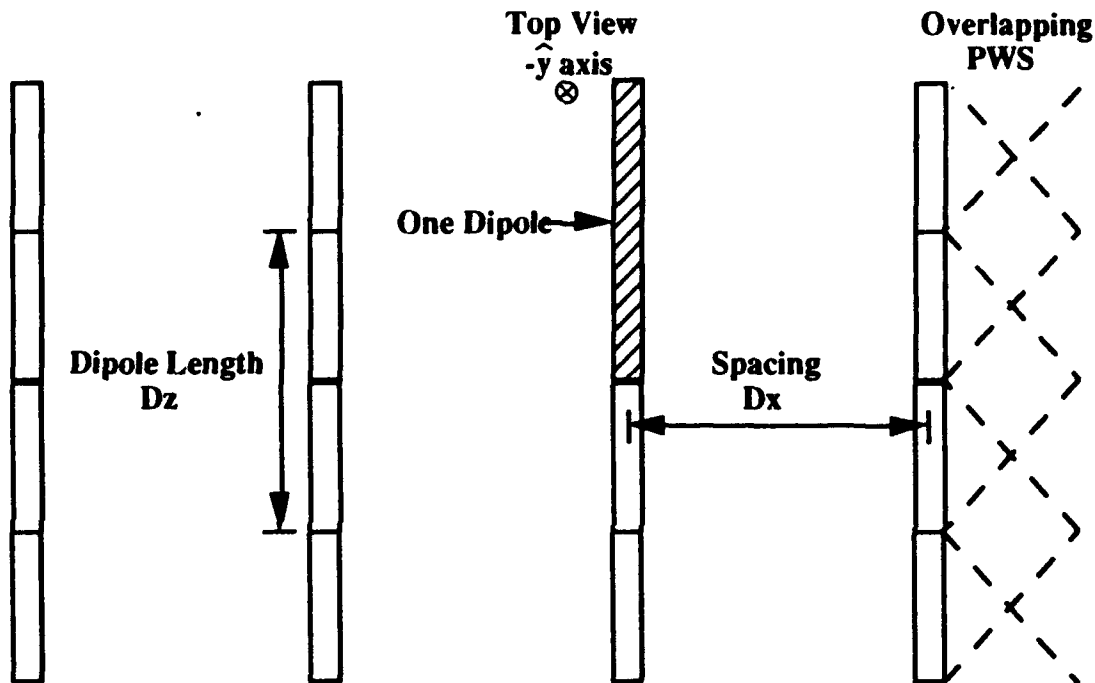


**Figure 21. PMM Model for Inductive Design #1.** This was the model for the parallel wire grid with variable spacing. The incident angle was defined by  $\alpha = 0$  and  $\eta = 80$ . The overlapping dipoles had PWS basis functions. To ensure that the PWS approximate triangular functions, the effective  $\epsilon$  was set to near zero.

The PMM code was then used to model the first capacitive taper. The first capacitive taper (thin strips) were modeled by thin dipoles placed 4 wire radii apart. The wire radii of the dipoles were set very small (0.025 mils) so that the length to width ratio could be kept greater than 8:1 (for PMM accuracy).  $D_x$  was set equal to the equivalent wire width of the wire (0.1 mil), this allowed the dipoles to approximate a continuous thin strip.  $D_z$  was set to the center-to-center spacing (6 mm at the ground plane edge). The current on each dipole was modeled using five overlapping PWS modes. Since these dipoles were

finite in extent, the  $\epsilon_r$  was not set near zero because PWS offered the best basis function model. The incidence angle was defined by  $\alpha = 90$  and  $\eta = 80$ . (See Figure 22)

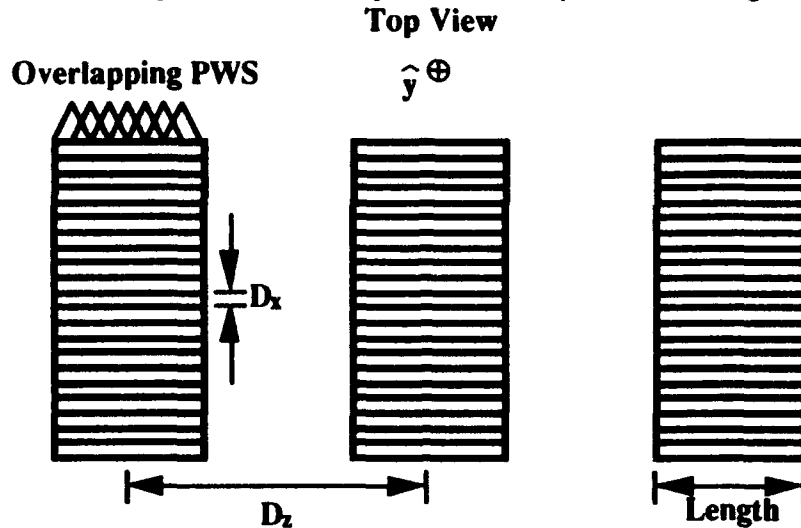


**Figure 22. PMM Model for Capacitive Design #1.** This was the model for the thin strip grid with constant center-to-center spacing and varying length. The incident angle was defined by  $\alpha = 90$  and  $\eta = 80$ .

The second inductive taper was then modeled using PMM. The skewed slot array kept a constant slot width (5 mils). The  $D_z$  was set equal to the length of the slot (350 mils at the free space end) plus the line width (5 mils). The  $D_x$  was set equal to the slot width plus the line width. The skewed array was modeled upon a thin (10 mils) dielectric slab ( $\epsilon_r = 4.5$ ). The current on each of the slots was modeled using five overlapping PWS modes. The incident angle was defined by  $\alpha = 90$  and  $\eta = 80$ . (See Figure 23)

The second capacitive taper was then modeled using PMM. The thin strips were modeled as dipoles placed 4 wire radii (0.025 mils) apart.  $D_x$  was set equal to the equivalent width of the dipoles (0.1 mils).  $D_z$  was set equal to the center-to-center spacing (350 mils at the ground plane edge) plus the minimum gap size (5 mils). Next a thin dielectric slab (10 mils) was placed under the first array ( $\epsilon_r = 4.5$ ). A second identical thin strip array was placed under the dielectric and offset by half of  $D_z$  (167.5 mils). The current on the dipoles was modeled using five overlapping PWS. The incident angle was defined by  $\alpha = 90$  and  $\eta = 80$ . (See Figure 24)

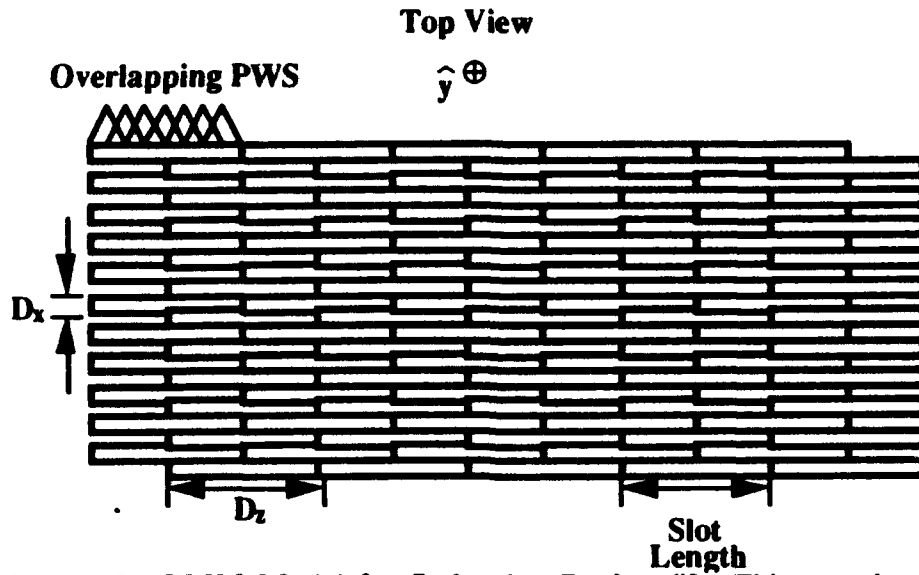


**Figure 23. PMM Model for Inductive Design #2.** This was the model for the skewed slot array. The incident angle was defined by  $\alpha = 90$  and  $\eta = 80$ .

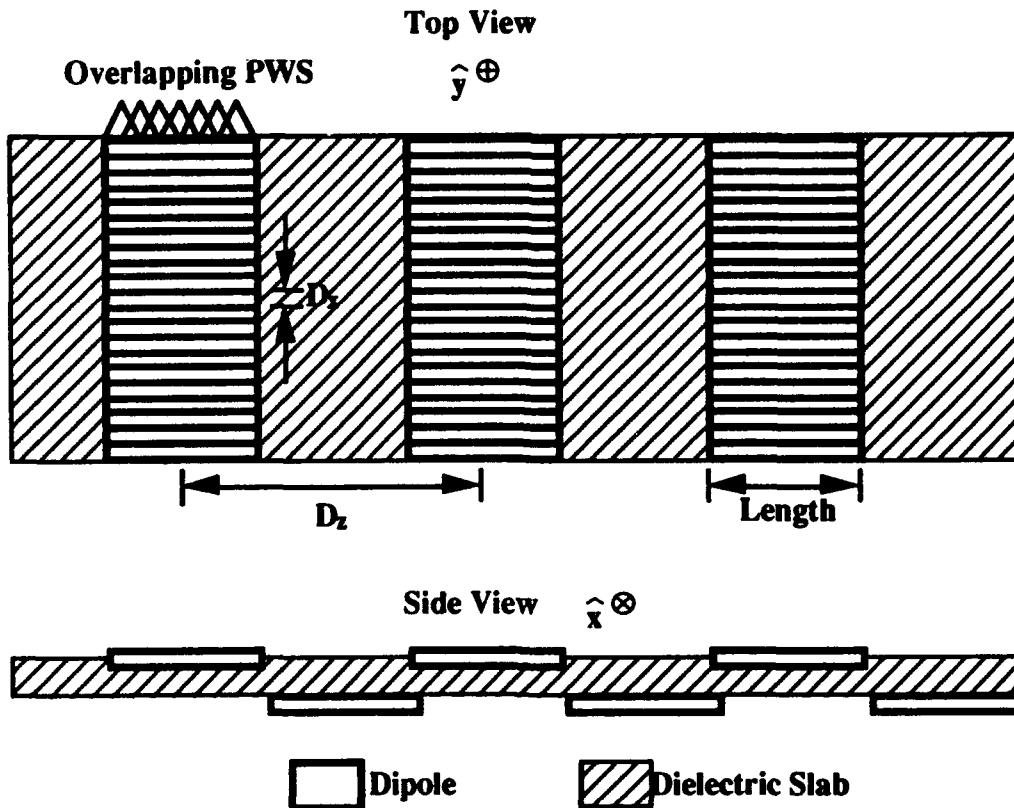


**Figure 24. PMM Model for Capacitive Design #2.** This was the model for the second capacitive design. The incident angle was defined by  $\alpha = 90$  and  $\eta = 80$ .

**Finite Difference Time Domain (FDTD).** Luebber's FDTD code [3] was then used to validate the second capacitive and inductive tapers. This code was run on a Silicon Graphics machine. To ensure that the dielectric slab (10 mils thick) could be modeled by the code the cell size was set to 0.4244 mm by 0.4244 mm which gave time steps of 1 psec. The dielectric constant for the styrofoam was set to 1.02 and the dielectric constant for the photo etch substrate was set to 4.5. The entire grid size for the FDTD run was 4300 by 700 (the Liao boundary condition is generally considered valid for grids which have less than a 10:1 rectangularity). The computer runs for this model required over 50 MB of RAM and several hours to run. The observation angles measured were  $90^\circ$ ,  $120^\circ$ ,  $150^\circ$ ,  $180^\circ$ ,  $210^\circ$ ,  $240^\circ$ , and  $270^\circ$ . The time domain results were then Fourier transformed to echo width using a companion program to the Luebber's code. The results from these runs are given in Chapter 4. (See Figure 25)

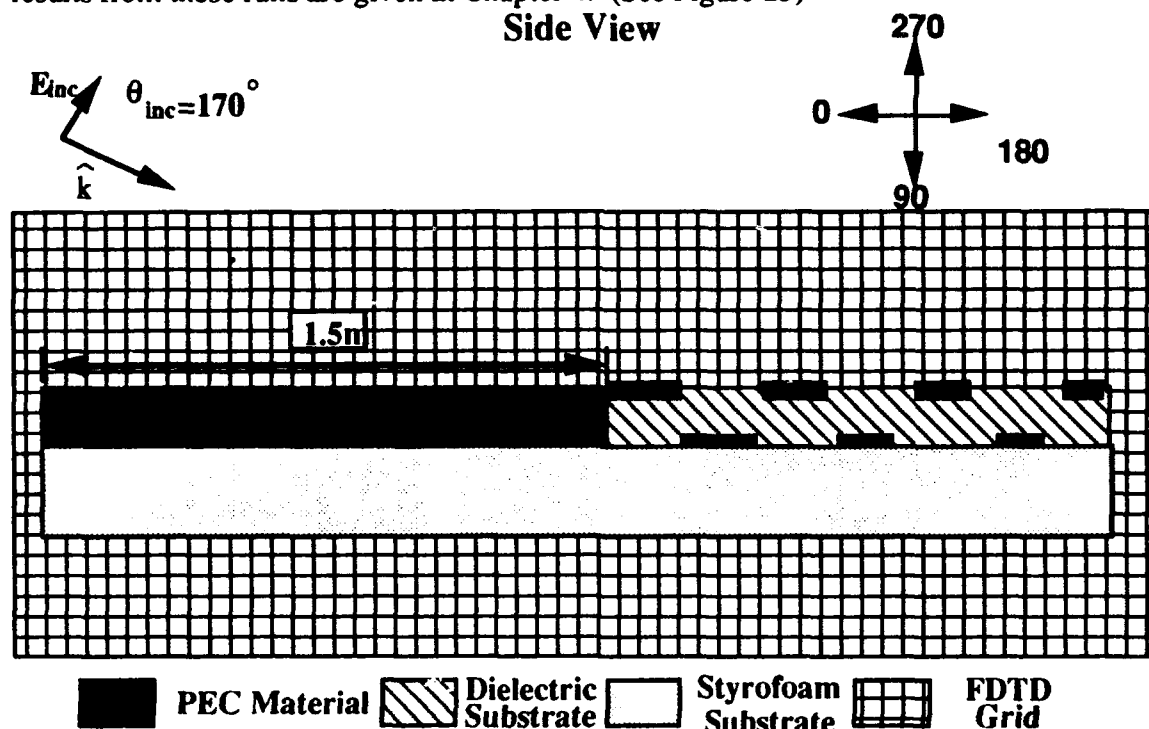


**Figure 25. FDTD Model for Capacitive Design #2.** This was the FDTD model for the second capacitive design. The cell size of the grid was 0.4244 mm by 0.4244 mm. The time step was 1 psec. The incident angle was  $170^\circ$  and the observation angles were  $90^\circ$ ,  $120^\circ$ ,  $150^\circ$ ,  $180^\circ$ ,  $210^\circ$ ,  $240^\circ$ , and  $270^\circ$ . The large strip was 1.5 m wide.

### ***Summary***

This chapter covered the methodology used in this study. The design methodology was examined and explained. The experimental setup used at OSU-ESL was detailed. The numerical models used were explained. The variables and angle definitions for numerical and experimental were explained. The results of the numerical and experimental analysis are given in Chapter 4.

## ***Chapter 4: Results and Analysis***

### ***Introduction***

**Overview.** This chapter reviews the results from the measurements and the numerical analysis done in this thesis. In the first section, the results from the PMM code are presented. In the next two sections, the results from the measurements of the first and second taper designs are outlined. The measurements and UTD validation are then given in the next section. In the last two sections, the results from the MoM code work and the FDTD code are presented. The only design not tested by numerical means was the second inductive taper. In each section, the sources of error and preliminary analysis of results are given.

### ***PMM Output***

**Overview.** This section covers the data generated by Henderson's PMM code. Specifically, the data was computed as a function of position on the taper and a function of frequency. The method of changing the PMM output from reflection coefficients to impedances through the first resonance was given in Chapter 3 (Equations 3.1 a-c). For additional results from PMM and PMM source code listings, see Appendix A.

***Impedance Taper Edges as a Function of Frequency.*** Each impedance design had a crucial side of the taper (free space side for inductive taper and ground plane side for capacitive taper). Henderson's PMM code was used to find the reflection and transmission coefficients as functions of frequencies for the crucial edges. The coefficients were then transformed to impedances. For the inductive tapers, the free space edge needed to have high impedance (high transmission coefficient) over the frequency range. For capacitive tapers the ground plane edge needed to have low impedance (high reflection coefficient) over the frequency range.



Modeling the termination edges made the assumption of local periodicity invalid. However, the grating lobe problems presented by completely periodic structures modeled in PMM, would not necessarily occur in a tapered periodic surface. Therefore, the assumption of local periodicity would predict a grating lobe condition in a completely periodic structure that would not occur in a tapered periodic structure. In predicting an upper limit of design, the taper should actually perform better than PMM predictions.

The first inductive design's crucial edge was the free space edge. The edge was modeled using PMM as defined in Chapter 3. The first inductive design free space edge had high impedance only at 15 GHz. After 15 GHz (the resonance), the method used to determine the sheet impedance of the structure was no longer valid. In the valid frequency range, the real impedance was very low in comparison to the imaginary impedance, which corresponded to a lossless impedance. (See Figure 26)

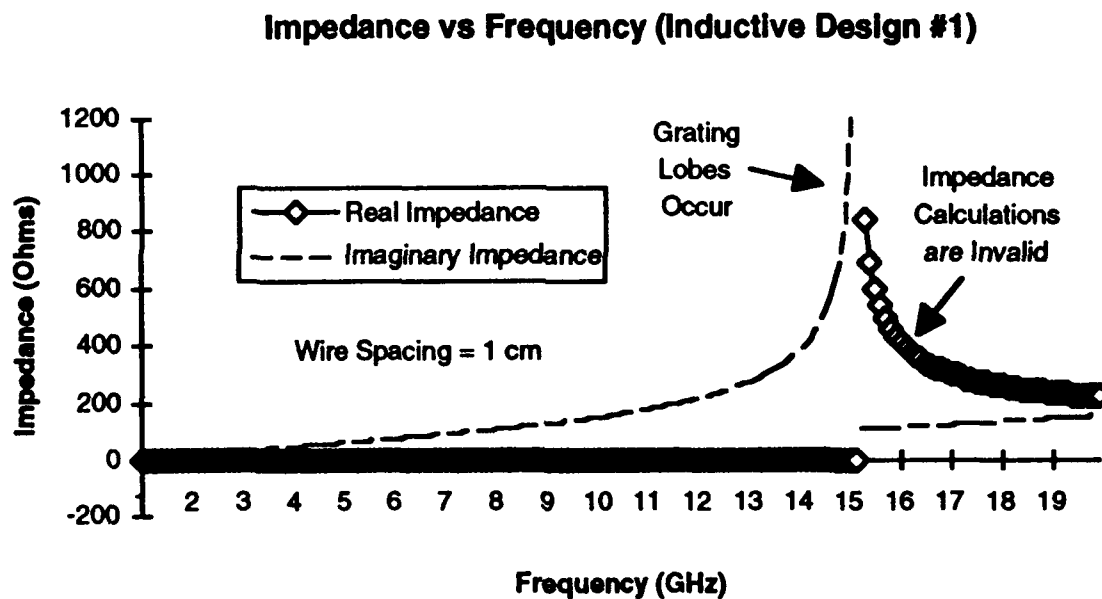


**Figure 26. Impedance vs Frequency for the Free Space Edge of Inductive Design #1.** Note that only at  $f = 15$  GHz does the first inductive taper have a high value of impedance.

The second inductive design's crucial edge was the free space edge. The edge was modeled using PMM as defined in Chapter 3. The edge displayed high impedance at 8.5 GHz. The bandwidth of this edge was much larger than for the first inductive design, meaning that the free space edge of this taper had high impedance over a wider range of frequencies compared to the first inductive taper. Also the real impedance was still much smaller than the imaginary impedance, making the design appear lossless. The change in sign of the impedance at 8.5 GHz corresponded to the change from inductive to capacitive impedance at the resonant frequency of the slots. This phase shift could cause time dispersion in the time domain, by causing a phase shift between frequencies (in the time domain signal) below 8.5 GHz and frequencies above 8.5 GHz. The phase shift should not be a problem for constant frequency applications. (See Figure 27)

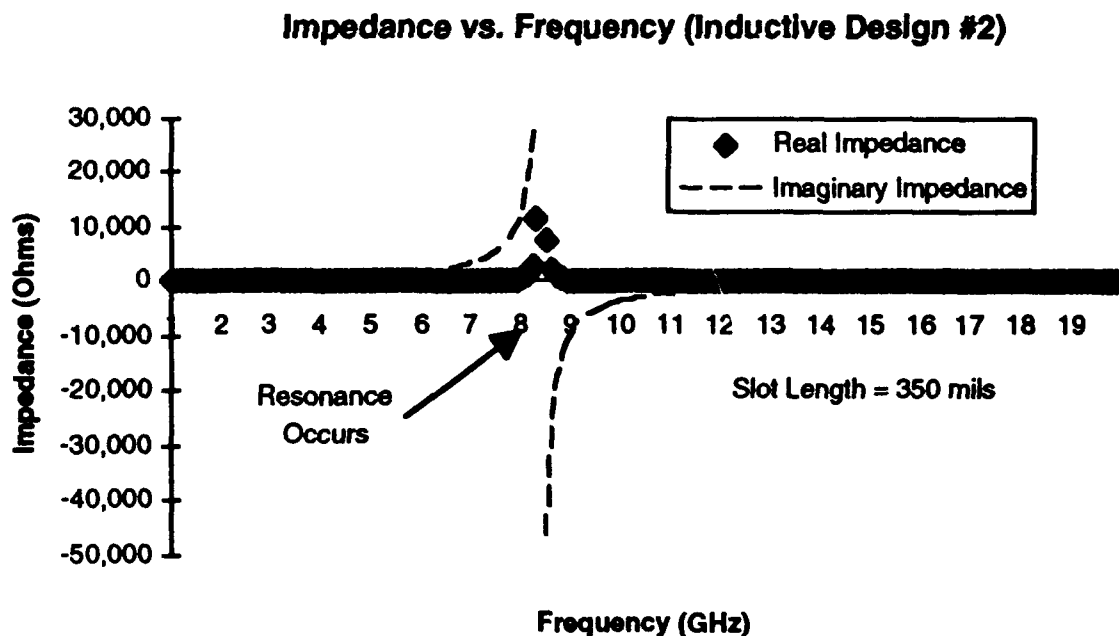


**Figure 27. Impedance vs Frequency for the Free Space Edge of Inductive Design #2.** Note that in this design, the resonant frequency occurred around 8.5 GHz.

The first capacitive design's crucial edge was the ground plane edge. The edge was modeled using PMM as defined in Chapter 3. The edge had low impedance (less than 100 ohms) over the frequency range 17-20 GHz. The taper appeared lossless due to very low real impedance over the entire frequency range. This taper was not resonant at the frequencies of interest and displayed no change in sign of the impedance. This design was constructed with a minimum line width of 0.5 mm. (See Figure 28)

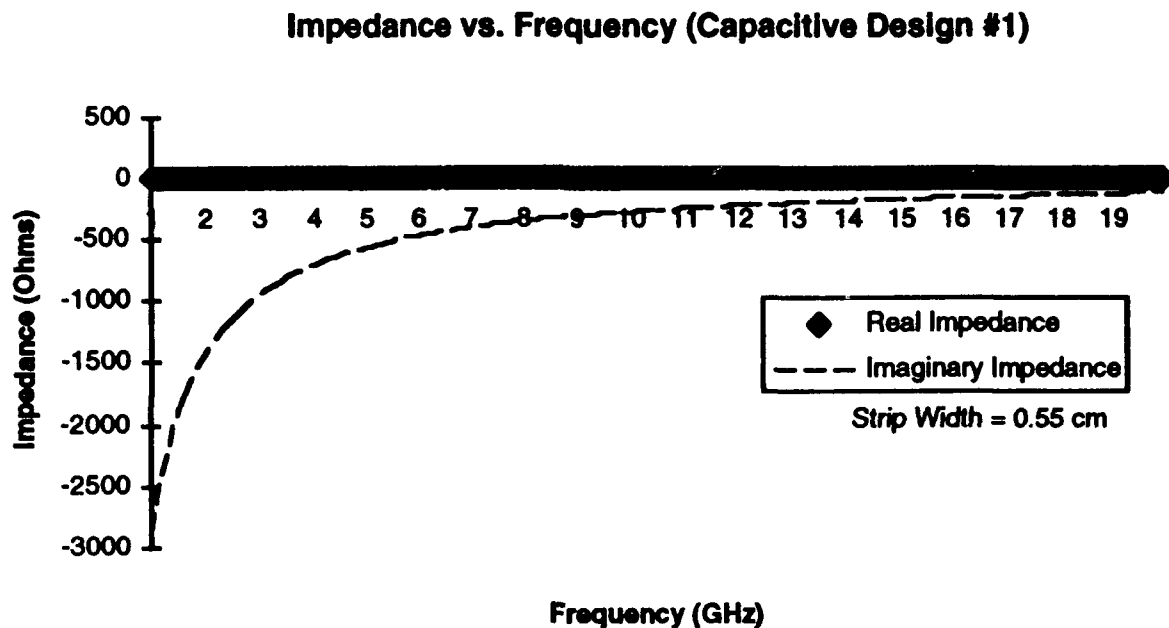


**Figure 28. Impedance vs Frequency for the Ground Plane Edge of Capacitive Design #1. Note the high impedance at lower frequencies.**

The second capacitive design's crucial edge was the ground plane edge. The edge was modeled using PMM as defined in Chapter 3. The edge in the second capacitive design had much better characteristics than the first capacitive design. The impedance was very low (less than 5 ohms) over the frequency range 6-10 GHz. The resonance of the strips occurred around 8.5 GHz and introduced a phase shift (which again could be a problem in the time domain). The anti-resonance at 16 GHz showed where the ground plane edge failed, as well as where the impedance conversion was invalid. (See Figure 29)

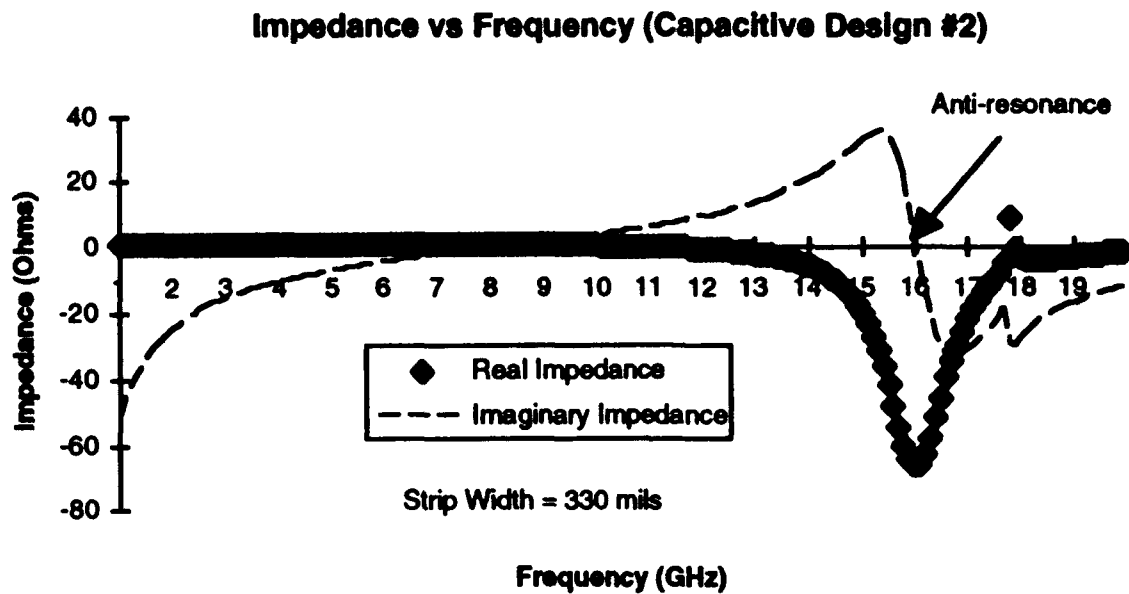


**Figure 29. Impedance vs Frequency for the Ground Plane Edge of Capacitive Design #2.** Note that in this design, low impedance occurred in the range 6-10 GHz.

These results showed how well the crucial edge of each taper worked. One important fact to notice is that the real part of the impedance in each taper was very low in comparison to the imaginary impedance in all of the tapers. Therefore, the real part of the impedance will be ignored for the remainder of this study. In the first inductive taper, the impedance of the free space side was low except at 15 GHz. The impedance of the second inductive design was much higher than the first inductive taper which should make for a better taper. The first capacitive taper had a high impedance at the ground plane edge, while the second capacitive taper more closely matched the ground plane edge. The second designs had much better impedance characteristics and a much larger bandwidth than the first designs, but the second designs would cause dispersion in the time domain due to the phase shifts.

***Impedance and Reflection Coefficient as a Function of Position on the Taper.*** By taking values along the taper and assuming local periodicity, the impedance as a function of position on the taper was found up to the first resonance. In each of these graphs, the reactance was graphed as a function of length from the ground plane side to the free space side. Due to the 8:1 length to width ratio required by PMM, impedances near free space on the capacitive side could not be calculated. Due to the equivalent wire width used by PMM, impedances near the ground plane side of the inductive tapers could not be calculated. Since the conversion method for impedances assumed a single resonance, the impedances could not be calculated for frequencies beyond than the first resonance. Also graphed are the reflection coefficients as a function of position on the taper, which were valid over the entire frequency range. The tapers are shown for frequencies 2, 6, 10, 14, and 18 GHz. Additional frequencies are given in Appendix A.

In the first inductive design, the spacing is varied from 0 to 1 cm over the length of the taper. From Figure 30, the taper impedance continuously increases from zero to the higher impedance of the taper edge. Note that for 18 GHz the inductive taper appeared to end early, this is due to the grating lobe situation that occurred at frequencies greater than 15 GHz preventing impedance calculations. The high impedance side of the taper over most of the frequency range was very low in comparison to free space. This low impedance at the free space edge indicated that this taper was very poor for frequencies below 15 GHz. Also note that this taper displayed no phase shift over the entire taper in the frequencies shown. The reflection coefficient as a function of position on the taper was valid over the entire frequency range (see Figure 31). Note that the reflection coefficient is high (near 7 dB) over the entire taper. The higher frequencies appeared to work better, but even the high frequencies did not have smooth gradual tapers to free space. (see Figures 30 and 31)

### Impedance vs. Length of Taper (Inductive Design #1)

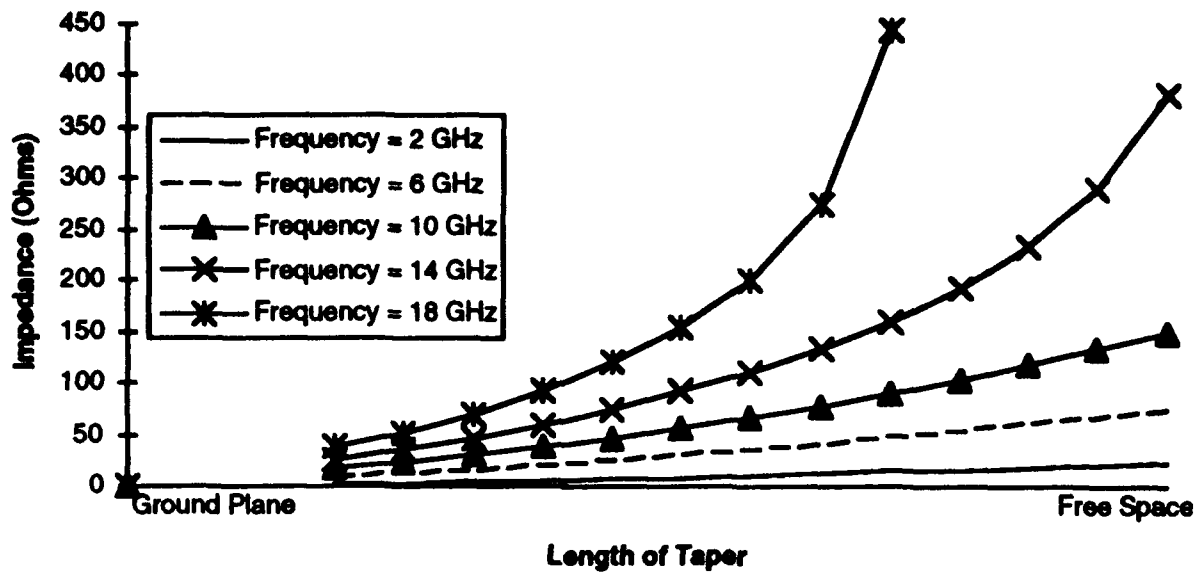


Figure 30. Impedance vs Length for Inductive Design #1. This has a relatively low impedance over the frequency range.

### Reflection Coefficient vs Length of Taper (Inductive Design #1)

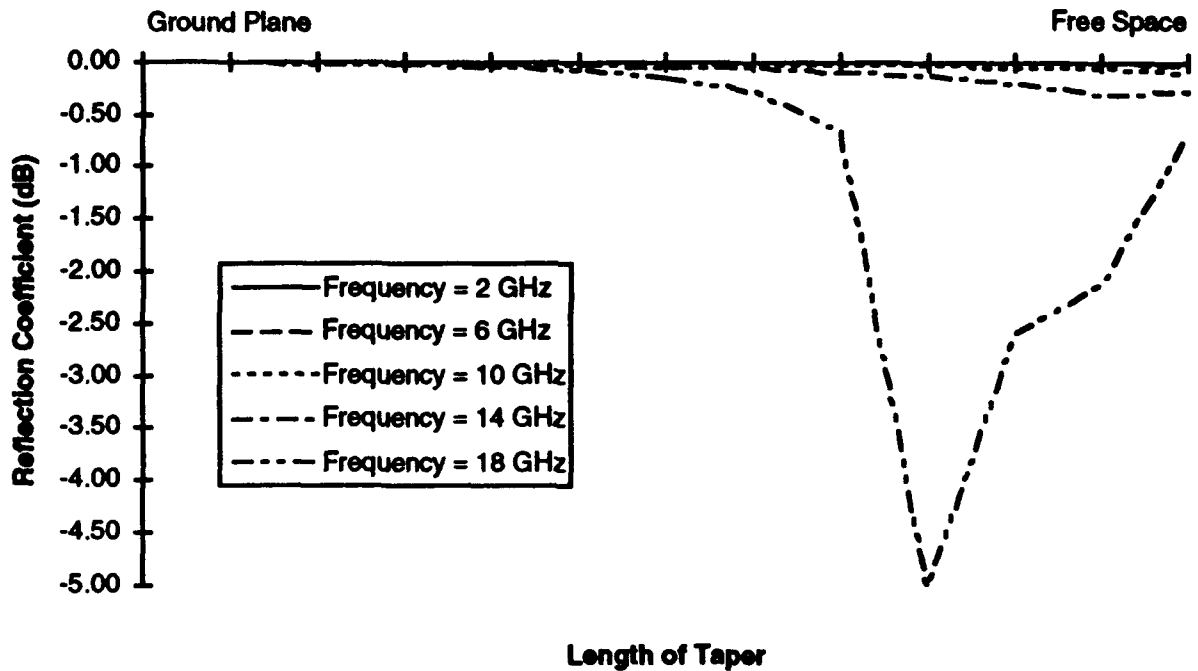
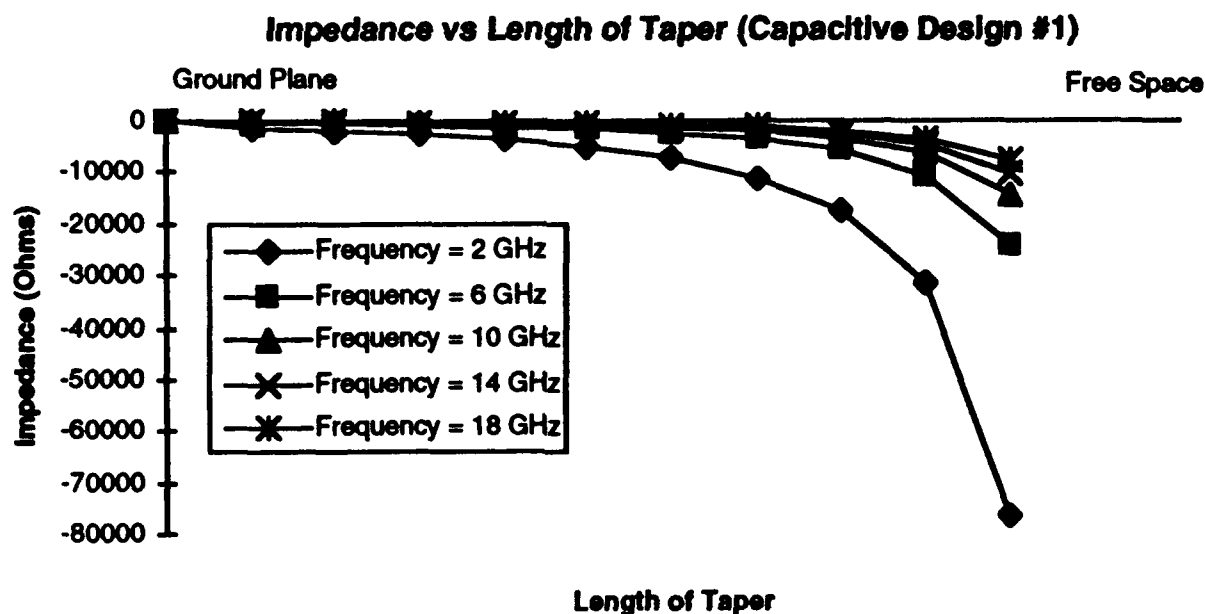
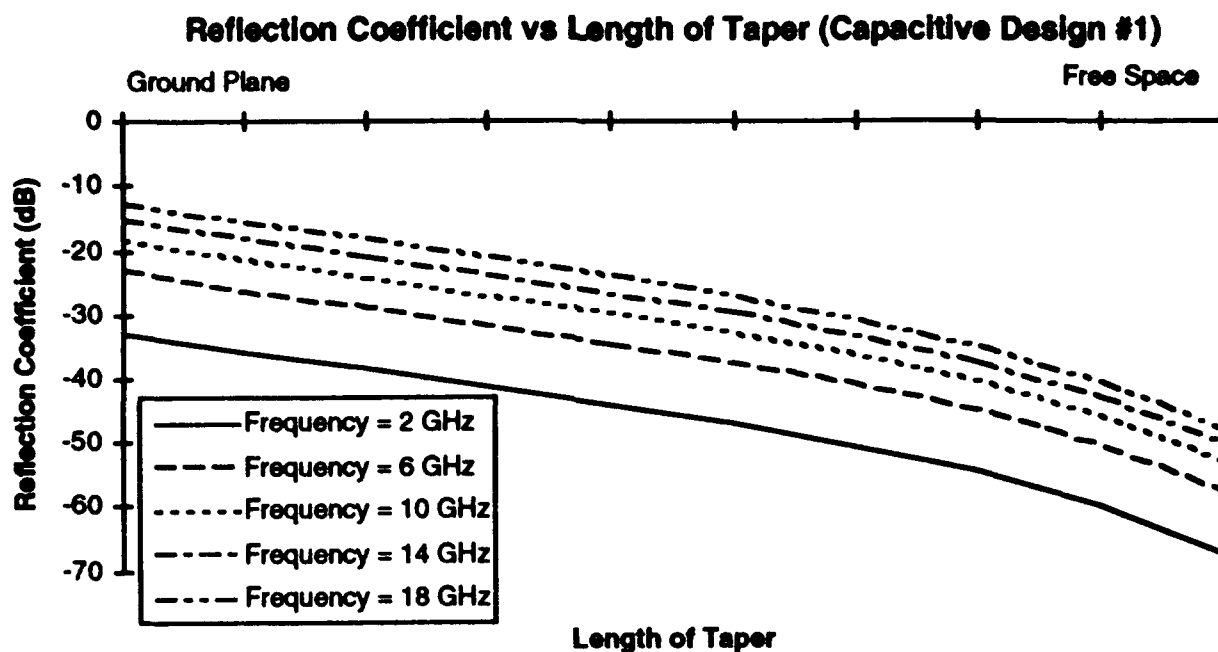


Figure 31. Reflection Coefficient vs Length for Inductive Design #1. Note the large discontinuity at the free space end.

The first capacitive design had the strip width varying from 5.5 mm to 0.5 mm over the length of the taper with a constant center-to-center spacing of 6 mm. From Figure 32, the taper did a nice continuous job of tapering the impedance from zero to near infinity. However, the ground plane edge had a significant discontinuity that is difficult to see in Figure 32. This taper displayed no phase shift over the frequency range and had high impedance values for the free space edge. The reflection coefficient as a function of position on the taper was valid over the entire frequency range (see Figure 33). The discontinuity between the ground plane and the taper were quite large (between 12 and 33 dB). The free space side was much more closely matched and should not provide as much scattering as from the ground plane and taper interface. (see Figures 32 and 33)



**Figure 32. Impedance vs Length for Capacitive Design #1.** This taper had large impedances at the free space edge.



**Figure 33. Reflection Coefficient vs Length for Capacitive Design #1. Note the large discontinuities at the ground plane edge.**

The second inductive taper was made by tapering slot lengths in a skewed array from 5 mils to 350 mils. Due to the finite length of the elements, resonances occurred in this taper. As the frequencies increased, the resonance slowly moved back (towards the ground plane) on the taper, because the slot lengths decreased in that direction. At the resonance, the impedance approaches positive infinity and the ground plane was exactly matched to free space (see Figure 34). On the free space side of the resonance, the reflection coefficient increased toward the free space edge of the taper (see Figure 35). The taper worked best when the resonance occurred near the end of the taper (around 8 GHz). When the resonance did not occur on the taper (frequencies less than 8 GHz), the taper did not work as well because of the high reflection coefficient at the free space edge. When the resonance occurs on the taper, but not on the end, there can additional scattering from the taper free space edge if the reflection coefficient at the free space end was not low enough (above 10 GHz). (See Figures 34 and 35)



### Impedance vs Length of Taper (Inductive Design #2)

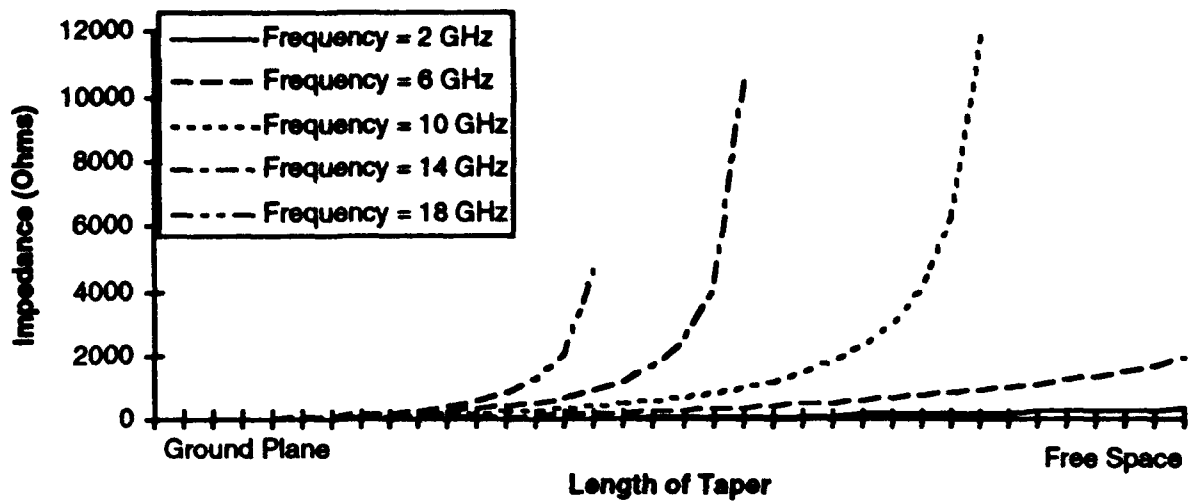


**Figure 34. Impedance vs Length for Inductive Design #2.** This taper did have resonances.

### Reflection Coefficient vs Length of Taper (Inductive Design #2)

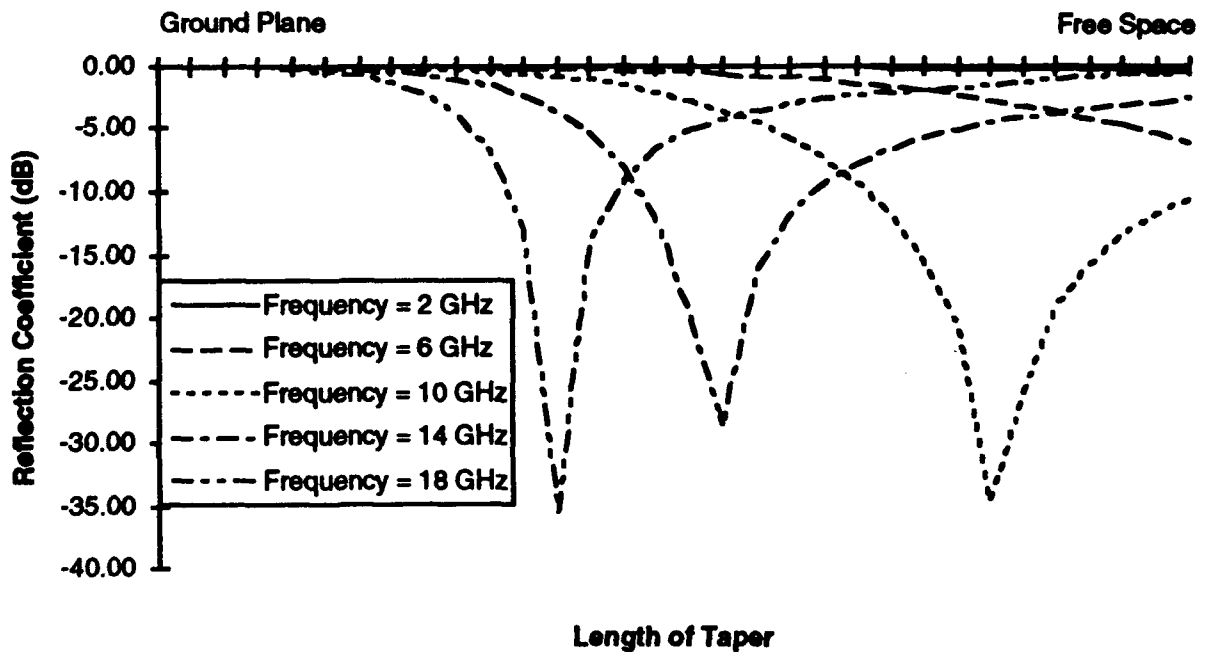


**Figure 35. Reflection Coefficient vs Length of Inductive Design #2.** Note that only around 8 GHz did the free space side have a low reflection coefficient.

The second capacitive design had tapered strip widths from 330 mils to 5 mils. The resonances occurred at approximately the same position on the taper. The lower frequencies approached the resonance at faster rate and have a more gradual taper (see Figure 36). At the resonance, the impedance approaches negative infinity and the ground plane was exactly matched to free space. On the ground plane side of the resonance, the reflection coefficient decreased from zero to large negative values (see Figure 37). On the free space side of the resonance, the reflection coefficient increased toward the free space edge. The reflection coefficient was still fairly low at the end of the taper over most of the frequency range. The ground plane interface was still a scattering source for low frequencies (due to low reflection coefficients) and high frequencies (due to a second resonance). This taper displayed the best reflection and impedance characteristics of all of the designs over the frequency range. (See Figures 36 and 37)

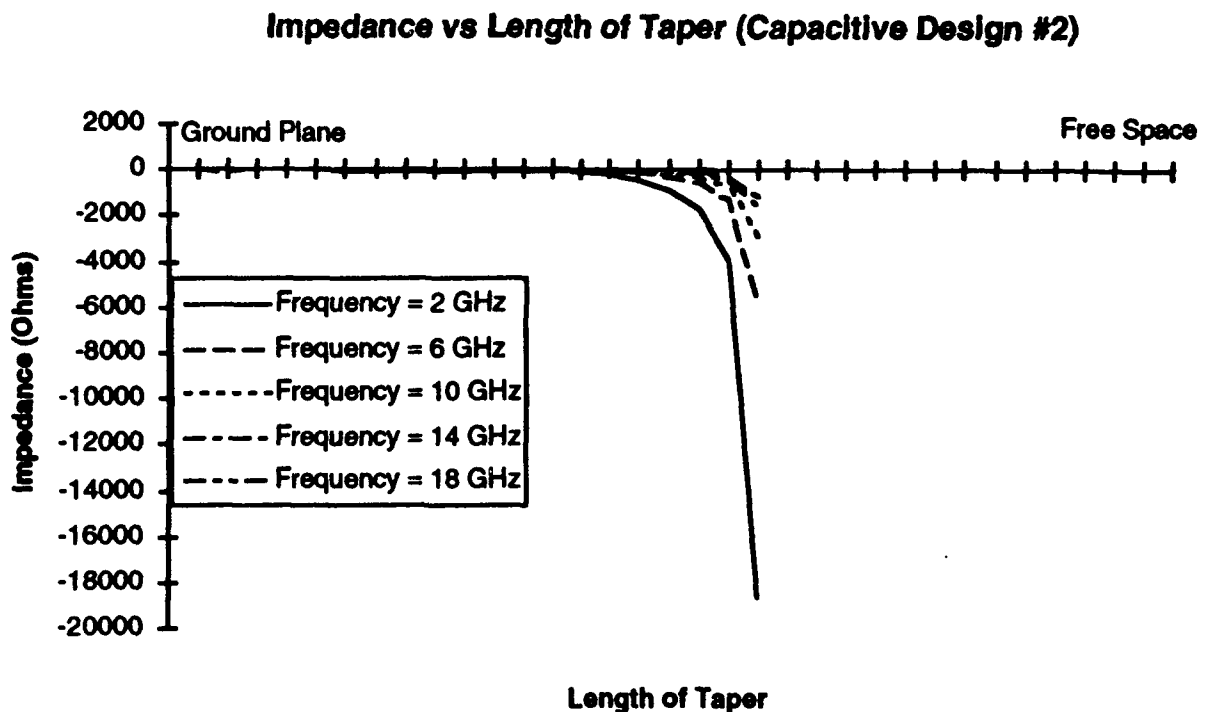


**Figure 36. Impedance vs Length for Capacitive Design #2.** This taper does have resonances, but has a higher bandwidth than the first capacitive taper.

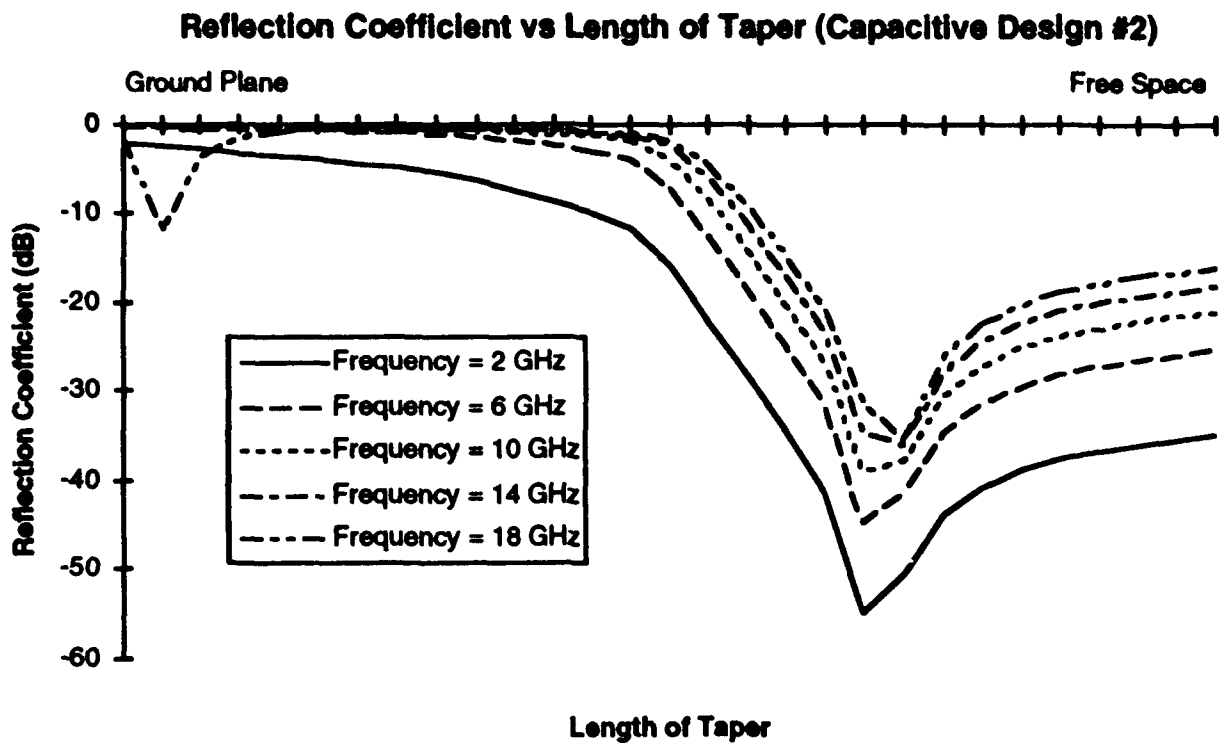


**Figure 37. Reflection Coefficient vs Length of Capacitive Design #2.** Note that this taper has a nice taper over most of the frequency range.

**Measurements Without the Dielectric Substrate.** Henderson's PMM code was then used to determine the effect of the dielectric slab on the second impedance designs. If the dielectric slab had no effect, then some of the mathematical methods mentioned in Chapter 2 could have been used to check the results from PMM. The results from the PMM code without the dielectric slab showed a marked difference in both of the second designs when the dielectric is removed (See Figures 38 and 39). Therefore, the mathematical methods mentioned in Chapter 2 were not used to solve the second impedance designs.

### Impedance vs Frequency (Inductive Design #2)

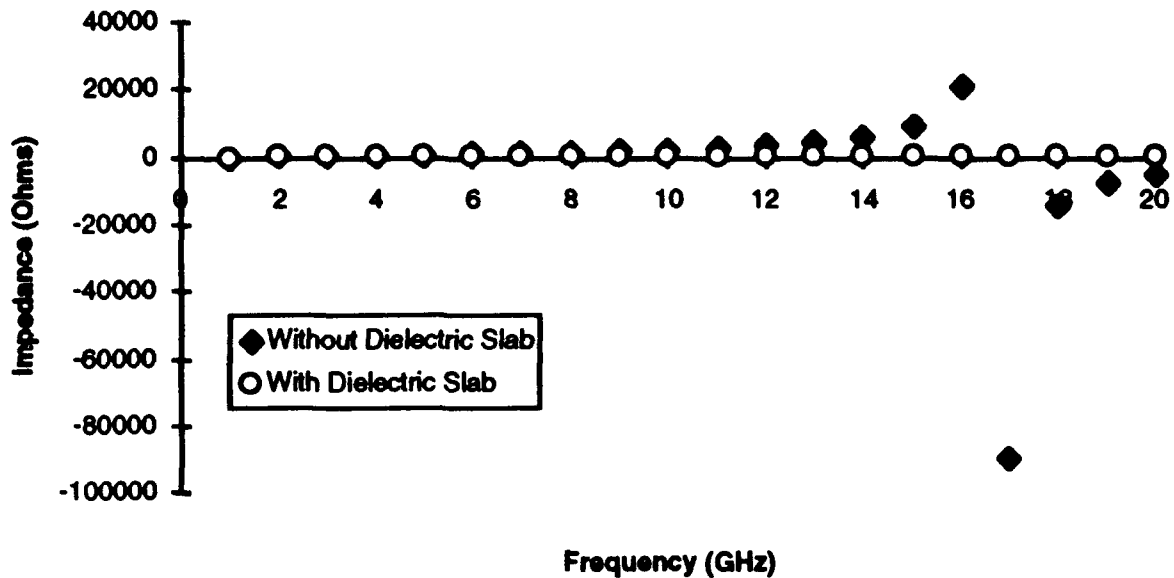


**Figure 38. Impedance vs Frequency for Free Space Edge of Inductive Design #2 Without the Dielectric Substrate.** Note that without the dielectric slab, the impedance changes dramatically especially at higher frequencies.

### Impedance vs Frequency (Capacitive Design #2)

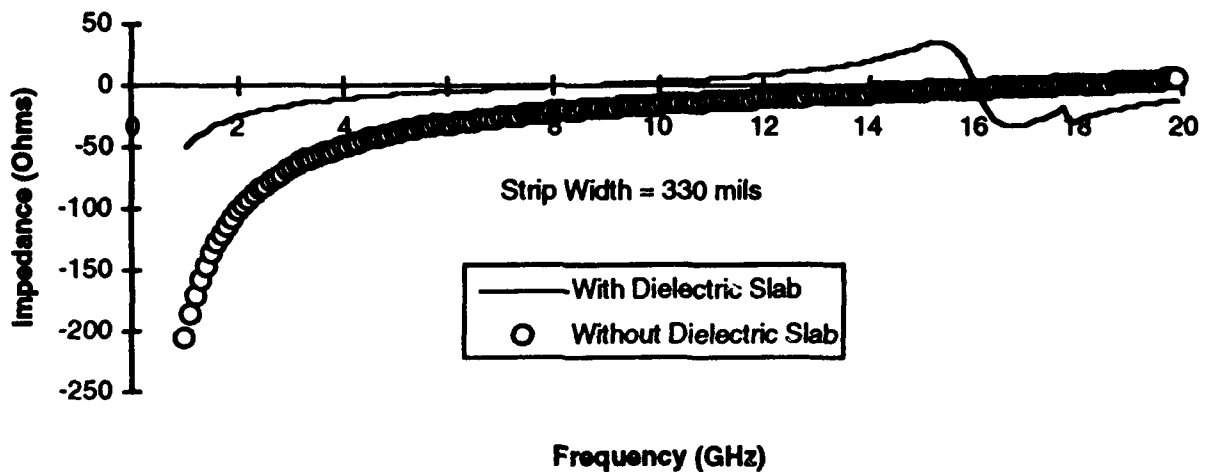


**Figure 39. Impedance vs Frequency for Ground Plane Edge of Capacitive Design #2 Without the Dielectric Substrate.** Note that without the dielectric slab, the impedance changes dramatically.

### ***Measured Results on the Impedance Taper Designs***

**Overview.** This section covers the results from the two separate days of testing at OSU-ESL. Since the power output of the American Electronics Laboratory (AEL) horn was not calibrated each day, the results from one day's experiment can only be compared to the same day's data. Each pattern without a taper was compared to UTD solutions to test the ability of the antenna platform to simulate an infinite 2D knife edge. To smooth the data, a moving median was taken every 7 data points ( $1.5^\circ$  on each side of the data point) for both the measured and computed data.

**First Inductive Taper.** The first inductive taper was measured and showed no improvement. There was no difference in the total field pattern except at 18 GHz. The improvement was slight at 18 GHz and only in the shallow shadow region (less than  $30^\circ$  in the shadow region). This improvement did correspond to the expectation from Figure 31 that 18 GHz would have the best results. For the other frequencies, the wires used were not able to produce high impedance and diffraction reduction was expected to be slight. The rest of the azimuth and frequency scans are in Appendix B.

**First Capacitive Taper.** The measurements made on the first capacitive taper design showed a very limited effect on the scattered field. The tapers were crudely made and therefore the results from these tapers are very questionable. Since the impedance of the strips was very high (some were open circuits), the PEC assumption no longer held true for these tapers. However, for 18 GHz there was a very slight reduction in the deep shadow region. This reduction was less than 5 dB and only appeared present at 18 GHz, which corresponded to the results present in Figure 33. The azimuth and frequency scans for the first capacitive taper are in Appendix B.

**Second Inductive Taper.** The second inductive taper was measured. The results of this taper were slightly better than the first inductive taper. First the soft edge diffraction from the platform with no taper was then compared to UTD results for a knife

edge (incidence angle =  $4.7^\circ$  off the ground plane). The comparison of the UTD and measured results showed additional scattering sources than the knife edge (Figure 40). The scattering from the knife edge was predominant more than  $30^\circ$  into the shadowed region. Figure 41 shows the azimuth cut of the second inductive design at 10 GHz. Limited improvement was displayed in the region less than  $30^\circ$  in the shadow region at 10 GHz. The improvement did correspond to the results from Figure 35. Figures 42, 43, and 44 give the frequency scans of the second inductive design at the observation angles  $90^\circ$ ,  $120^\circ$ , and  $150^\circ$  respectively. The only reduction in diffraction occurred in the near shadow region ( $30^\circ$  in the shadow region or  $150^\circ$  observation angle). This taper might have worked better in the region less than  $30^\circ$  in the shadow region, but the additional scattering sources in the shallow shadow region might have overshadowed the effectiveness of the taper. The power levels for the deeper shadow region were very low and reduction in the far shadow region was difficult to determine. The taper seemed to be ineffective at most look angles and frequencies. The rest of the azimuth and frequency scans for the second inductive taper are in Appendix C.

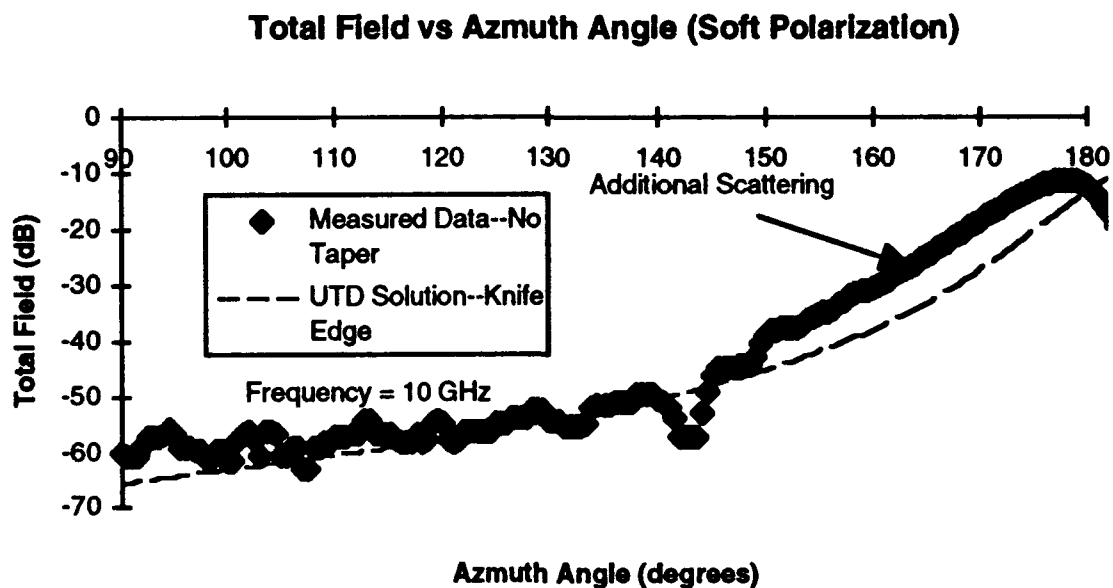


**Figure 40. Comparison of UTD and Measured Results From the Knife Edge.** Note the additional scattering in the region less than  $30^\circ$  in the shadow region.

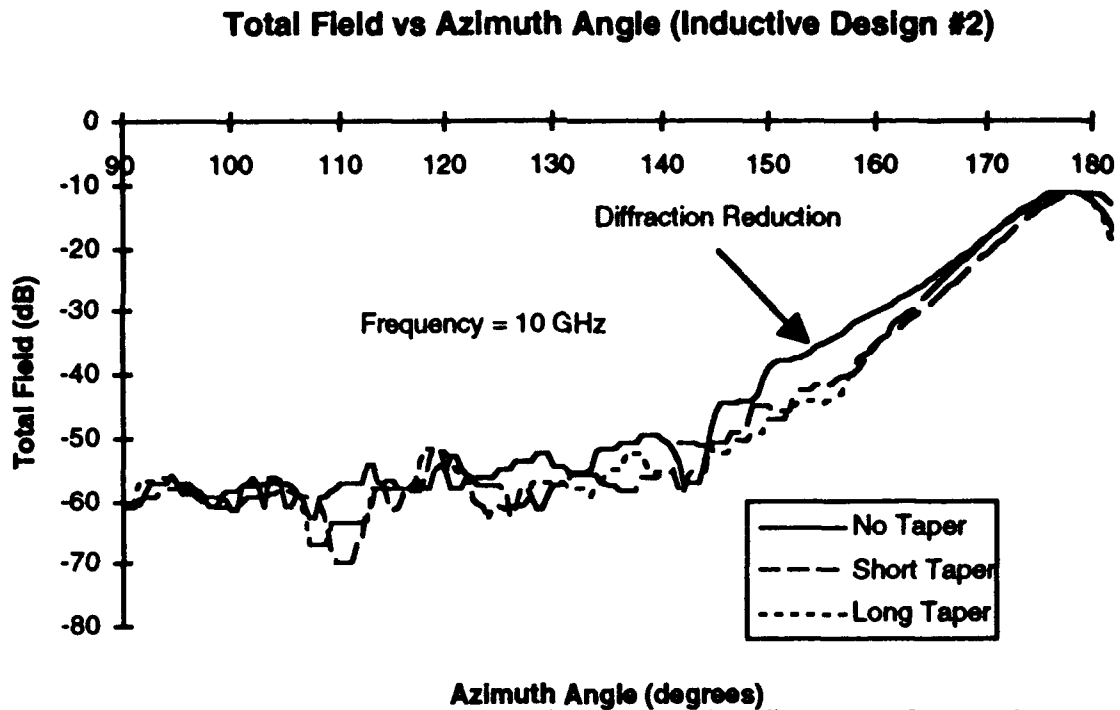


**Figure 41. Azimuth Cut of Inductive Design #2 at 10 GHz.** Note that this design had a limited improvement in the range  $150^{\circ}$  to  $170^{\circ}$  in the shadow region.

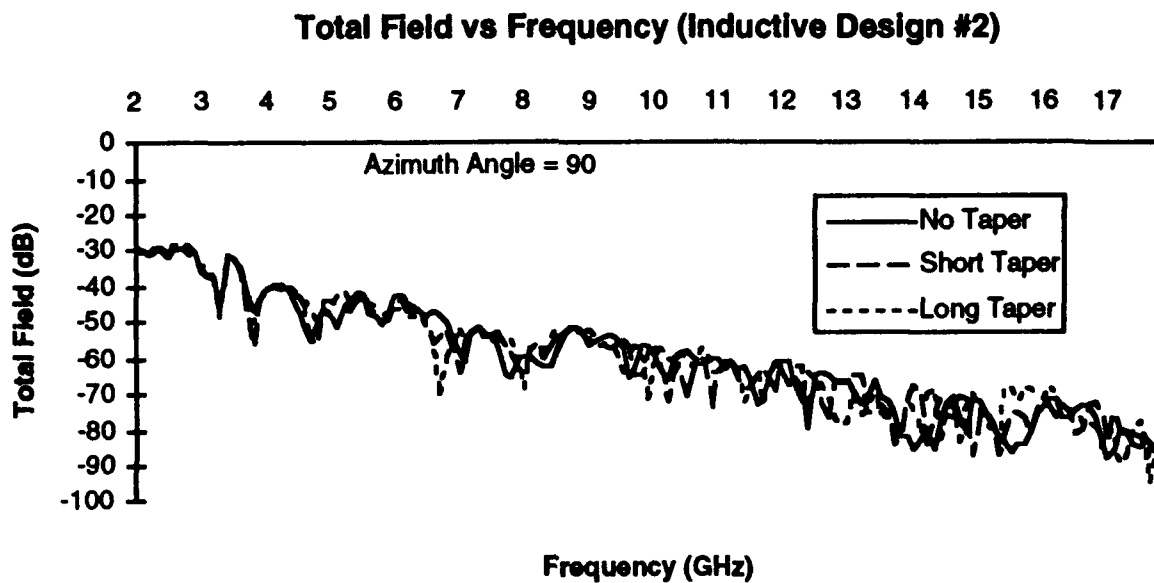


**Figure 42. Frequency Sweep for Inductive Design #2 at  $90^{\circ}$  in the Shadow Region.** This graph showed no improvement over the entire frequency range at  $90^{\circ}$  in the shadow region.

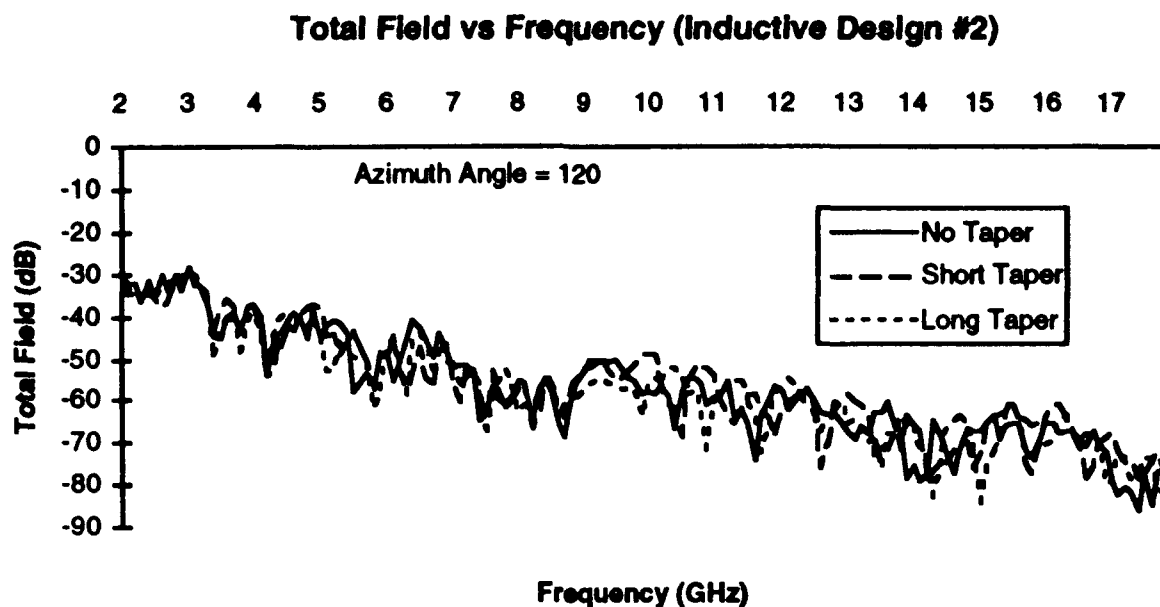


**Figure 43. Frequency Sweep for Inductive Design #2 at 120° in the Shadow Region.** This graph showed no improvement over the entire frequency range at 120° in the shadow region.

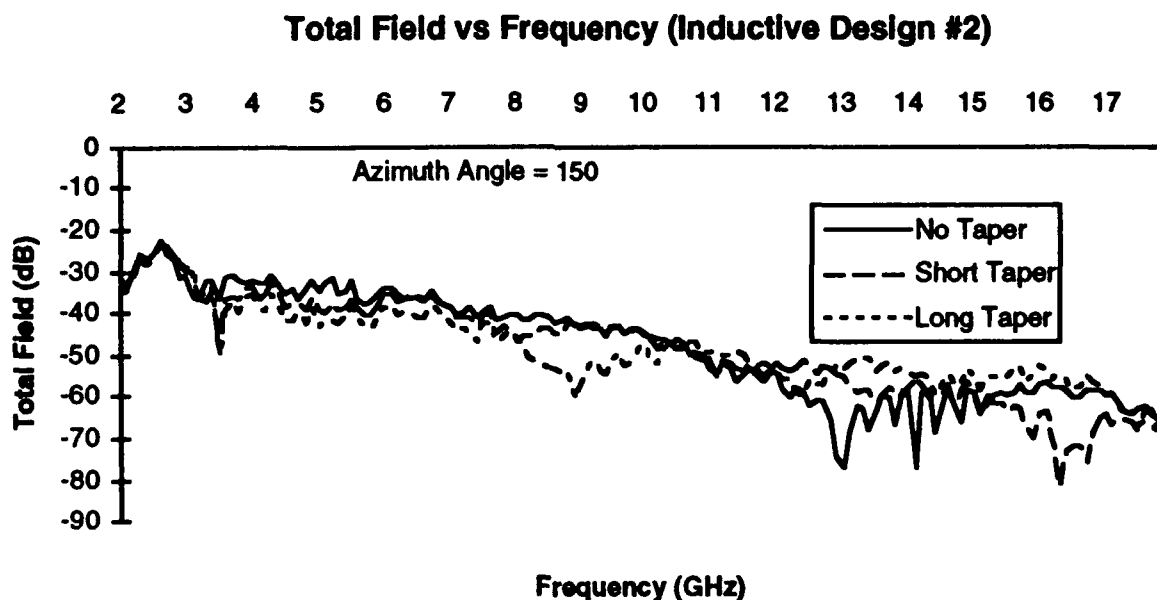


**Figure 44. Frequency Sweep for Inductive Design #2 at 150° in the Shadow Region.** This graph showed no improvement over most of the frequency range at 150° in the shadow region. Only the frequency range 3-10 GHz showed moderate improvement.



**Second Capacitive Taper.** The second capacitive taper showed a marked improvement over a bare edge. First the hard edge diffraction from the platform with no taper was then compared to UTD results for a knife edge (incidence angle =  $4.7^\circ$  off the ground plane). The comparison of the UTD and measured results showed additional scattering sources than the knife edge (Figure 45) in the region less than  $30^\circ$  into the shadowed region. Figure 46 shows the azimuth cut of the second inductive design at 10 GHz. Marked improvement was displayed in the region more than  $30^\circ$  in the shadow region for both the long and short tapers. Figures 47, 48, and 49 give the frequency scans of the second capacitive design at the observation angles  $90^\circ$ ,  $120^\circ$ , and  $150^\circ$  respectively. The second capacitive design seemed to work well over a wide frequency range, 5-15 GHz, which agreed with the results from Figure 37. The taper did not seem to be effective in the region less than  $30^\circ$  in the shadow region possibly due to the additional scattering sources. The rest of the azimuth and frequency scans are in Appendix C.

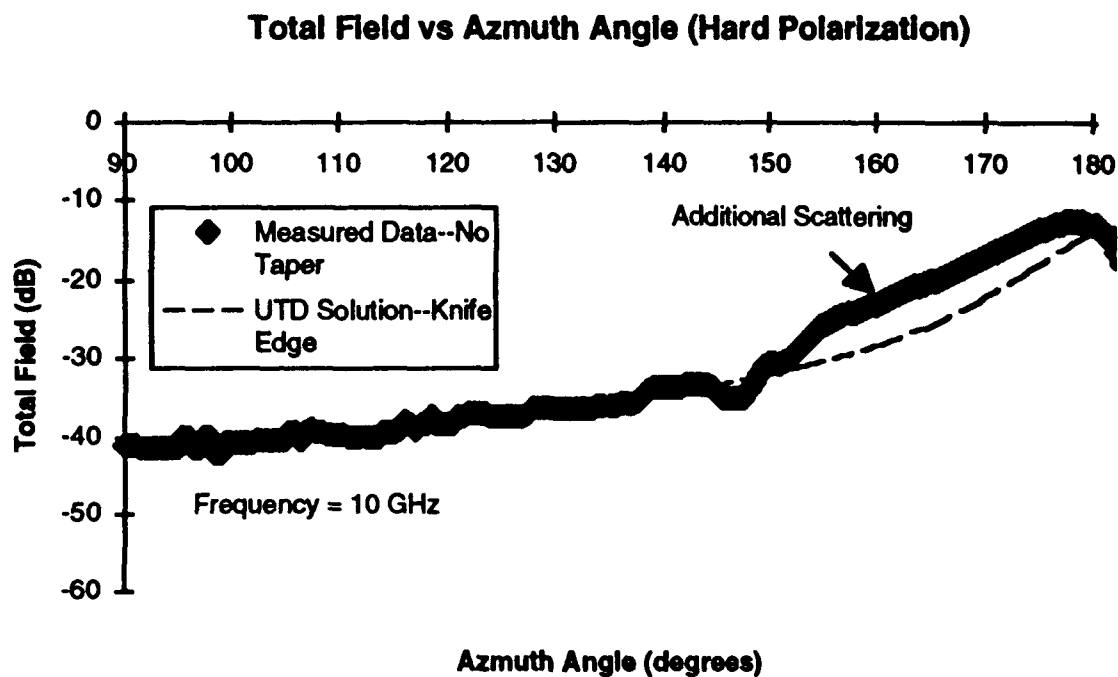


**Figure 45.** Comparison of UTD and Measured Results From the Knife Edge. The results showed additional scattering when the observation was less than  $30^\circ$  in the shadowed region.

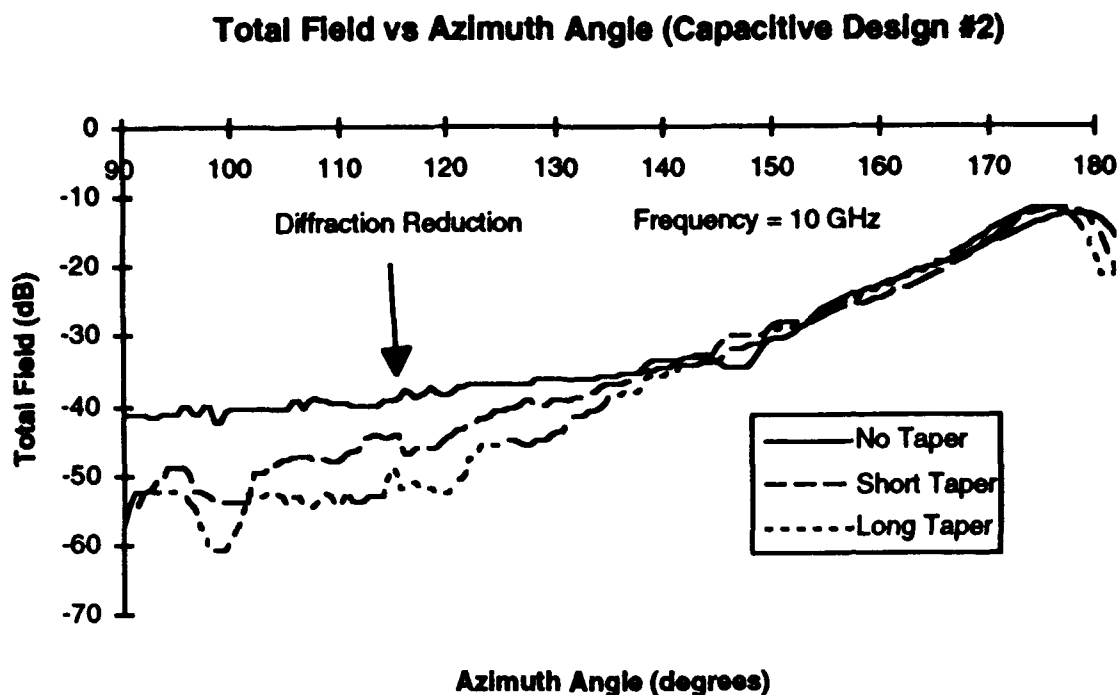


**Figure 46. Azimuth Cut of Capacitive Design #2 at 10 GHz.** Note that this design showed improvement more than  $30^\circ$  in the shadow region.

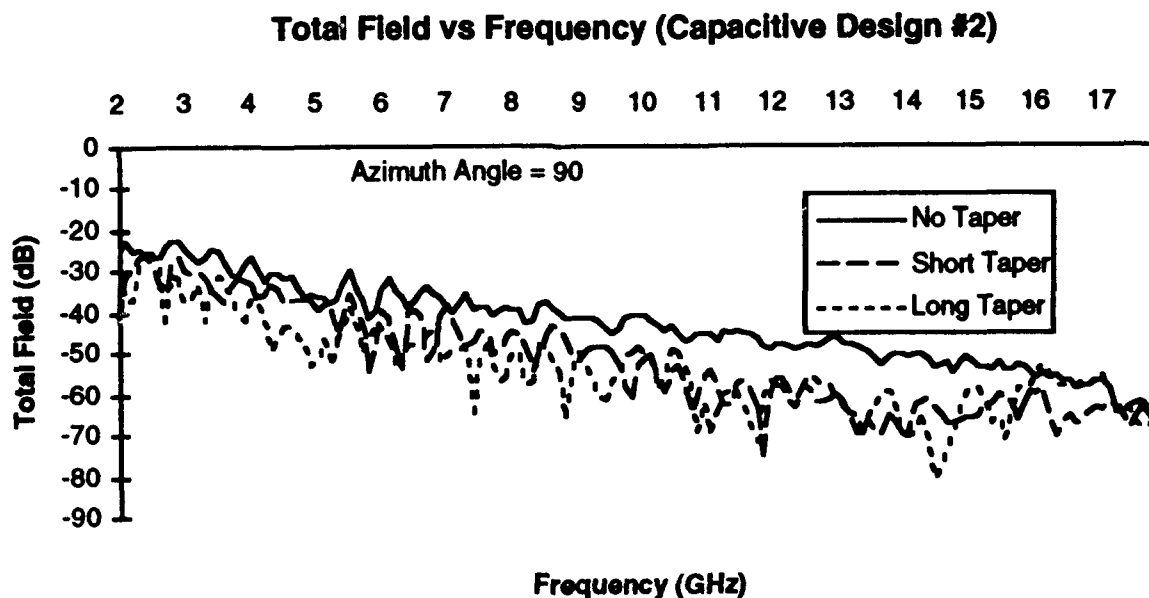


**Figure 47. Frequency Sweep for Capacitive Design #2 at  $90^\circ$  in the Shadow Region.** This graph showed a 10 dB reduction over the frequency range 6-16 GHz at  $90^\circ$  in the shadow region.

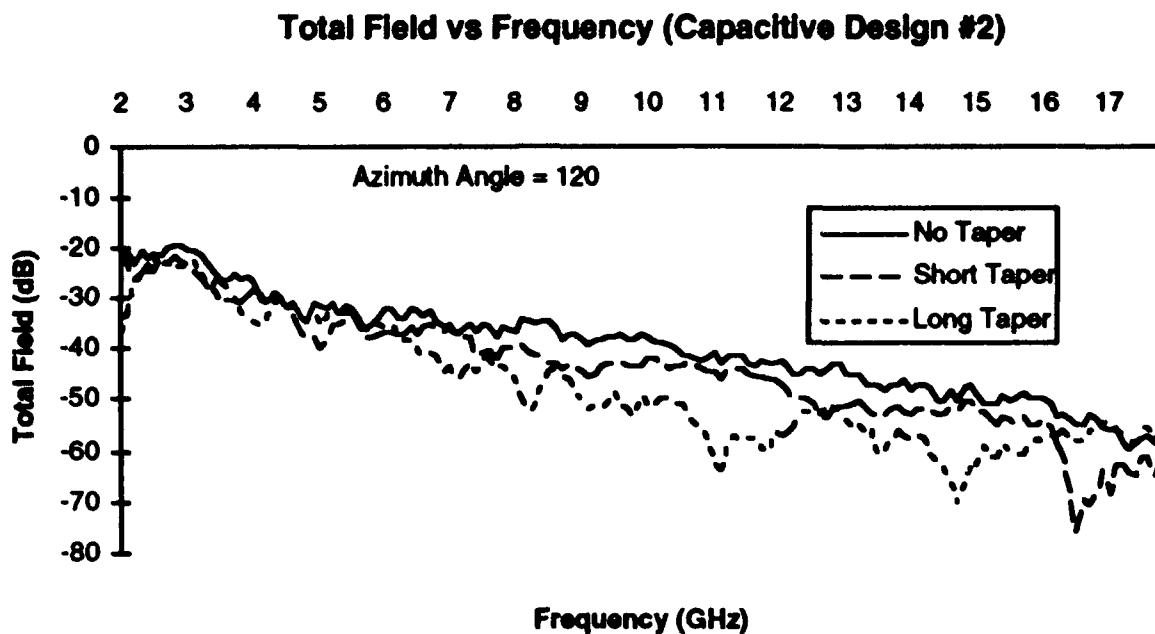


**Figure 48. Frequency Sweep for Capacitive Design #2 at 120° in the Shadow Region.** This graph showed a 5 dB improvement over the frequency range 6-16 GHz at 120° in the shadow region.

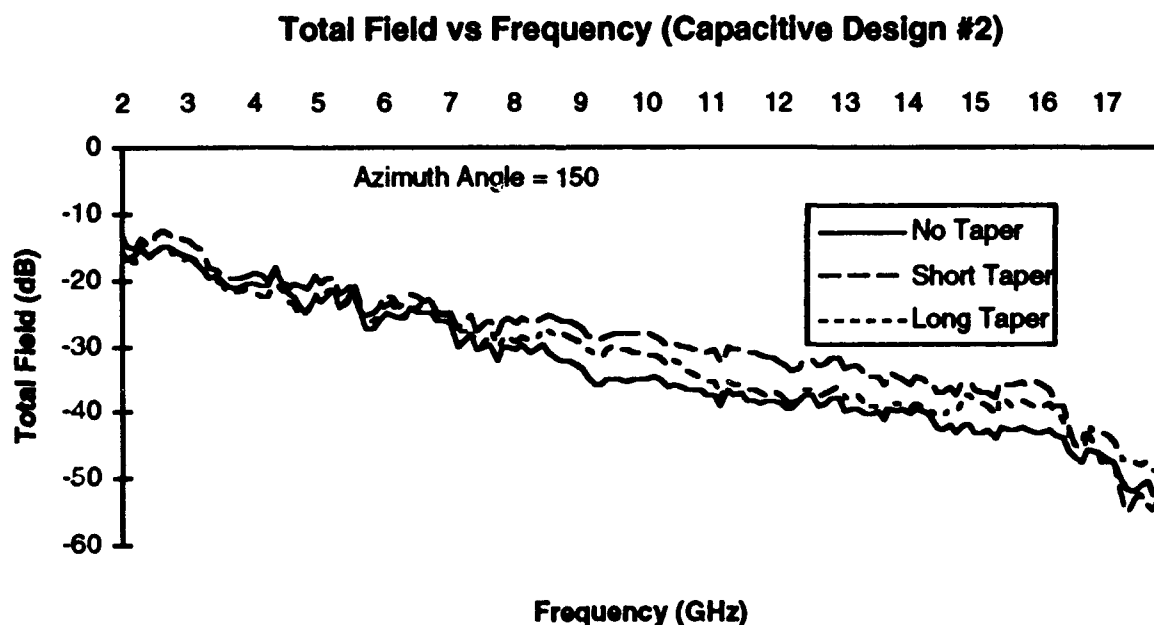


**Figure 49. Frequency Sweep for Inductive Design #2 at 150° in the Shadow Region.** This graph showed no improvement over the entire frequency range at 150° in the shadow region.

### **MoM Results on First Taper Designs**

**First Inductive Taper.** The first inductive taper was then modeled using a MoM code developed by myself with pulse basis functions and point testing functions. To model the effectiveness of the taper, a long (1m) thin strip was modeled using the code both with one edge tapered and without any edge tapers. The scattered fields from the large strip (1m) were then compared with modifications using short and long tapers. The MoM measurements were bistatic azimuth cuts at every  $0.5^\circ$  (incident field at  $10^\circ$  from grazing). The measurements were made at 2, 10, 18 GHz. Each TMz MoM computer run took about 10 minutes on a Sun workstation. The results at 10 GHz showed negligible improvement over the bistatic scans (See Figure 50). The remainder of the MoM data showed no improvement (See Appendix D for the rest of the data).

#### **Scattered Field vs Azimuth Angle (Inductive Design #1)**

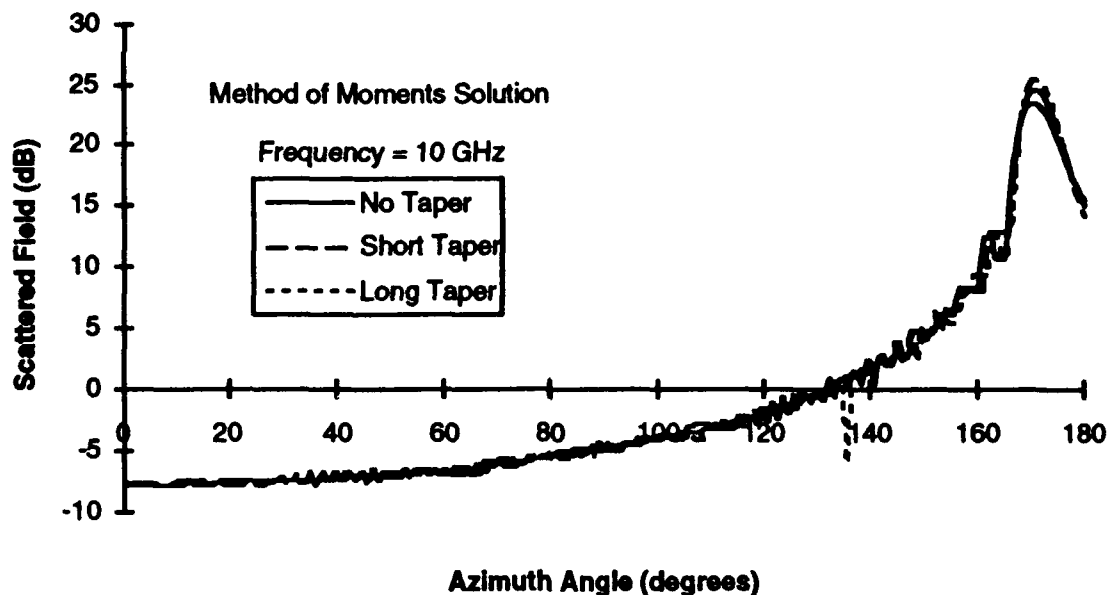


**Figure 50. Comparison of MoM Results for Inductive Design #1.**  
The graph above shows no improvement for inductive taper design #1 at 10 GHz.

***First Capacitive Taper.*** The first capacitive taper was then modeled using the TEz MoM code developed by Skinner [19]. The comparison was made between the long thin strip (1m) with no edge taper and the long thin strip with one edge tapered (30 cm taper). The MoM measurements were bistatic azimuth cuts at every  $0.5^\circ$  (incident field at  $10^\circ$  off grazing). The measurements were made at 2, 10, 18 GHz. Each TEz MoM run took about 15 minutes on a Sun workstation. The calculations at 10 GHz showed an improvement for the first capacitive taper (See Figure 51). The capacitive taper seemed to work especially well at 18 GHz. (See Appendix D for the rest of the data)

The MoM results followed the measured data. The first inductive taper did not work very well, because of the inability to increase inductance enough with straight wires. The TMz MoM code showed no positive effect on the bistatic scattering from the first inductive taper. One possible source of error in the TMz code was the use of the thin wire approximation with the close proximity of the wires. The first capacitive taper appeared from the early PMM work to be an effective taper design. The TEz MoM results validated that the first capacitive taper could work as a taper design. The MoM results could not be experimentally validated, due to the crude manufacturing of the first capacitive taper making the measurements dubious.

### Scattered Field vs Azimuth Angle (Capacitive Design #1)

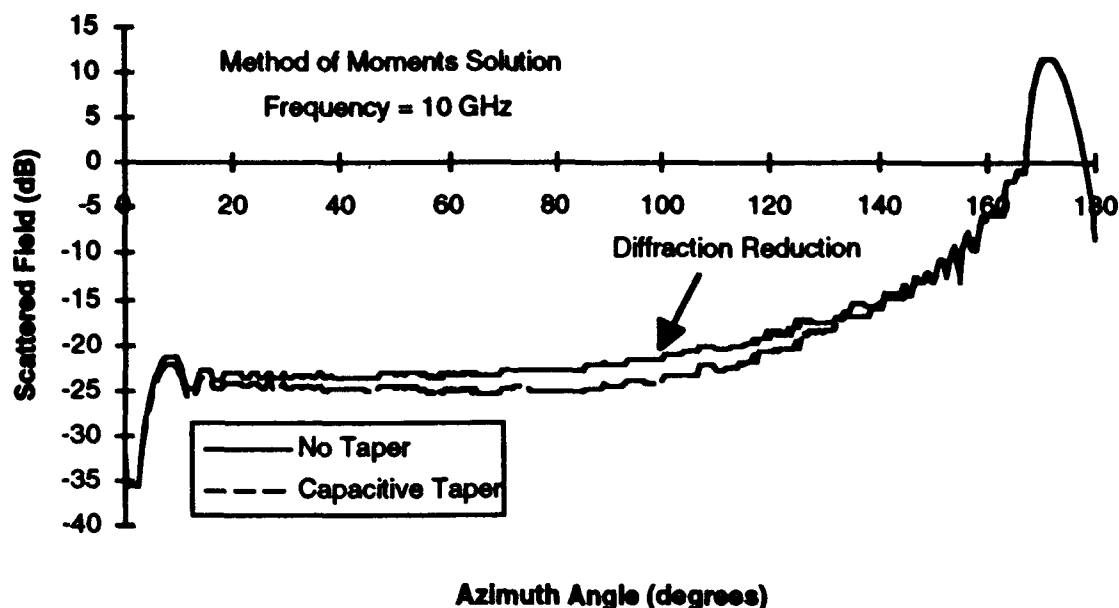


**Figure 51. Comparison of MoM Results for Capacitive Design #1.** The graph above showed improvement for capacitive taper design #1 at 10 GHz. The taper seemed to be effective from 20° to 140°.

#### ***FDTD Results on Second Capacitive Taper Design***

***Second Capacitive Taper.*** The second capacitive taper was modeled using the FDTD code developed by Luebbers. The model used to study the capacitive taper is given in Chapter 3. The result from the FDTD code for the 90° observation angle is given in Figure 48. The FDTD data did support the measurements that showed a reduction in diffraction due to the second capacitive taper.

Also FDTD supported the measurements since no noticeable reduction was made in diffraction until the observation was greater than 30° in the shadow region in both the FDTD model and the measurements. The FDTD results showed improvement for the long taper over the short taper only at lower frequencies (less than 6 GHz). This result agreed with the measurements. The type of taper (linear, binomial, triangular, etc.) should only matter when the taper is shorter electrically. The FDTD results suggested that the second

capacitive taper was effective in the range 2-13 GHz. This result tended to support the experimental data, where the second capacitive taper was effective in reducing deep shadow fields in the frequency range 6-16 GHz.

Also the FDTD results showed additional scattering for the no taper design in the shallow shadow region (which are noted in Figures 16 and 17). FDTD was then used to try and isolate the sources of additional scattering. First slope diffraction was considered, but since the source was a simple source, no slope diffraction could occur. Second, the scattering from the 2 inch thick styrofoam was considered. In the FDTD measurements of the entire antenna platform, the dielectric constant of the styrofoam was assumed to be 1.02. However, the actual dielectric constant of the styrofoam used was too low for measurement accuracy. Therefore, the dielectric constant could have much higher than 1.02 (possibly as high as 1.2). Therefore, FDTD was used to determine the scattering from the 2 inch thick styrofoam alone (without the ground plane or taper design) as a function of the dielectric constant. The values of 1.02, 1.1 and 1.2 were used for the dielectric constant. The FDTD results from the dielectric substrate alone showed considerable scattering in the region less than  $30^\circ$  in the shadow region (see Figure 53) for all three dielectric constants. Figure 53 shows the scattered field as a function of observation angle and dielectric constant and the scattered field was above 5 dB for most of the shallow shadow region. The observation angles were taken from  $45^\circ$  to  $-45^\circ$  in  $5^\circ$  increments. The cell size was made much larger (1.5 mm by 1.5 mm), since there was no thin dielectric substrate to model. The FDTD results also showed that this additional scattering occurred over the entire frequency range of interest (see Figure 54). Therefore, at least part of the additional scattering was due to scattering from the styrofoam substrate.

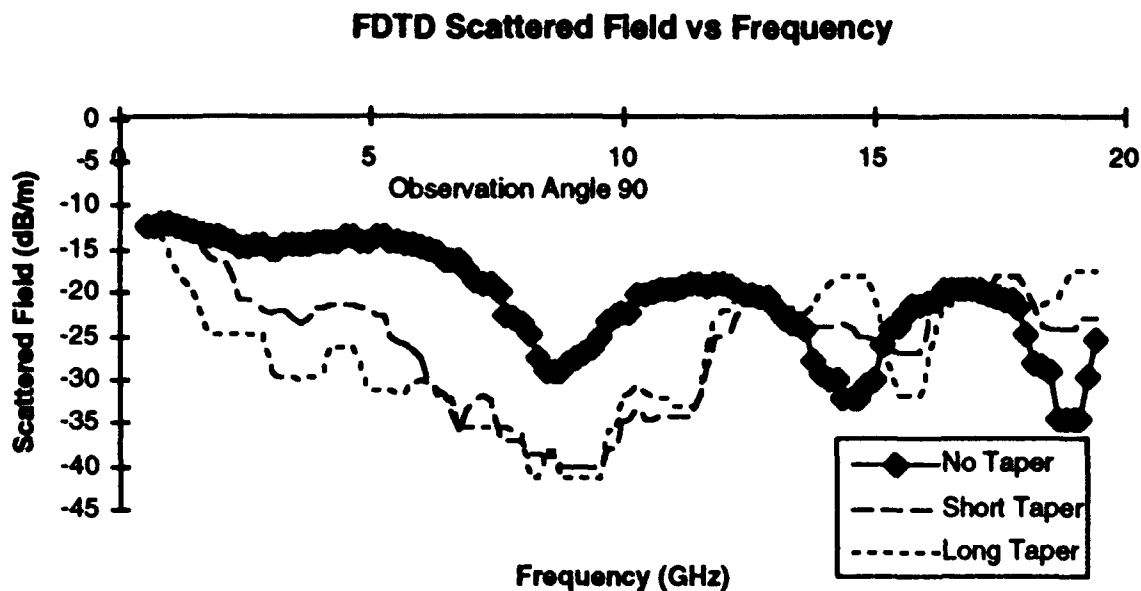


**Figure 52. Comparison of FDTD Results for Capacitive Design #2.** The graph above shows improved for the second capacitive taper design up to 13 GHz. The incident field was at  $10^\circ$  and the far field observation angle was  $90^\circ$ .

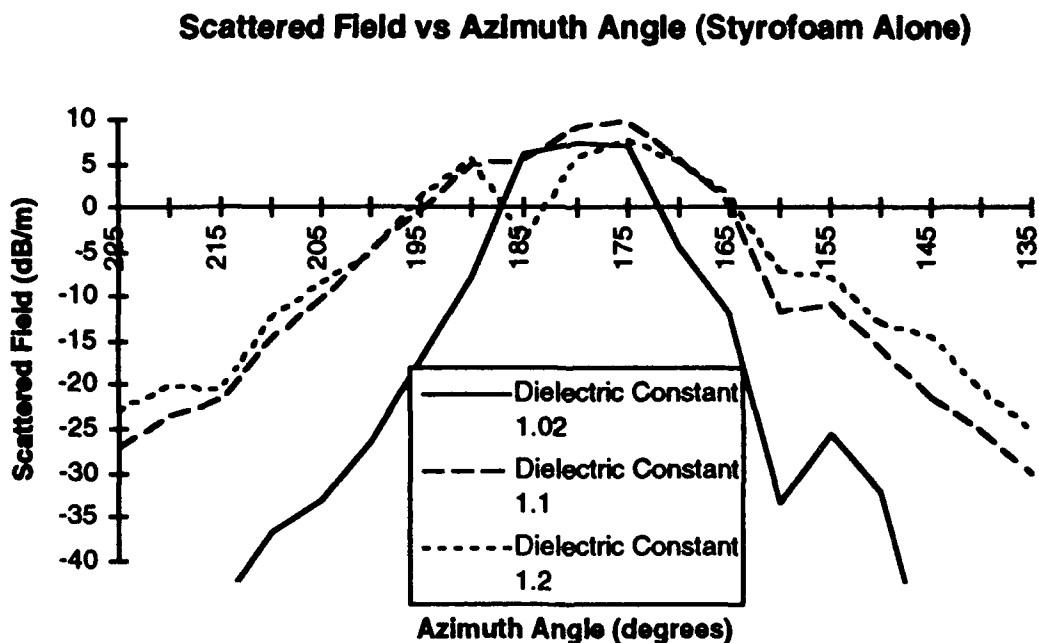


**Figure 53. Scattered Field from the Styrofoam Substrate Alone as a Function of Observation Angle.** The graph above shows the scattering from the 2 inch thick styrofoam alone for different dielectric constants at 10 GHz.



### Scattered Field vs Frequency (Styrofoam Alone)

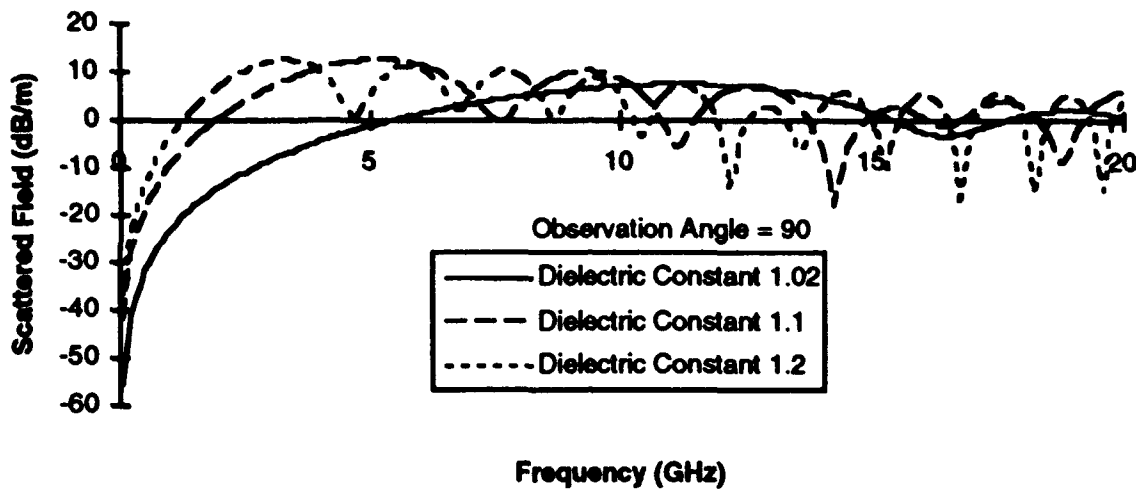


**Figure 54. Scattered Field from the Styrofoam Substrate Alone as a Function of Frequency.** The graph above shows the scattering from the 2 inch thick styrofoam alone for different dielectric constants at a look angle of 90°.

### Summary

This chapter covered the results and analysis of this study. The tapers were designed using Henderson's PMM code and were tested at a compact range. The tapers were also modeled using UTD, MoM and FDTD codes. The inductive tapers did not work very well. The first capacitive taper was crudely made and showed only limited improvement. The second capacitive taper worked very well over a wide frequency range in both the measurements and numerical data. The FDTD code was also used to try to identify sources of additional scattering.

## *Chapter 5: Conclusions and Future Studies*

### *Introduction*

**Overview.** This chapter covers the conclusions from the results of the study and suggests future work for periodic tapers. The success of all four taper designs used in this study are covered in the first section. The future work section covers suggestions for different taper designs and better methodology for studying tapered periodic surfaces.

### *Success of the Taper Designs*

**Inductive Tapers.** The inductive taper designs were not very successful. The first inductive taper's experimental results showed very limited diffraction reduction in the shallow shadow region at 18 GHz. The TMz MoM analysis of the first inductive taper showed the design had a very small diffraction reduction. The large diameter wires in the first taper were a problem, since the inductance of the free space edge could not be increased enough by spacing alone (due to grating lobe problems). The second inductive taper showed more promise to work as a taper design from the PMM results. The experimental measurements showed a larger reduction in the shallow shadow region for the second inductive taper as compared to the first inductive taper. However, the reduction was still slight and only over a small frequency range (8-10 GHz). The slot array was also unable to impedance match the free space end.

**Capacitive Tapers.** The capacitive tapers were more successful in reducing edge diffraction. The first capacitive taper measurements displayed a small reduction in the scattering, but the crude manufacturing made these results highly suspect. The TEz MoM code model of this taper did show a slight improvement for the first capacitive design. One good characteristic of this first capacitive design was that the impedance was entirely capacitive over the entire frequency range. This characteristic is good for time domain applications, due to the fact that the phase shift by the taper is constant and will not produce

time dispersion. The second capacitive taper was highly effective over a large frequency bandwidth (6-16 GHz). The long version of the second capacitive taper did work better than the short version of the second capacitive taper, but only for low frequencies. The second capacitive taper had the best match of all the tapers for both the ground plane and free space edges. The second taper did have resonances which would produce dispersion in a time domain signal. This property, while unwanted for time domain applications, is not terrible for continuous frequency applications.

### *Future Work*

*Overview.* This section covers future work suggested by the results to further the development and understanding of periodic taper design. There are limitless types of periodic structures which could be used for their inductive or capacitive properties. Improvements could also have been made in the measurements and modeling used in this thesis. There are also several different applications which were not studied in this paper.

*Inductive Tapers.* The inductive taper designs were not successful, but future designs might be effective. One improvement to the first inductive design would be to load the parallel wire grid at the free space edge. If these wires were loaded, the free space edge of the taper would have a higher impedance and match free space better. A loaded taper may still have high power applications. The power of the antenna should be reduced at the free space end of the taper so that a high resistive (or inductive) wire would not heat up a great amount. Also, the heat dissipated in a transient antenna would be reduced, because the average power of a transient antenna is much lower than for a continuous wave antenna. The parallel wire grid would not have a phase shift over the frequency range and would work well for time domain applications. Another improvement to the first design, would be to use thinner wires (which have more inductance and can be spaced closer together). To improve the second inductive design, a lower dielectric constant dielectric might improve the inductive capabilities of the taper. The thin dielectric slab acted as a

capacitive sheet and by reducing the dielectric constant, the capacitance of the design would be reduced. Another improvement might be to increase the width of the slots, which would increase the transmission coefficient at the free space end of the taper. Wider slots would also result in a decrease in the bandwidth. Finally, for future inductive tapers, other designs need to be tested. There are several ways to create inductance with periodic geometries and these geometries can easily be tapered to create new inductive tapers.

**Capacitive Tapers.** The capacitive tapers were successful in reducing edge diffraction. One improvement to the first capacitive taper would be to change from constant center-to-center spacing to constant gap size (the gap size is the length of the gap between strips). This change would make for a more continuous taper design and increase the bandwidth of the taper. Another improvement to the first taper would be to load the free space edge of the taper. This would reduce the scattering from the free space end of the taper. Due to the success of the second capacitive taper, this type of design shows good possibilities. To improve the second capacitive taper, one might try the changes mentioned above for the first capacitive taper. Another taper improvement would be to try different periodic geometries that create capacitive impedance. Discrete capacitive elements would be better for bandwidth and continuous tapers, however, these discrete elements would resonate and prevent time domain applications. Therefore, depending upon the application, the taper could be improved in a variety of ways.

**Measurements.** The measurements in this study were bistatic measurements. Monostatic (or backscatter) measurements would also be of interest especially for RCS reduction. Monostatic measurements would be much easier to perform and would not require such a large structure for measurements. Also monostatic measurements would not require all the assumptions that were needed in a bistatic study. If a similar antenna platform was to be used in a future study, the dielectric constant of the styrofoam must be measured for proper modeling. For a dielectric constant so close to unity, a cavity

resonance method of measuring the dielectric constant would be needed instead of the waveguide method. Other future work would be to attach the tapers directly to antennas much like edge cards. Another major area of study for these periodic tapers would be in the reduction in edge scattering from a finite size radome. For better modeling of the tapers, singly-periodic PMM codes could be used instead of Henderson's PMM code. This would allow the tapers be designed without having to assume local periodicity. To improve the modeling of the platform using FDTD, the entire structure (including the source antenna) should be modeled using a 3D total field FDTD code. This would get rid of the plane wave incidence approximation and the 2D approximation. By modeling the entire structure, the additional sources of scattering would be easier to determine. There are many different measurements that could be of interest using these periodic tapers.

### ***Overview***

This study was a preliminary review of the use of capacitive and inductive periodic structures as impedance tapers. In this study, effective tapers were designed, built, modeled, and measured. MoM provided a valid model for the first capacitive and inductive designs. FDTD provided a valid model for the more complex second capacitive taper. The design technique of using Henderson's PMM code and assuming local periodicity seemed to model the impedance tapers well. Future work would include better measurement techniques and better periodic taper designs.

## APPENDIX A

### RESULTS FROM PMM OUTPUT

This appendix contains the all the results from PMM. The first results are the PMM source code listings. Also in this appendix are all the impedance and reflection coefficient values calculated from the PMM codes.

This is the PMM code listing for the first inductive taper.

```
TITLE "Inductive Design #1"
PLOTFILE wire100.plt
FREQUENCY 1,20,.1
ETA =80
ALPHA = 0
!      This is the first inductive design composed
!      of parallel wires of constant radius with a
!      varying spacing. In this study the radius
!      is 1/32 of an inch and the spacing is varied
!      from .3 to 1 cm.

!      the spacing is given in centimeters
ANGLE ALPHA, ETA
SPACING = 1.00
DX = SPACING
DZ = .25
SET MODE SINE
NONSKEWED GRID DX, DZ = DZ
!      width in centimeters
RADIUS=2.54/32
WIDTH =4*RADIUS
DIPOLE ARRAY WIDTH, .001, (.001,0.)
  NODE 10,0,0
  NODE 20,0,DZ
  NODE 30,0,-DZ
  SEGMENT 20,10,20
  SEGMENT 30,10,30
  MODE 10,20,30
END ARRAY
XEQ
EXIT
```

This is the PMM code listing for the first capacitive taper.

TITLE "Capacitive Design #1 "

PLOTFILE slot055.plt

FREQUENCY 1,20,1

ETA = 80

ALPHA=90

! This is the first capacitive design composed of  
! parallel thin strips which have constant center to  
! center spacing and varying length. The length is varied  
! from .5 cm to .55 cm and the spacing is .6 cm.

! the length is given in cm

LENGTH=.55

HALFLENGTH=LENGTH/2.

QUARTERLENGTH=LENGTH/4.

THIRDLLENGTH=LENGTH/3.

EIGHTHLENGTH=LENGTH/8.

SIXLENGTH=LENGTH/6.

WIREDWIDTH=0.001\*2.54

DX=WIREDWIDTH

DZ=.6

HALFDZ=DZ/2.

ANGLE ALPHA, ETA

SET MODE SINE

NONKEWED GRID DX, DZ = DZ

DIPOLE ARRAY WIREDWIDTH, .001

NODE 1,0,HALFLENGTH

NODE 2,0,THIRDLLENGTH

NODE 3,0,SIXLENGTH

NODE 4,0,0

NODE 5,0,-SIXLENGTH

NODE 6,0,-THIRDLLENGTH

NODE 7,0,-HALFLENGTH

SEGMENT 1,1,2

SEGMENT 2,2,3

SEGMENT 3,3,4

SEGMENT 4,4,5

SEGMENT 5,5,6

SEGMENT 6,6,7

MODE 2,1,2

MODE 3,2,3

MODE 4,3,4

MODE 5,4,5

MODE 6,5,6

END ARRAY

PMM\$ACCURACY=50000

XEQ

EXIT

This is the PMM code listing for the second inductive taper.

```
TITLE "Inductive Design #2"
PLOTFILE IND350.PLT
NOSHOW ALL
SHOW COEFFICIENTS
FREQUENCY 1,20.,1
ETA = 80
ALPHA = 90
!      This is the second inductive design composed of single skewed slot
!      array on a thin (10 mil) dielectric substrate. The width of the slots is kept
!      to the minimum line width (5 mil). The length of the slots is varied from
!      5 mil to 350 mil. The spacing from each slot to the next is the average length
!      of the slots plus the minimum line width.
!      the length is given in inches
LENGTHIN=0.350
LENGTH=LENGTHIN*2.54
INMIN = 0.005
CMMIN=INMIN*2.54
WIDTH=0.005*2.54
HALFLENGTH=LENGTH/2.
QUARTERLENGTH=LENGTH/4.
THIRDLLENGTH=LENGTH/3.
EIGHTHLENGTH=LENGTH/8.
SIXLENGTH=LENGTH/6.
ANGLE ALPHA, ETA
DX = WIDTH+CMMIN
DZ = LENGTH+CMMIN
SET MODE SINE
SKEWED GRID DX, DZ = DZ
SLOT ARRAY WIDTH, .001
  NODE 1,0,HALFLENGTH
  NODE 2,0,THIRDLLENGTH
  NODE 3,0,SIXLENGTH
  NODE 4,0,0
  NODE 5,0,-SIXLENGTH
  NODE 6,0,-THIRDLLENGTH
  NODE 7,0,-HALFLENGTH
SEGMENT 1,1,2
SEGMENT 2,2,3
SEGMENT 3,3,4
SEGMENT 4,4,5
SEGMENT 5,5,6
SEGMENT 6,6,7
MODE 2,1,2
MODE 3,2,3
MODE 4,3,4
MODE 5,4,5
MODE 6,5,6
END ARRAY
SLAB 0.010*2.54,(4.5,0.),(1.,0.)
XEQ
EXIT
```



This is the PMM code listing for the second capacitive taper.

```
TITLE "Capacitive Design #2"
PLOTFILE cap330.plt
NOSHOW ALL
SHOW COEFFICIENTS
FREQUENCY 1,20,.1
ETA = 80
ALPHA=90
!   This is the second capacitive design composed of two arrays of thin
!   strips with constant center to center spacing with a thin (10mil) dielectric
!   in between the arrays. The strip length is varied from .005 mil to .330 mil.
!   The spacing is held constant to .335 mil.
!
!   The length is given in mils.
LENGTHIN=0.330
LENGTH=LENGTHIN*2.54
HALFLENGTH=LENGTH/2.
QUARTERLENGTH=LENGTH/4.
THIRDLLENGTH=LENGTH/3.
EIGHTHLENGTH=LENGTH/8.
SIXLENGTH=LENGTH/6.

WIREWIDTH=0.001*2.54
DX=WIREWIDTH
DZ=(0.335*2.54)
HALFDZ=DZ/2.
ANGLE ALPHA, ETA
SET MODE SINE
NONSKEWED GRID DX, DZ = DZ

DIPOLE ARRAY WIREWIDTH, .001
  NODE 1,0,HALFLENGTH
  NODE 2,0,THIRDLLENGTH
  NODE 3,0,SIXLENGTH
  NODE 4,0,0
  NODE 5,0,-SIXLENGTH
  NODE 6,0,-THIRDLLENGTH
  NODE 7,0,-HALFLENGTH
  SEGMENT 1,1,2
  SEGMENT 2,2,3
  SEGMENT 3,3,4
  SEGMENT 4,4,5
  SEGMENT 5,5,6
  SEGMENT 6,6,7
  MODE 2,1,2
  MODE 3,2,3
  MODE 4,3,4
  MODE 5,4,5
  MODE 6,5,6
END ARRAY
]
SLAB 0.010*2.54,(4.5,0.),(1.,0.)
```

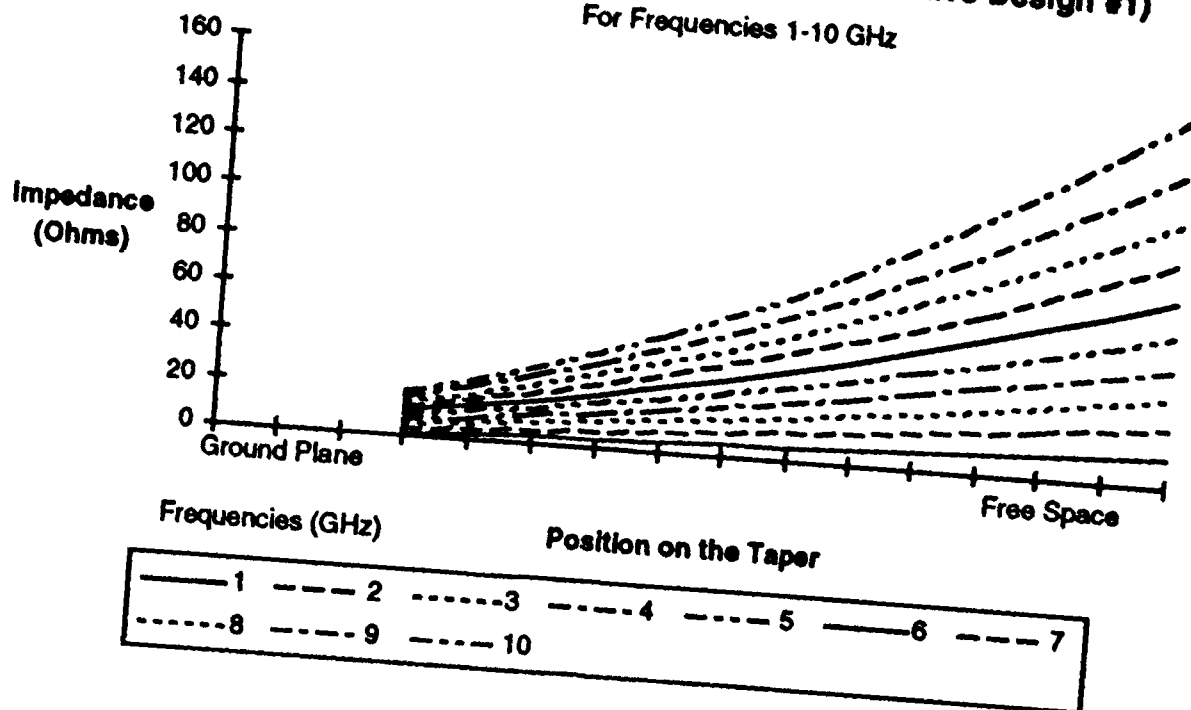
```

DIPOLE ARRAY WIREWIDTH, .001
  NODE 1,0,HALFLENGTH+HALFDZ
  NODE 2,0,THIRDLLENGTH+HALFDZ
  NODE 3,0,SIXLENGTH+HALFDZ
  NODE 4,0,HALFDZ
  NODE 5,0,-SIXLENGTH+HALFDZ
  NODE 6,0,-THIRDLLENGTH+HALFDZ
  NODE 7,0,-HALFLENGTH+HALFDZ
SEGMENT 1,1,2
SEGMENT 2,2,3
SEGMENT 3,3,4
SEGMENT 4,4,5
SEGMENT 5,5,6
SEGMENT 6,6,7
MODE 2,1,2
MODE 3,2,3
MODE 4,3,4
MODE 5,4,5
MODE 6,5,6
END ARRAY
PMM$ACCURACY=50000
XEQ
EXIT

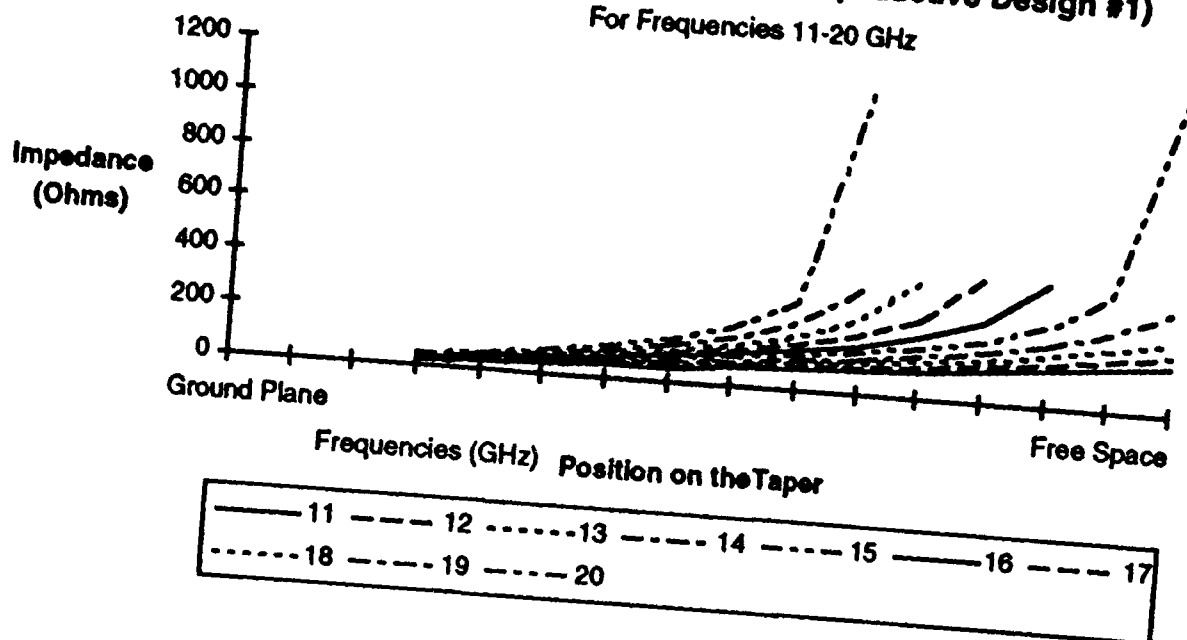
```

The following are the graphs of the impedance and reflection coefficients vs position on the taper for all four of the designs tested in this study. The different series represent the frequency for the calculations.

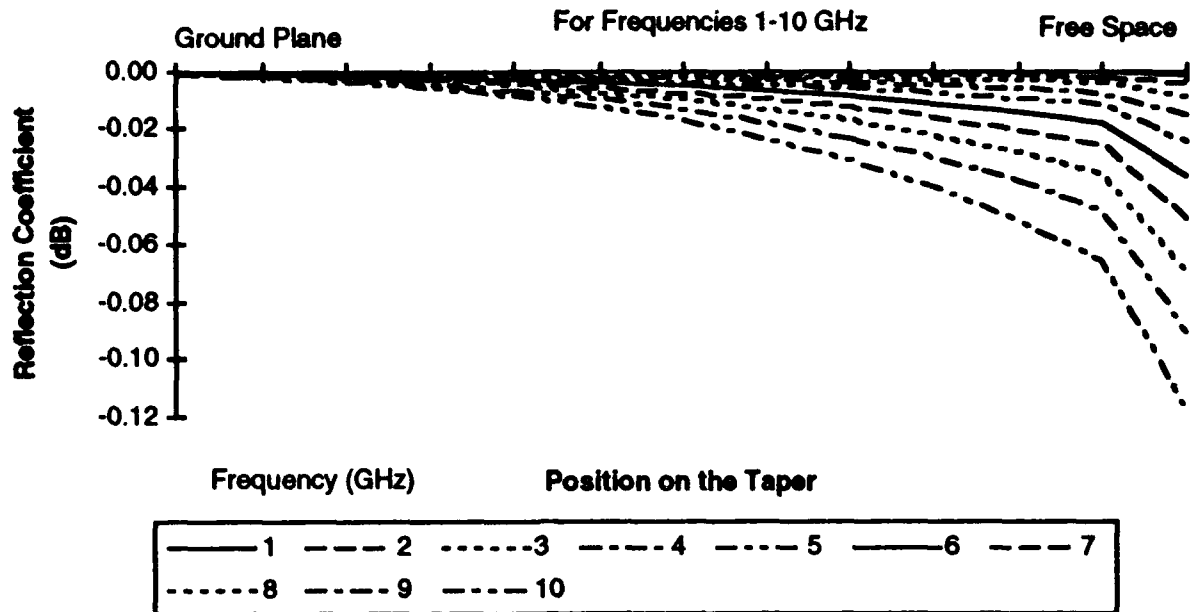
**Impedance vs Length of the Taper (Inductive Design #1)**  
For Frequencies 1-10 GHz



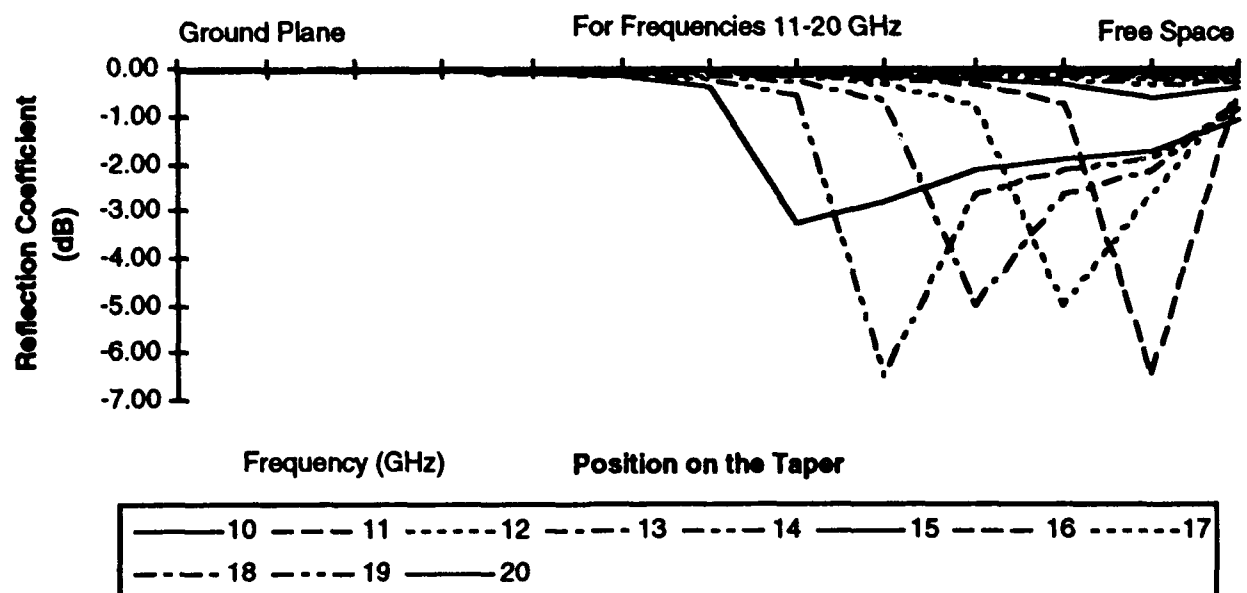
**Impedance vs Length of the Taper (Inductive Design #1)**  
For Frequencies 11-20 GHz

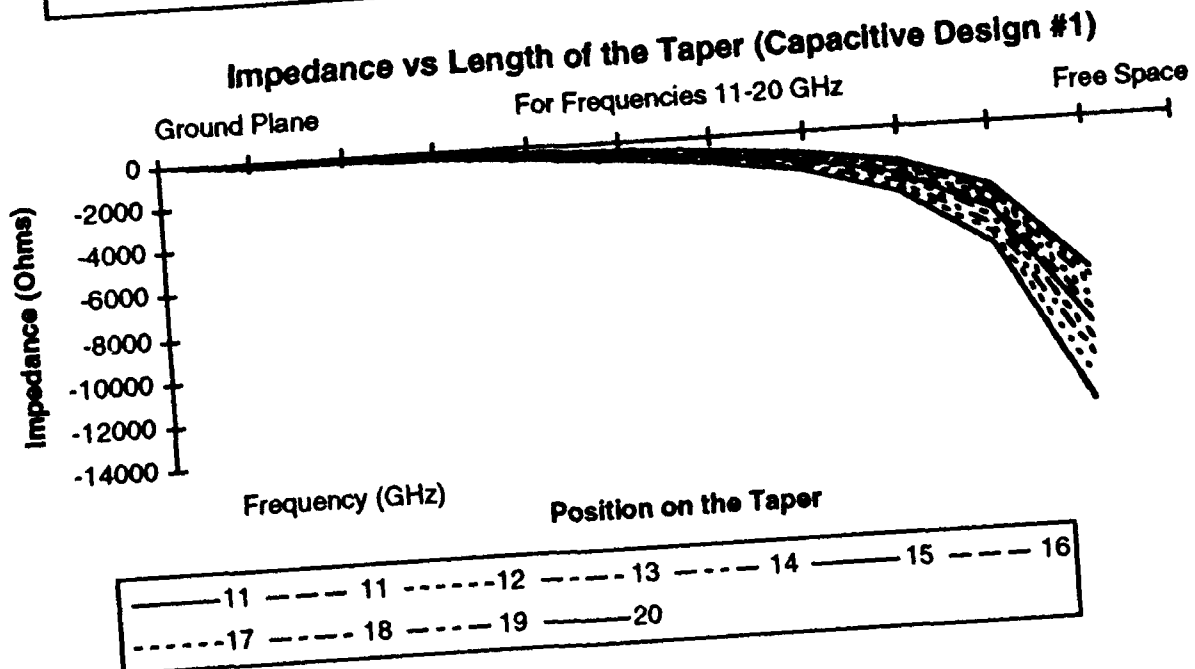
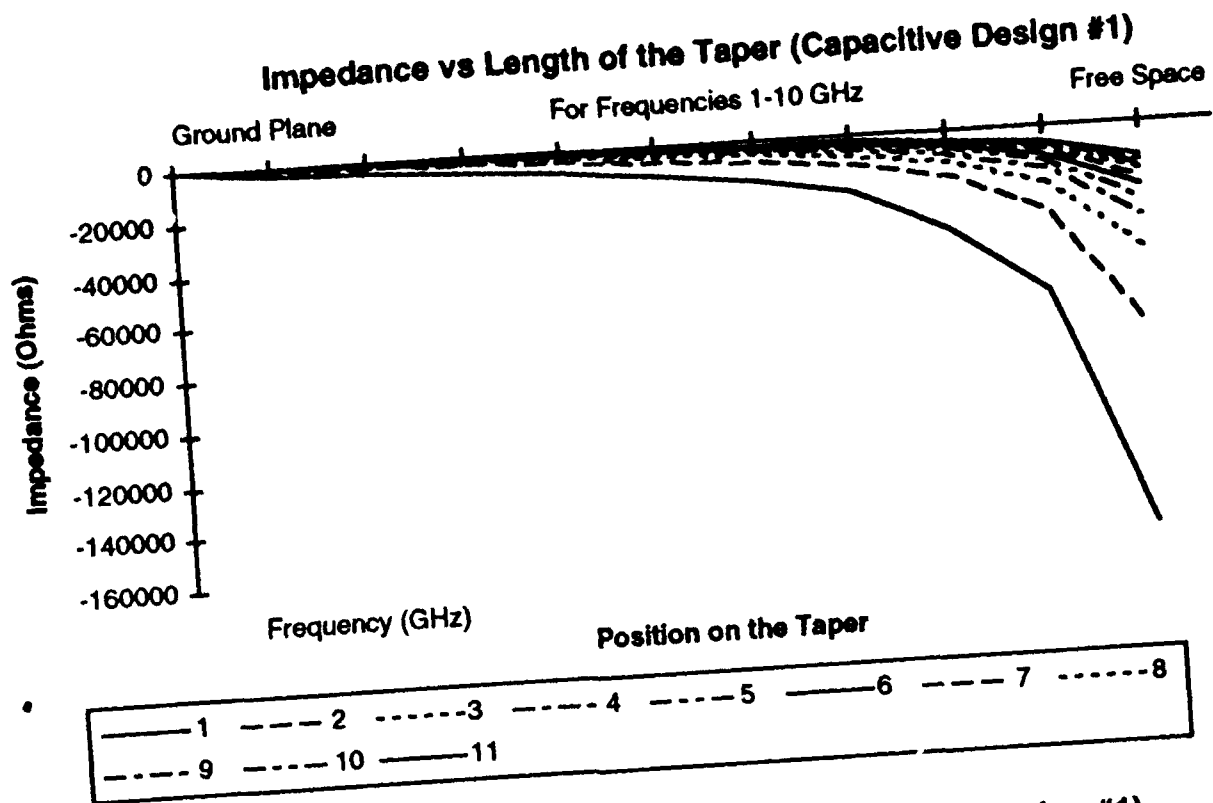


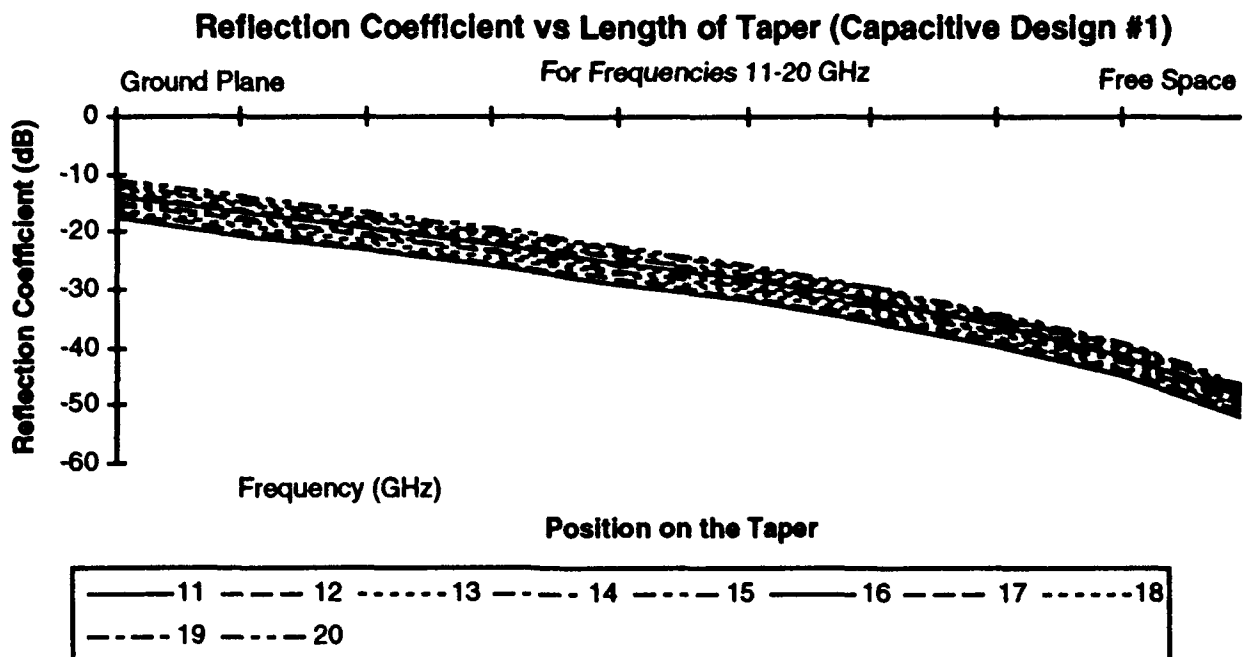
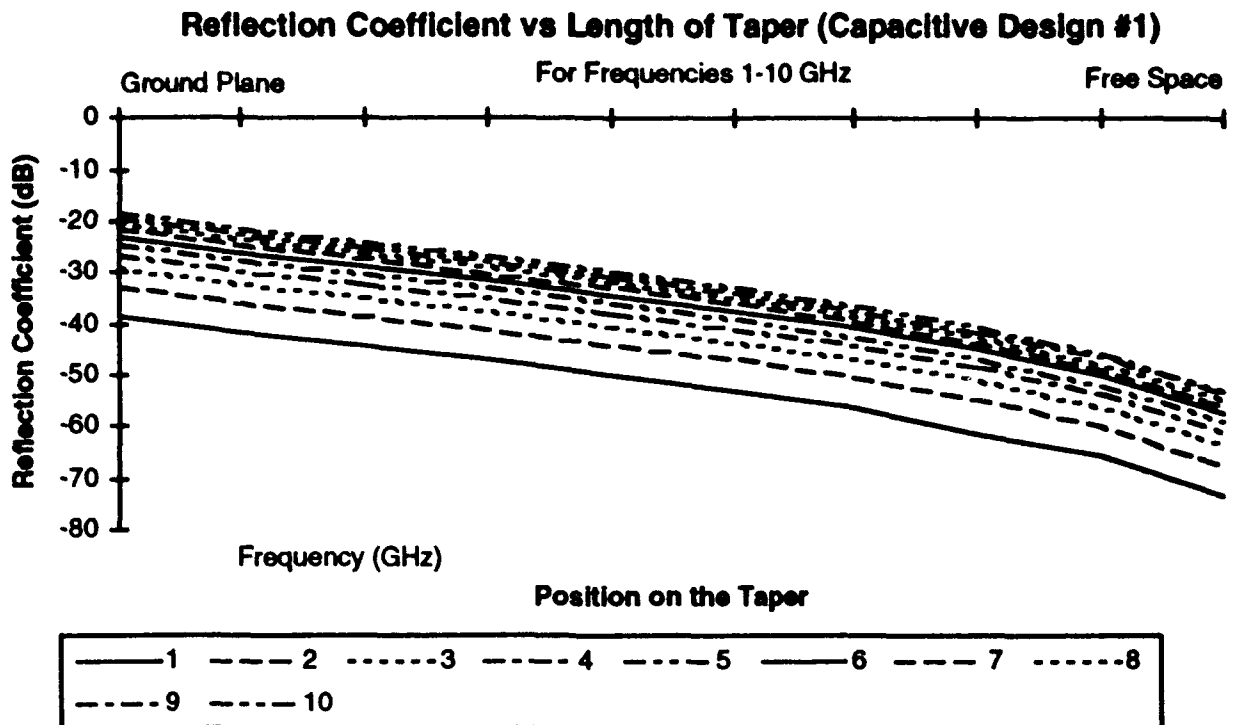
### Reflection Coefficient vs Length of Taper (Inductive Design #1)



### Reflection Coefficient vs Length of Taper (Inductive Design #1)

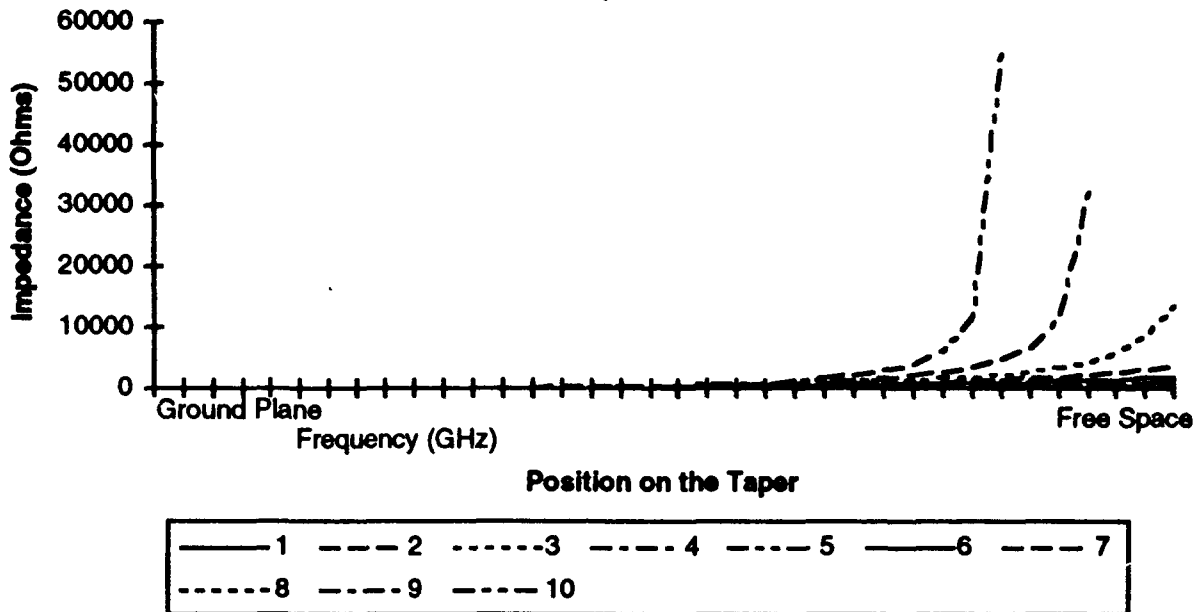






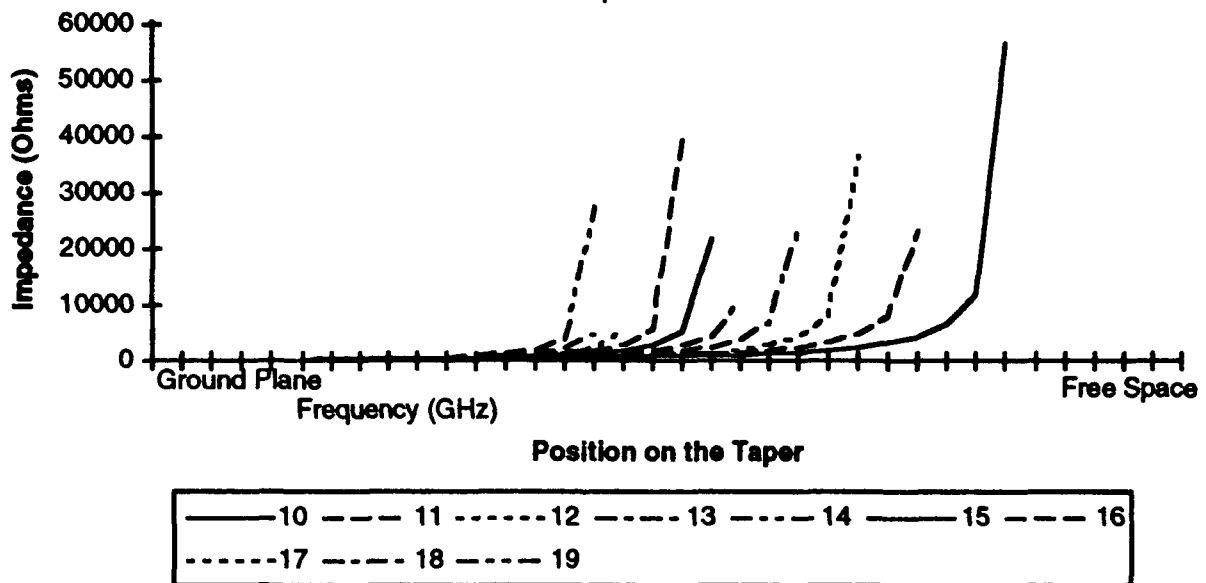
### Impedance vs Length of the Taper (Inductive Design #2)

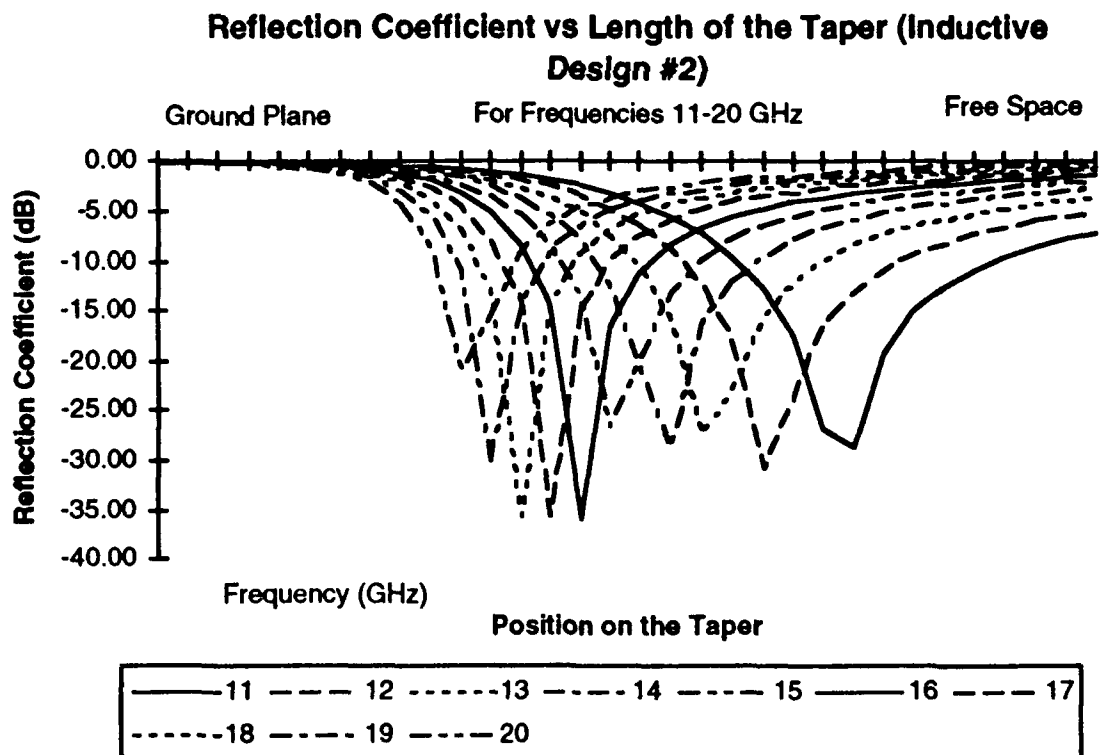
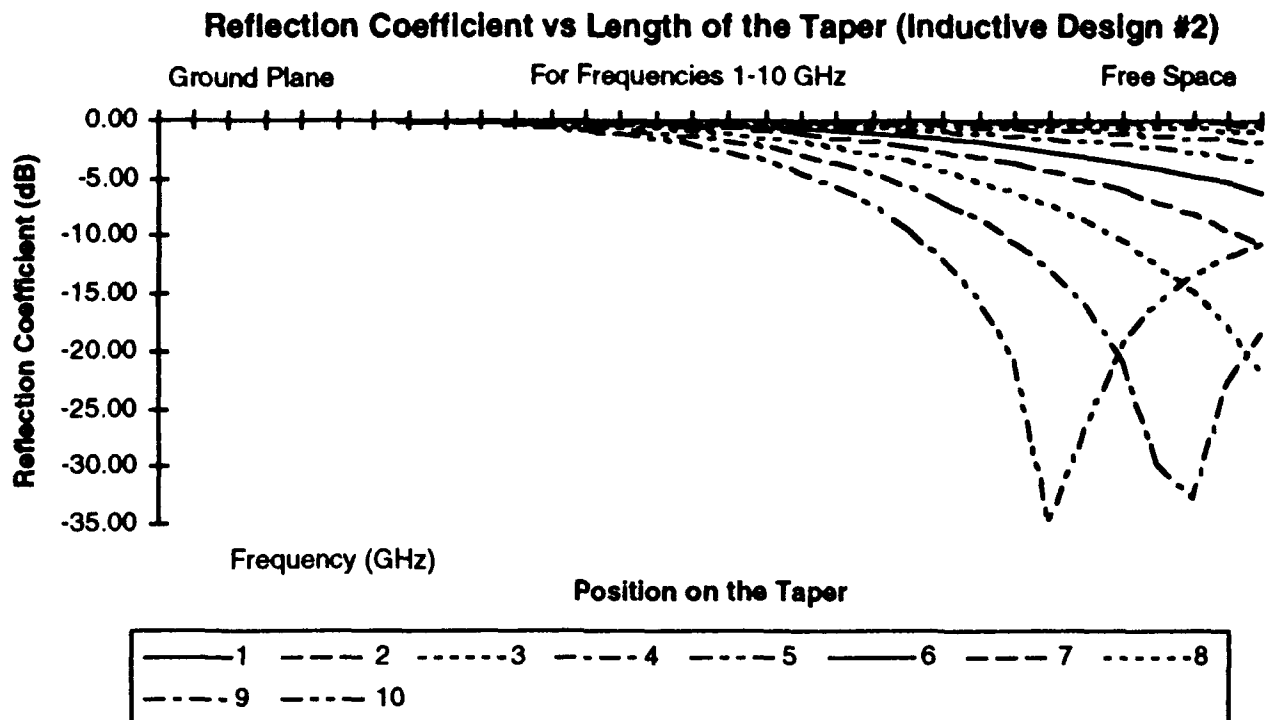
For Frequencies 1-10 GHz



### Impedance vs Length of the Taper (Inductive Design #2)

For Frequencies 11-20 GHz

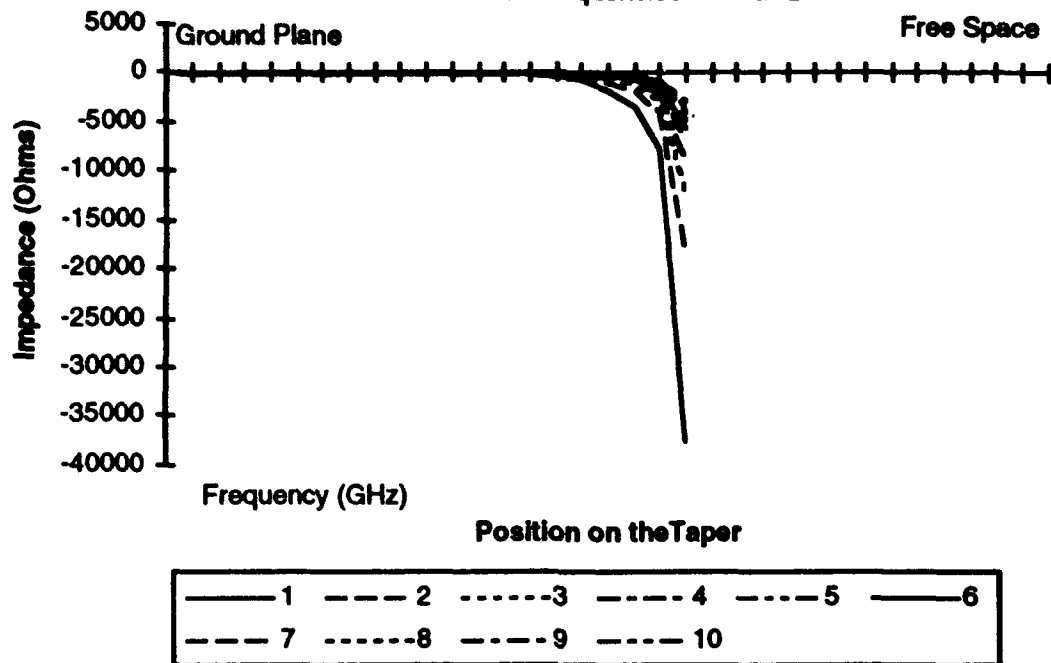






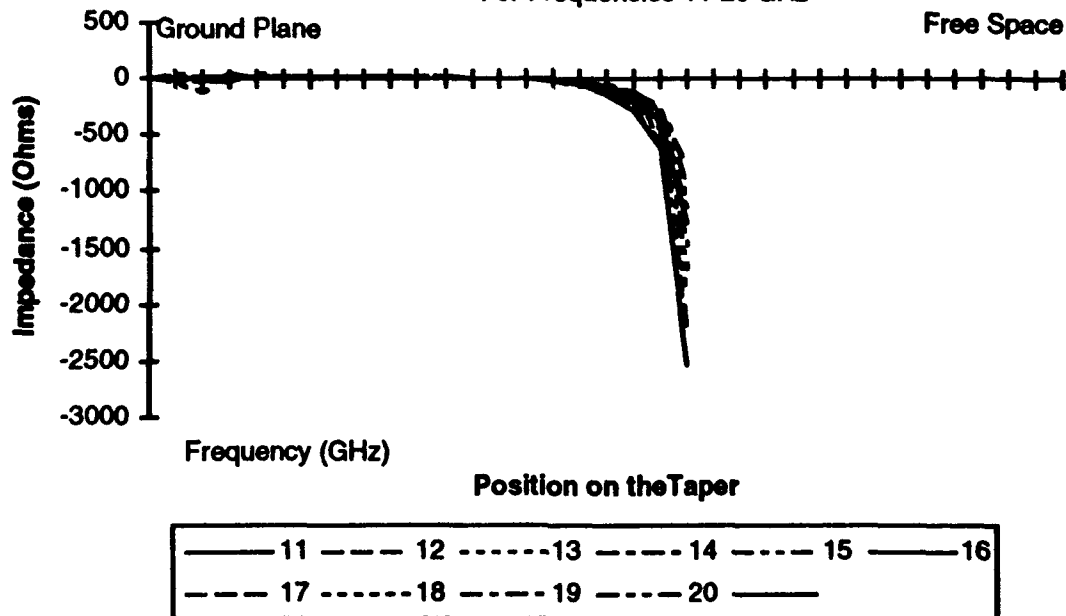
### Impedance vs Length of Taper (Capacitive Design #2)

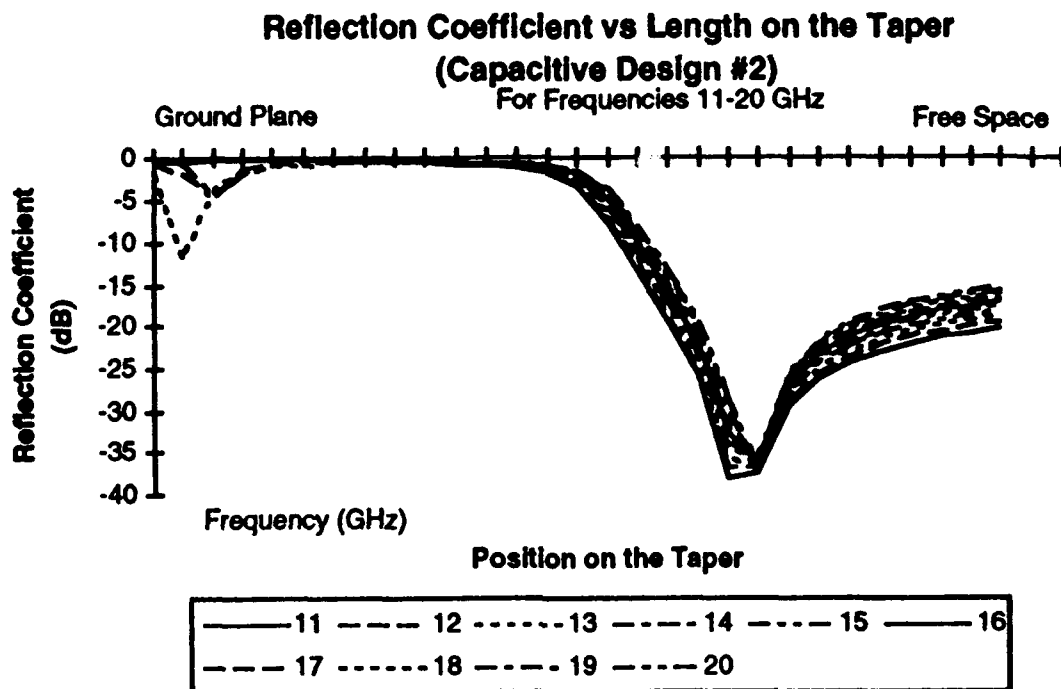
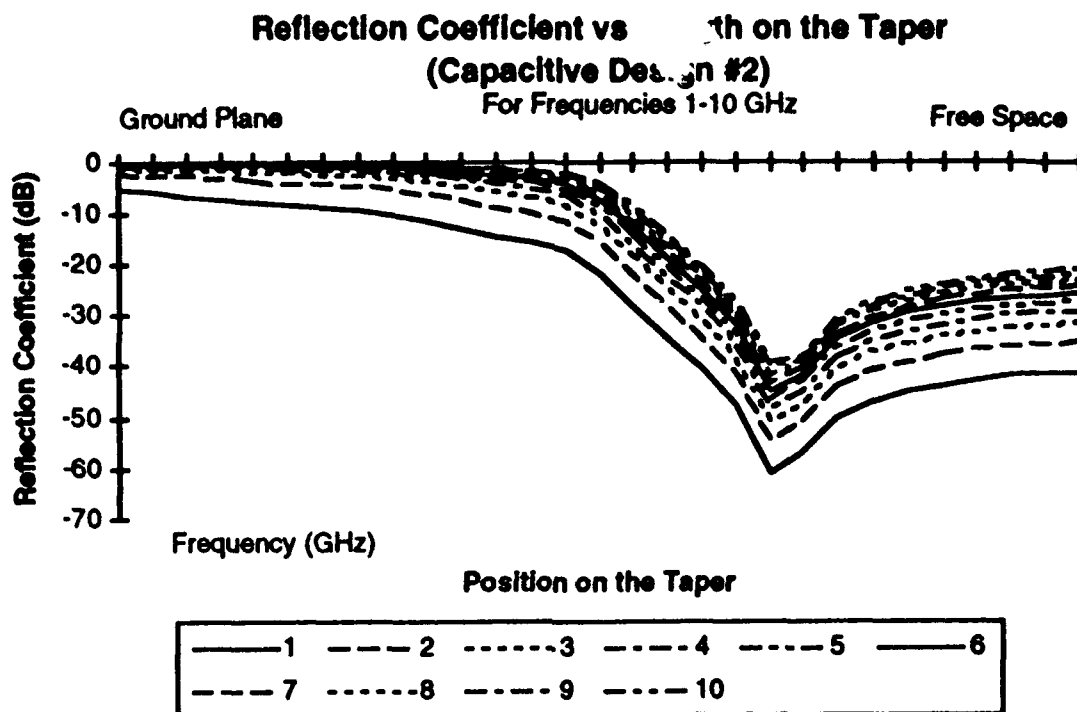
For Frequencies 1-10 GHz



### Impedance vs Length of Taper (Capacitive Design #2)

For Frequencies 11-20 GHz





## **APPENDIX B**

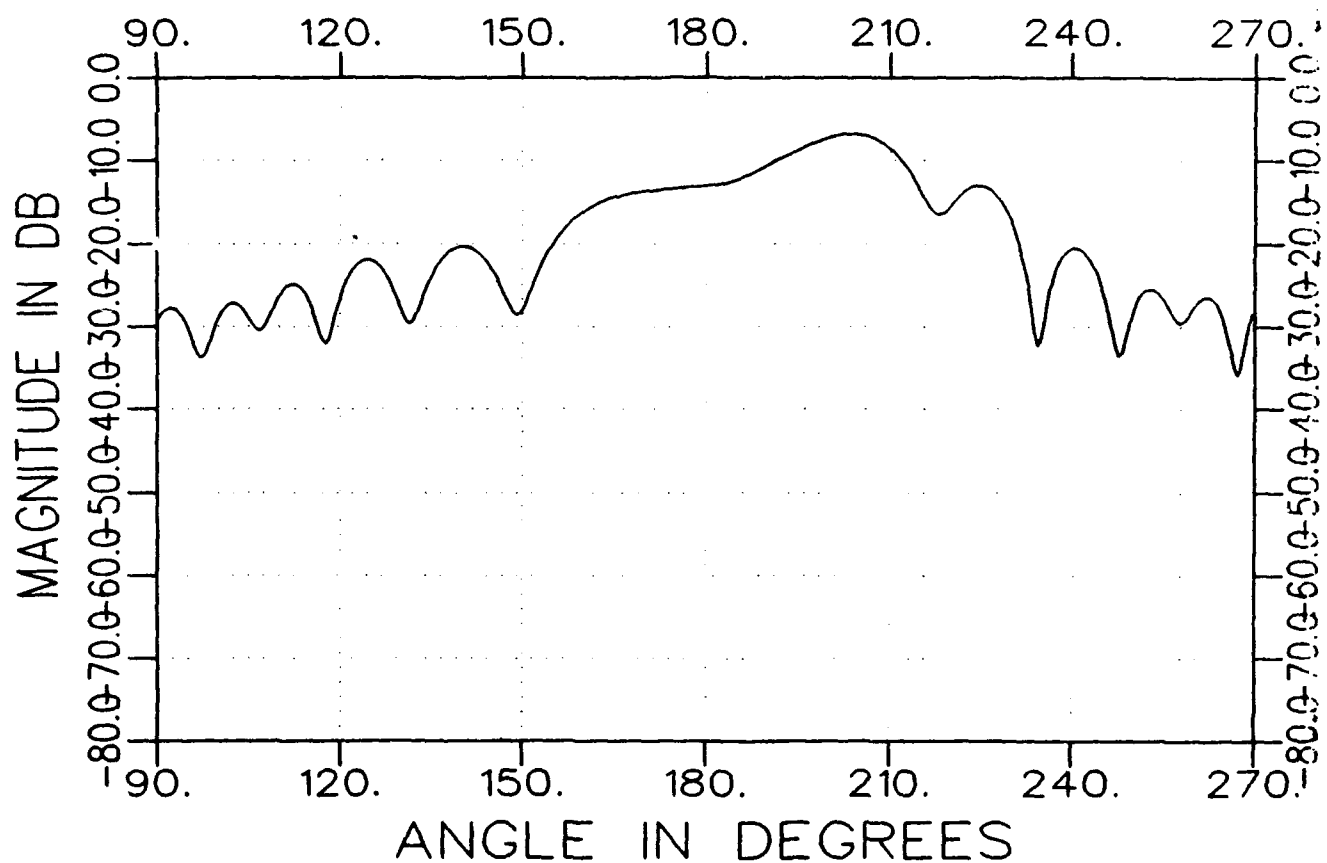
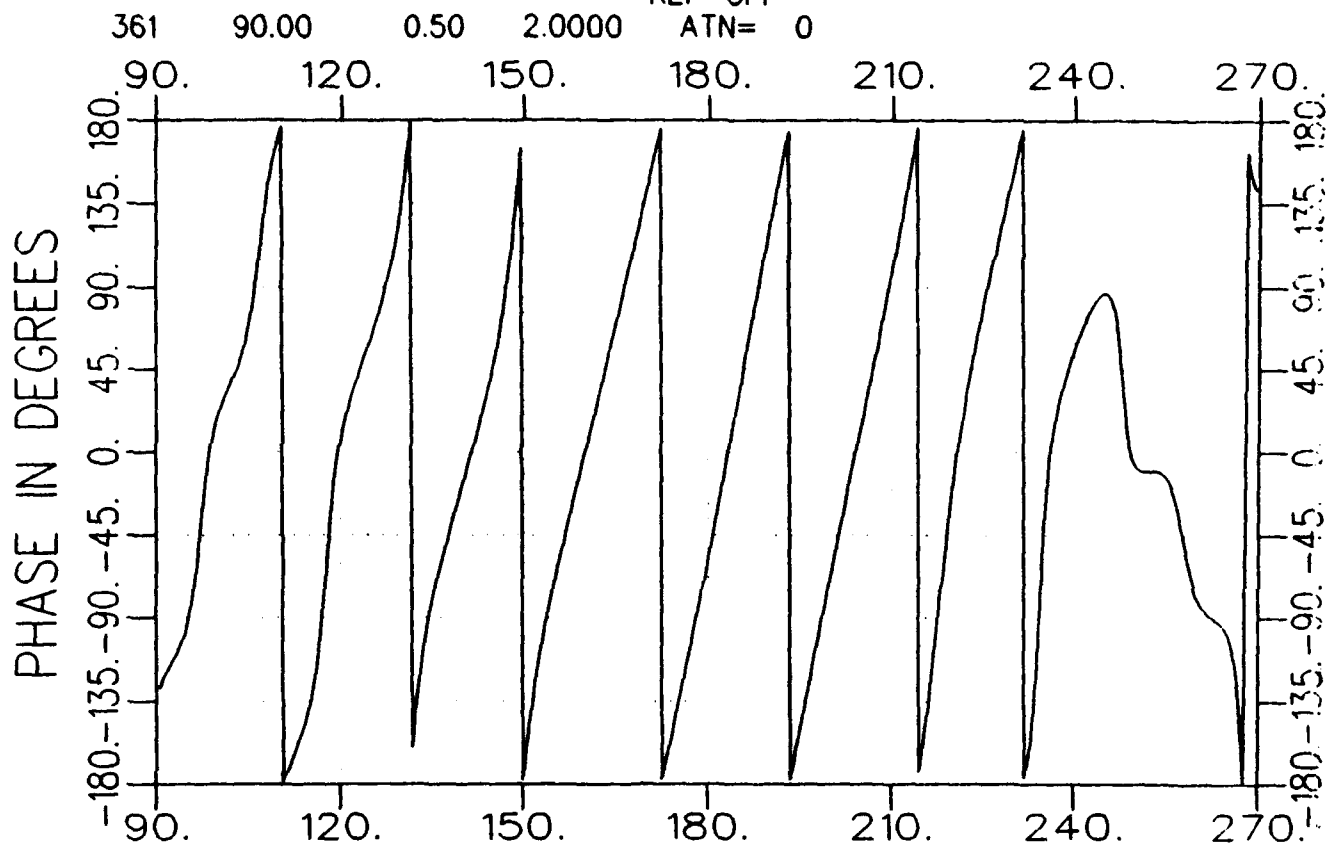
### **FIRST MEASURED DATA**

The first data in this appendix are the magnitude and phase azimuth cuts at frequencies 2, 10, and 18 GHz. The second data in this appendix are the frequency sweeps and time domain plots at azimuth angles 90°, 120°, and 150°. The OSU-ESL designator system used letters to designate which taper was measured. The following letters correspond to the OSU-DATA for the first impedance designs.

a3204----Capacitive Taper #1  
b3204----No Taper for Hard Polarization  
c3204----Long Inductive Taper #1  
d3204----Short Inductive Taper #1  
e3204----No Taper for Soft Polarization

a3204dh0200-a.trq  
TARGET

AZIM. 07/23/93 09:27  
CAP. SLOT GRID AVE= 1  
REF=OFF

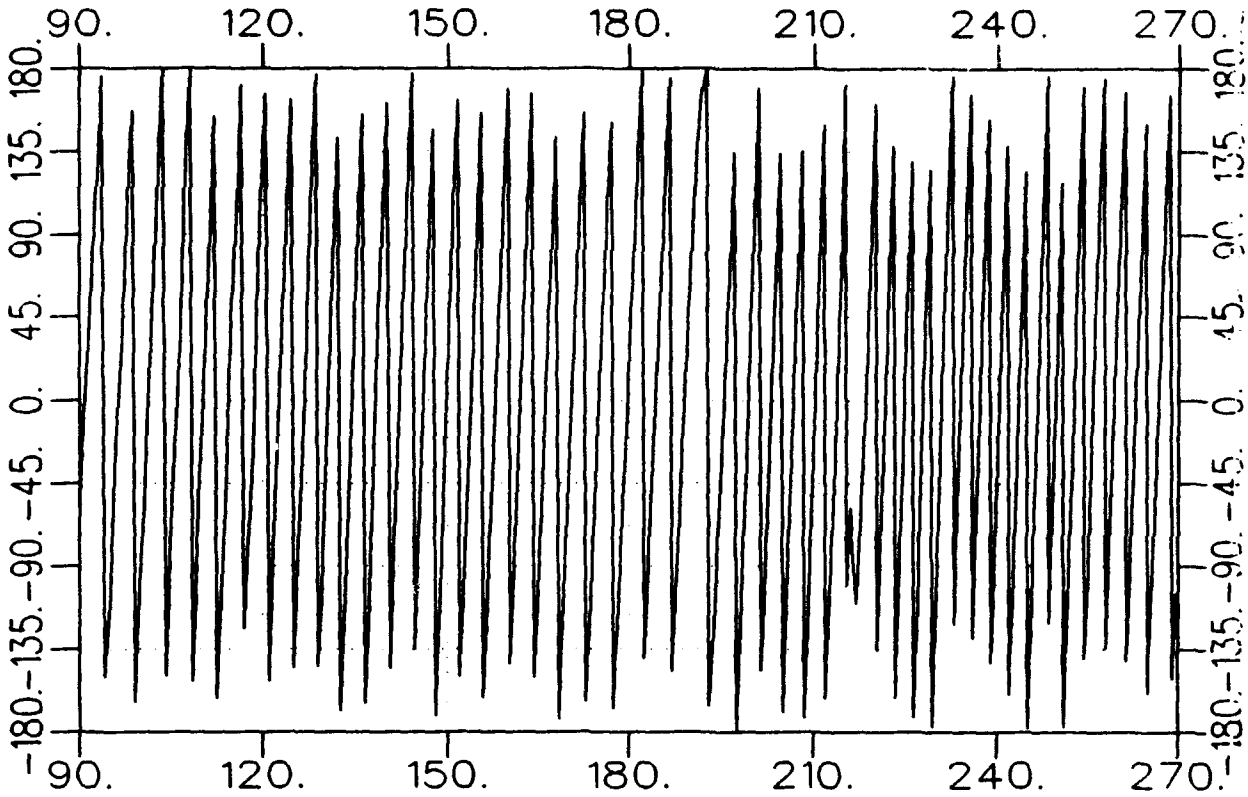


a3204ah1000-a.frq  
TARGET

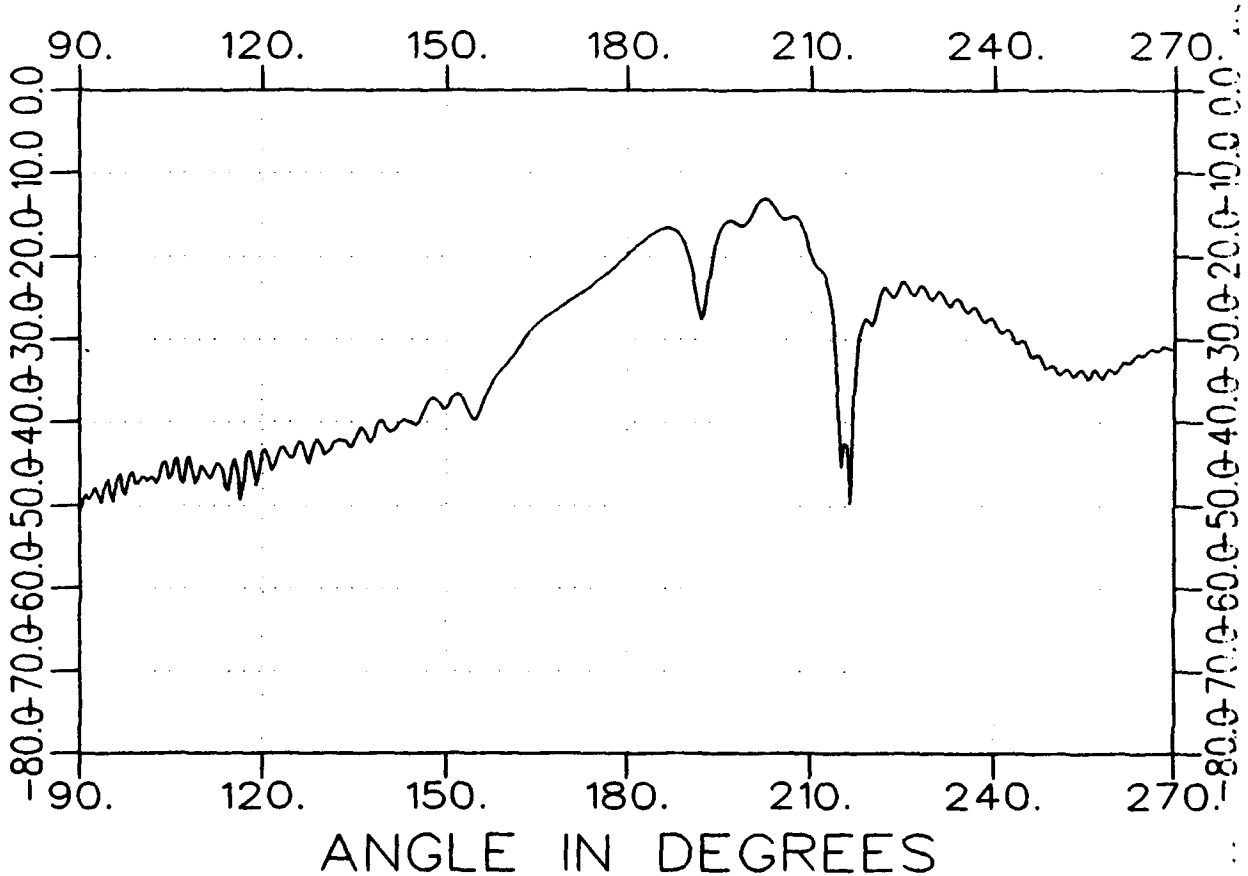
AZIM. 07/23/93 09:27  
CAP. SLOT GRID AVE= 1  
REF=OFF

361 90.00 0.50 10.0000 ATN= 0

PHASE IN DEGREES



MAGNITUDE IN DB

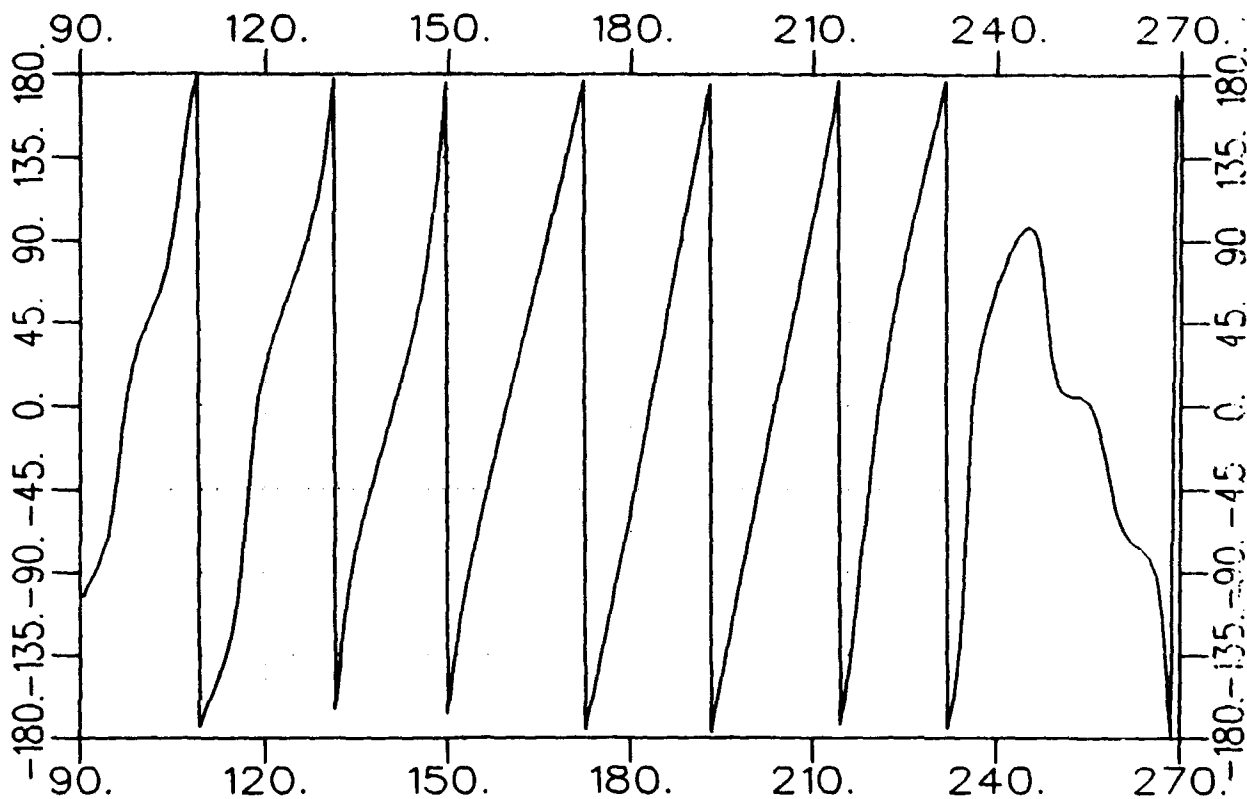


b3204ah0200-a.freq  
TARGET

AZIM. 07/23/93 09:43  
CAP. SLOT GRID AVE= 1  
REF=OFF

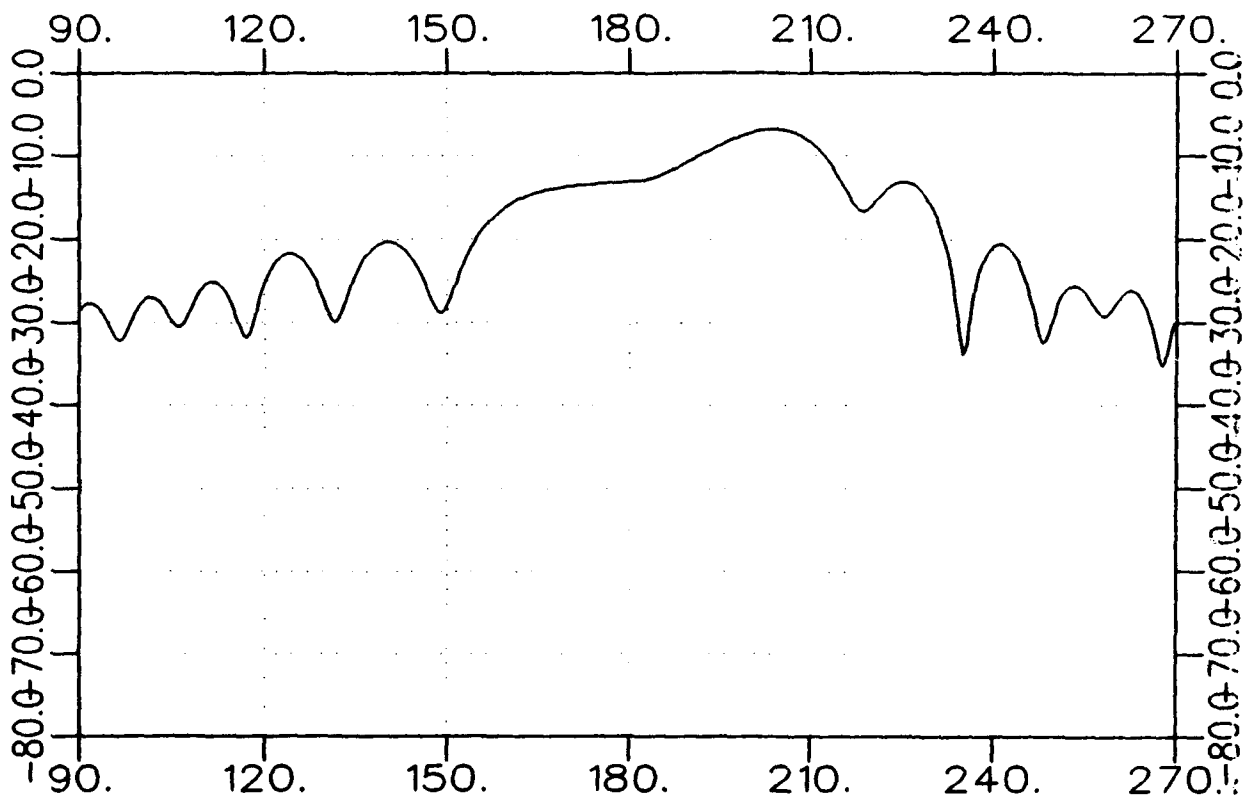
361 90.00 0.50 2.0000 ATN= 0

PHASE IN DEGREES



ANGLE IN DEGREES

MAGNITUDE IN DB



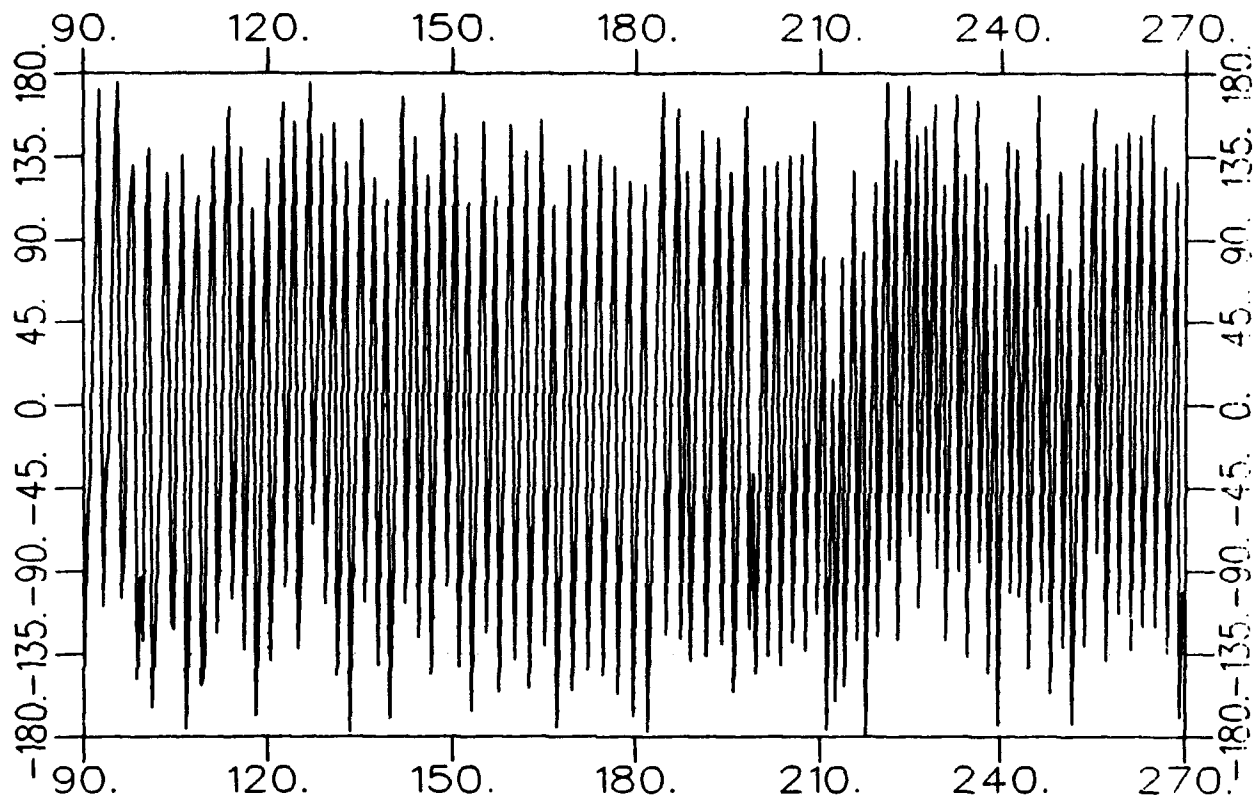
ANGLE IN DEGREES

a3204ah1800-a.freq  
TARGET

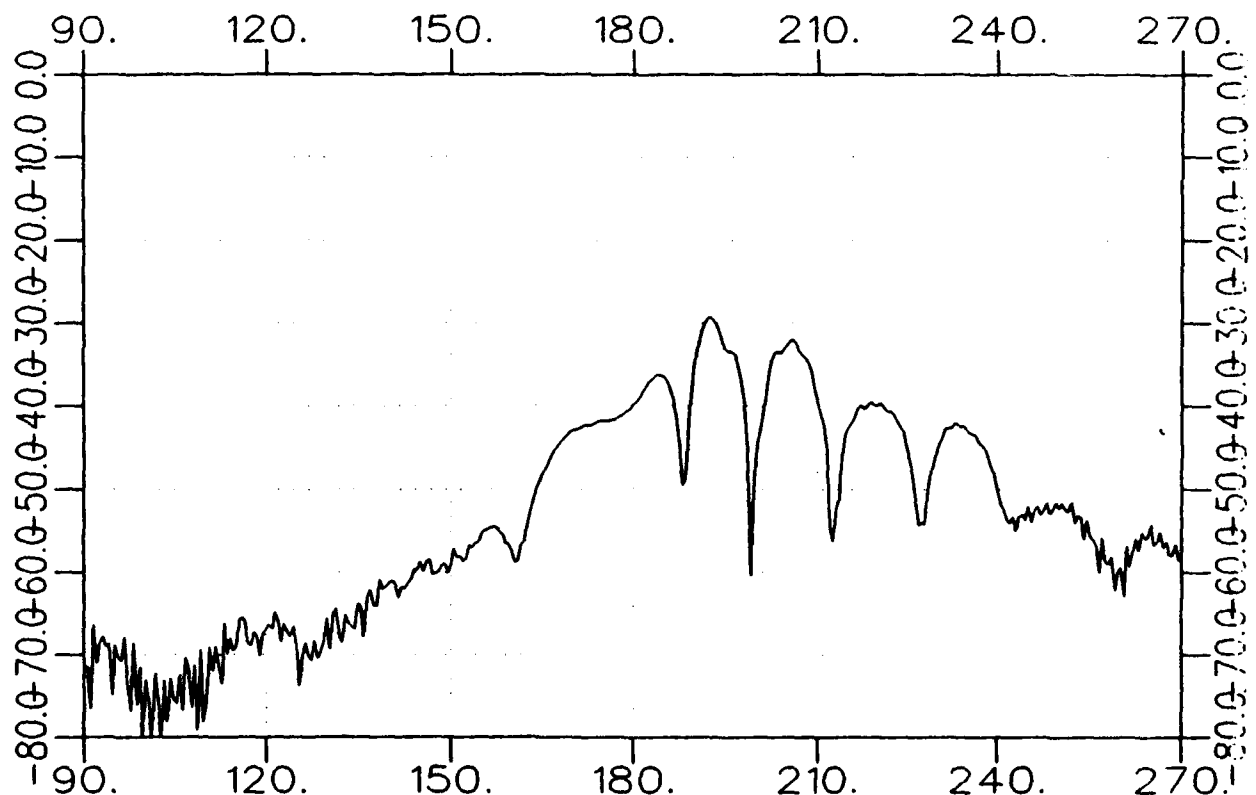
AZIM. 07/23/93 09:27  
CAP. SLOT GRID AVE= 1  
REF=OFF

361 90.00 0.50 18.0000 ATN= 0

PHASE IN DEGREES



MAGNITUDE IN DB



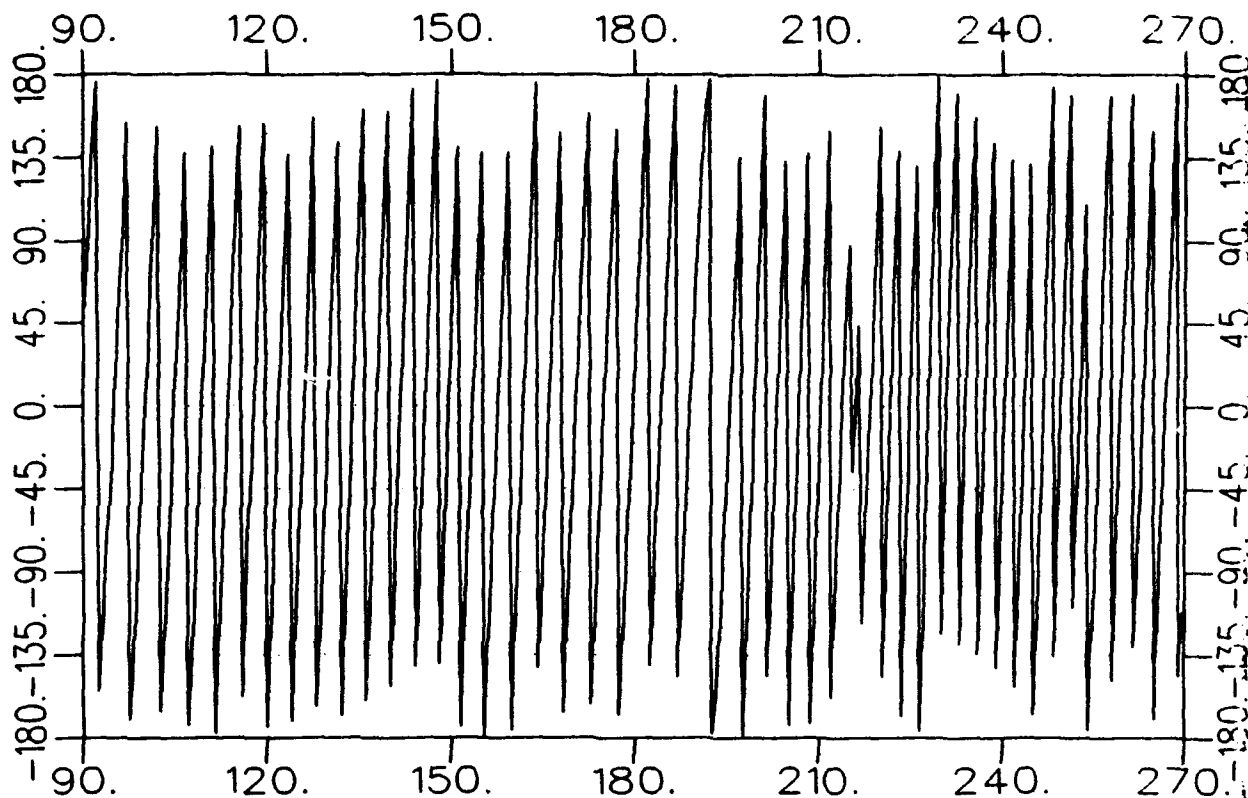
ANGLE IN DEGREES

b3204dh1000-a.freq  
TARGET

AZIM. 07/23/93 09:43  
CAP. SLOT GRID AVE= 1  
REF=OFF

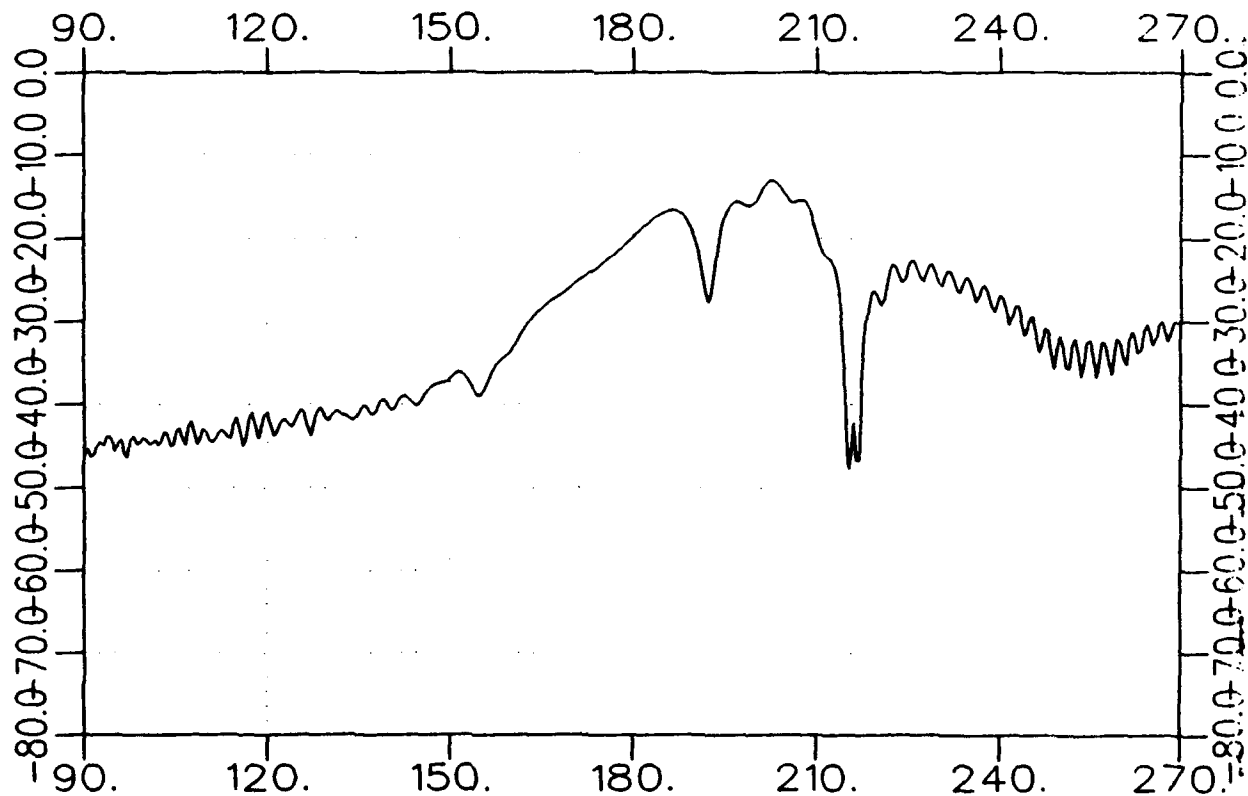
361 90.00 0.50 10.0000 ATN= 0

PHASE IN DEGREES



ANGLE IN DEGREES

MAGNITUDE IN DB



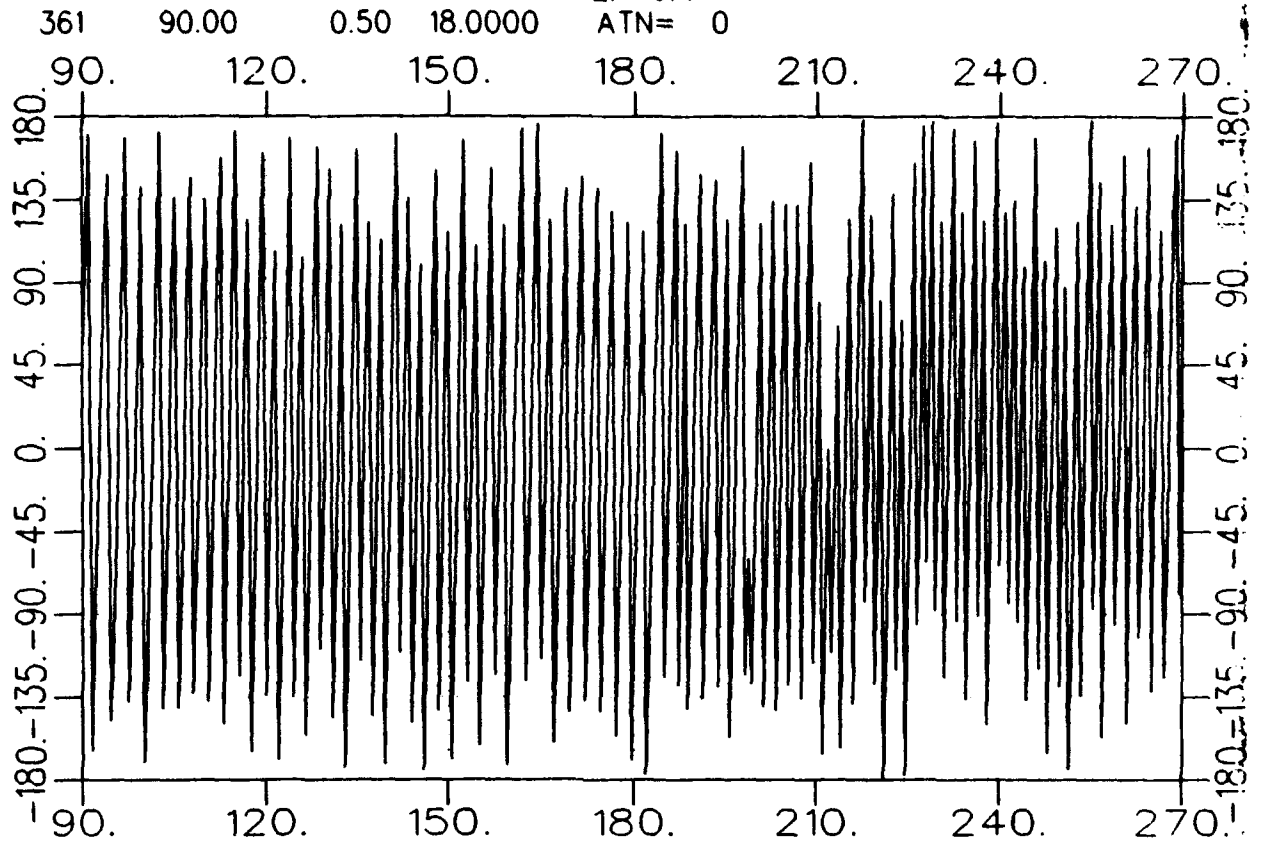
ANGLE IN DEGREES



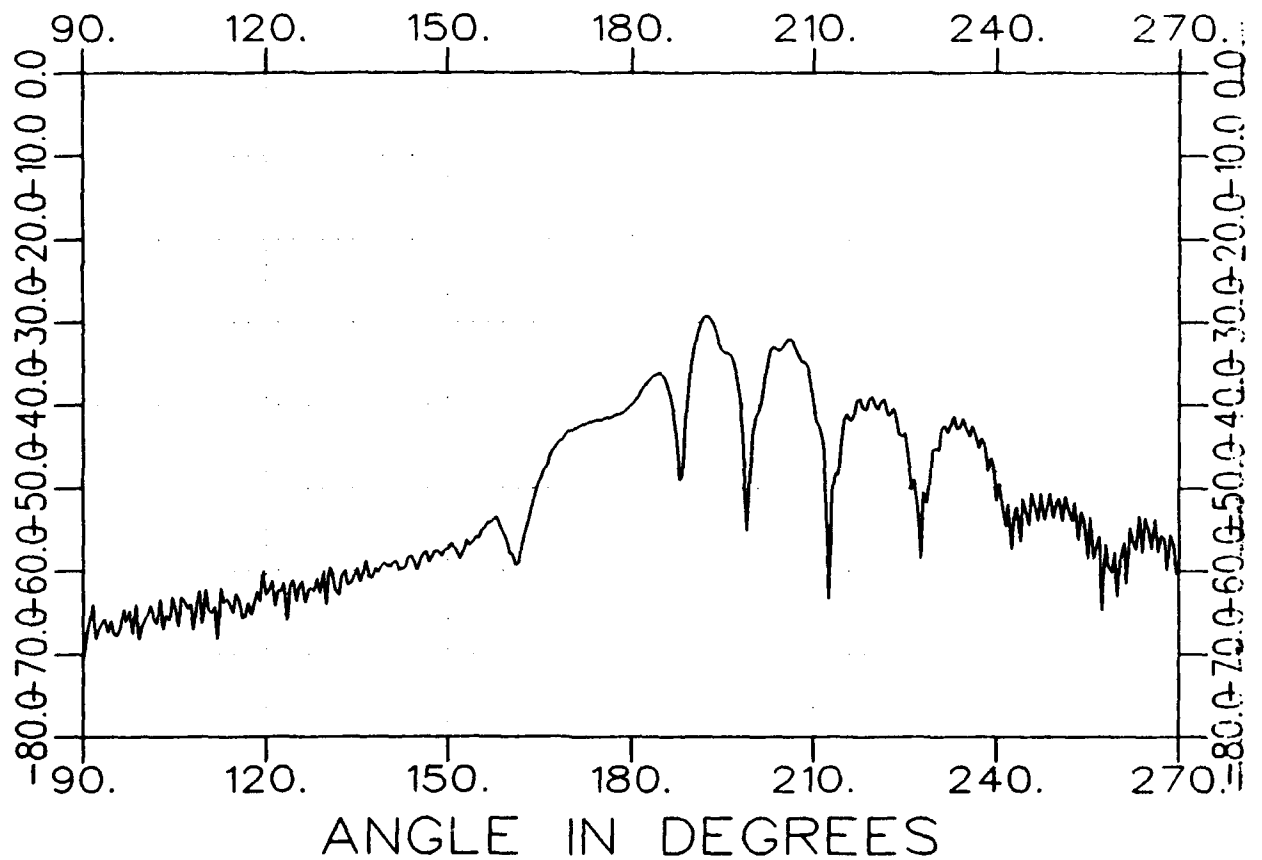
b3204ah1800-a.frq  
TARGET

AZIM. 07/23/93 09:43  
CAP. SLOT GRID AVE= 1  
REF=OFF  
ATN= 0

PHASE IN DEGREES



MAGNITUDE IN DB

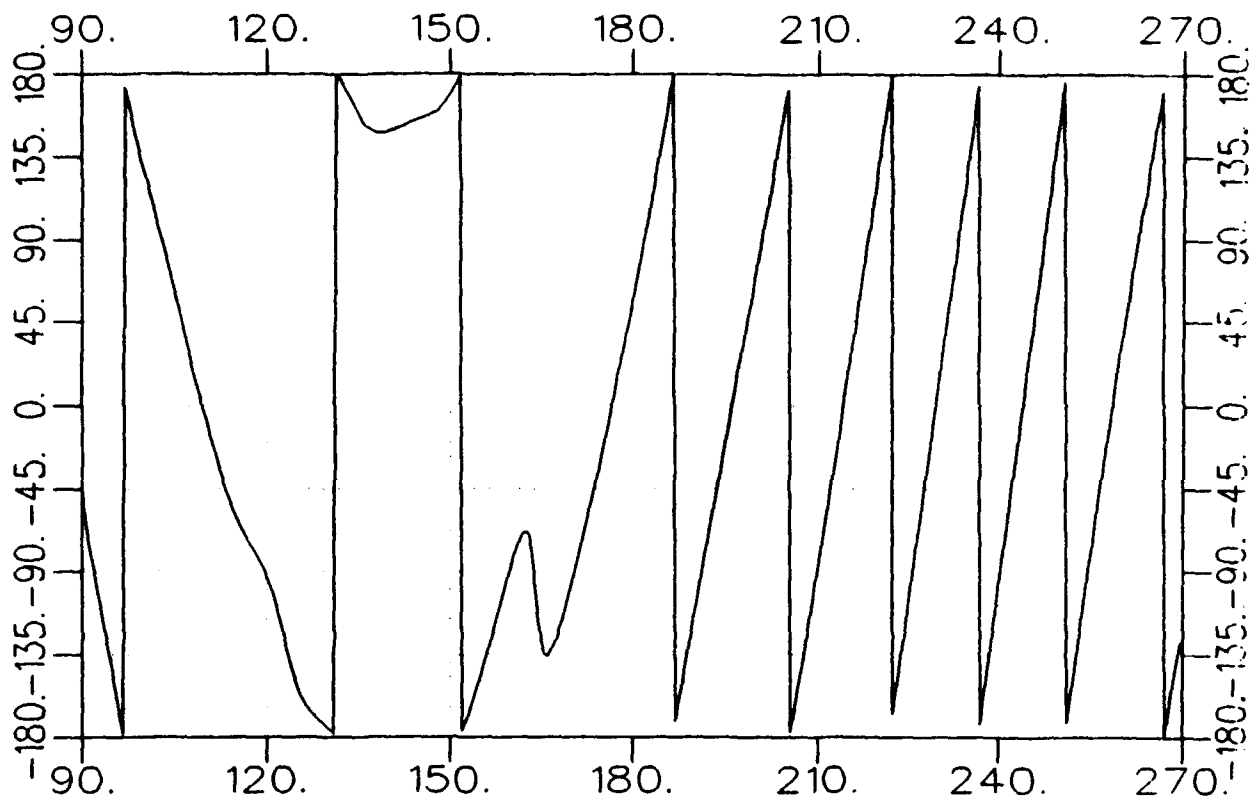


c3204av0200-a.frq  
TARGET

AZIM. 07/23/93 10:17  
CAP. SLOT GRID AVE= 1  
REF=OFF

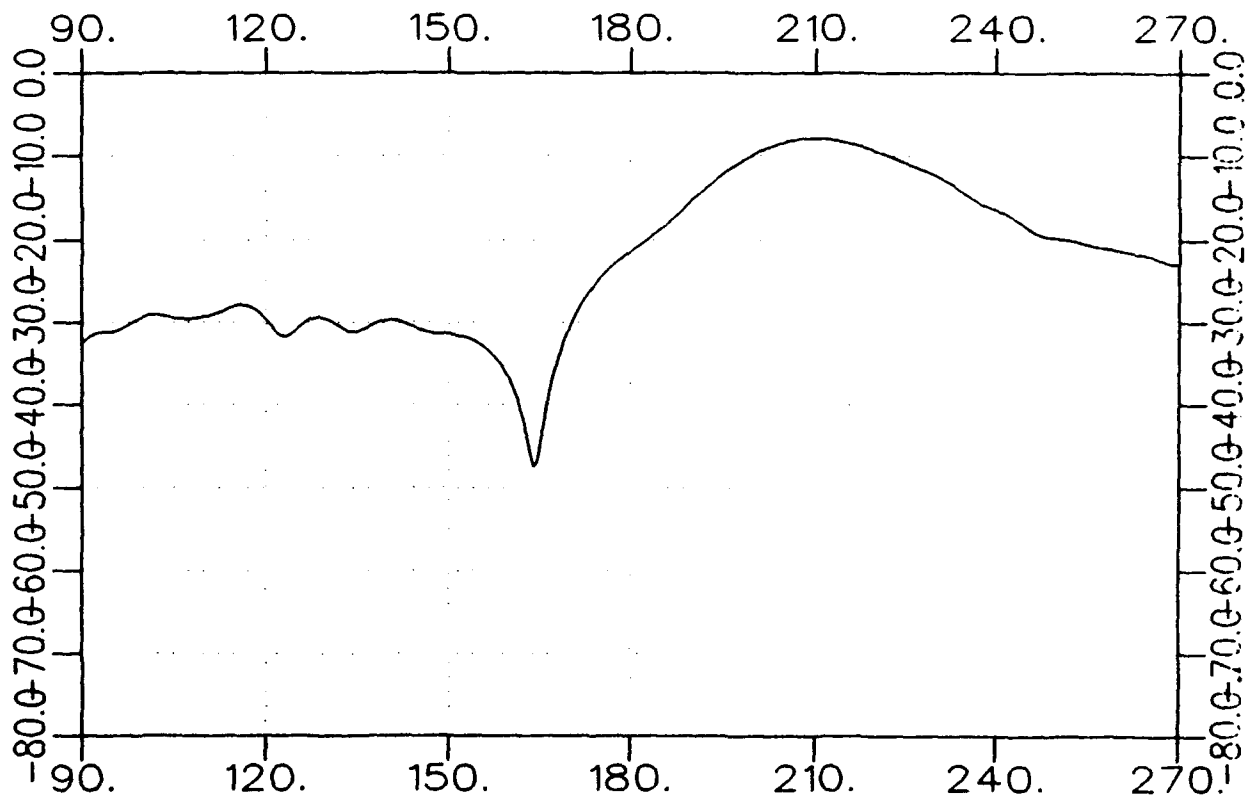
361 90.00 0.50 2.0000 ATN= 0

PHASE IN DEGREES



ANGLE IN DEGREES

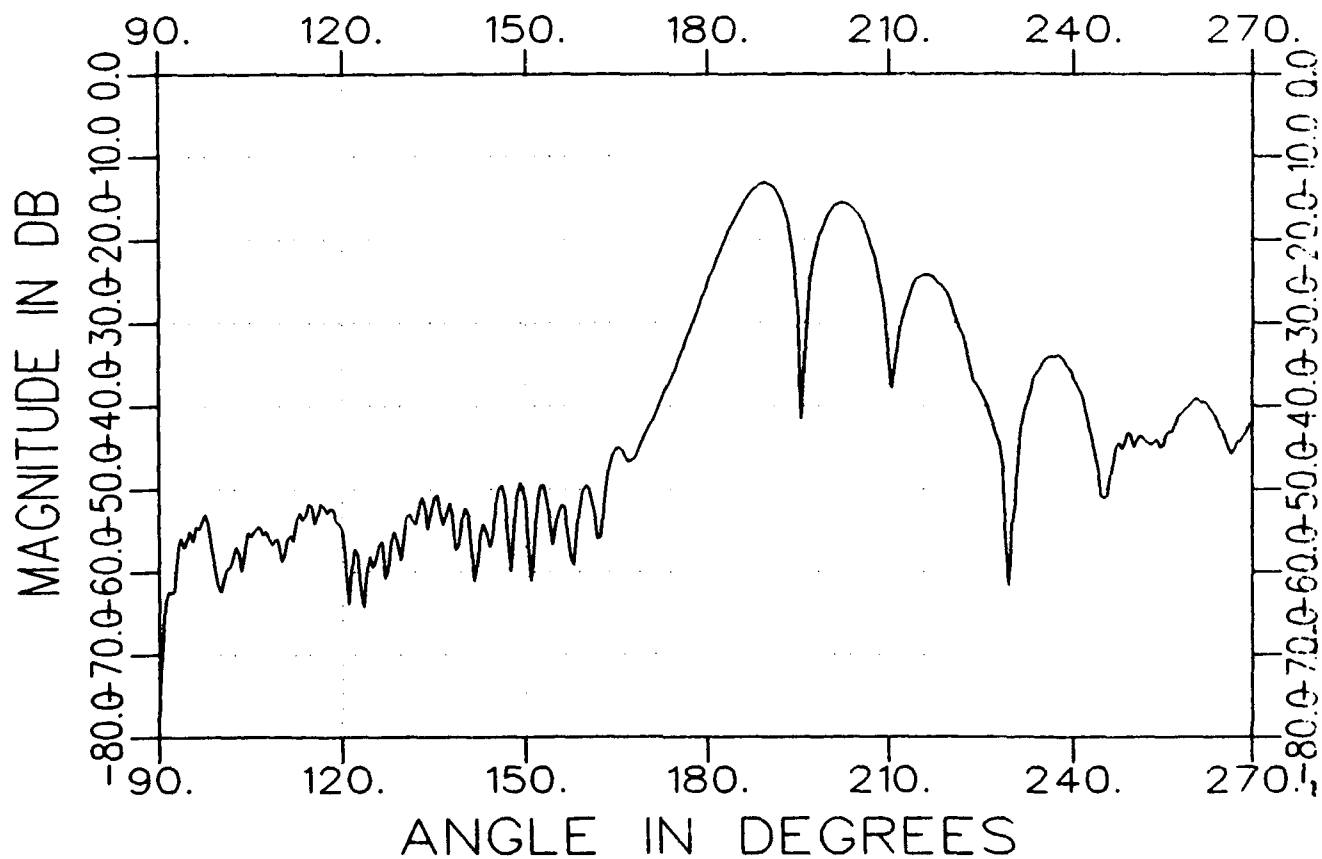
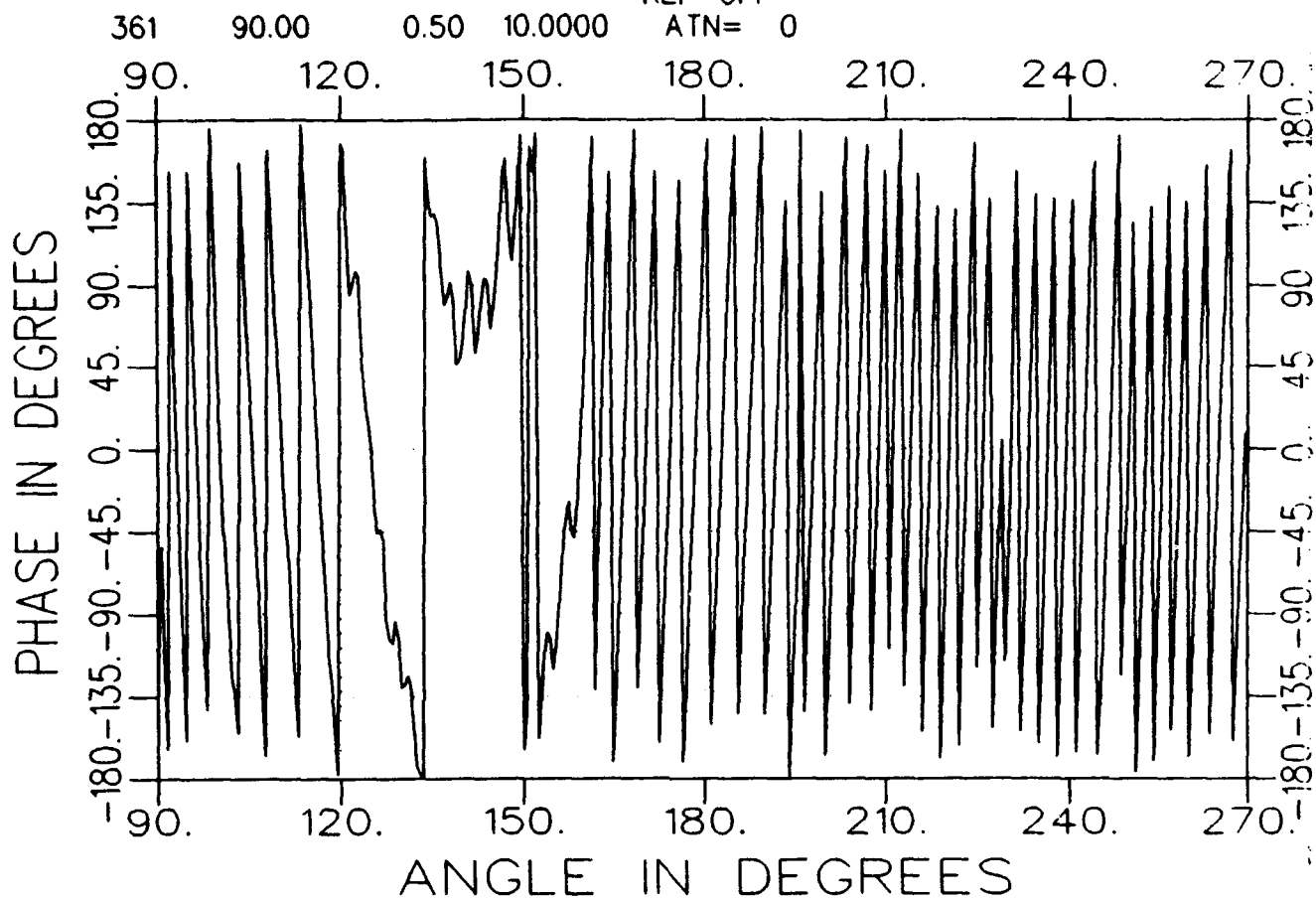
MAGNITUDE IN DB



ANGLE IN DEGREES

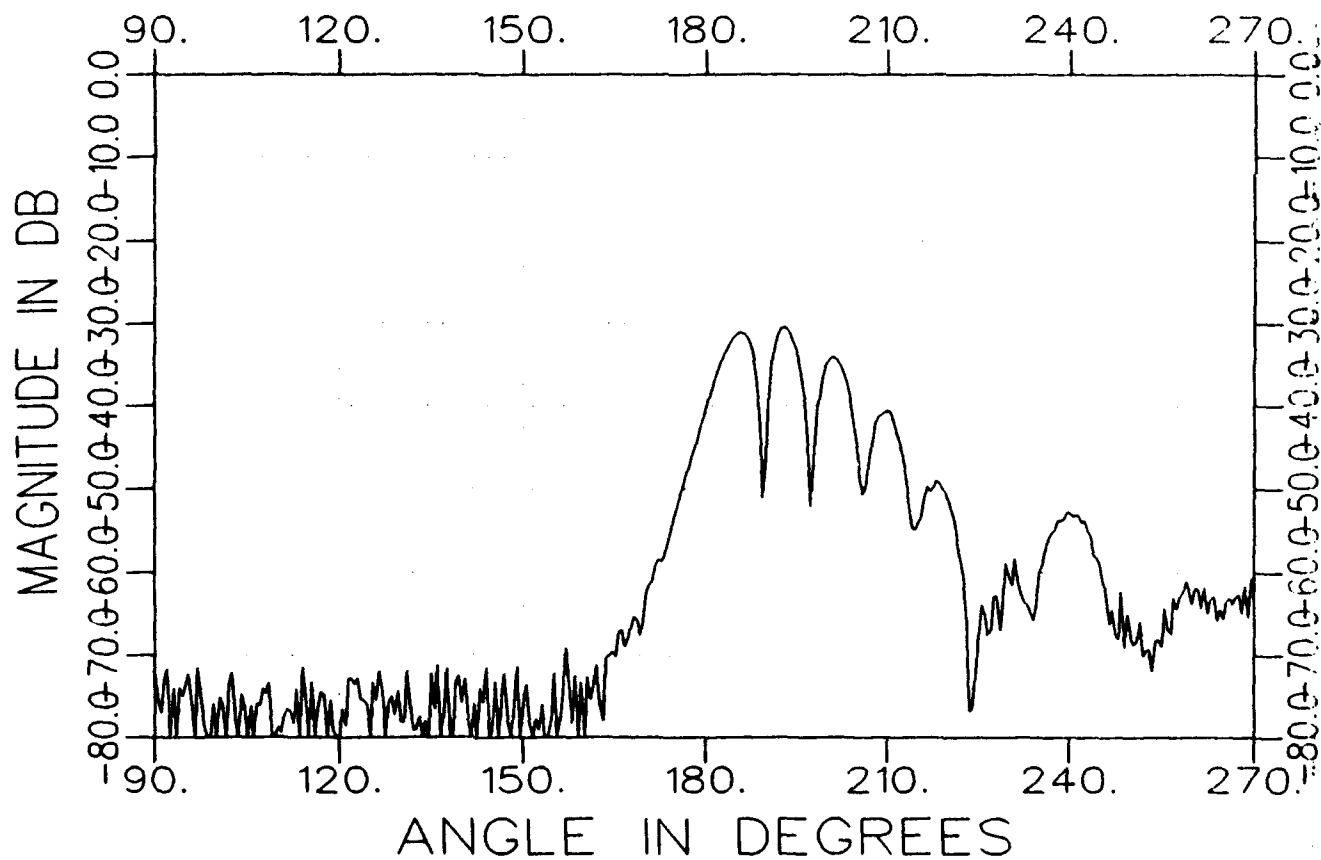
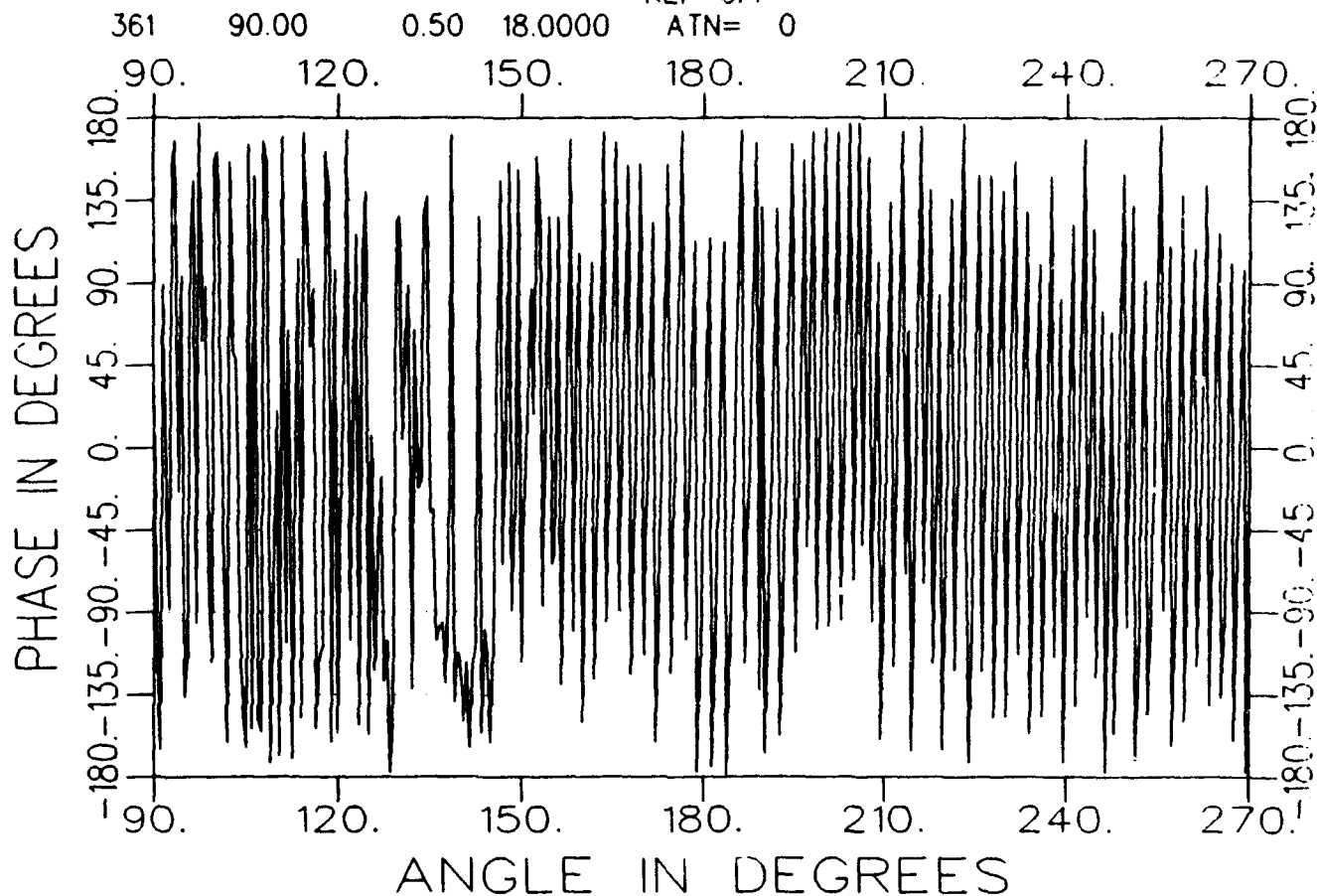
c3204av1000-a.frq  
TARGET

AZIM. 07/23/93 10:17  
CAP. SLOT GRID AVE= 1  
REF=OFF  
ATN= 0



c3204av1800-a.frq  
TARGET

AZIM. 07/23/93 10:17  
CAP. SLOT GRID AVE= 1  
REF=OFF  
ATN= 0

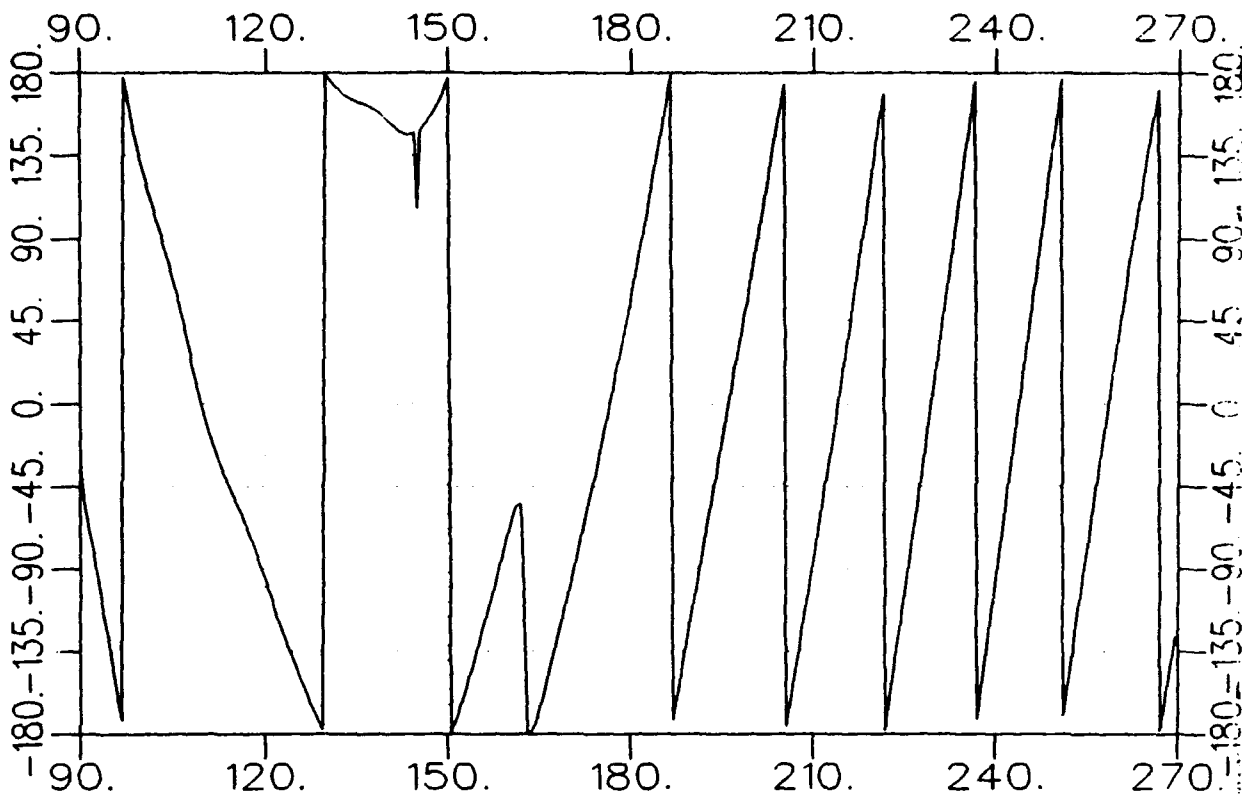


d3204av0200-a.frq  
TARGET

AZIM. 07/23/93 10:35  
CAP. SLOT GRID AVE= 1  
REF=OFF

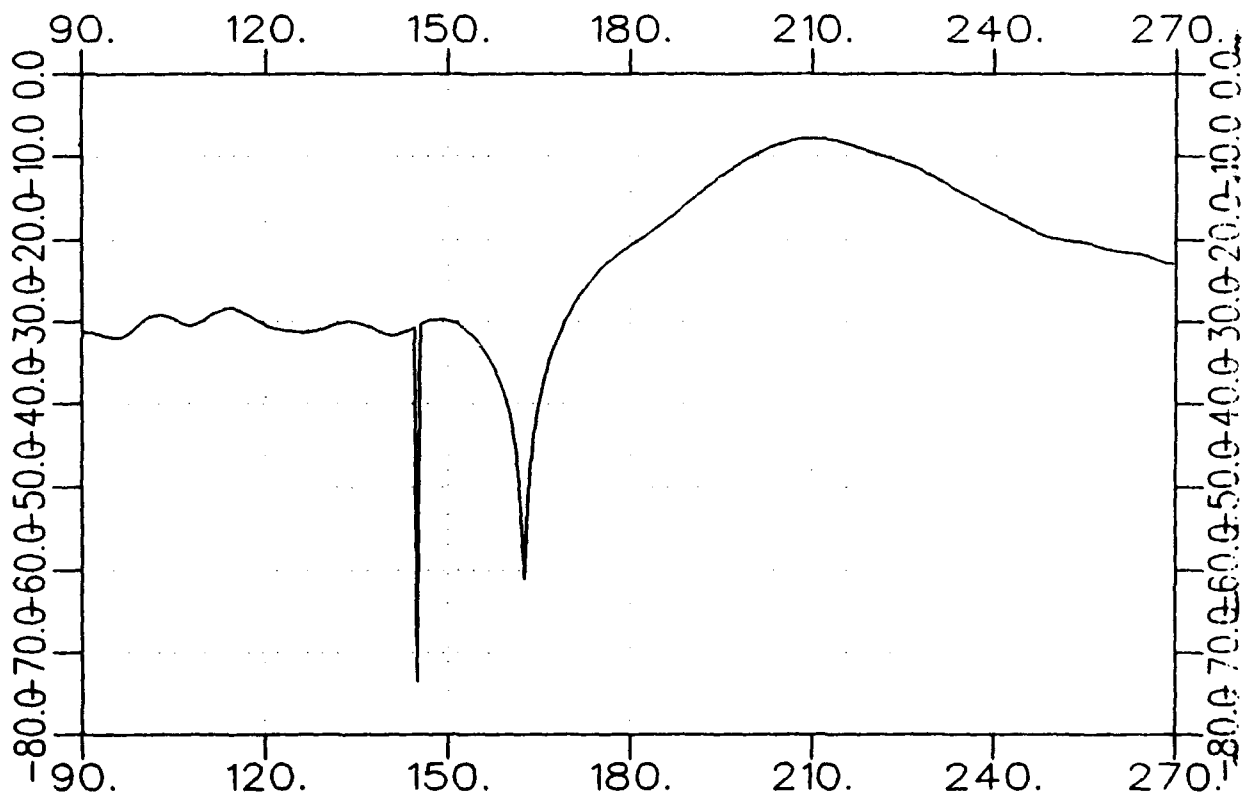
361 90.00 0.50 2.0000 ATN= 0

PHASE IN DEGREES



ANGLE IN DEGREES

MAGNITUDE IN DB

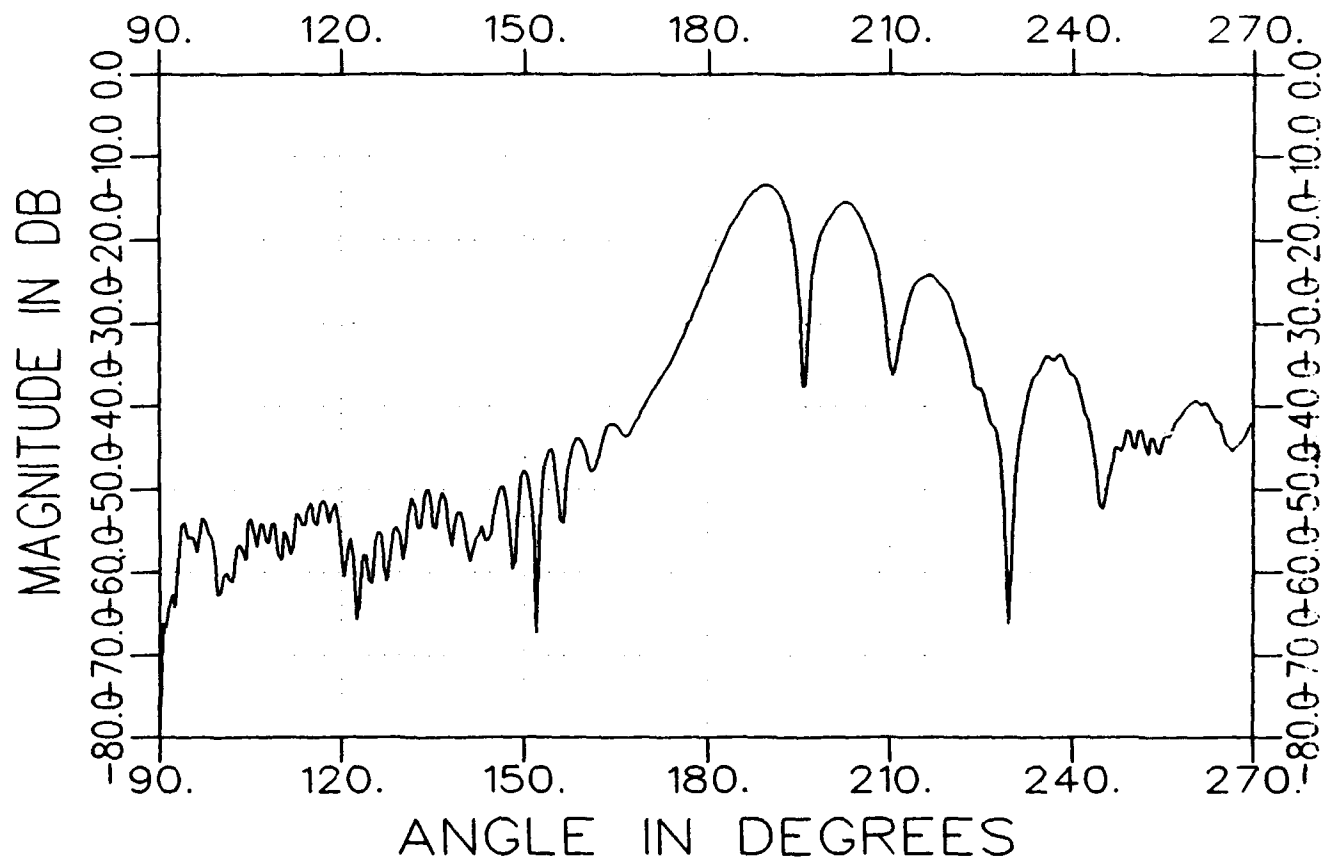
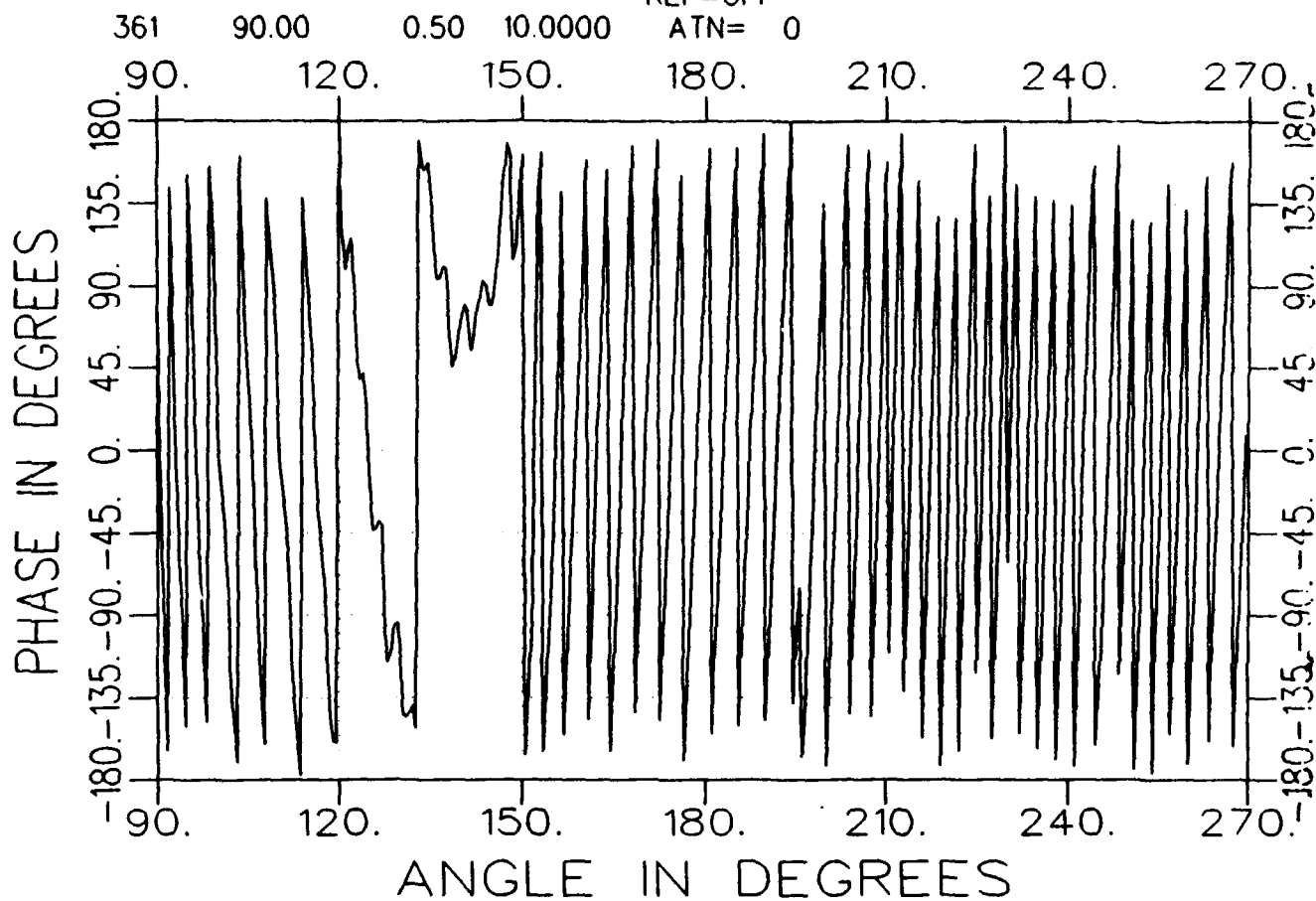


ANGLE IN DEGREES

33204av1000-a.frq  
TARGET

AZIM. 07/23/93 10:35  
CAP. SLOT GRID AVE= 1  
REF=OFF

1

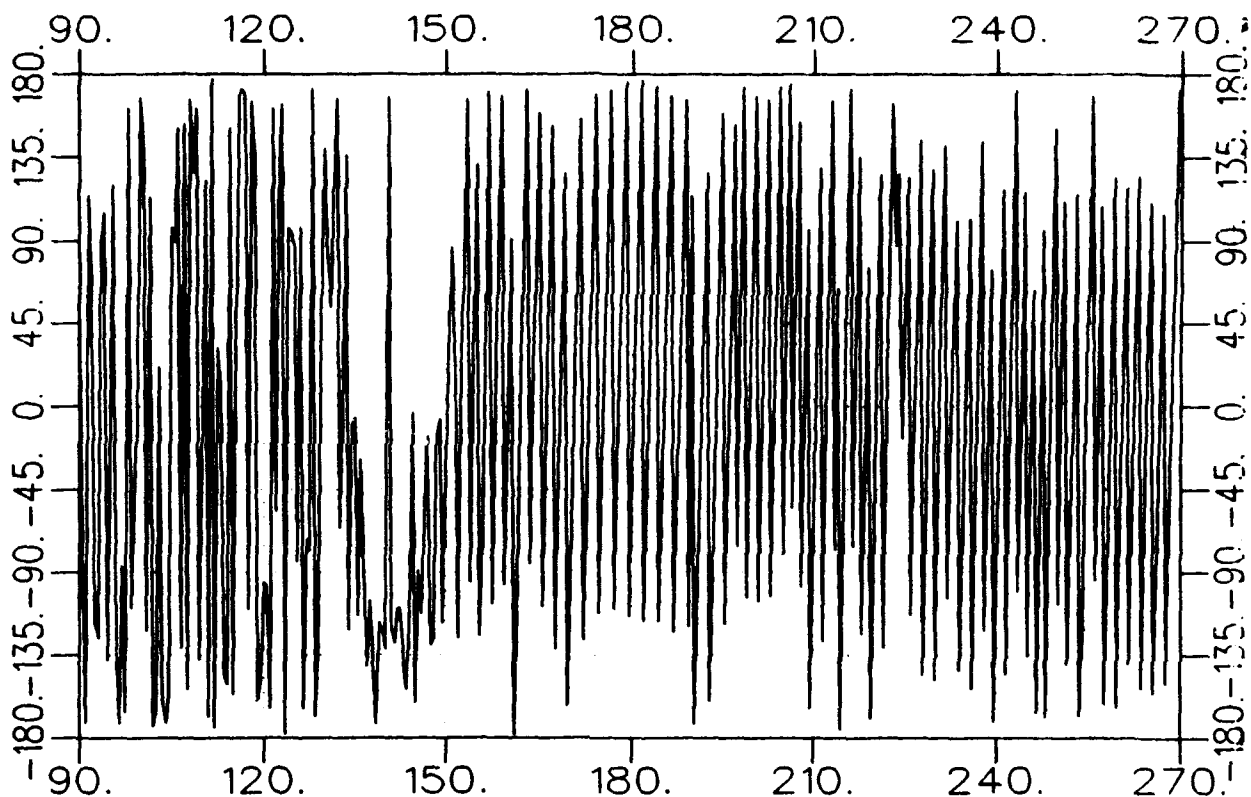


d3204av1800-a.frq  
TARGET

AZIM. 07/23/93 10:35  
CAP. SLOT GRID AVE= 1  
REF=OFF

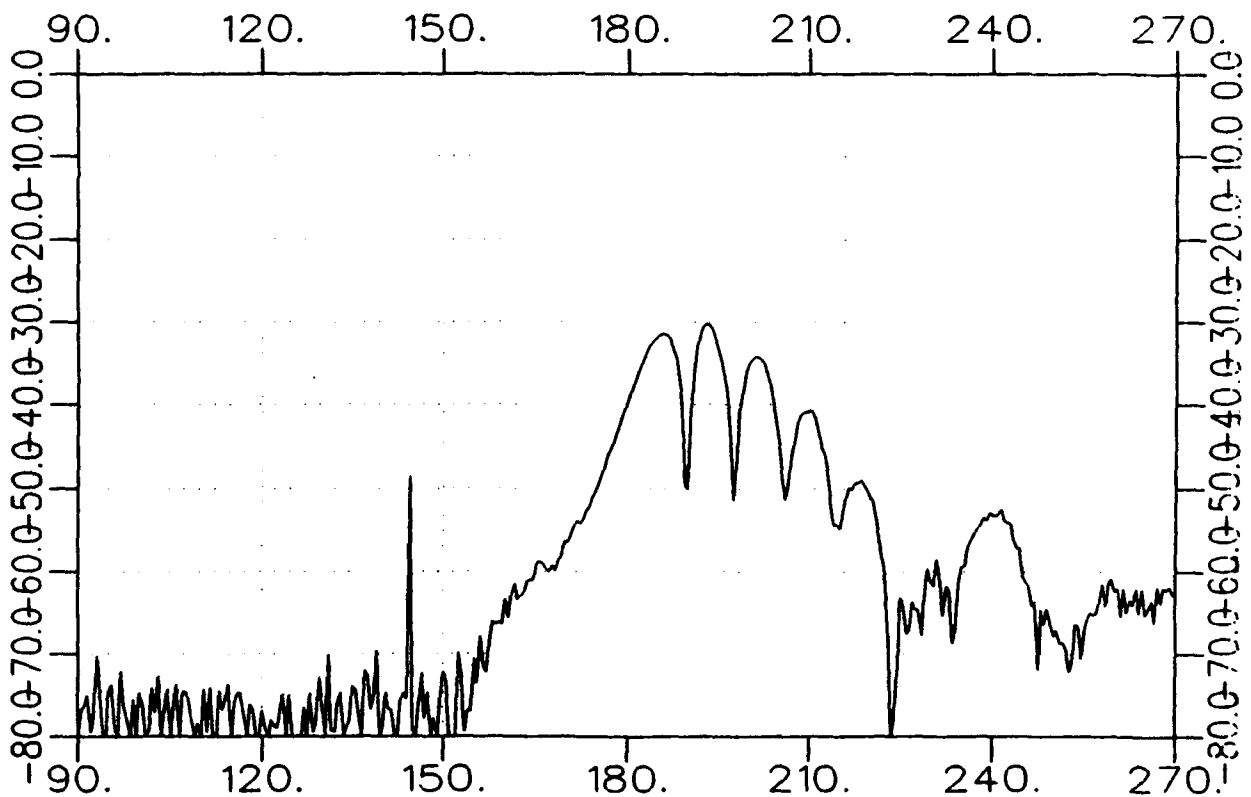
361 90.00 0.50 18.0000 ATN= 0

PHASE IN DEGREES



ANGLE IN DEGREES

MAGNITUDE IN DB



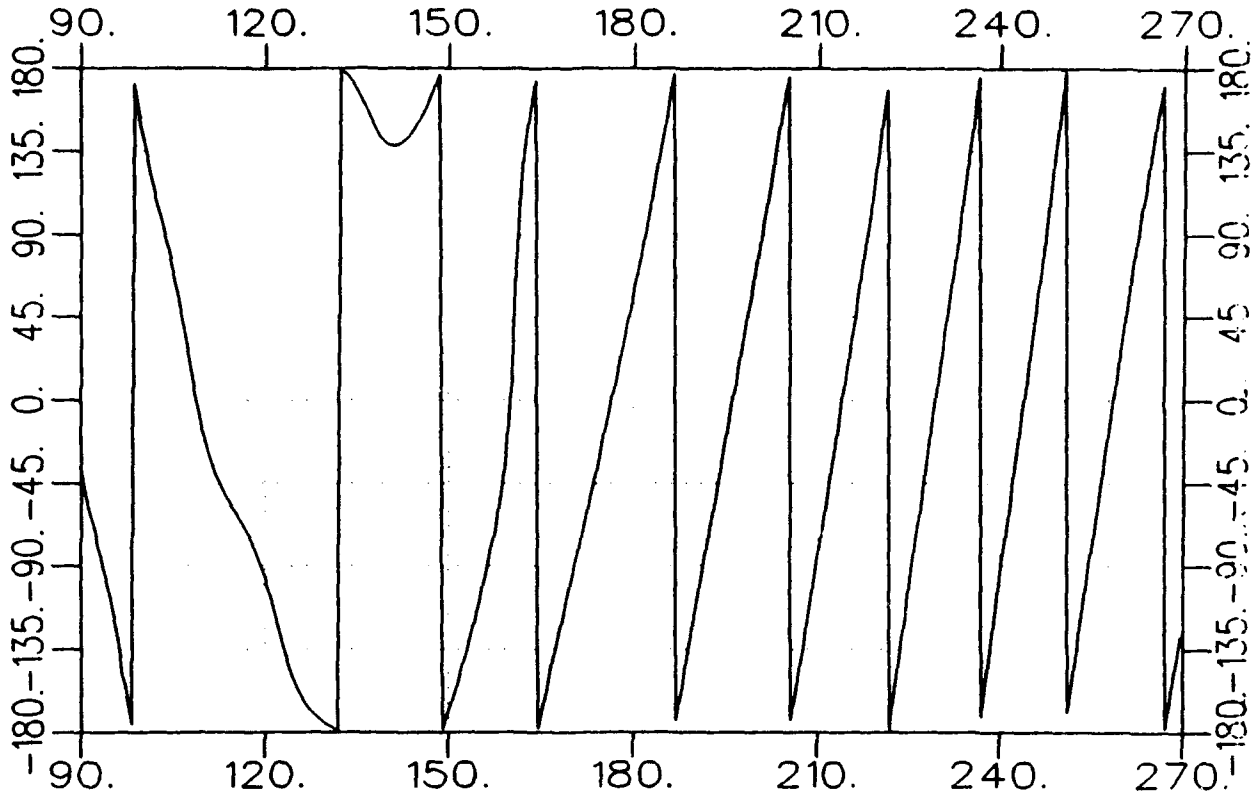
ANGLE IN DEGREES

e3204av0200-a.frq  
TARGET

AZIM. 07/23/93 10:49  
CAP. SLOT GRID AVE= 1  
REF=OFF

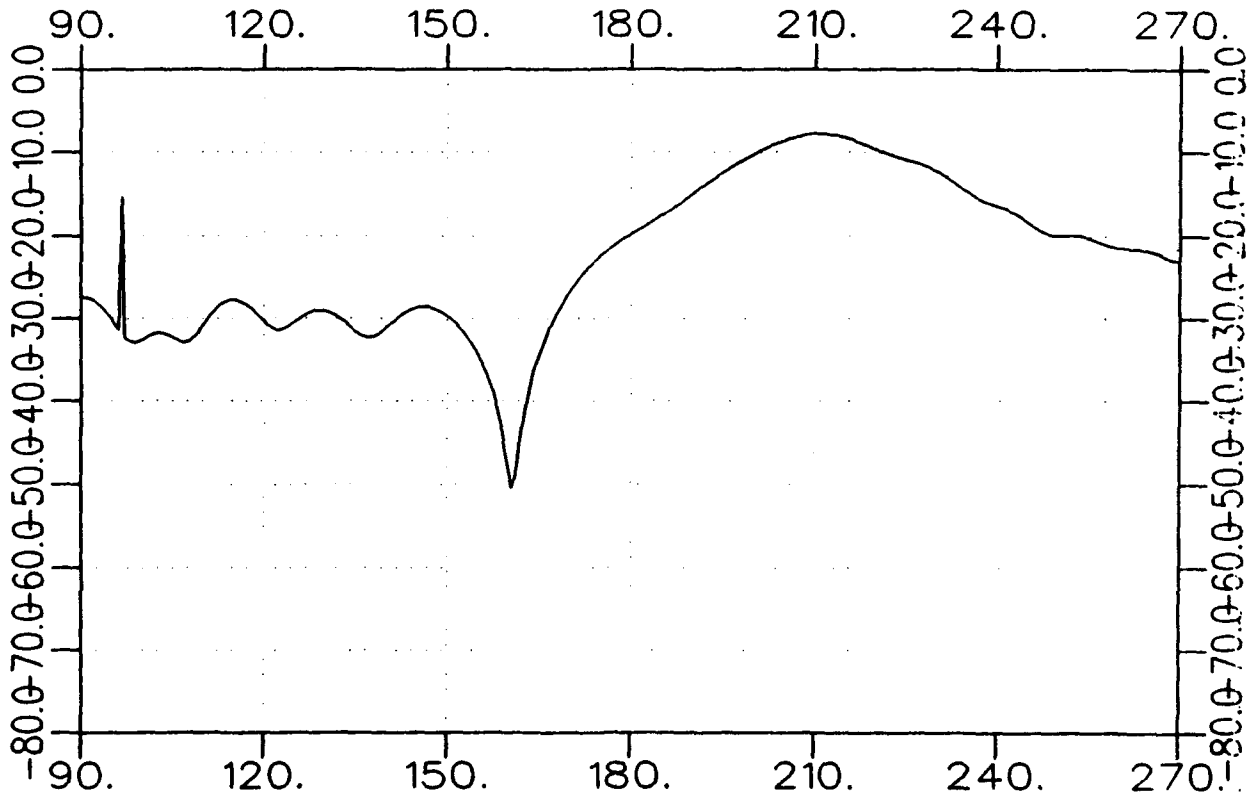
361 90.00 0.50 2.0000 ATN= 0

PHASE IN DEGREES



ANGLE IN DEGREES

MAGNITUDE IN DB

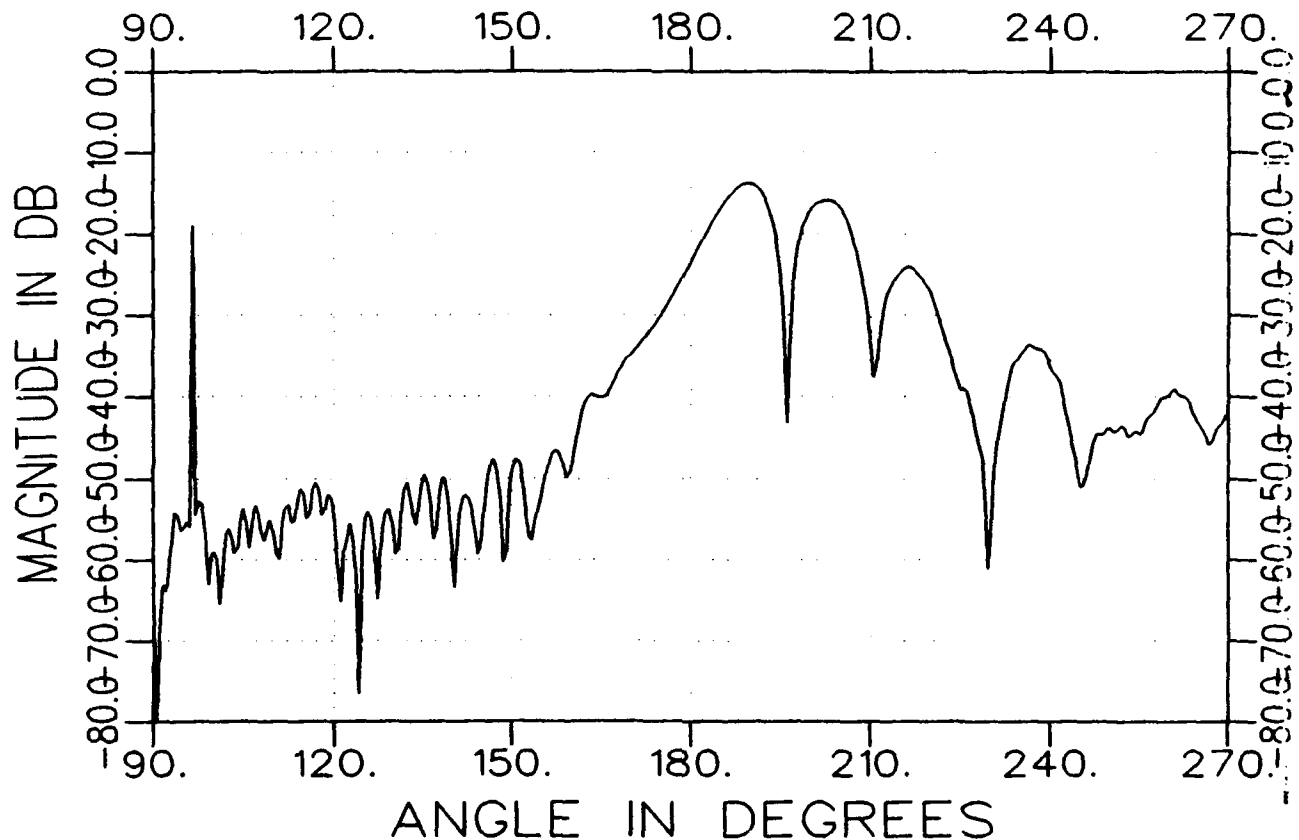
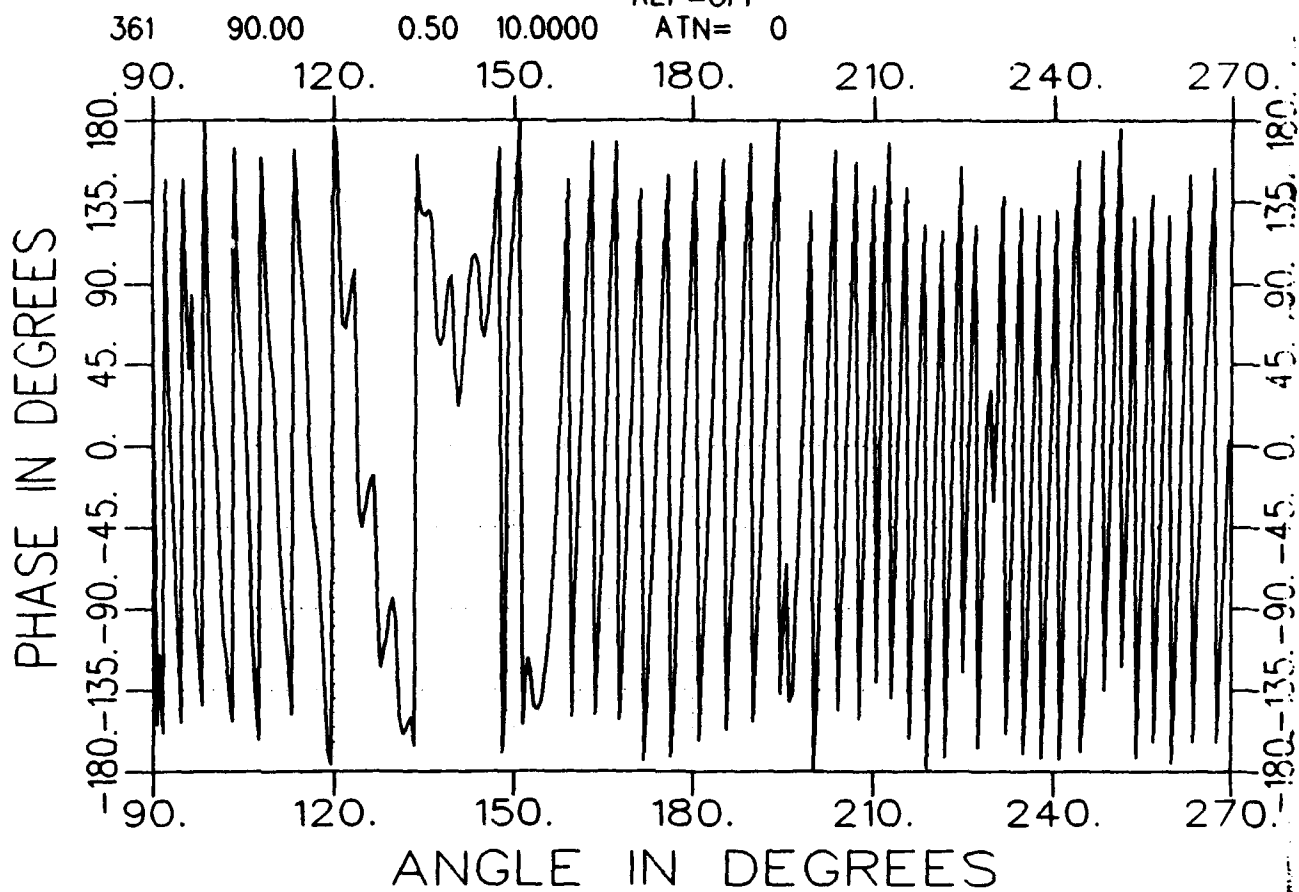


ANGLE IN DEGREES



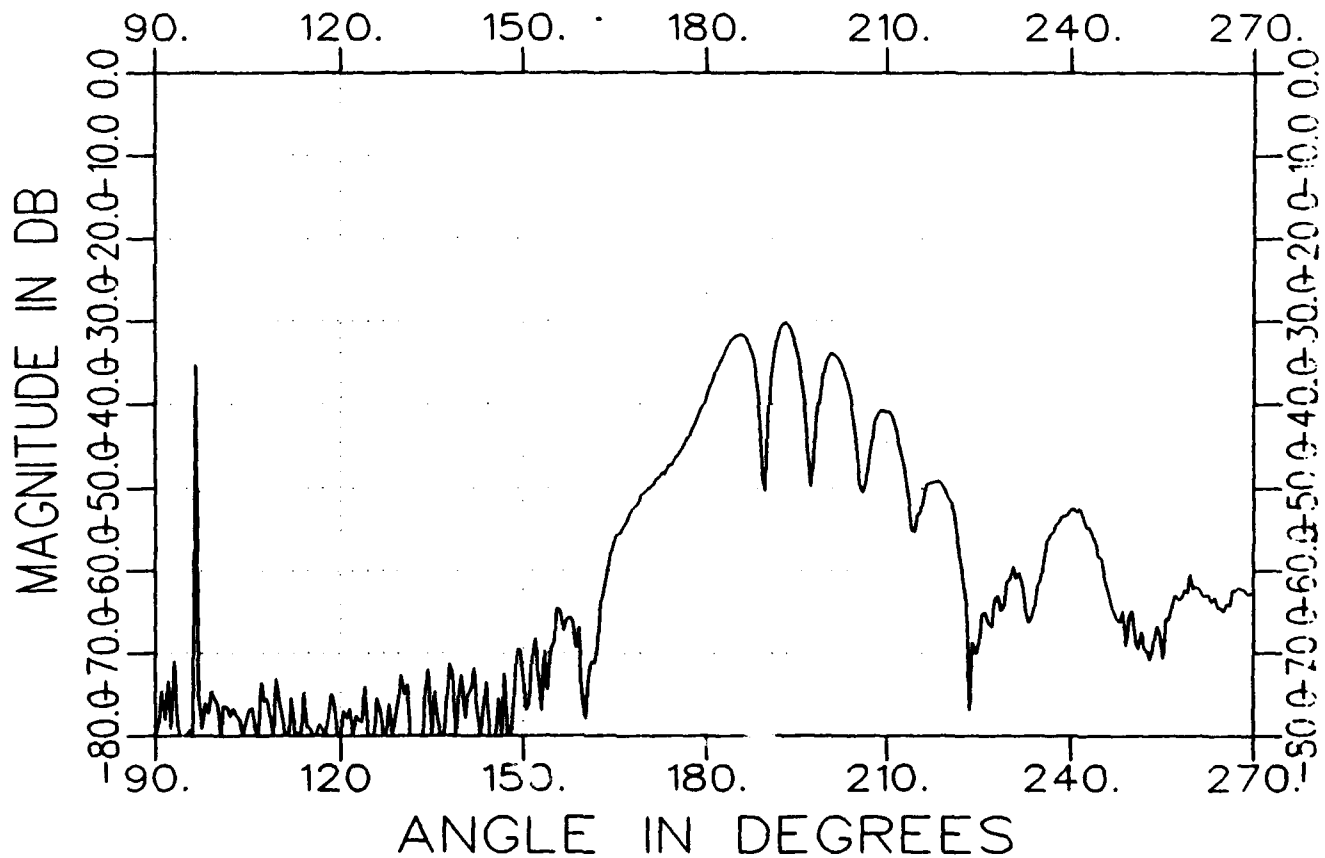
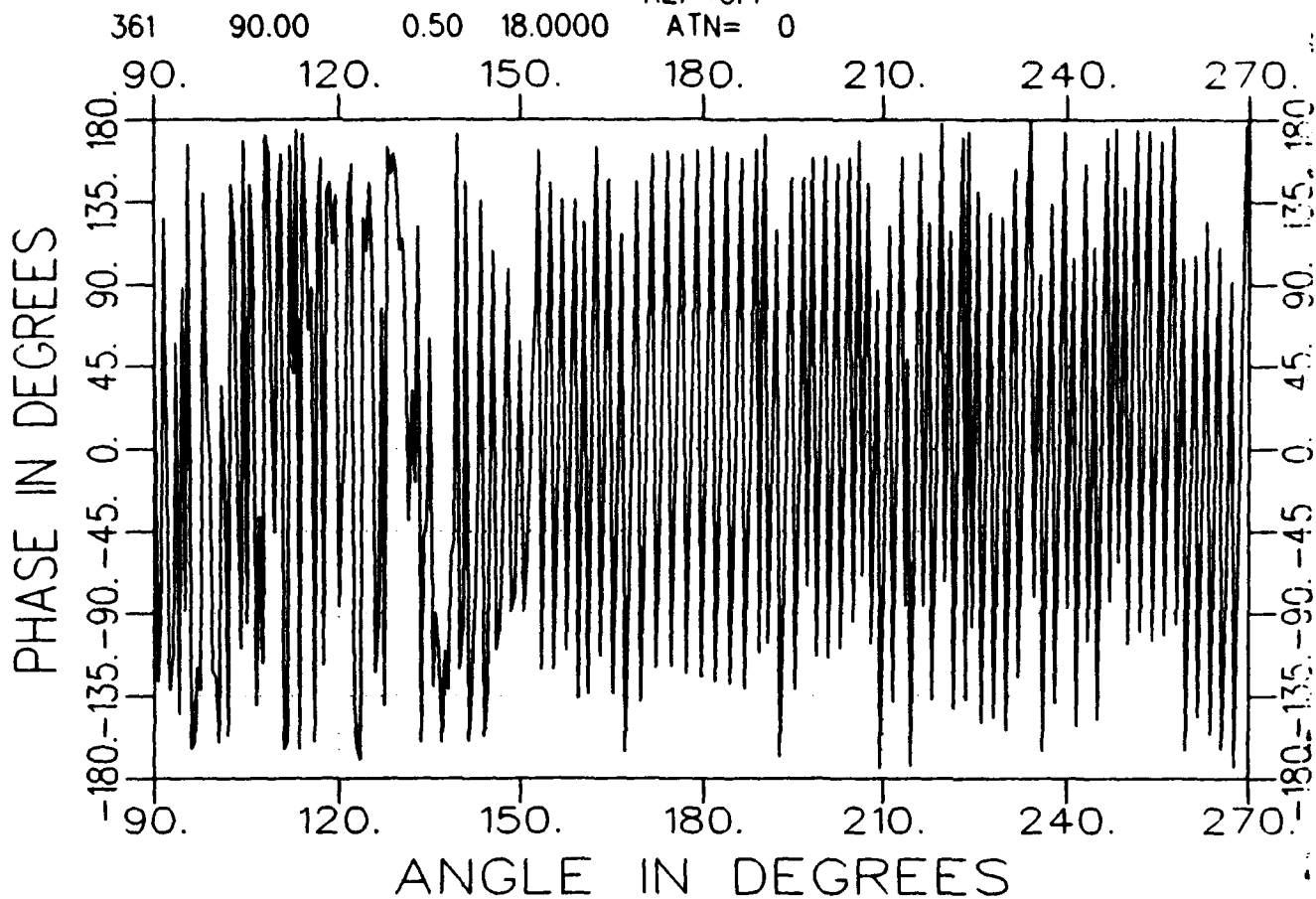
e3204av1000-a.frq  
TARGET

AZIM. 07/23/93 10:49  
CAP. SLOT GRID AVE= 1  
REF=OFF



e3204av1800-a.frq  
TARGET

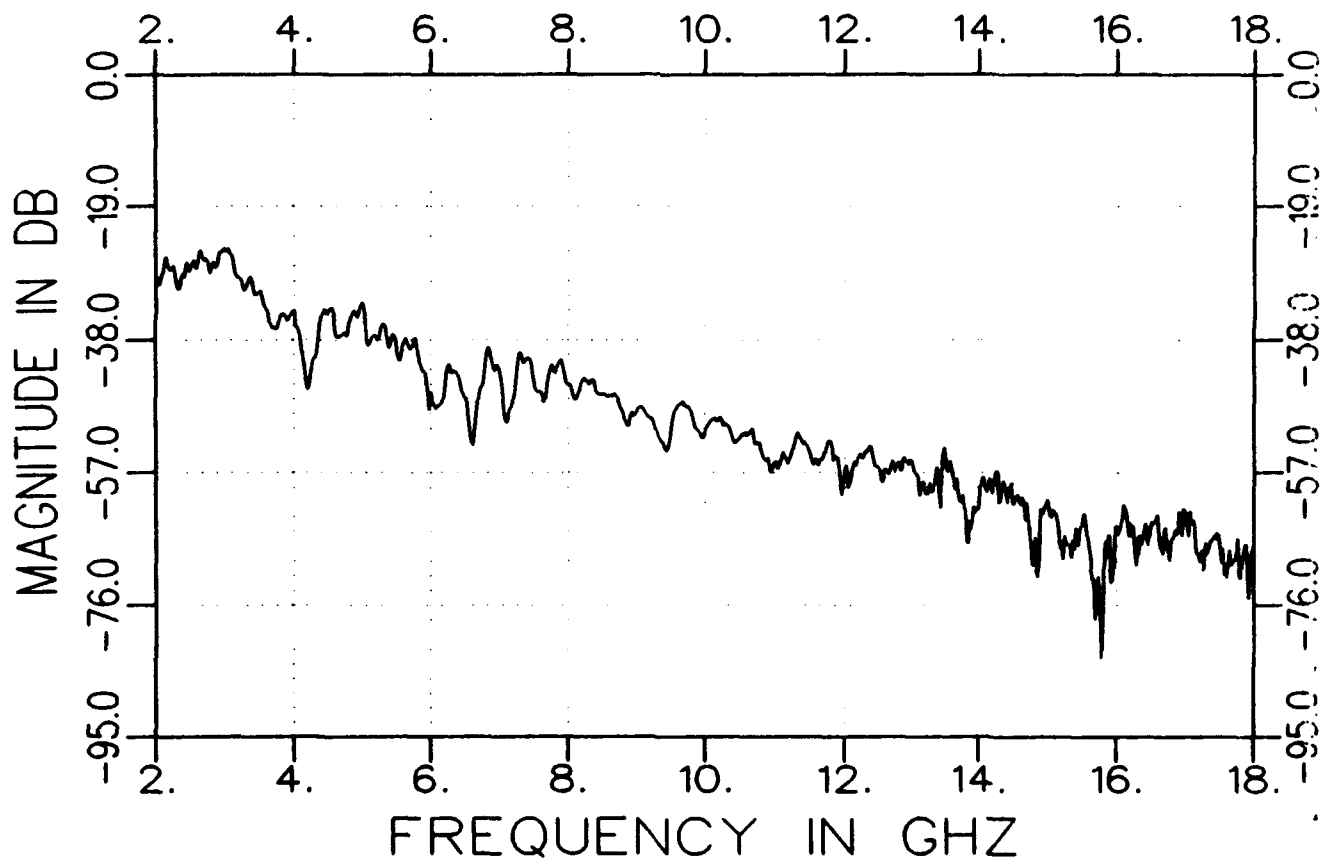
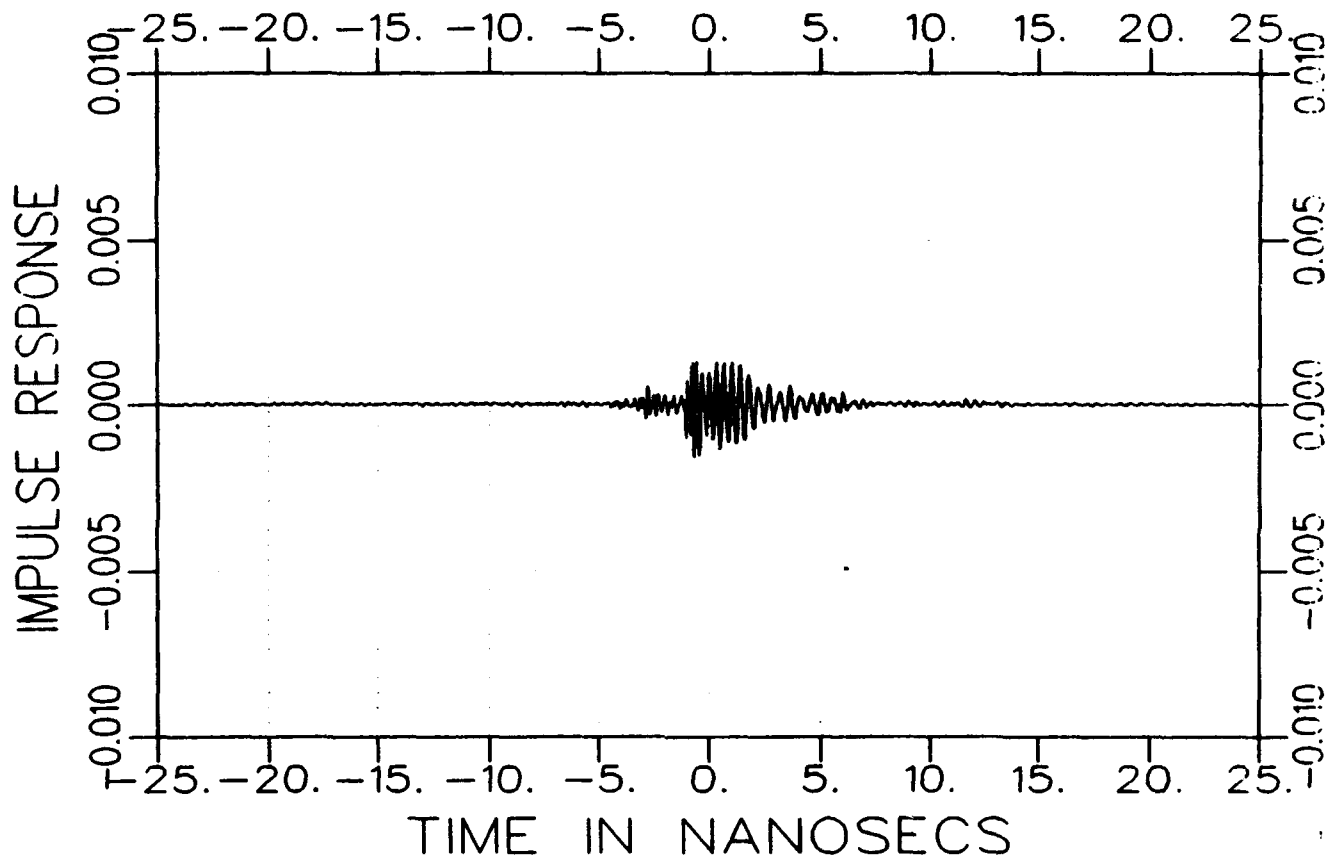
AZIM. 07/23/93 10:49  
CAP. SLOT GRID AVE= 1  
REF=OFF  
ATN= 0



a3204fh0900-a  
TARGET

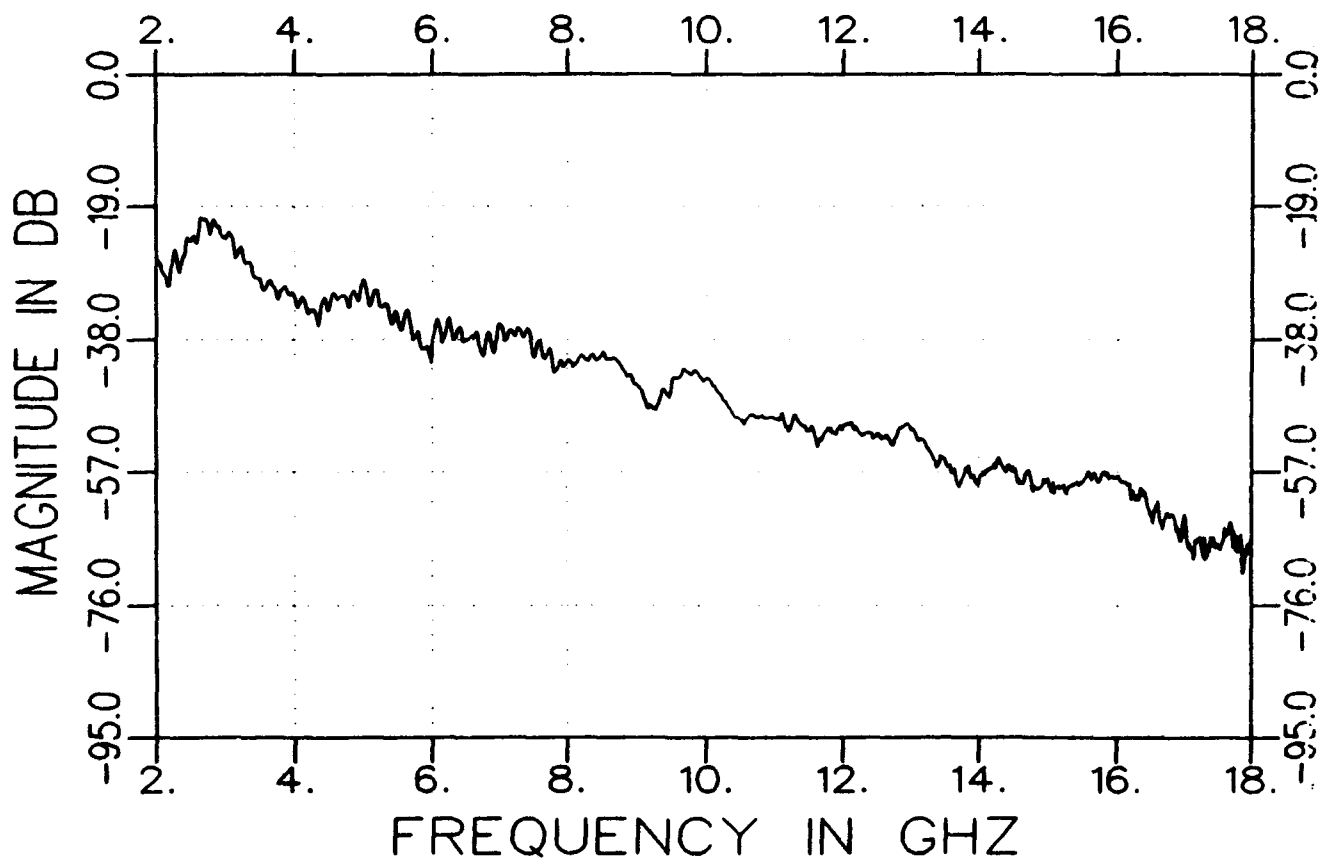
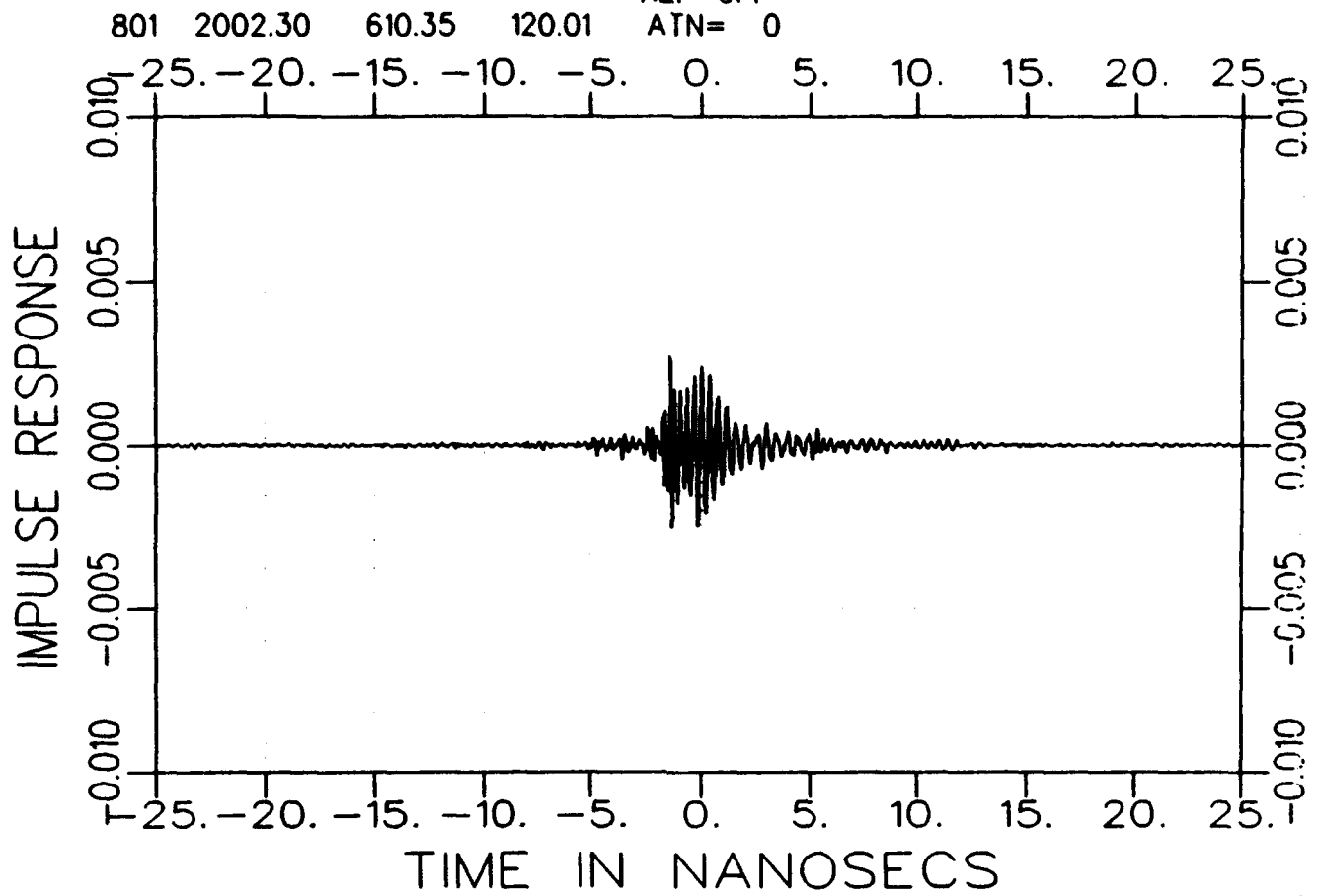
FR&AZ 07/23/93 09:27  
CAP. SLOT GRID AVE= 1  
REF=OFF

801 2002.30 610.35 90.00 ATN= 0



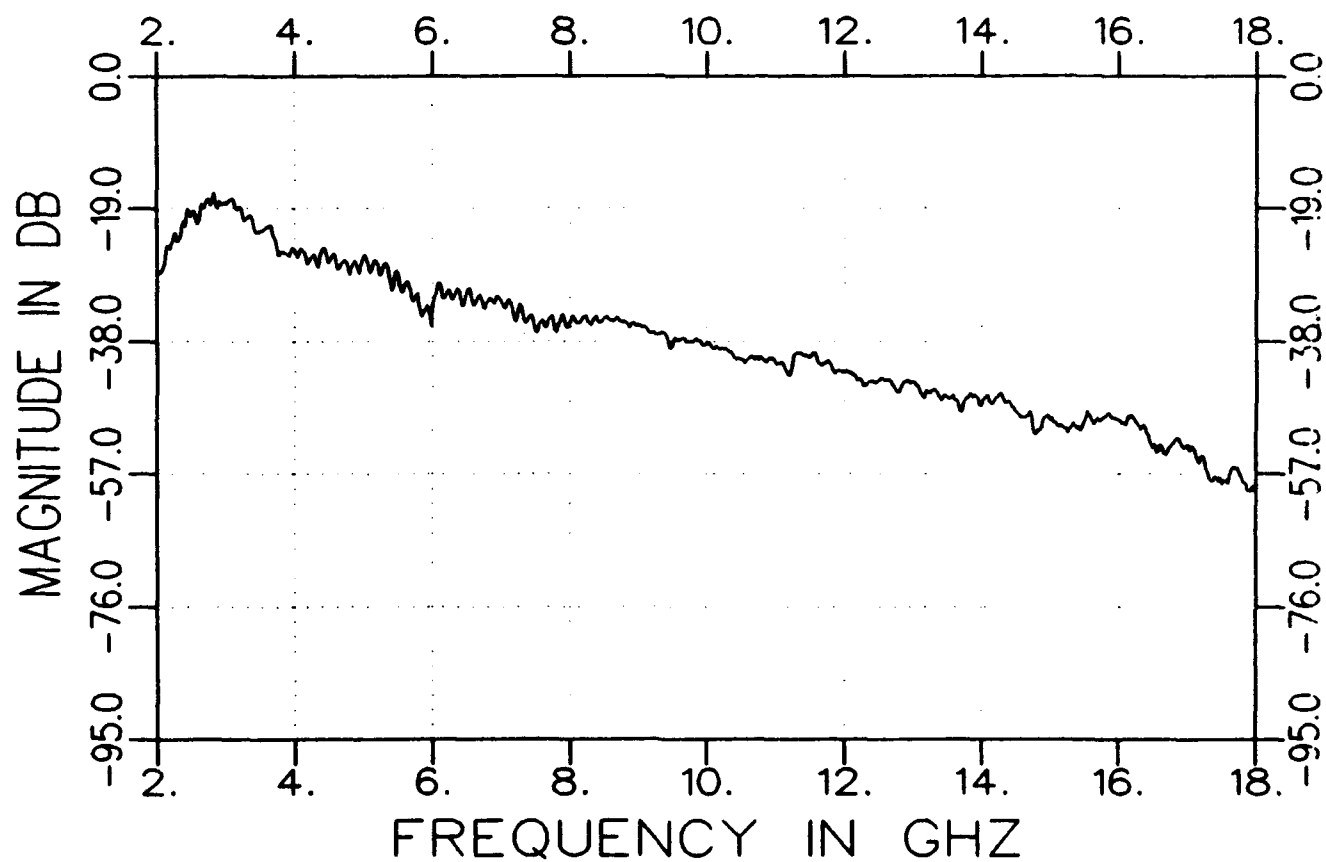
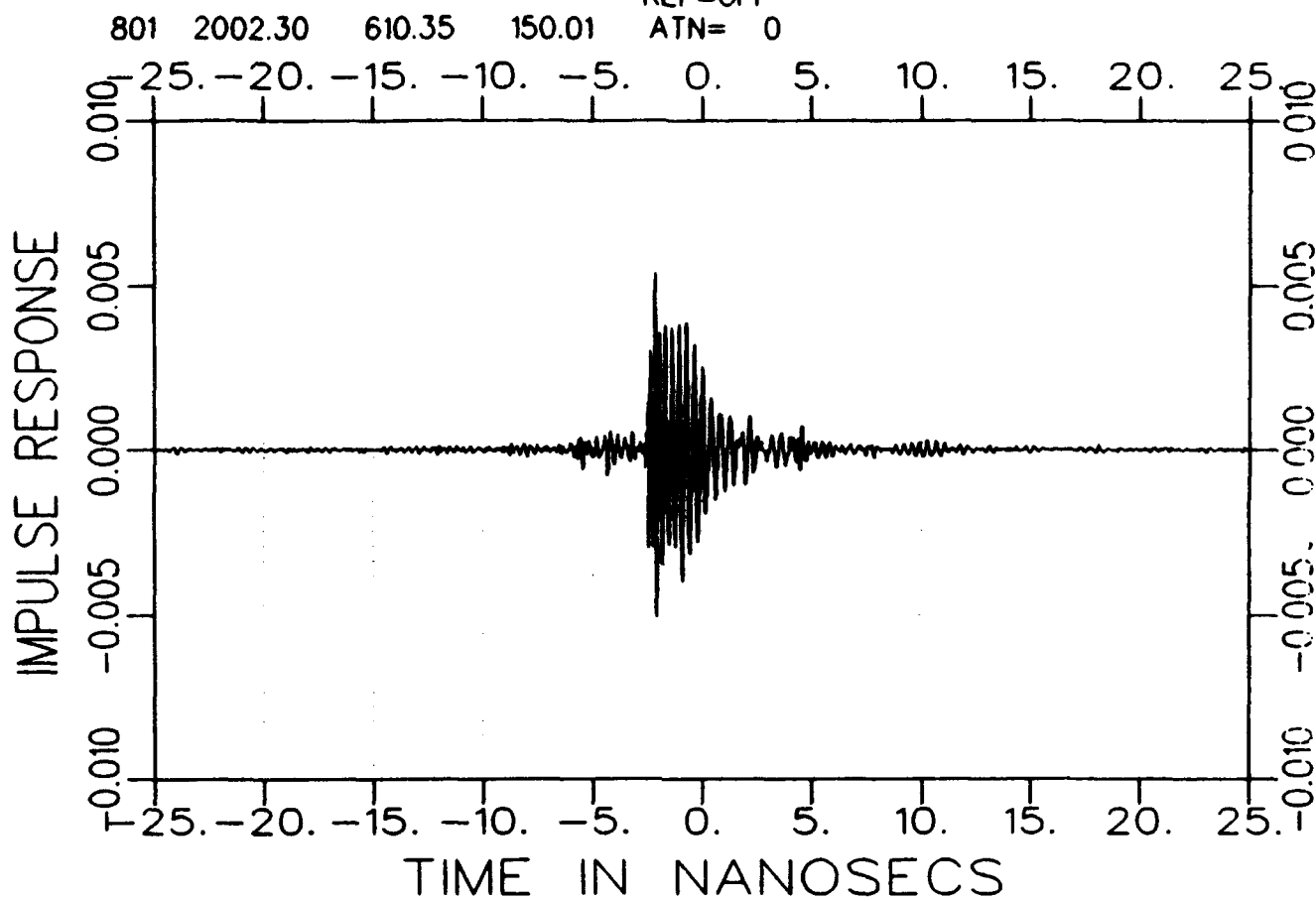
03204fh1200-a  
TARGET

FR&AZ 07/23/93 09:27  
CAP. SLOT GRID AVE= 1  
REF=OFF  
ATN= 0



a3204fh1500-a  
TARGET

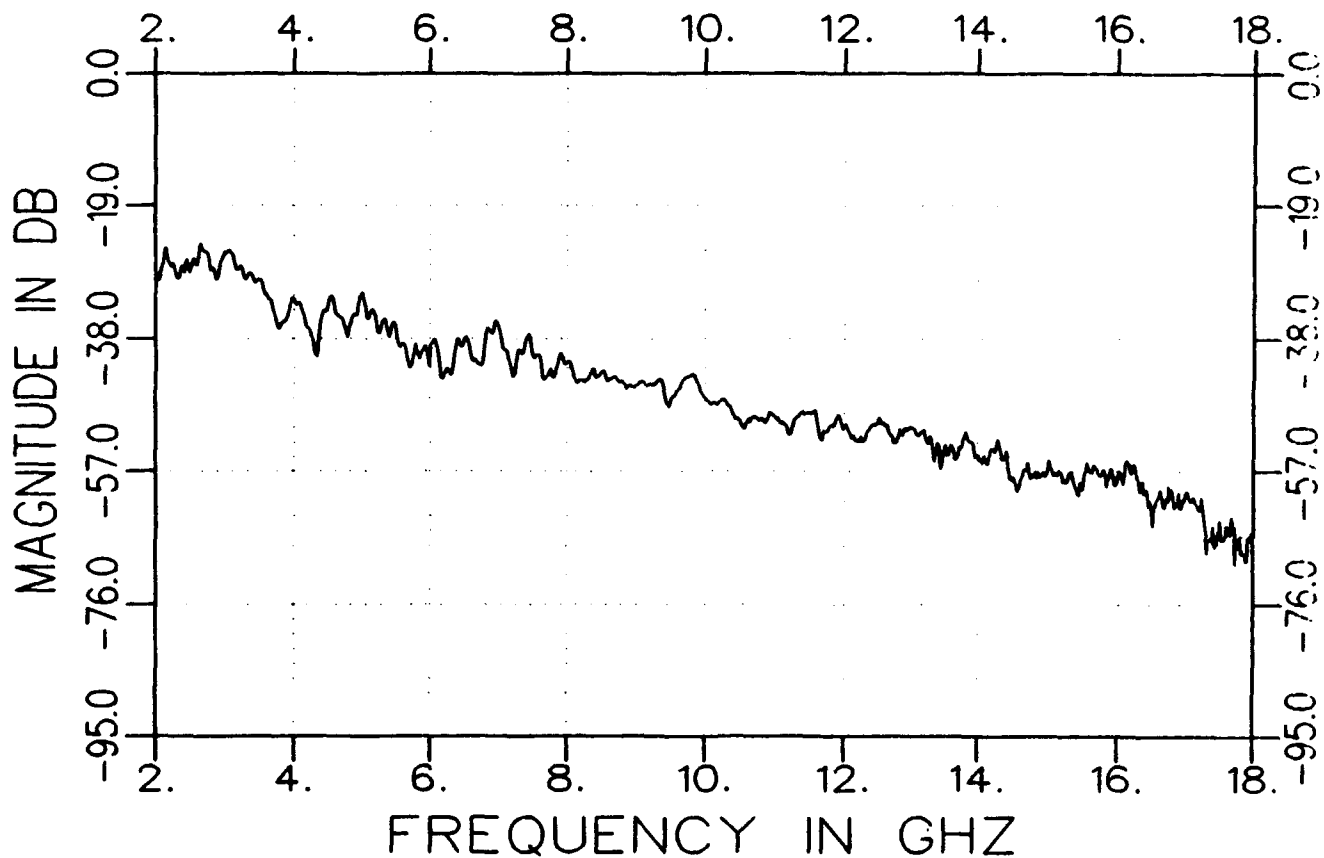
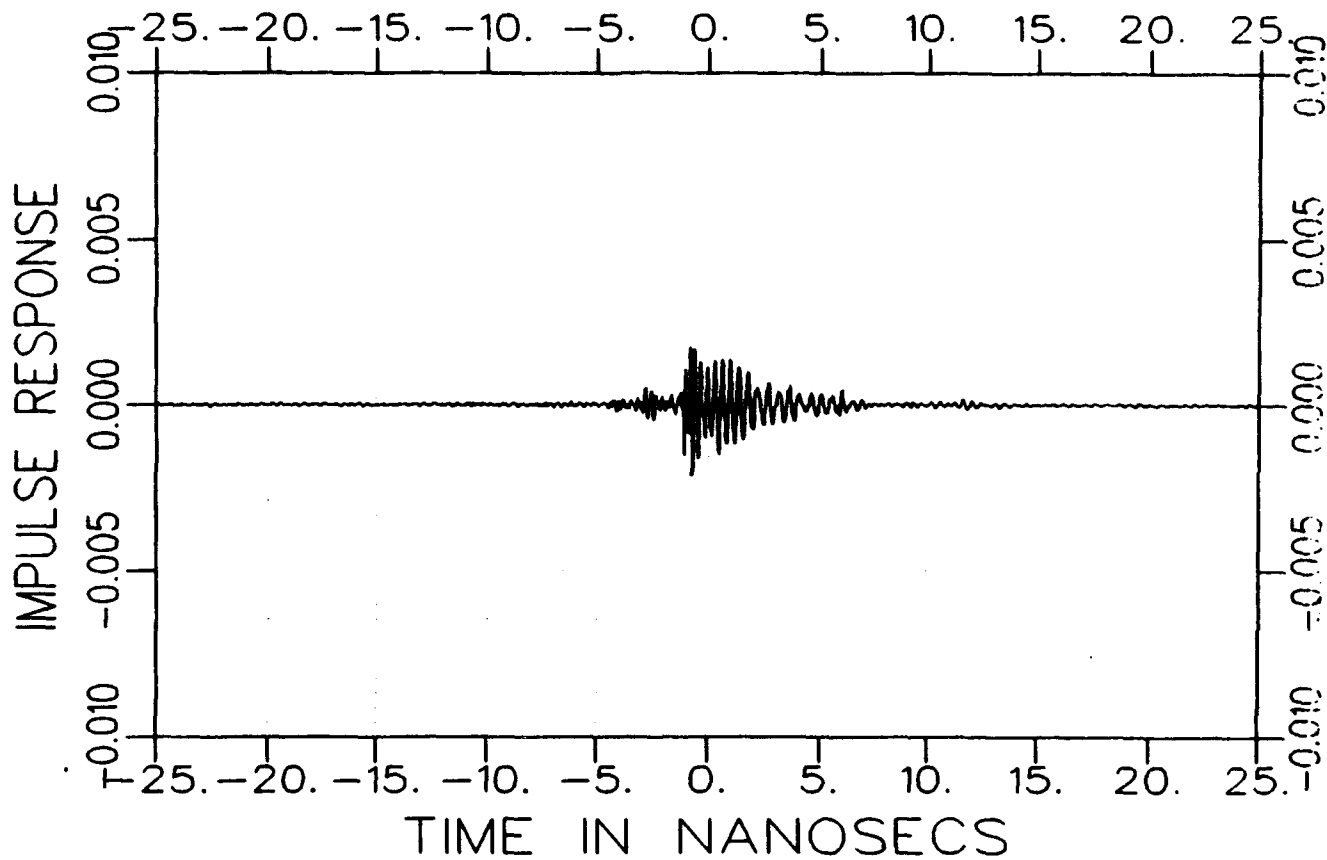
FR&AZ 07/23/93 09:27  
CAP. SLOT GRID AVE= 1  
REF=OFF  
ATN= 0



b3204fh0900-a  
TARGET

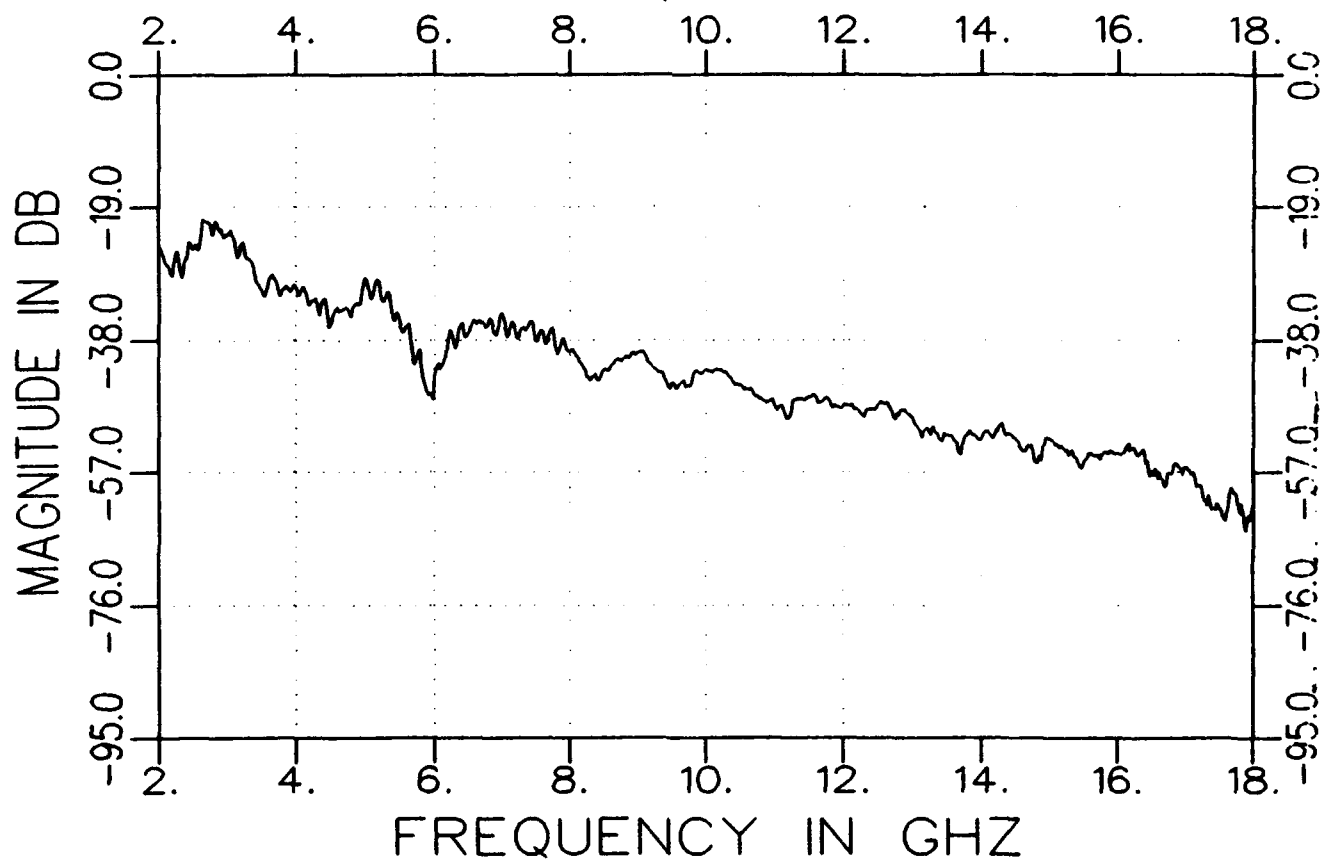
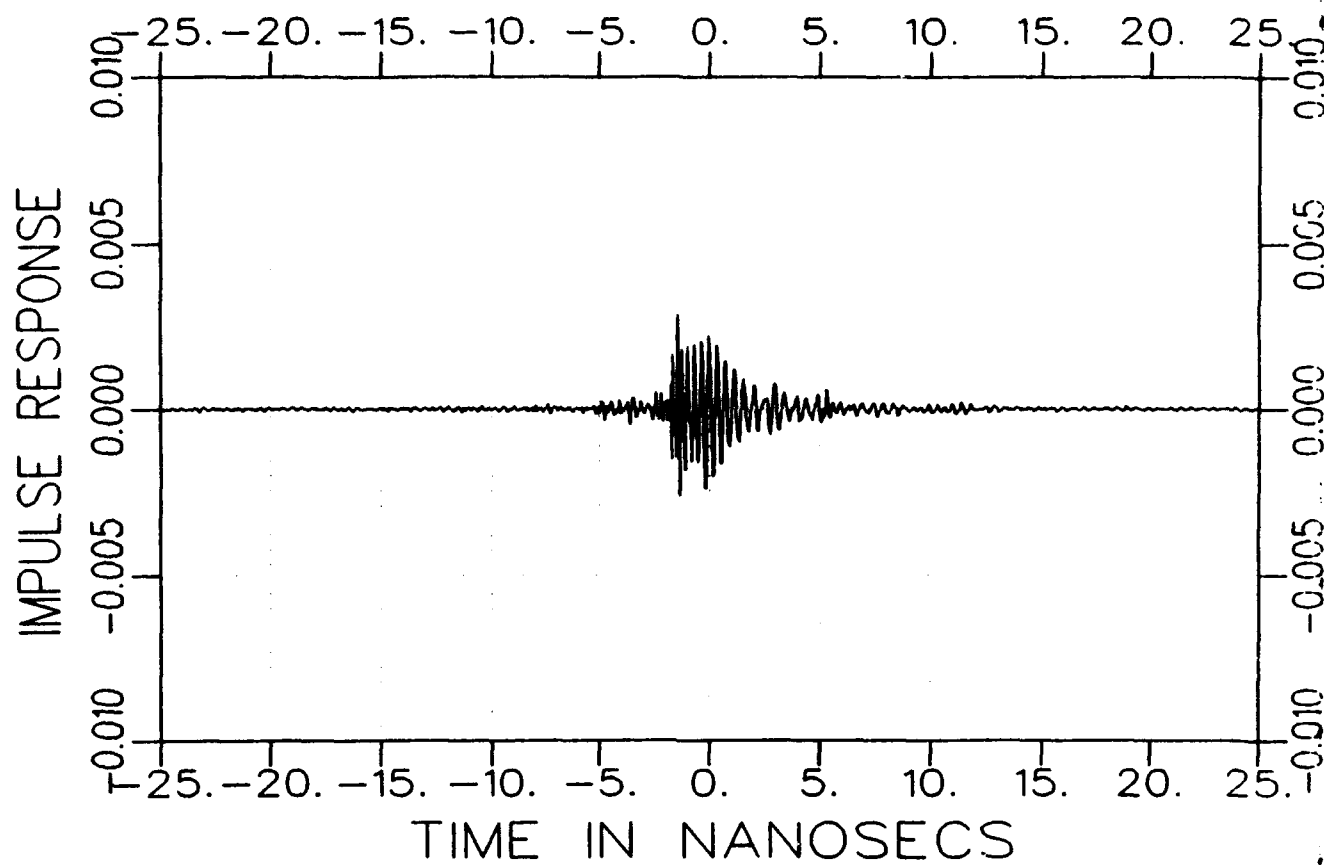
FR&AZ 07/23/93 09:43  
CAP. SLOT GRID AVE= 1  
REF=OFF

801 2002.30 610.35 90.00 ATN= 0



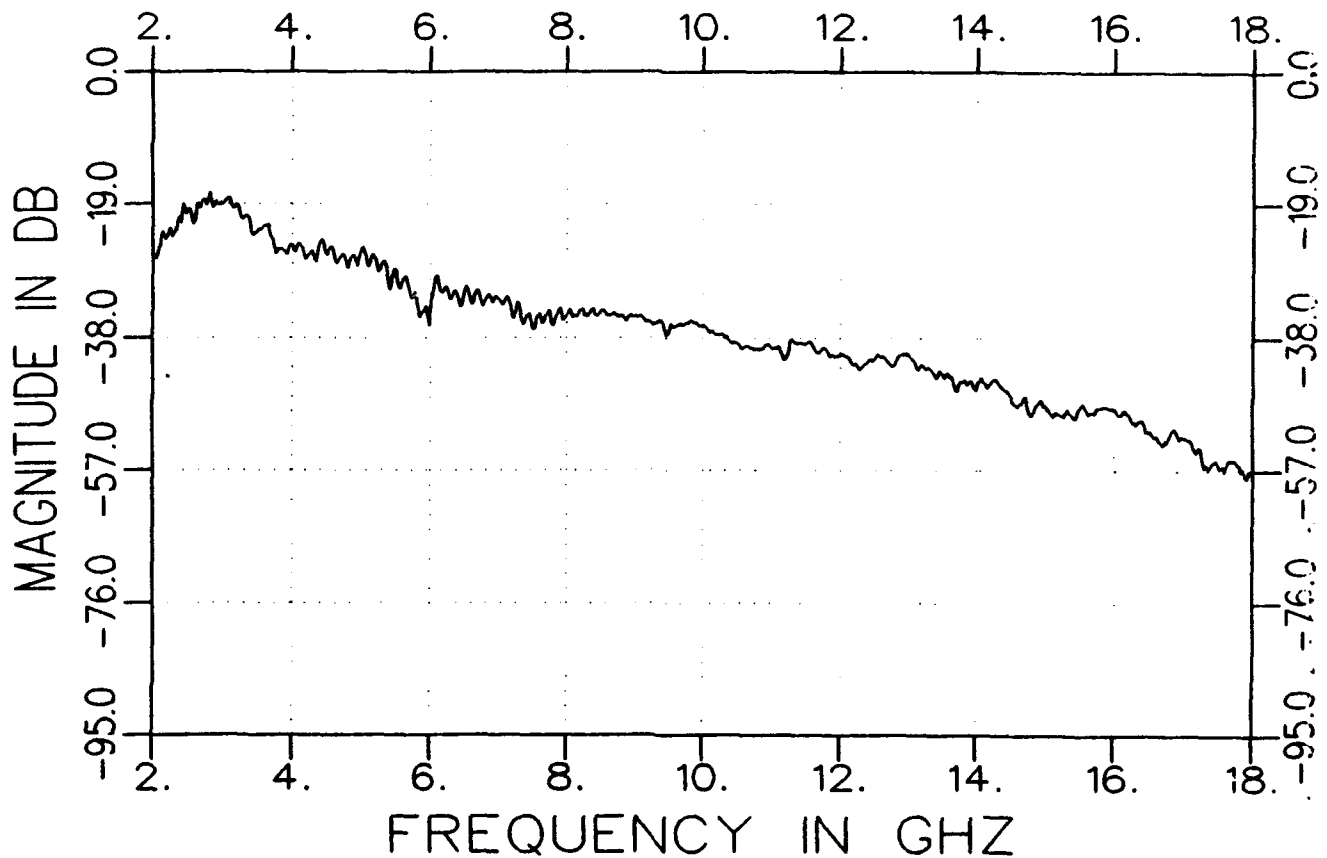
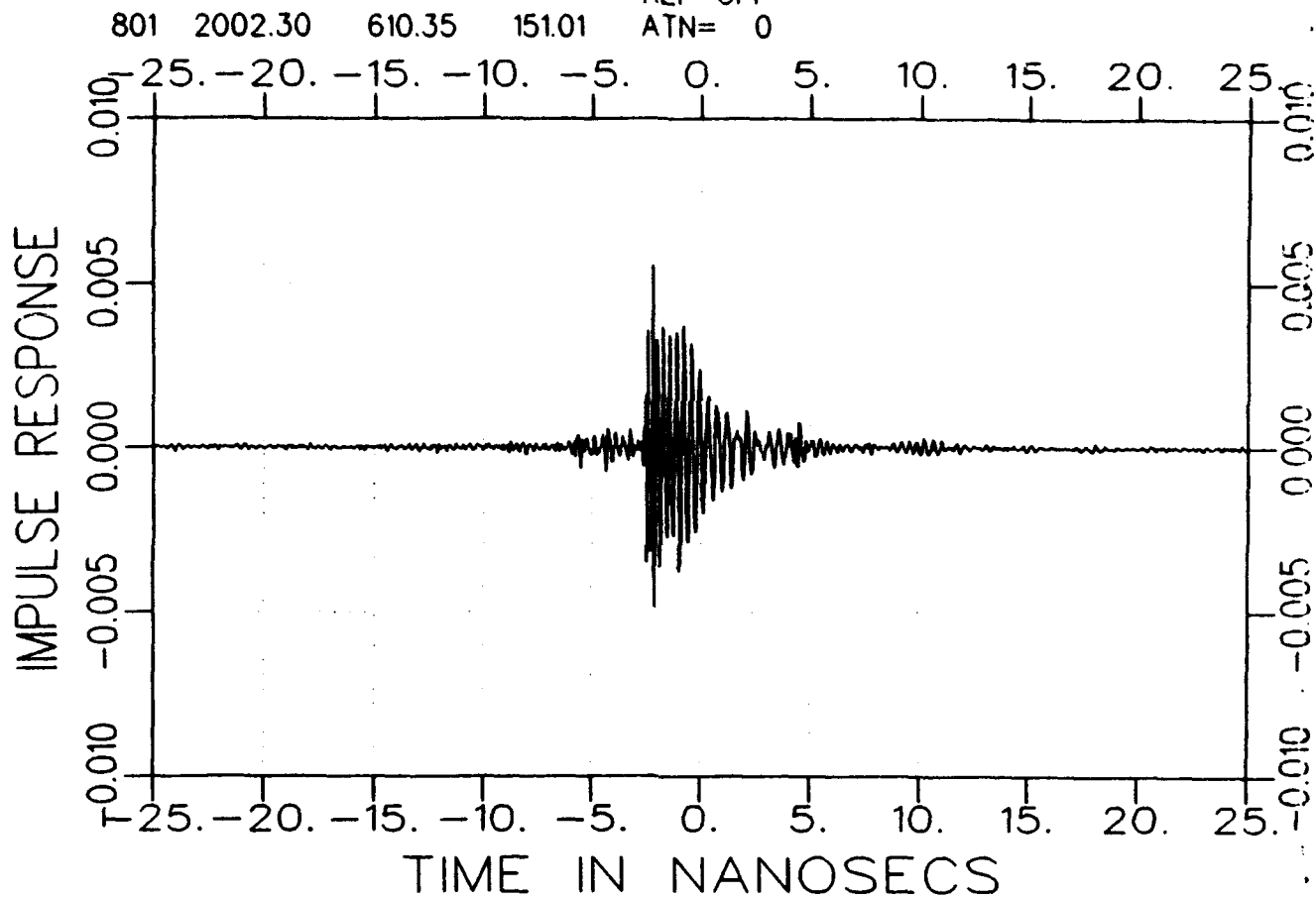
b3204fh1205-a  
TARGET

FR&AZ 07/23/93 09:43  
CAP. SLOT GRID AVE= 1  
REF=OFF  
801 2002.30 610.35 120.51 ATN= 0



b3204fh1510-a  
TARGET

FR&AZ 07/23/93 09:43  
CAP. SLOT GRID AVE= 1  
REF=OFF  
ATN= 0

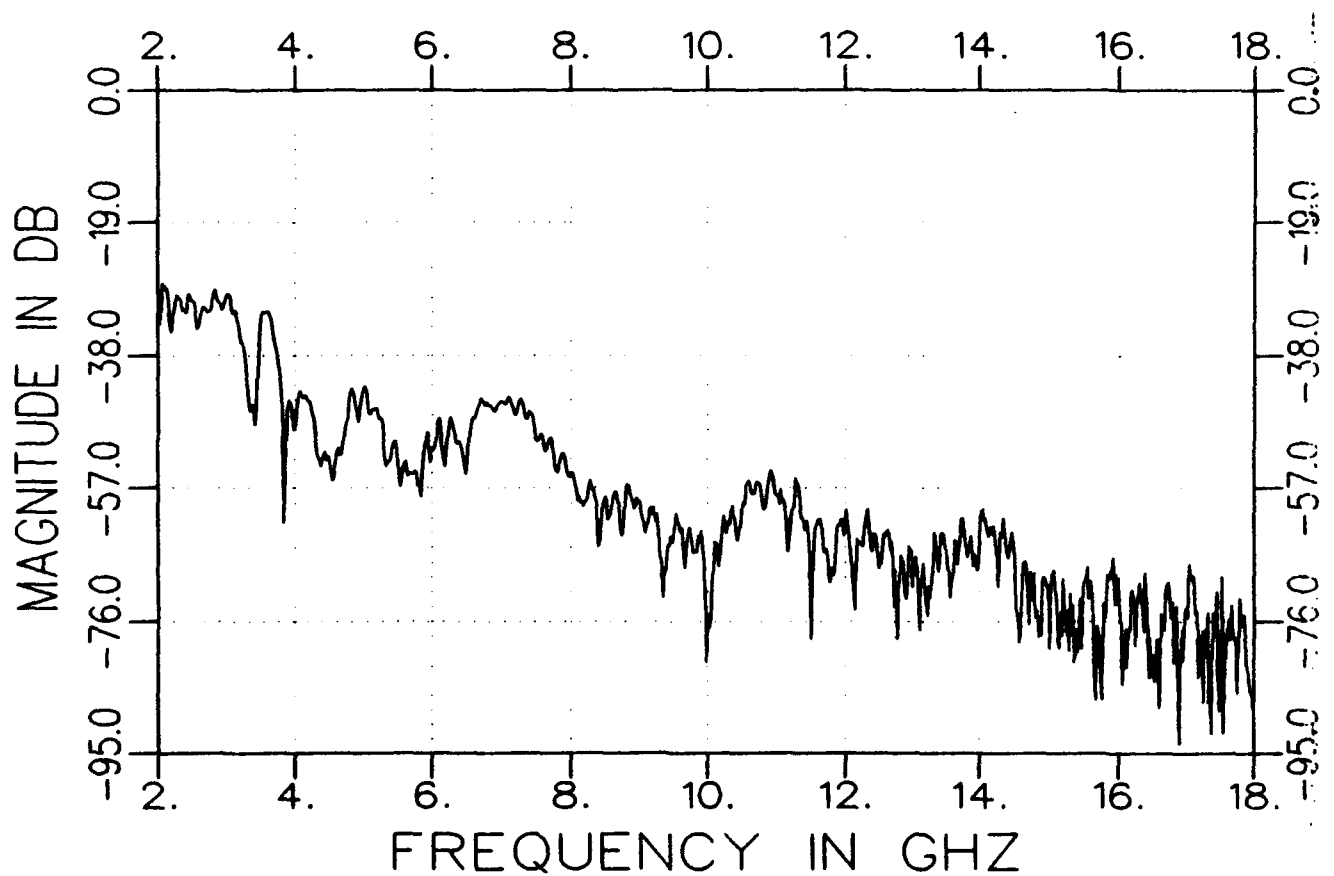
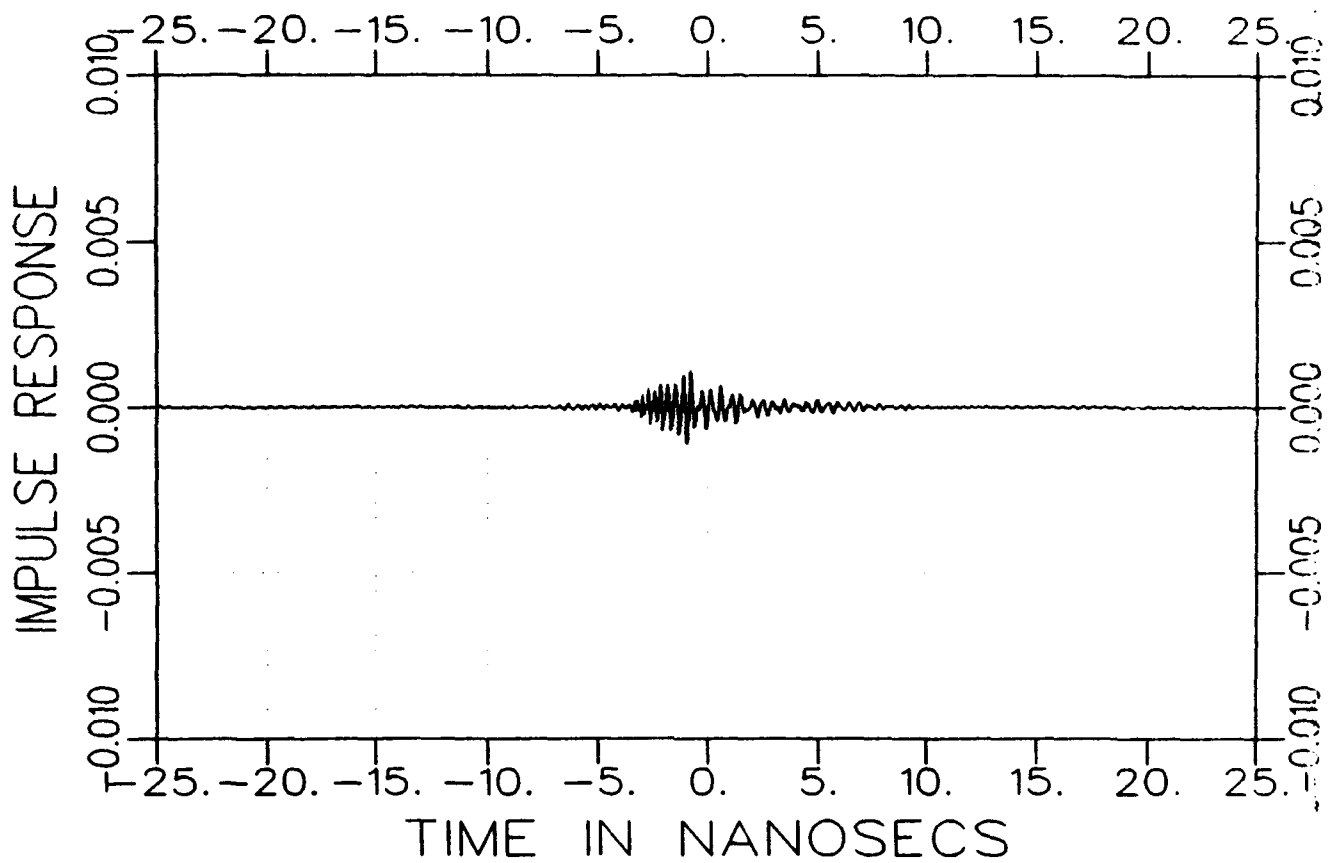




c3204fv0900-a  
TARGET

FR&AZ 07/23/93 10:17  
CAP. SLOT GRID AVE= 1  
REF=OFF

801 2002.30 610.35 90.00 ATN= 0



c3204fv1205-a

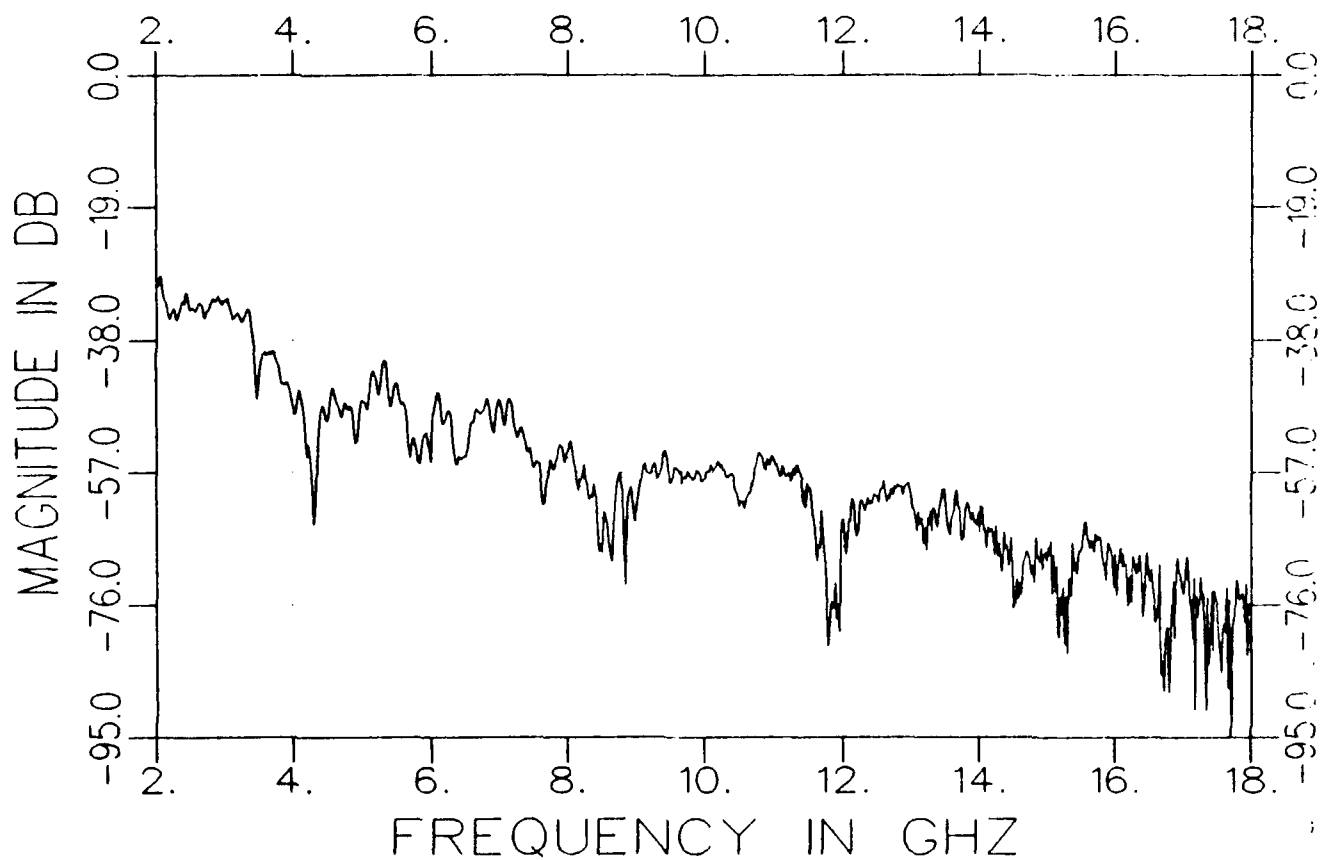
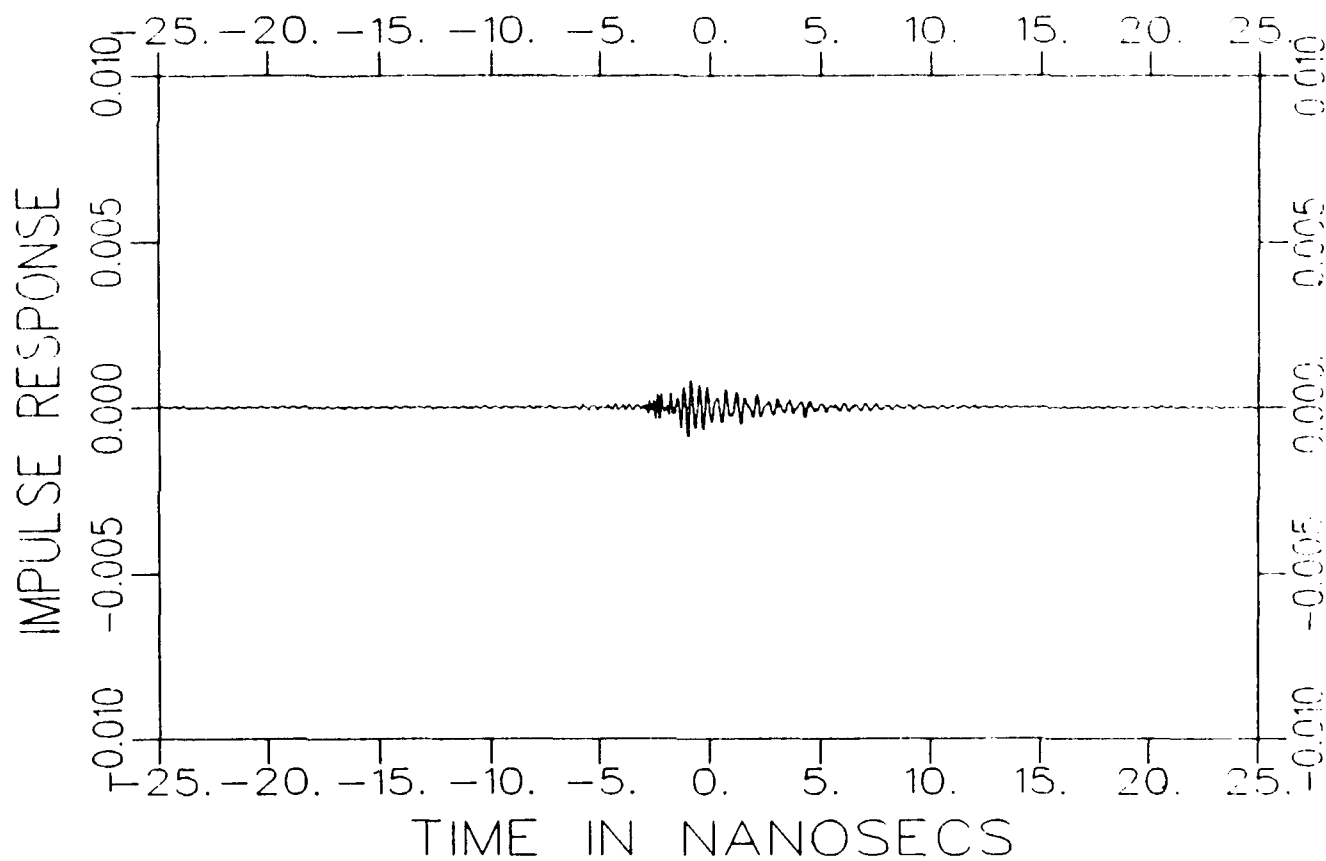
TARGET

FR&AZ 07/23/93 10:17

CAP. SLOT GRID AVE= 1

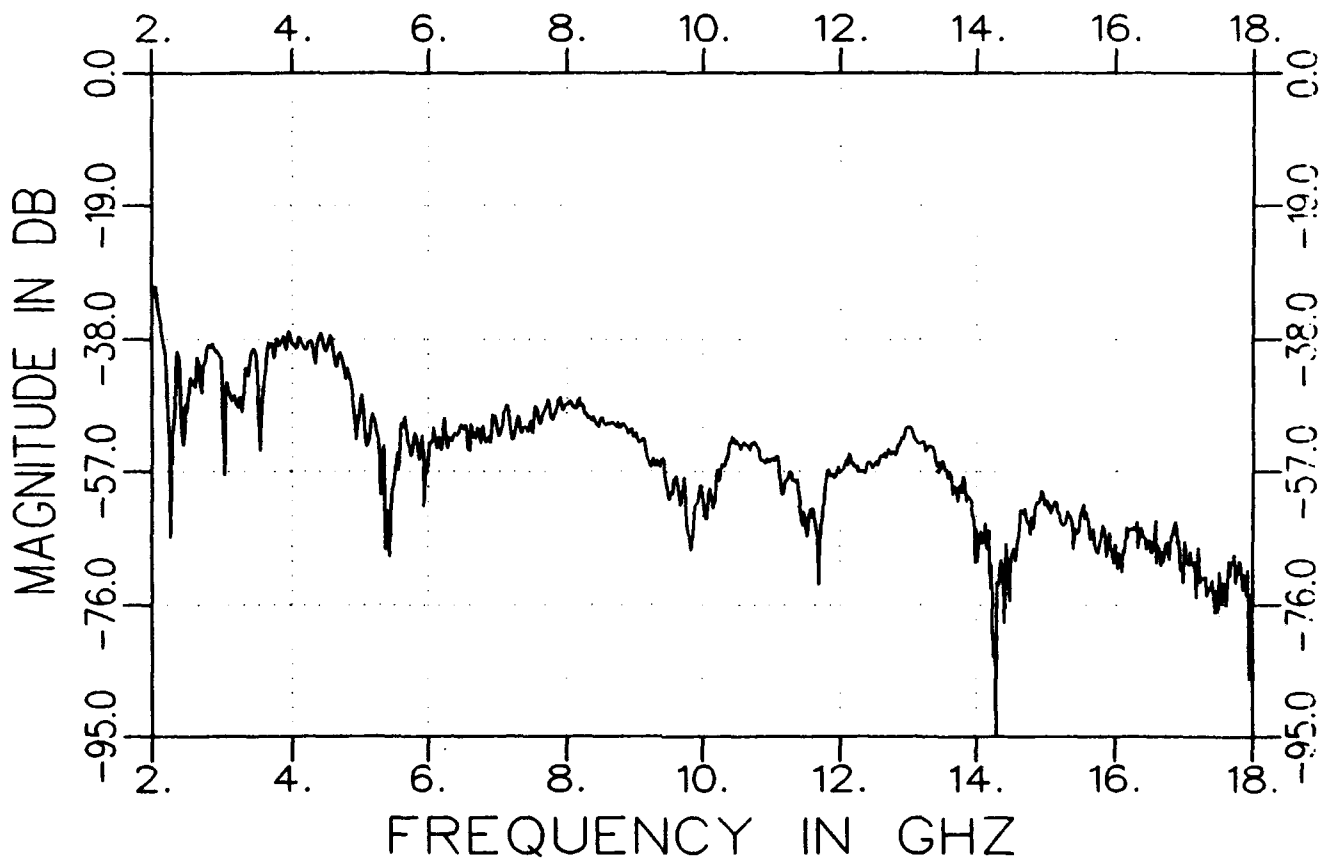
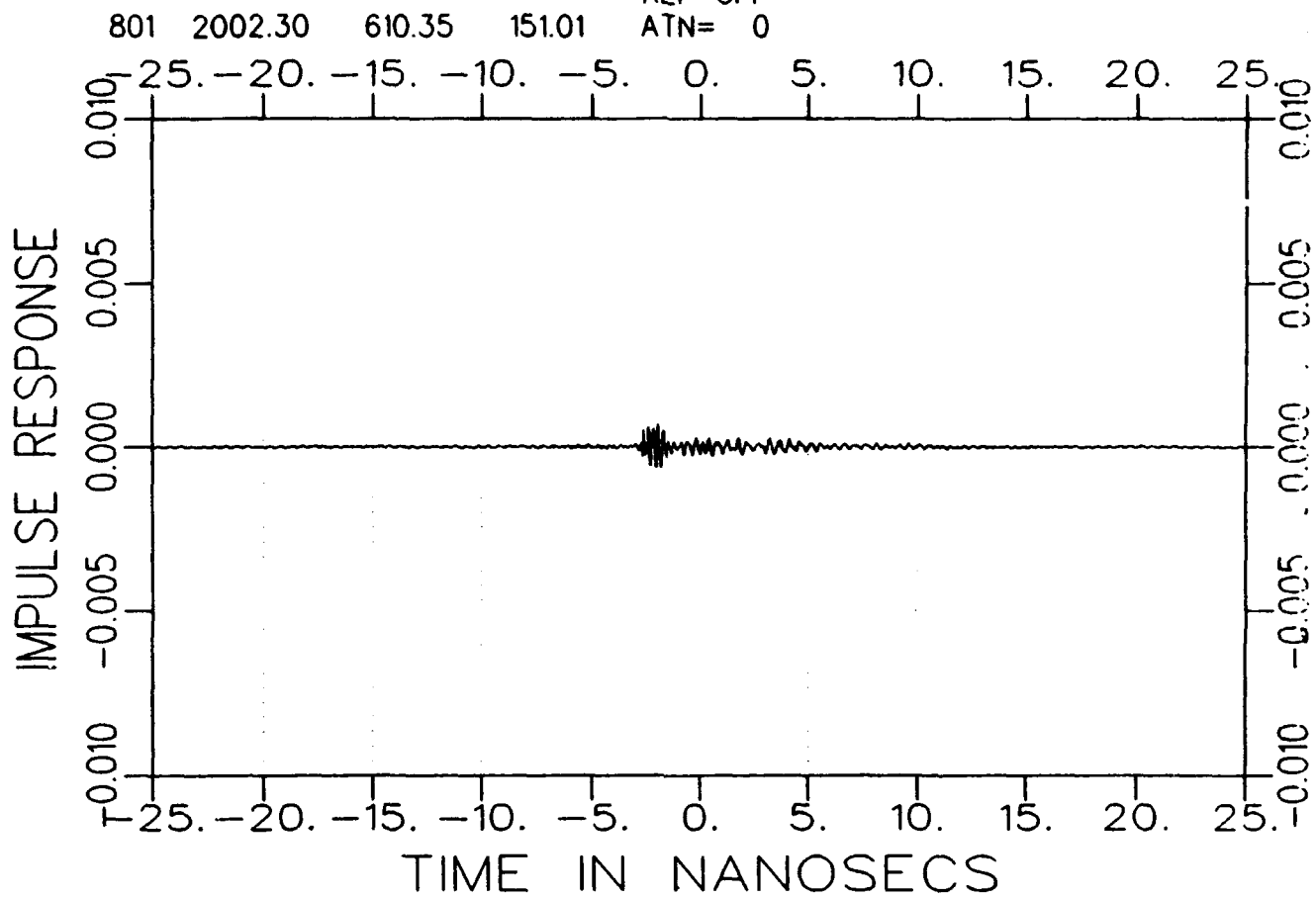
REF=OFF

801 2002.30 610.35 120.51 ATN= 0



c3204fv1510-a  
TARGET

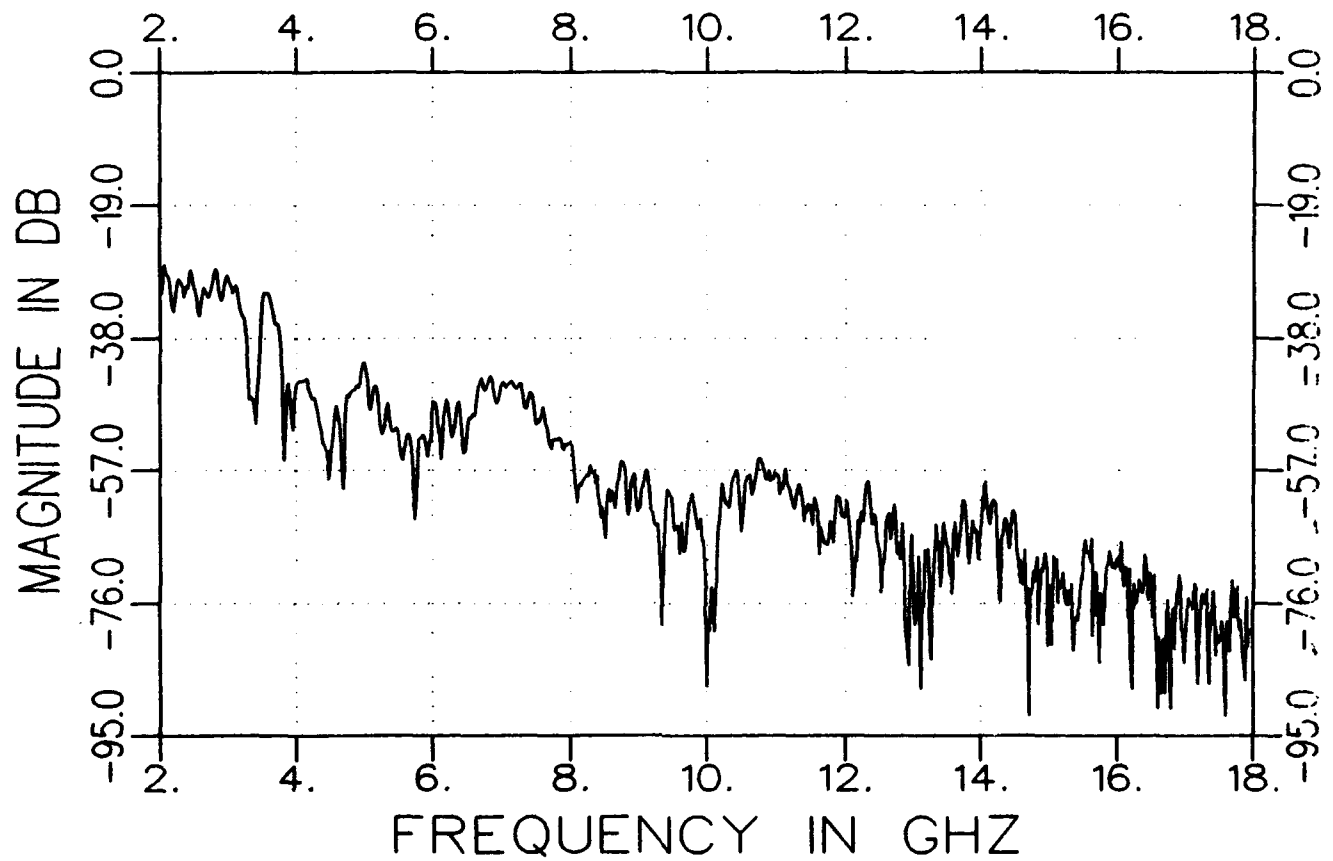
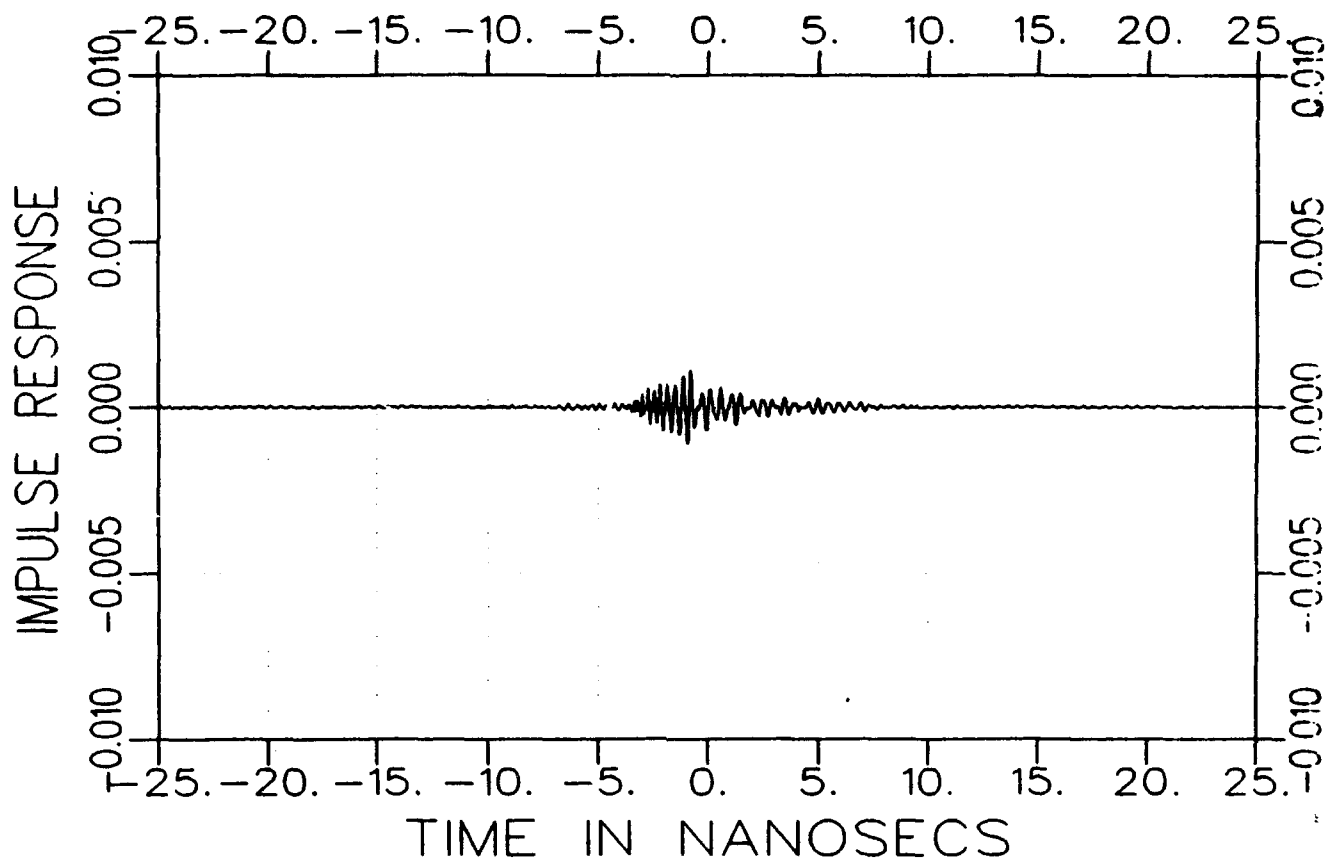
FR&AZ 07/23/93 10:17  
CAP. SLOT GRID AVE= 1  
REF=OFF  
ATN= 0



d3204fv0900-a  
TARGET

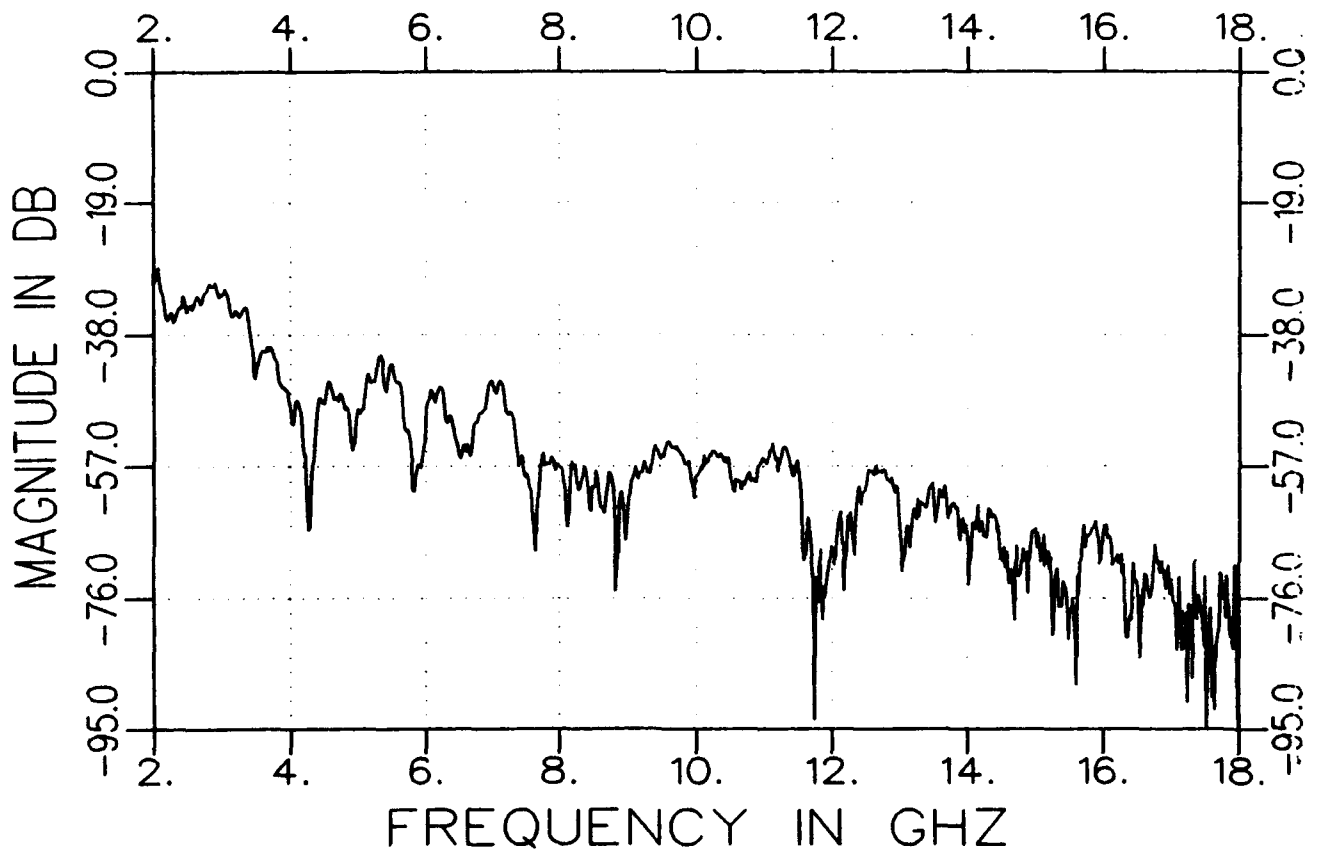
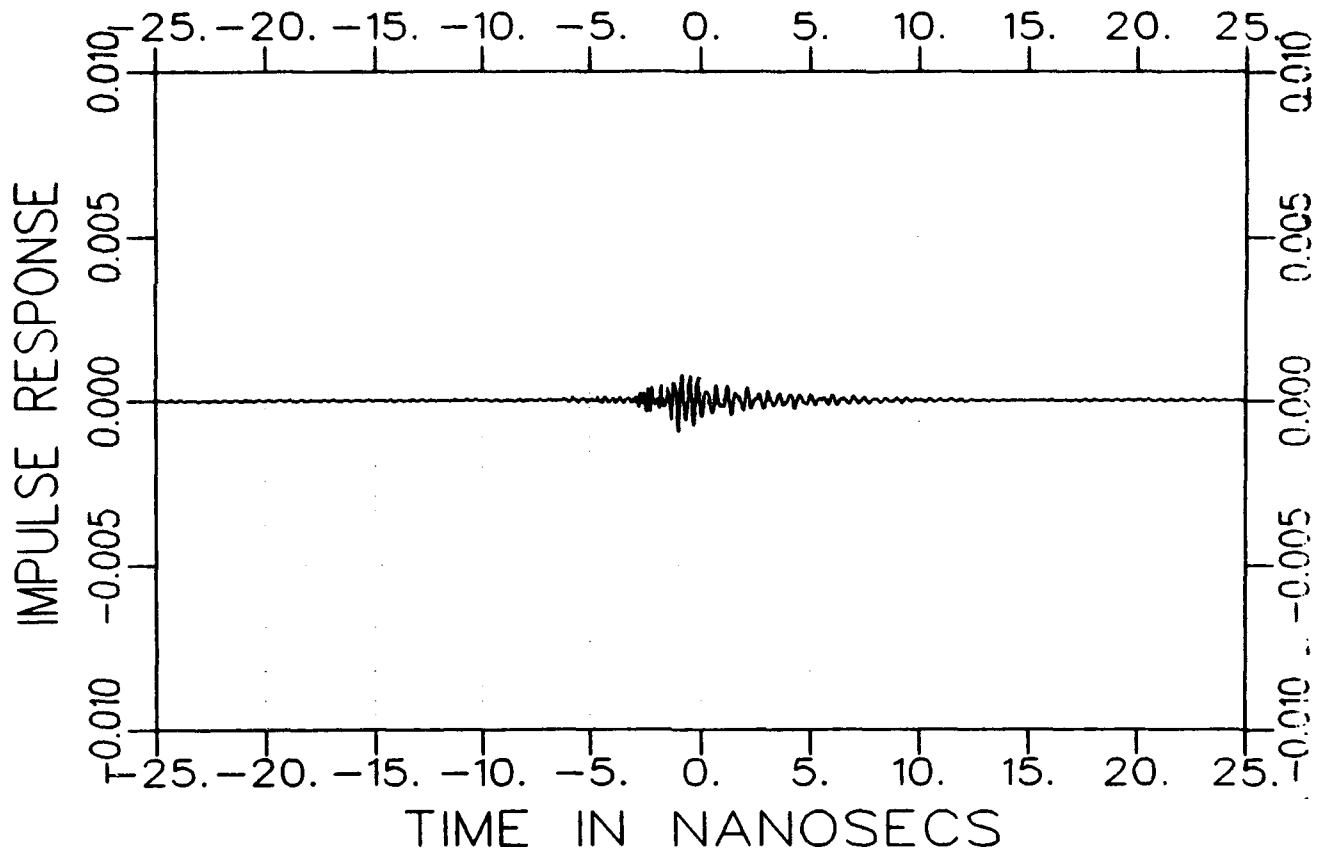
FR&AZ 07/23/93 10:35  
CAP. SLOT GRID AVE= 1  
REF=OFF

801 2002.30 610.35 90.00 ATN= 0



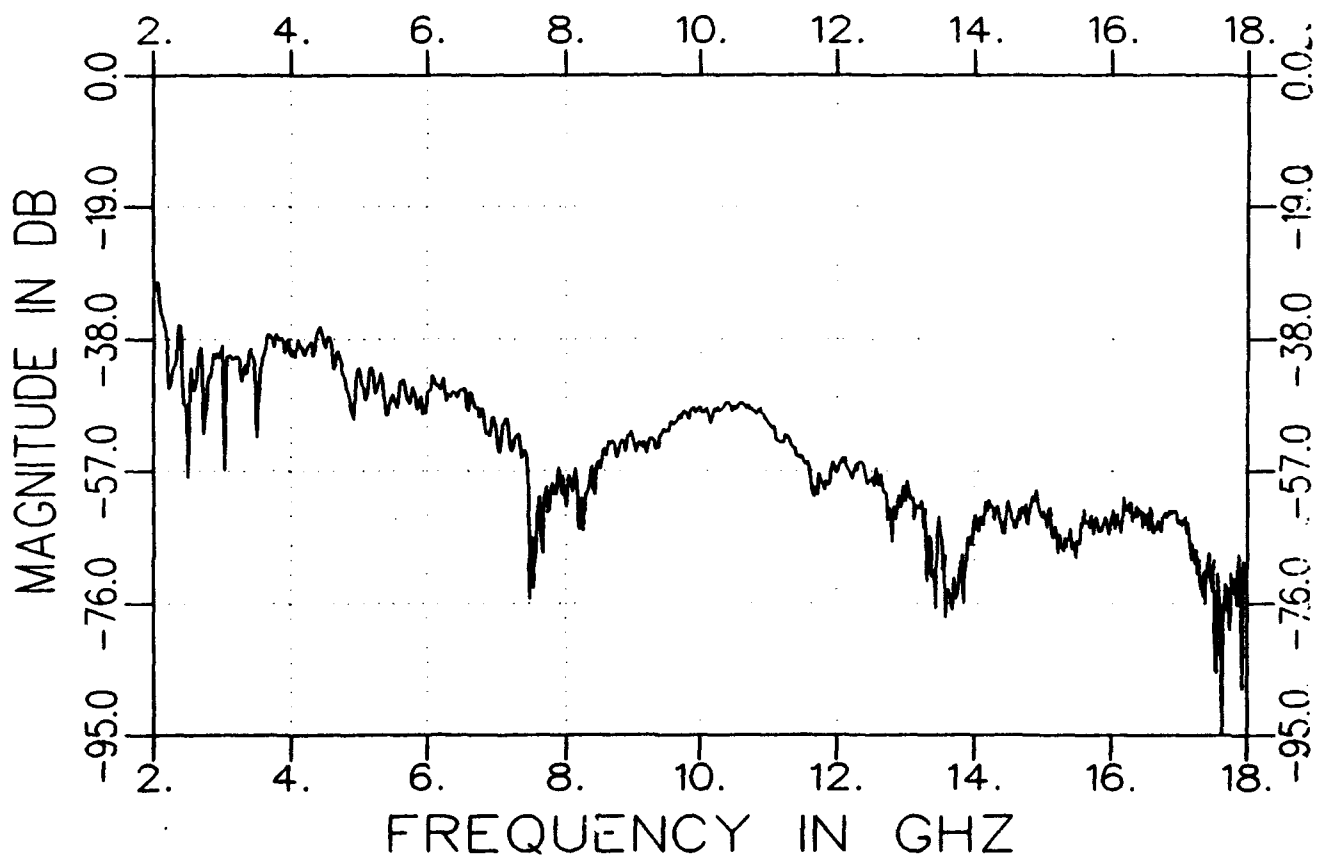
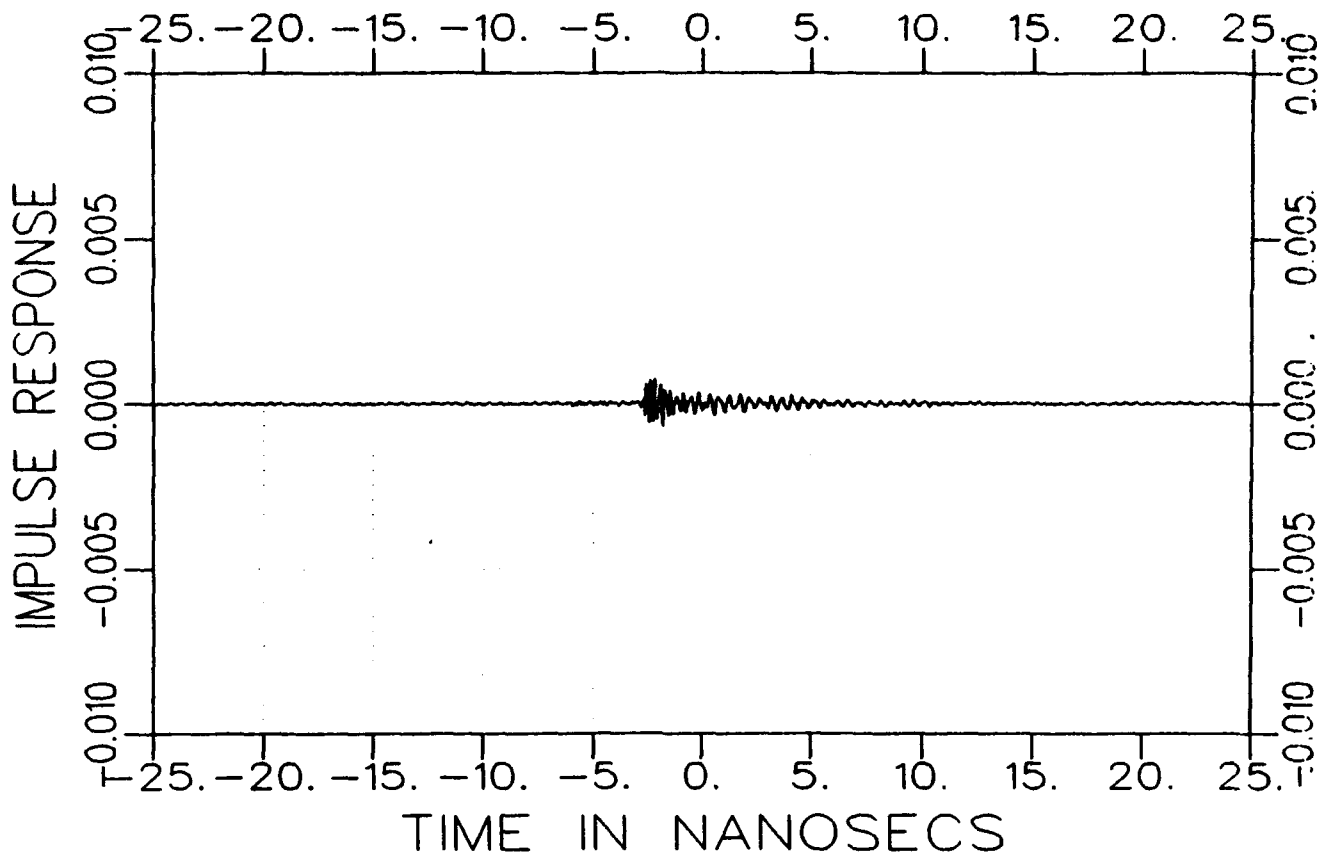
d3204fv1200-a  
TARGET

FR&AZ 07/23/93 10:35  
CAP. SLOT GRID AVE= 1  
REF=OFF  
801 2002.30 610.35 120.01 ATN= 0



d3204fv1500-a  
TARGET

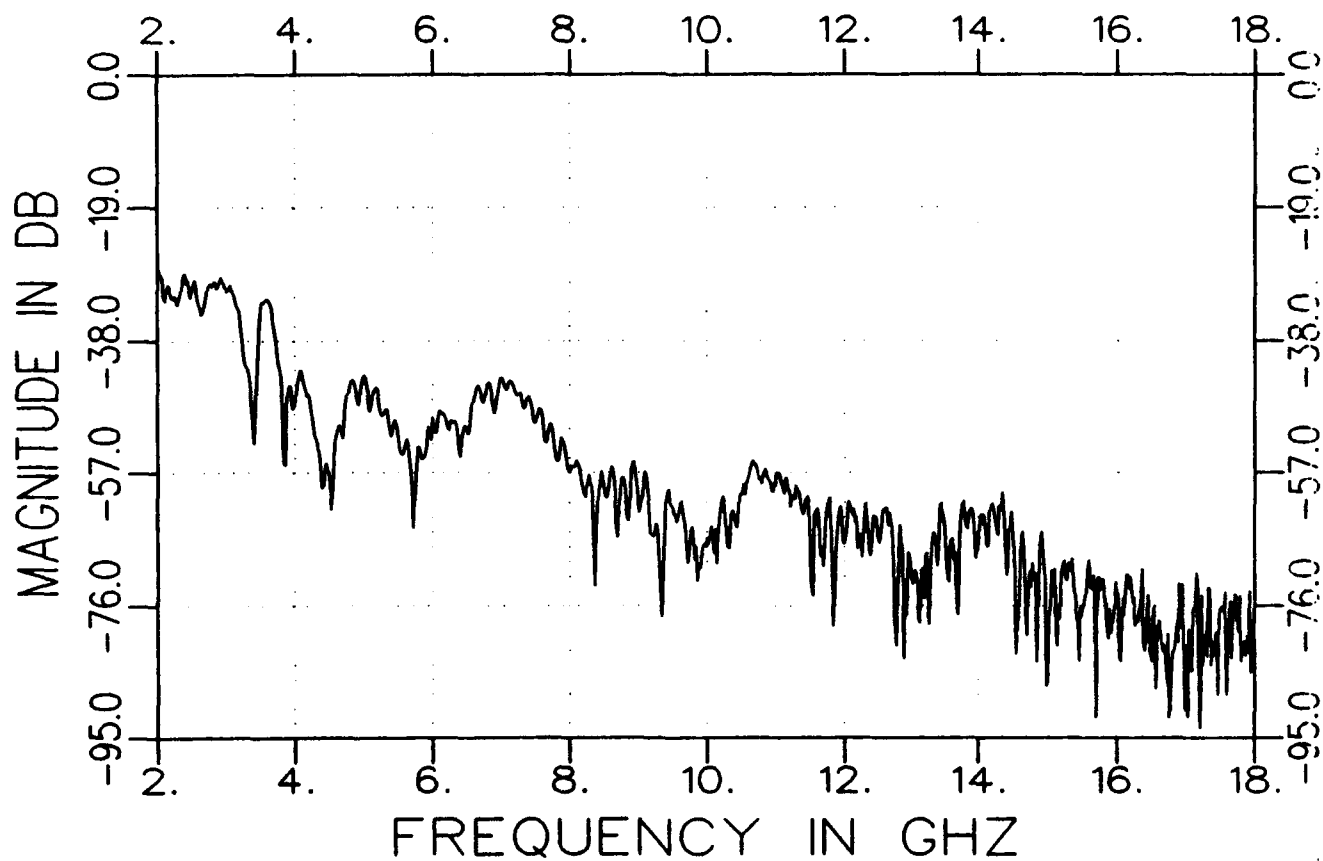
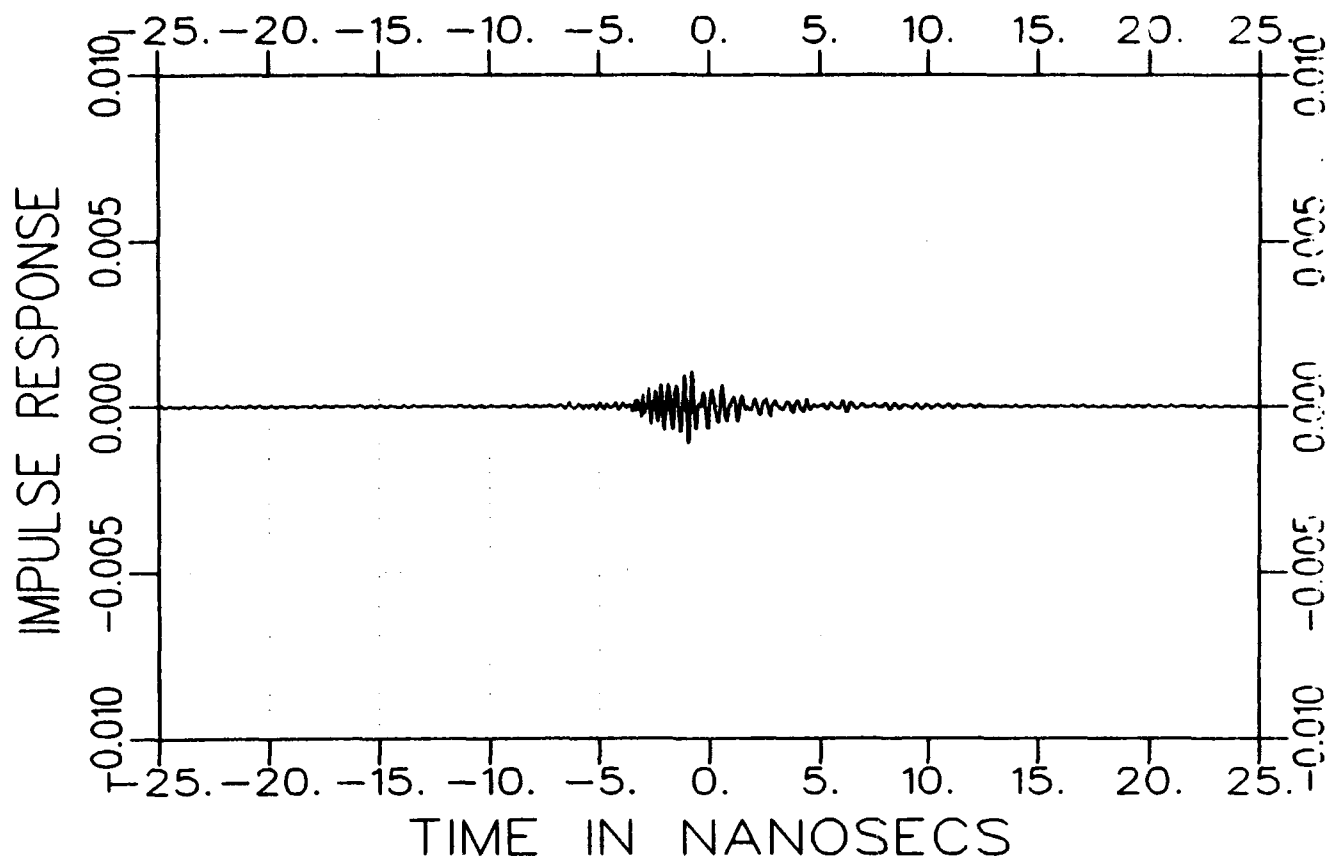
FR&AZ 07/23/93 10:35  
CAP. SLOT GRID AVE= 1  
REF=OFF  
ATN= 0



e3204fv0900-a  
TARGET

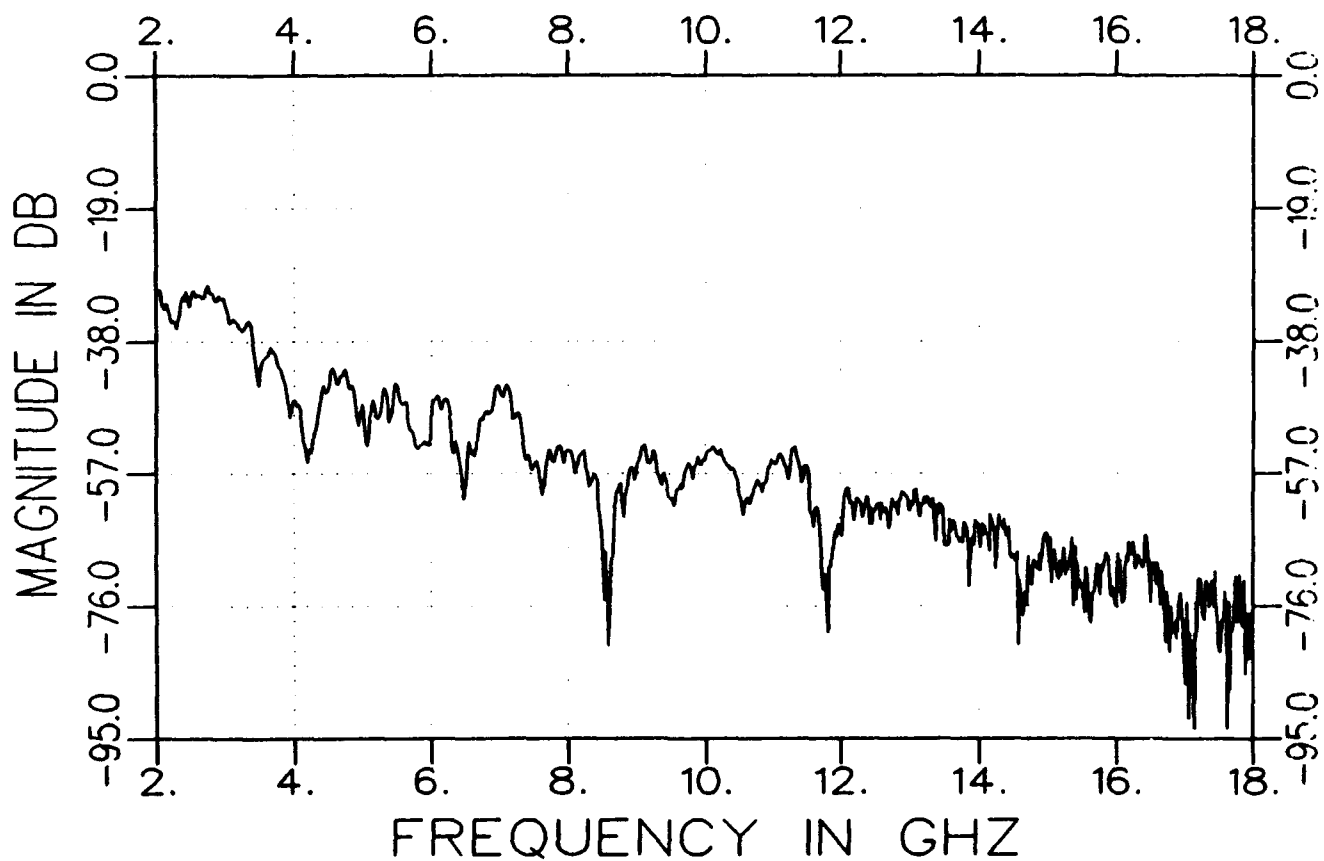
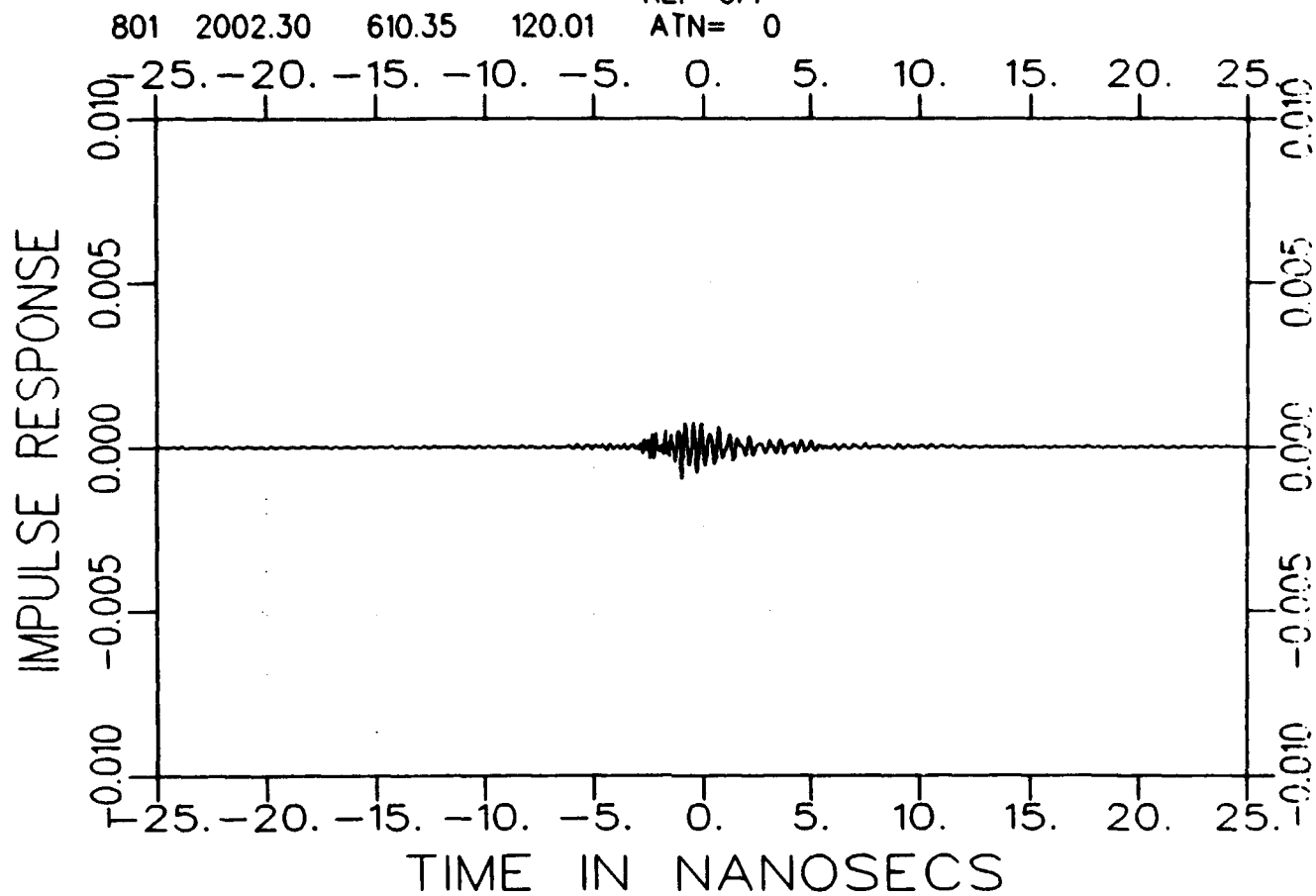
FR&AZ 07/23/93 10:49  
CAP. SLOT GRID AVE= 1  
REF=OFF

801 2002.30 610.35 90.00 ATN= 0



e3204fv1200-a  
TARGET

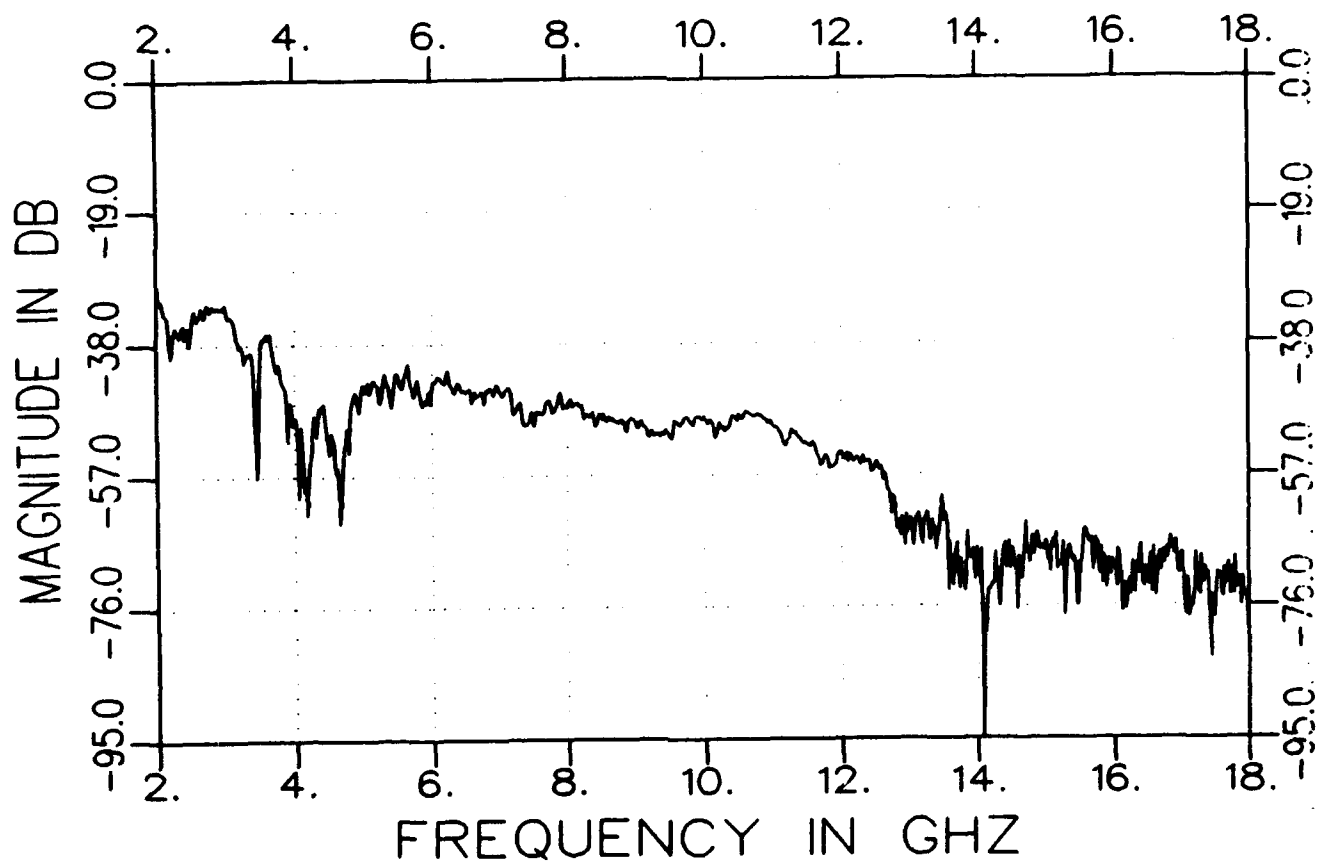
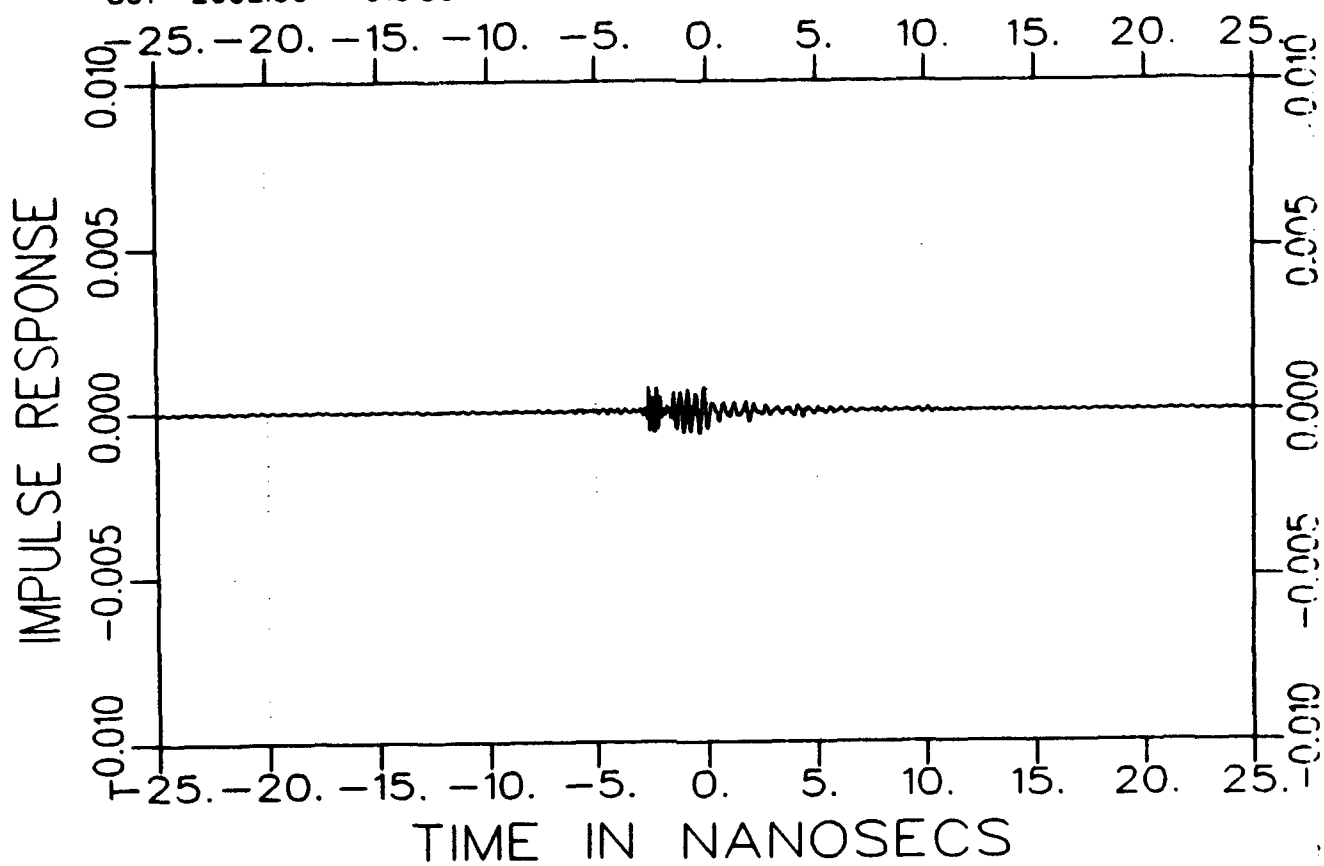
FR&AZ 07/23/93 10:49  
CAP. SLOT GRID AVE= 1  
REF=OFF  
ATN= 0





e3204fv1500-a  
TARGET

FR&AZ 07/23/93 10:49  
CAP. SLOT GRID AVE= 1  
REF=OFF  
801 2002.30 610.35 150.01 ATN= 0



## APPENDIX C

### SECOND MEASURED DATA

This appendix contains the UTD codes and data as well as the second impedance designs experimental results. The first set of data is the source codes for the UTD calculation for both principle polarizations. The second set of data is the UTD calculated data for both principle polarizations at frequencies 2, 10, and 18 GHz. The third set of data is the azimuth cuts of the second impedance designs at frequencies 2, 4, 6, 8, 10, 12, 14, 16, and 18 GHz. The last set of data is the frequency sweeps and time domain response of the second impedance designs at azimuth angles  $90^\circ$ ,  $120^\circ$ , and  $150^\circ$ .

The UTD source code for soft polarization (electric line source) is the following:

```
PROGRAM SOFTPOLARIZATION_DIFFRACTION
C
C   THIS PROGRAM WORKS FOR AN ELECTRIC LINE SOURCE IN THE
C   PRESENCE OF A 2D
C   WEDGE. N IS THE WEDGE FACTOR. RHO IS THE OBSERVATION
C   DISTANCE IN WAVELENGTHS
C   RHOP IS THE DISTANCE FROM THE SOURCE TO THE EDGE IN
C   WAVELENGTHS
C
C   COMPLEX J,UI,UR,UGTD,UUTD,UIO,UIQR,DS,DH,U1,U2,U3,Z
C   REAL PHI,PHIP,PHID,PHIPD,RHO,RHOP,DI,S,L,QR,K,N,RSB,ISB,X
C   REAL E1,E2,E3,offset
C
C   OPEN(UNIT=21,FILE='GO_db_s.XL1',STATUS='UNKNOWN')
C   OPEN(UNIT=22,FILE='GTD_db_S.XL1',STATUS='UNKNOWN')
C   OPEN(UNIT=24,FILE='UTD_DB_S.XL1',STATUS='UNKNOWN')
C   open(unit=25,file='utdnor_s.xl1',status='unknown')
C   J=(0.,1.)
C   PI=3.14592654
C   K=2.*PI
C   offset=0.
C
C   N=2.
C   write(*,*)'How far away is the source in wavelengths? '
```

```

read(*,*)RHOP
write(*,*)'What is the offset in dB? '
read(*,*)offset

c  RHOP=5.
   PHIPD=atan(2.5/30)*180/PI
   RHO=1000.

   RSB=180.-PHIPD
   ISB=180.+PHIPD
   PHIP=PHIPD*PI/180

   UIO=EXP(-(J*K*RHOP))/SQRT(RHOP)

   DO 100 I=0,360
   PHID=270.-I/2.
   PHI=PHID*PI/180
   X1=(RHO*COS(PHI)-RHOP*COS(PHIP))**2
   X=X1+(RHO*SIN(PHI)-RHOP*SIN(PHIP))**2
   DI=SQRT(X)
   QR=RHO*RHOP*SIN(PHI+PHIP)/(RHO*SIN(PHI)+RHOP*SIN(PHIP))
   L=SQRT((RHOP*SIN(PHIP))**2+(QR-(RHOP*COS(PHIP)))**2)
   S=SQRT((RHO*SIN(PHI))**2+((RHO*COS(PHI)-QR)**2)

   UIQR=EXP(-(J*K*L))/SQRT(L)
   IF (PHID.GE.ISB) THEN
   UI=0.
   GOTO 10
   ELSE
   UI=EXP(-(J*K*DI))/SQRT(DI)
10  END IF

   IF (PHID.GE.RSB) THEN
   UR=0.
   GOTO 20
   ELSE
   UR=-UIQR*EXP(-(J*K*S))*SQRT(L/(L+S))
20  END IF

   Z=UIO*EXP(-J*PI/4)/SQRT(2*PI*K)*(-.5)*EXP(-J*K*RHO)/SQRT(RHO)
   UGTD=Z*((1/COS((PHI-PHIP)/2))-(1/COS((PHI+PHIP)/2)))
   L=RHO*RHOP/(RHO+RHOP)

   CALL WDC(DS,DH,L,PHID,PHIPD,90.,N)
   UUTD=UIO*DS*EXP(-(J*K*RHO))/SQRT(RHO)

   U1=UI+UR
   U2=UI+UR+UGTD
   U3=UI+UR+UUTD

   E1=CABS(U1)*SQRT(RHOP)
   E2=CABS(U2)*SQRT(RHOP)

```

```

E3=CABS(U3)*SQRT(RHOP)

if (e1.eq.0) then
  e1db=-80
else
  e1db=20*log10(e1)
end if
if (e2.eq.0) then
  e2db=-80.
else
  e2db=20*log10(e2)
end if
if (e3.eq.0) then
  e3db=-80.
else
  e3db=20*log10(e3)
end if

c  WRITE(21,*)PHID,e1db
c  WRITE(22,*)PHID,e2db
   WRITE(24,*)(180.-PHID),',',e3db+offset
c  write(25,*)PHID,E3
100 CONTINUE
   STOP
   END

```

The UTD code used for hard polarization was the following:

```

PROGRAM HARDPOLARIZATION_DIFFRACTION

C
C  THIS PROGRAM WORKS FOR AN MAGNETIC LINE SOURCE IN THE
C  PRESENCE OF A 2D
C  WEDGE. N IS THE WEDGE FACTOR. RHO IS THE OBSERVATION
C  DISTANCE IN WAVELENG
C  RHOP IS THE DISTANCE FROM THE SOURCE TO THE EDGE IN
C  WAVELENGTHS
C  this program gives out UTD solutions but can also give GO and GTD as
c  well
C
C  COMPLEX J,UI,UR,UGTD,UUTD,UIO,UIQR,DS,DH,U1,U2,U3,Z
C  REAL PHI,PHIP,PHID,PHIPD,RHO,RHOP,DI,S,L,QR,K,N,RSB,ISB,X
C  REAL E1,E2,E3,offset

c  OPEN(UNIT=21,FILE='GO_DB_H.XL1',STATUS='UNKNOWN')
c  OPEN(UNIT=22,FILE='GTD_DB_H.XL1',STATUS='UNKNOWN')
   OPEN(UNIT=24,FILE='UTD_DB_H.XL1',STATUS='UNKNOWN')
c  open(unit=25,file='utdnor_h.xl1',status='unknown')
   J=(0.,1.)
   PI=3.14592654

```

```

K=2.*PI
offset=0.

C
N=2.
write(*,*)'How far away is the source in wavelengths? '
read(*,*)RHOP
write(*,*)'What is the offset in dB? '
read(*,*)offset
c RHOP=5.
  PHIPD=atan(2.5/30.)*180/PI
  RHO=1000.

  RSB=180.-PHIPD
  ISB=180.+PHIPD
  PHIP=PHIPD*PI/180

  UIO=EXP(-(J*K*RHOP))/SQRT(RHOP)

  DO 100 I=0,360
    PHID=270.-I/2.
    PHI=PHID*PI/180
    X1=(RHO*COS(PHI)-RHOP*COS(PHIP))**2
    X=X1+(RHO*SIN(PHI)-RHOP*SIN(PHIP))**2
    DI=SQRT(X)
    QR=RHO*RHOP*SIN(PHI+PHIP)/(RHO*SIN(PHI)+RHOP*SIN(PHIP))
    L=SQRT((RHOP*SIN(PHIP))**2+(QR-(RHO*COS(PHIP)))**2)
    S=SQRT((RHO*SIN(PHI))**2+((RHO*COS(PHI))-QR)**2)

    UIQR=EXP(-(J*K*L))/SQRT(L)
    IF (PHID.GE.ISB) THEN
      UI=0.
      GOTO 10
    ELSE
      UI=EXP(-(J*K*DI))/SQRT(DI)
10  END IF

    IF (PHID.GE.RSB) THEN
      UR=0.
      GOTO 20
    ELSE
      UR=UIQR*EXP(-(J*K*S))*SQRT(L/(L+S))
20  END IF

    Z=UIO*EXP(-J*PI/4)/SQRT(2*PI*K)*(-.5)*EXP(-J*K*RHO)/SQRT(RHO)
    UGTD=Z*((1/COS((PHI-PHIP)/2))+(1/COS((PHI+PHIP)/2)))
    L=RHO*RHOP/(RHO+RHOP)

    CALL WDC(DS,DH,L,PHID,PHIPD,90.,N)
    UUTD=UIO*DH*EXP(-(J*K*RHO))/SQRT(RHO)

    U1=UI+UR
    U2=UI+UR+UGTD

```

```

U3=U1+UR+UUTD

E1=CABS(U1)*SQRT(RHOP)
E2=CABS(U2)*SQRT(RHOP)
E3=CABS(U3)*SQRT(RHOP)
if (e1.eq.0) then
  e1db=-80
else
  e1db=20*log10(e1)
end if
if (e2.eq.0) then
  e2db=-80
else
  e2db=20*log10(e2)
end if
if (e3.eq.0) then
  e3db=-80.
else
  e3db=20*log10(e3)
end if

c  WRITE(21,*)PHID,E1db
c  WRITE(22,*)PHID,E2db
  WRITE(24,*)(180.-PHID),',',E3db+offset
c  write(25,*)PHID,e3
100 CONTINUE
  STOP
  END

```

The two subroutines used with these codes were the following:

```

C  SUBROUTINE WDC(CDCS,CDCH,R,PHID,PHIPD,BTD,FN)
C  UTD WEDGE DIFFRACTION COEFFICIENT
C  THIS ROUTINE IS IN BALANIS, P.848
C  IT CALLS FUNCTION FTF(X)
C  INPUTS: R (REAL) =DISTANCE PARAMETER L IN WAVELENGTHS
C  PHID (REAL) = OBSERV. ANGLE PHI IN DEGREES
C  PHIPD (REAL) = INCIDENT ANGLE PHI-PRIME IN DEGREES
C  BTD (REAL) = OBLIQUE INCIDENT ANGLE BETA IN DEGREES
C  SEE BALANIS P.827 FOR PICTURE OF BETA ANGLE
C  FN (REAL) = WEDGE FACTOR N (DIMENSIONLESS)
C  OUTPUTS:
C  CDCS (COMPLEX) = SOFT POL. DIFF. COEFFICIENT
C  CDCH (COMPLEX) = HARD POL. DIFF. COEFFICIENT

```

```

C
  COMPLEX D(4),CT,TERM,FT(4),FTF,CDCS,CDCH
  DATA CT,UTPI/(-0.05626977,0.05626977),0.15915494/
  DATA PI,TPI,SML/3.14159265,6.28318531,0.001/
  DTOR=PI/180.
  PHR=PHID*DTOR
  PHPR=PHIPD*DTOR
  SBO=SIN(DTOR*BTD)
  IF(ABS(FN-0.5).LT.SML)GOTO 10
  DKL=TPI*R
  UFN=1./FN
  BETAR=PHR-PHPR
  TERM=CT/(FN*SBO)
  SGN=1.
  I=0
2 I=I+1
  DN=UFN*(0.5*SGN+UTPI*BETAR)
  N=DN+SIGN(0.5,DN)
  ANG=TPI*FN*N-BETAR
  A=2.*(COS(0.5*ANG)**2)
  X=DKL*A
  Y=PI+SGN*BETAR
  IF(ABS(X).LT.1.E-10) GOTO 3
  FT(I)=FTF(X)/TAN(.5*Y*UFN)
  GOTO 4
3 FT(I)=(0.,0.)
  IF(ABS(COS(0.5*Y*UFN)).LT.1.E-3)GOTO 4
  FT(I)=(1.7725,1.7725)*SIGN(SQRT(DKL),Y)
  FT(I)=(FT(I)-(0.,2.)*DKL*(PI-SGN*ANG))*FN
4 SGN=-SGN
  D(I)=TERM*FT(I)
  IF(SGN.LT.0.)GOTO 2
  BETAR=PHR+PHPR
  IF(1.LE.3)GOTO 2
  CDCS=(D(1)+D(2))-(D(3)+D(4))
  CDCH=(D(1)+D(2))+(D(3)+D(4))
  RETURN
10 CDCS=(0.,0.)
  CDCH=(0.,0.)
  RETURN
  END

```

#### COMPLEX FUNCTION FTF(XF)

```

C
C   THIS IS THE FRESNEL TRANSITION FUNCTION USED IN UTD.
C
C   THIS CODE COMES FROM BALANIS, P. 850
C   SEE COMMENTS THERE
C   COMPLEX FXX(8),FX(8),C

```

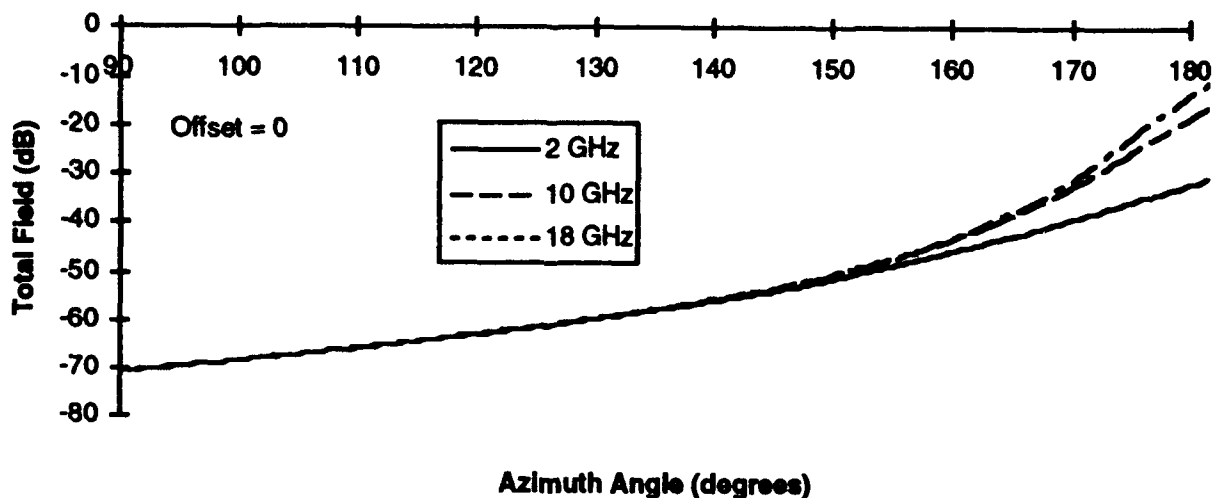
```

J  DIMENSION XX(8)
   DATA XX/.3,.5,.7,1.,1.5,2.3,4.,5.5/
   DATA CJ/(0.,1.)
   DATA FX/(0.5729,0.2677),(0.6768,0.2682),(0.7439,0.2549),
1(0.8095,0.2322),(0.873,0.1982),(0.9240,0.1577),(0.9658,0.1073),
2(0.9797,0.0828)
   DATA FXX/(0.,0.),(0.5195,0.0025),(0.3355,-0.0665),
1(0.2187,-0.0757),(0.127,-0.068),(0.0638,-0.0506),
2(0.0246,-0.0296),(0.0093,-0.0163)
   X=ABS(XF)
   IF(X.GT.5.5)GOTO 1
   IF(X.GT.0.3)GOTO 10
   FTF=((1.253,1.253)*SQRT(X)-(0.,2.)*X-0.6667*X*X)*CEXP(CJ*X)
   GOTO 20
10 DO 11 N=2,7
11 IF(X.LT.XX(N))GOTO 12
12 FTF=FXX(N)*(X-XX(N))+FX(N)
   GOTO 20
1 FTF=1.+(75./(16.*X*X)-0.75)/X/X+CJ*(0.5-15./(8.*X*X))/X
20 IF(XF.GE.0.)RETURN
   FTF=CONJG(FTF)
   RETURN
   END

```

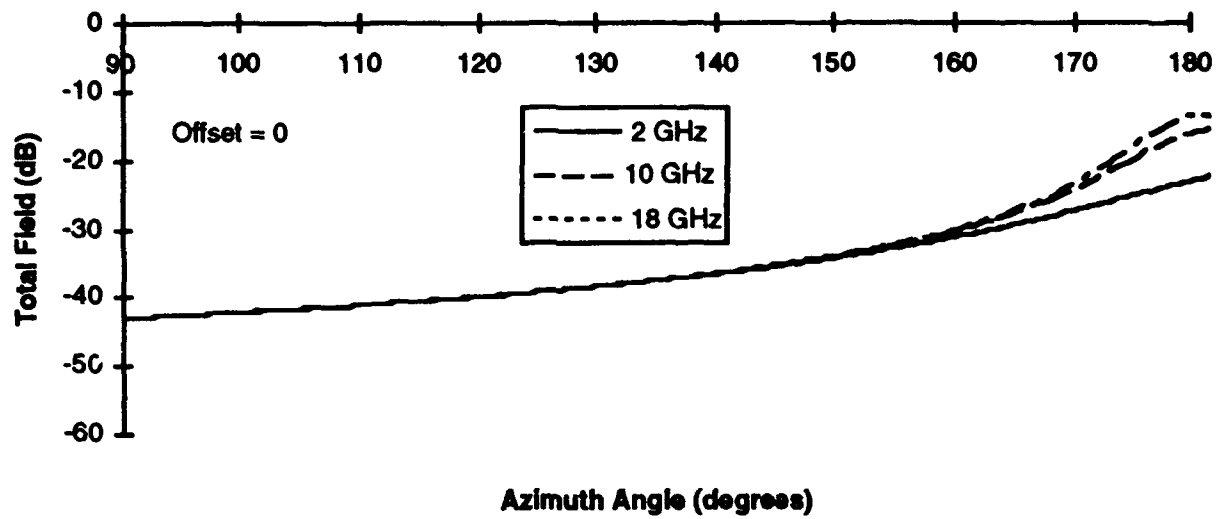
The following graphs are the results from the previous UTD codes for frequencies 2, 10, 18 GHz. The first one is for an infinite electric line source (soft polarization) and the second one is for an infinite magnetic line source (hard polarization).

#### UTD Calculations for Soft Polarization





### UTD Calculations for Hard Polarization



The next set of data is the magnitude and phase azimuth cuts at different angles taken of the second impedance designs. The last set of data is the frequency sweeps and time domain response of the second impedance designs. The OSU-ESL designator system used letters to designate which taper was measured. The following letters correspond to the OSU-DATA taken on the second impedance designs.

The azimuth scans for the second designs have the following designations:

- a3225----No Taper for Hard Polarization
- b3225----Long Capacitive Taper #2
- c3225----Short Capacitive Taper #2
- d3225----No Taper for Soft Polarization
- e3225----Long Inductive Taper #2
- f3225----Short Inductive Taper #2

The frequency scans for the second designs have the following designations:

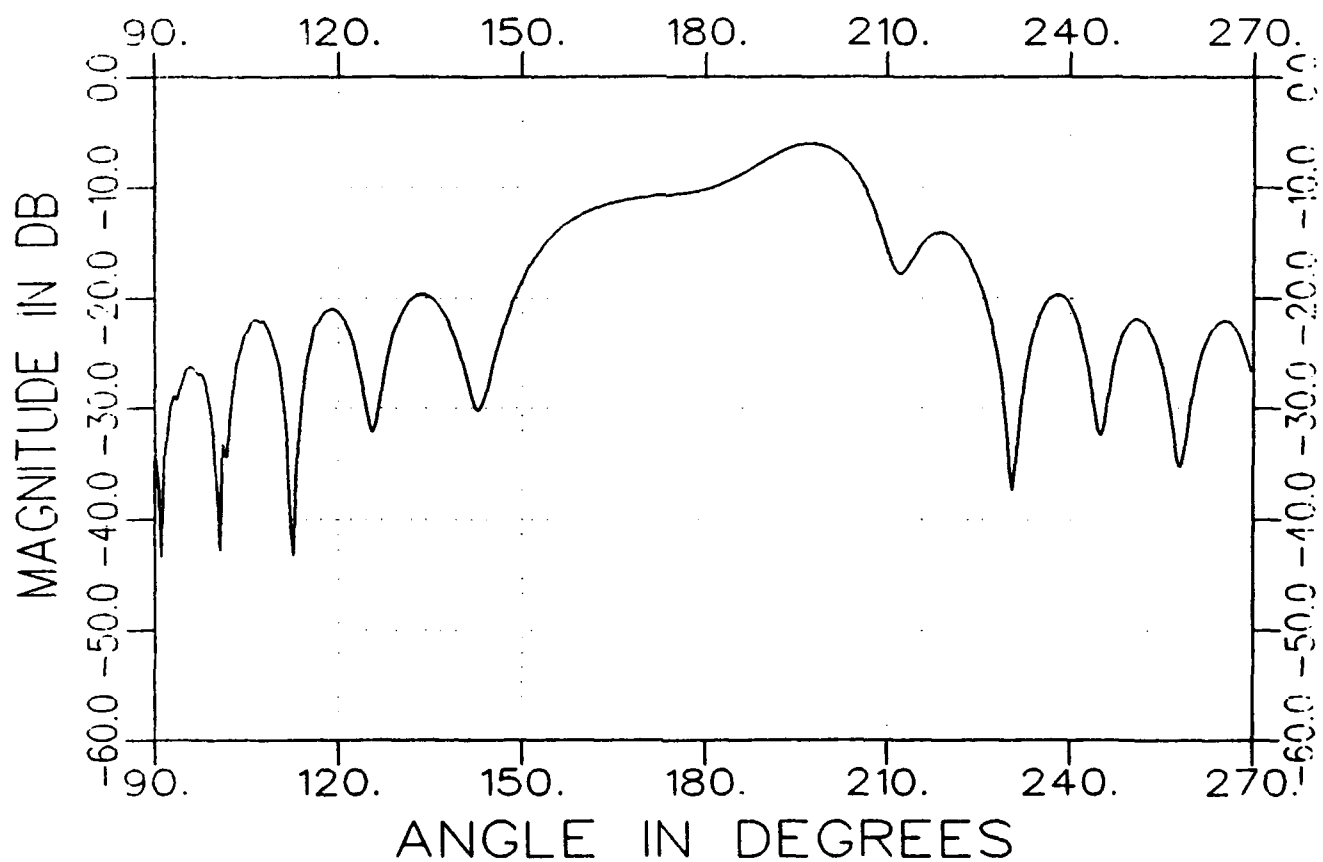
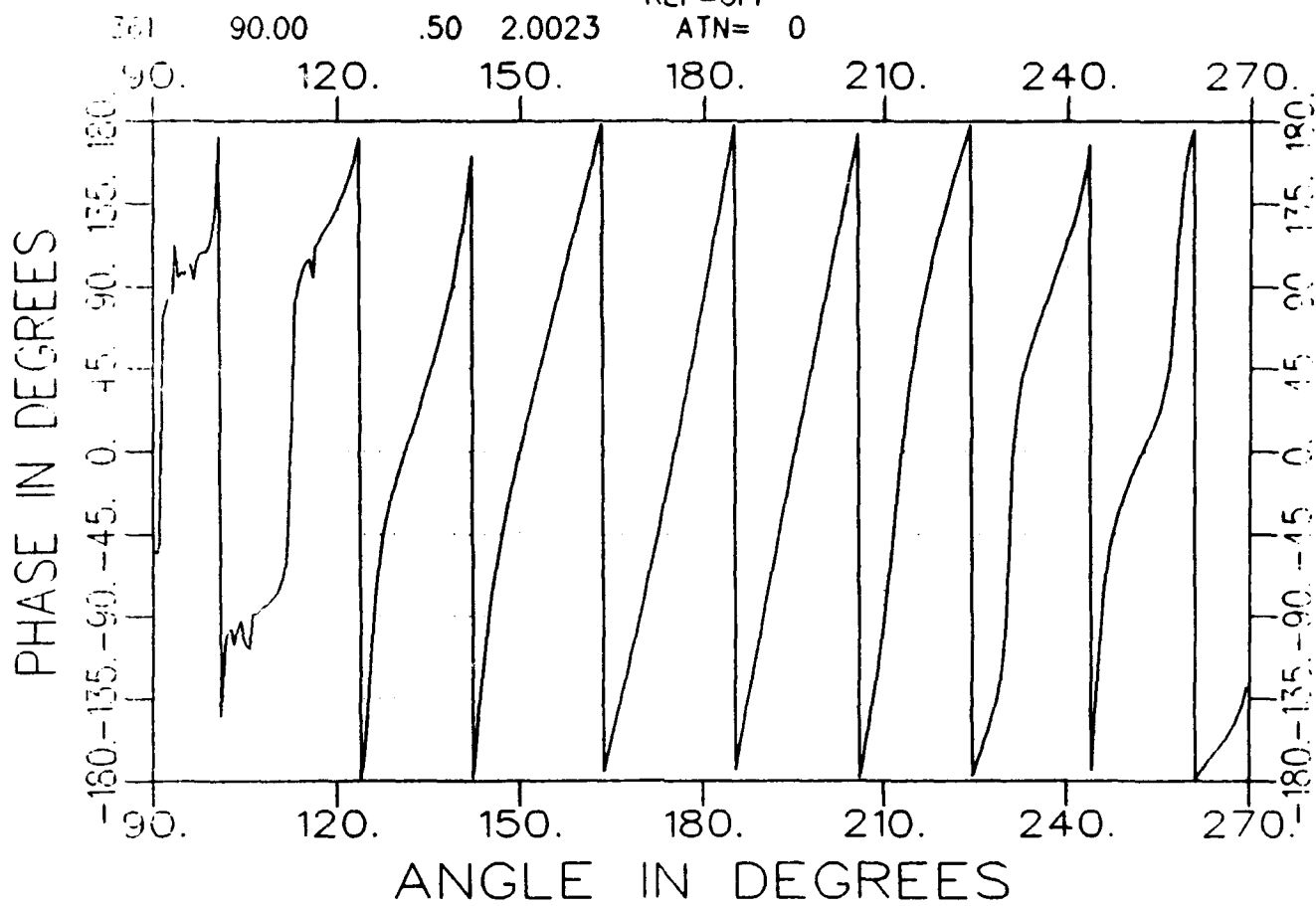
- g3225----Short Inductive Taper #2
- h3225----Long Inductive Taper #2
- i3225----No Taper for Soft Polarization
- j3225----No Taper for Hard Polarization
- k3225----Long Capacitive Taper #2
- l3225----Short Capacitive Taper #2

03225ah0200-a.tar  
TARGET

AZIM. 08/13/93 10:31  
cap grid

AVE= 82  
REF=OFF

ATN= 0

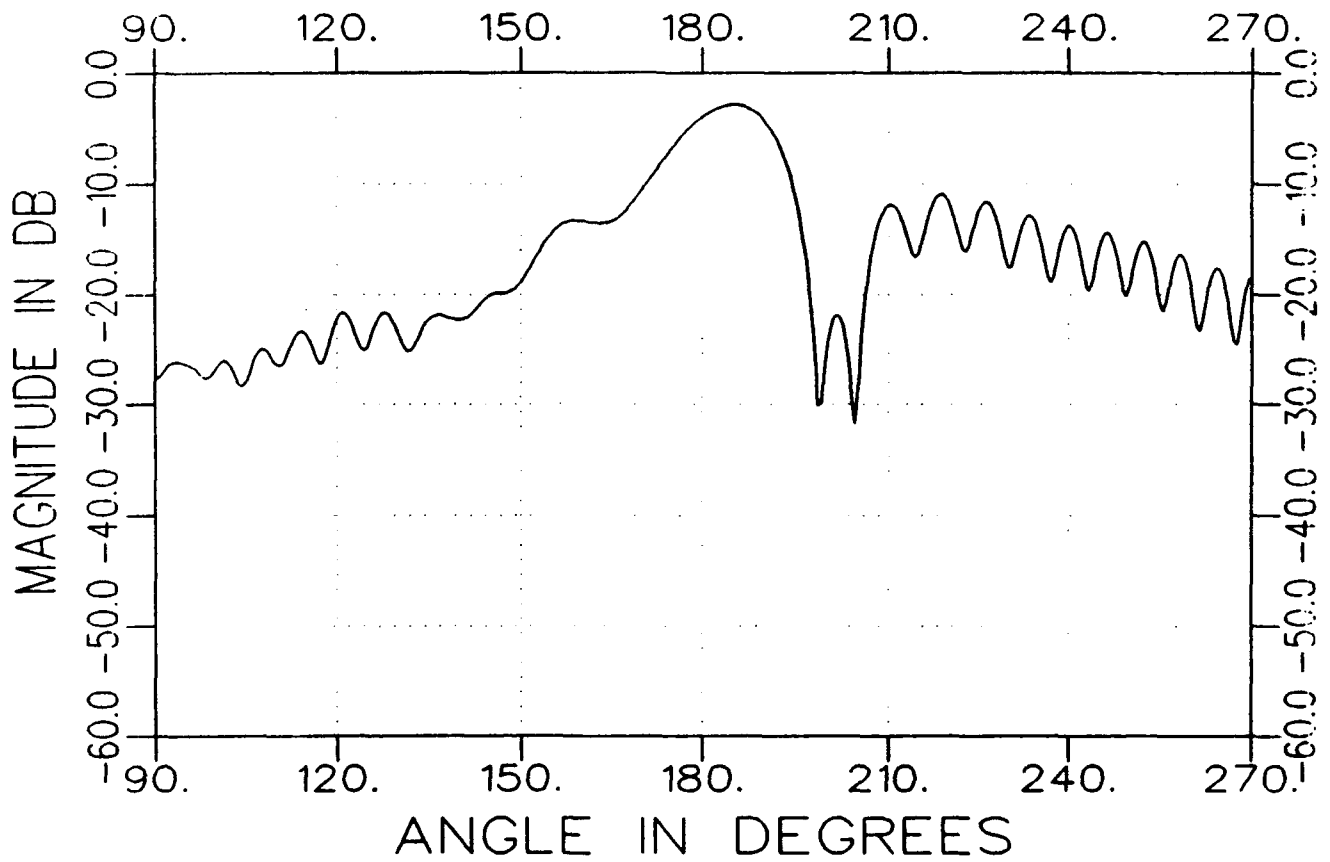
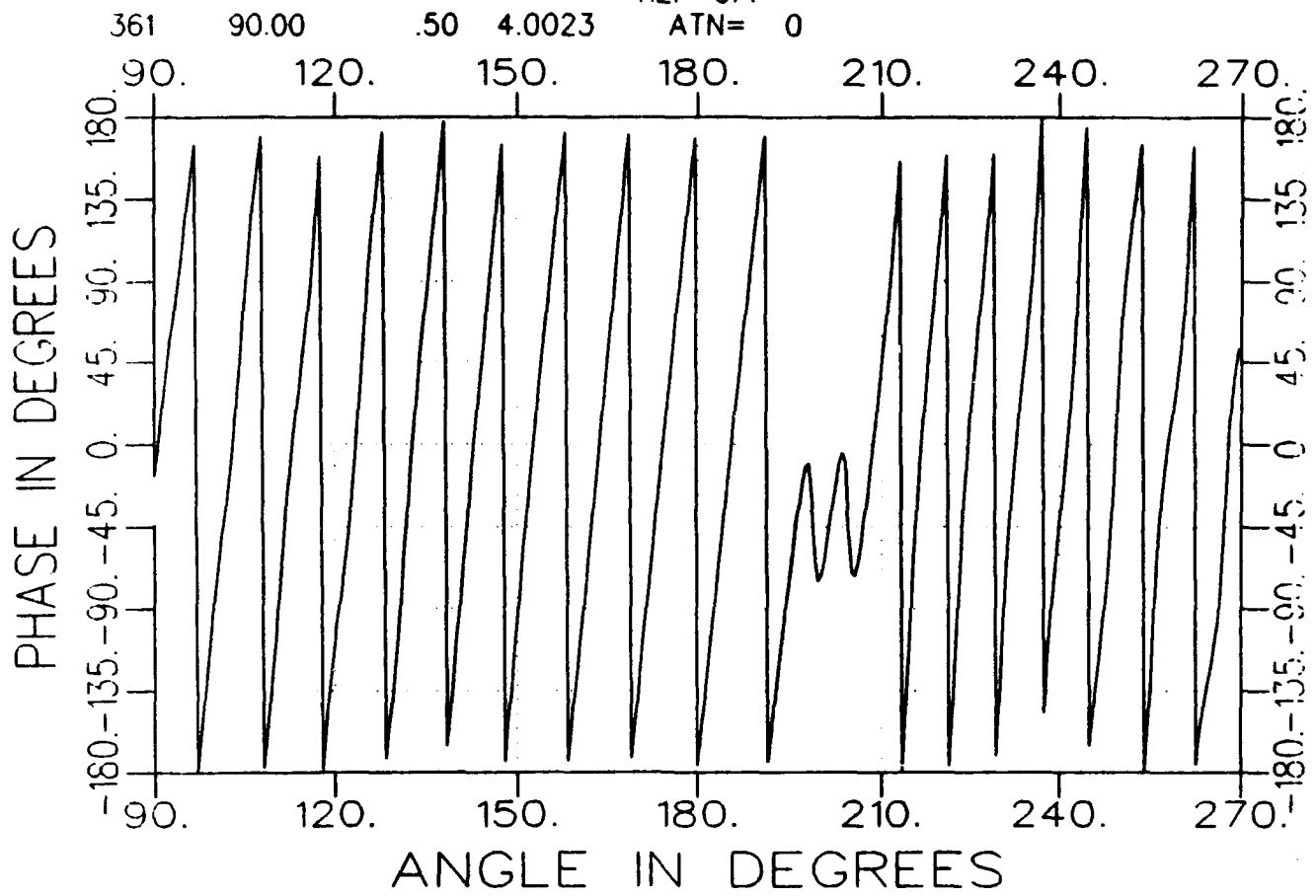


a3225ah0400-a.tar  
TARGET

AZIM. 08/13/93 10:33  
cap grid

AVE= 82  
REF=OFF

ATN= 0



a3225ah0600-a.tar  
TARGET

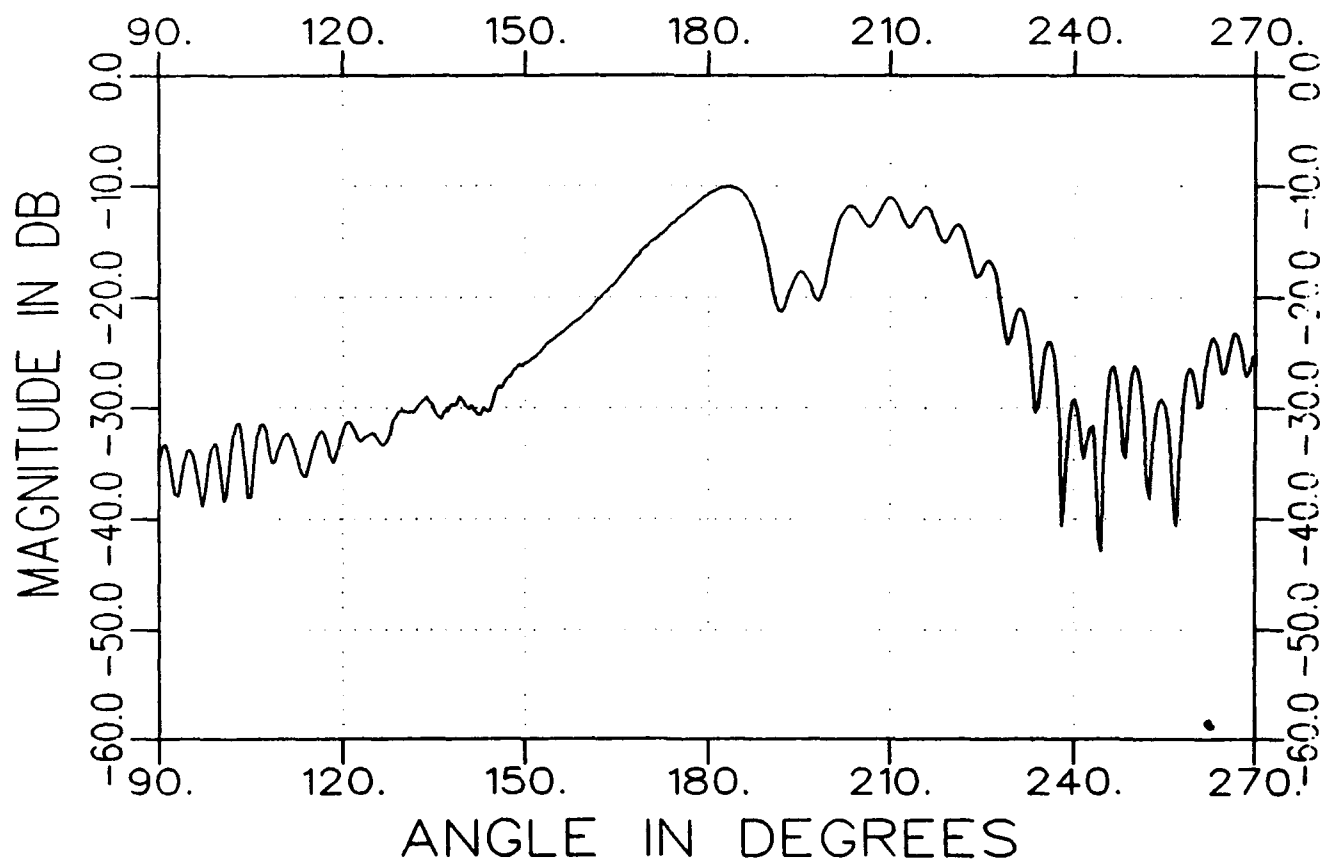
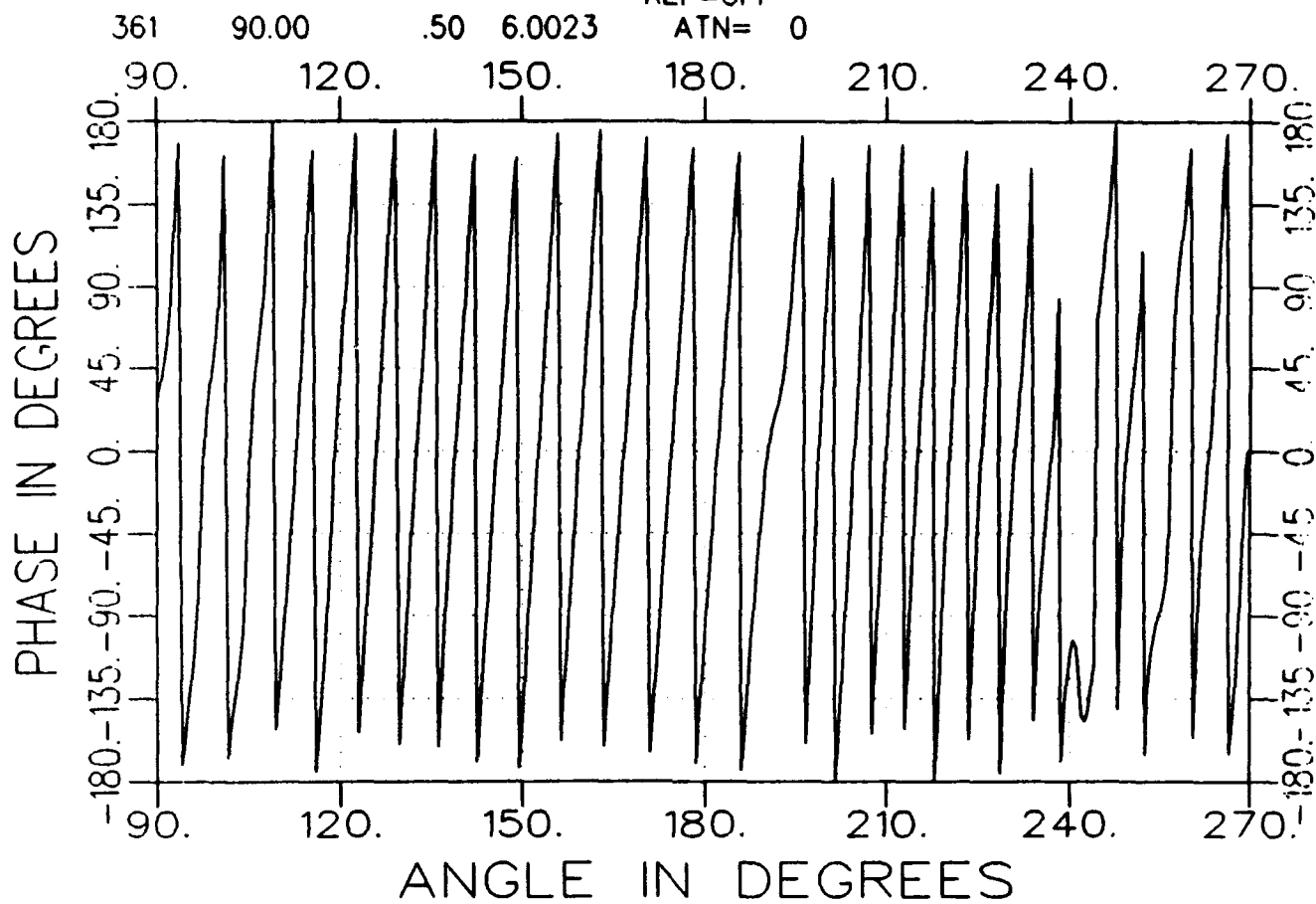
cap grid

AZIM. 08/13/93 10:35

AVE= 82

REF=OFF

ATN= 0



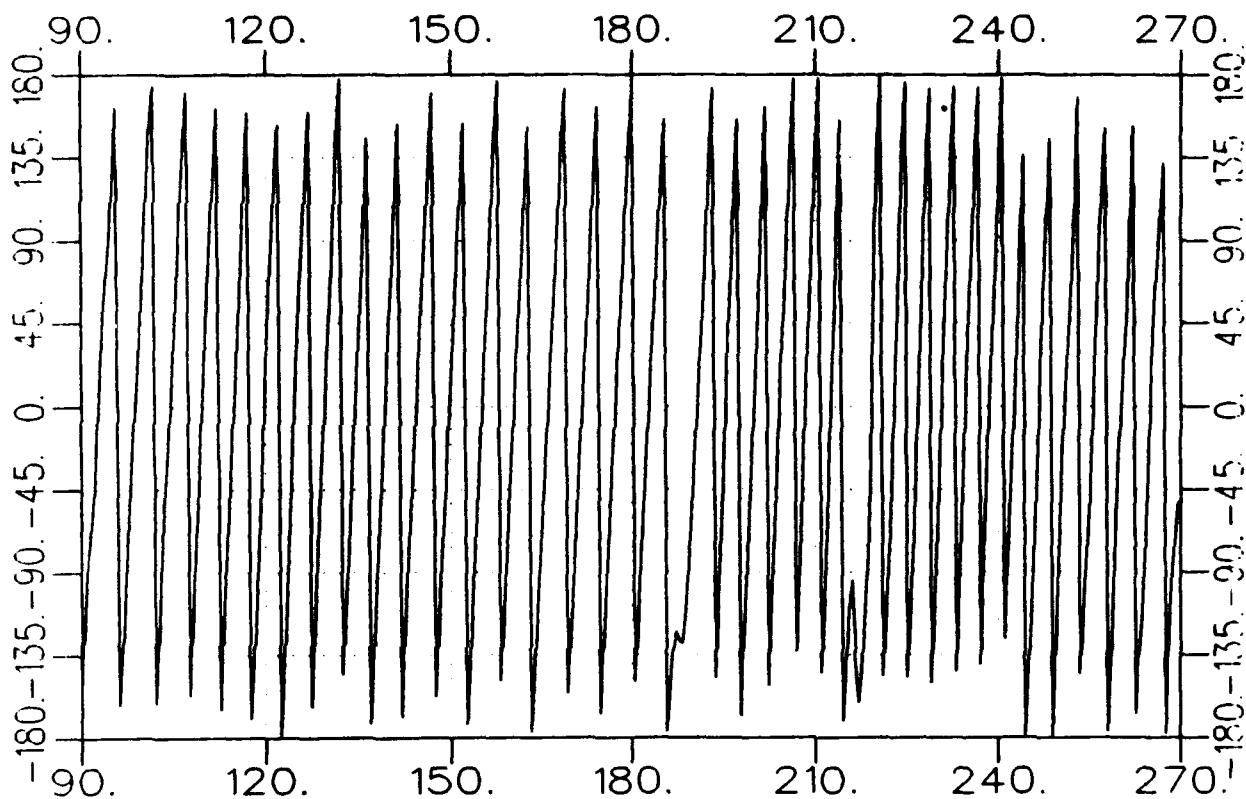
a3225ah0800-a.tar  
TARGET

AZIM. 08/13/93 10:37  
cap grid

AVE= 82  
REF=OFF  
ATN= 0

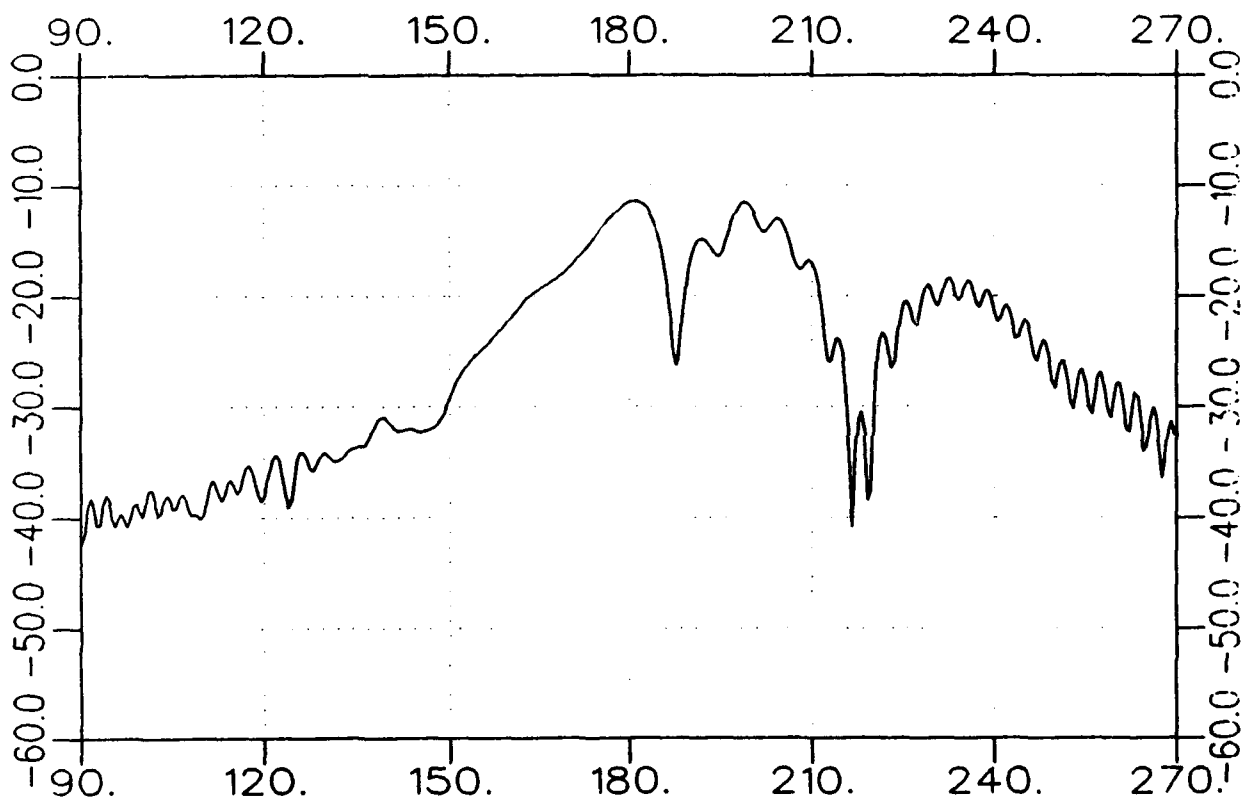
361 90.00 .50 8.0023

PHASE IN DEGREES



ANGLE IN DEGREES

MAGNITUDE IN DB



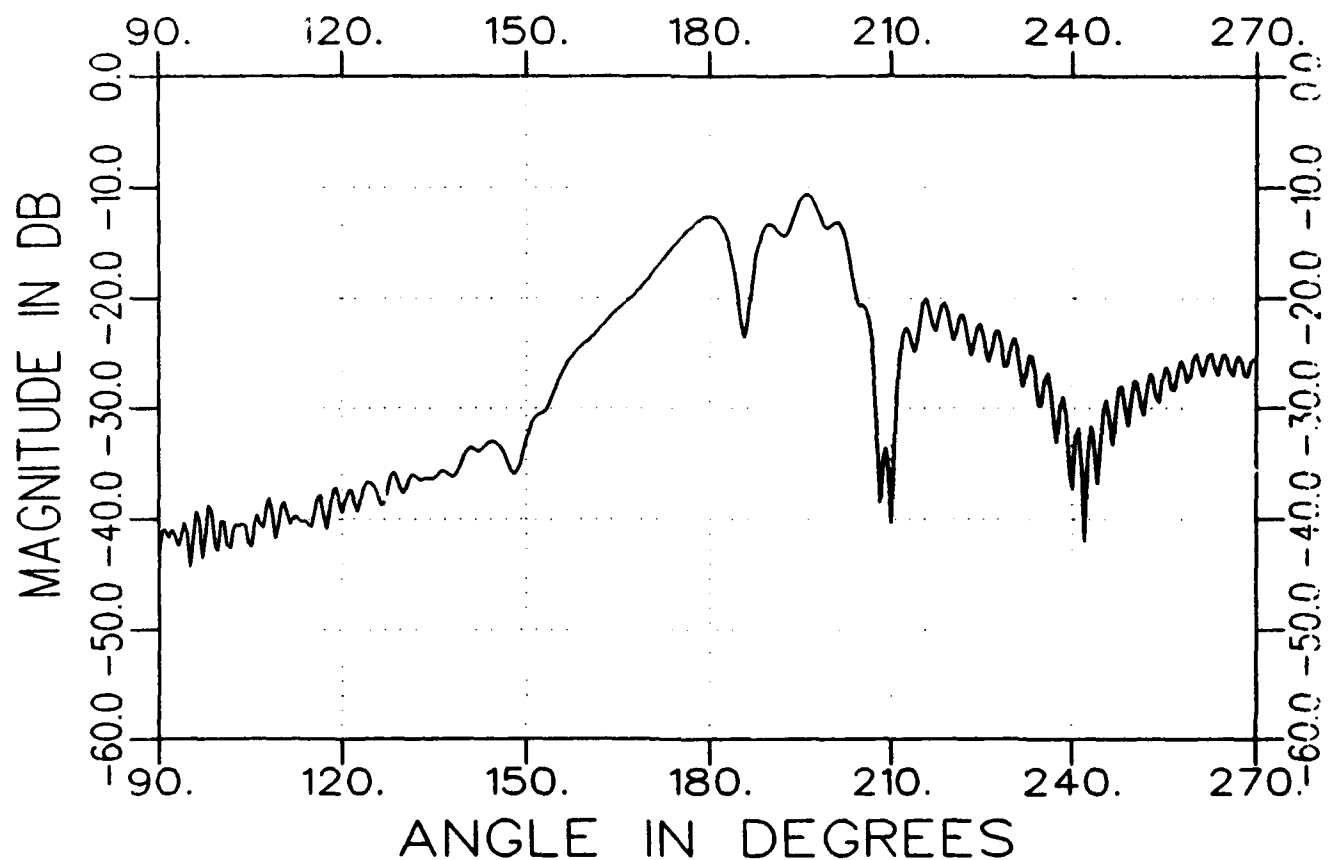
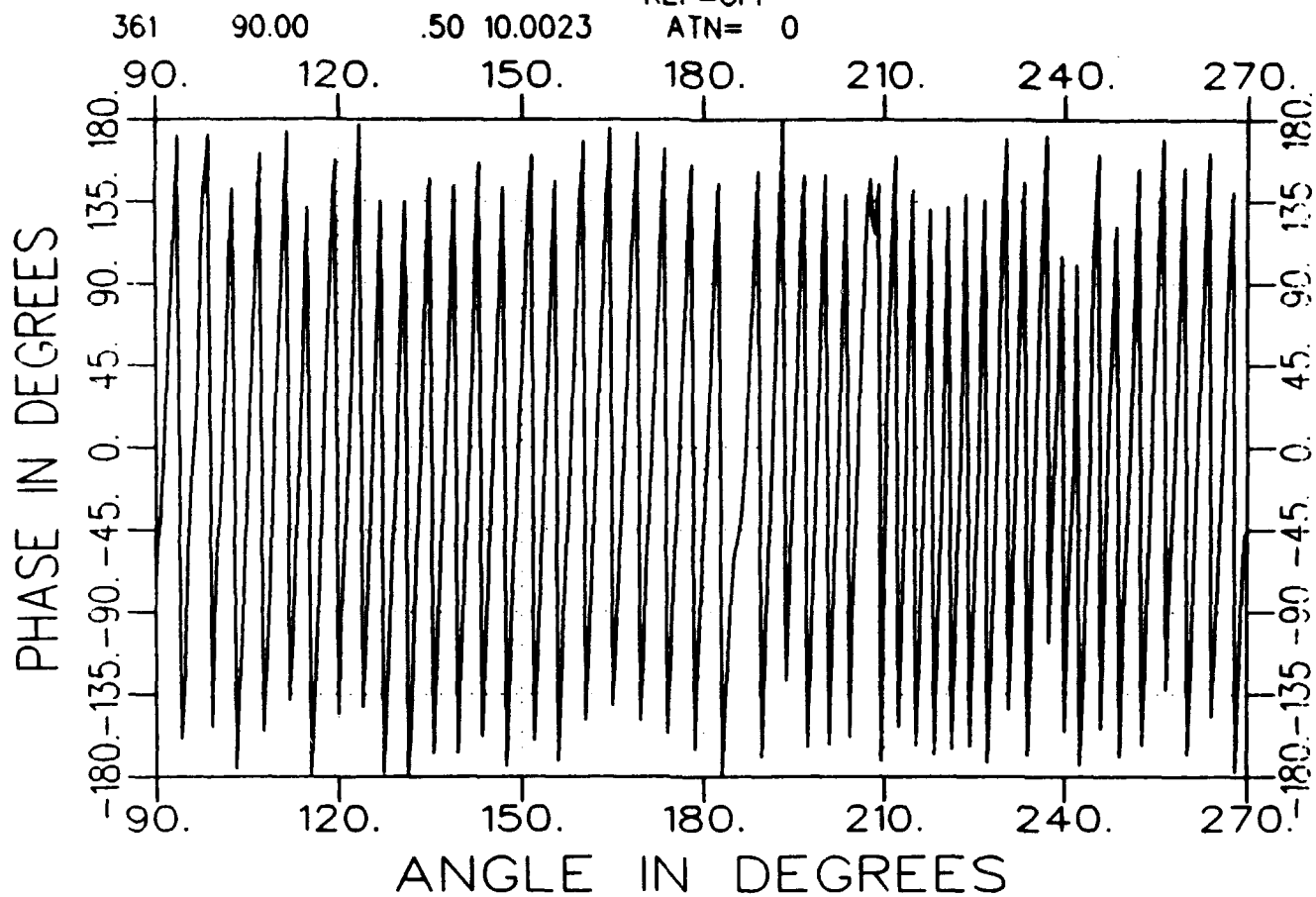
ANGLE IN DEGREES

a3225ah1000-a.tar  
TARGET

AZIM. 08/13/93 10:39  
cap grid

AVE= 82  
REF=OFF

ATN= 0

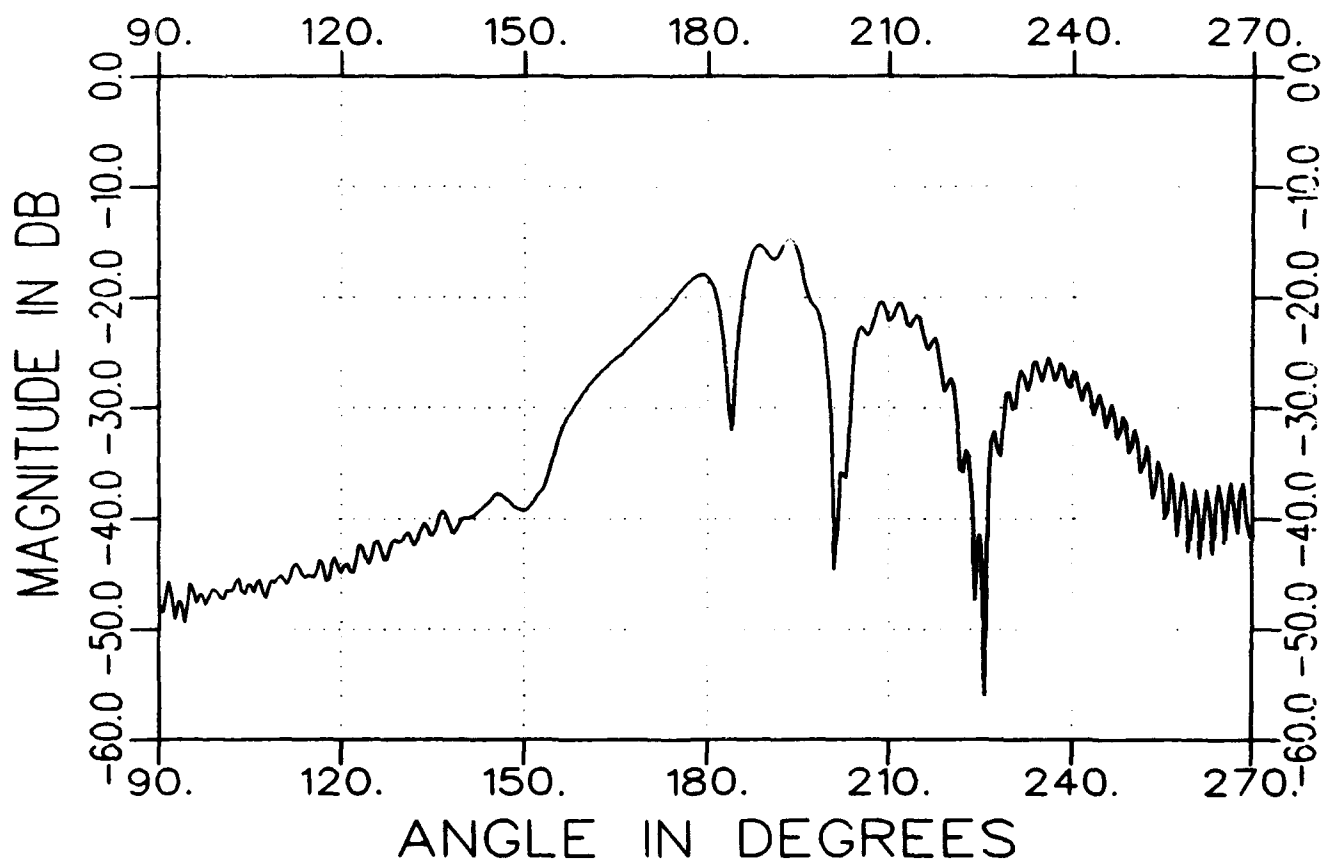
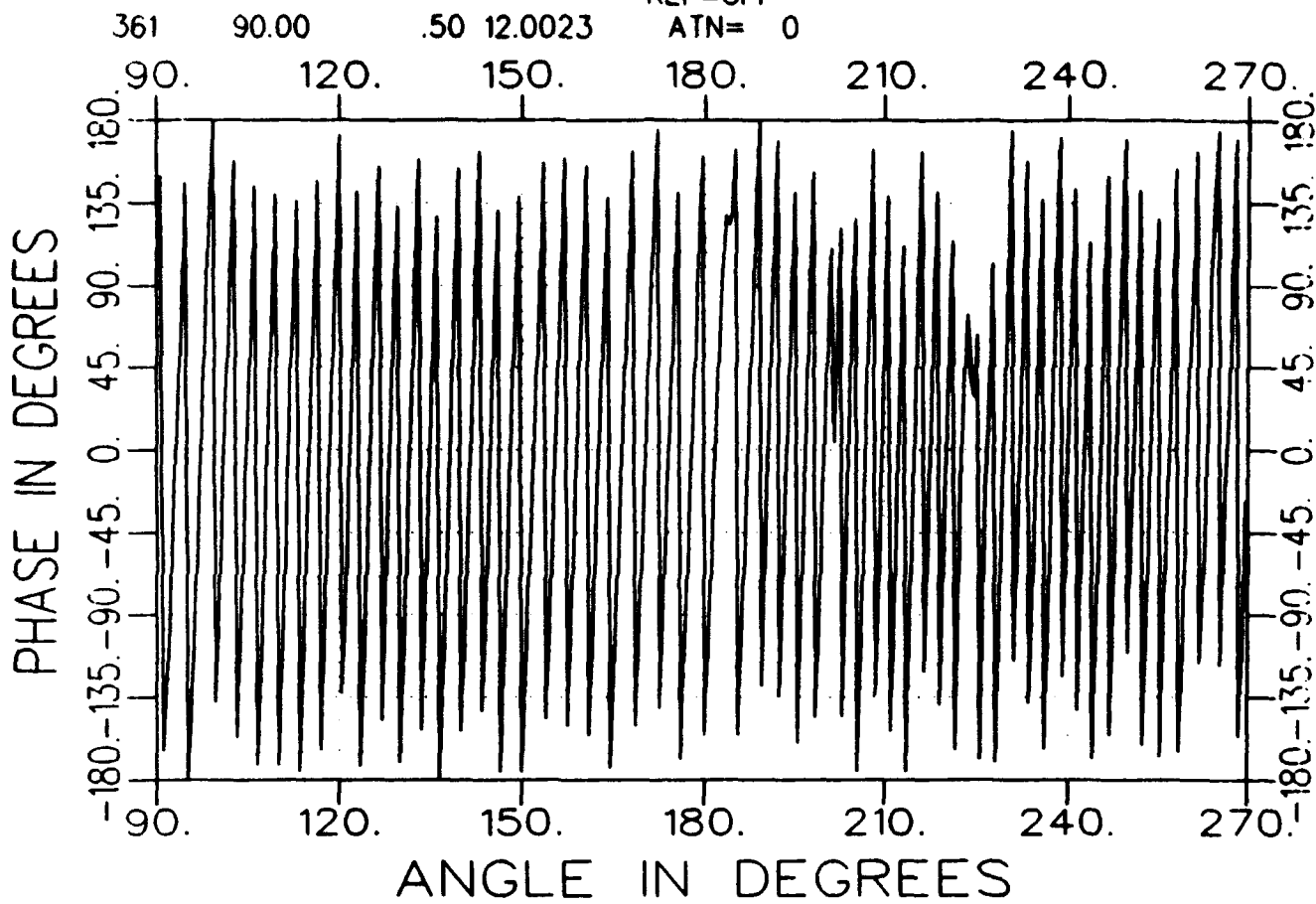


a3225ah1200-a.tar  
TARGET

AZIM. 08/13/93 10:41  
cap grid

AVE= 82  
REF=OFF

ATN= 0



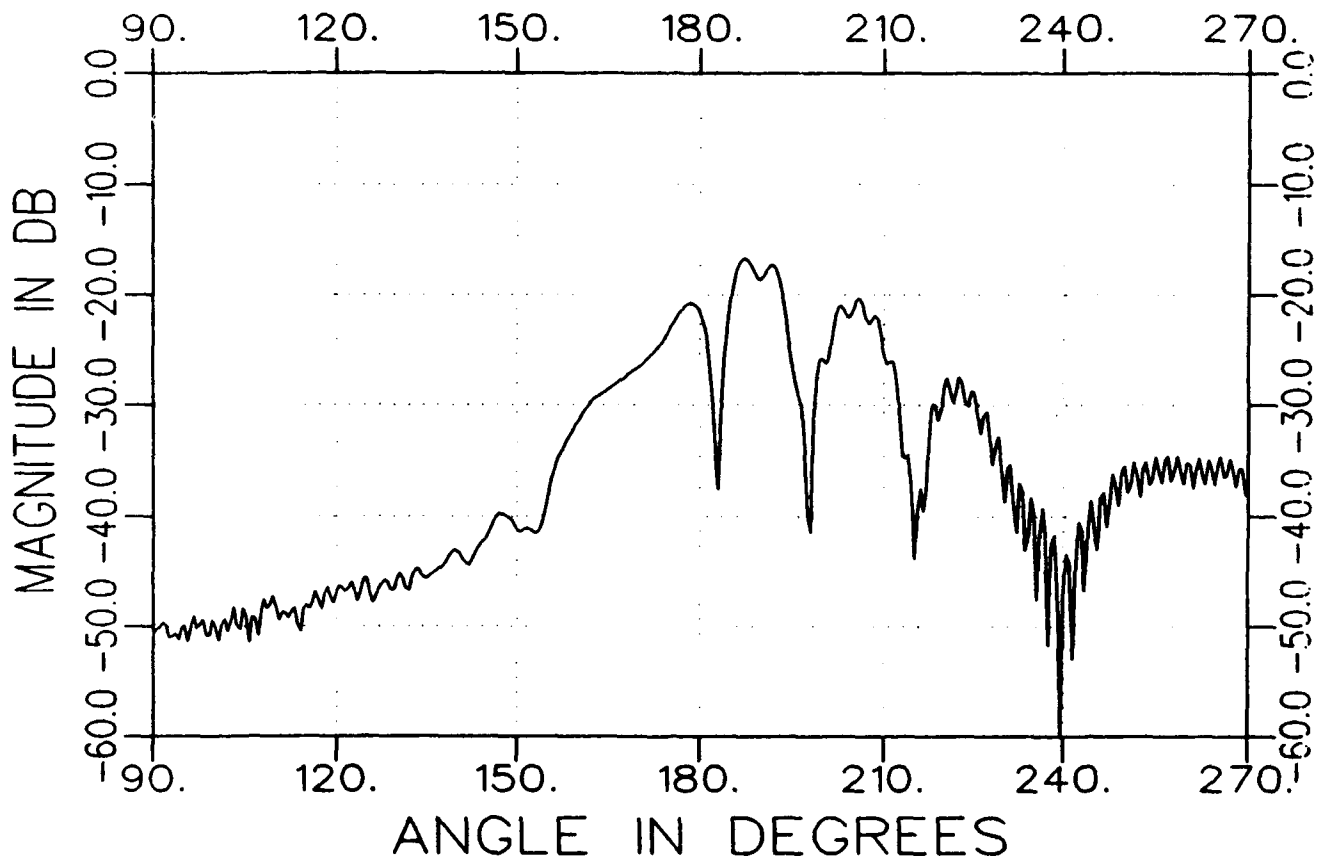
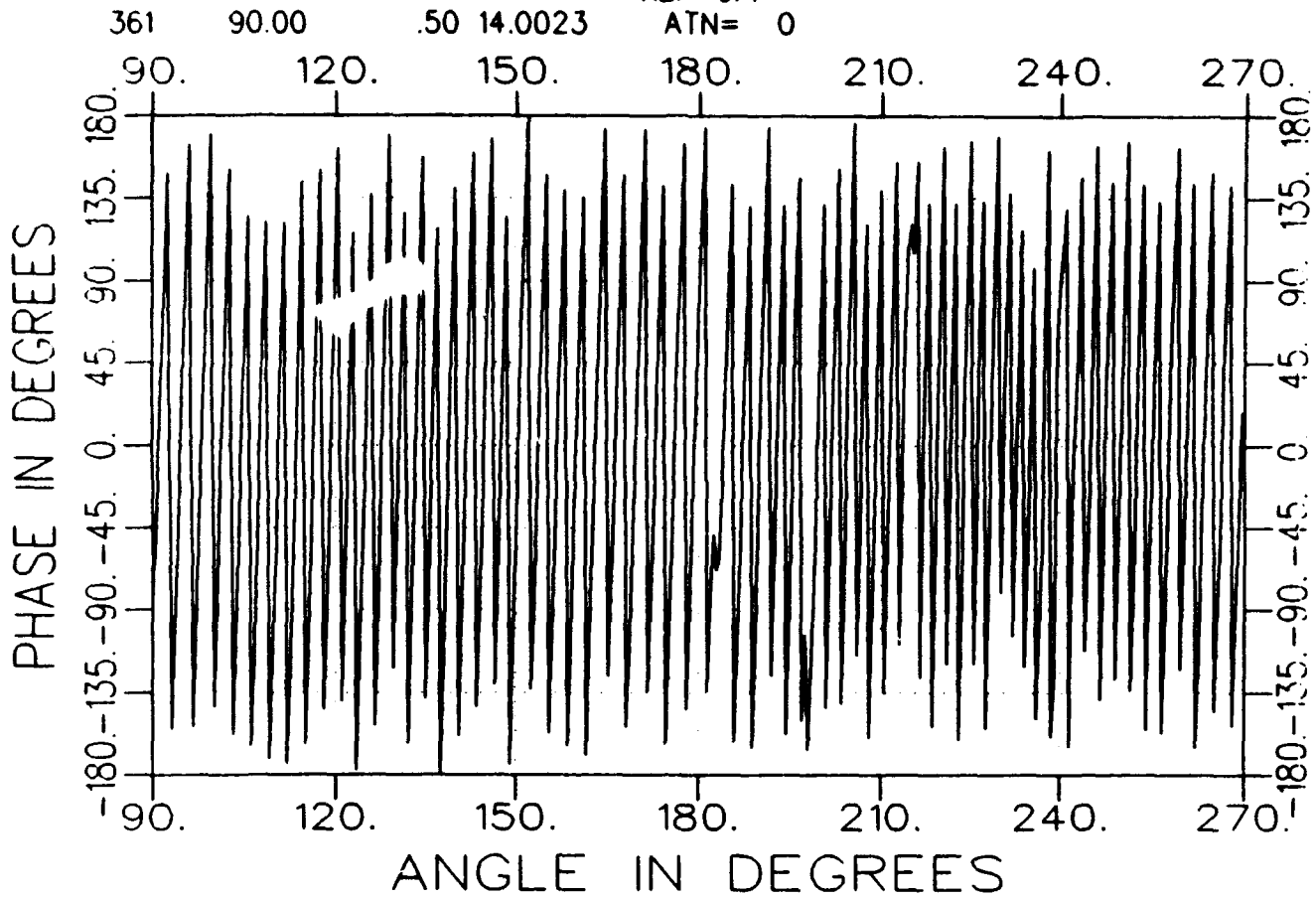


a3225ah1400-a.tar  
TARGET

AZIM. 08/13/93 10:43  
cap grid

AVE= 82  
REF=OFF

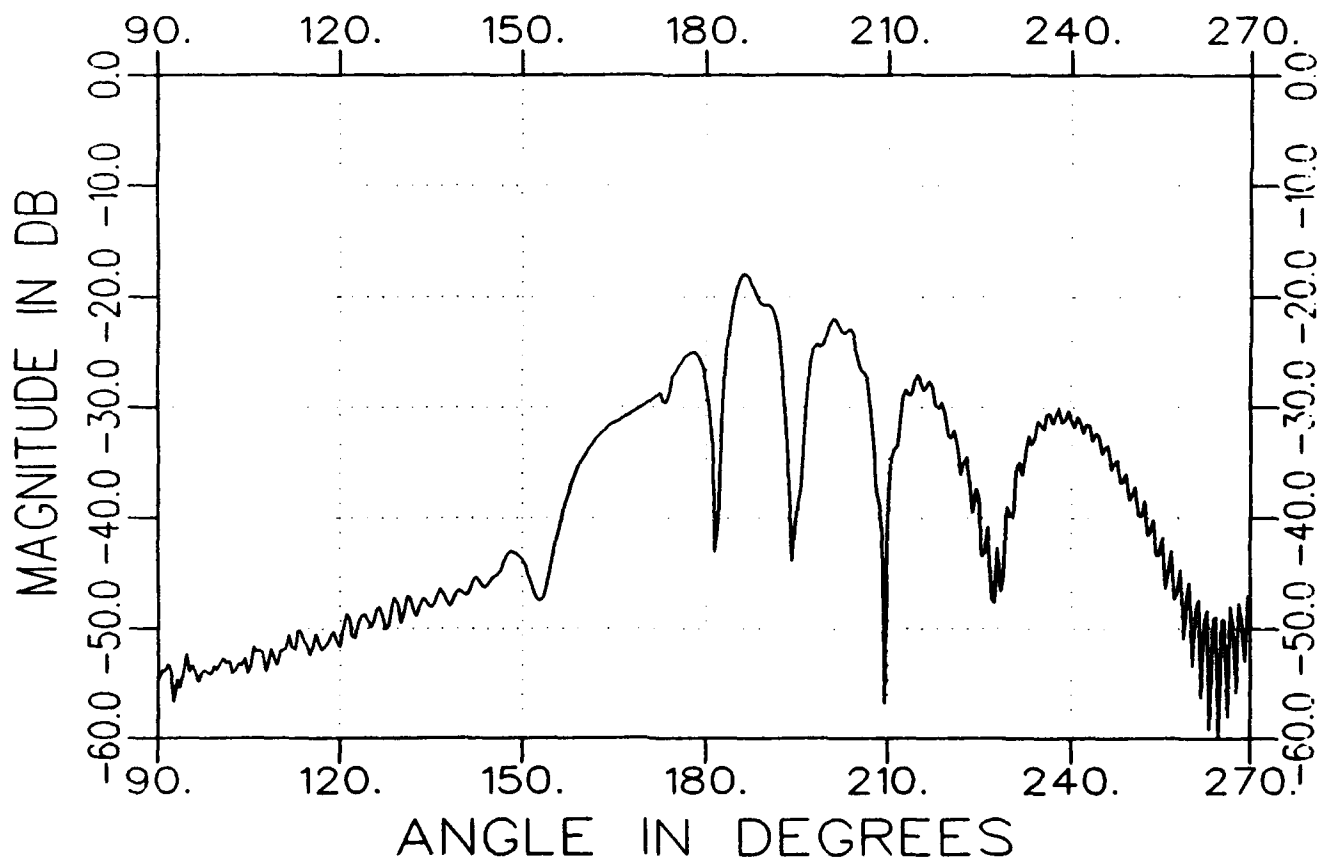
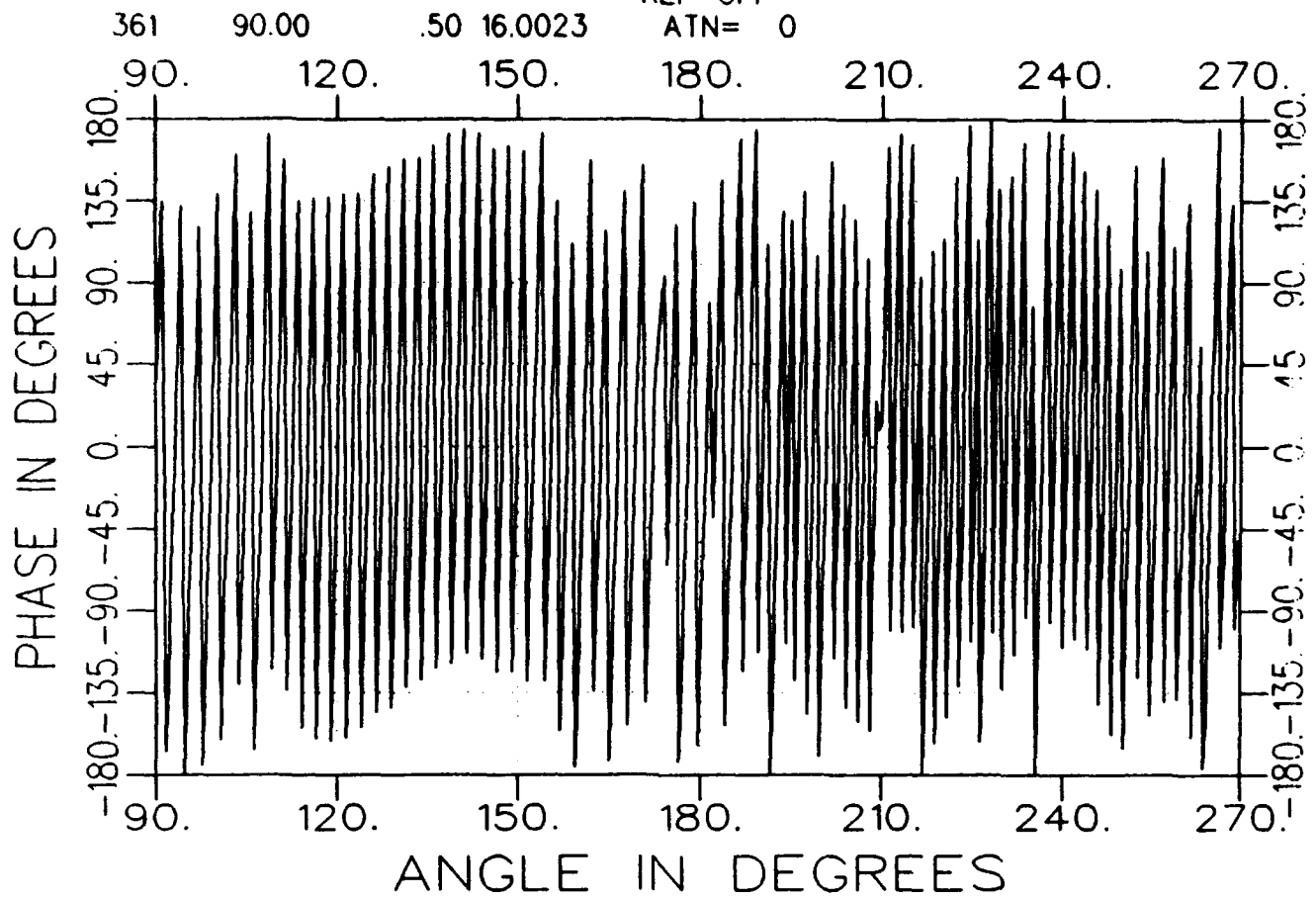
ATN= 0



a3225ah1600-a.tar  
TARGET

AZIM. 08/13/93 10:45  
cap grid

AVE= 82  
REF=OFF  
ATN= 0

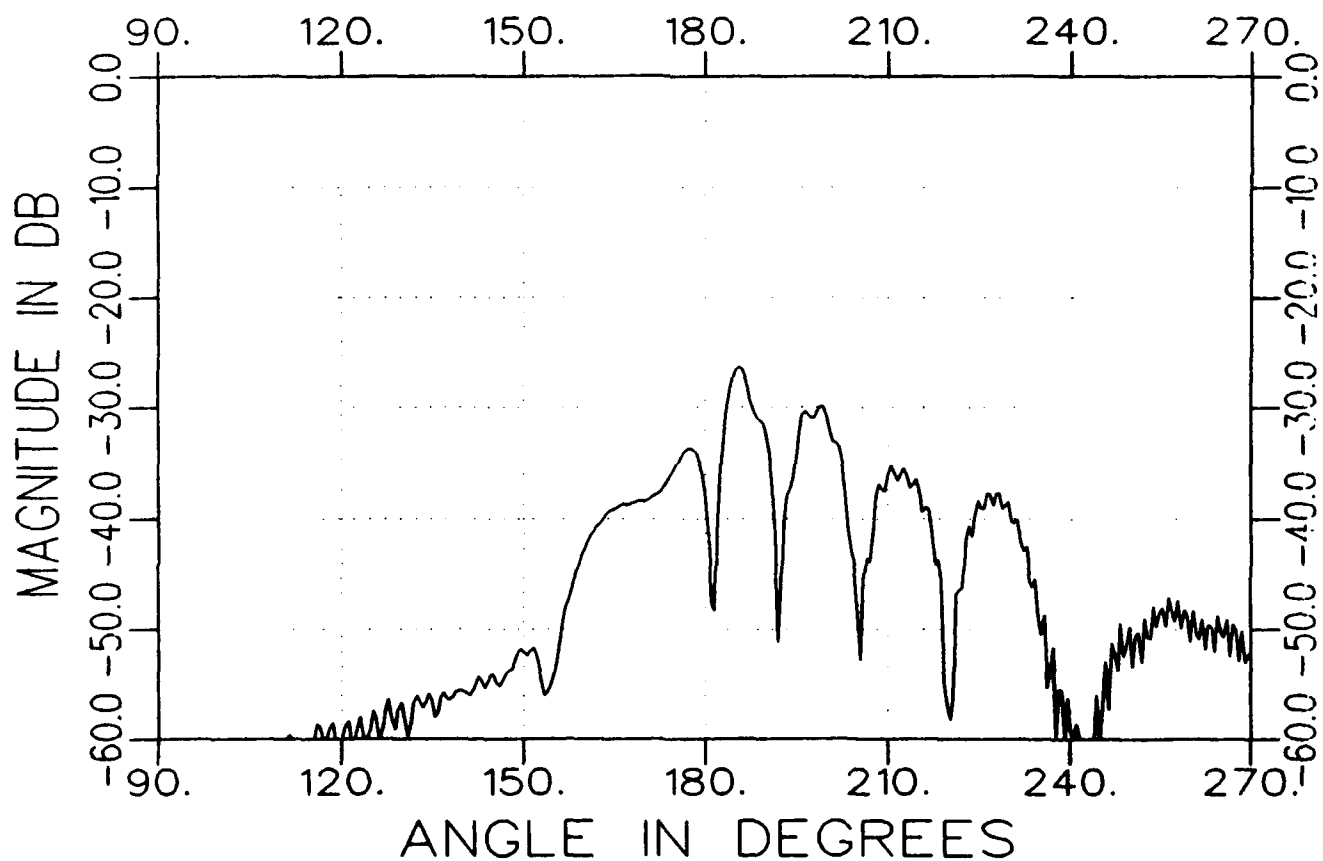
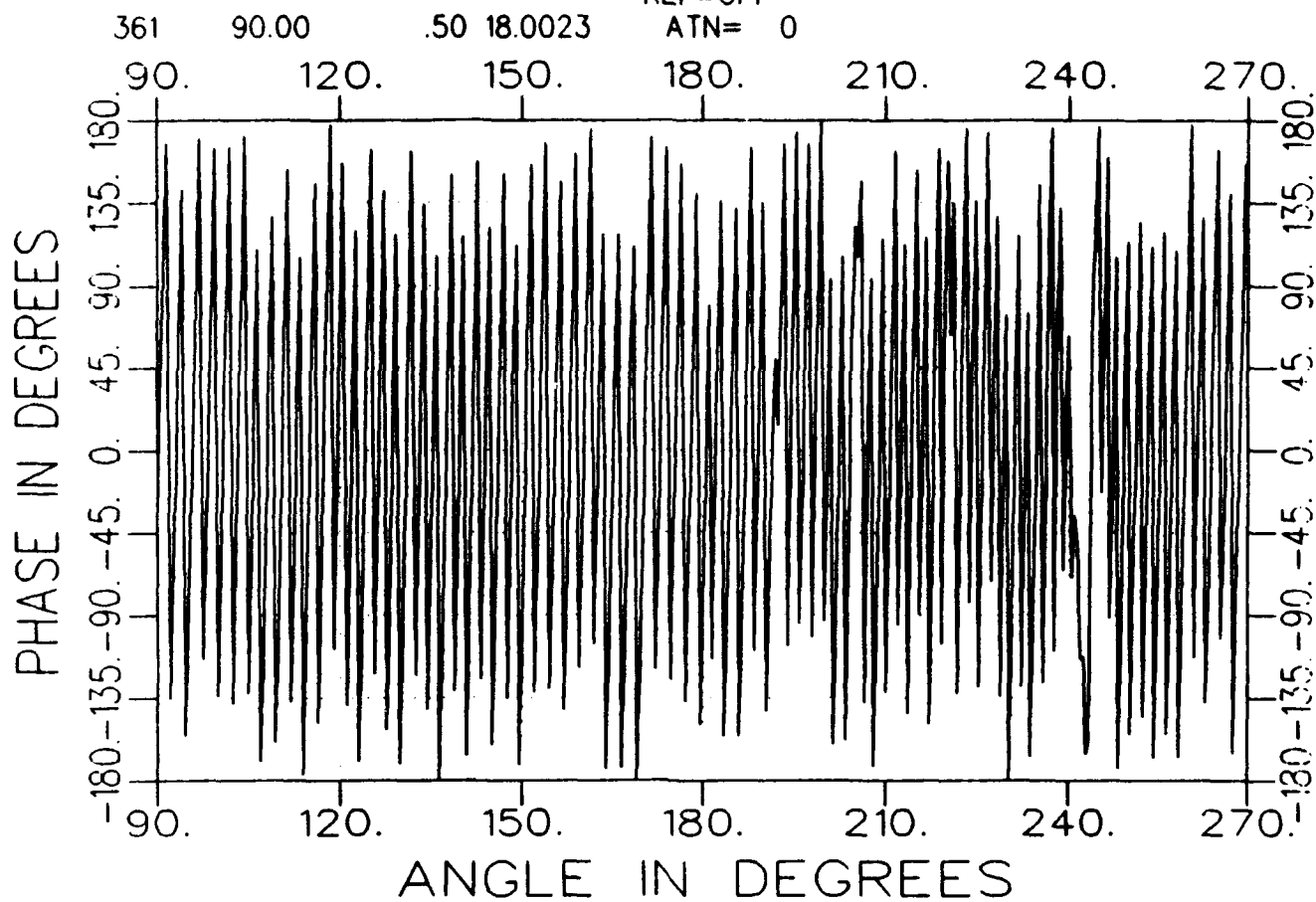


a3225ah1800-a.tar  
TARGET

AZIM. 08/13/93 10:47  
cap grid

AVE= 82  
REF=OFF

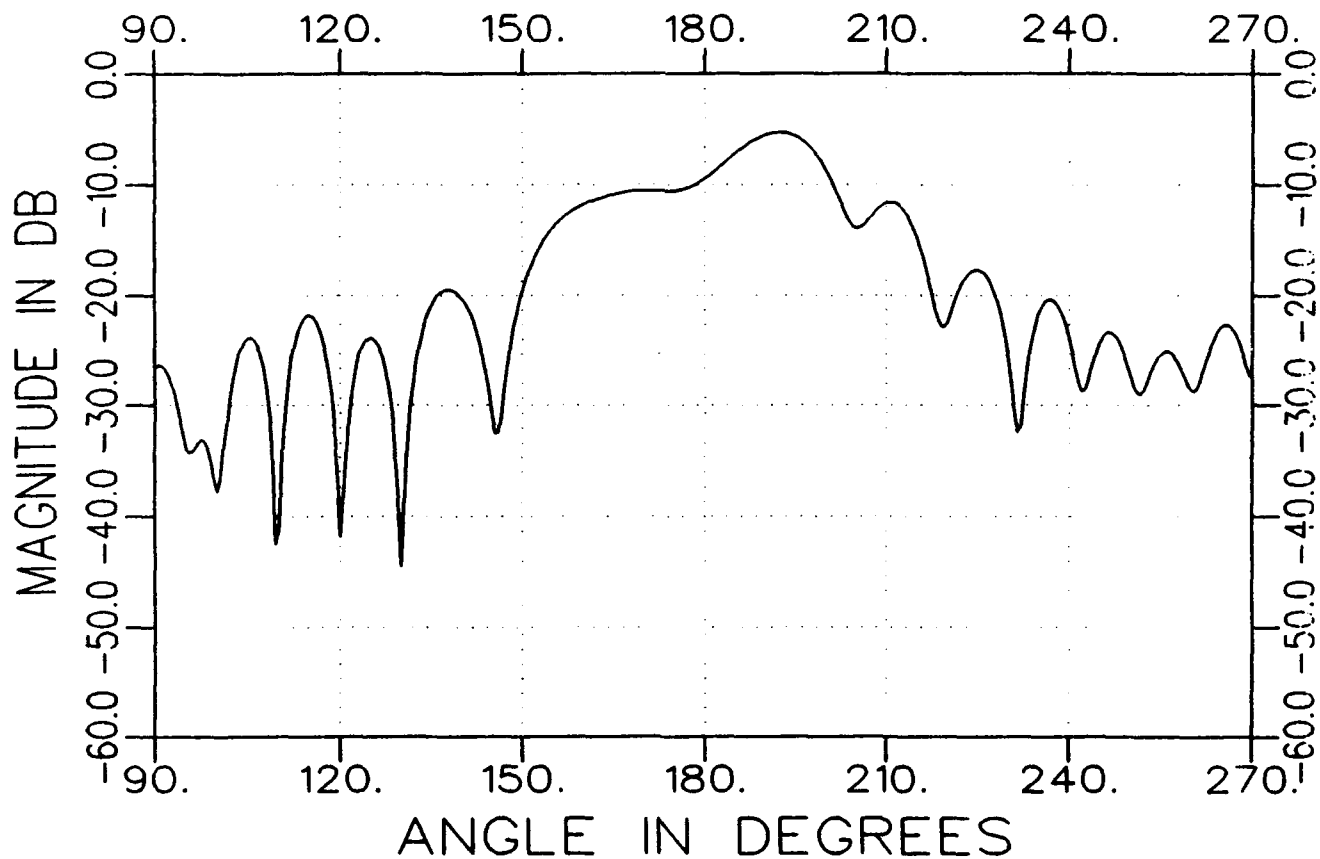
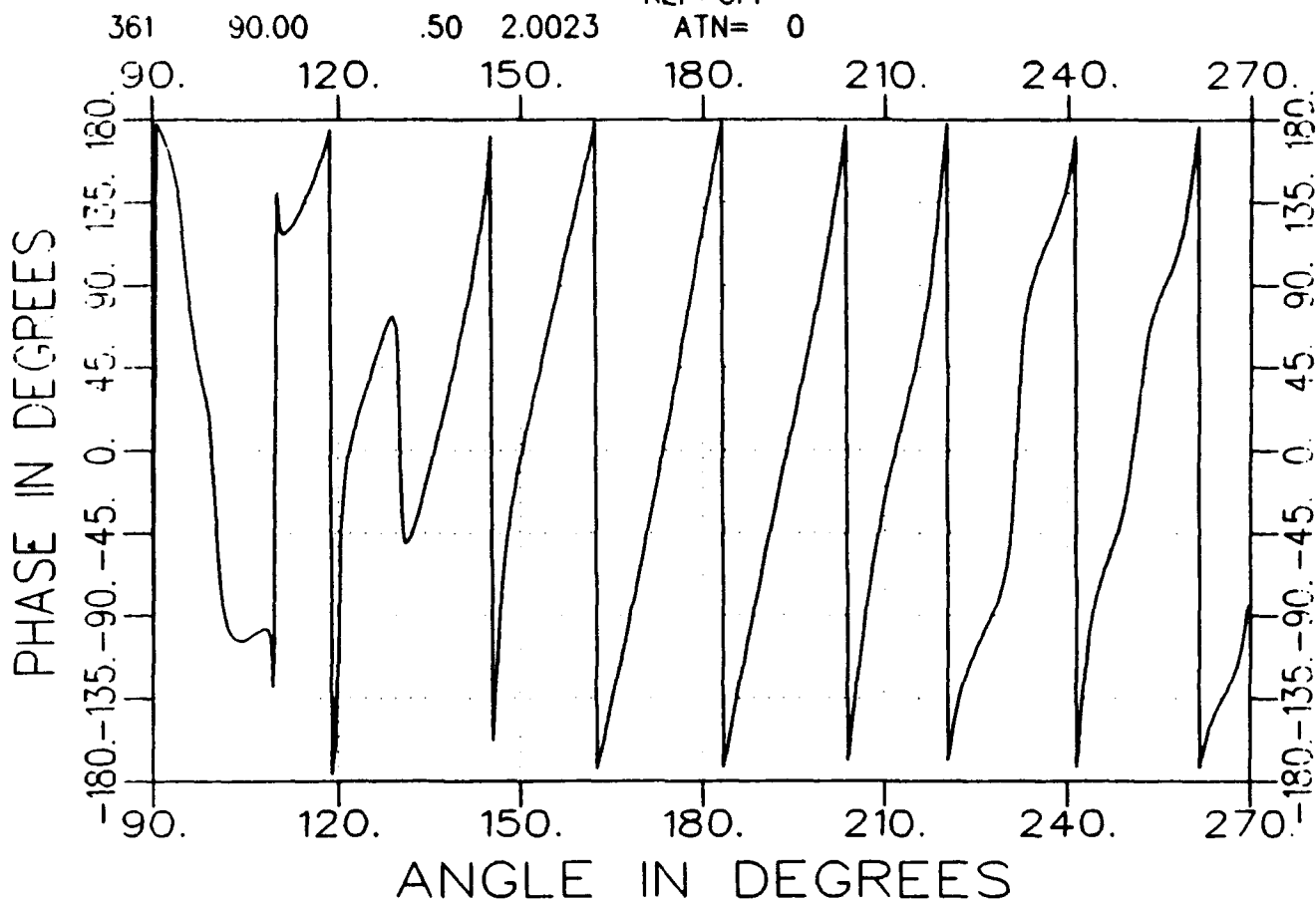
ATN= 0



b3225ah0200-a.tar  
TARGET

AZIM. 08/13/93 12:01  
long cap grid AVE= 82  
REF=OFF

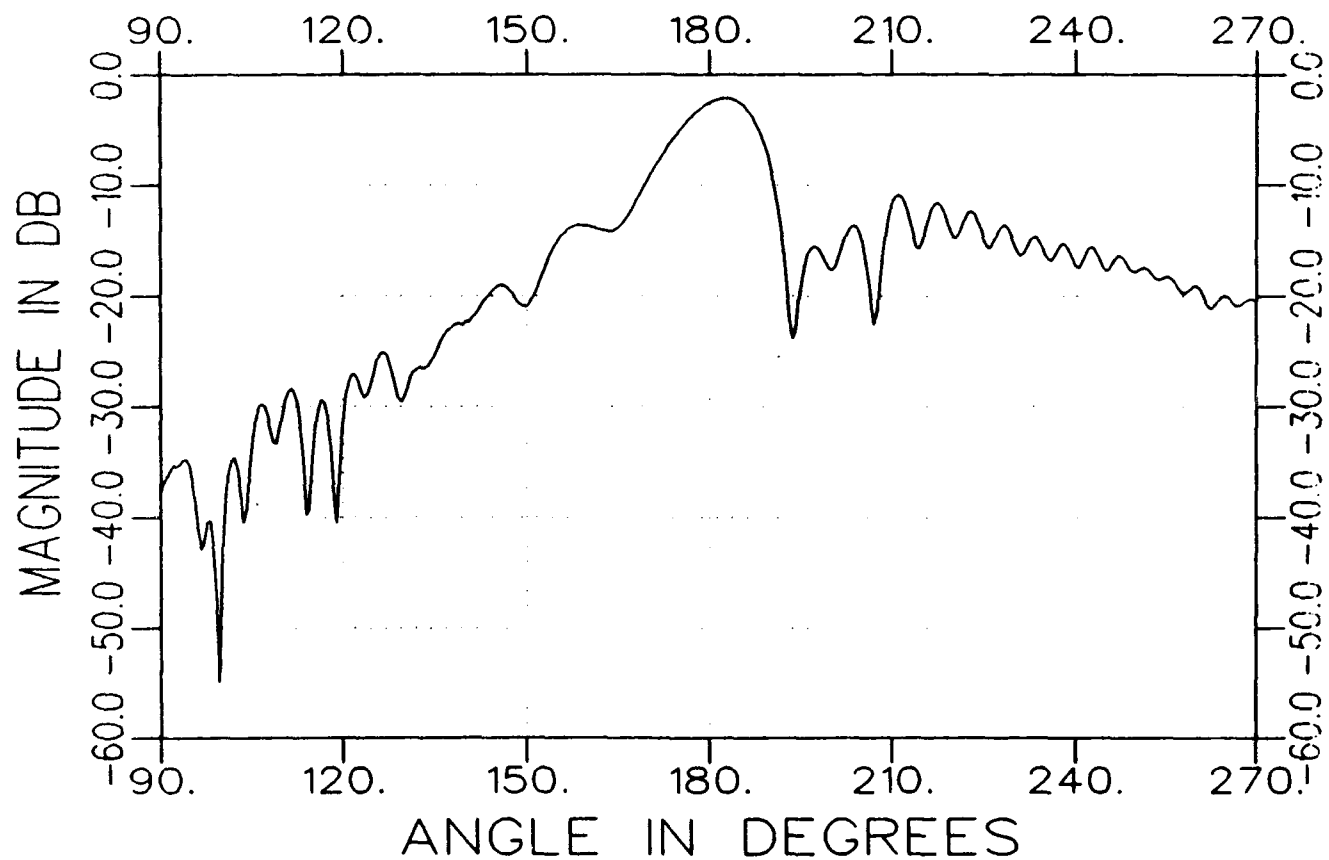
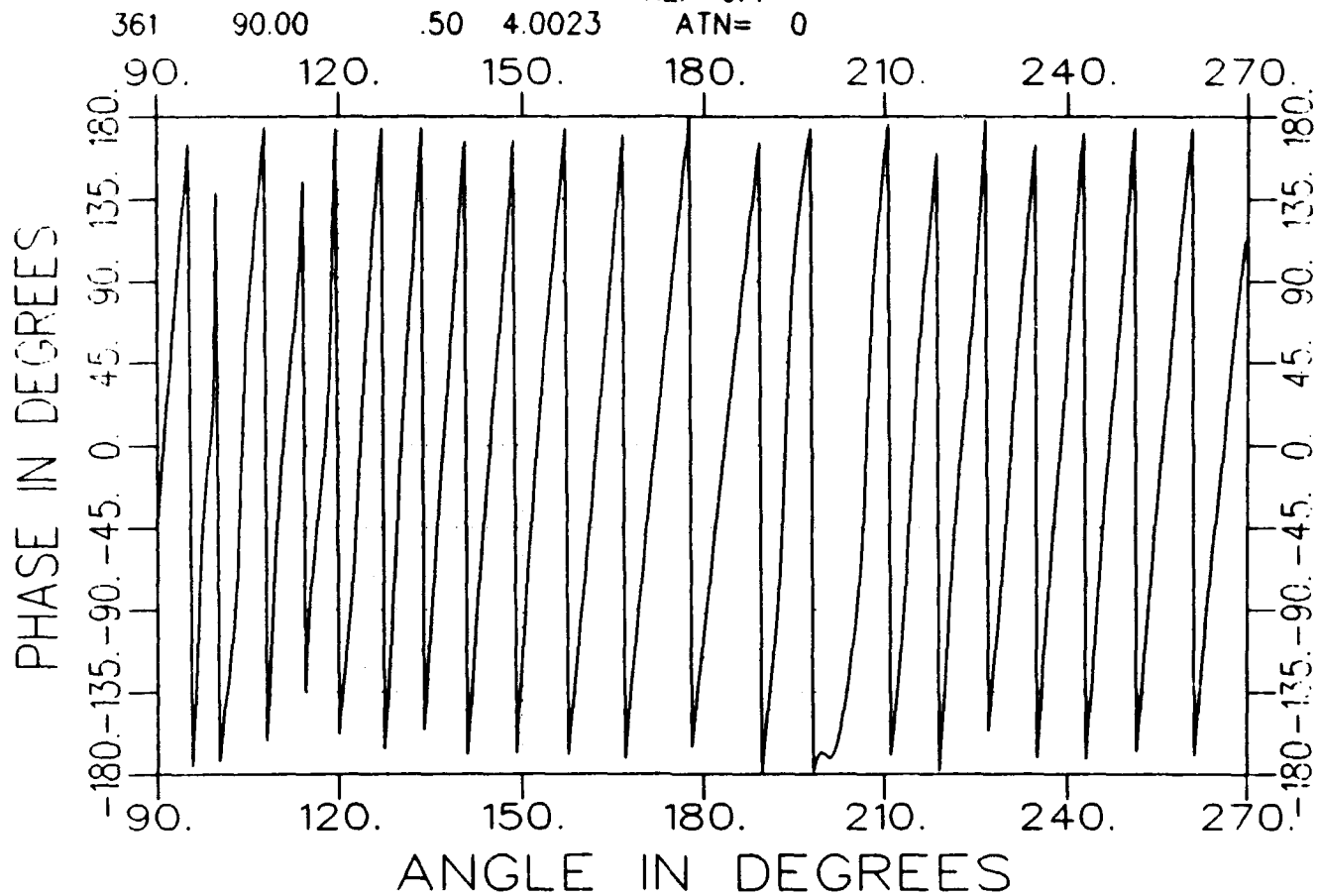
ATN= 0



b3225ah0400-a.tar  
TARGET

AZIM. 08/13/93 12:03  
long cap grid AVE= 82  
REF=OFF

ATN= 0



b3225ah0600--a.tar  
TARGET

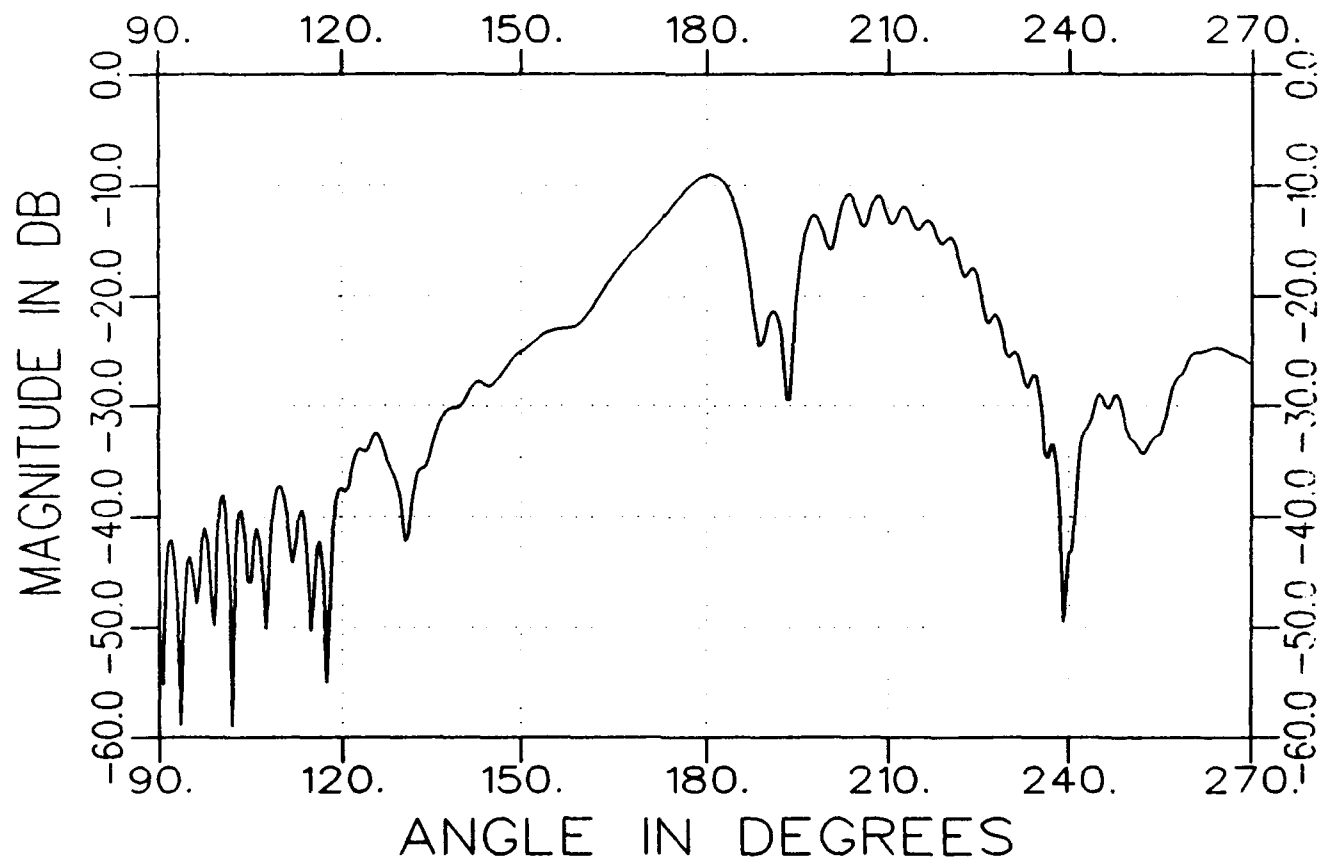
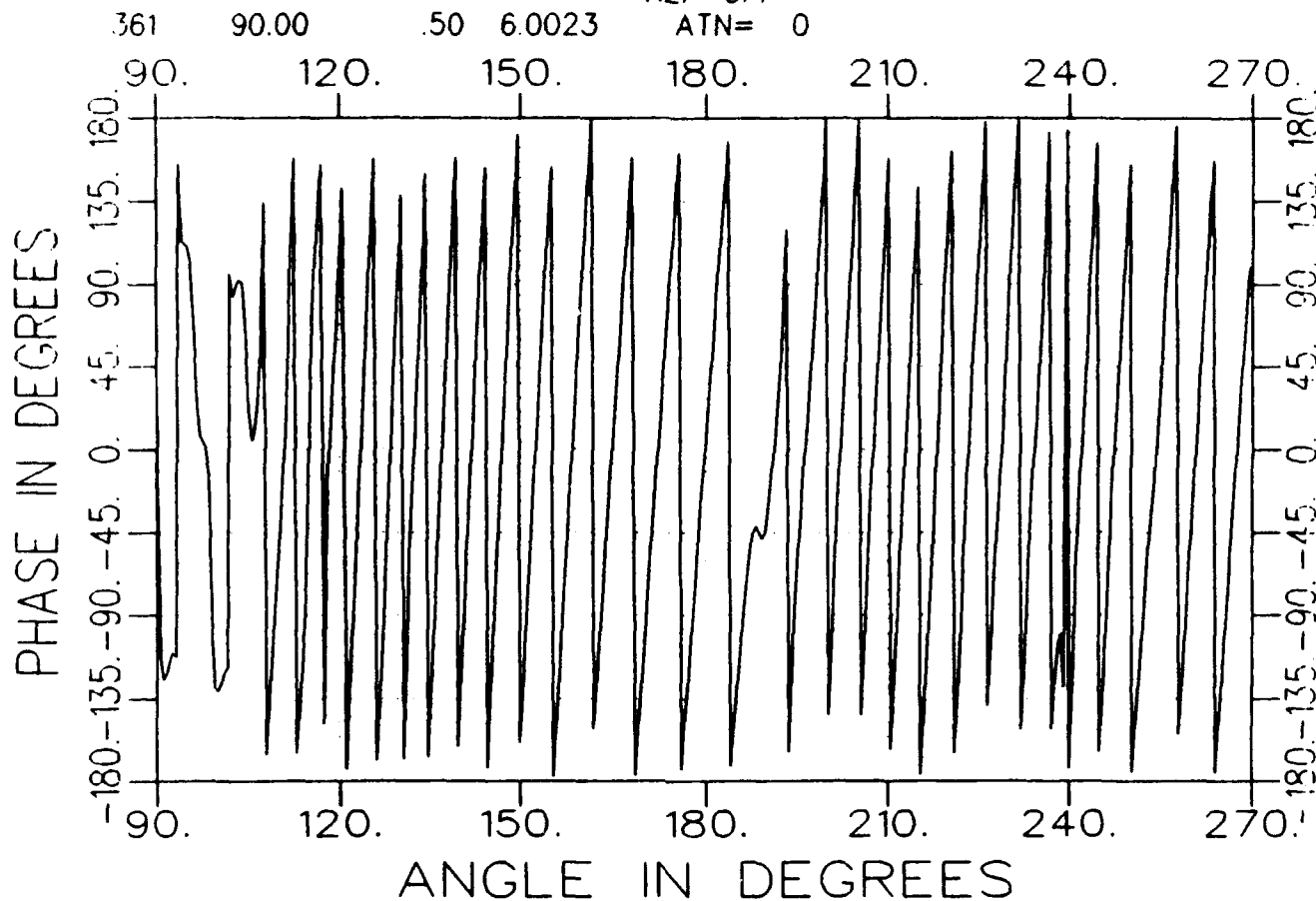
AZIM. 08/13/93 12:05

long cap grid

AVE= 82

REF=OFF

ATN= 0

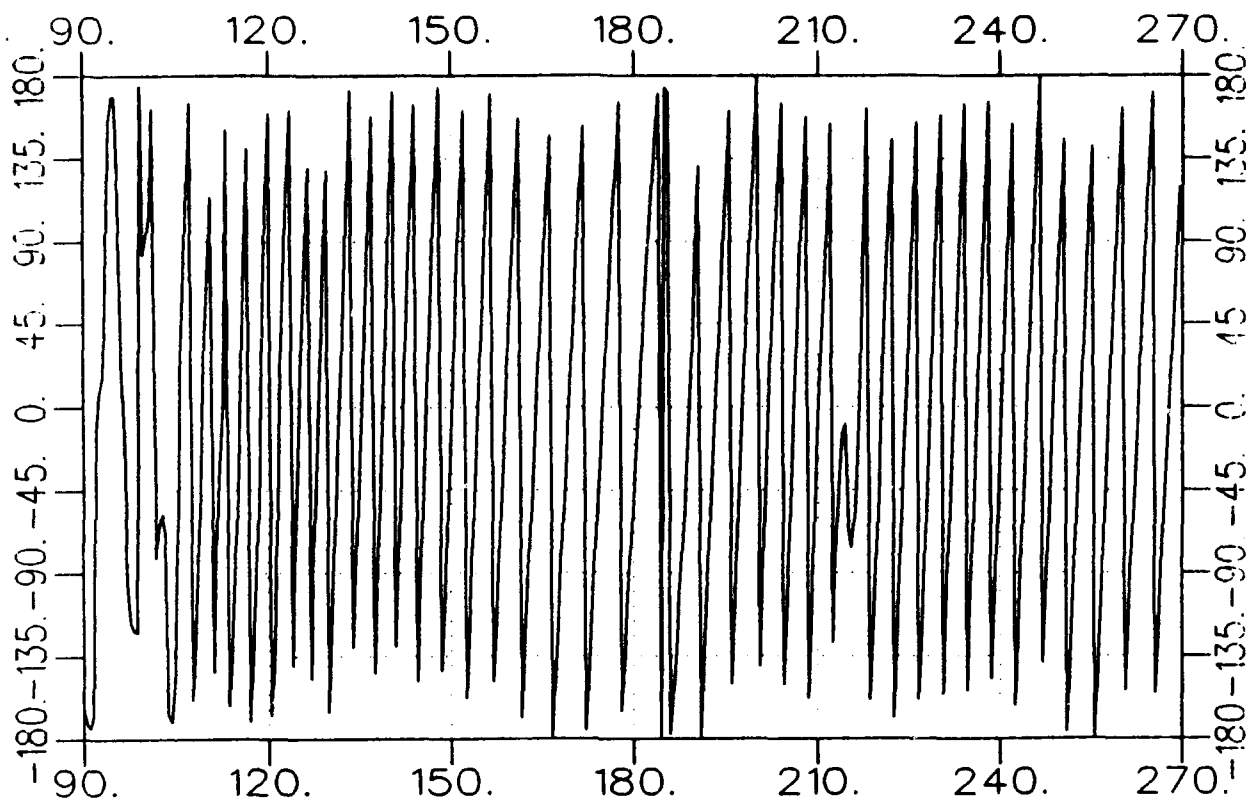


b3225ah0800-a.tar  
TARGET

AZIM. 08/13/93 12:07  
long cap grid AVE= 82  
REF=OFF

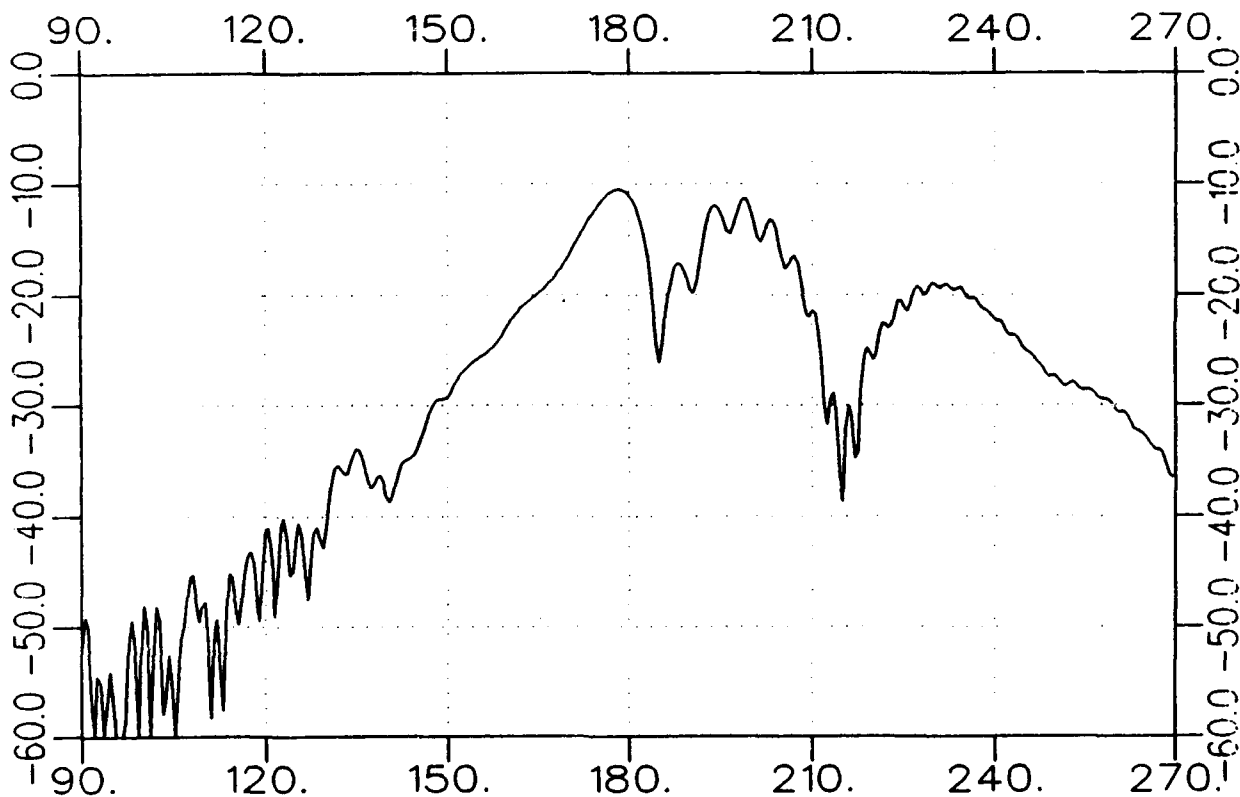
361 90.00 .50 8.0023 ATN= 0

PHASE IN DEGREES



ANGLE IN DEGREES

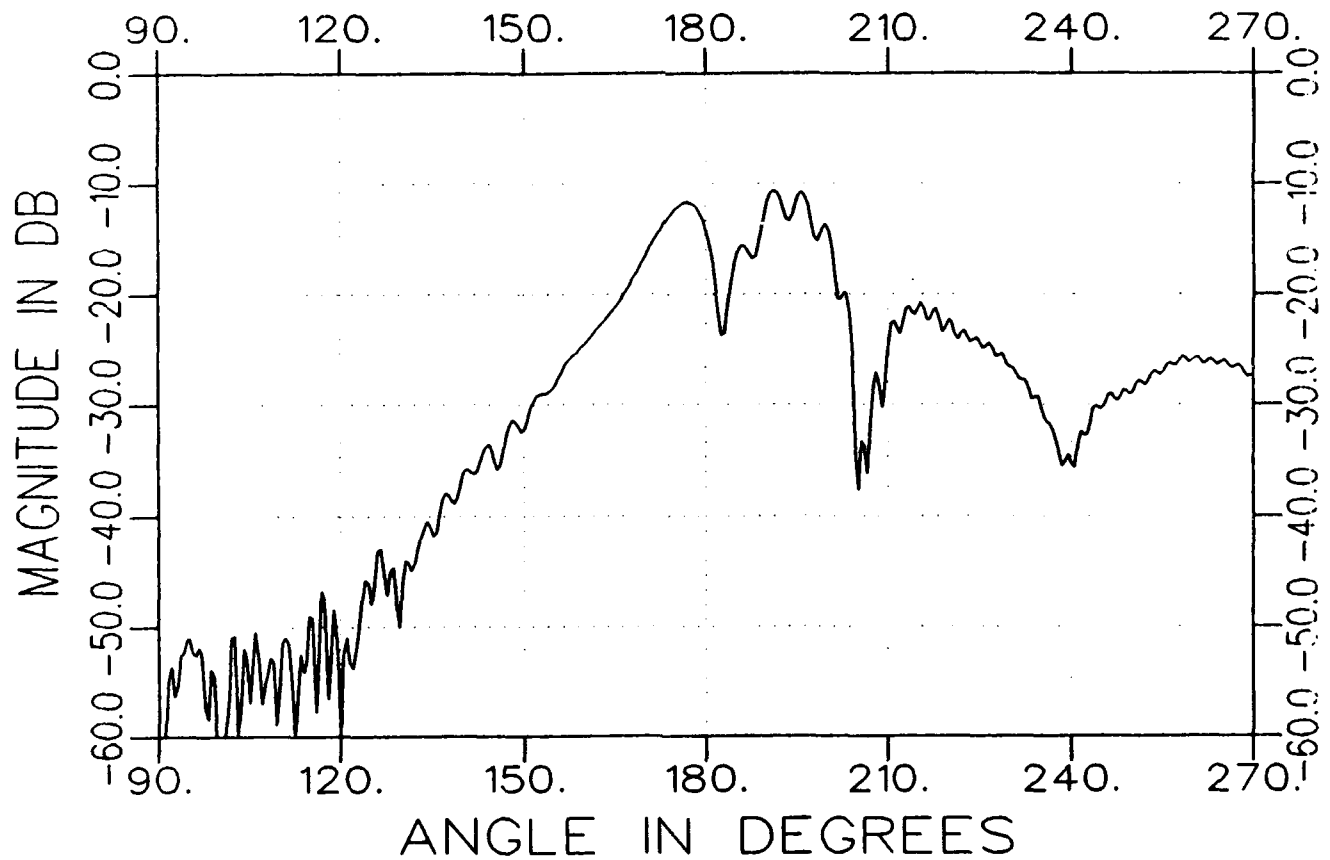
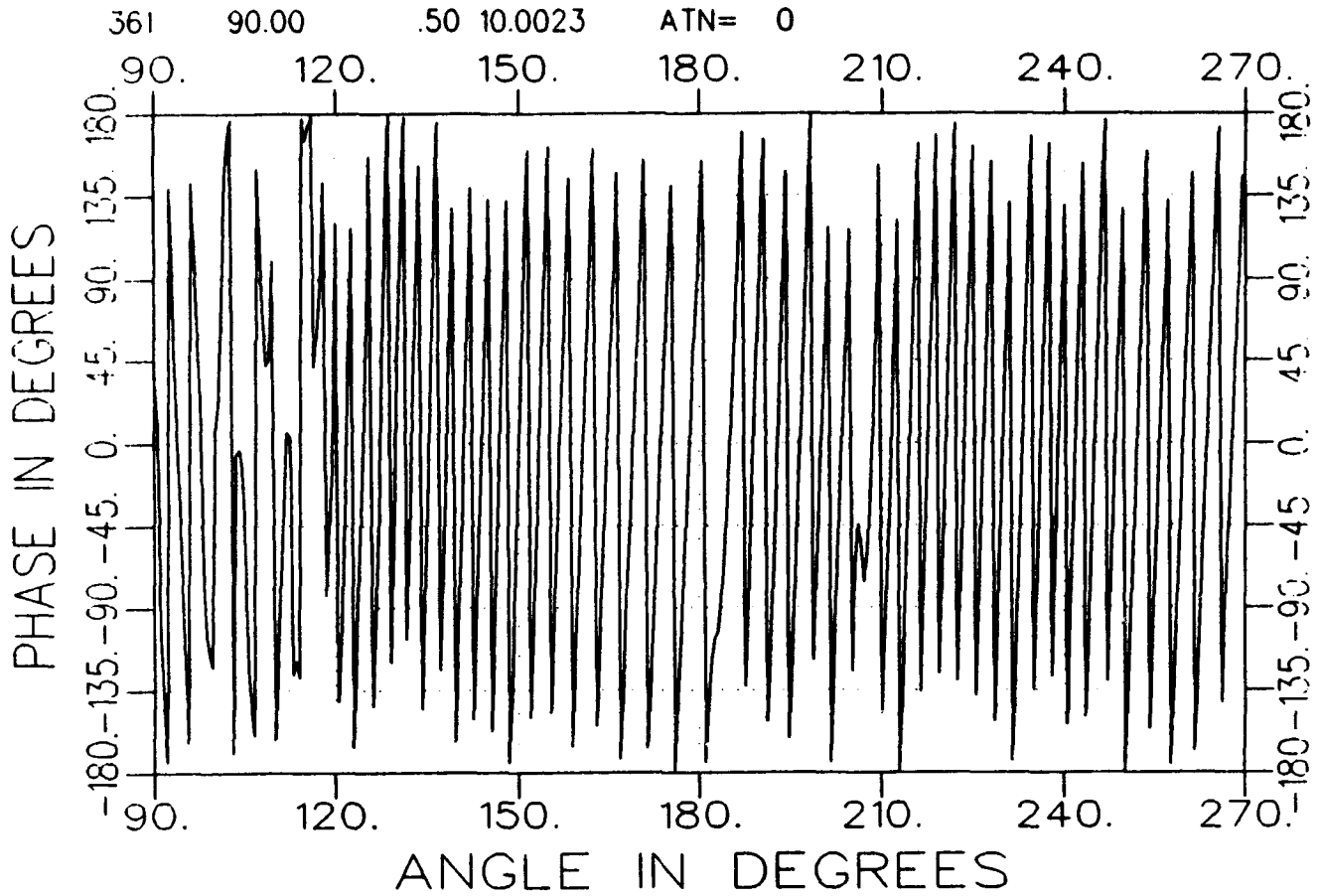
MAGNITUDE IN DB



ANGLE IN DEGREES

b3225gh1000-a.tar  
TARGET

AZIM. 08/13/93 12:09  
long cap grid AVE= 82  
REF=OFF  
ATN= 0



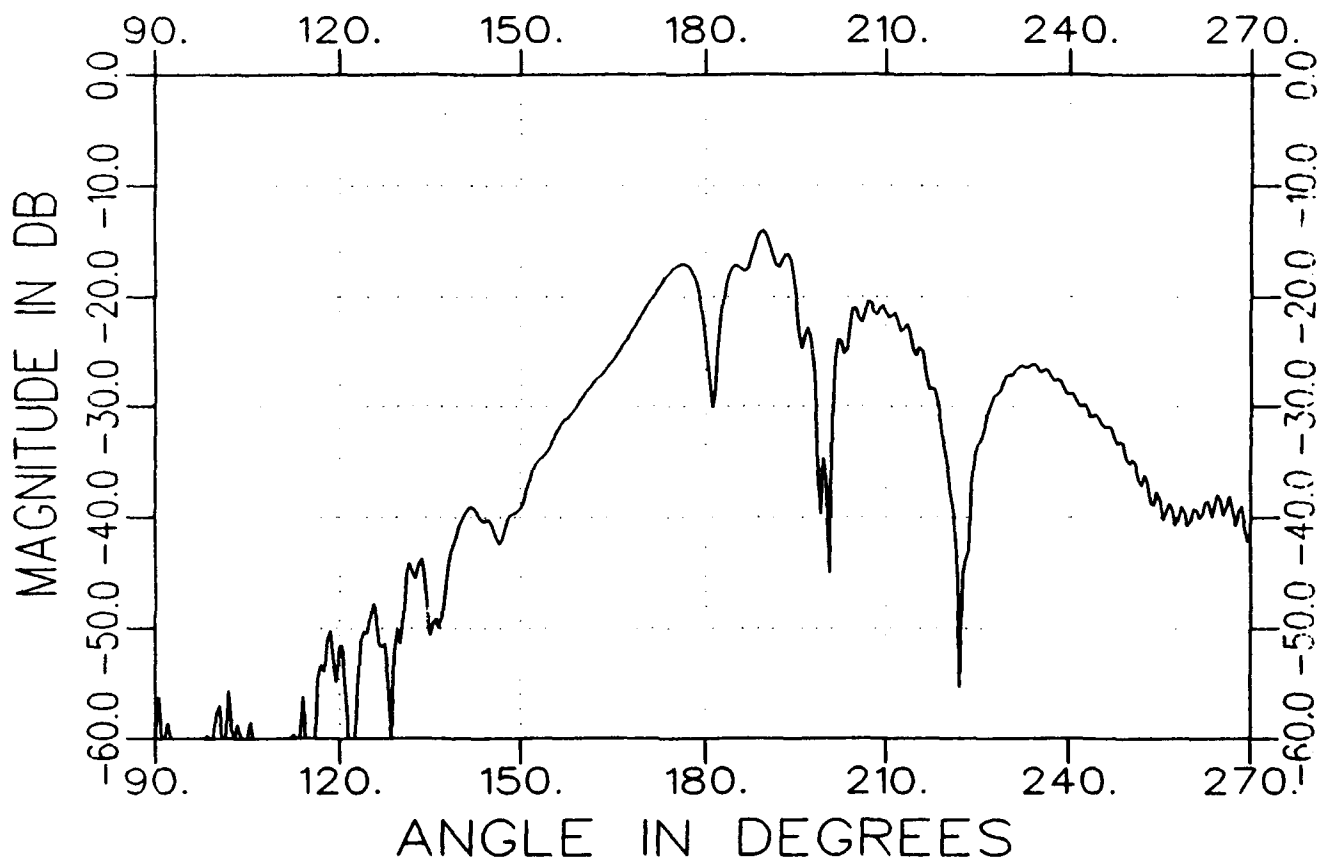
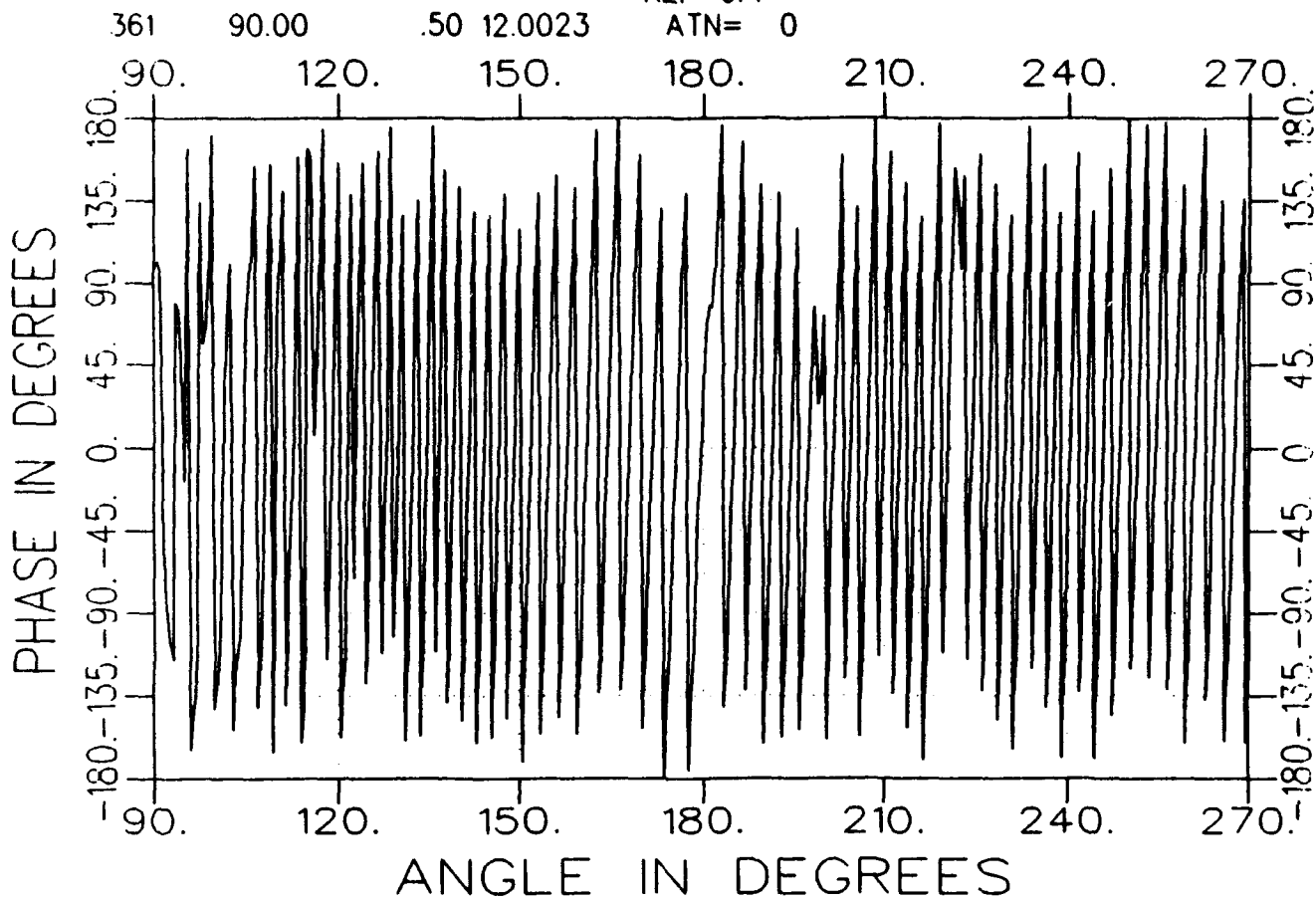


b3225ah1200-a.tar  
TARGET

AZIM. 08/13/93 12:11  
long cap grid

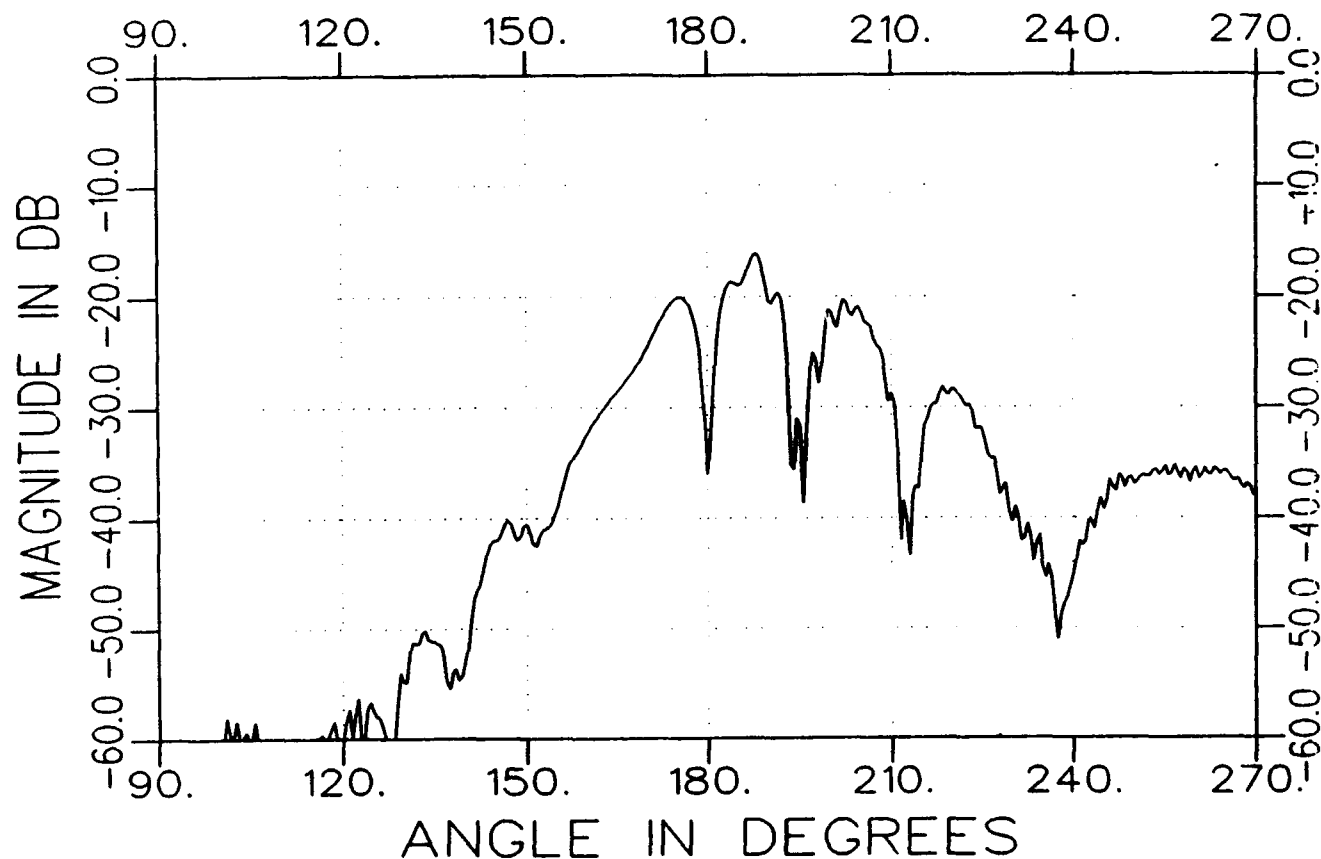
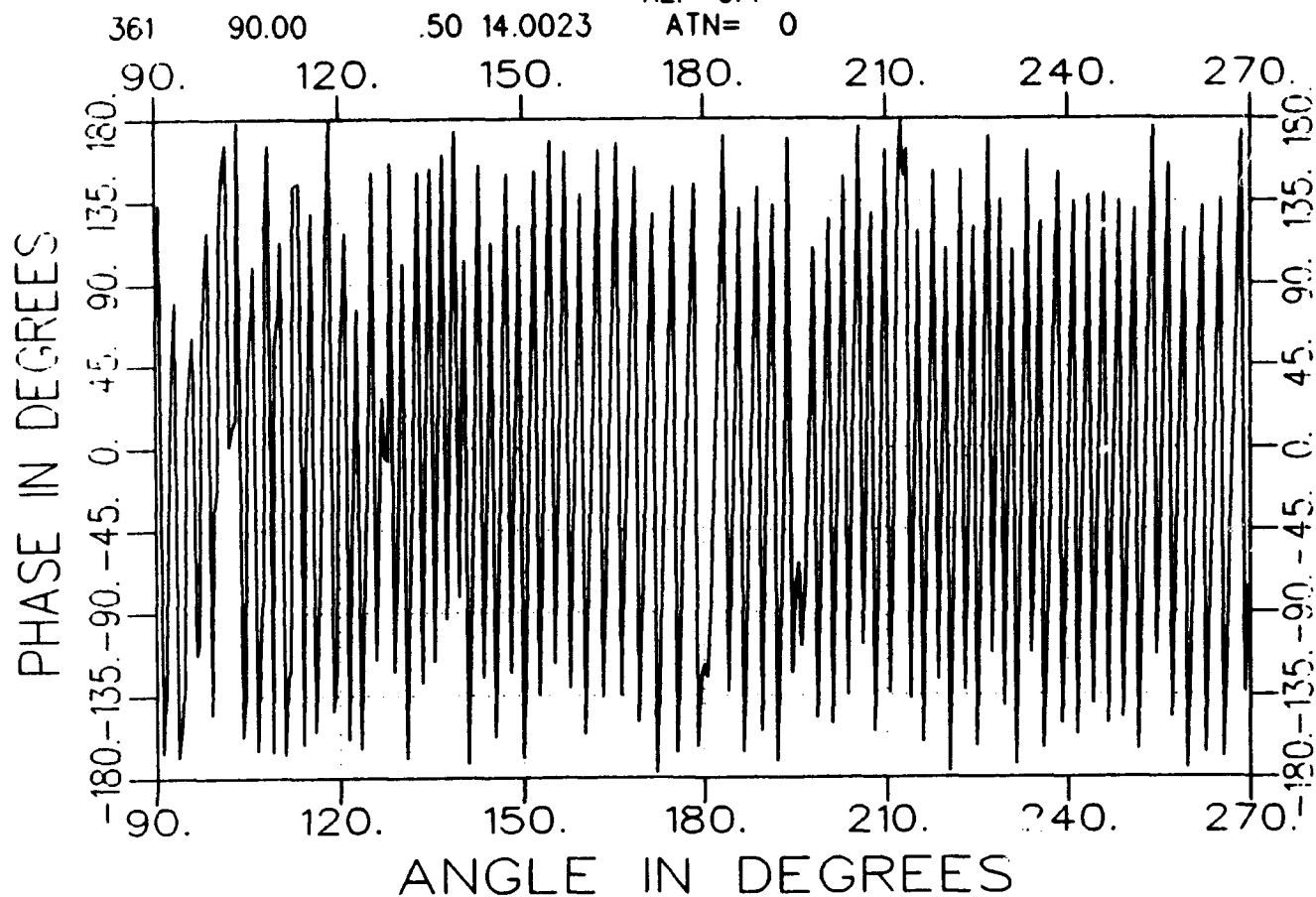
AVE= 82  
REF=OFF

ATN= 0



b3225ah1400-a.tar  
TARGET

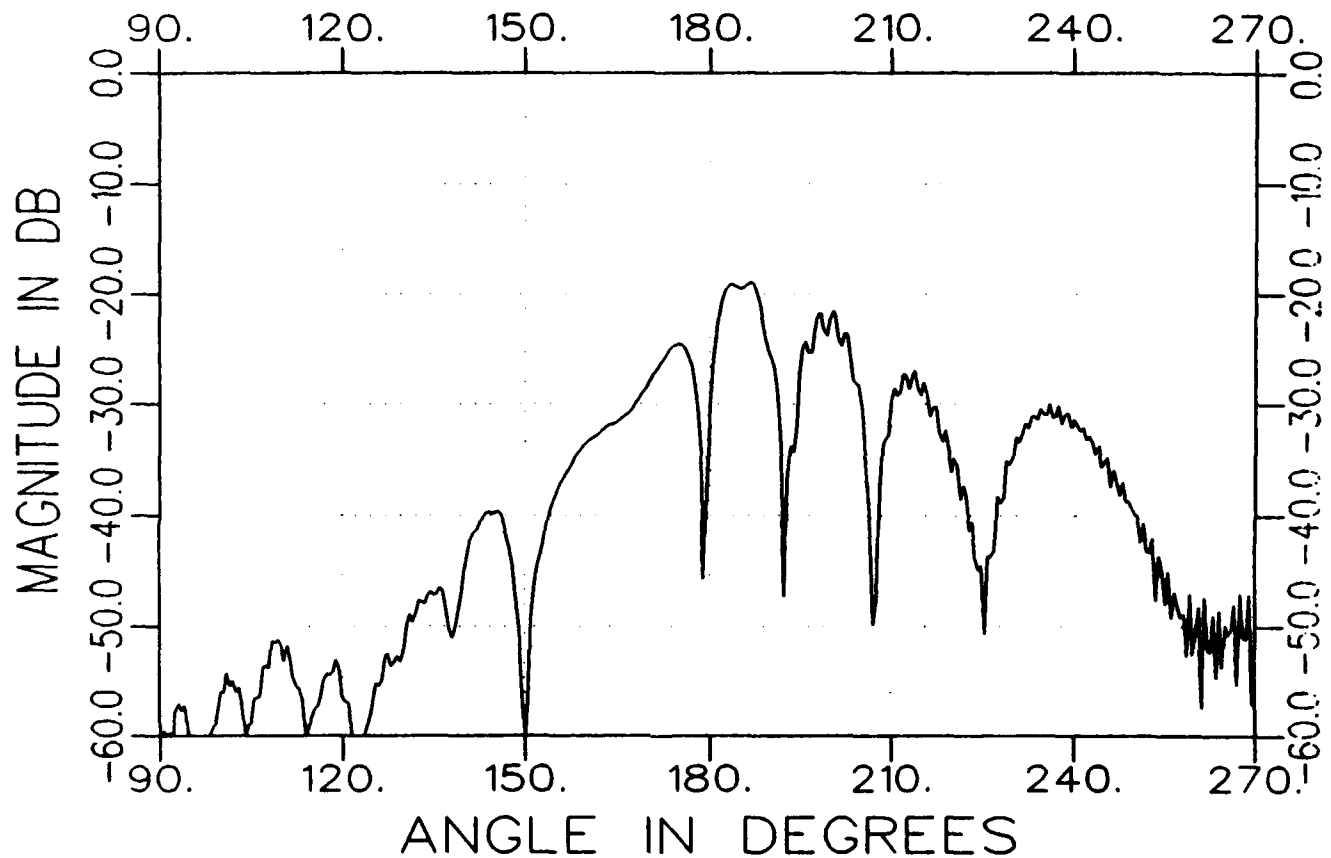
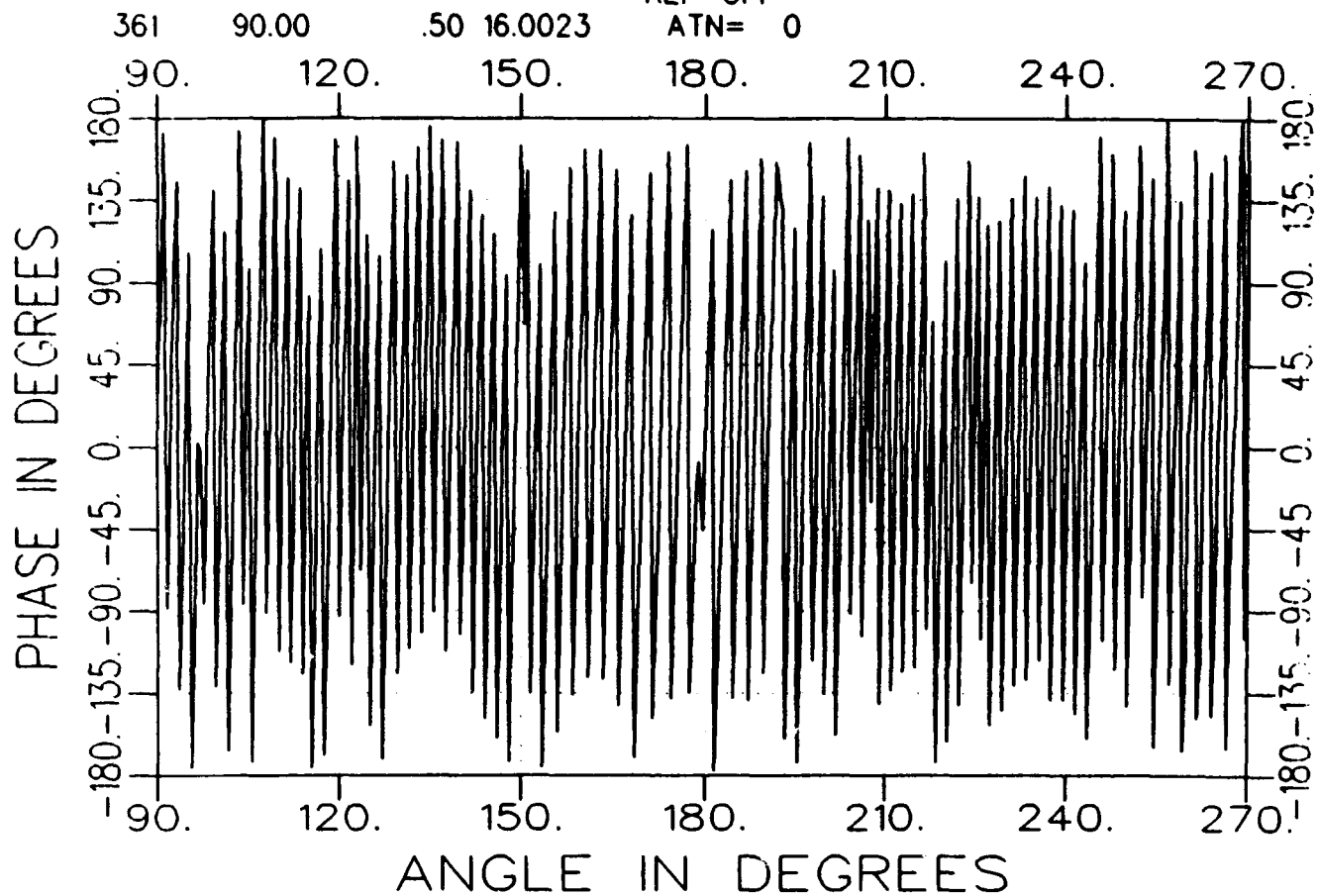
AZIM. 08/13/93 12:13  
long cap grid AVE= 82  
REF=OFF  
ATN= 0



b3225ahl600-a.tar  
TARGET

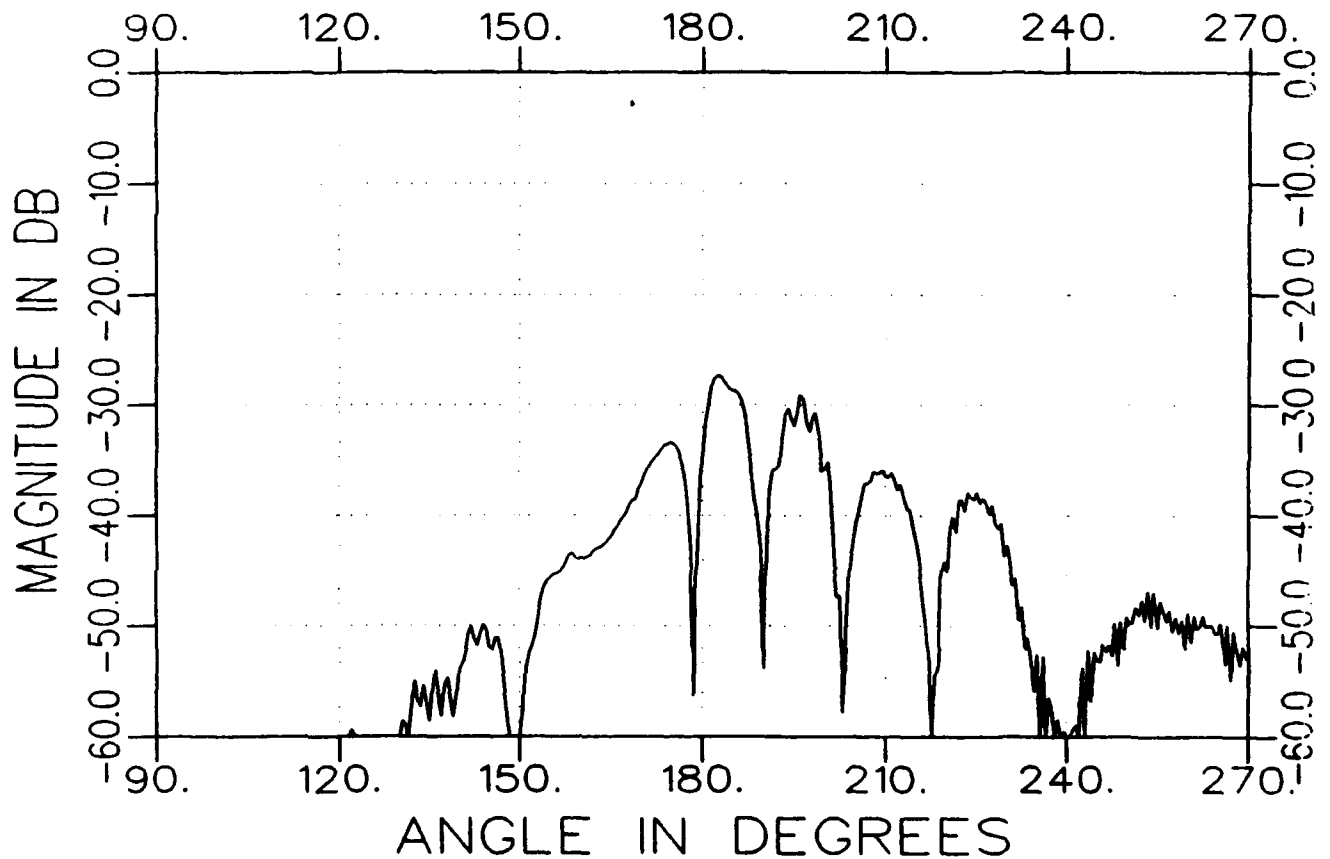
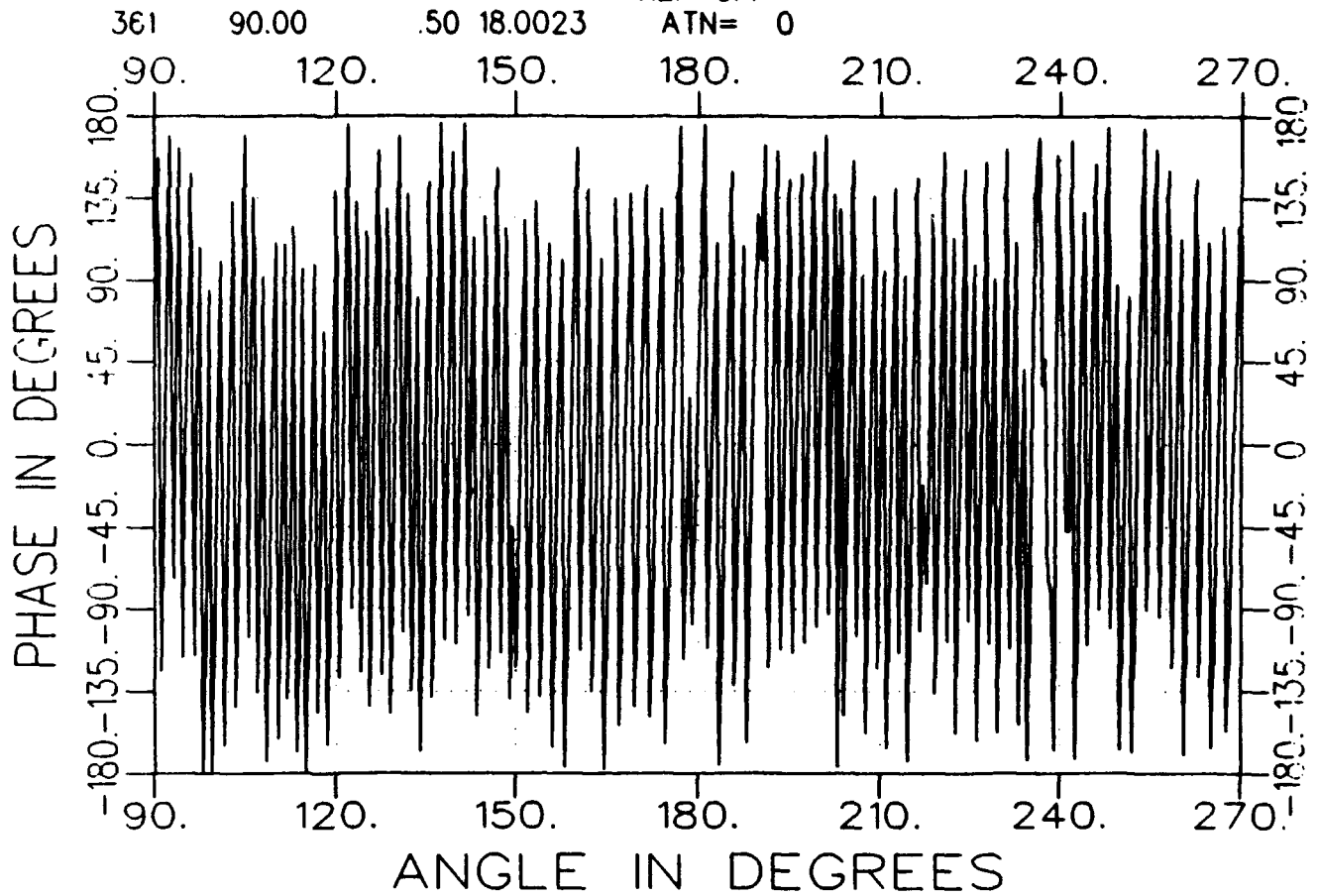
AZIM. 08/13/93 12:15  
long cap grid

AVE= 82  
REF=OFF  
ATN= 0



b3225ah1800-a.tar  
TARGET

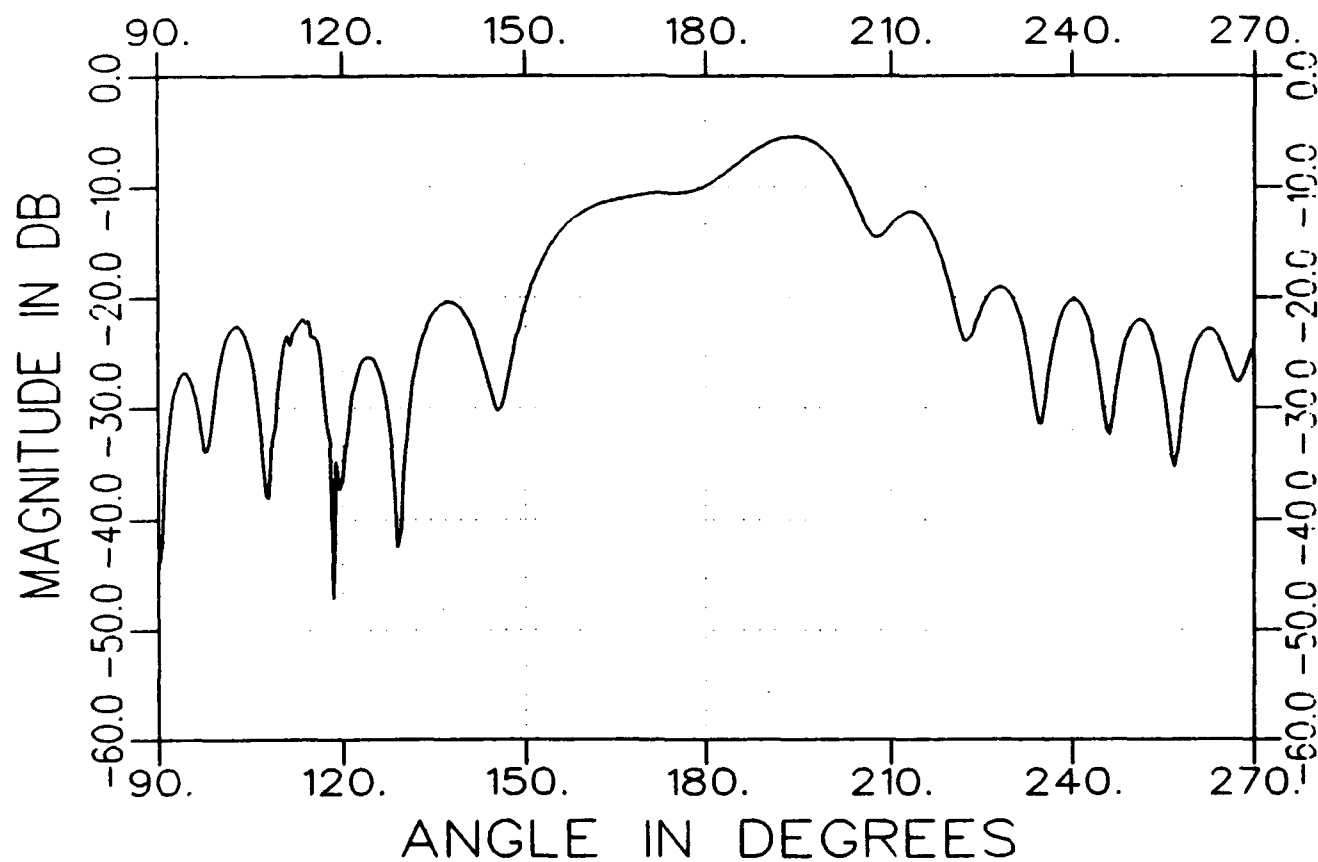
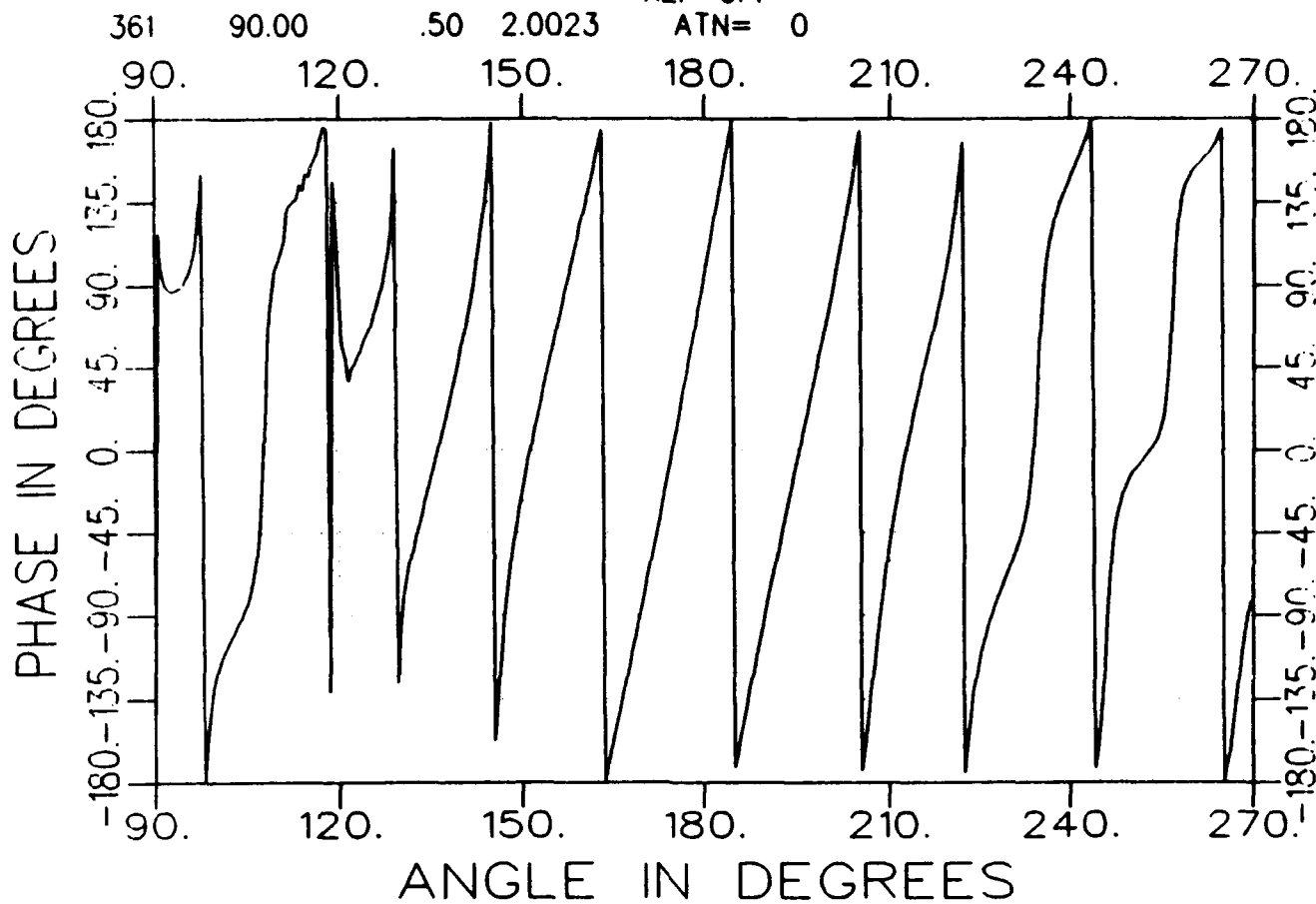
AZIM. 08/13/93 12:17  
long cap grid AVE= 82  
REF=OFF  
ATN= 0



c3225:0200-a:tar  
TARGET

AZIM. 08/13/93 12:25  
short cap grid AVE= 82  
REF=OFF

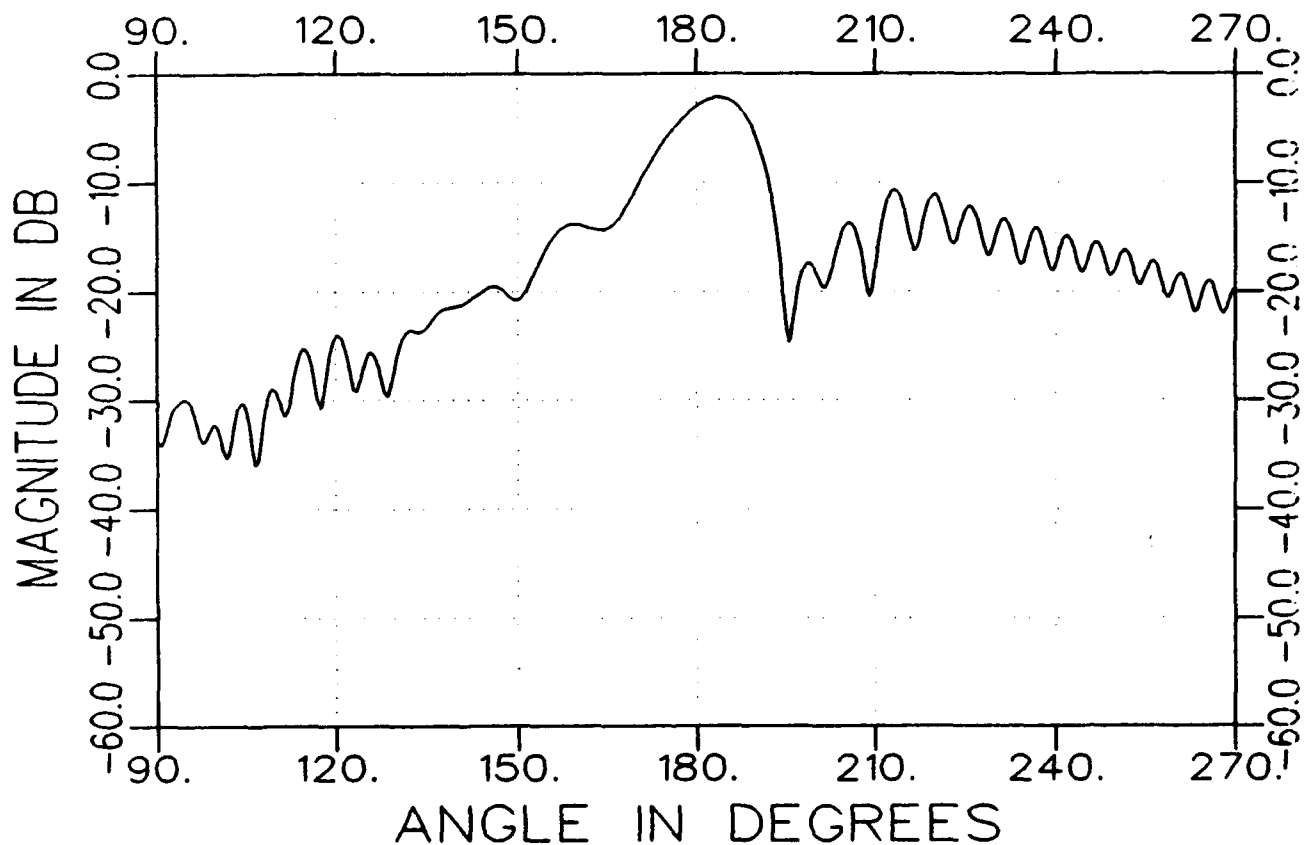
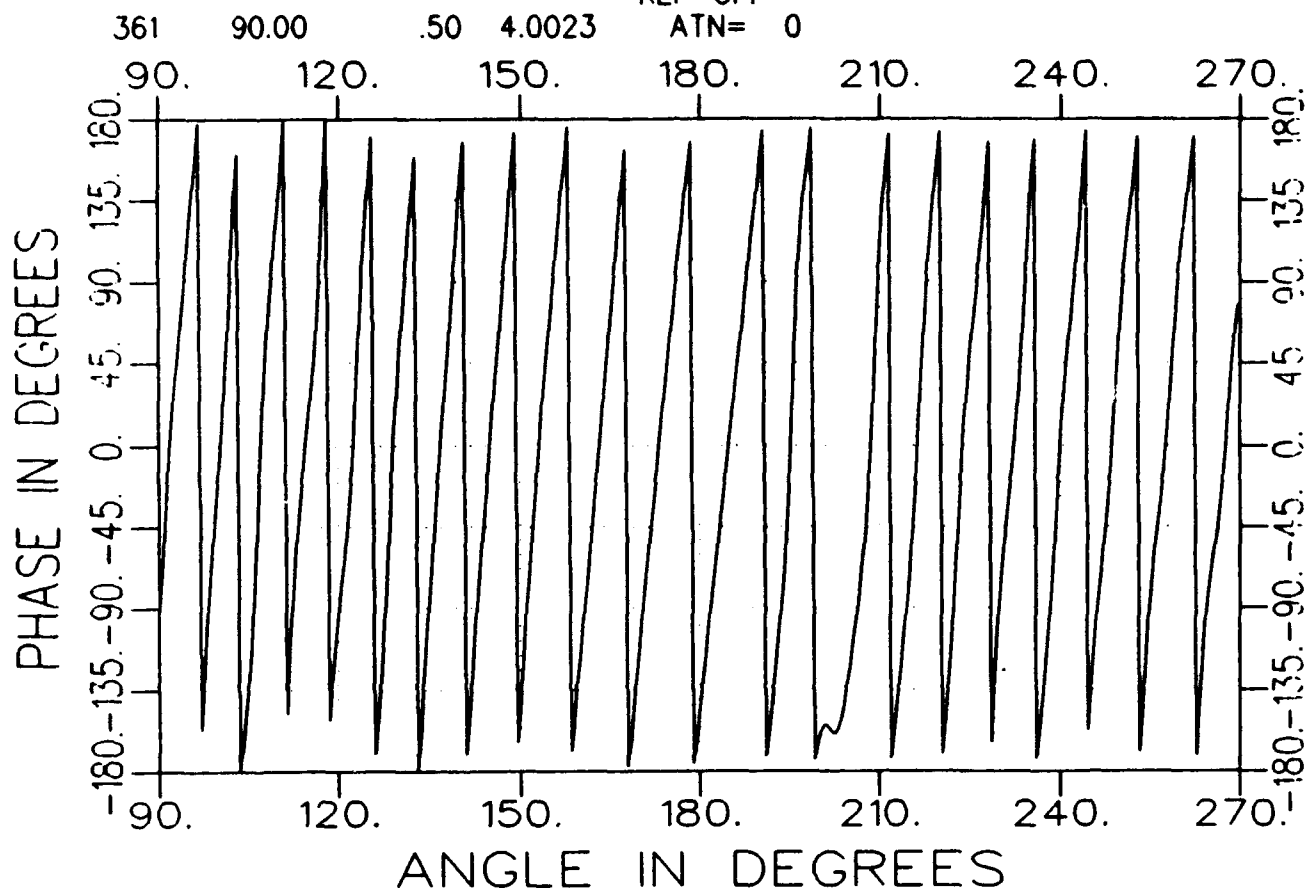
ATN= 0



c3225ah0400-a.tar  
TARGET

AZIM. 08/13/93 12:27  
short cap grid AVE= 82  
REF=OFF

ATN= 0

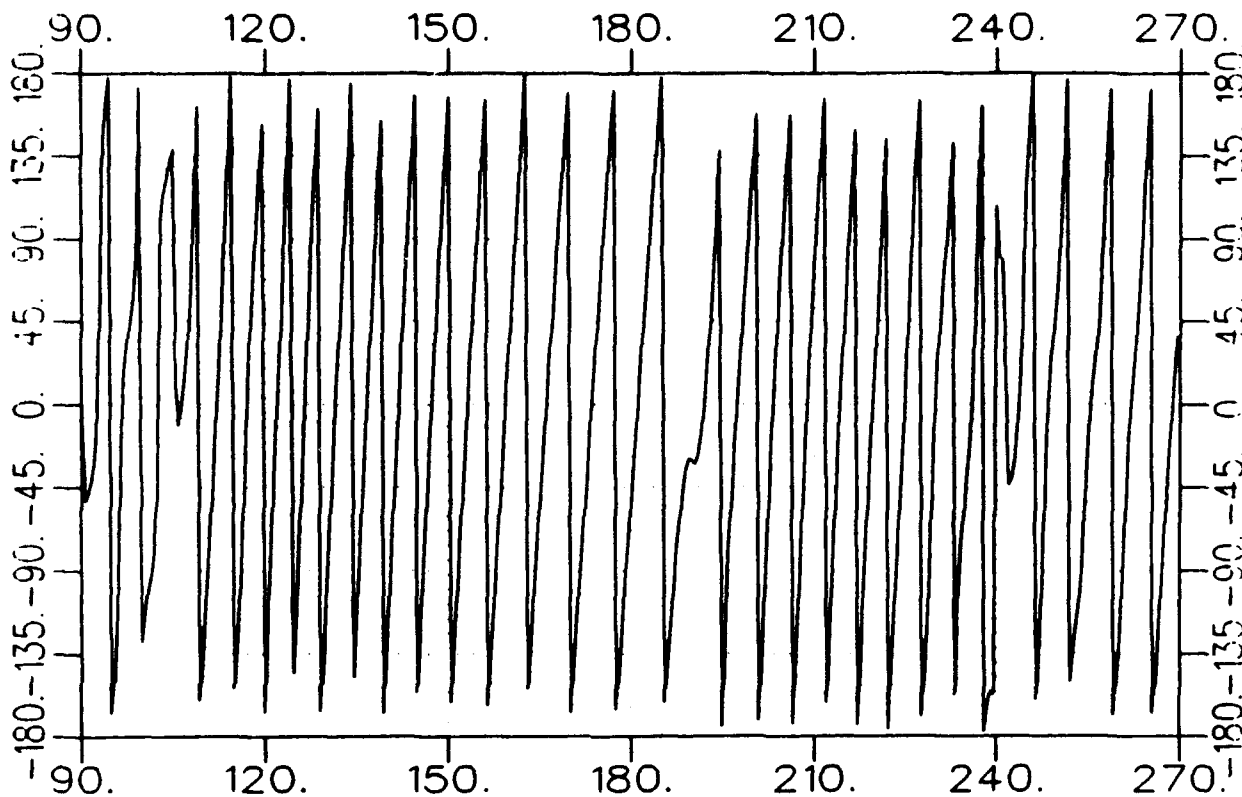


c3225ah0600-a.tar  
TARGET

AZIM. 08/13/93 12:29  
short cap grid AVE= 82  
REF=OFF

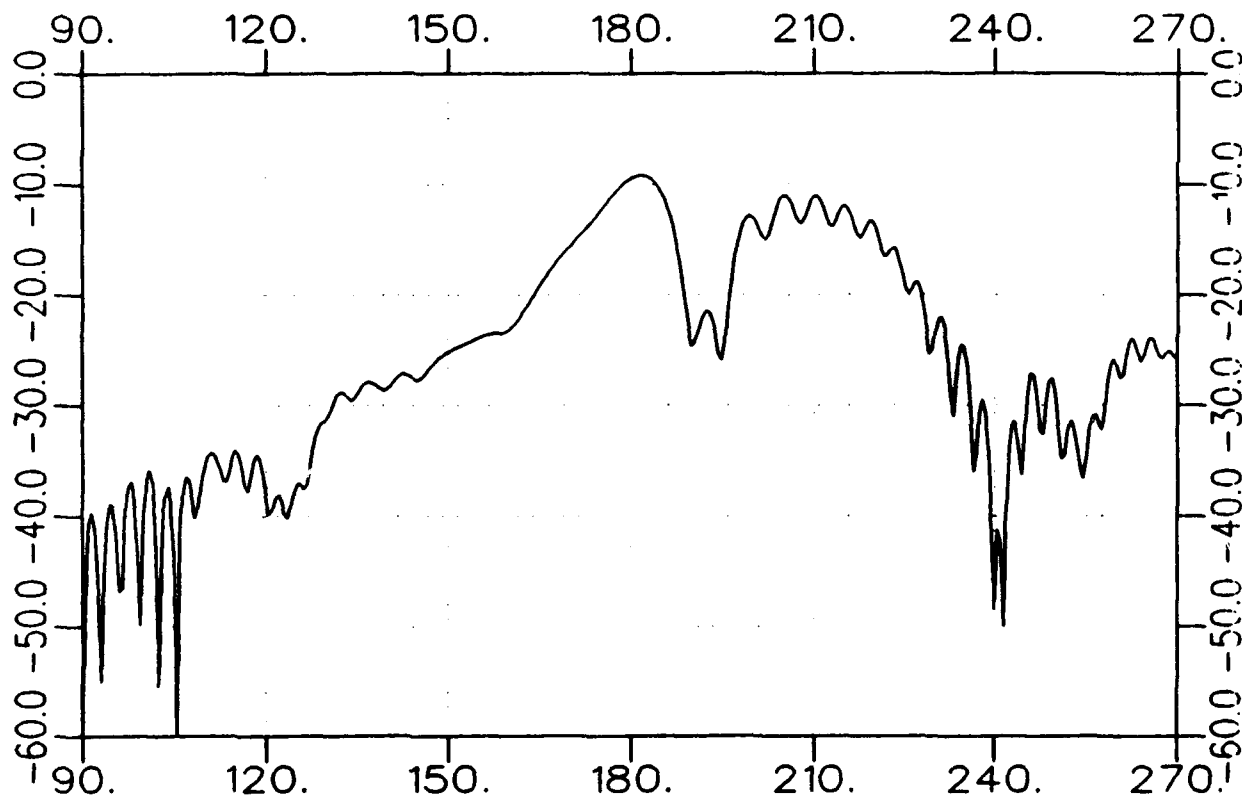
361 90.00 .50 6.0023 ATN= 0

PHASE IN DEGREES



ANGLE IN DEGREES

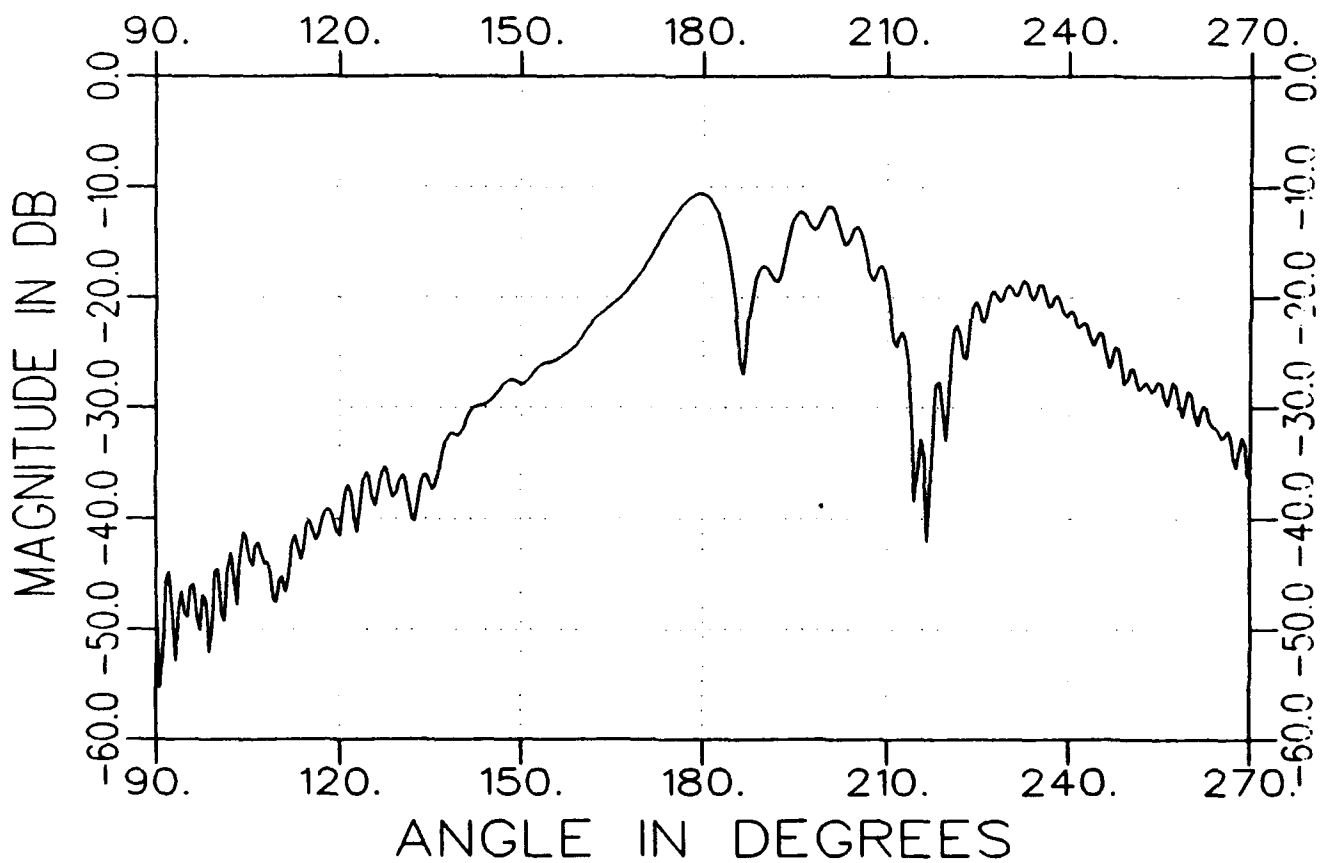
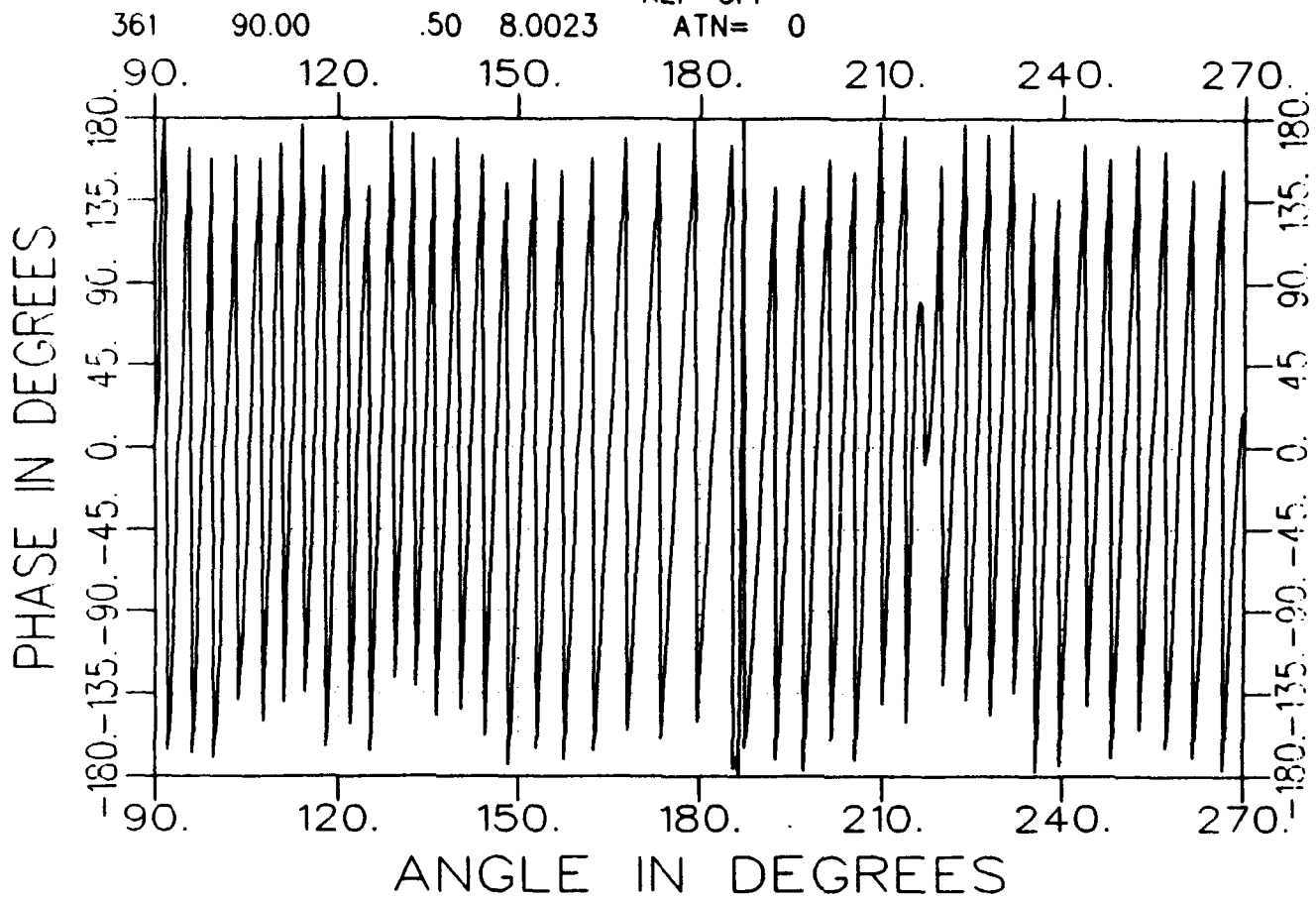
MAGNITUDE IN DB



ANGLE IN DEGREES

c3225ah0800-a.tar  
TARGET

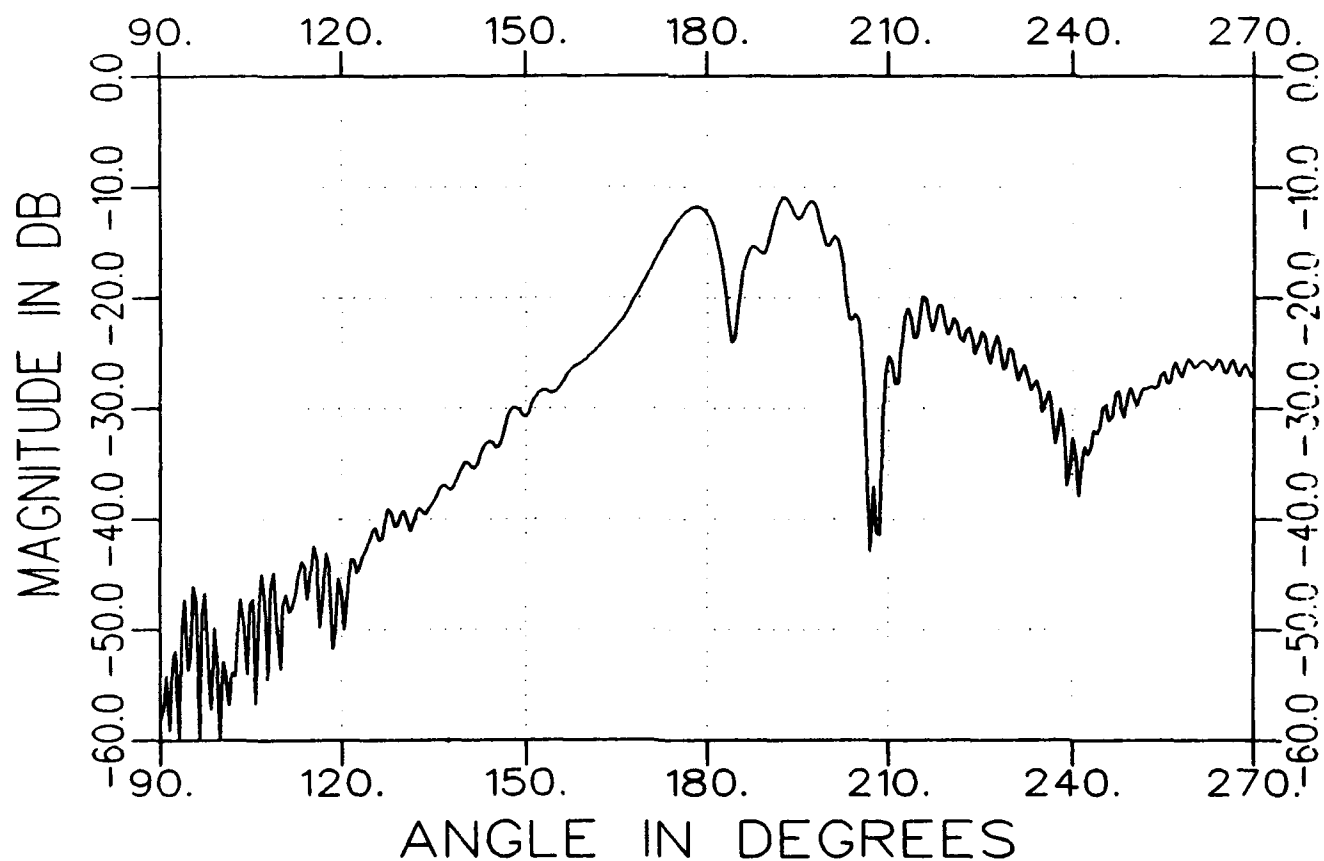
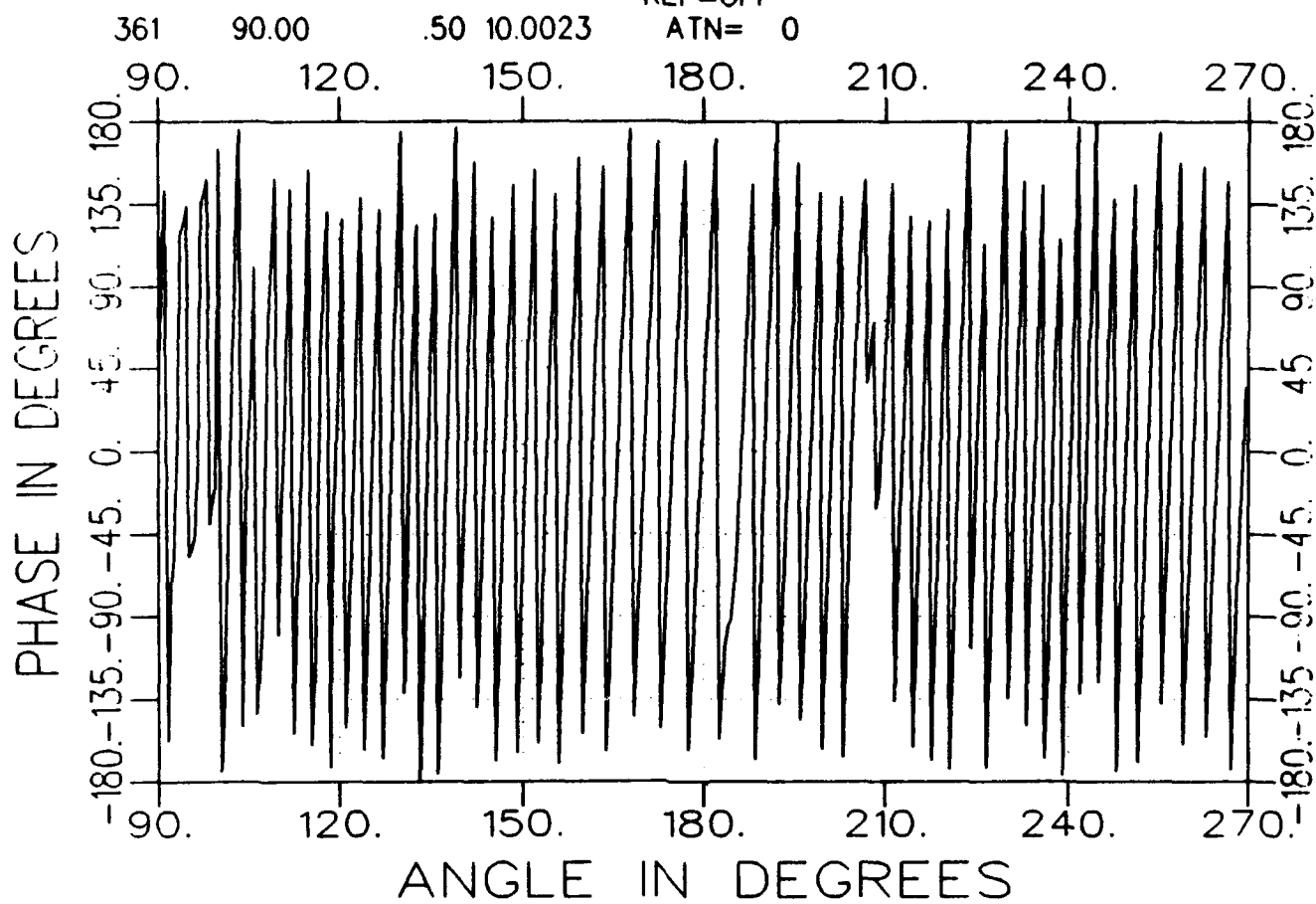
AZIM. 08/13/93 12:31  
short cap grid AVE= 82  
REF=OFF  
ATN= 0





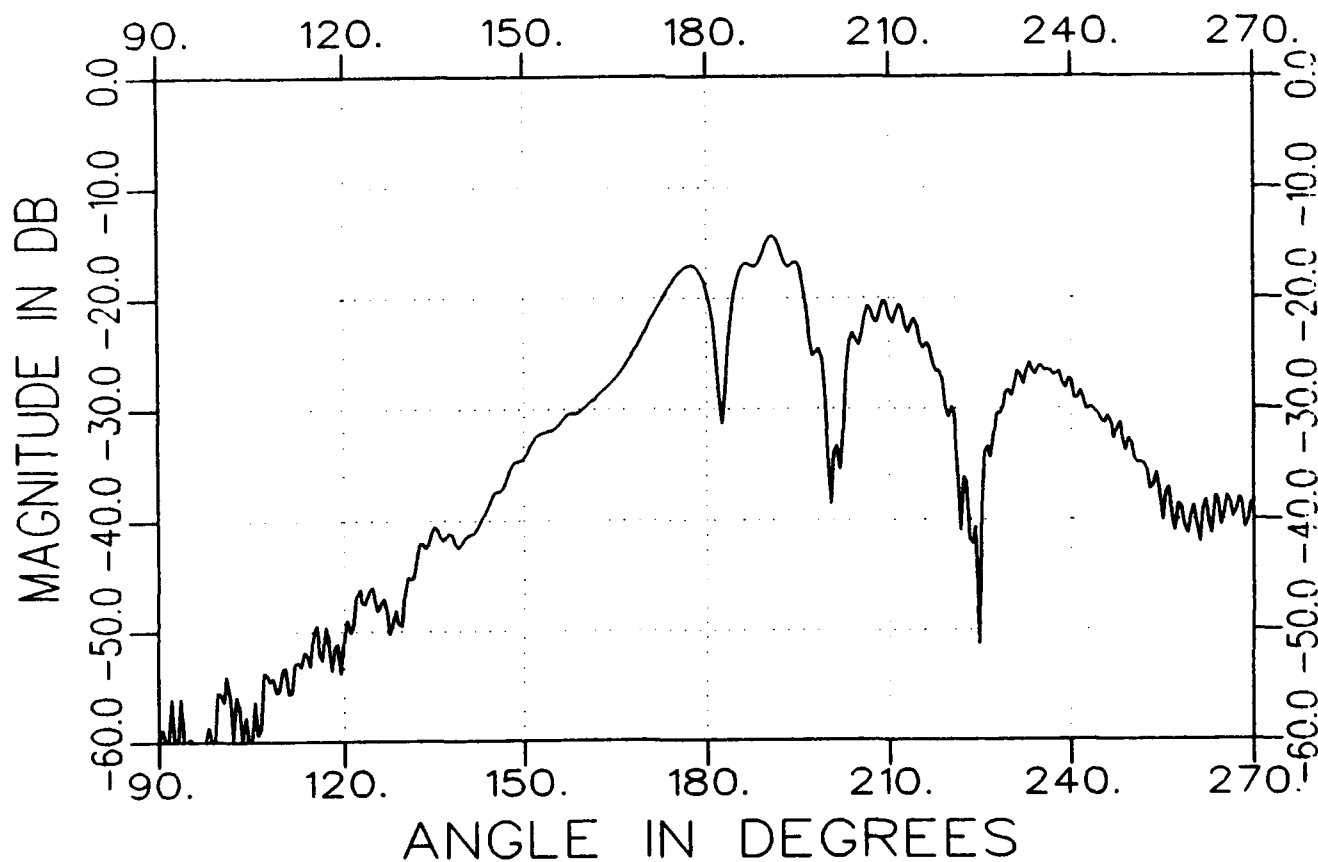
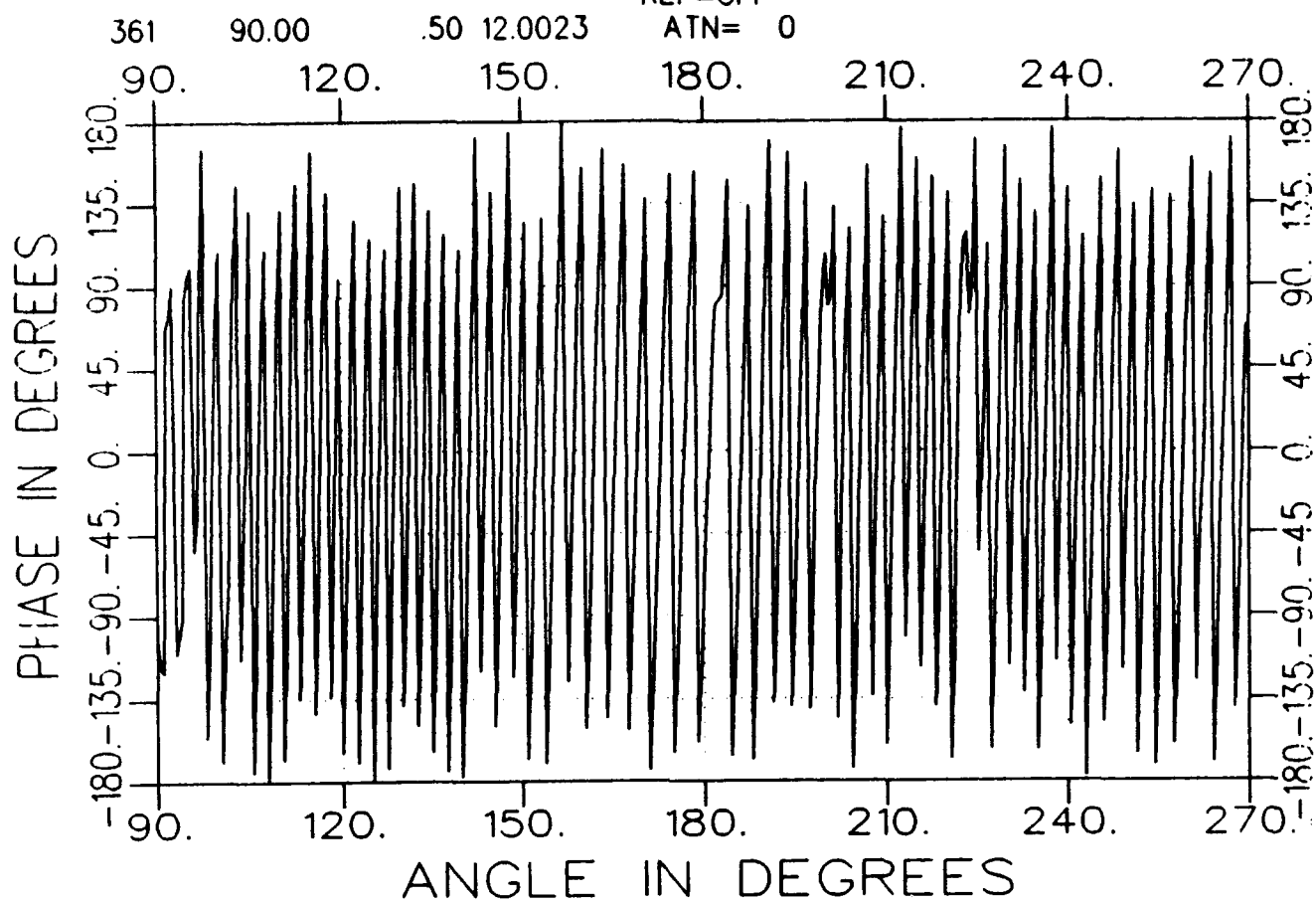
c3225ah1000-a.tar  
TARGET

AZIM. 08/13/93 12:33  
short cap grid AVE= 82  
REF=OFF  
ATN= 0



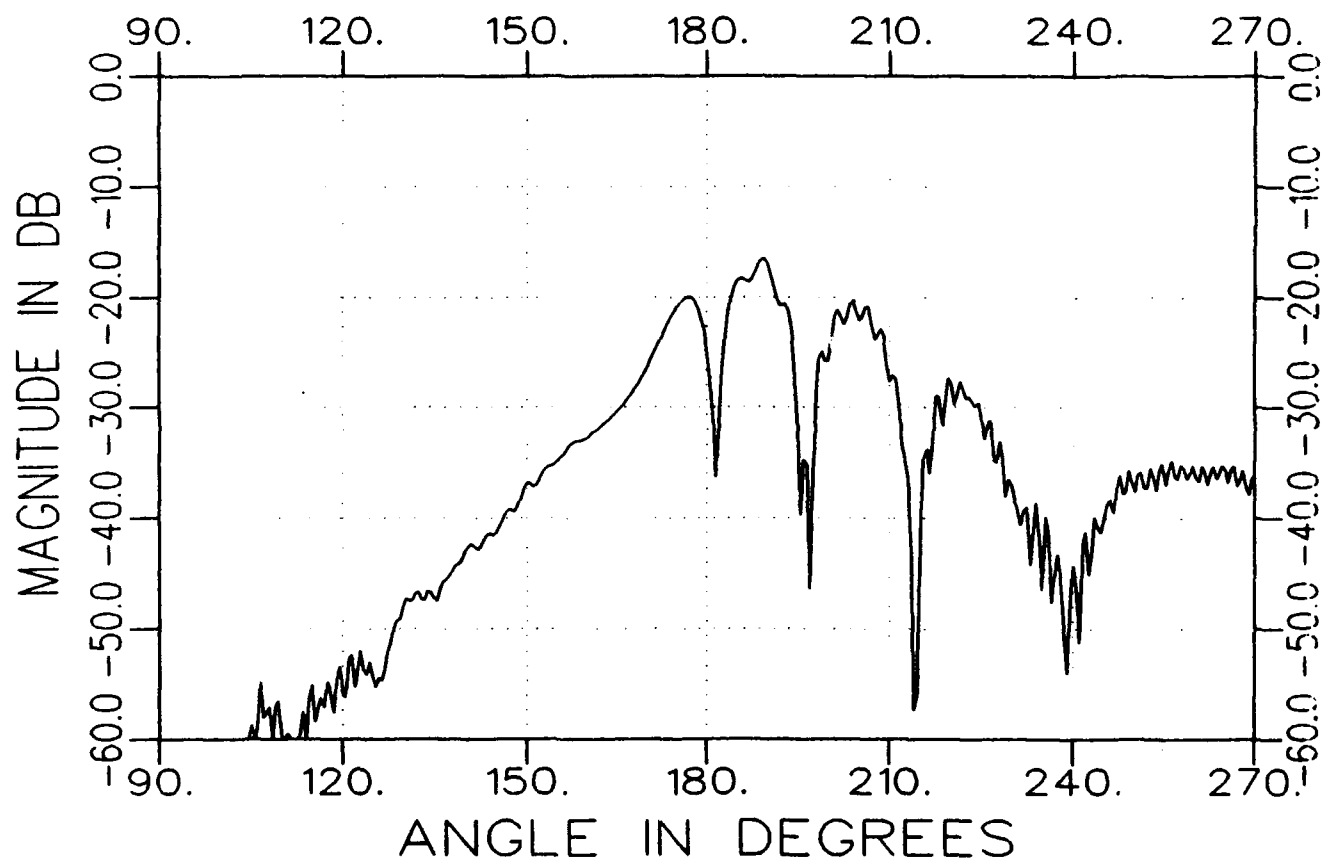
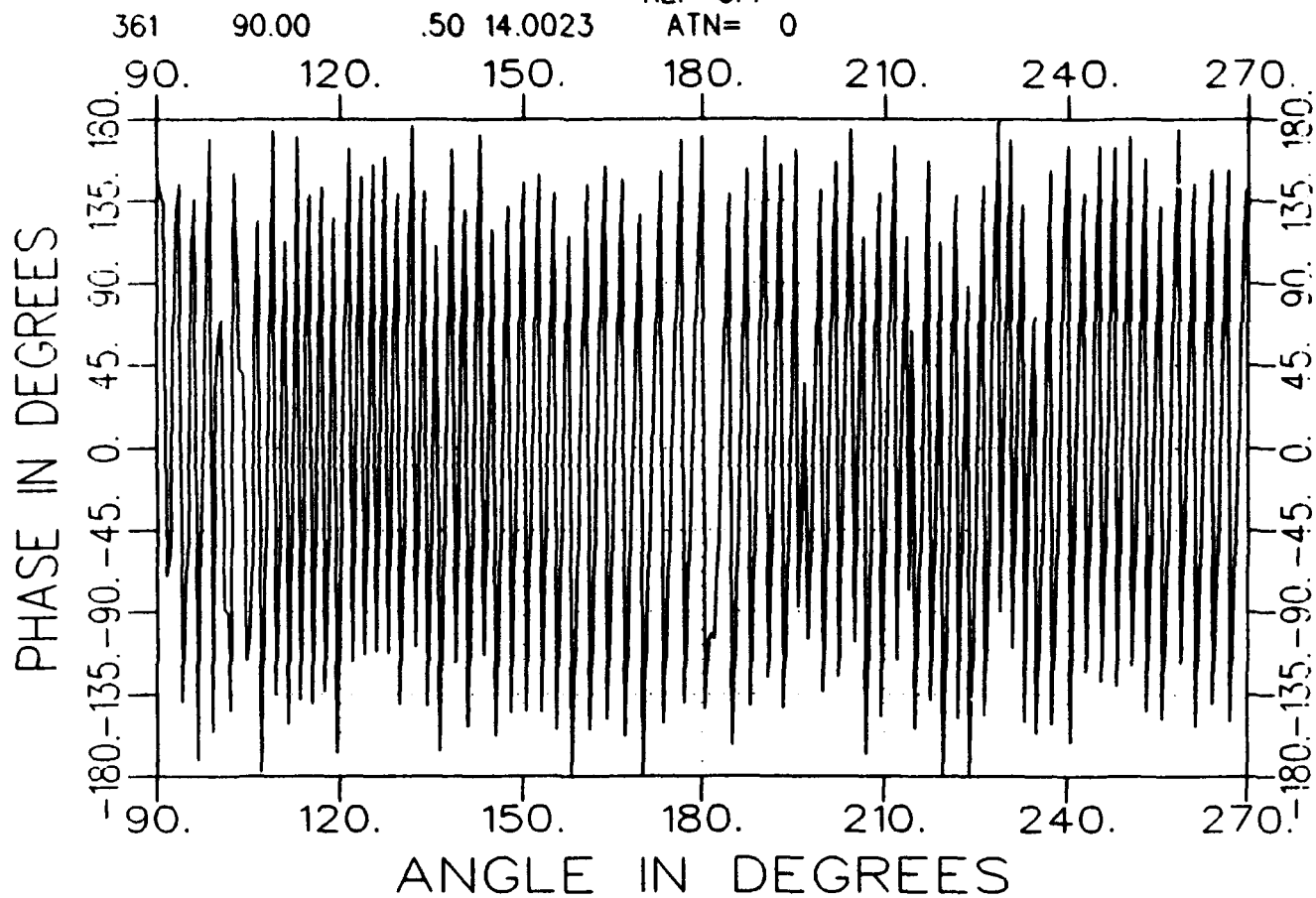
c3225ah1200-a.tar  
TARGET

AZIM. 08/13/93 12:35  
short cap grid AVE= 82  
REF=OFF  
ATN= 0



c3225ah1400-a.tar  
TARGET

AZIM. 08/13/93 12:37  
short cap grid AVE= 82  
REF=OFF  
ATN= 0

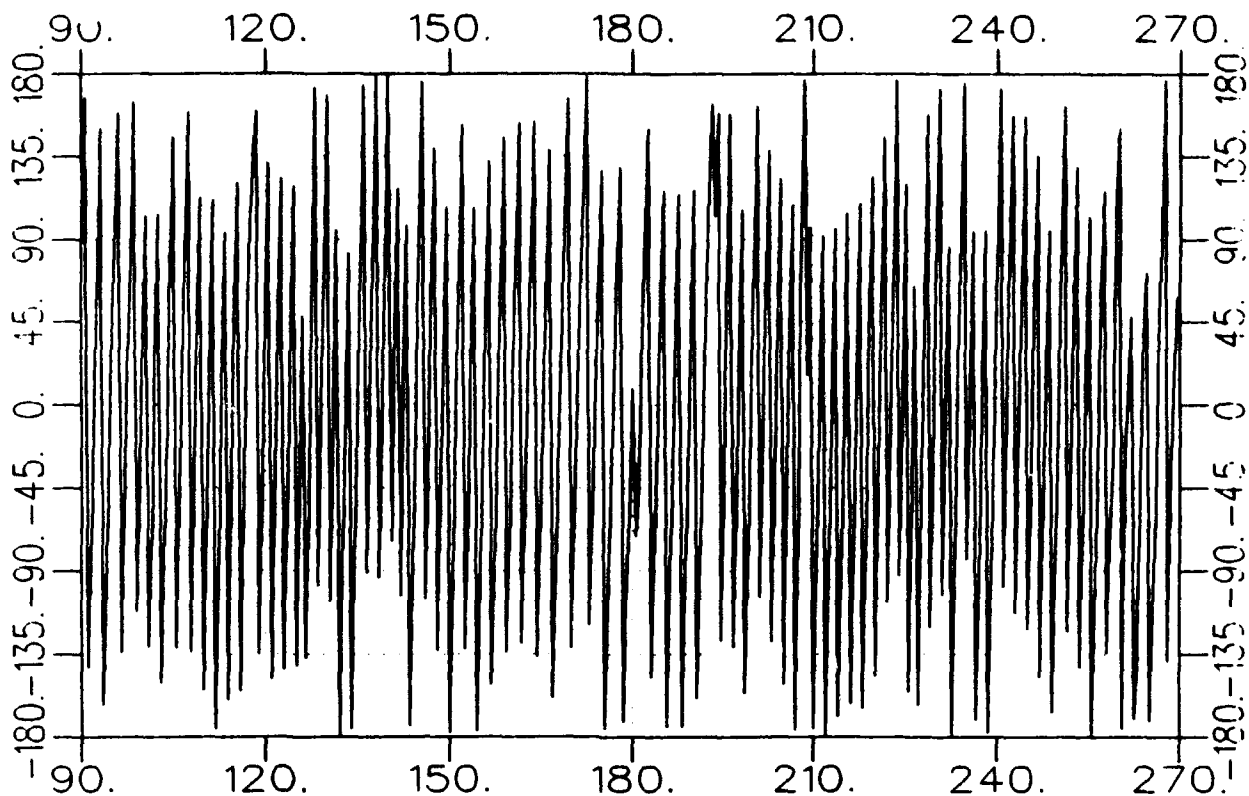


c3225ah1600-a.tar  
TARGET

AZIM. 08/13/93 12:39  
short cap grid AVE= 82  
REF=OFF

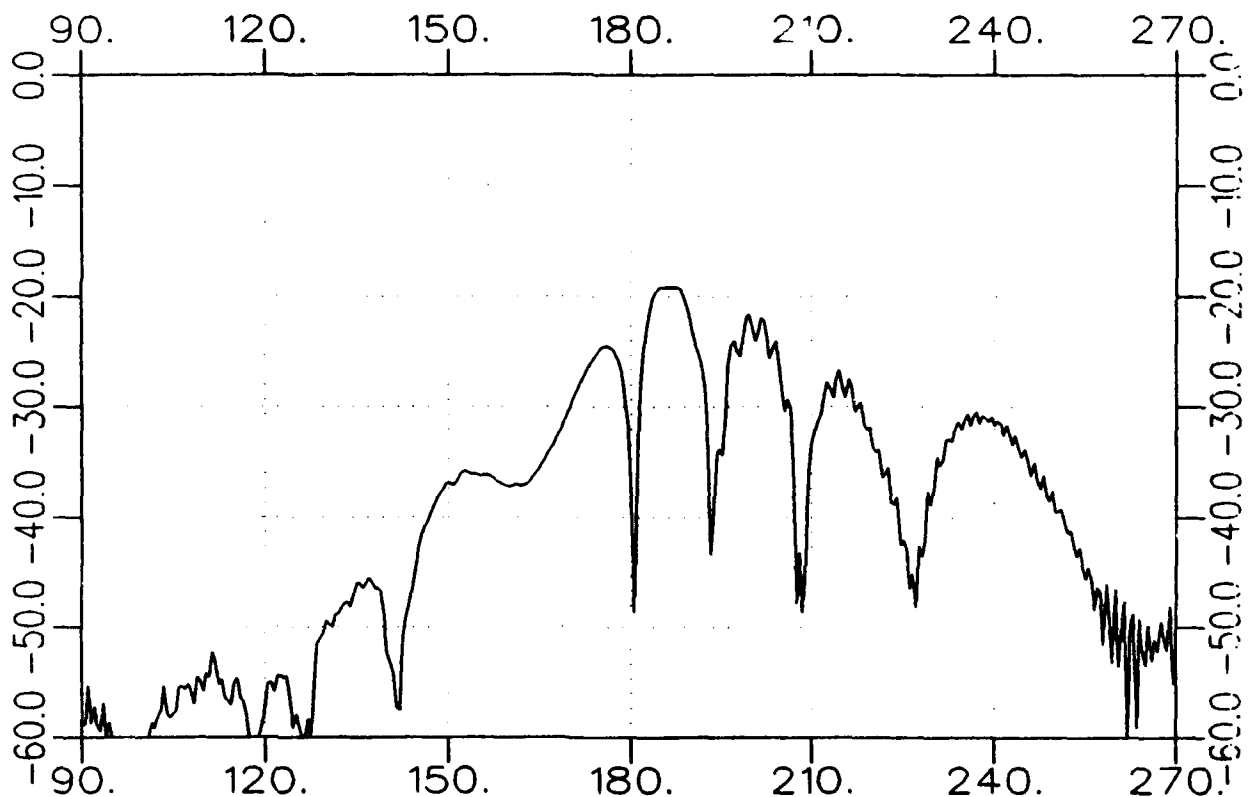
361 90.00 .50 16.0023 ATN= 0

PHASE IN DEGREES



ANGLE IN DEGREES

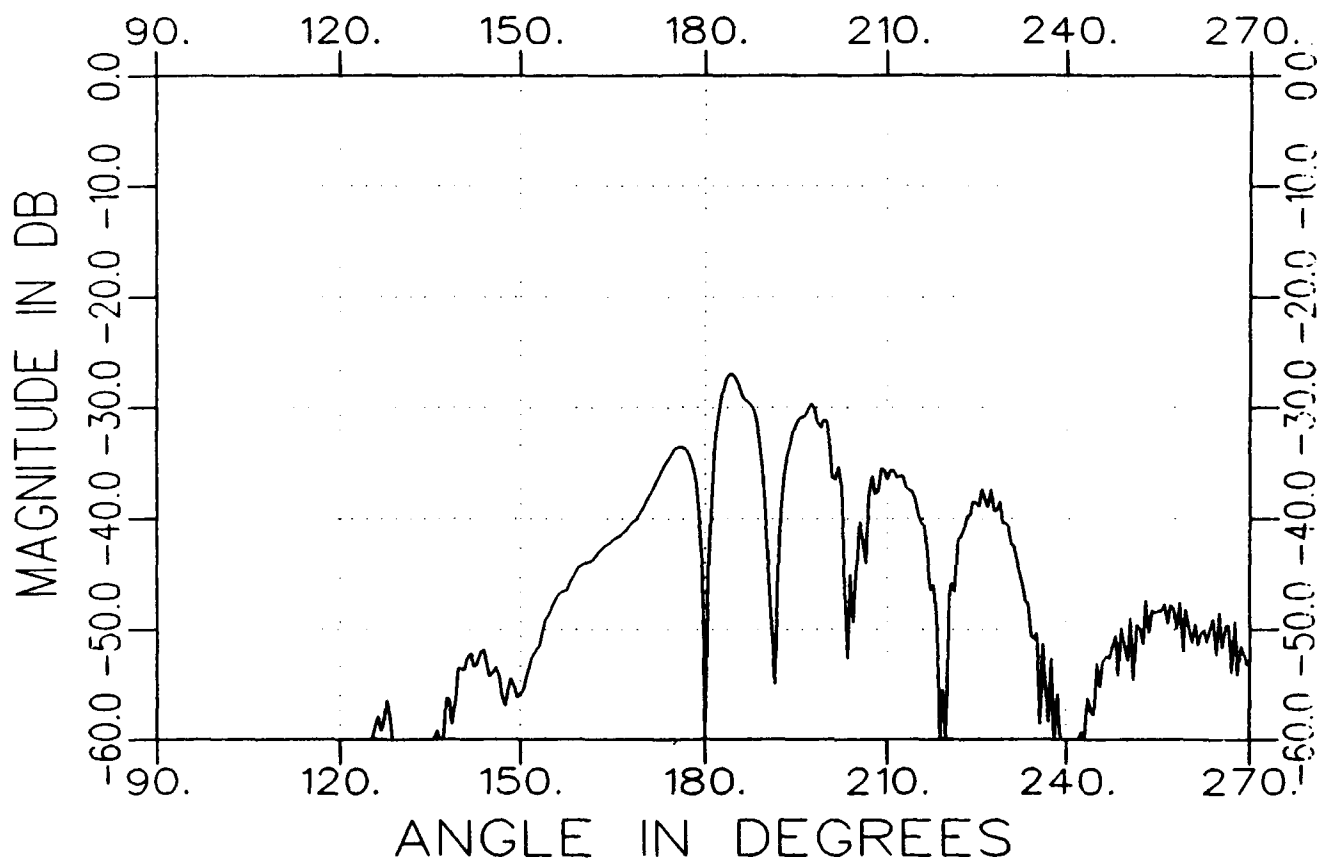
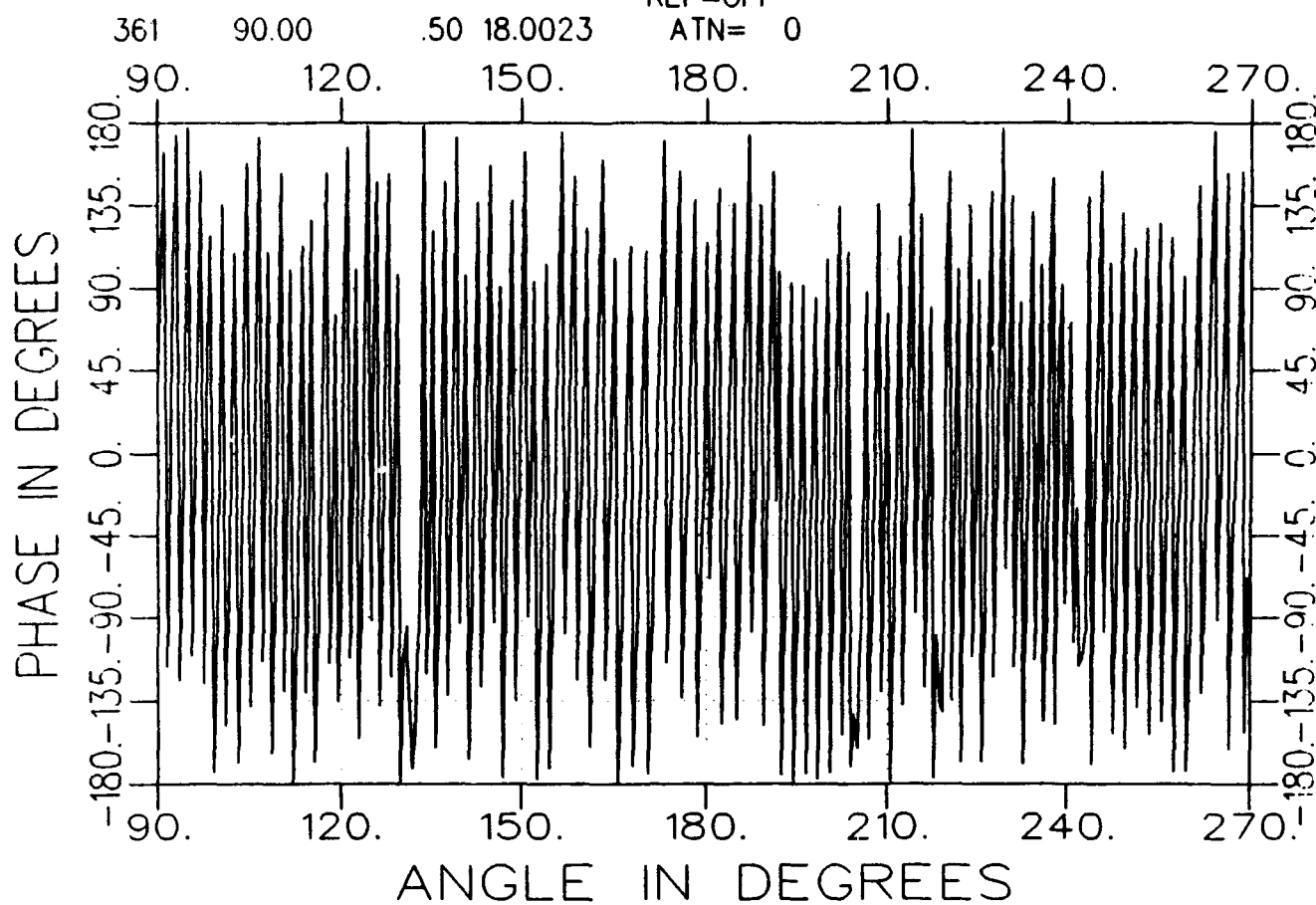
MAGNITUDE IN DB



ANGLE IN DEGREES

c3225ah1800-a.tar  
TARGET

AZIM. 08/13/93 12:41  
short cap grid AVE= 82  
REF=OFF  
ATN= 0

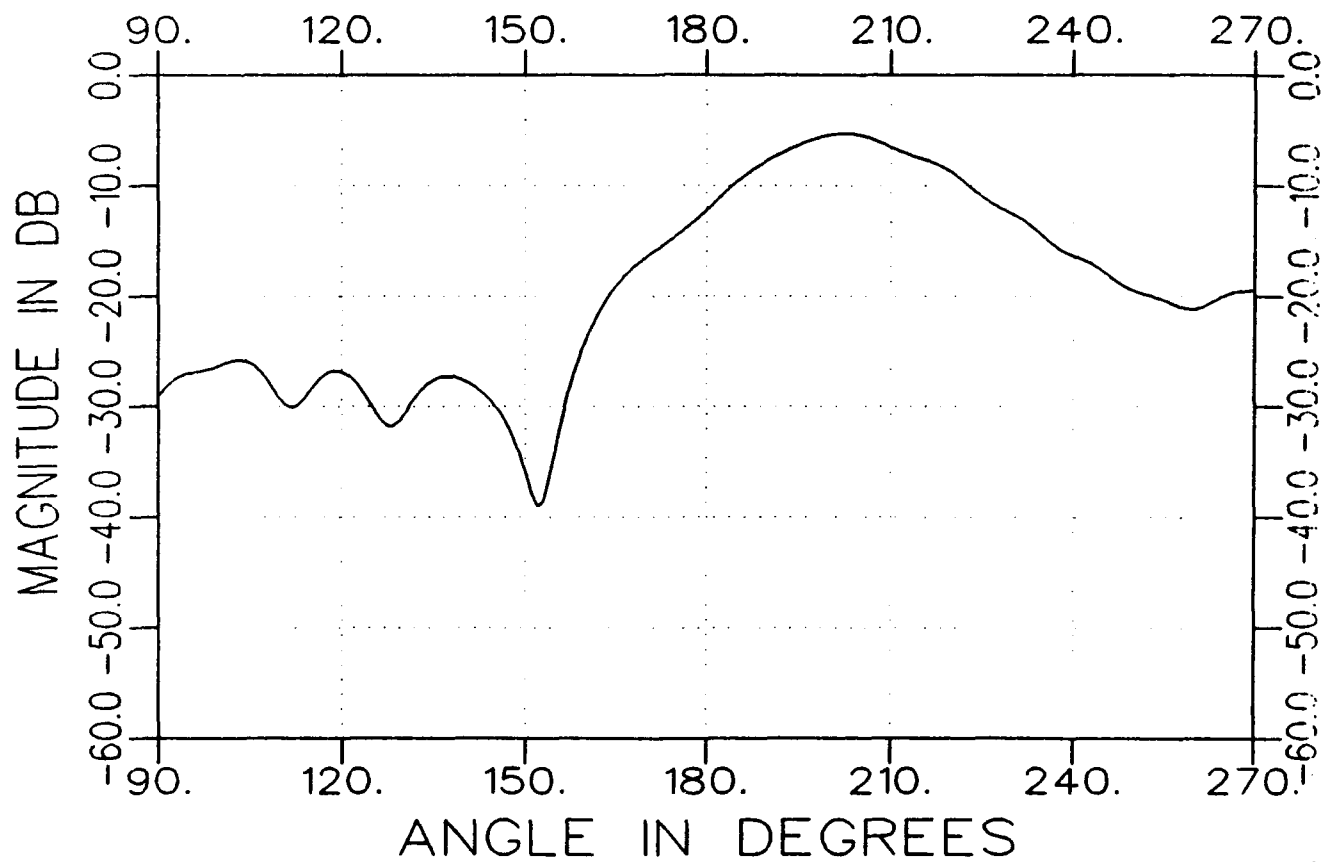
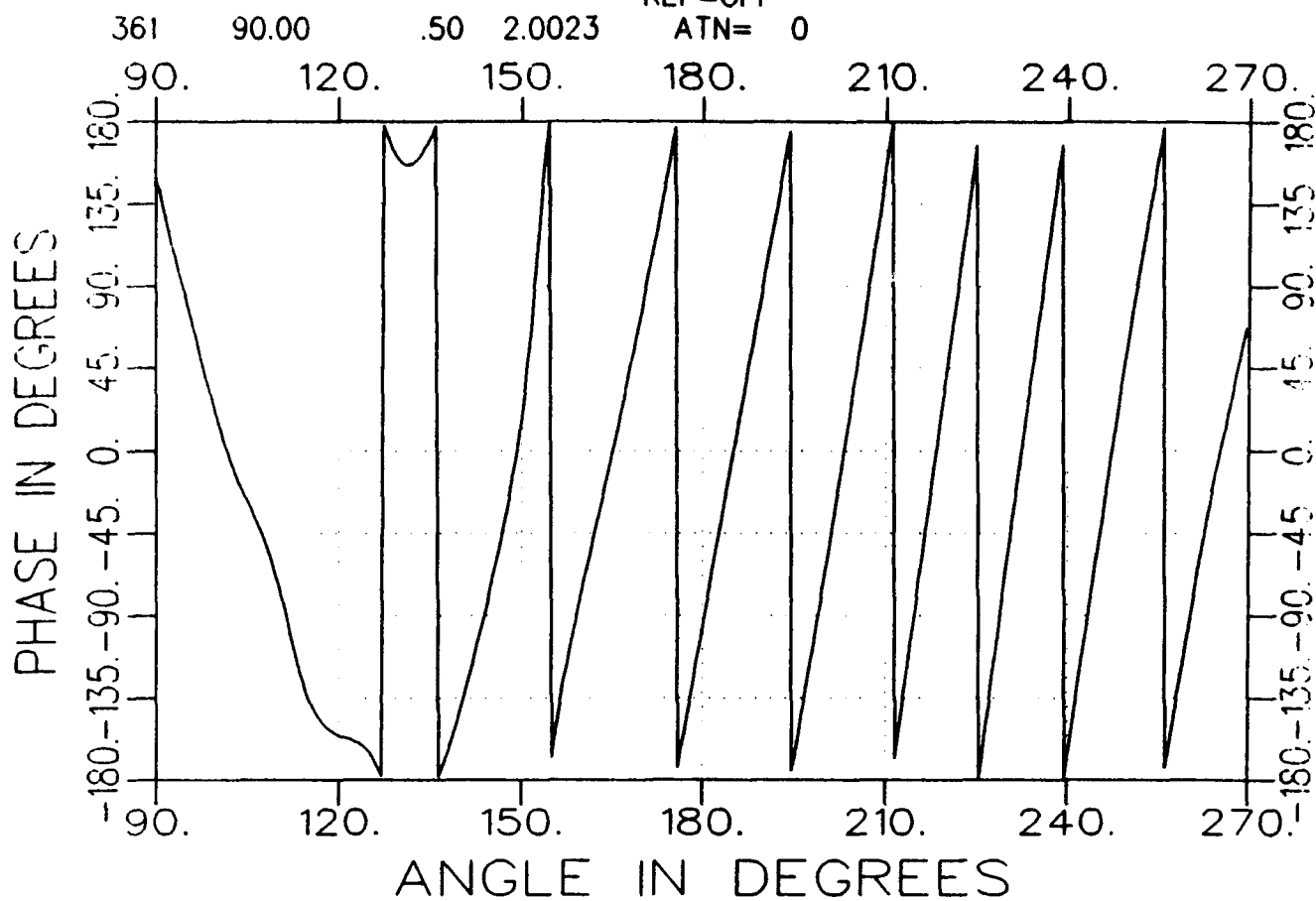


d3225aa0200-a.tar  
TARGET

AZIM. 08/13/93 13:10  
bare v

AVE= 82  
REF=OFF

ATN= 0



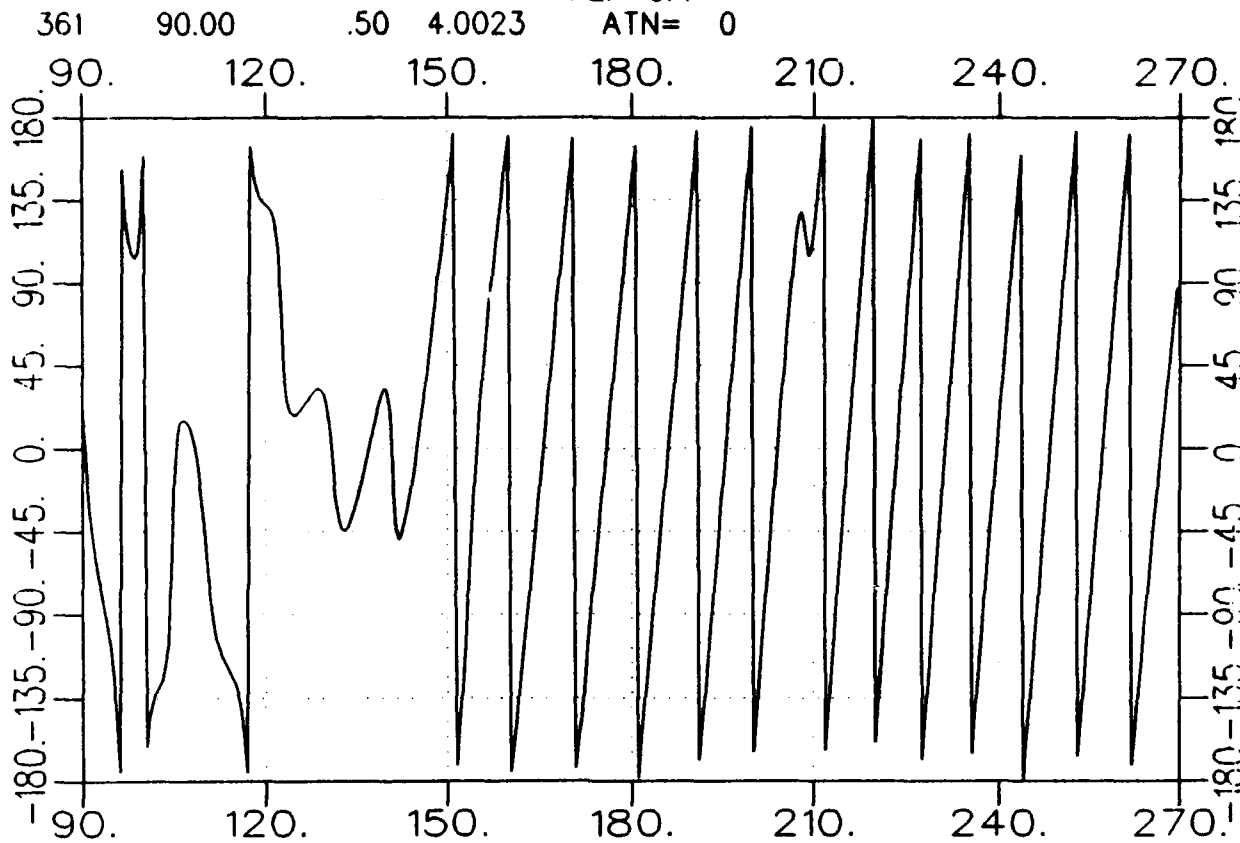
d3225aa0400-a.tar  
TARGET

AZIM. 08/13/93 13:12  
bare v

AVE= 82  
REF=OFF

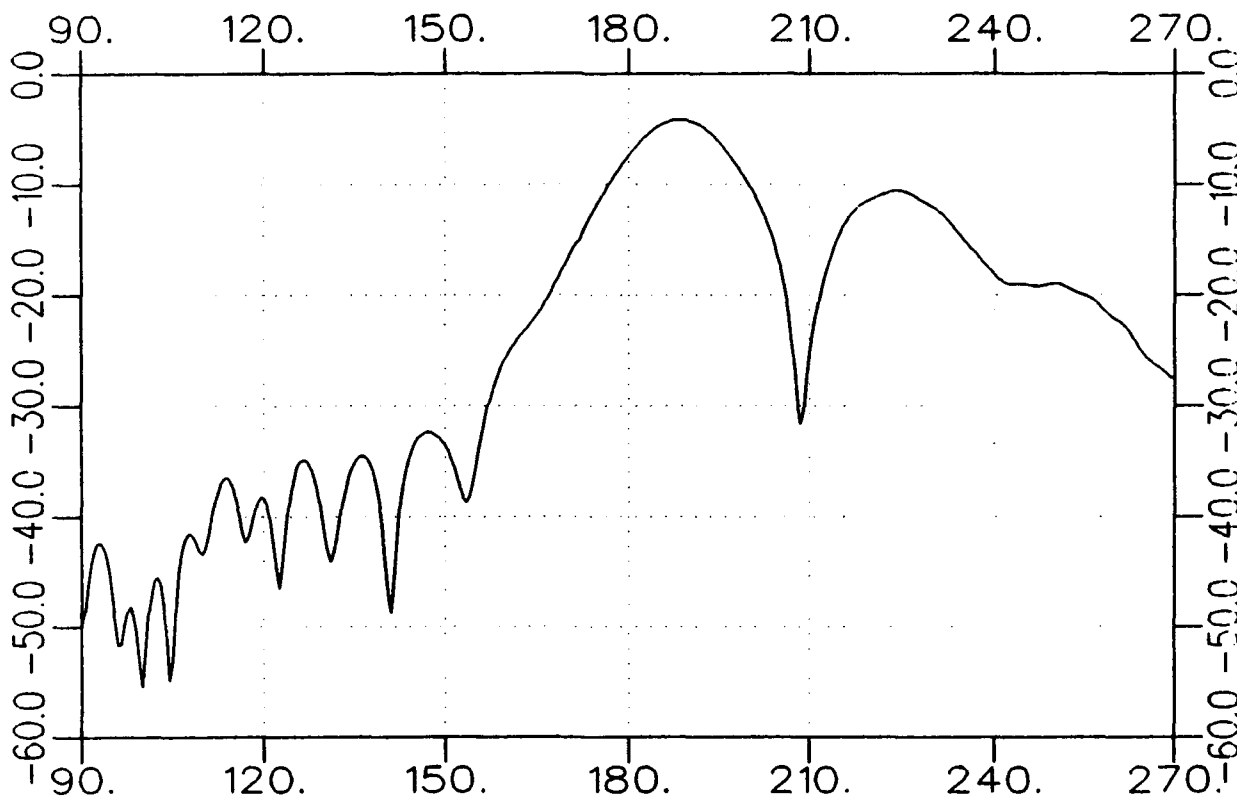
ATN= 0

PHASE IN DEGREES



ANGLE IN DEGREES

MAGNITUDE IN DB

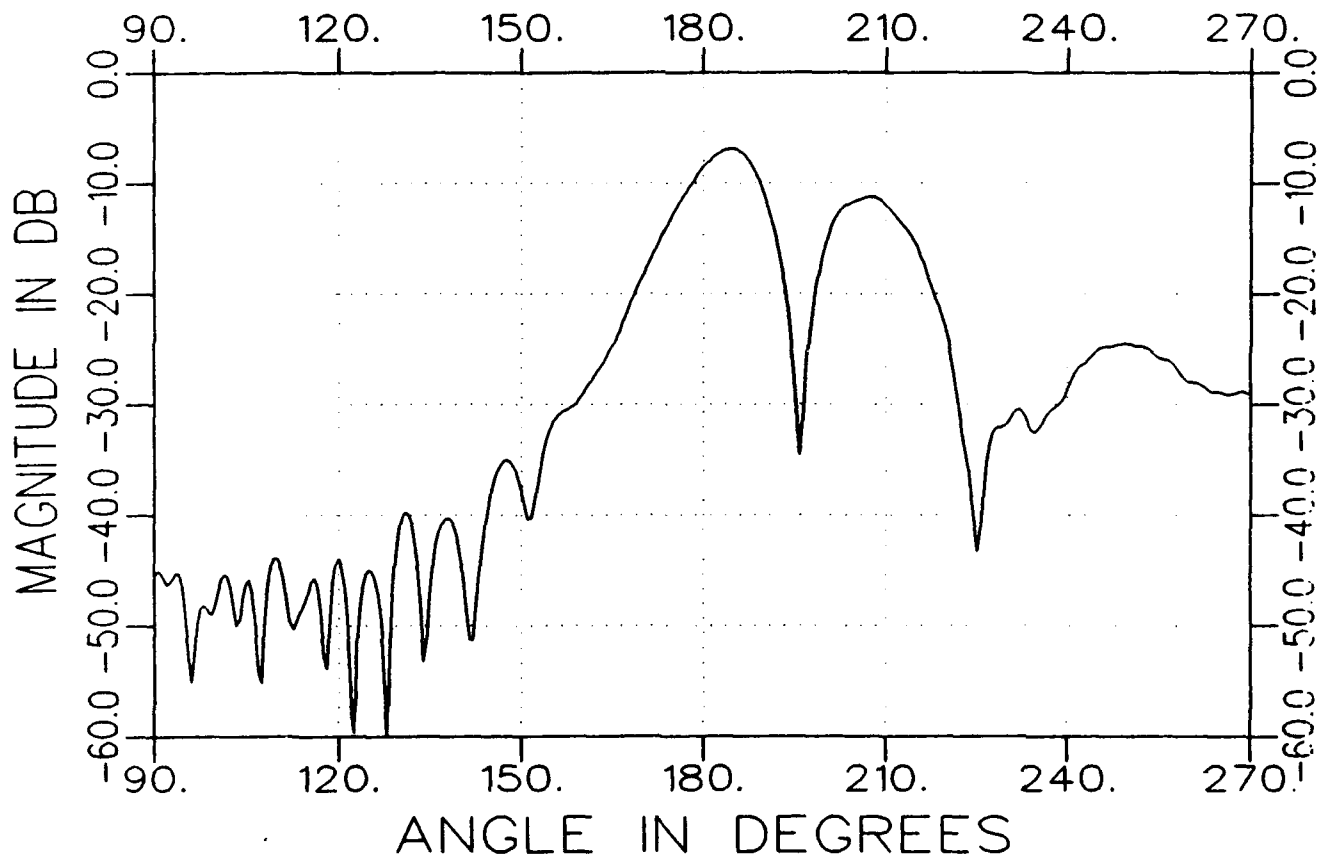
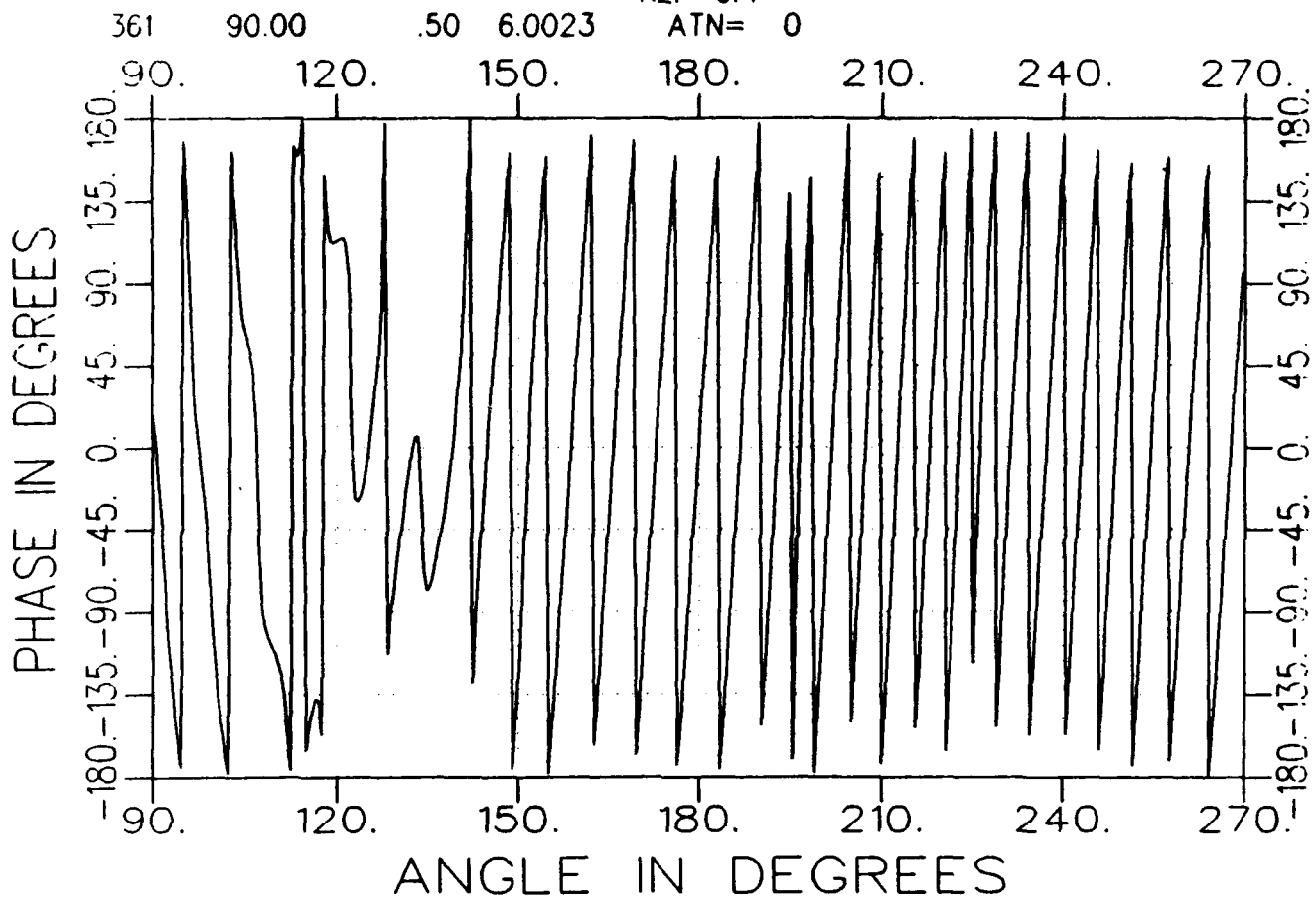


ANGLE IN DEGREES

d3225aa0600-a.tar  
TARGET

AZIM. 08/13/93 13:14  
bare v

AVE= 82  
REF=OFF  
ATN= 0



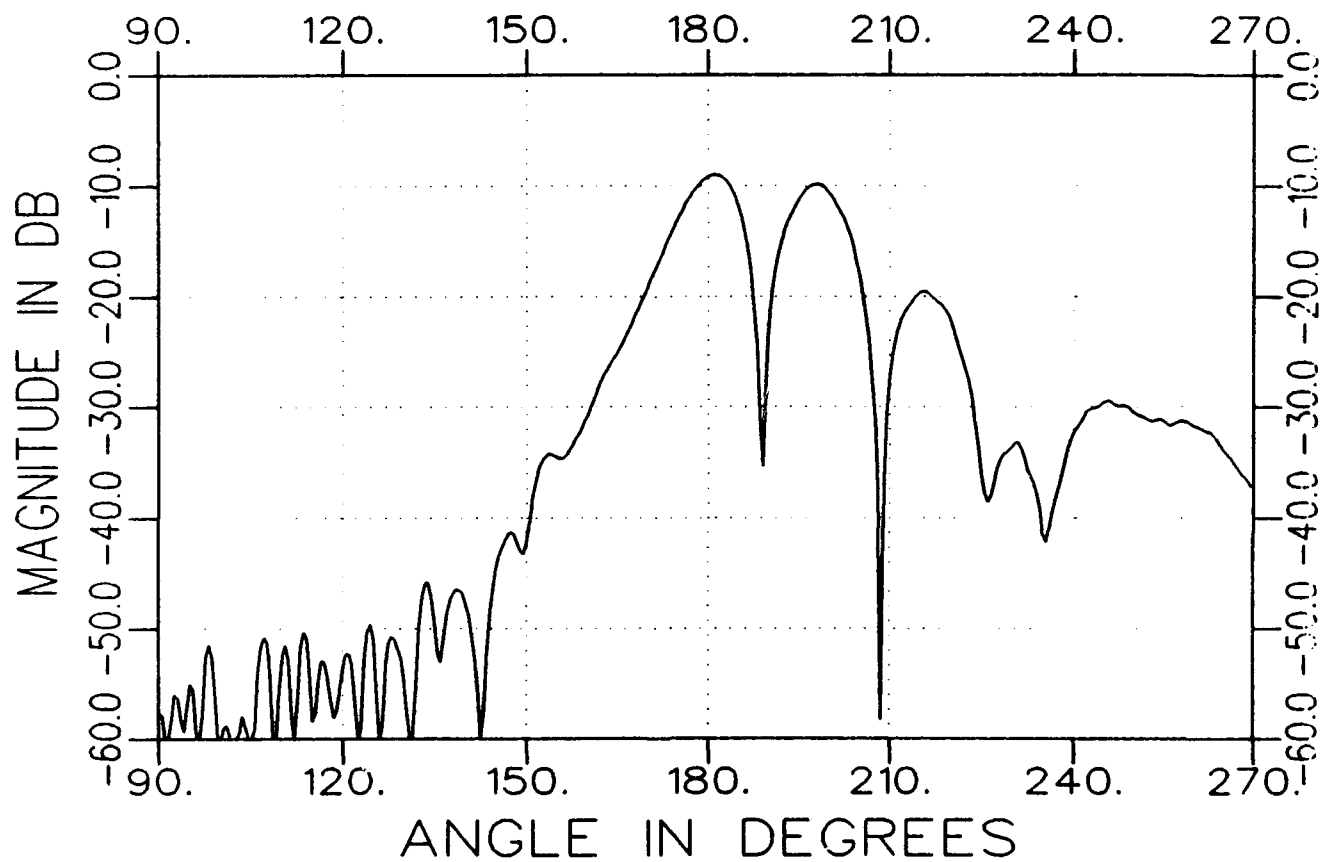
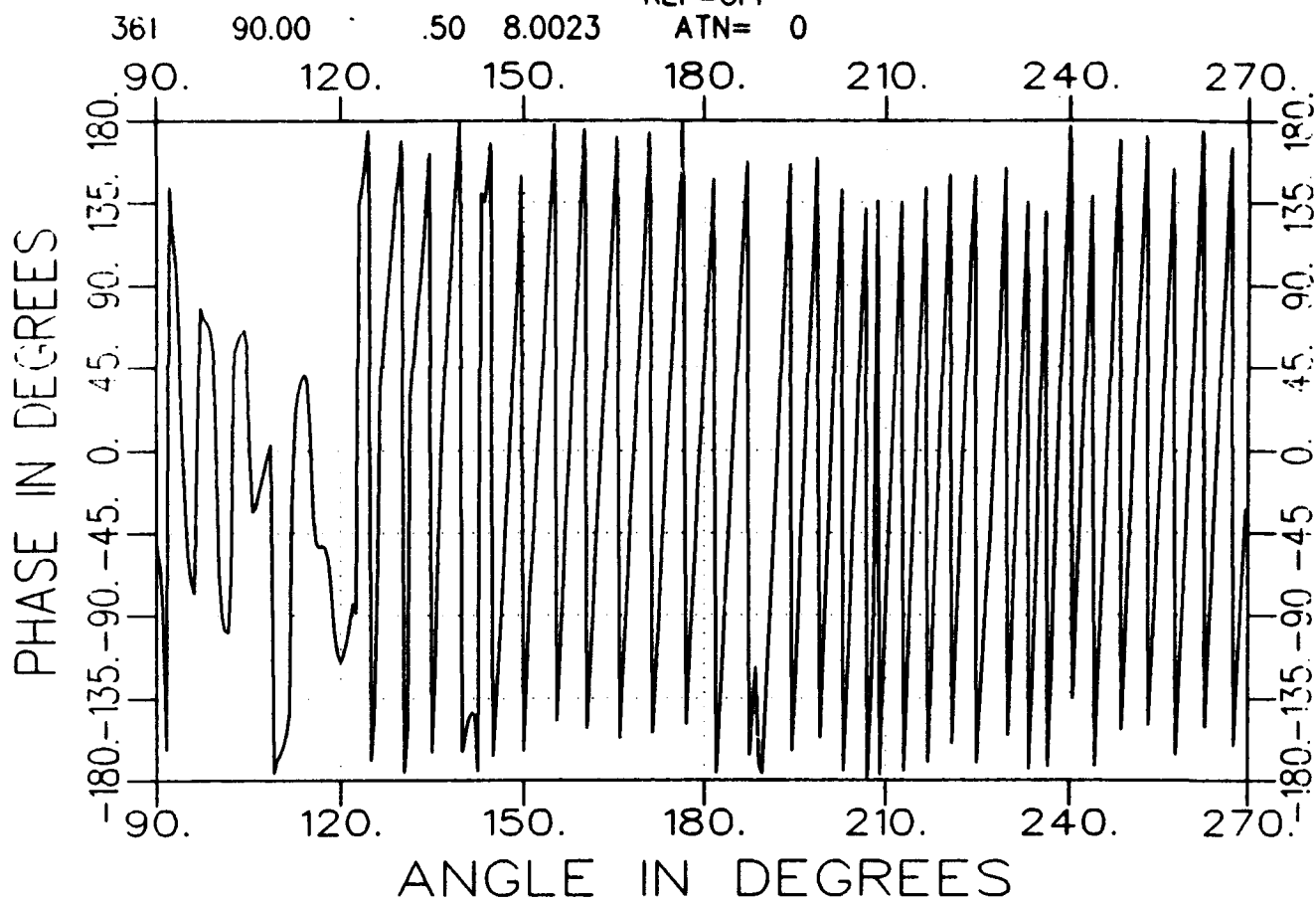


d3225000800-a.tar  
TARGET

AZIM. 08/13/93 13:16  
bare v

AVE= 82  
REF=OFF

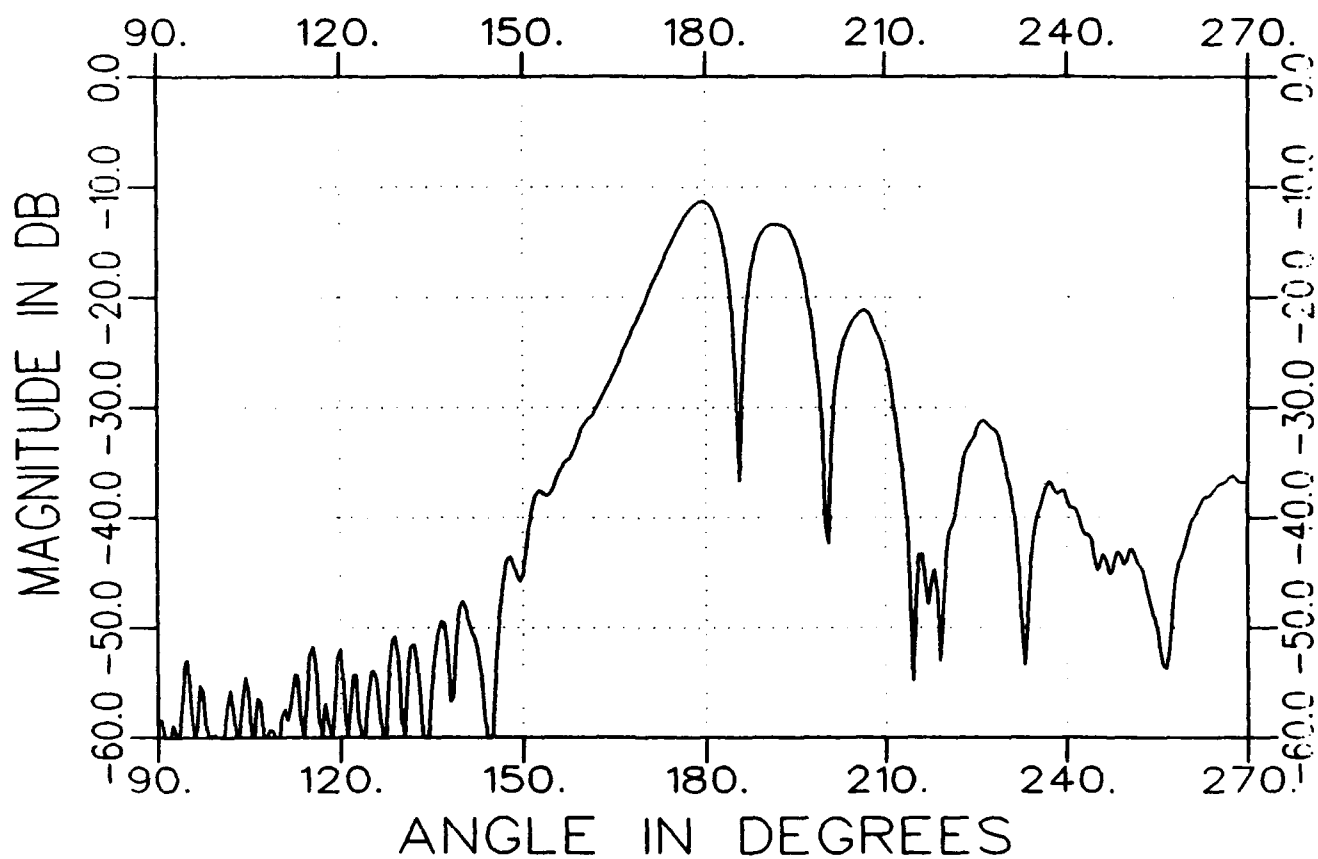
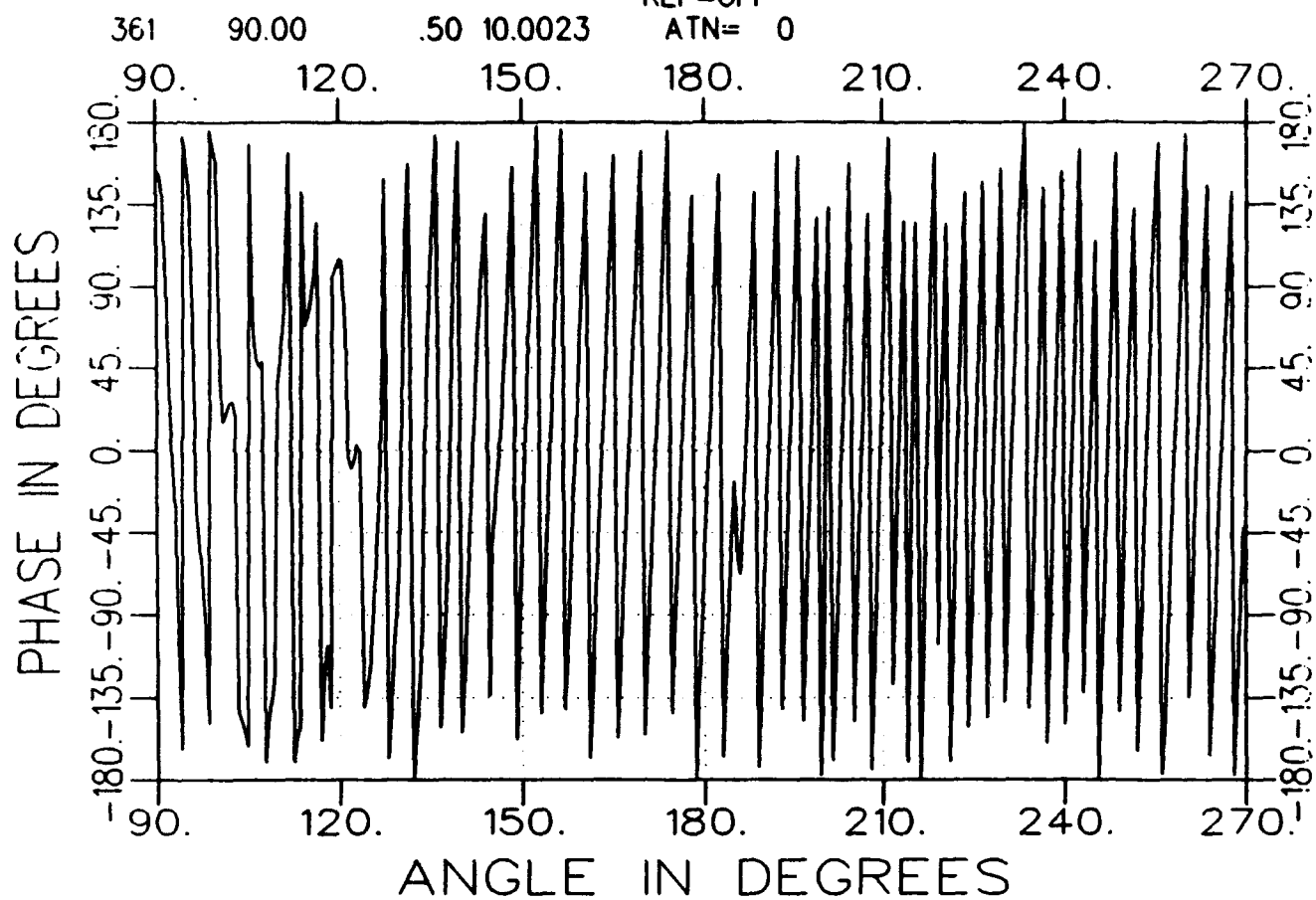
ATN= 0



d3225aa1000-a.tar  
TARGET

AZIM. 08/13/93 13:18  
bare v

AVE= 82  
REF=OFF  
ATN= 0

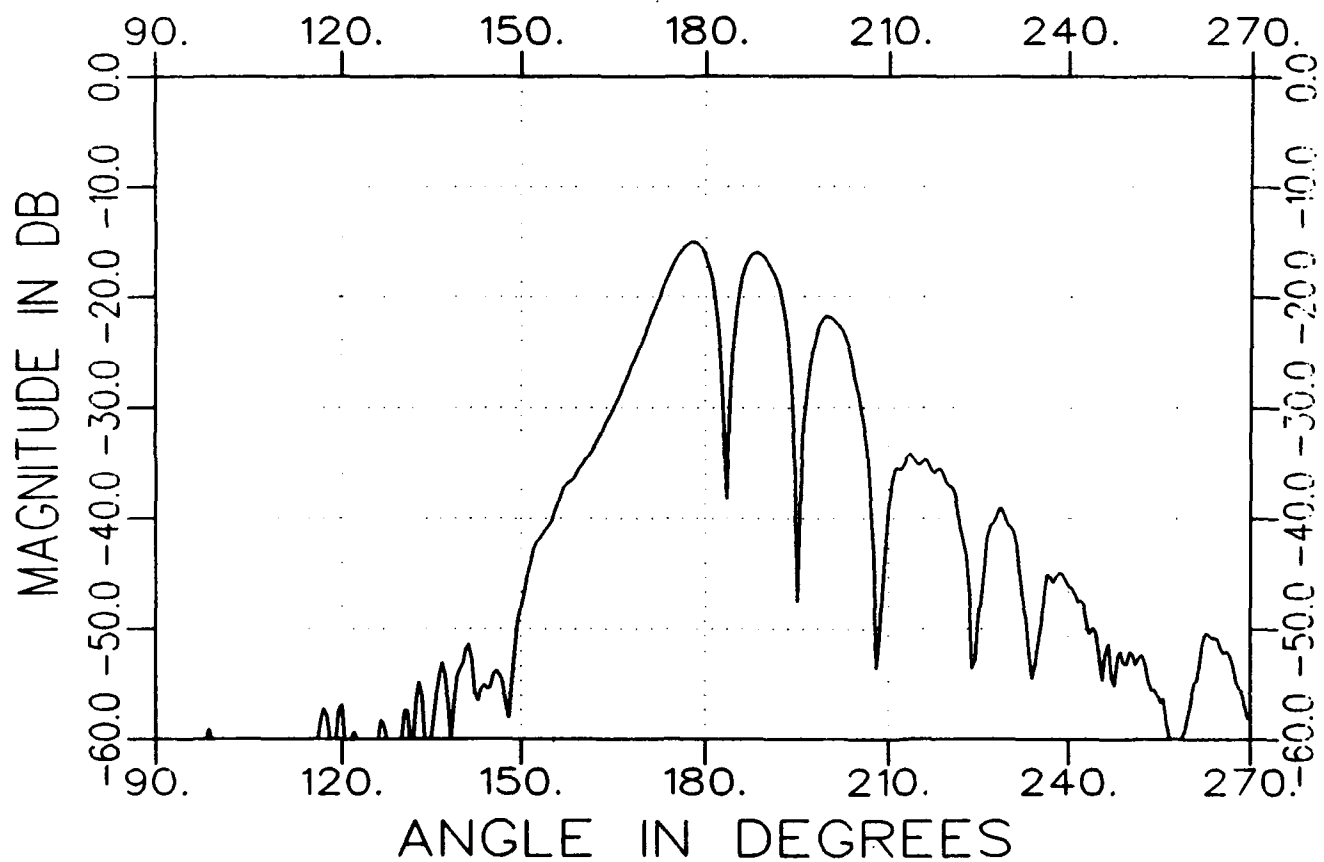
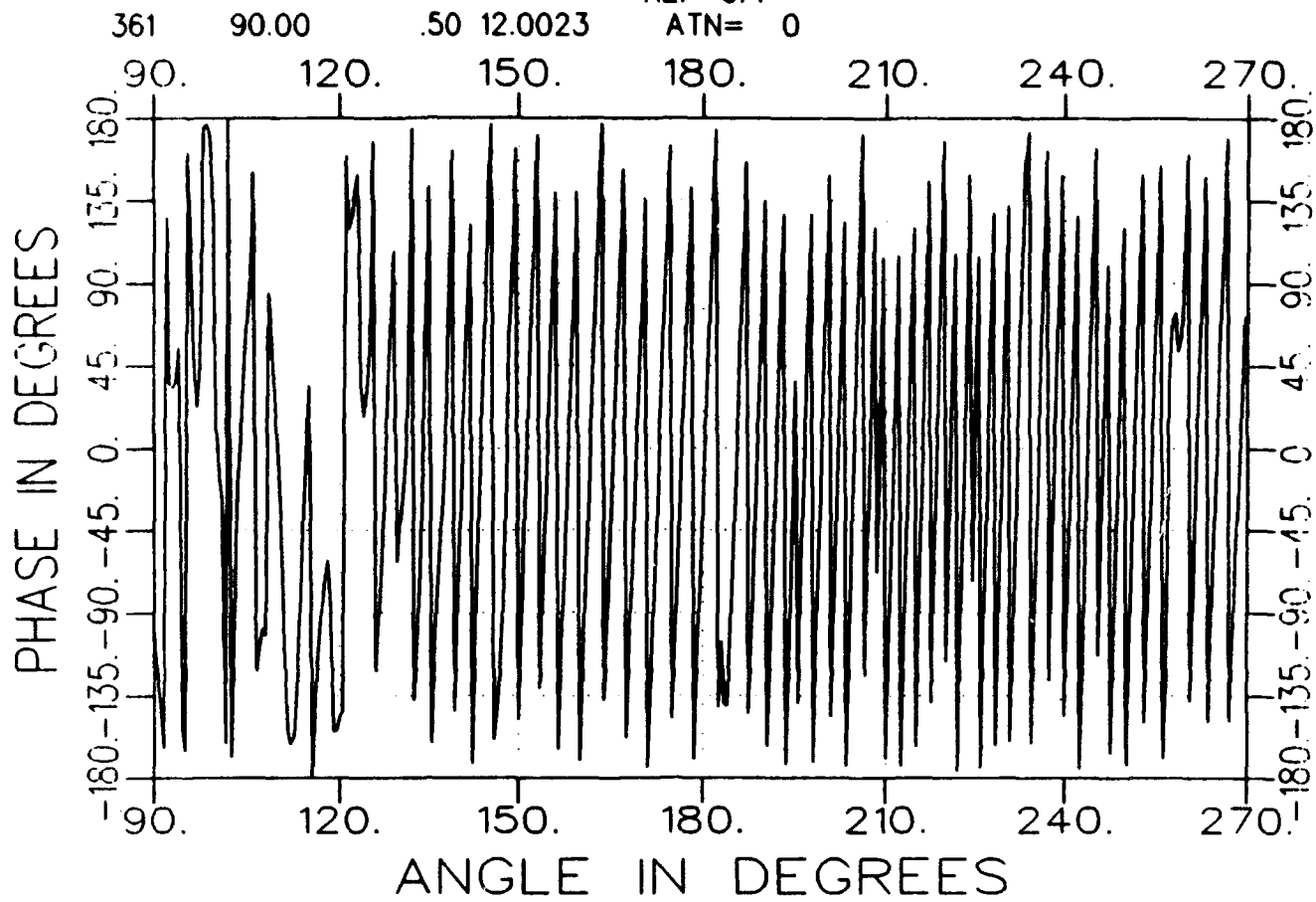


d3225aa1200-a.tar  
TARGET

AZIM. 08/13/93 13:20  
bare v

AVE= 82  
REF=OFF

ATN= 0

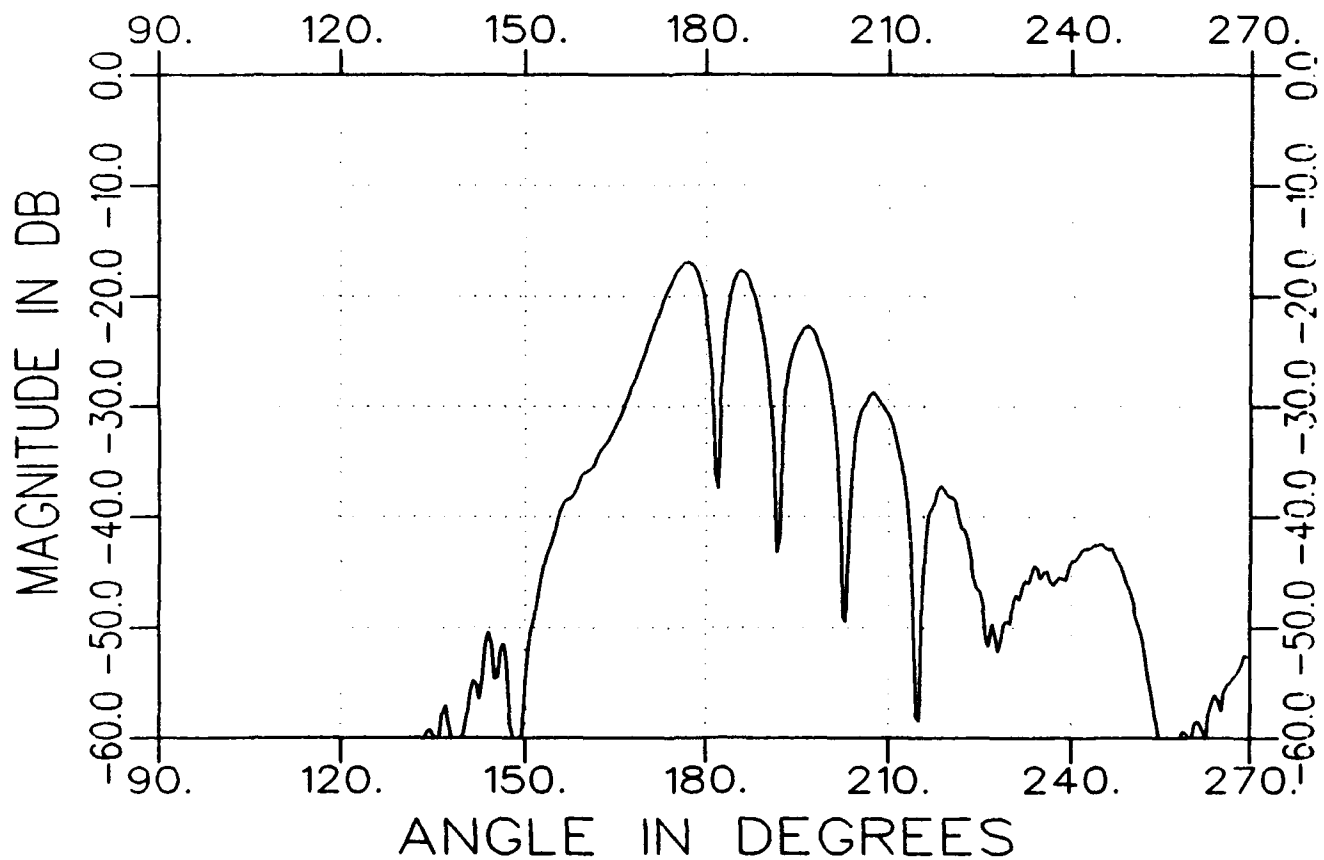
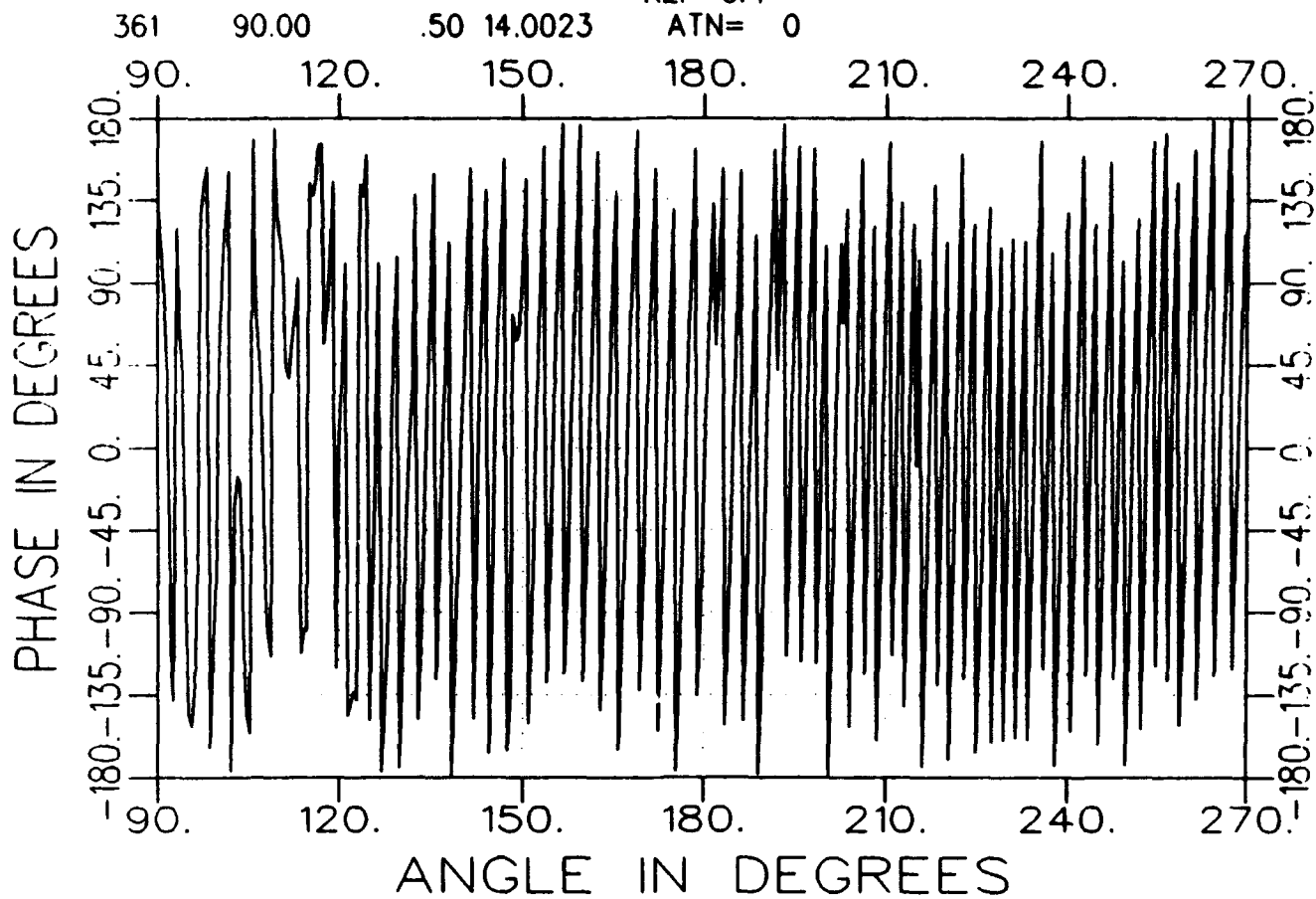


d3225au1400-a.tar  
TARGET

AZIM. 08/13/93 13:22  
bare v

AVE= 82  
REF=OFF

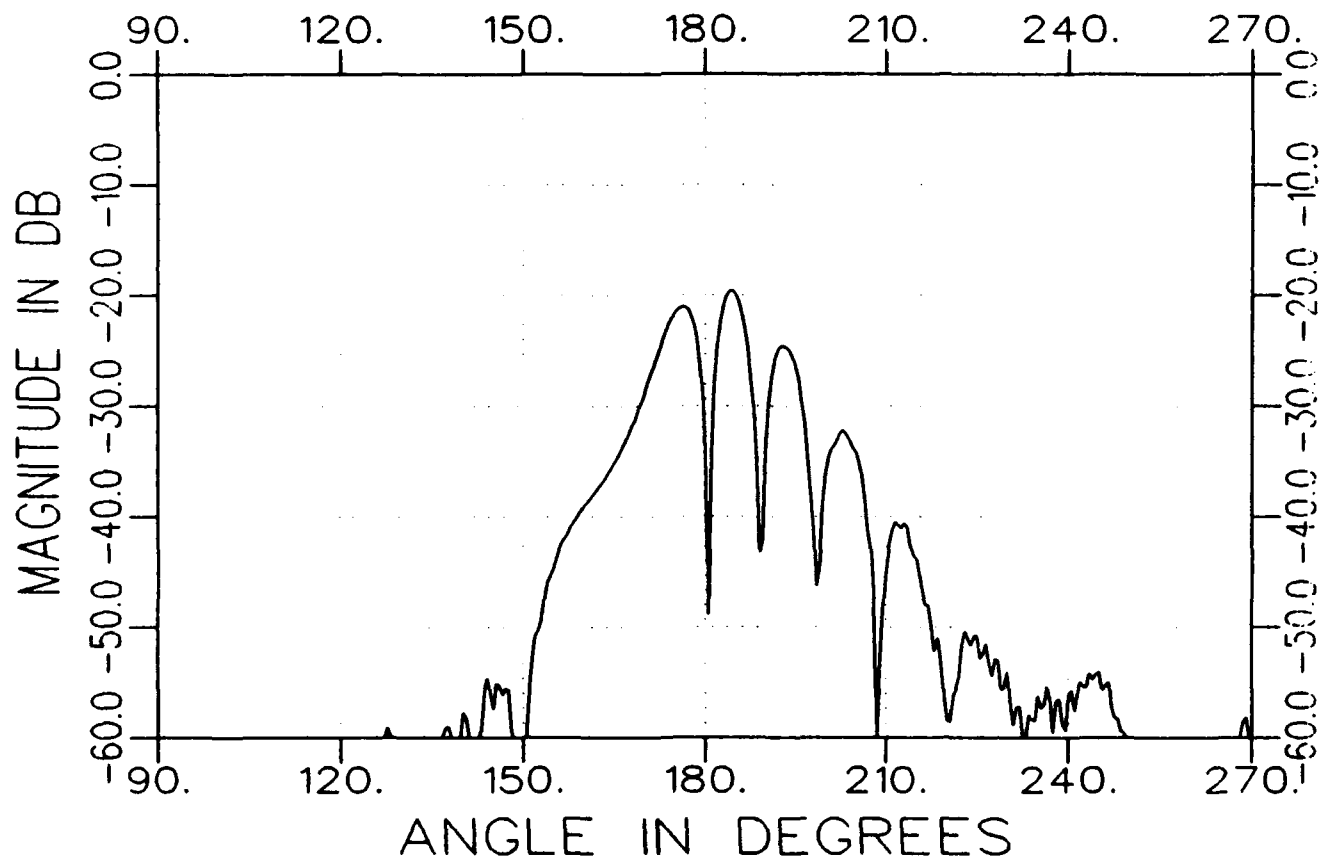
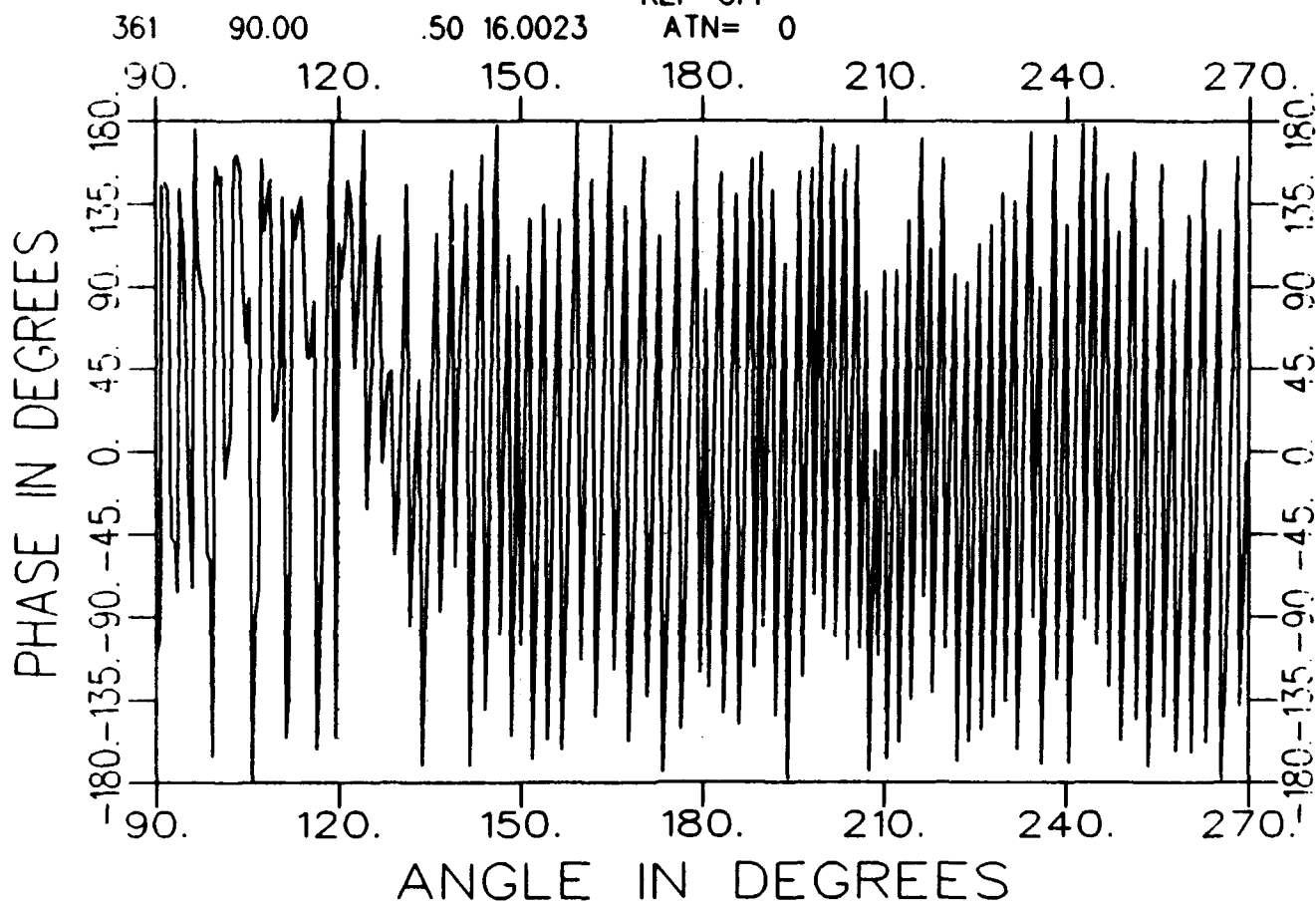
ATN= 0



d3225aa1600-a.tar  
TARGET

AZIM. 08/13/93 13:24  
bare v

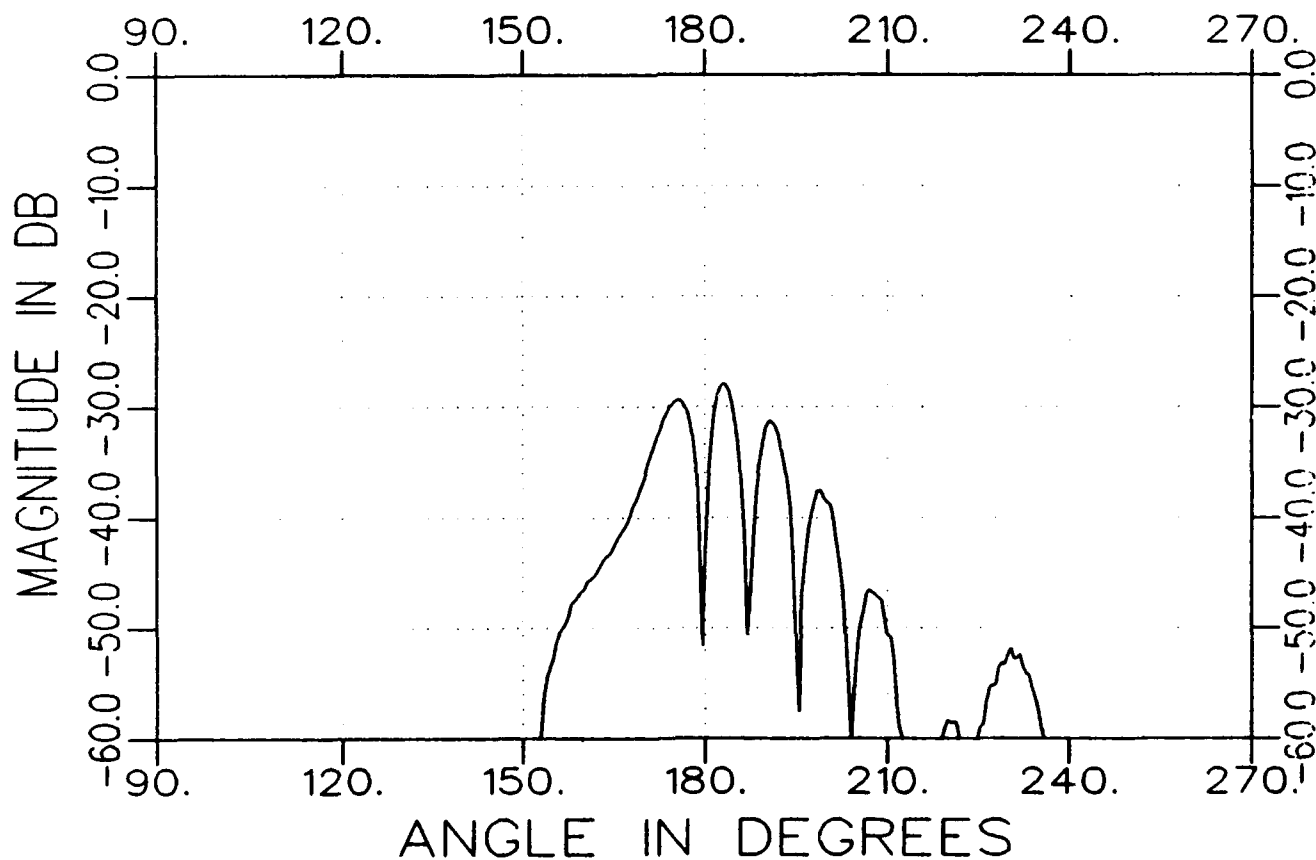
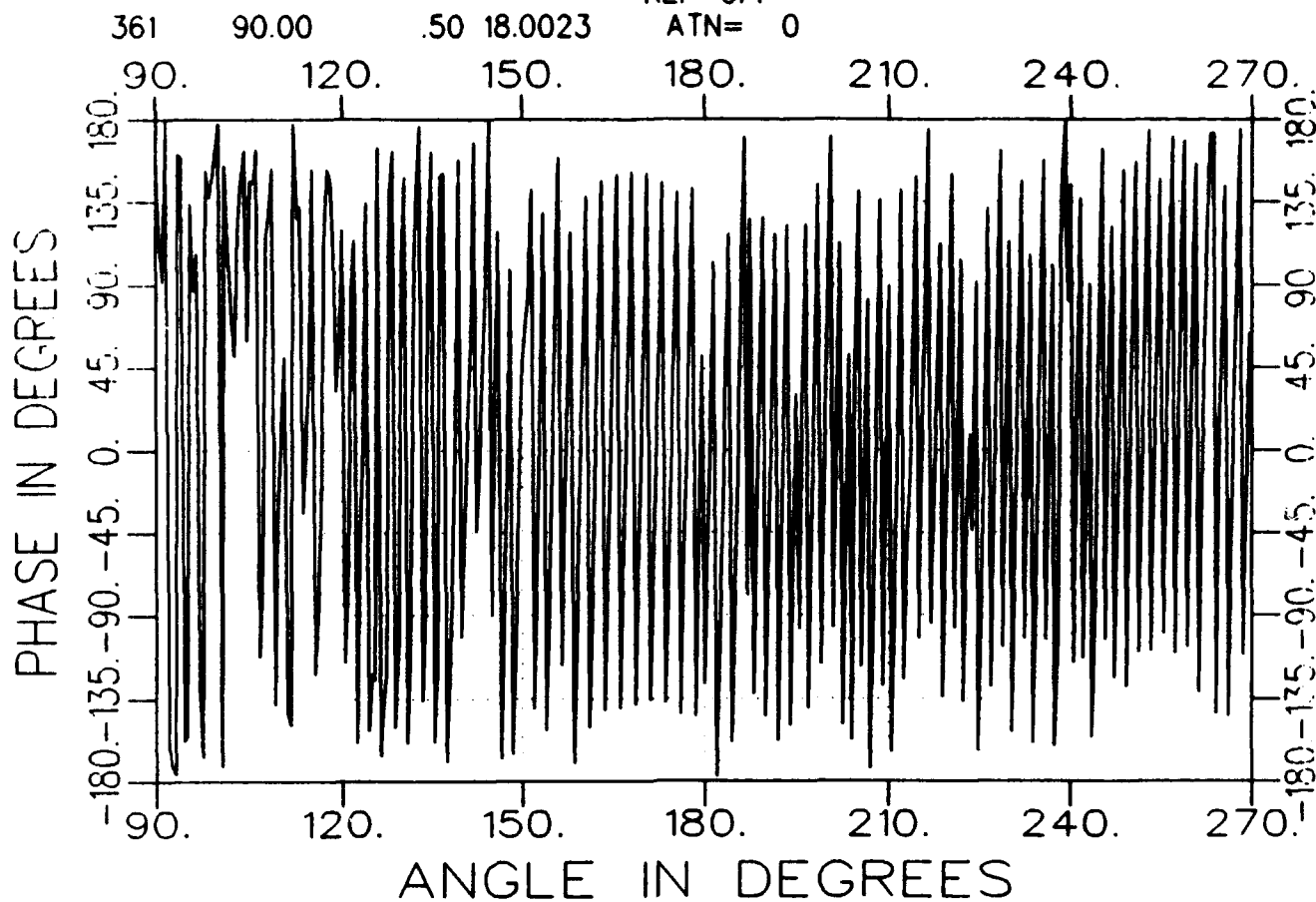
AVE= 82  
REF=OFF  
ATN= 0



d3225aa1800-a.tar  
TARGET

AZIM. 08/13/93 13:26  
bare v

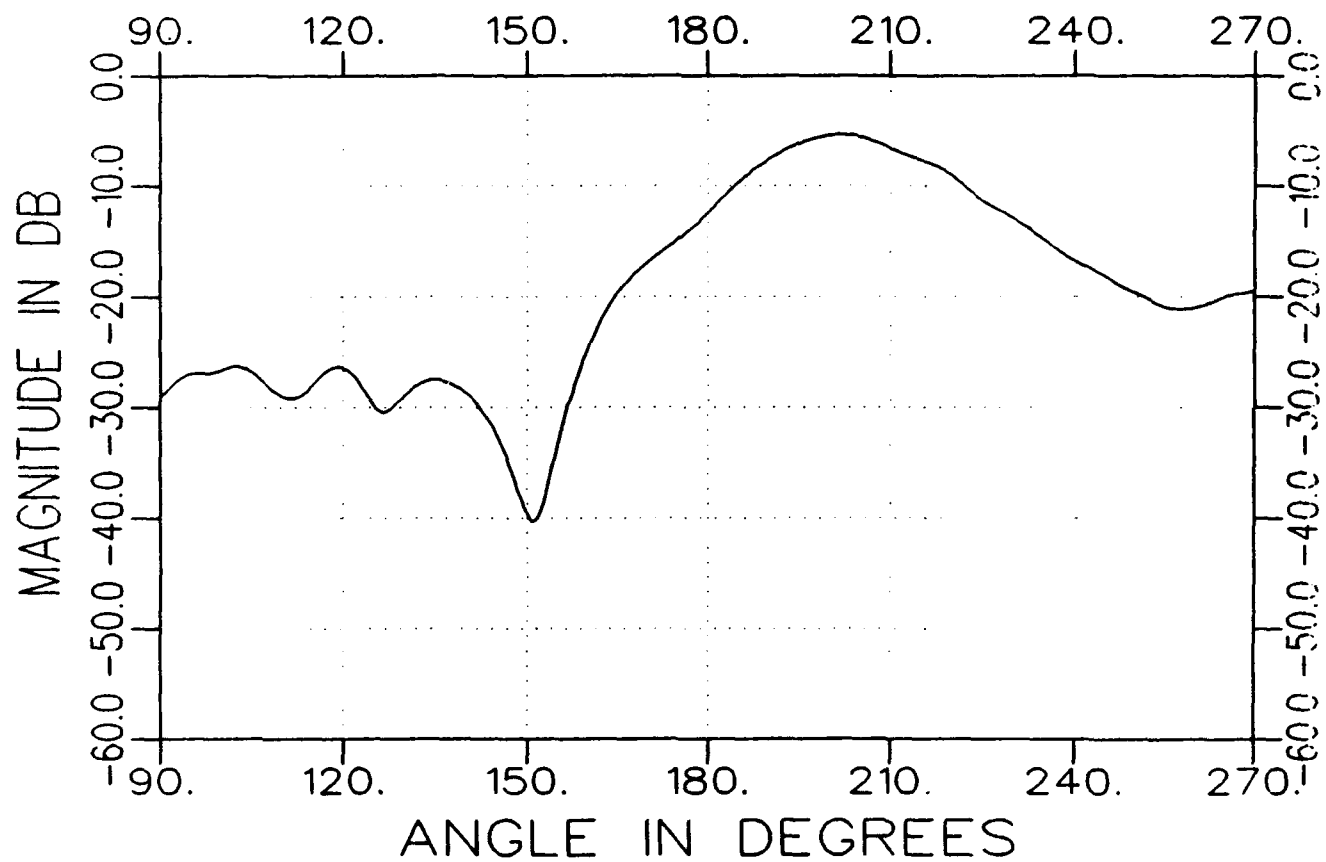
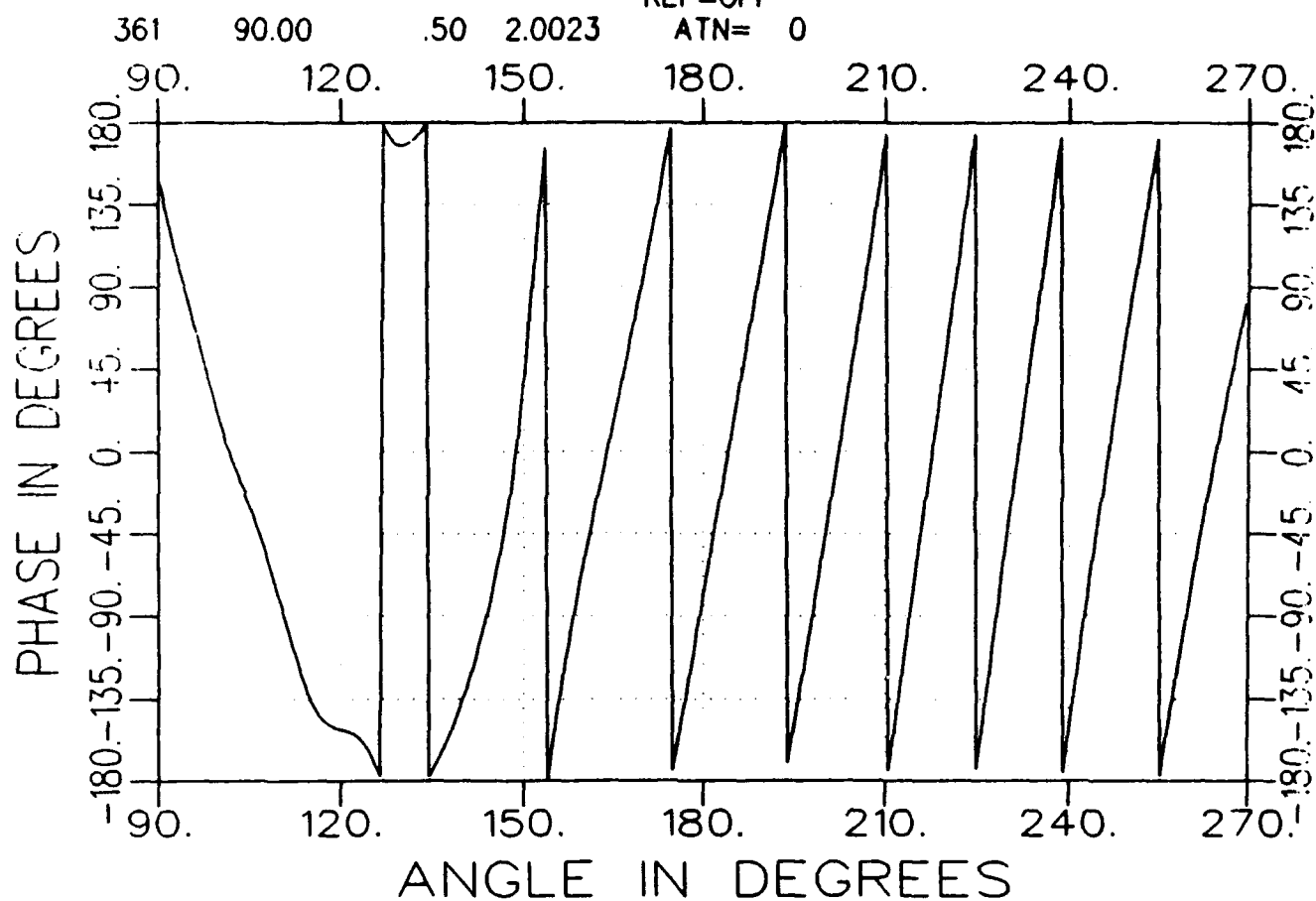
AVE= 82  
REF=OFF  
ATN= 0



e3225aa0200-a.tar  
TARGET

AZIM. 08/13/93 13:35  
long ind. grid AVE= 82  
REF=OFF

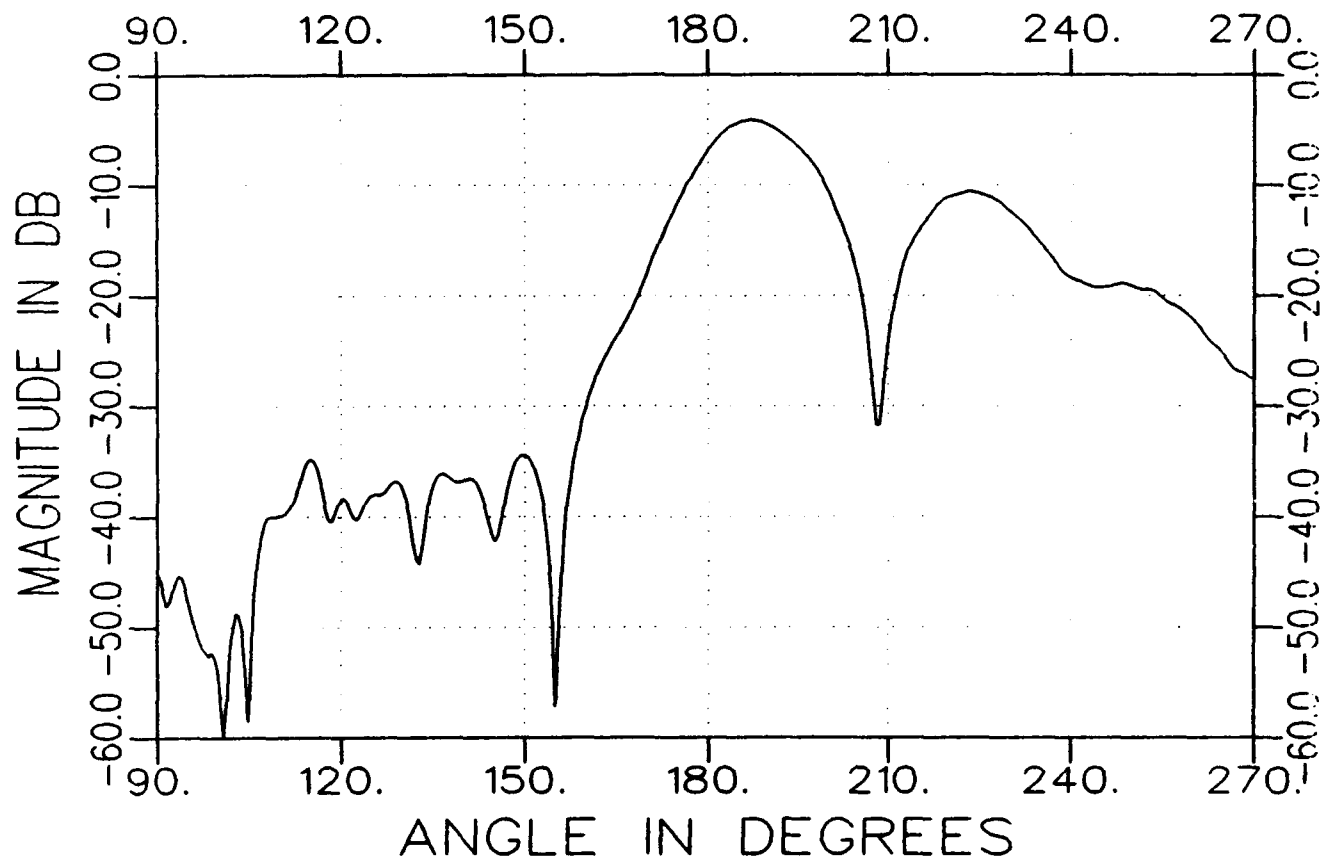
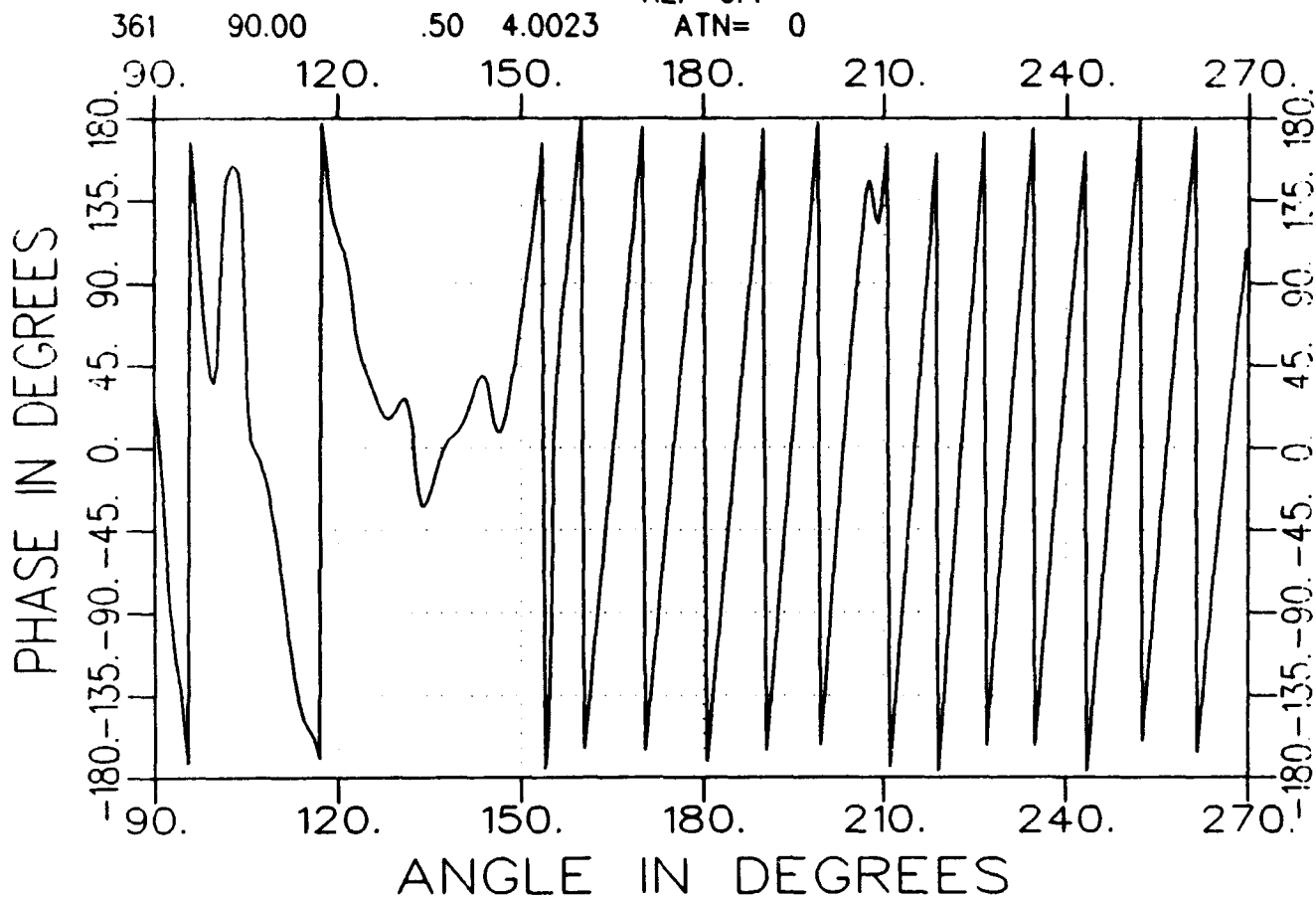
ATN= 0



e3225aa0400-a.tar  
TARGET

AZIM. 08/13/93 13:37  
long ind. grid AVE= 82  
REF=OFF

ATN= 0



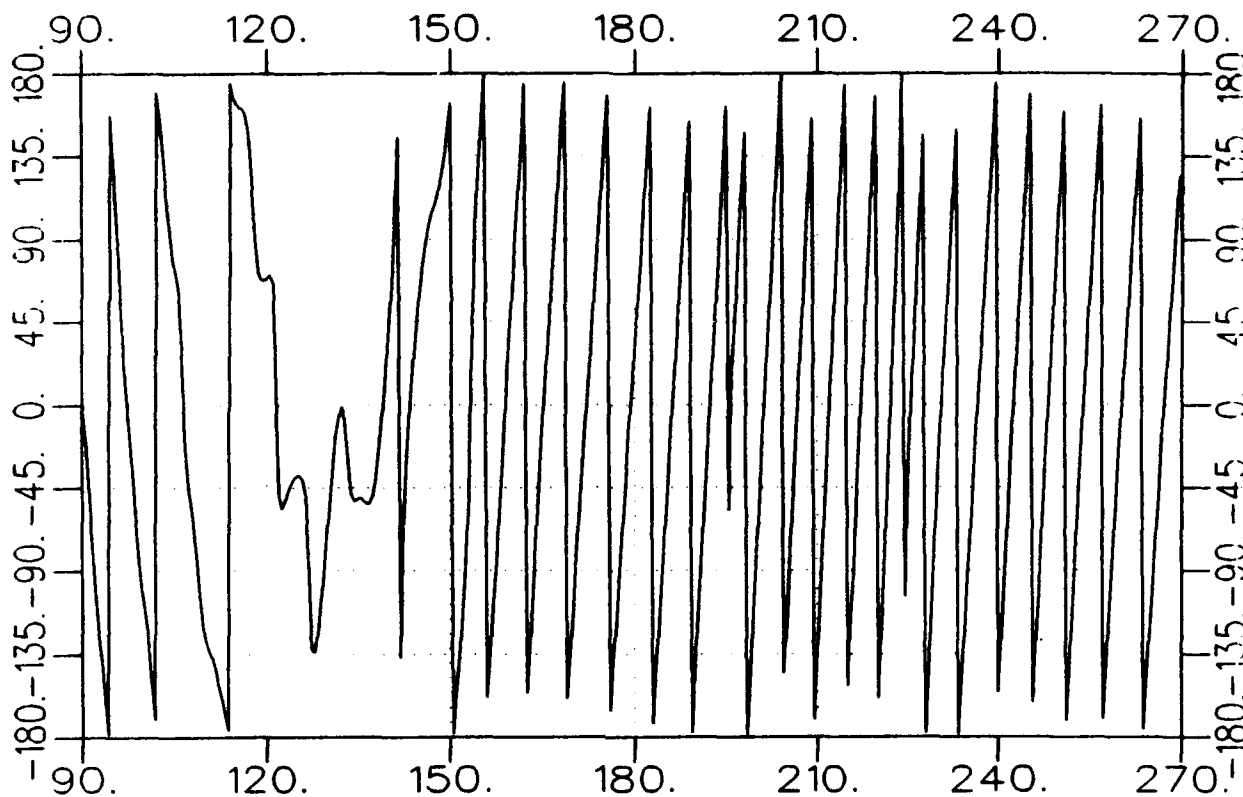


e3225aa0600-a.tar  
TARGET

AZIM. 08/13/93 13:39  
long ind. grid AVE= 82  
REF=OFF

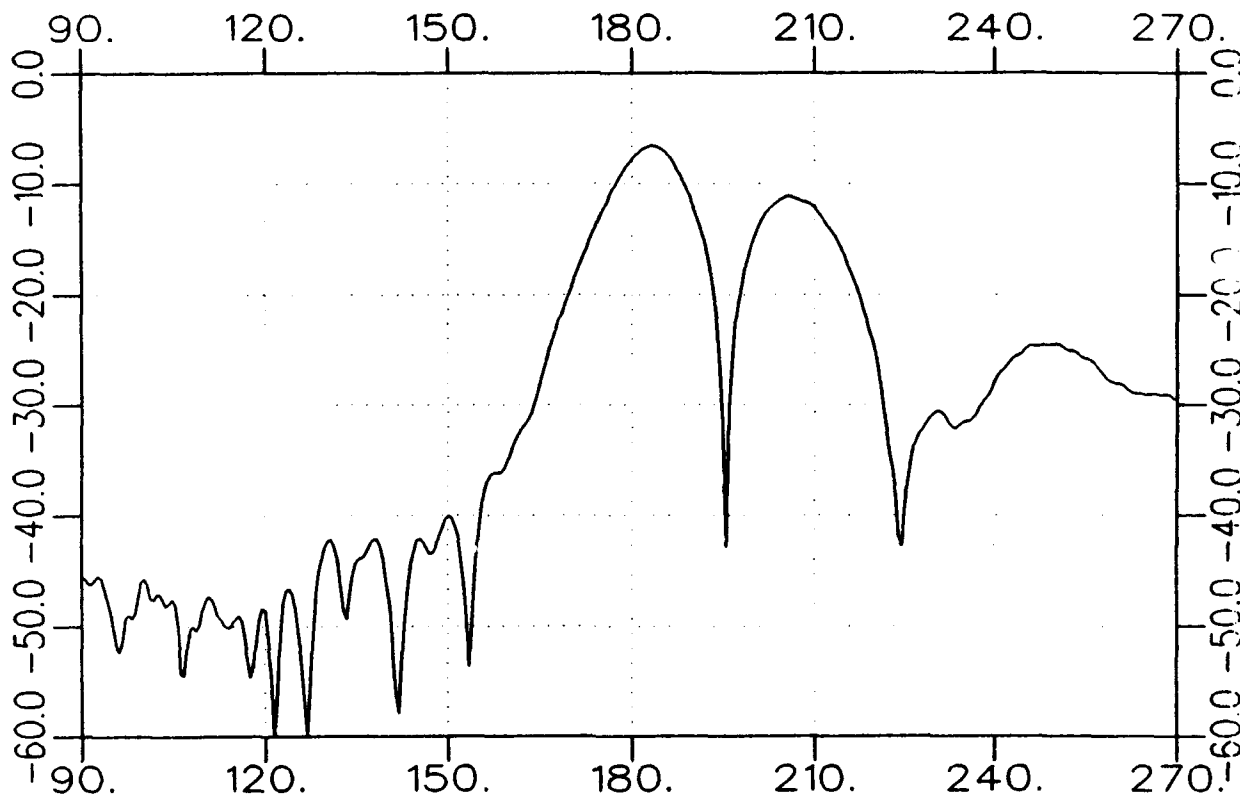
361 90.00 .50 6.0023 ATN= 0

PHASE IN DEGREES



ANGLE IN DEGREES

MAGNITUDE IN DB

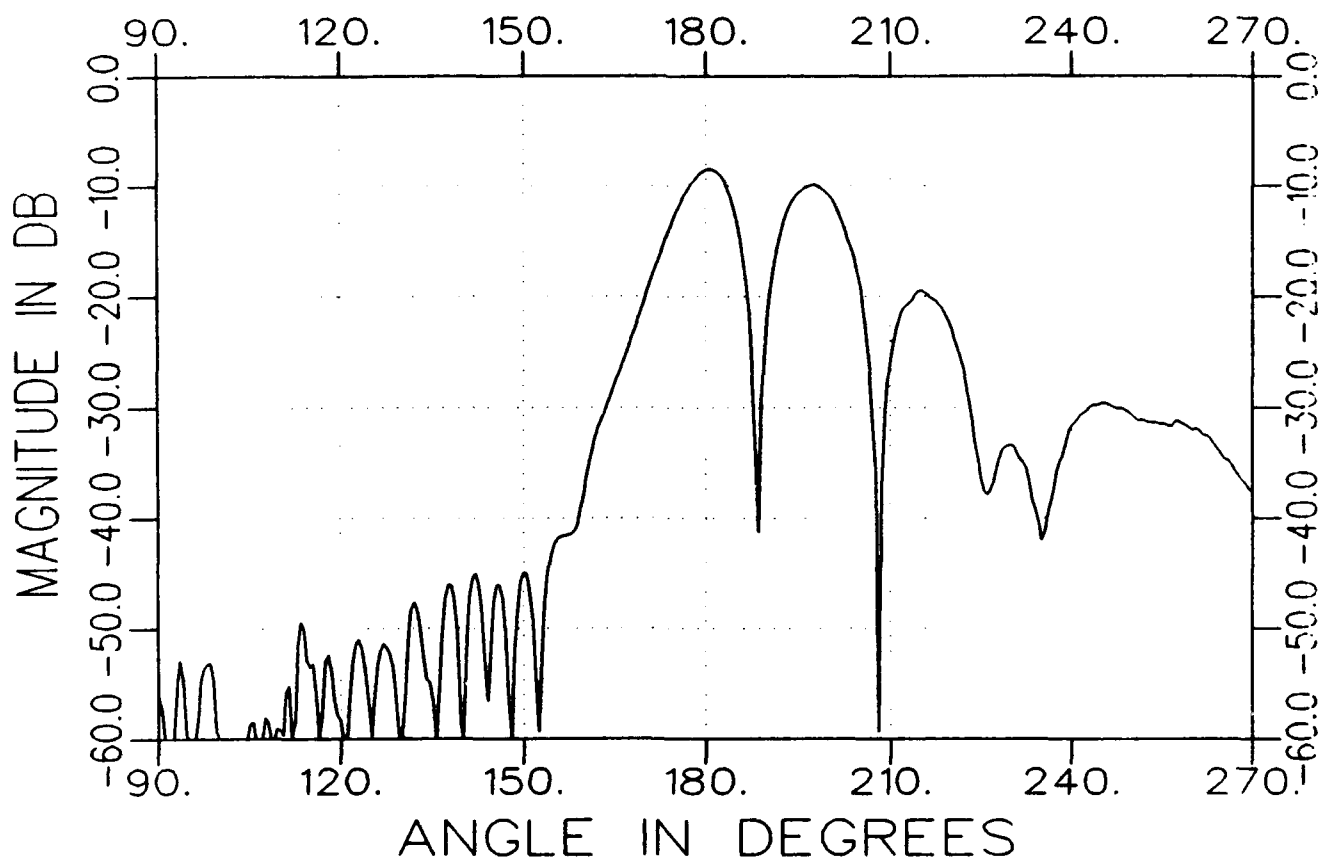
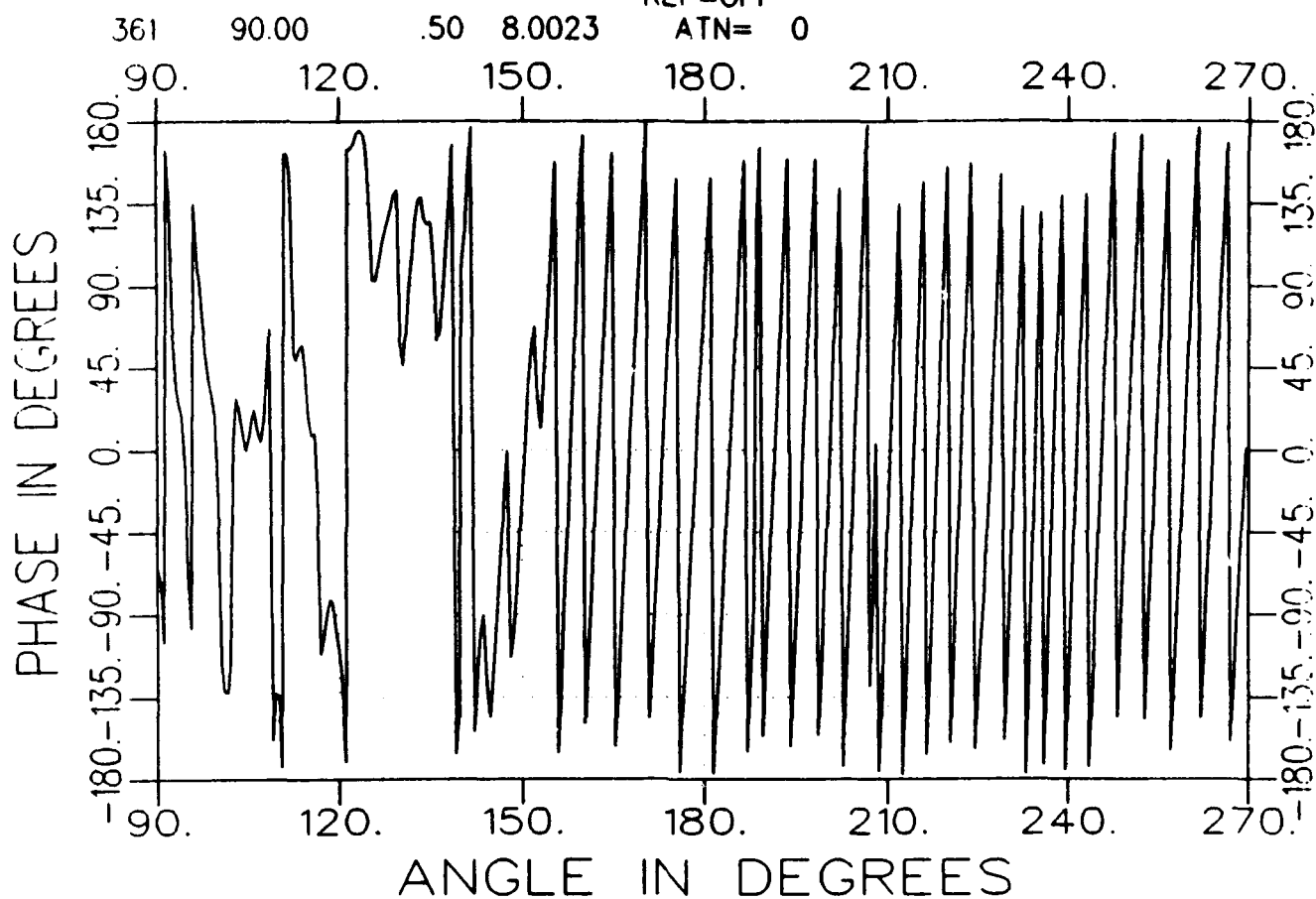


ANGLE IN DEGREES

e3225aa0800-a.tar  
TARGET

AZIM. 08/13/93 13:41  
long ind. grid AVE= 82  
REF=OFF

ATN= 0

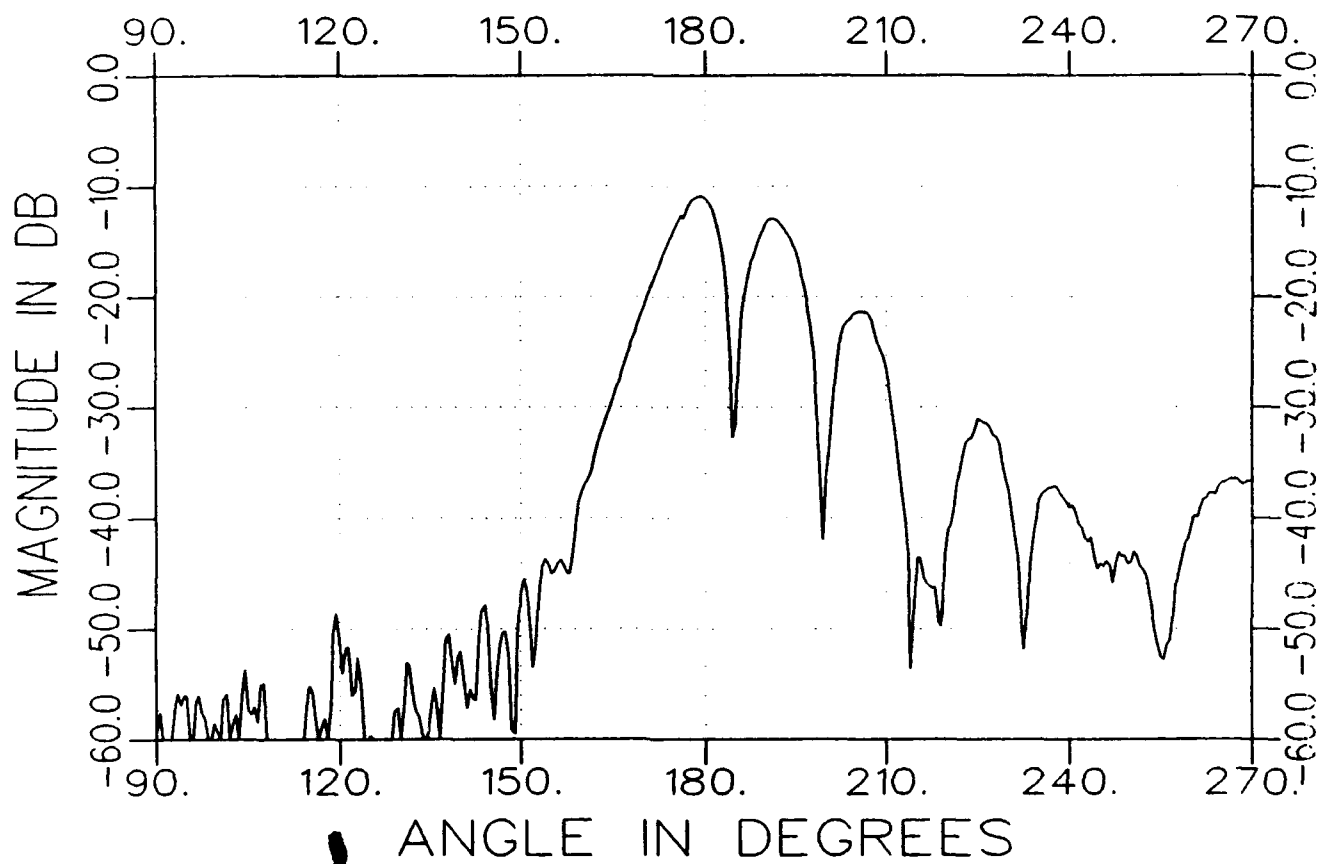
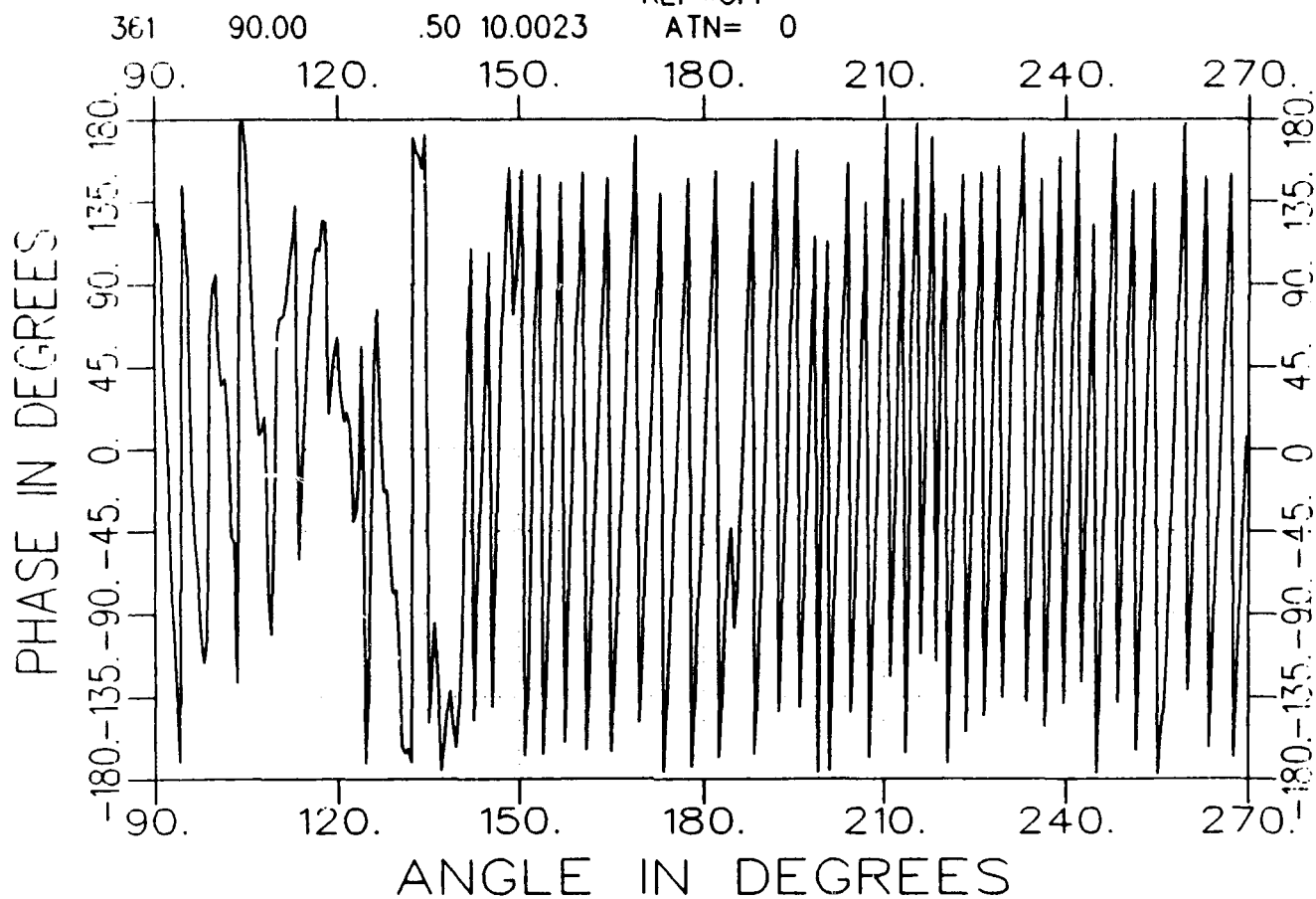


e3225au1000-a.tar  
TARGET

AZIM. 08/13/93 13:43  
long ind. grid AVE= 82

REF=OFF

ATN= 0

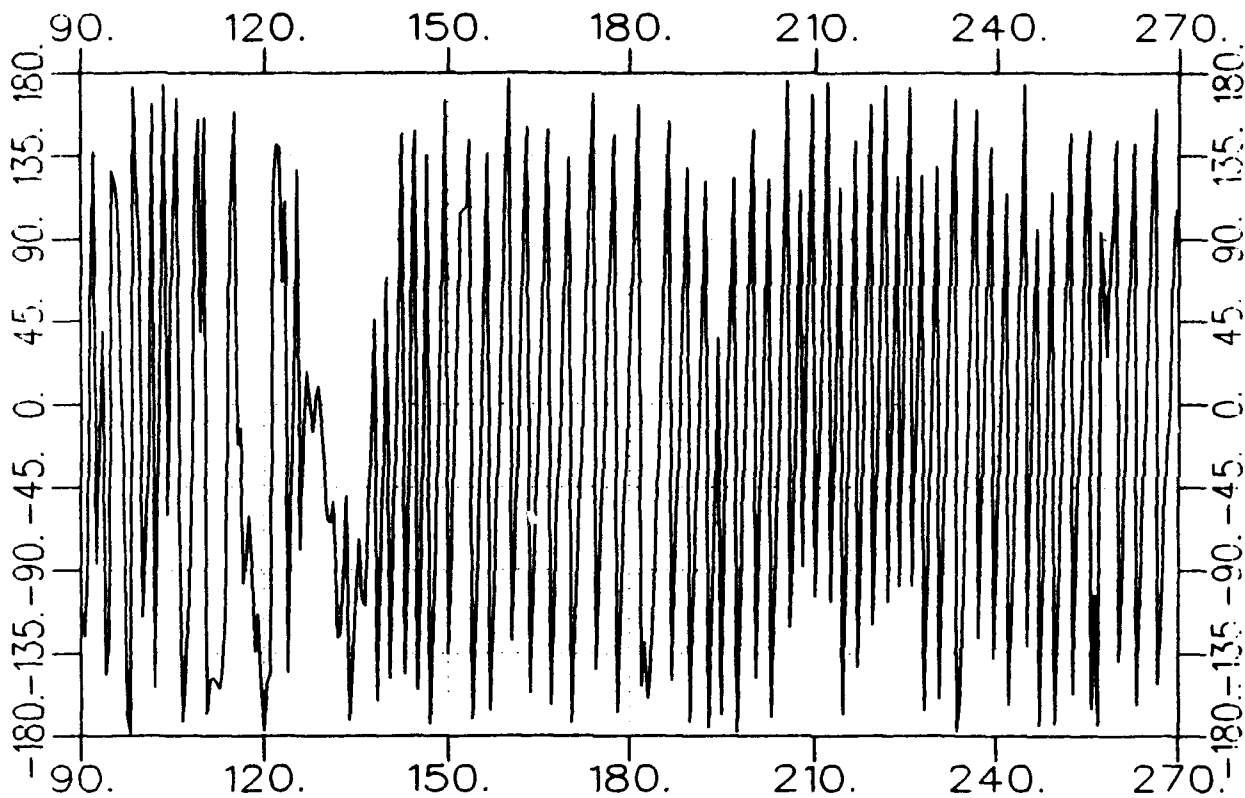


e3225aal200-a.tar  
TARGET

AZIM. 08/13/93 13:45  
long ind. grid AVE= 82  
REF=OFF

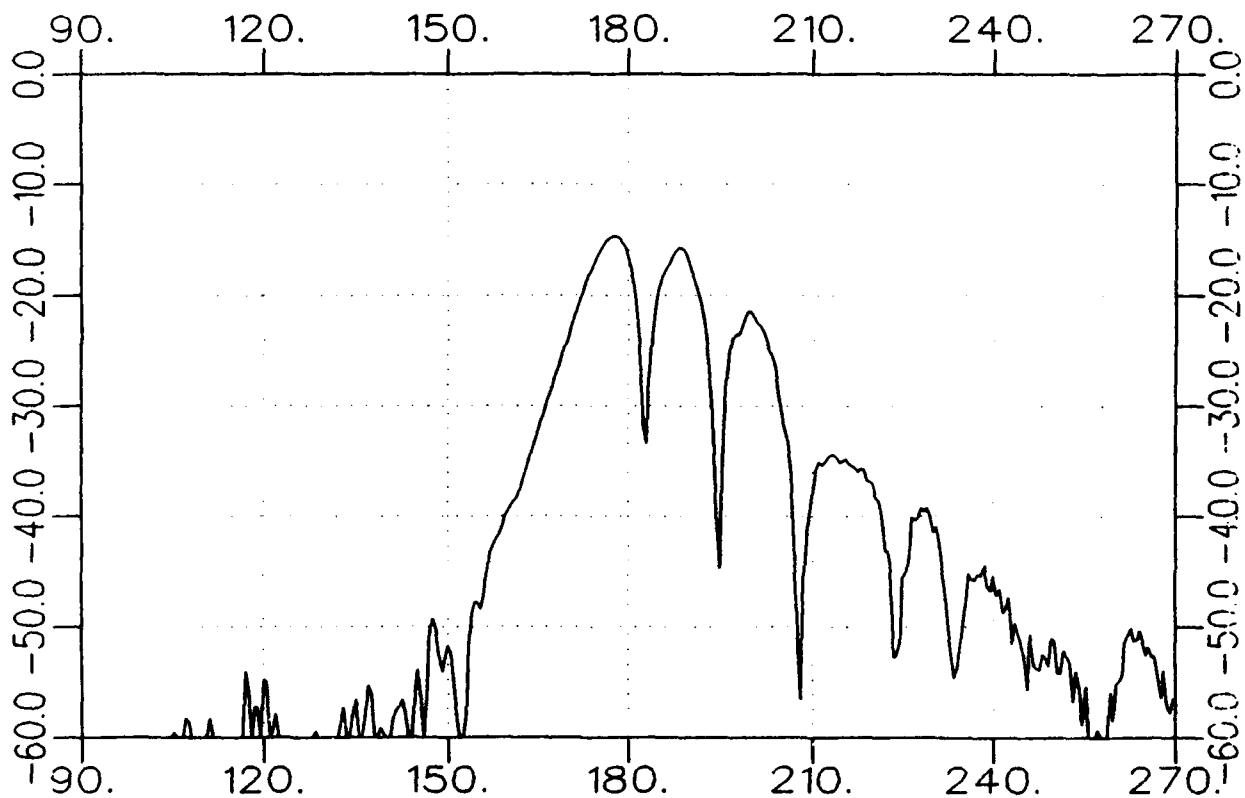
361 90.00 .50 12.0023 ATN= 0

PHASE IN DEGREES



ANGLE IN DEGREES

MAGNITUDE IN DB



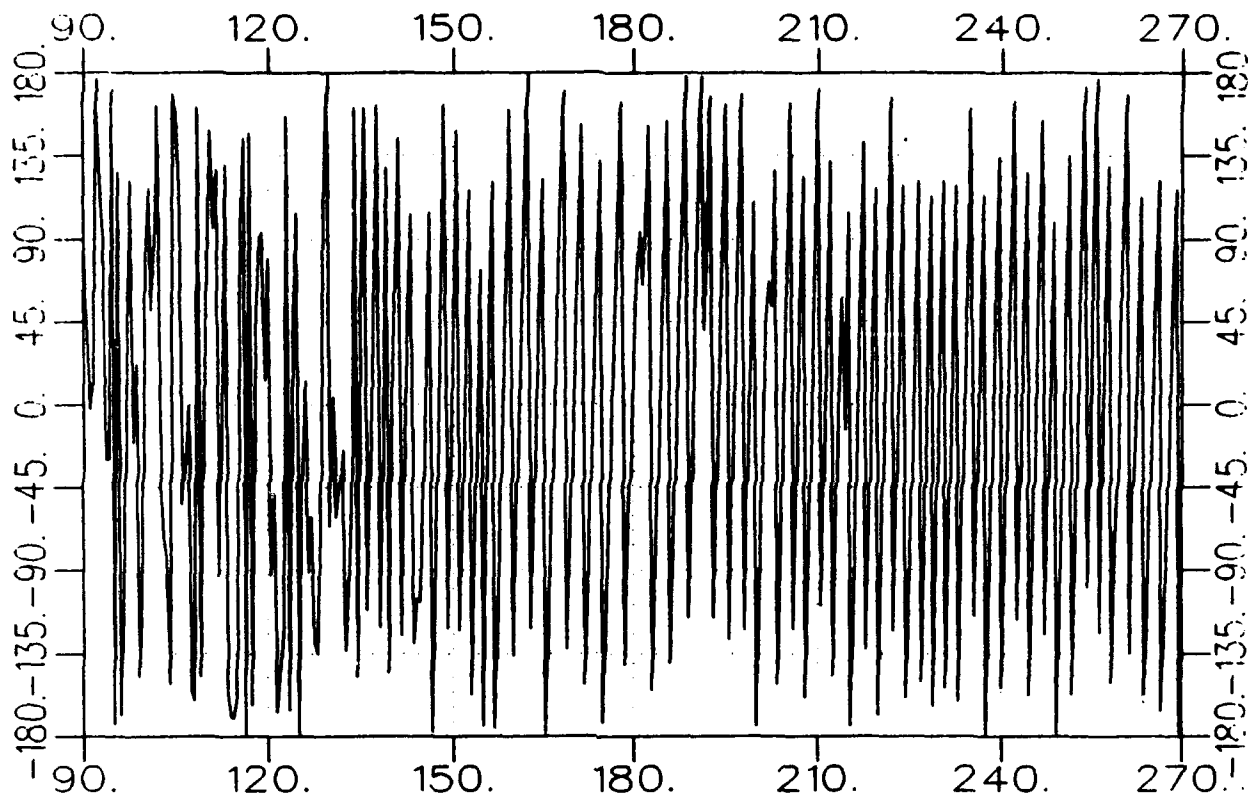
ANGLE IN DEGREES

e3225aa1400-a.tar  
TARGET

AZIM. 08/13/93 13:47  
long ind. grid AVE= 82  
REF=OFF

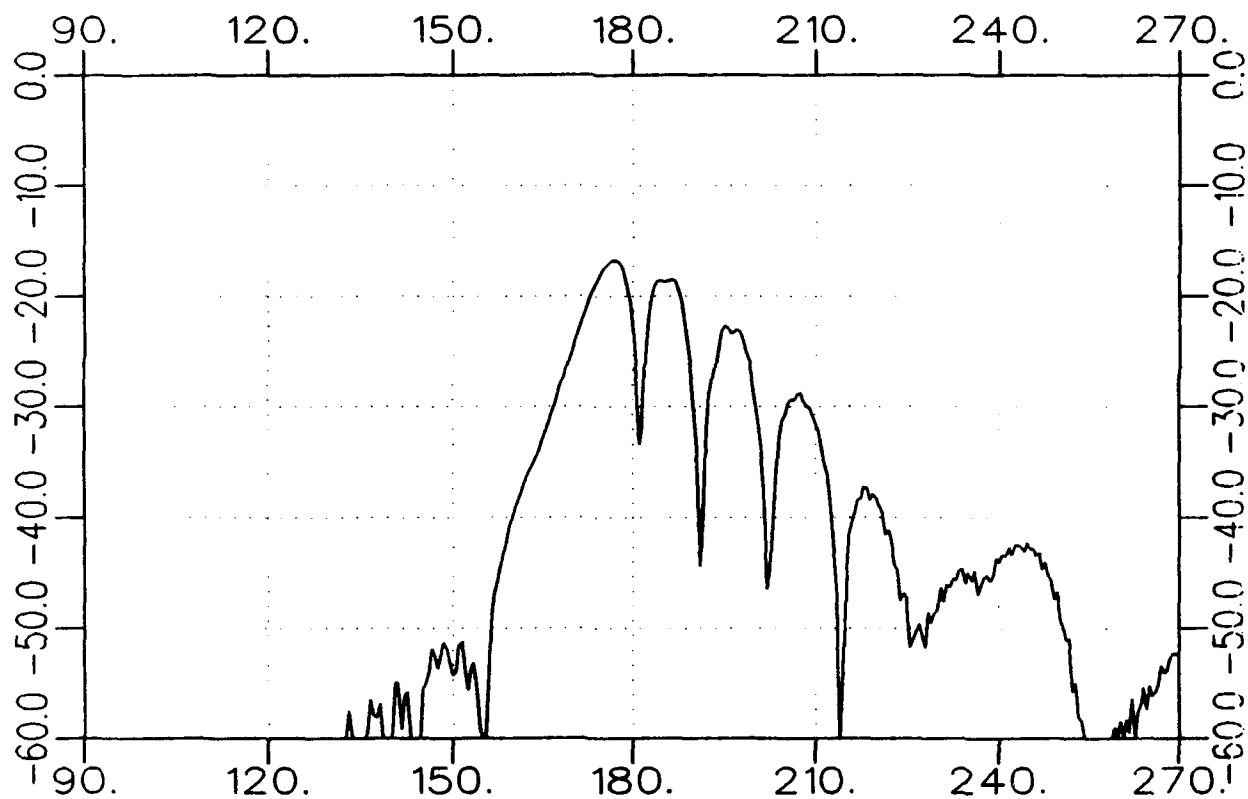
361 90.00 .50 14.0023 ATN= 0

PHASE IN DEGREES



ANGLE IN DEGREES

MAGNITUDE IN DB

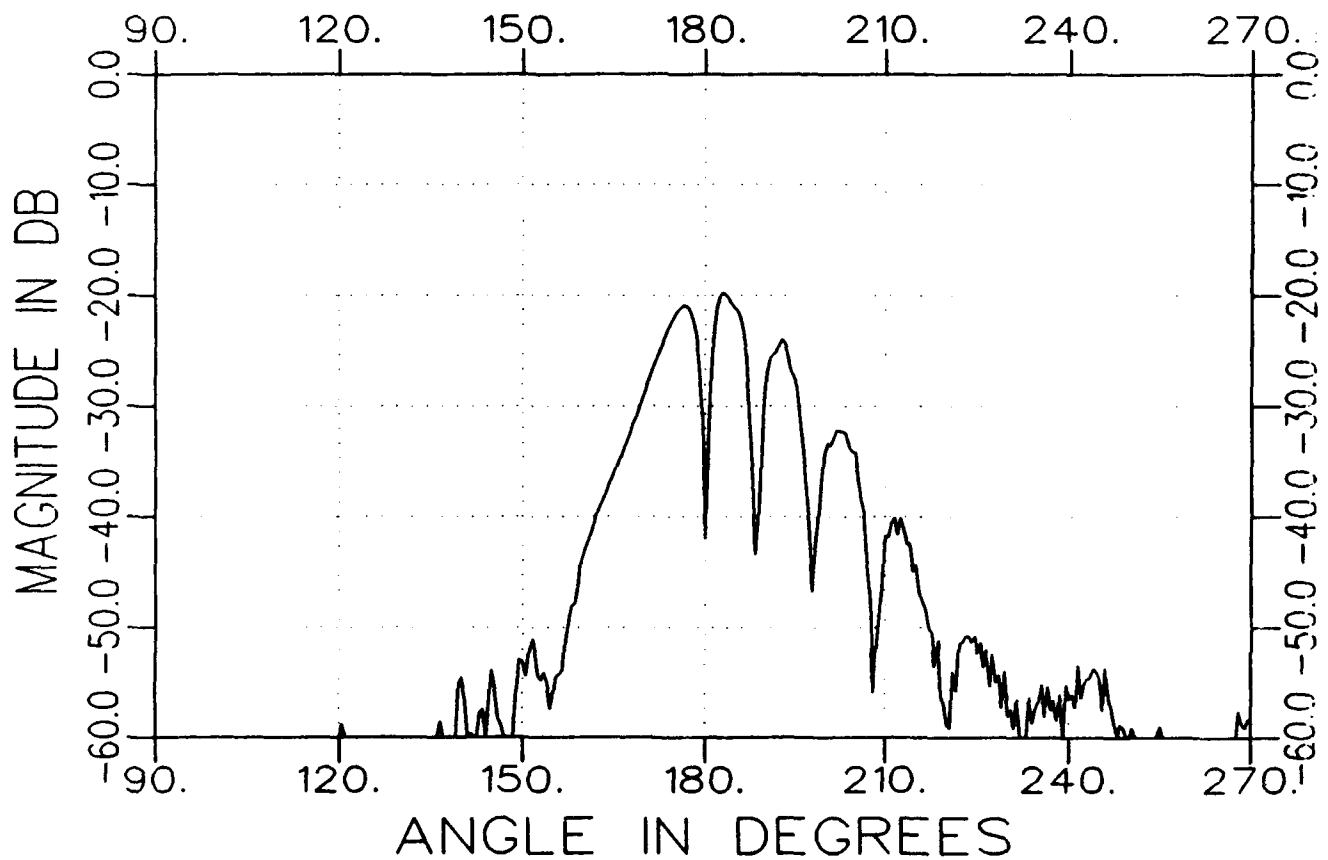
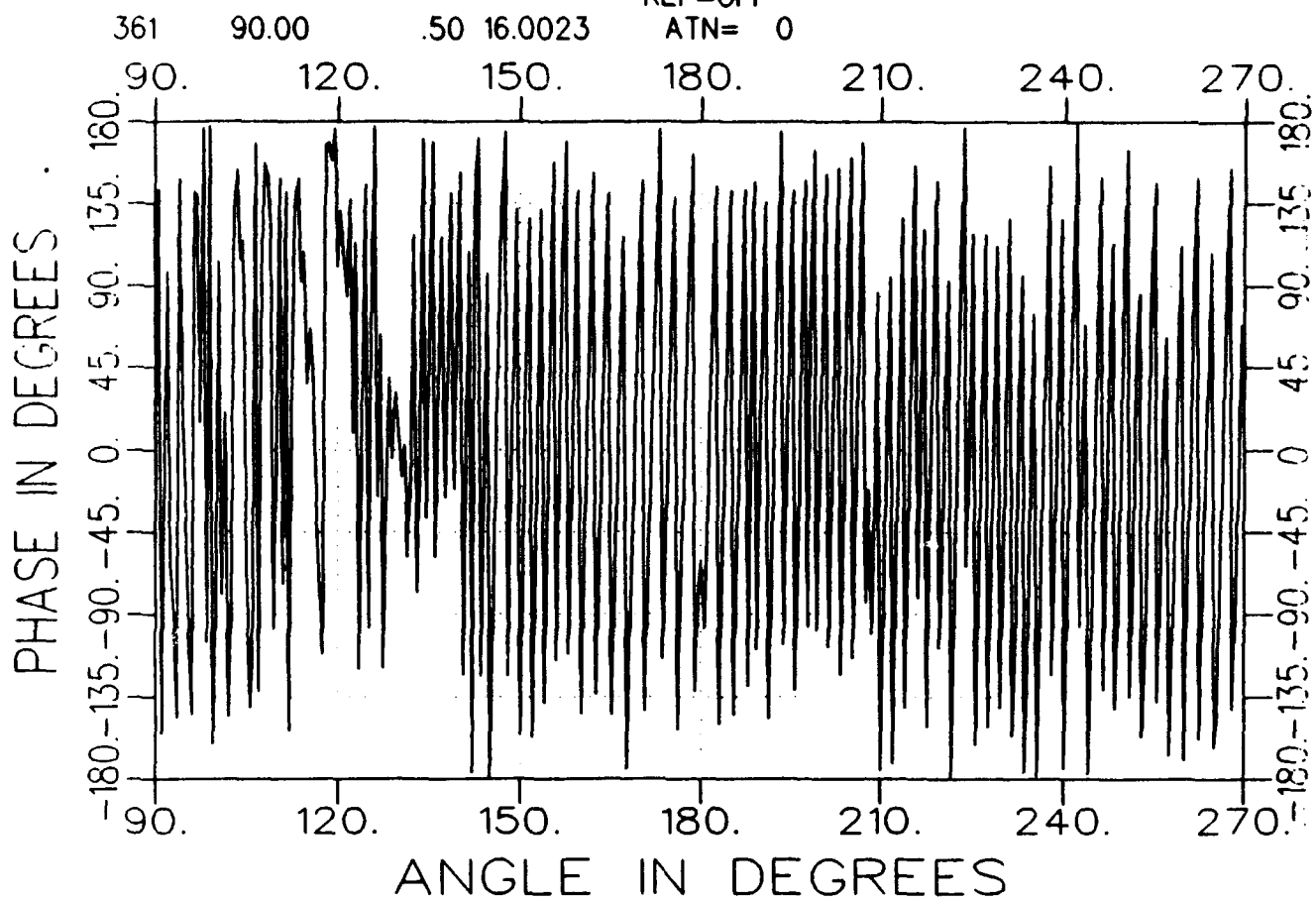


ANGLE IN DEGREES

e3225aal600-a.tar  
TARGET

AZIM. 08/13/93 13:49  
long ind. grid AVE= 82

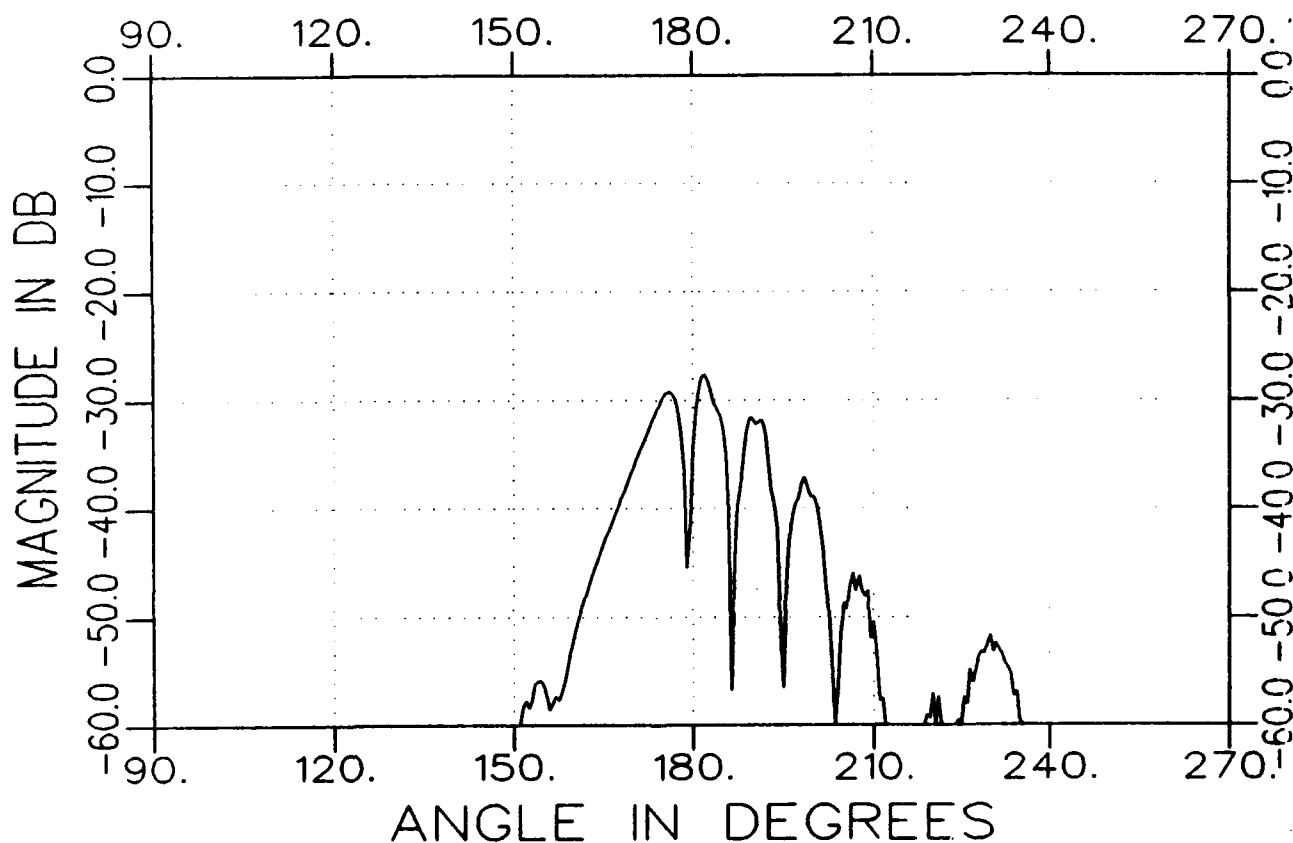
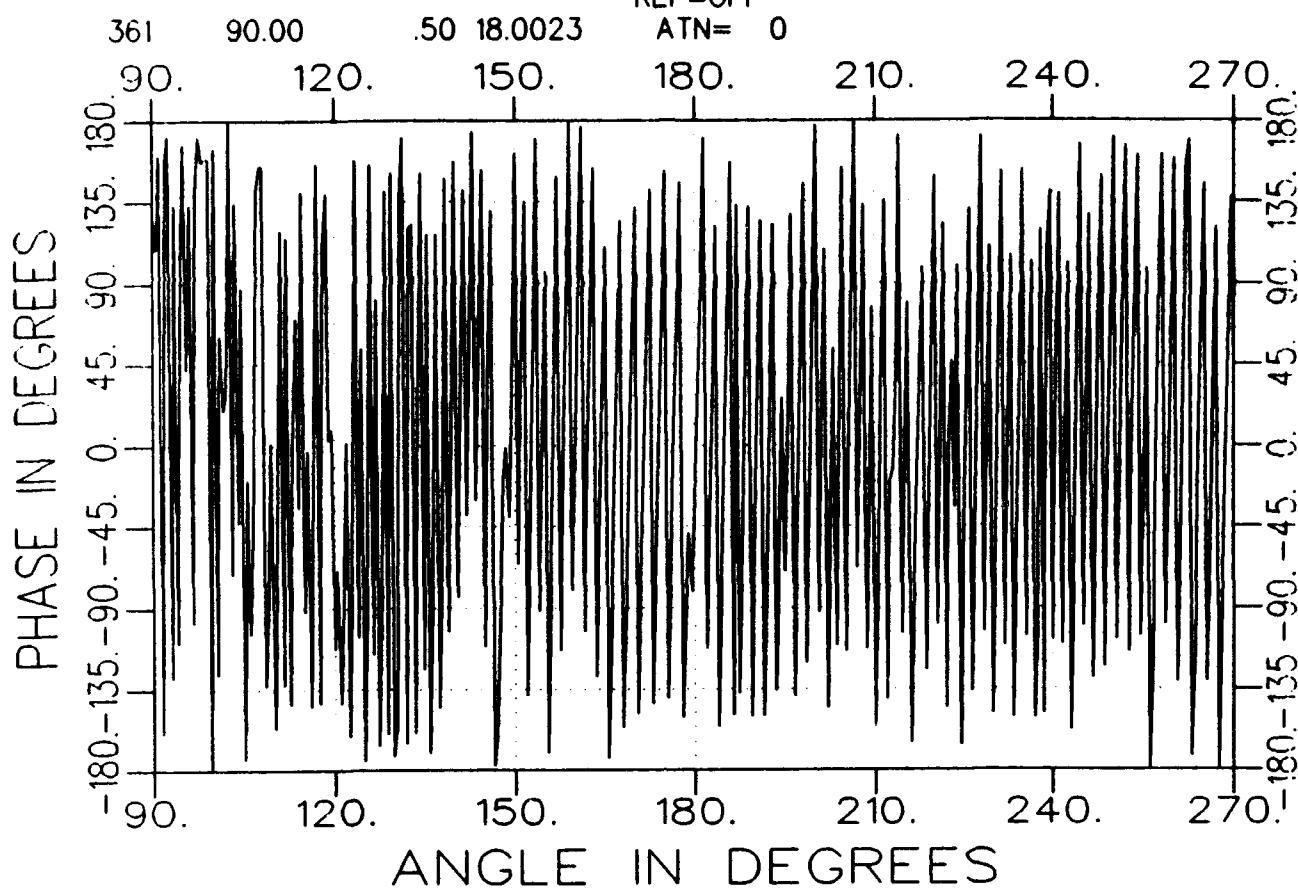
REF=OFF  
ATN= 0



e3225aa1800-a.tar  
TARGET

AZIM. 08/13/93 13:51  
long ind. grid AVE= 82  
REF=OFF

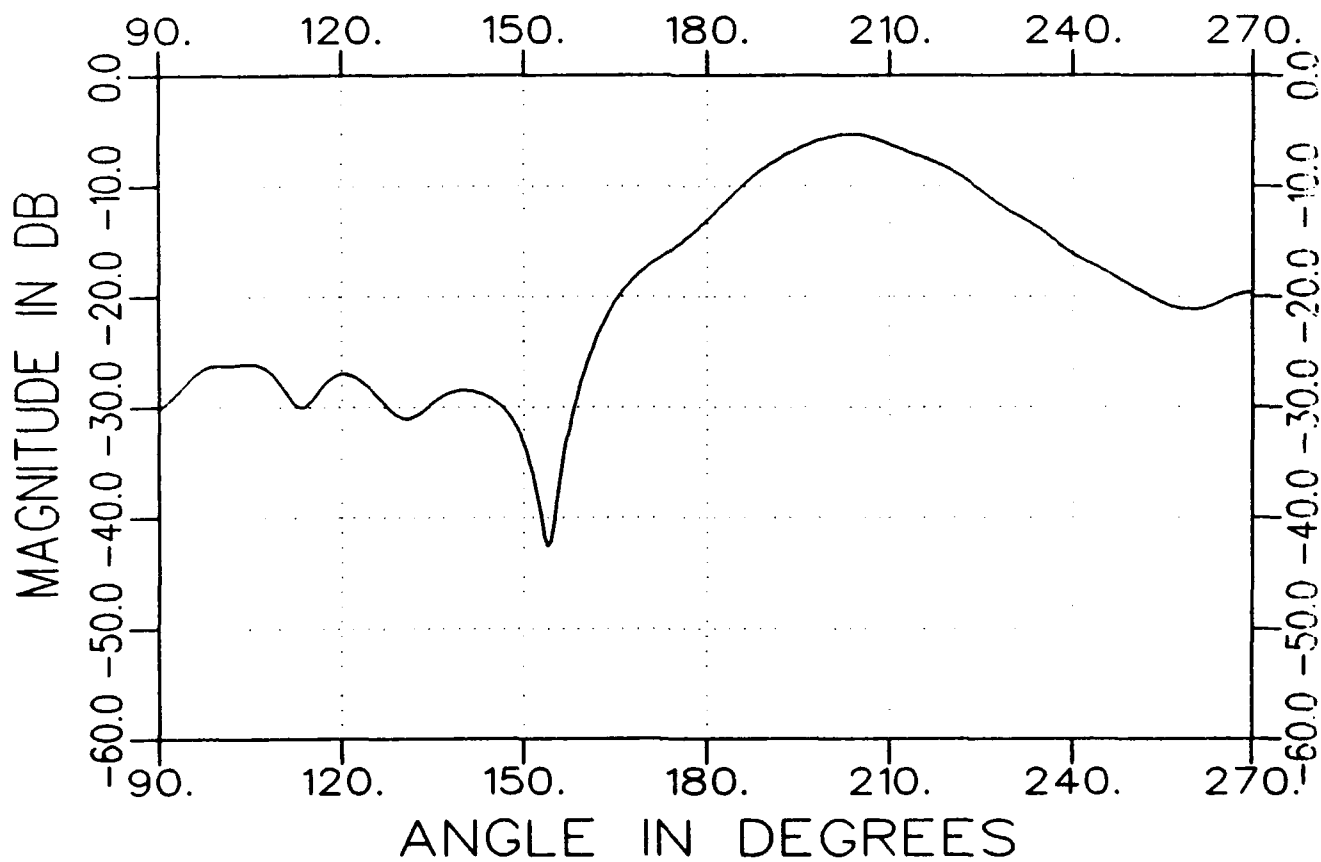
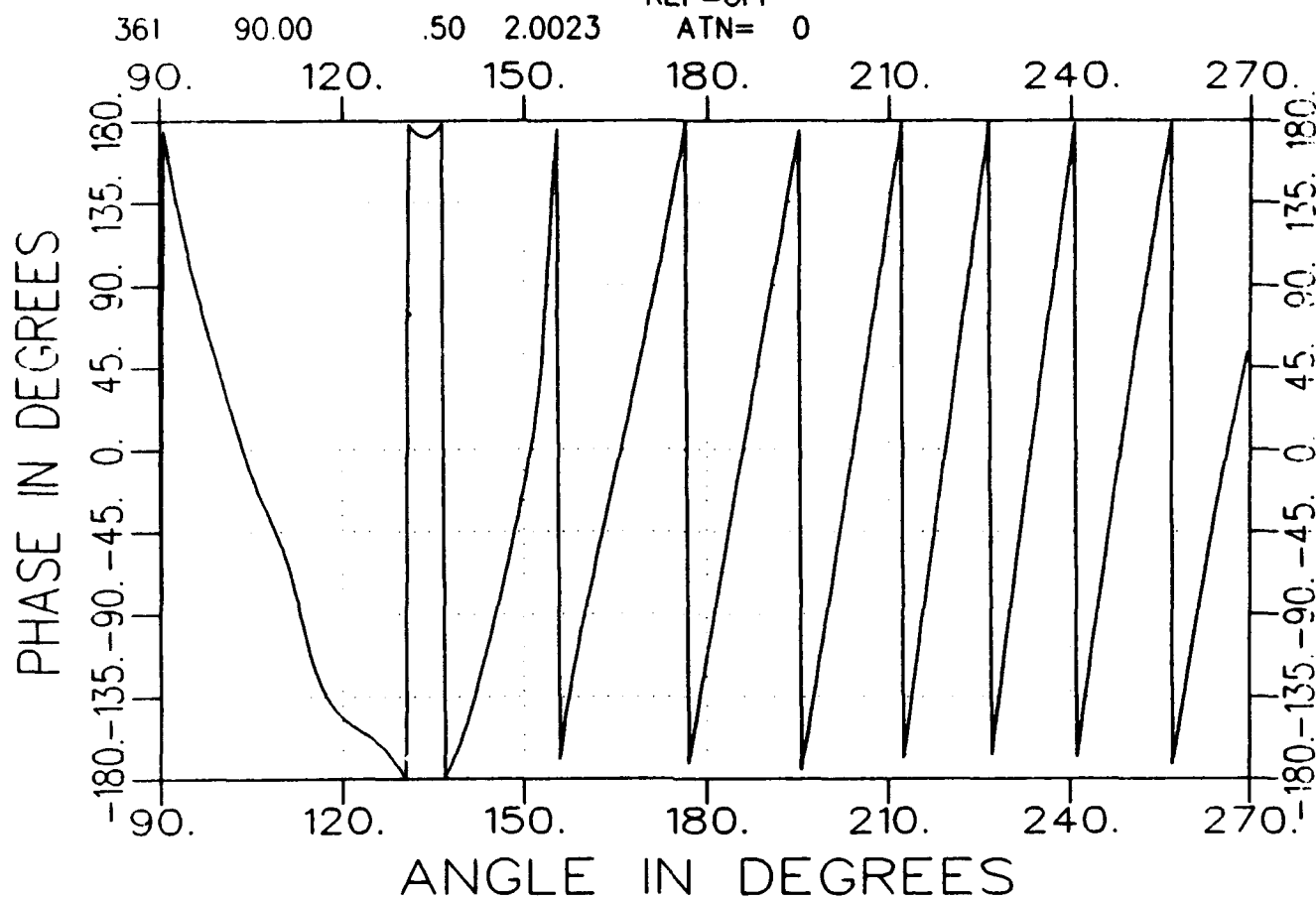
ATN= 0



f3225aa0200-a.tar  
TARGET

AZIM. 08/13/93 13:59  
short ind. grid AVE= 82  
REF=OFF

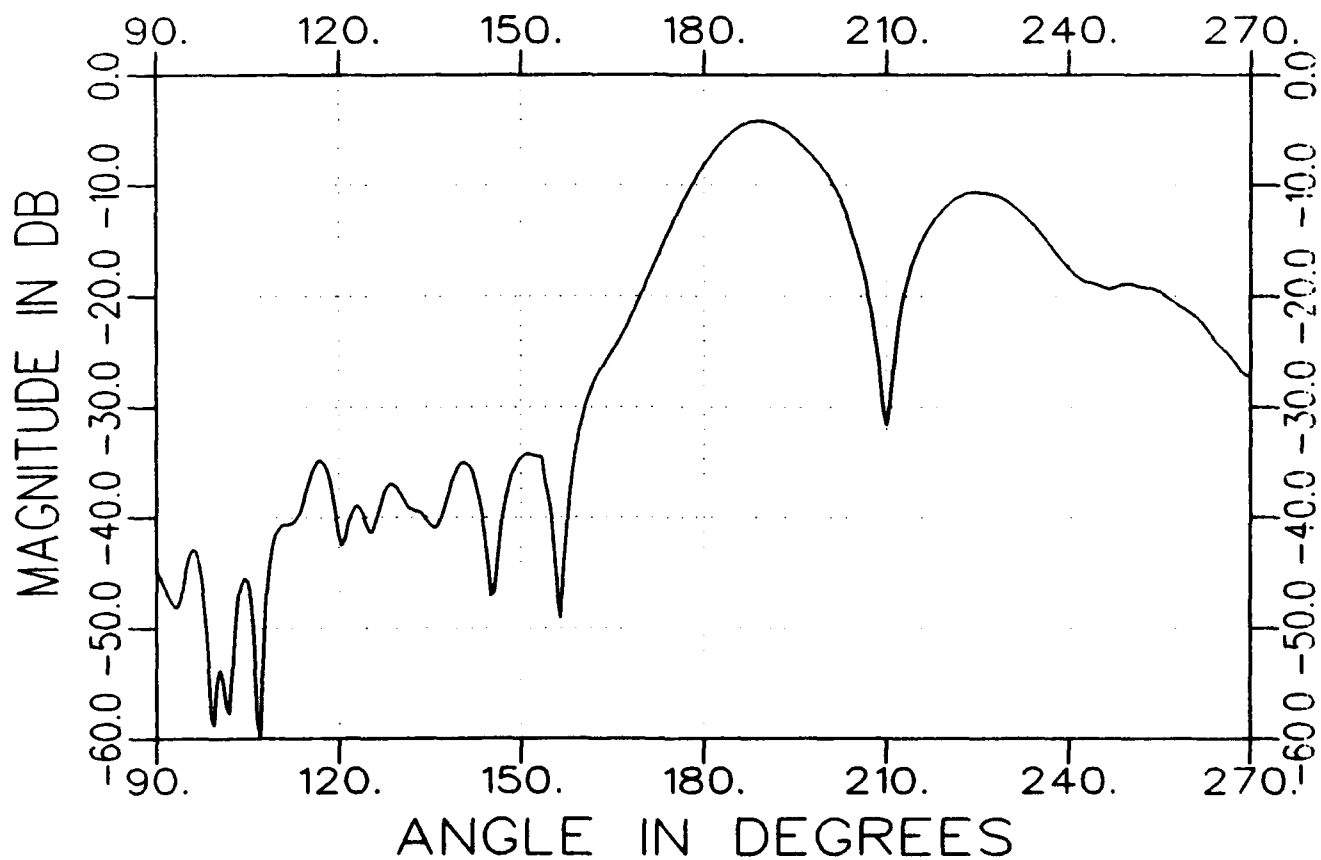
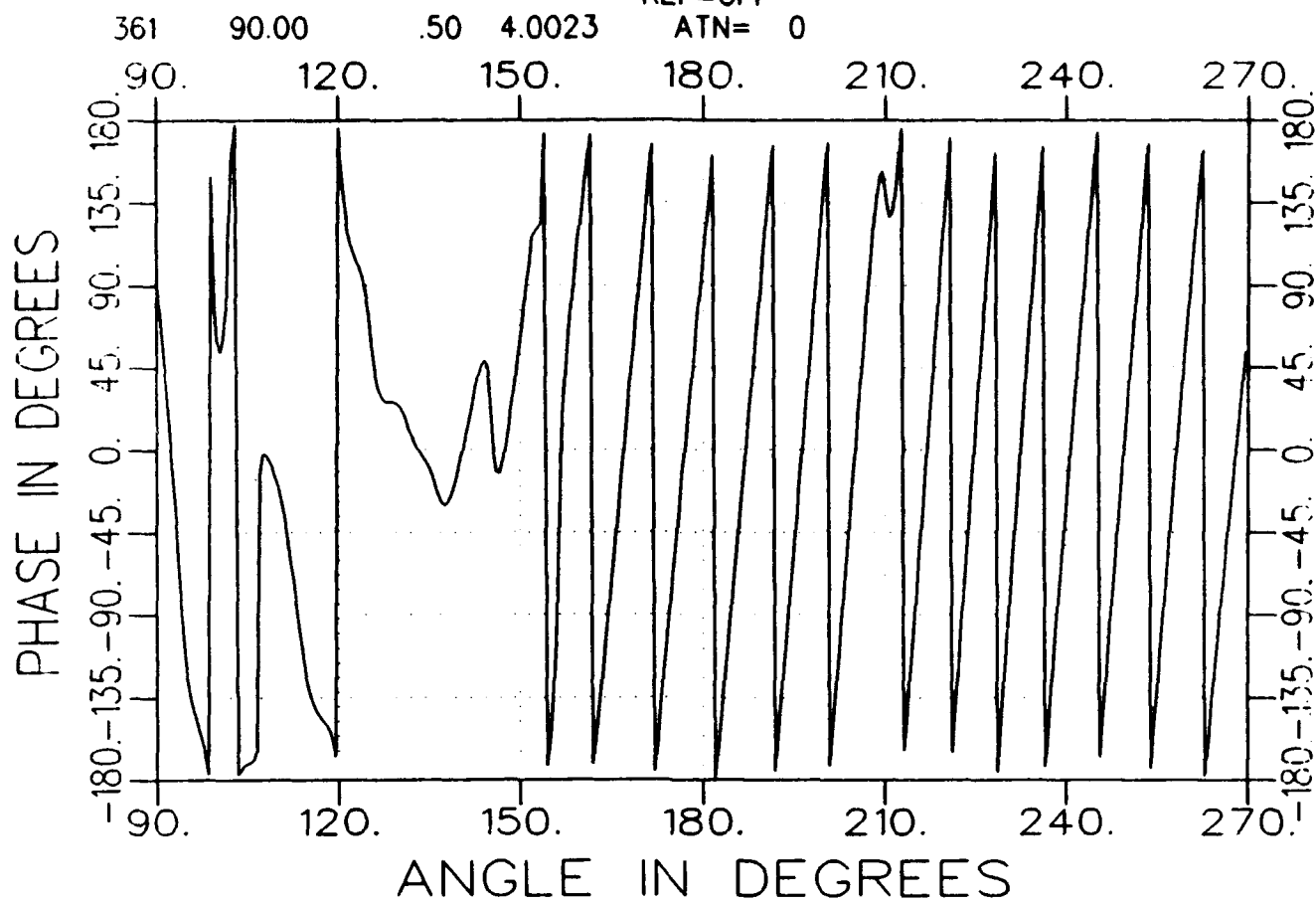
ATN= 0





f3225aa0400-a.tar  
TARGET

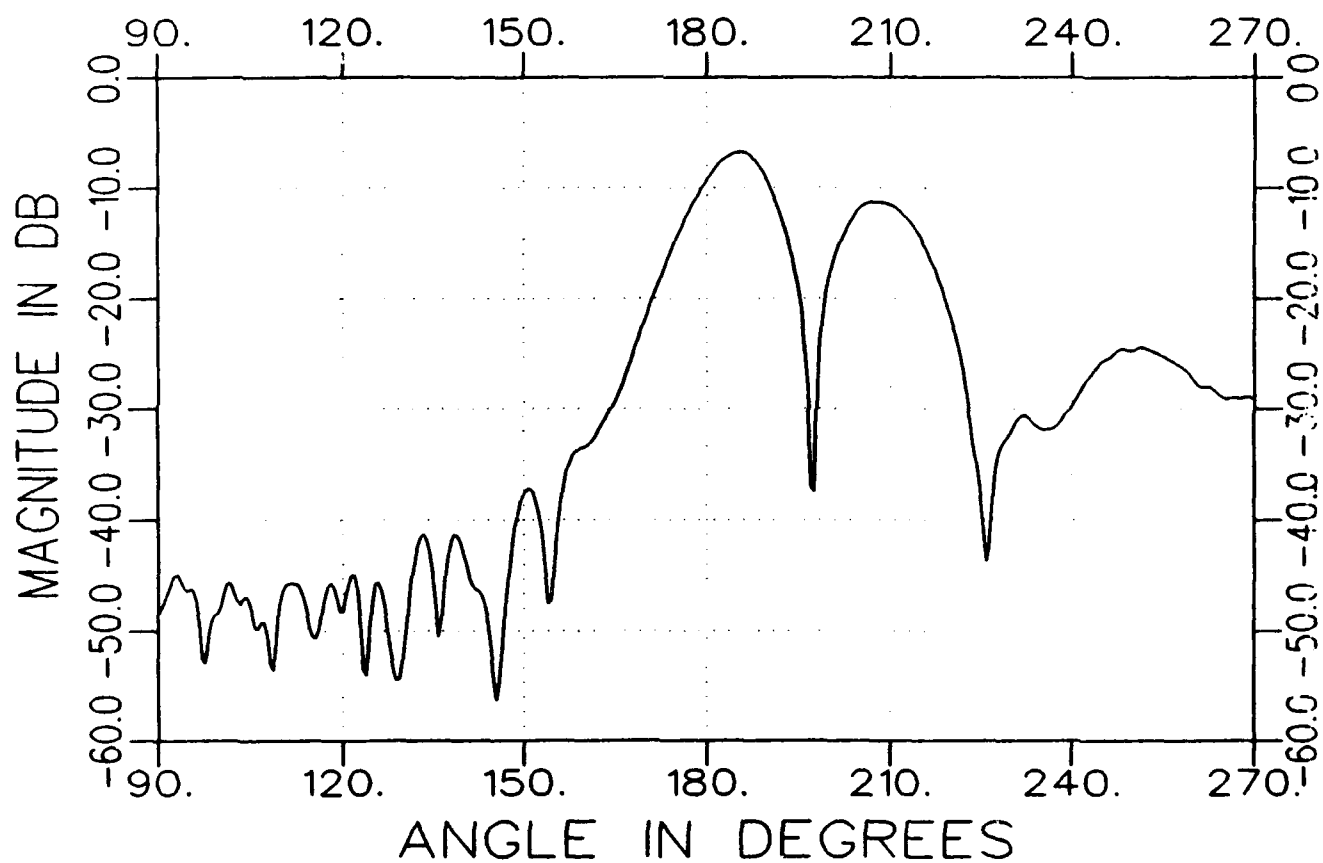
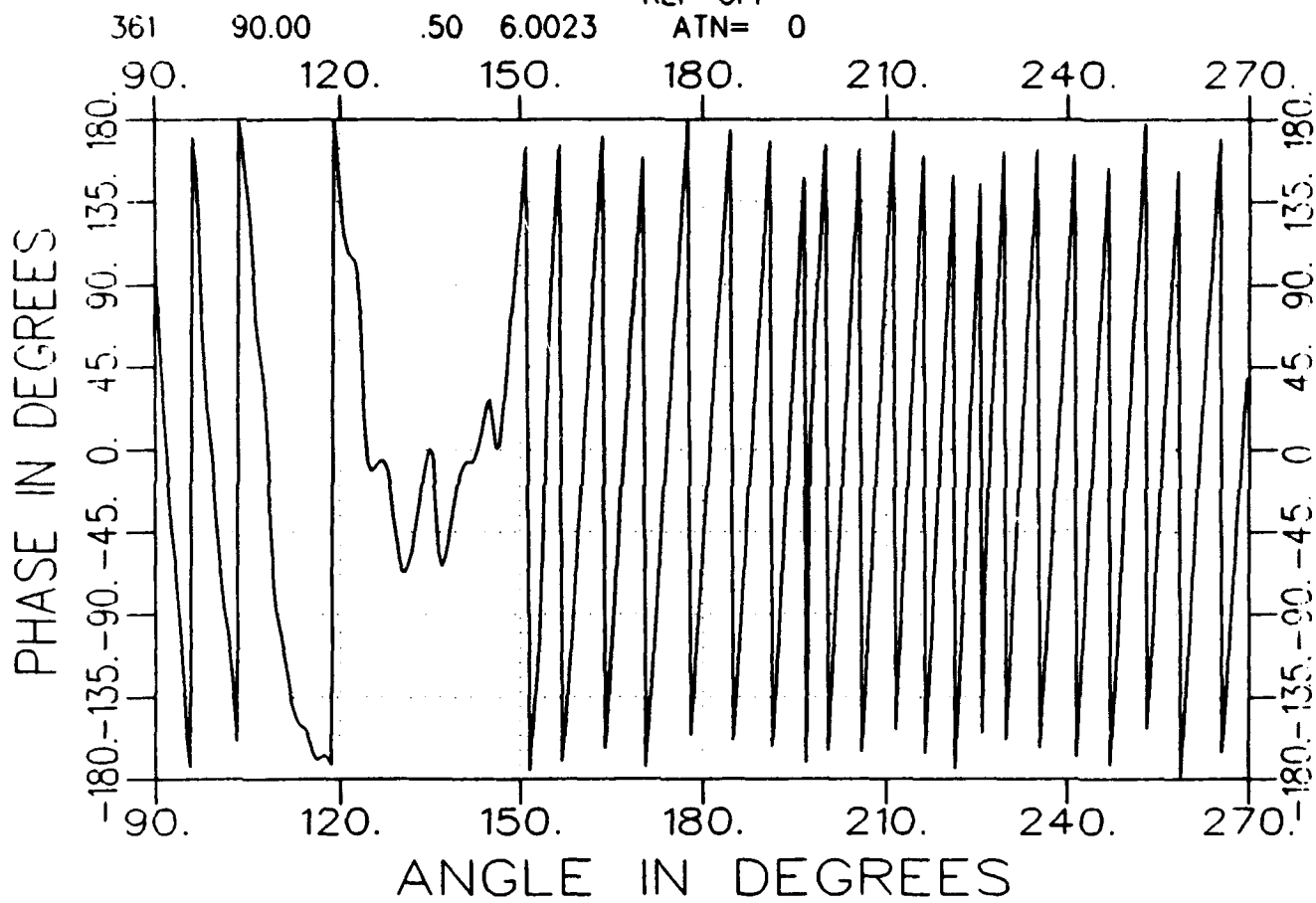
AZIM. 08/13/93 14:01  
short ind. grid AVE= 82  
REF=OFF  
ATN= 0



f3225aa0600-a.tar  
TARGET

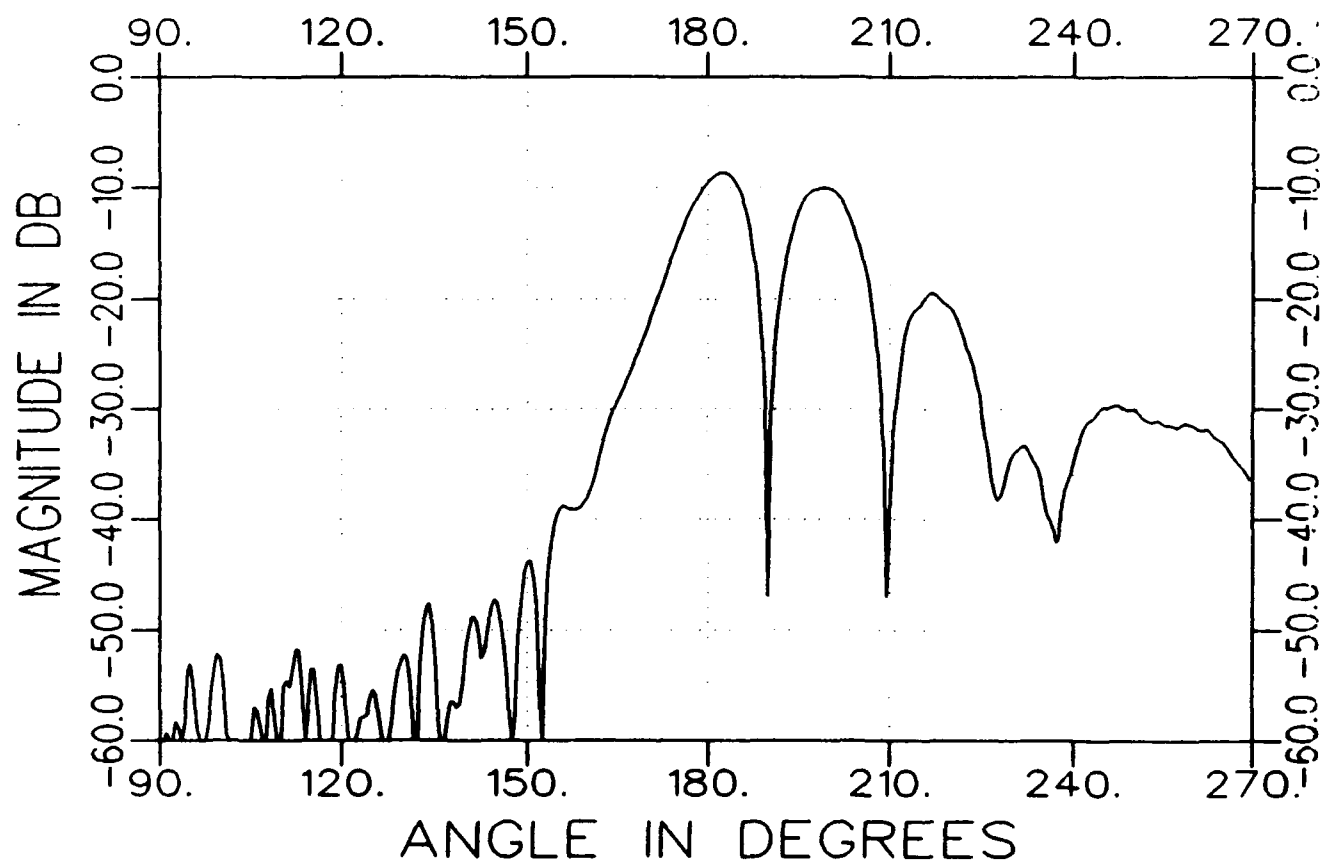
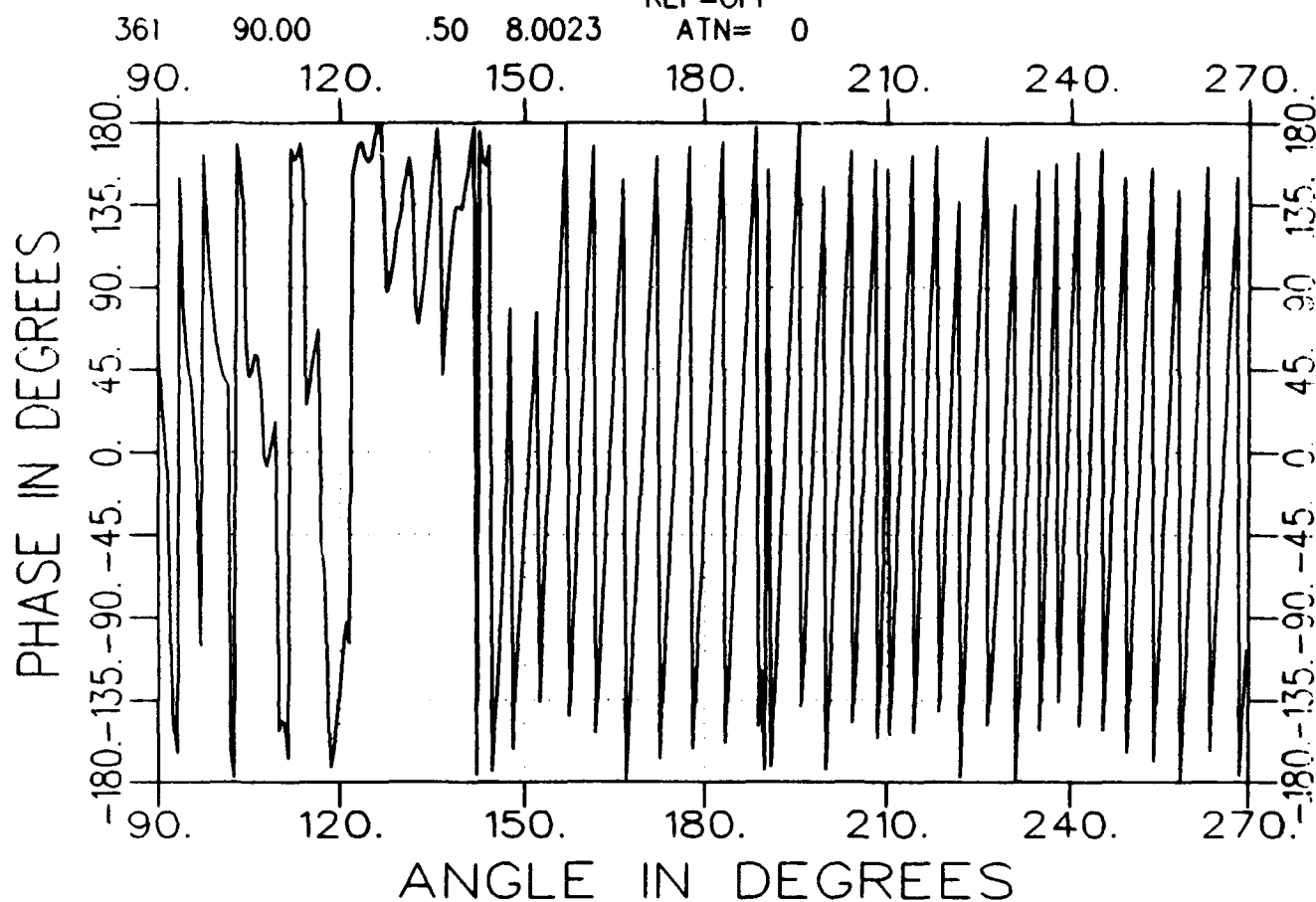
AZIM. 08/13/93 14:03  
short ind. grid AVE= 82  
REF=OFF

ATN= 0



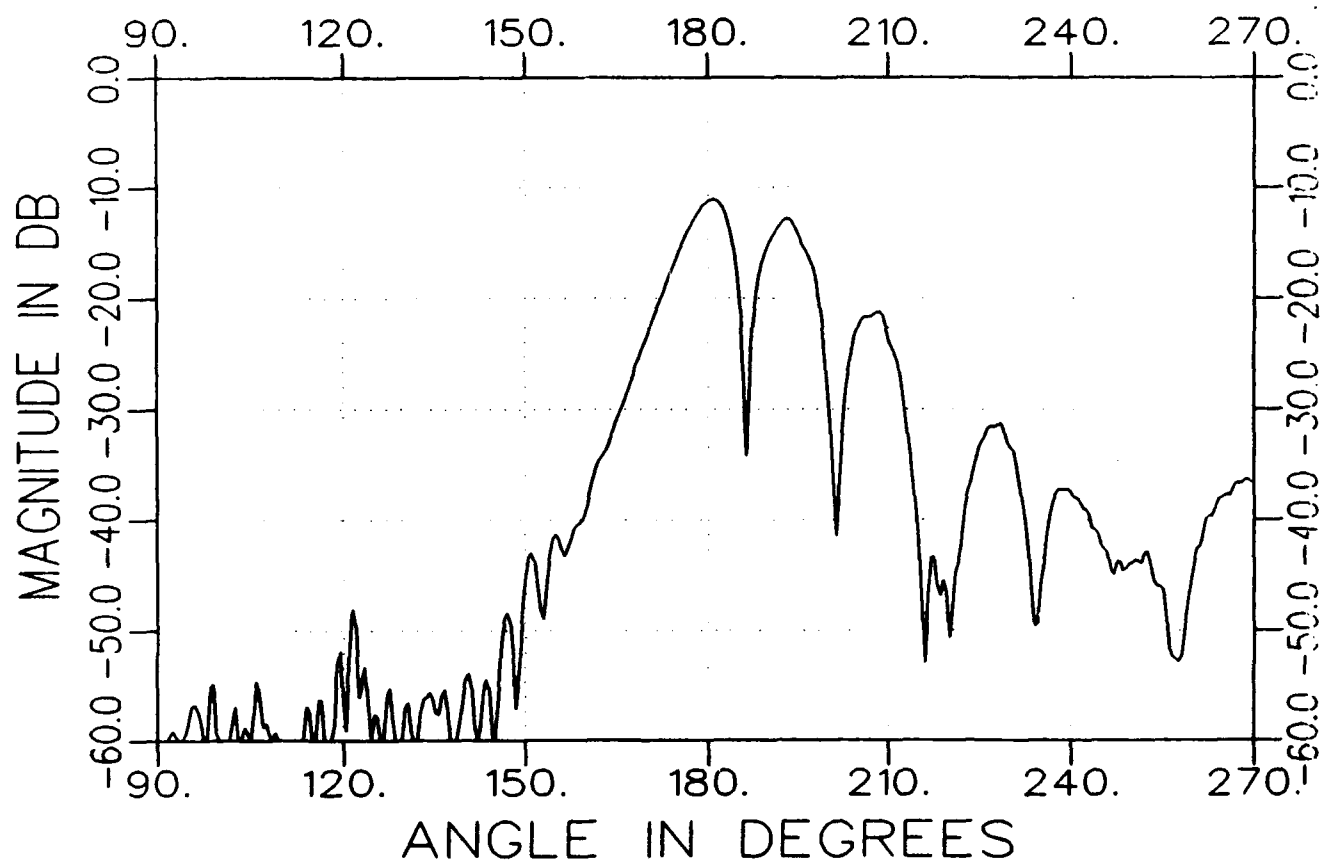
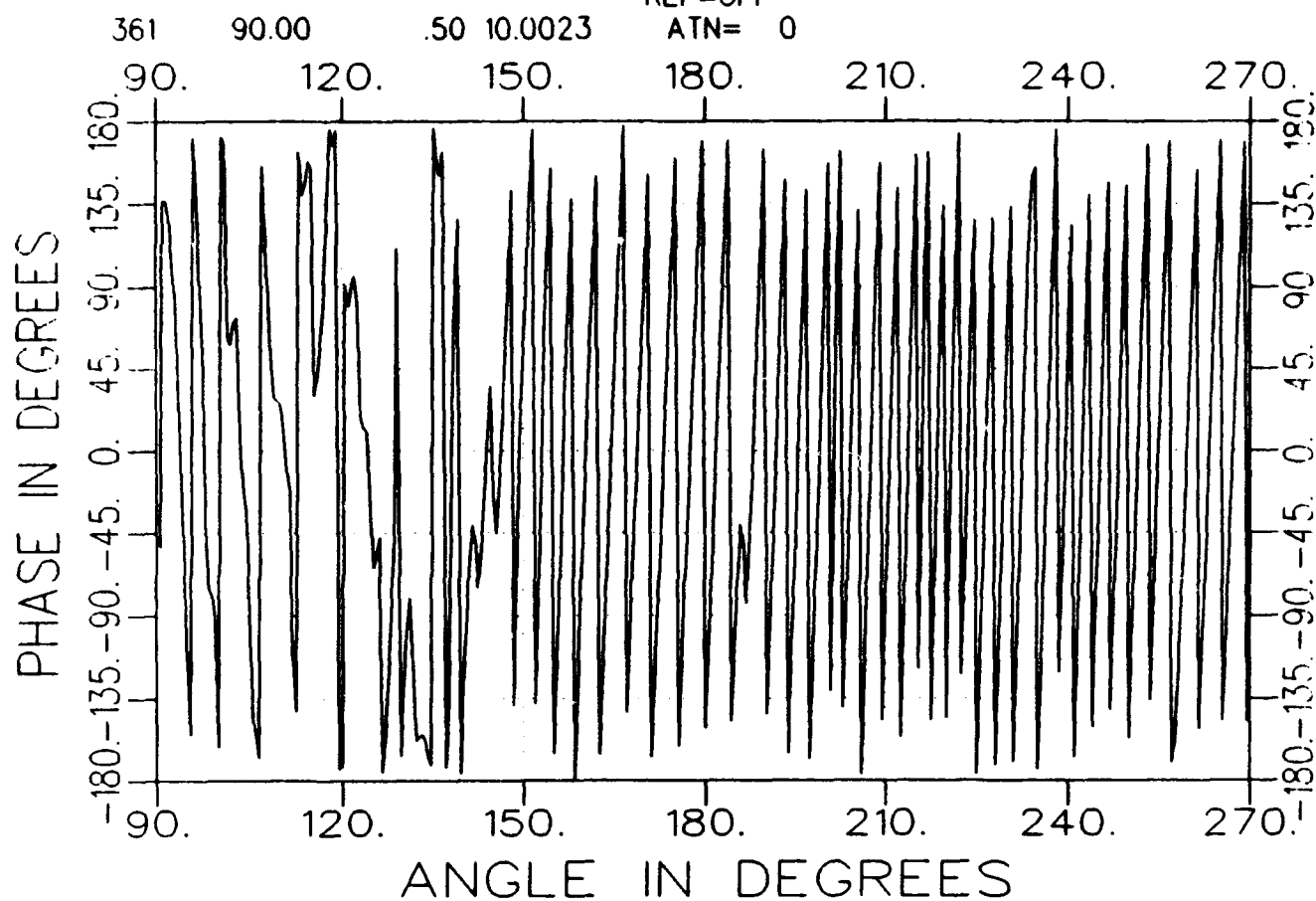
f3225aa0800-a.tar  
TARGET

AZIM. 08/13/93 14:05  
short ind. grid AVE= 82  
REF=OFF  
ATN= 0



f3225aal000-a.tar  
TARGET

AZIM. 08/13/93 14:07  
short ind. grid AVE= 82  
REF=OFF  
ATN= 0

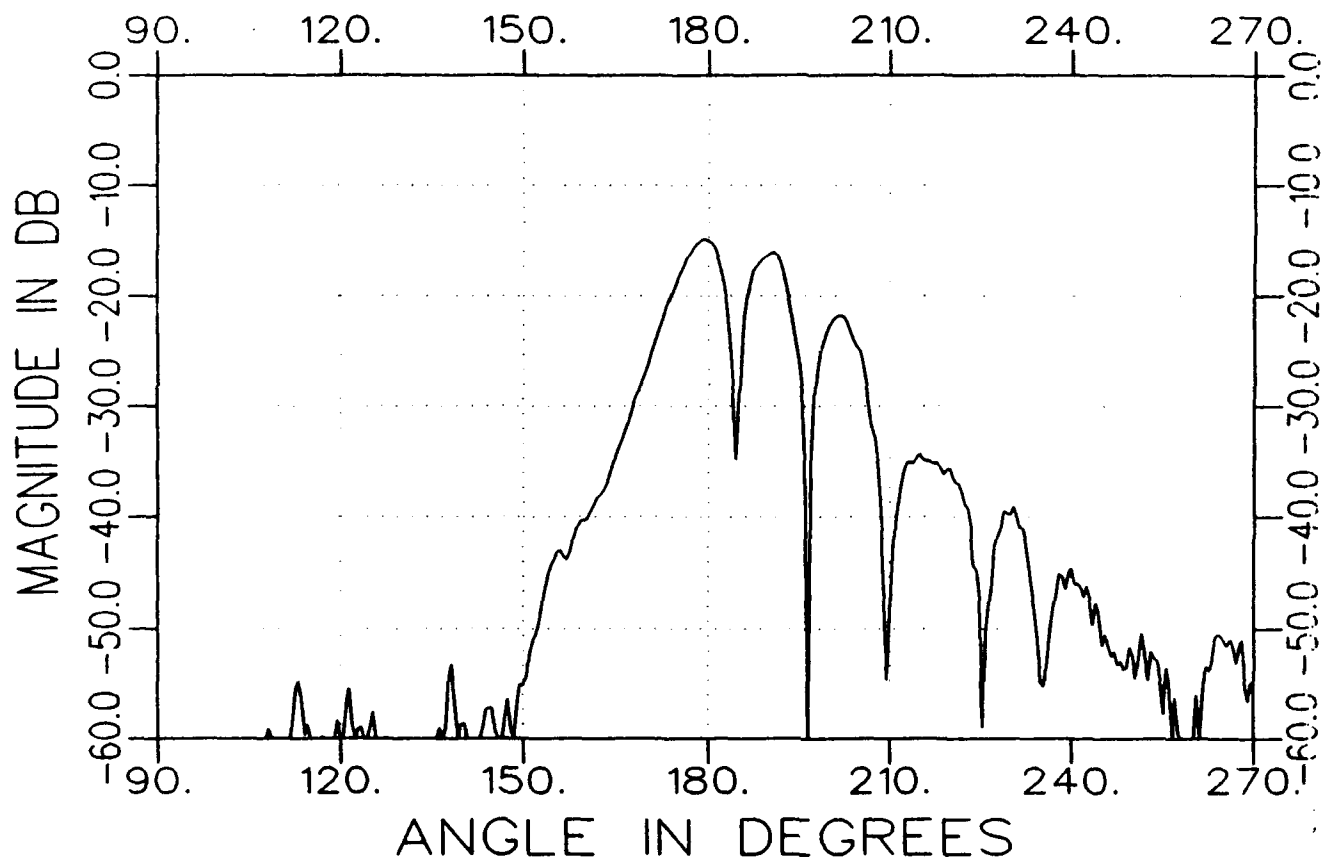
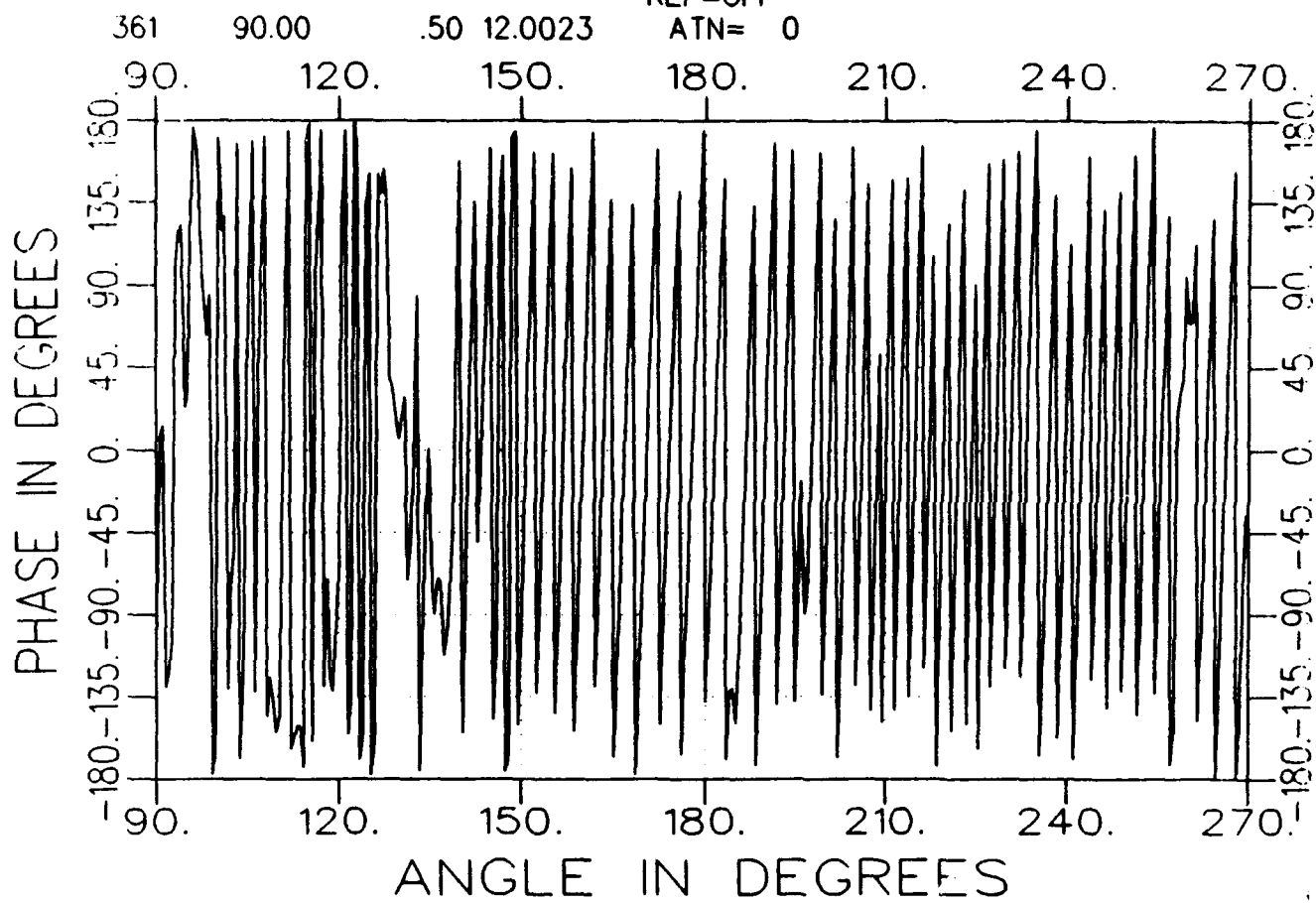


f3225aa1200-a.tar  
TARGET

AZIM. 08/13/93 14:09  
short ind. grid AVE= 82

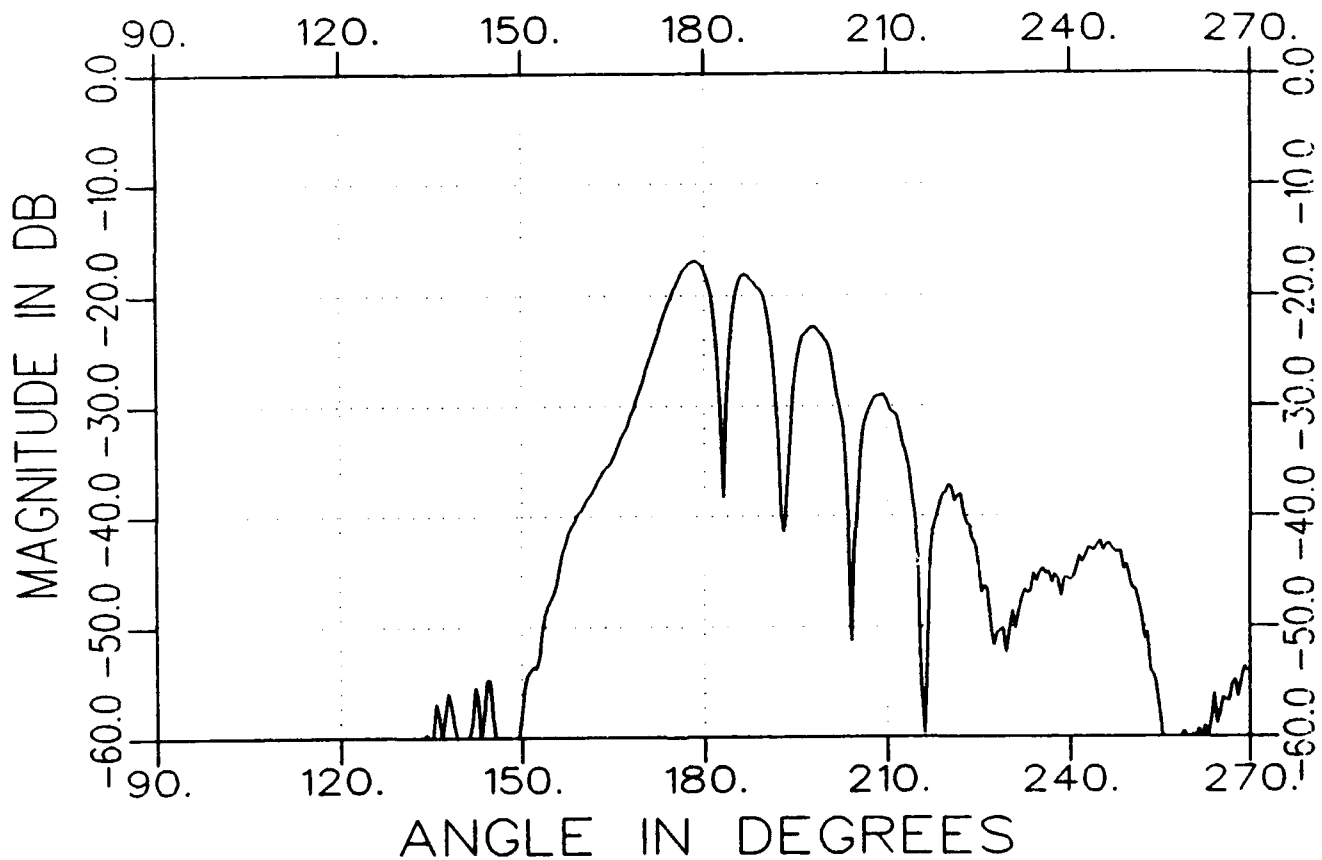
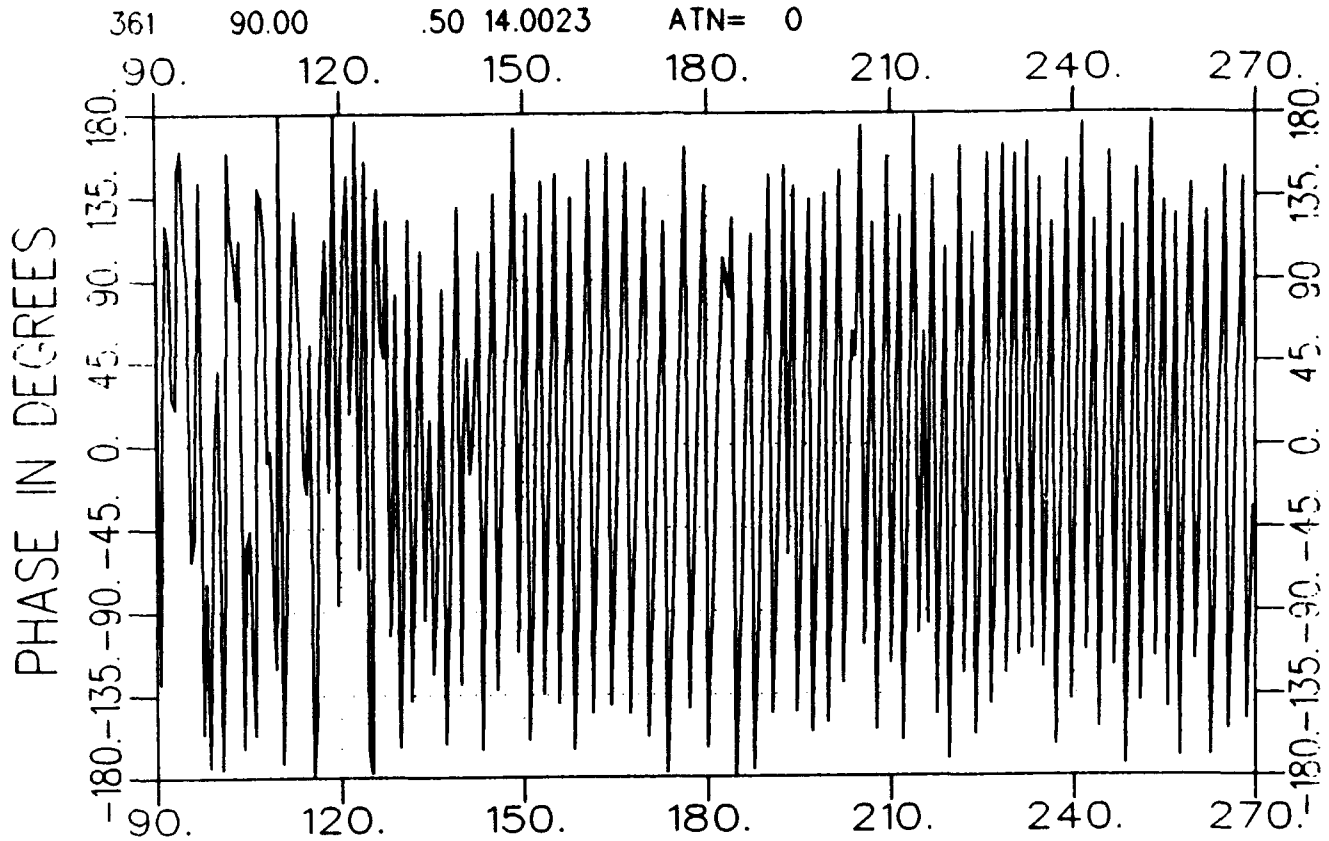
REF=OFF

ATN= 0



f3225aal400-a.tar  
TARGET

AZIM. 08/13/93 14:11  
short ind. grid AVE= 82  
REF=OFF  
ATN= 0

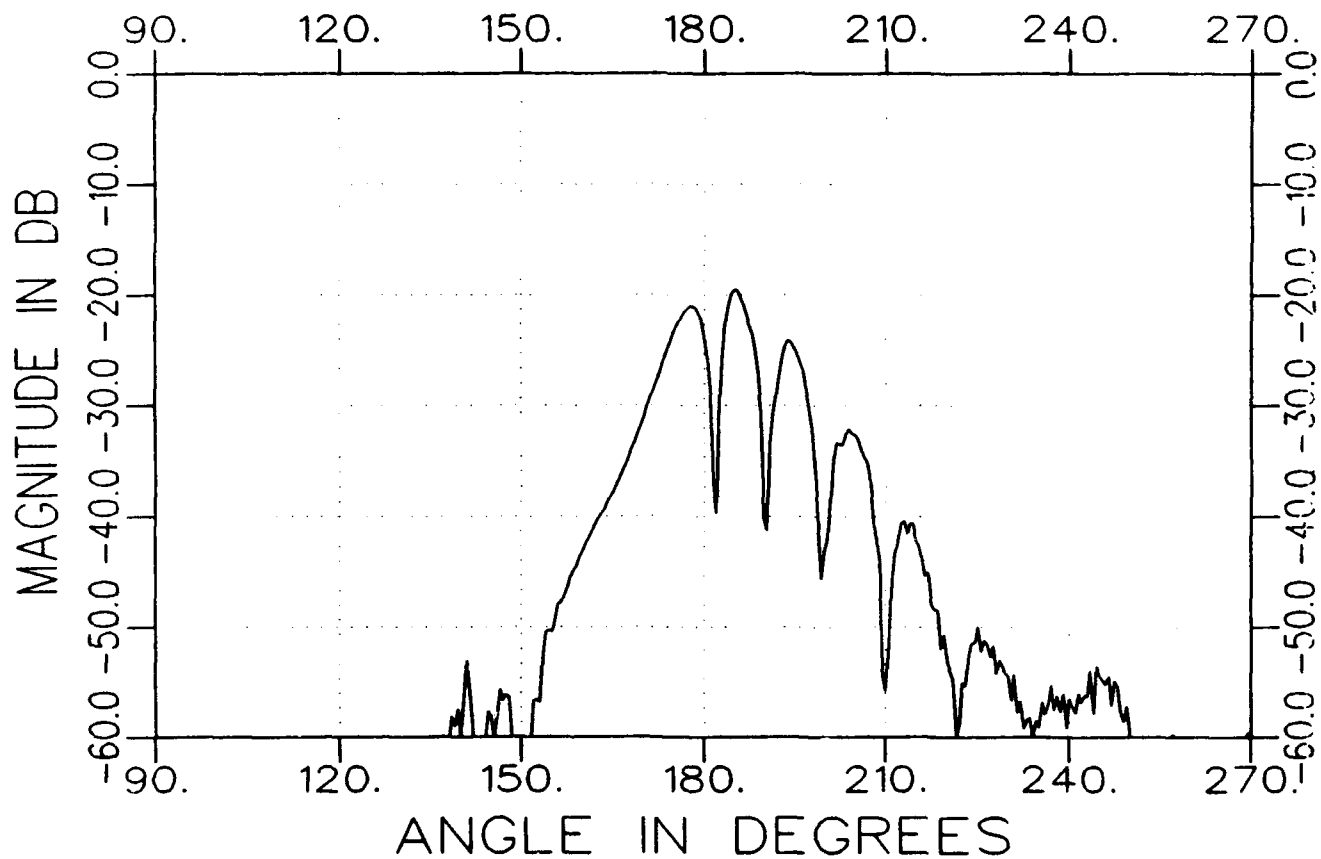
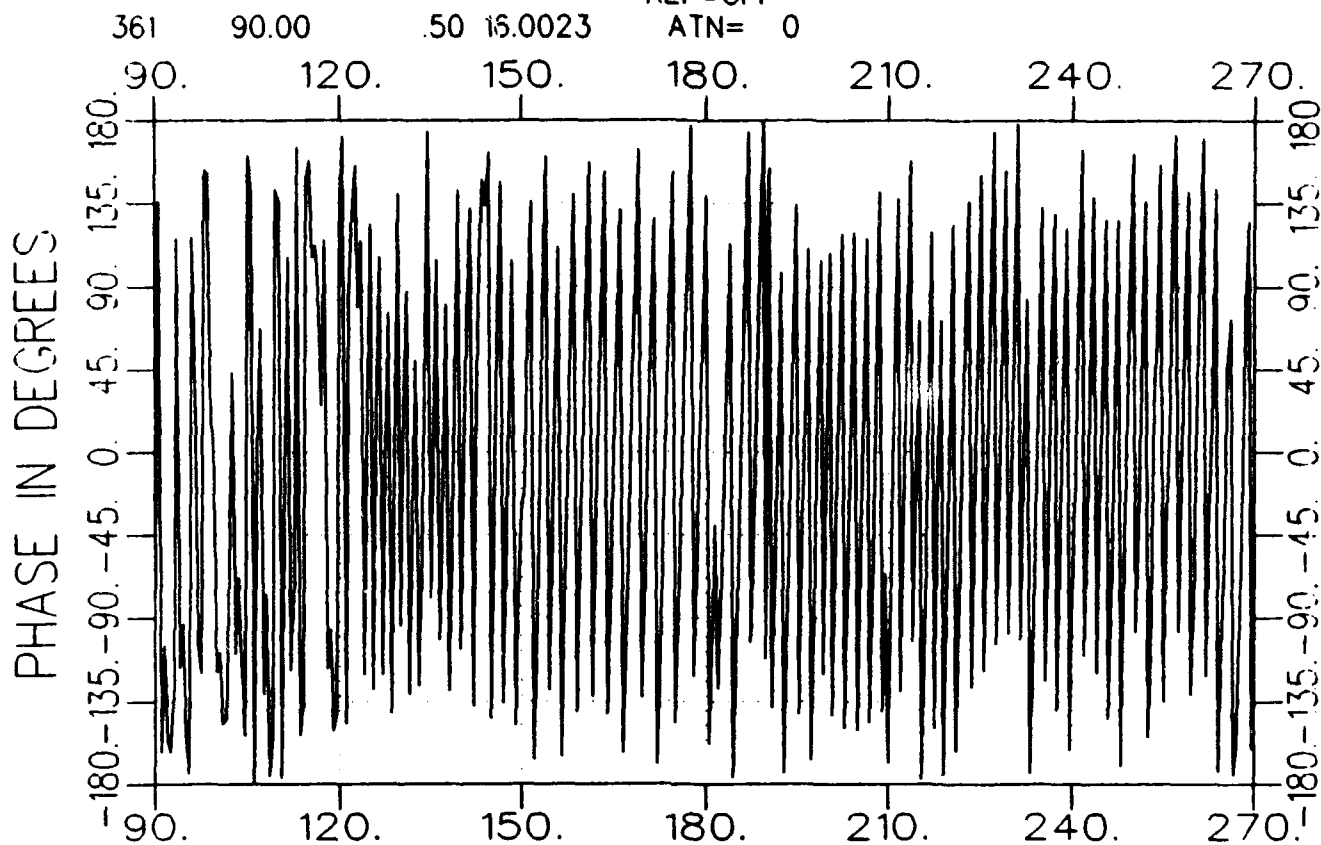


f3225aa1600-a.tar  
TARGET

AZIM. 08/13/93 14:13  
short ind. grid AVE= 82

REF=OFF

ATN= 0

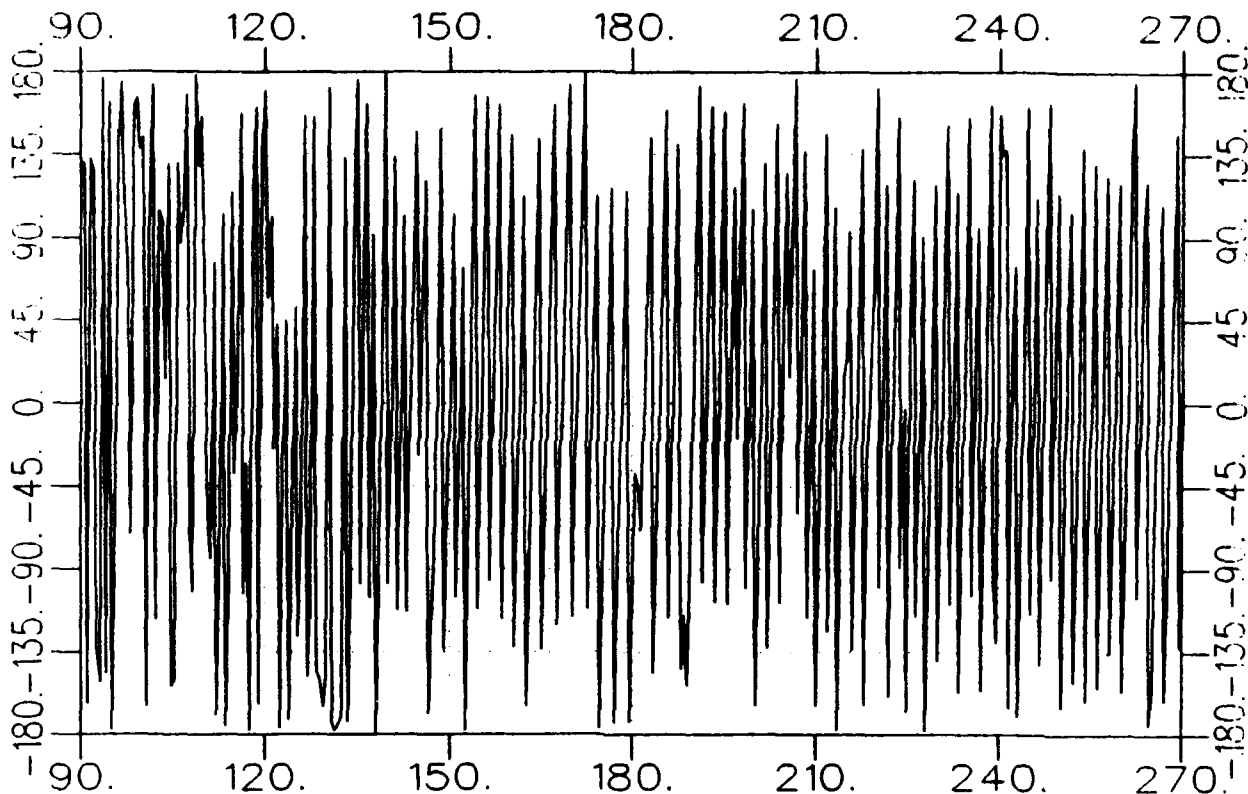


f3225aal800-a.tar  
TARGET

AZIM. 08/13/93 14:15  
short ind. grid AVE= 82  
REF=OFF

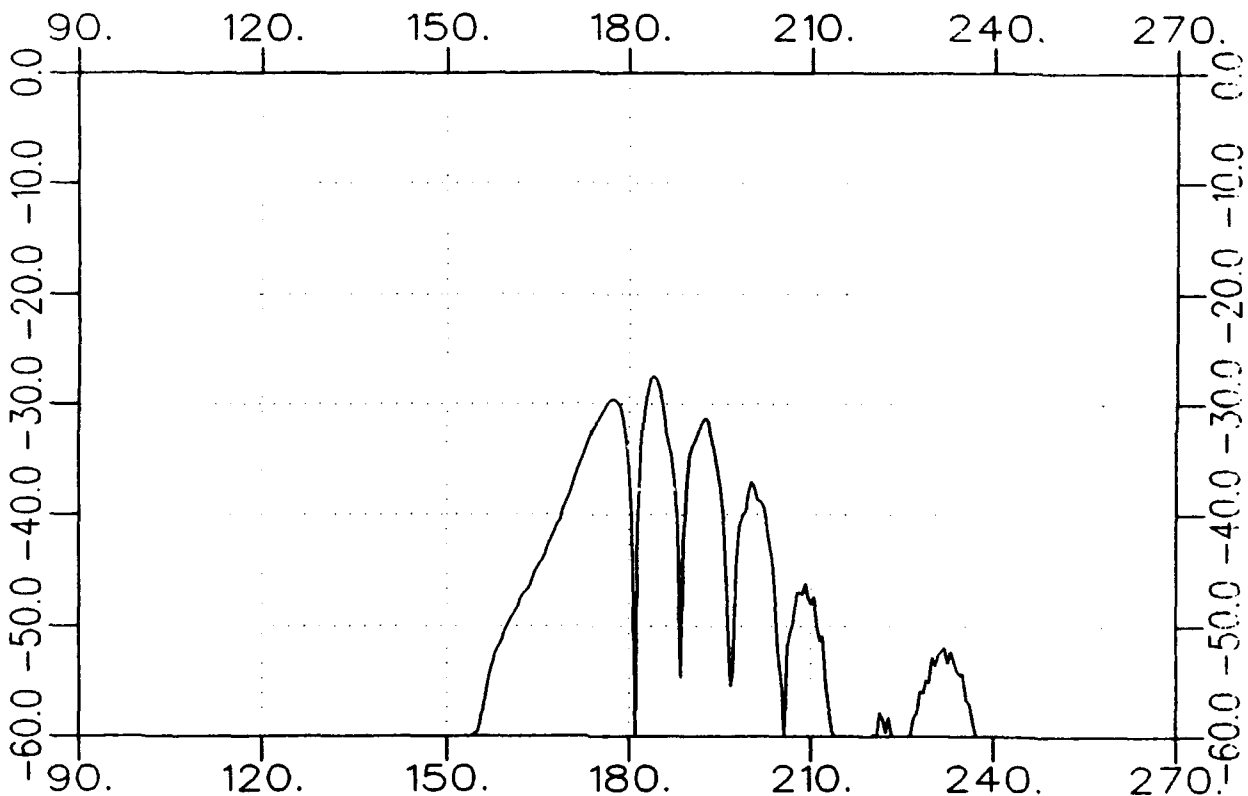
361 90.00 .50 18.0023 ATN= 0

PHASE IN DEGREES



ANGLE IN DEGREES

MAGNITUDE IN DB



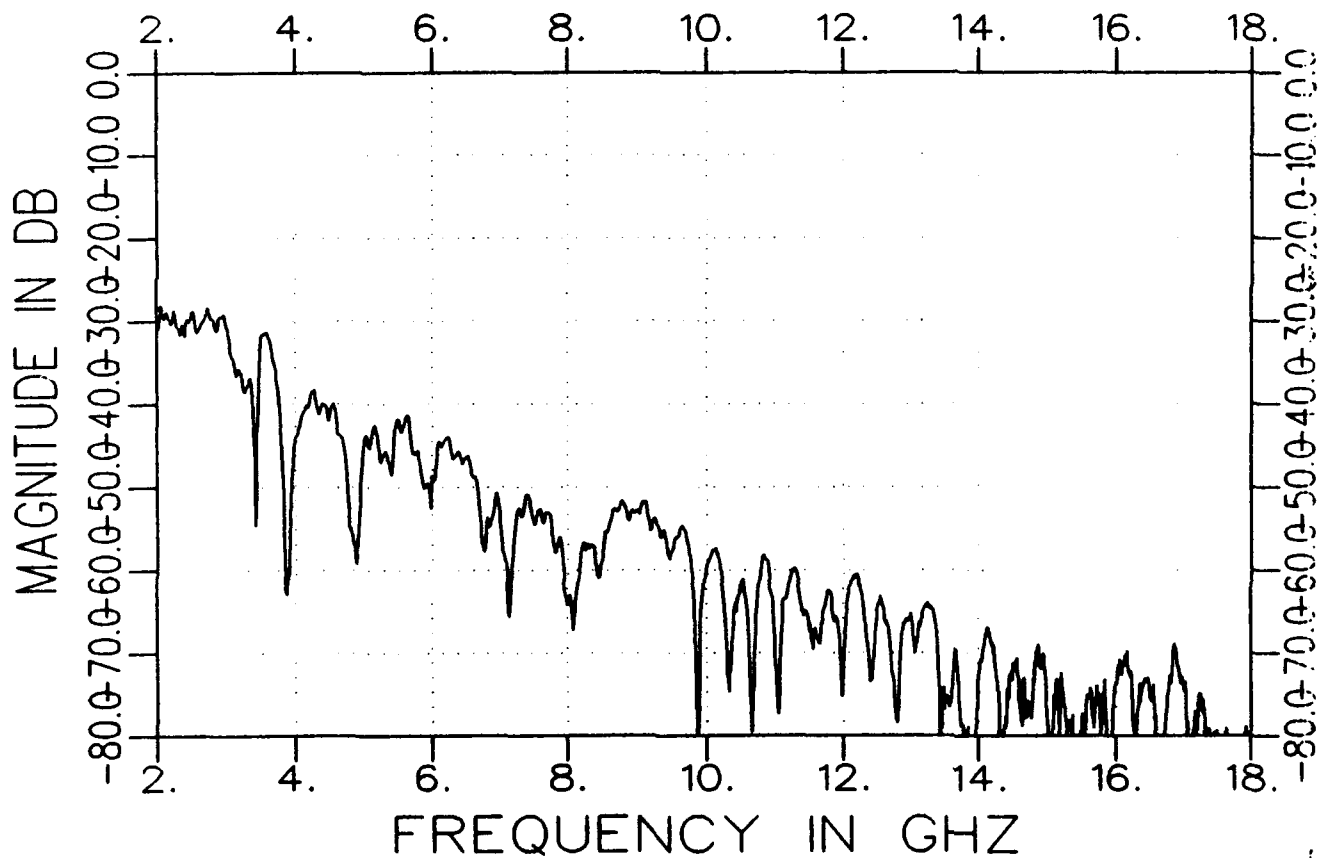
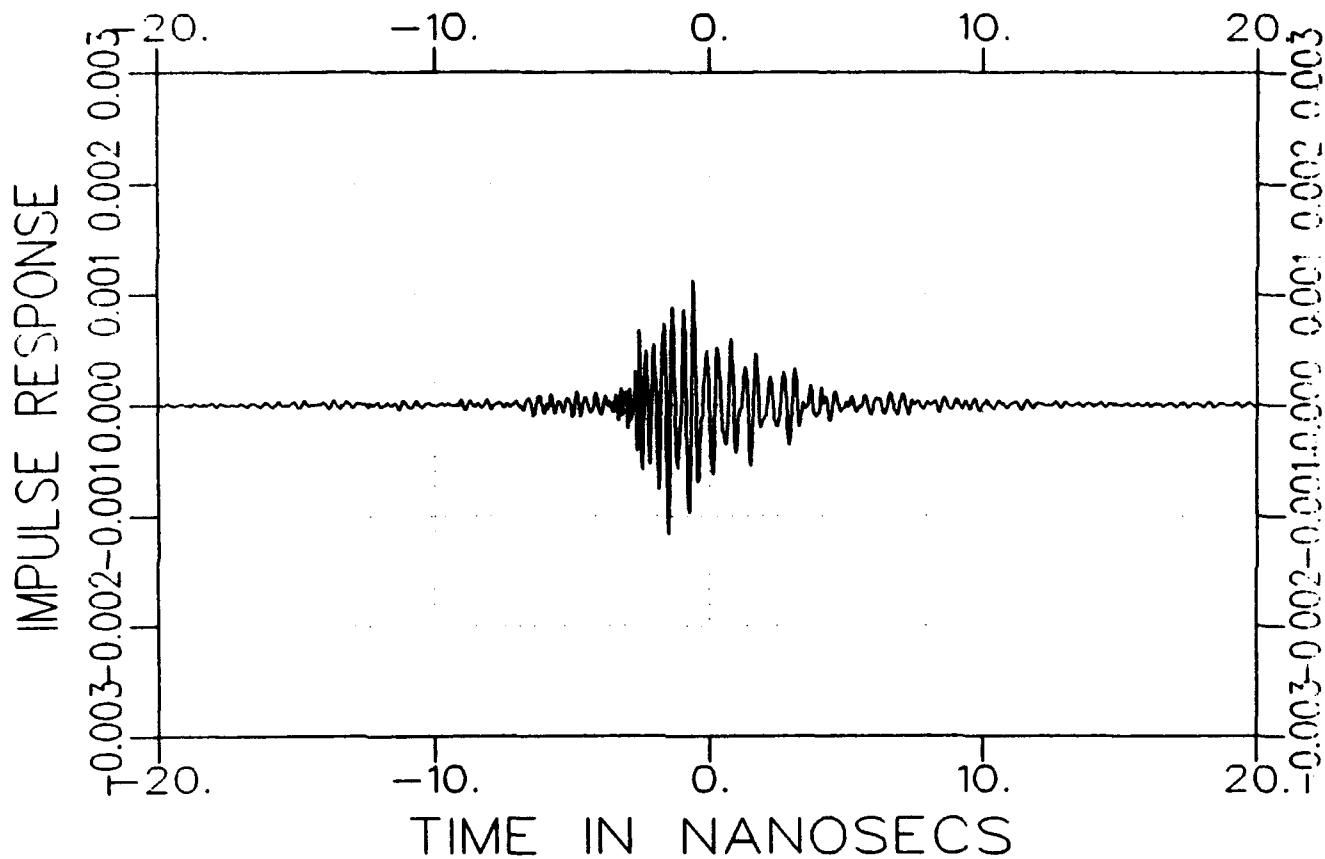
ANGLE IN DEGREES



g3225fa0900-a.tar  
TARGET

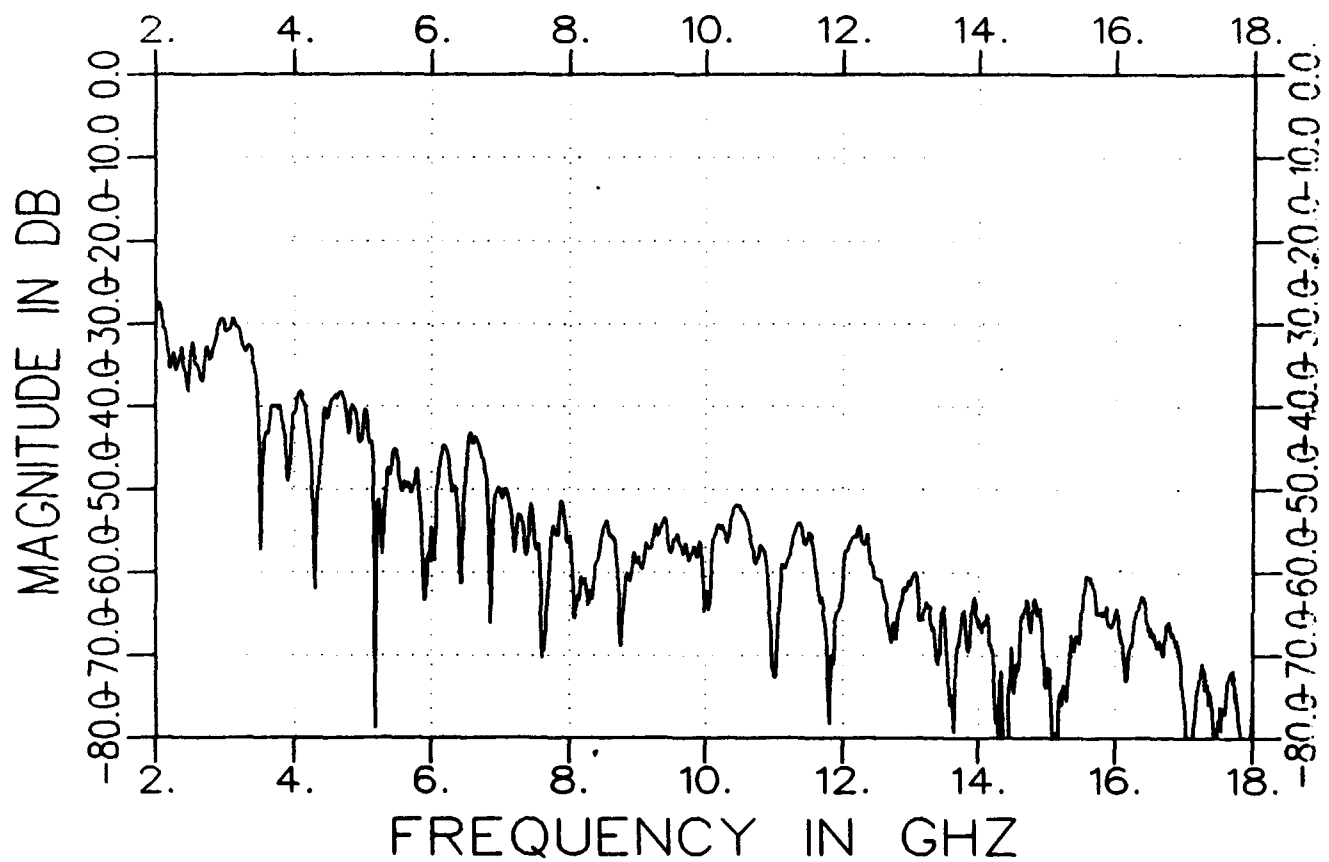
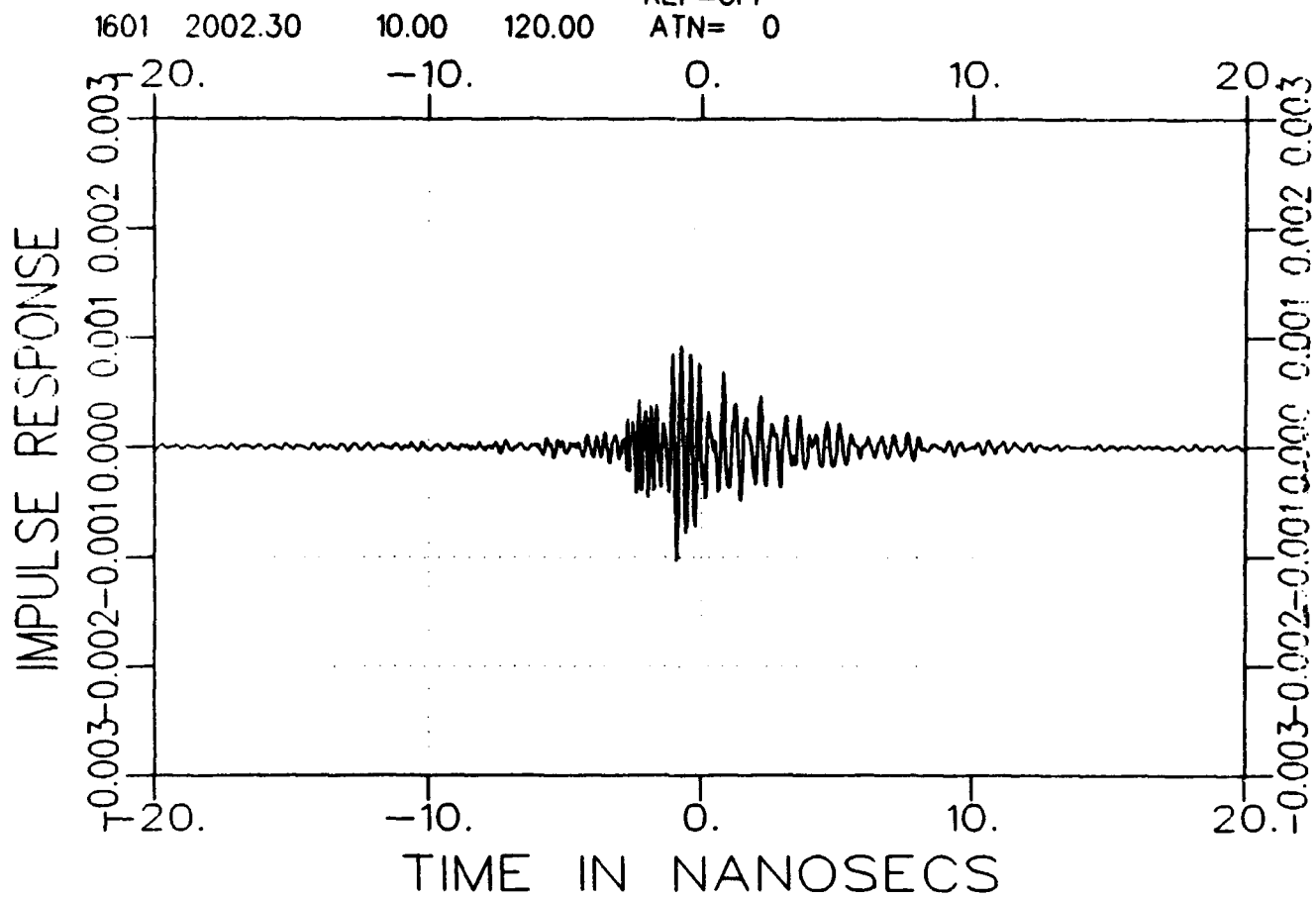
FREQ. 08/13/93 14:20  
freq s ind grid AVE= 82  
REF=OFF

1601 2002.30 10.00 90.00 ATN= 0



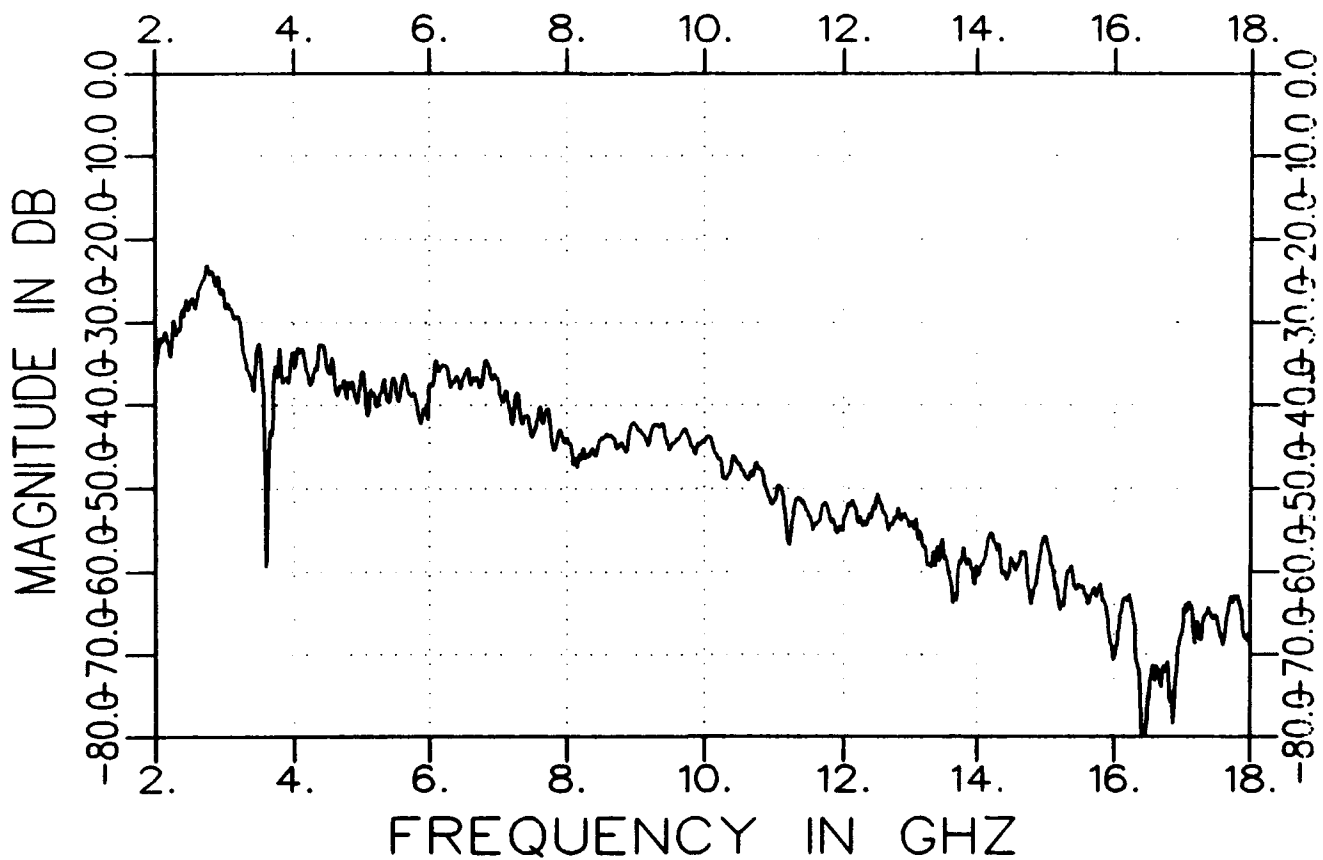
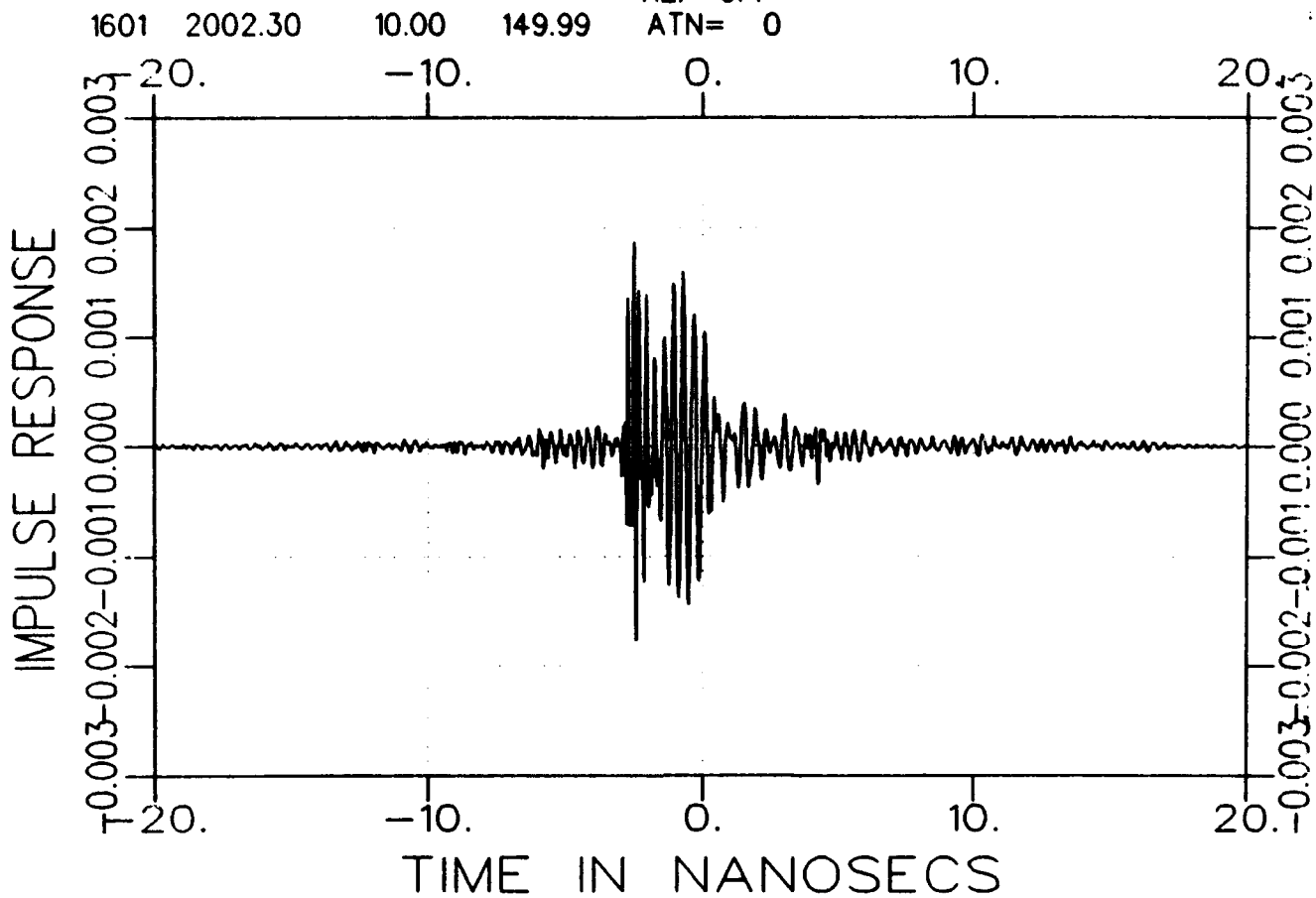
g3225fa1200-a.tar  
TARGET

FREQ. 08/13/93 14:22  
freq s ind grid AVE= 82  
REF=OFF  
ATN= 0



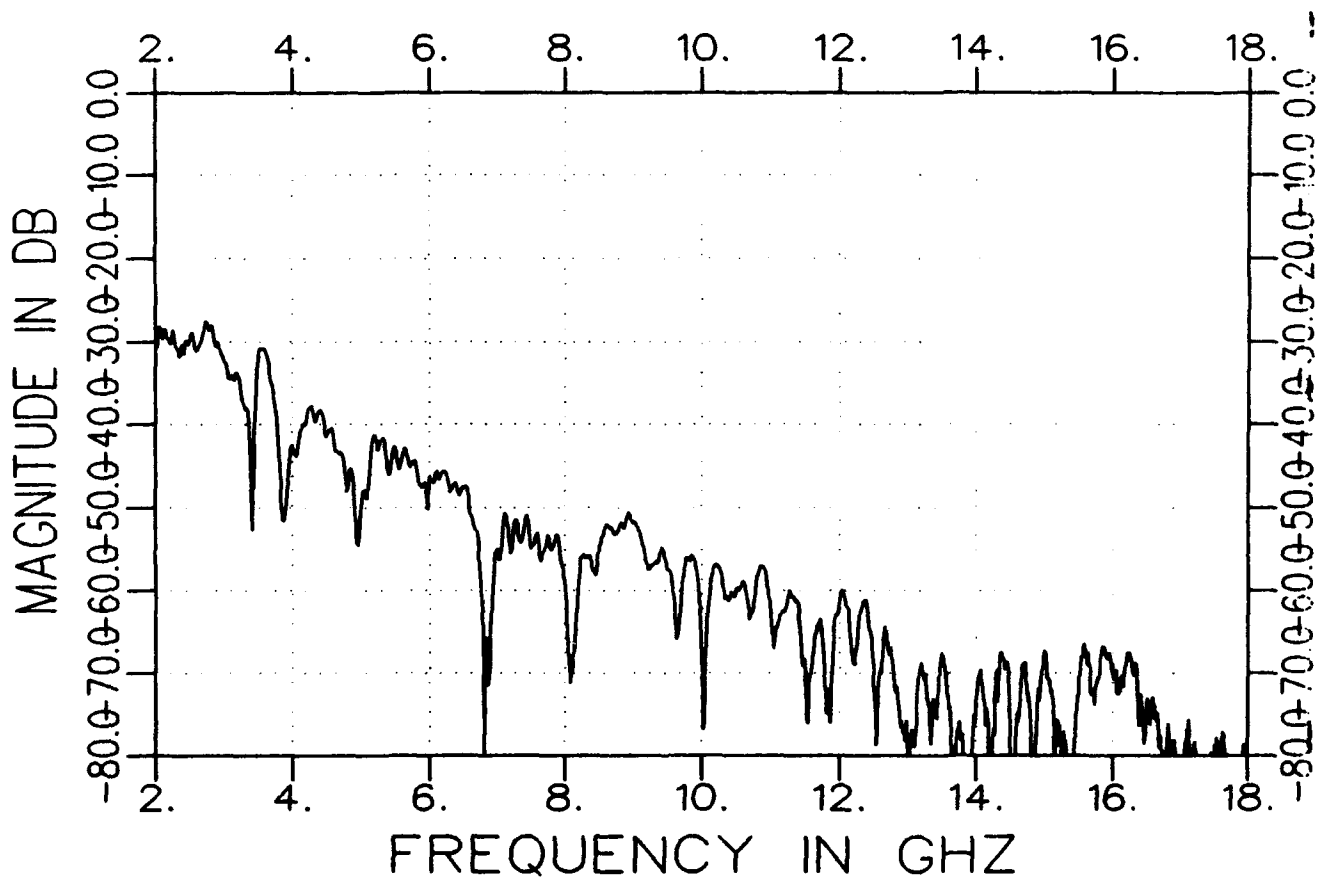
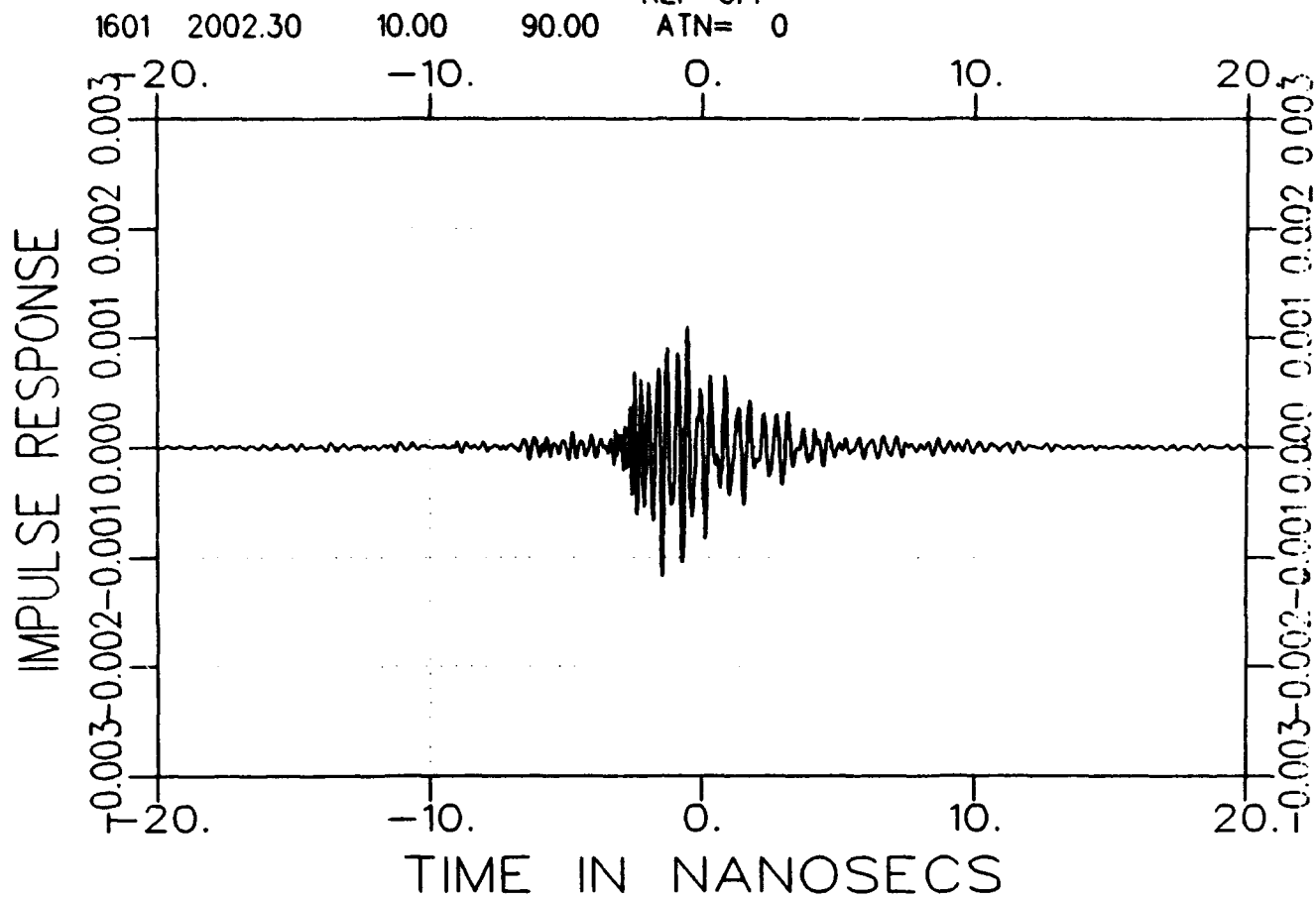
g3225fa1500-a.tar  
TARGET

FREQ. 08/13/93 14:23  
freq s ind grid AVE= 82  
REF=OFF  
ATN= 0



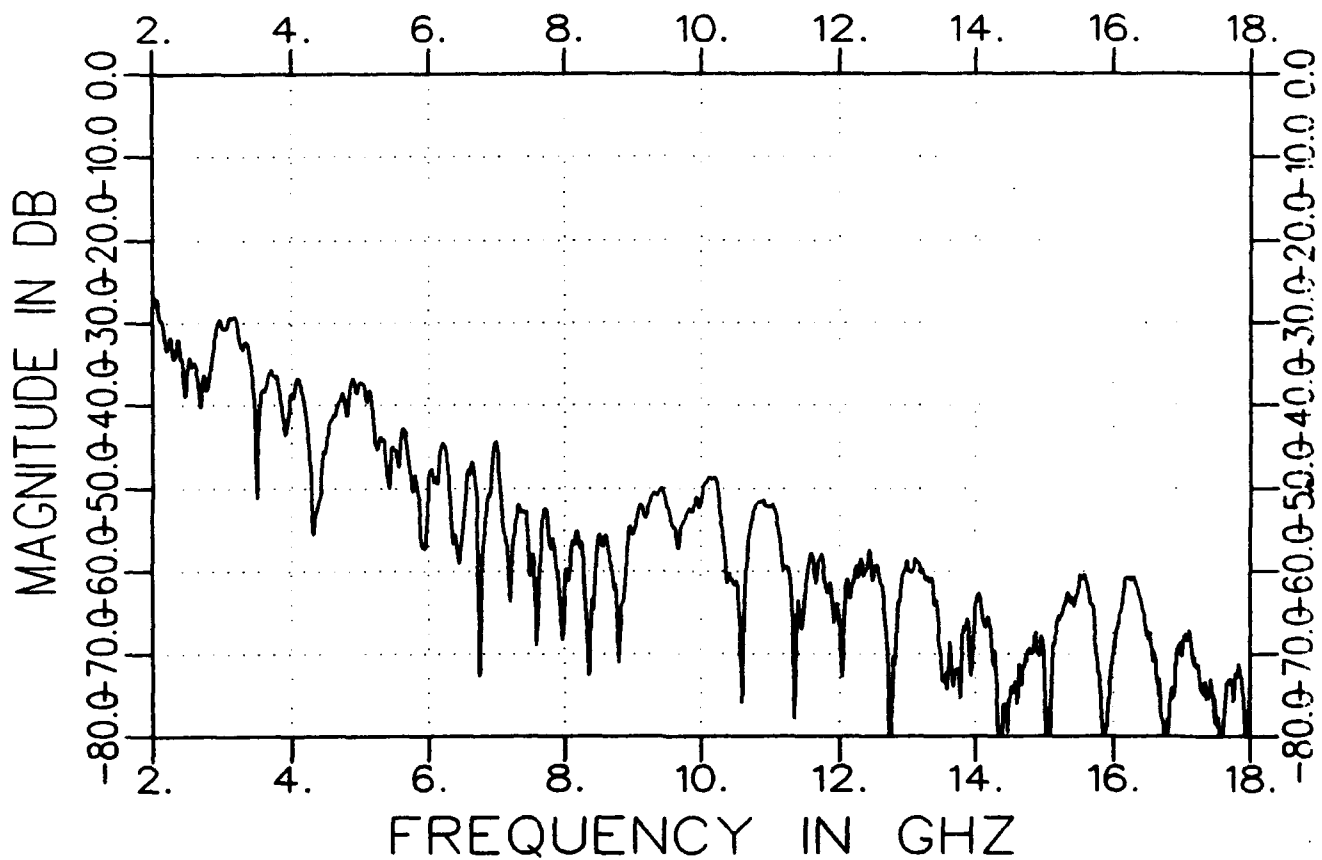
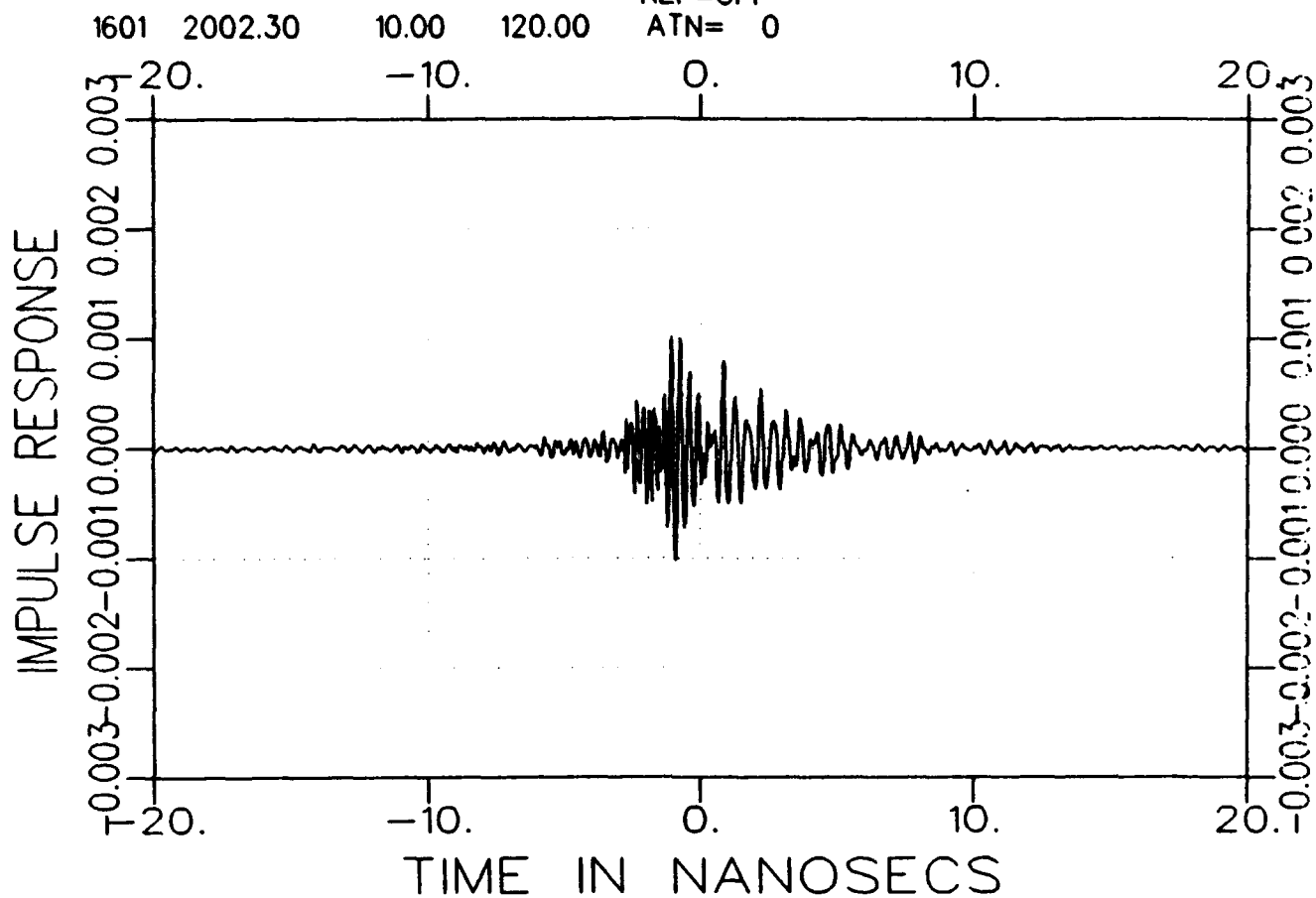
h3225fa0900-a.tar  
TARGET

FREQ. 08/13/93 14:34  
freq l ind grid AVE= 82  
REF=OFF  
ATN= 0



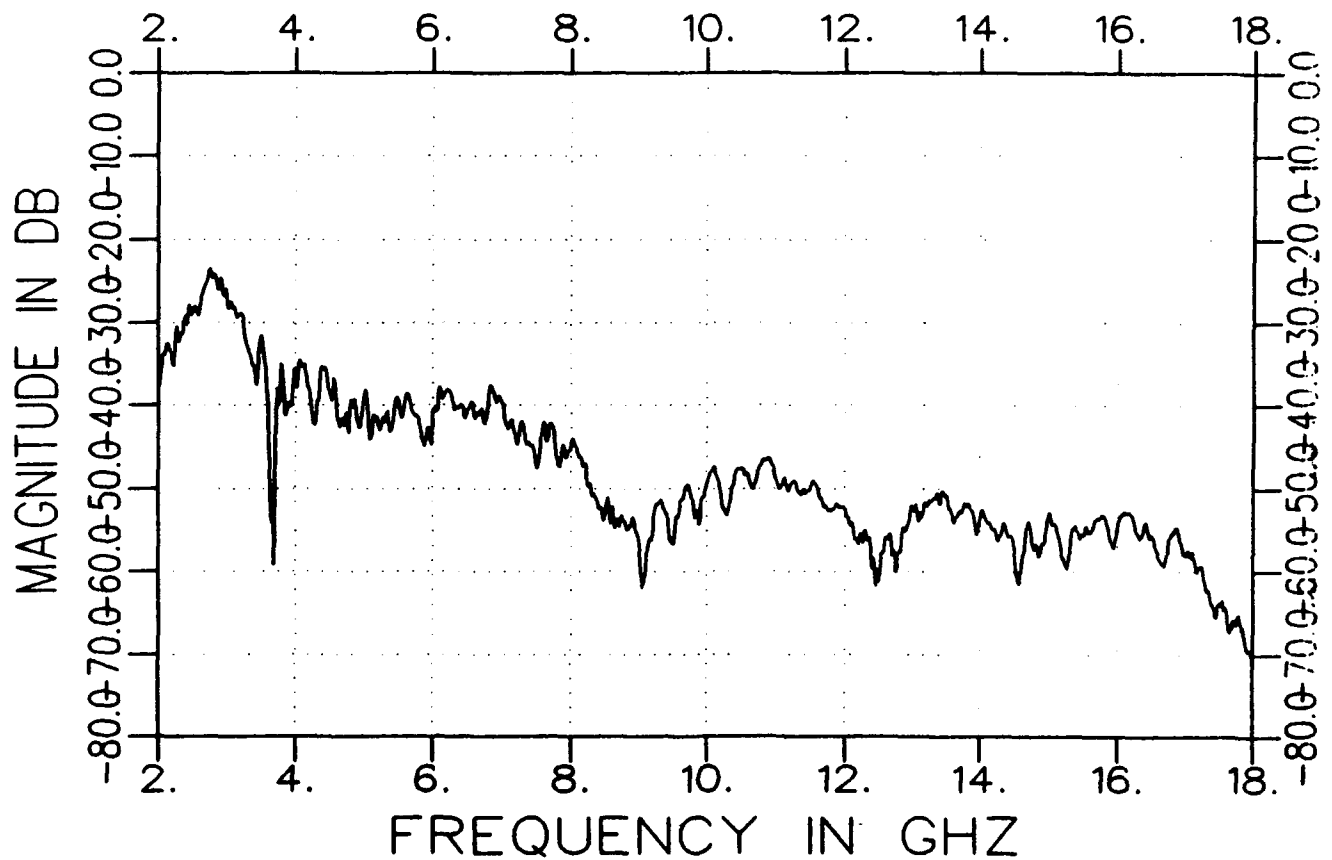
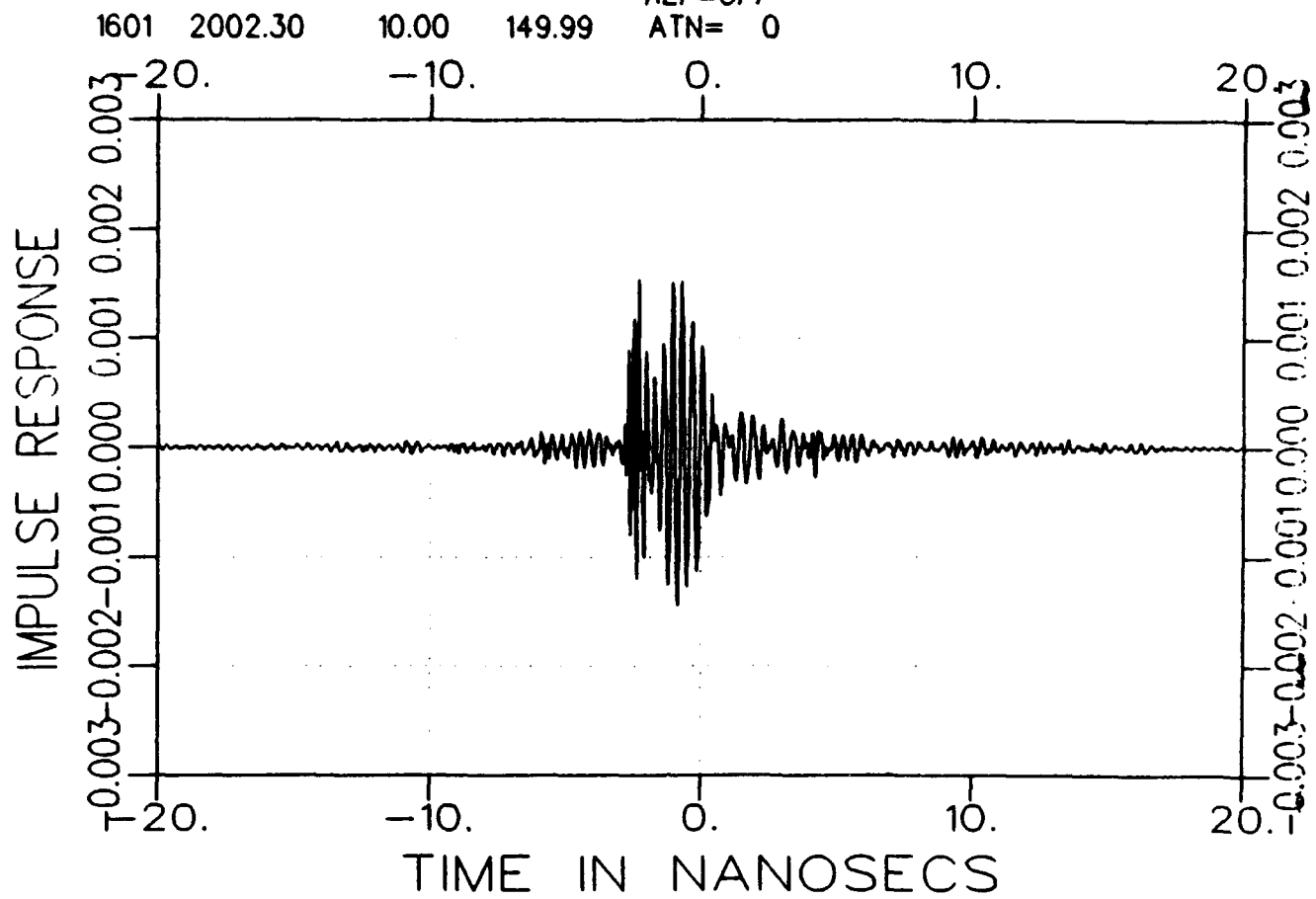
h3225fa1200-a.tar  
TARGET

FREQ. 08/13/93 14:35  
freq 1 ind grid AVE= 82  
REF=OFF  
ATN= 0



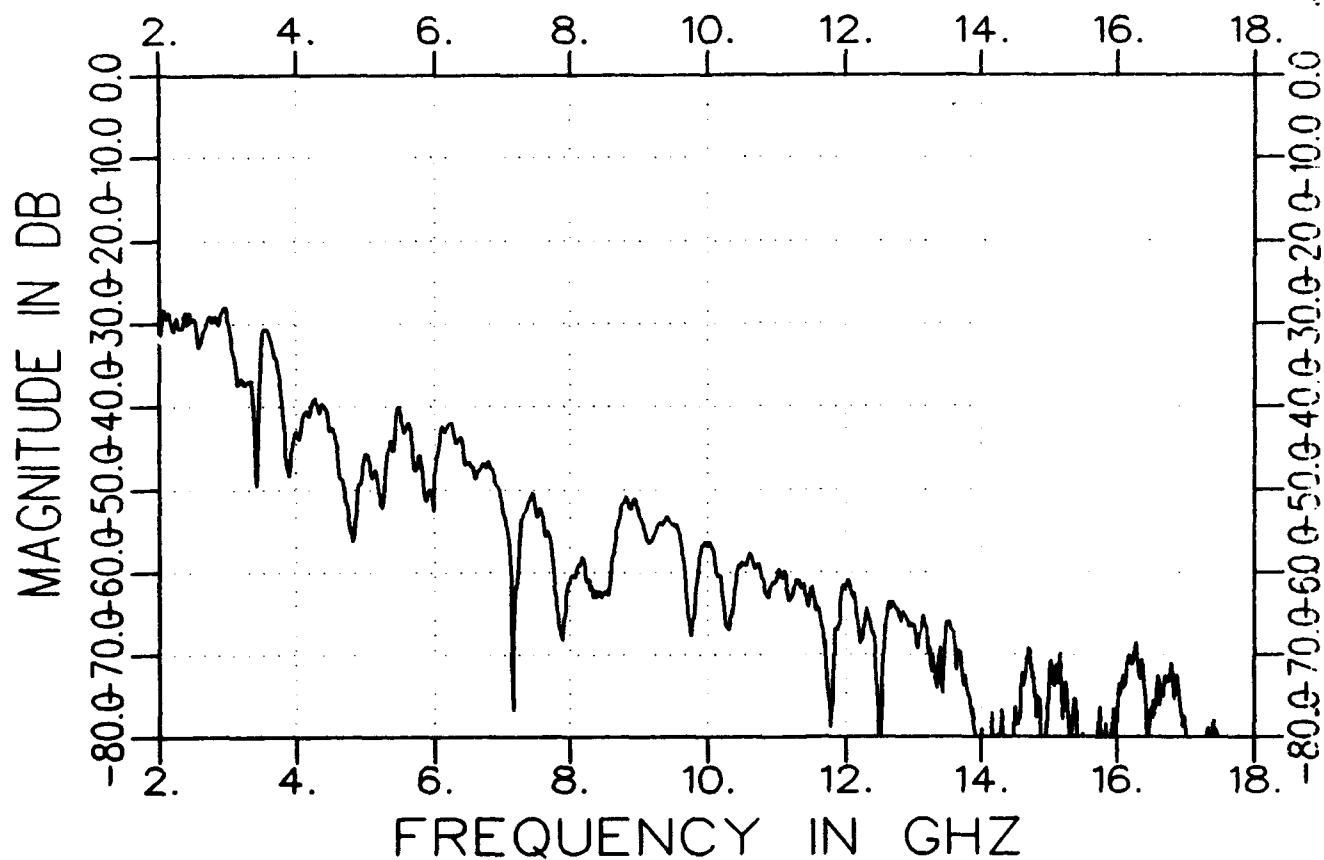
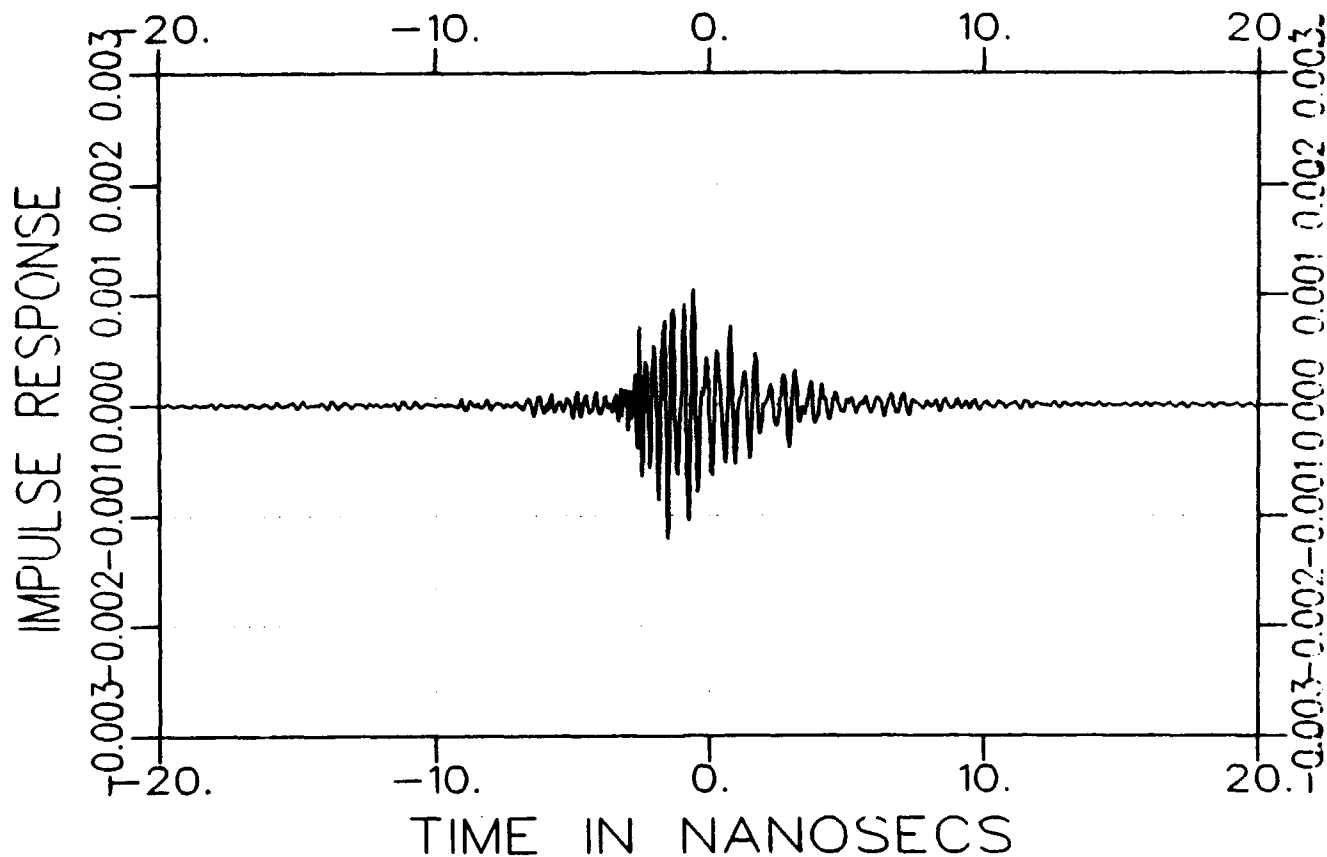
h3225fa1500-a.tar  
TARGET

FREQ. 08/13/93 14:36  
freq 1 ind grid AVE= 82  
REF=OFF  
ATN= 0



13225fa0900-a.tar  
TARGET

FREQ. 08/13/93 14:43  
freq naked v AVE= 82  
REF=OFF  
ATN= 0



i3225fa1200-a.tar  
TARGET

FREQ. 08/13/93 14:40

freq naked v

AVE= 82

REF=OFF

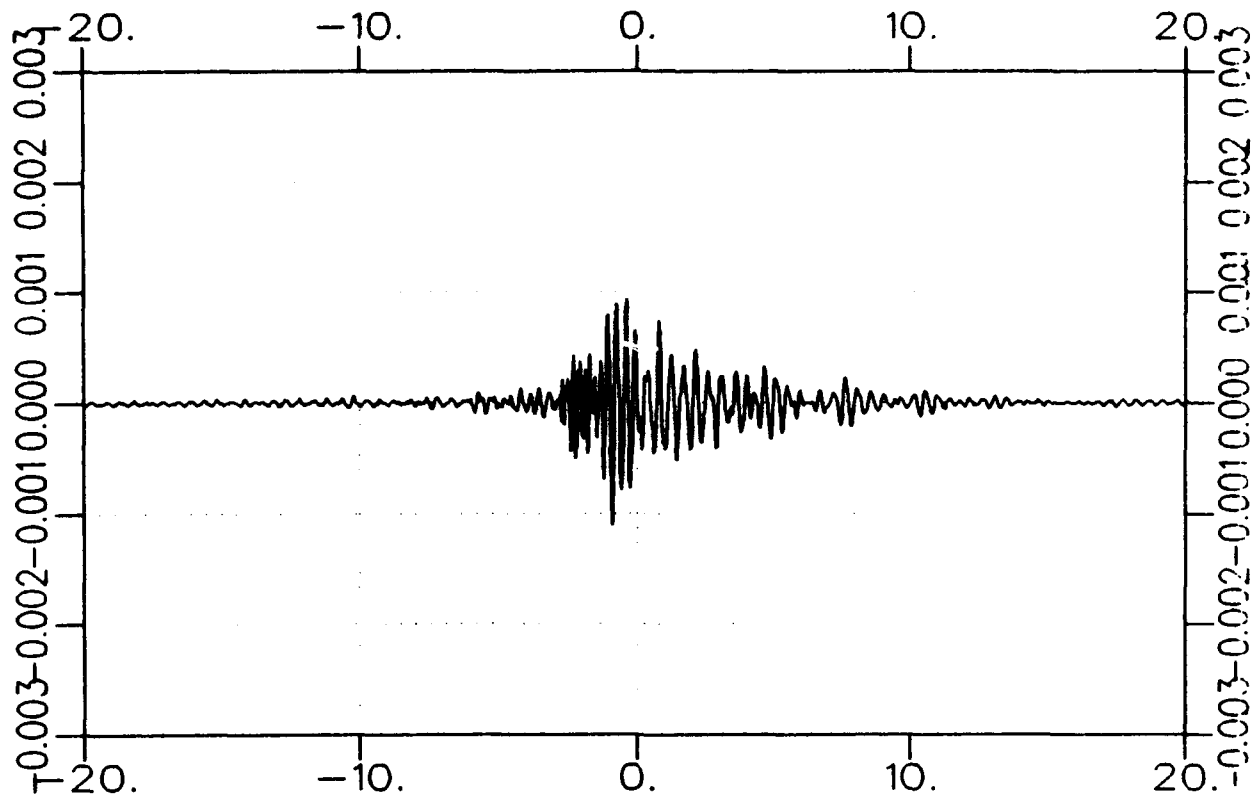
ATN= 0

1601 2002.30

10.00

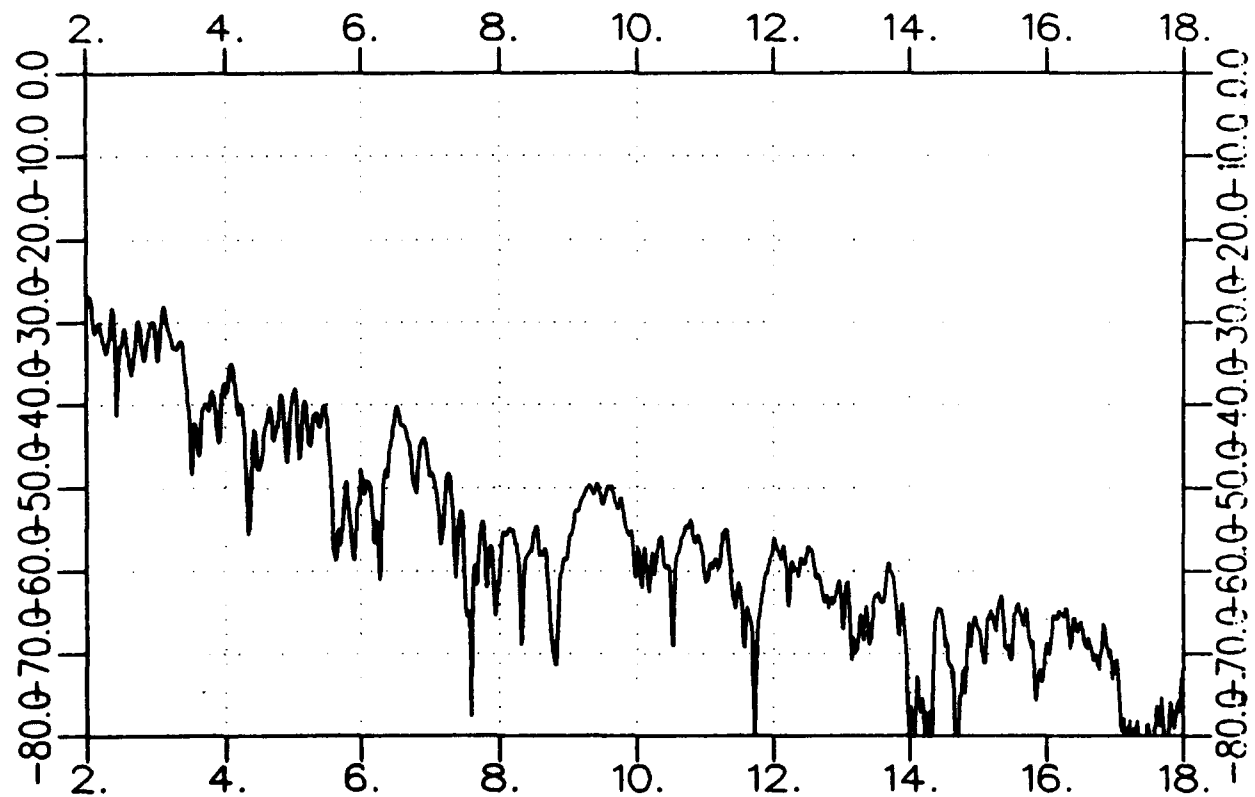
120.00

IMPULSE RESPONSE



TIME IN NANOSECS

MAGNITUDE IN DB



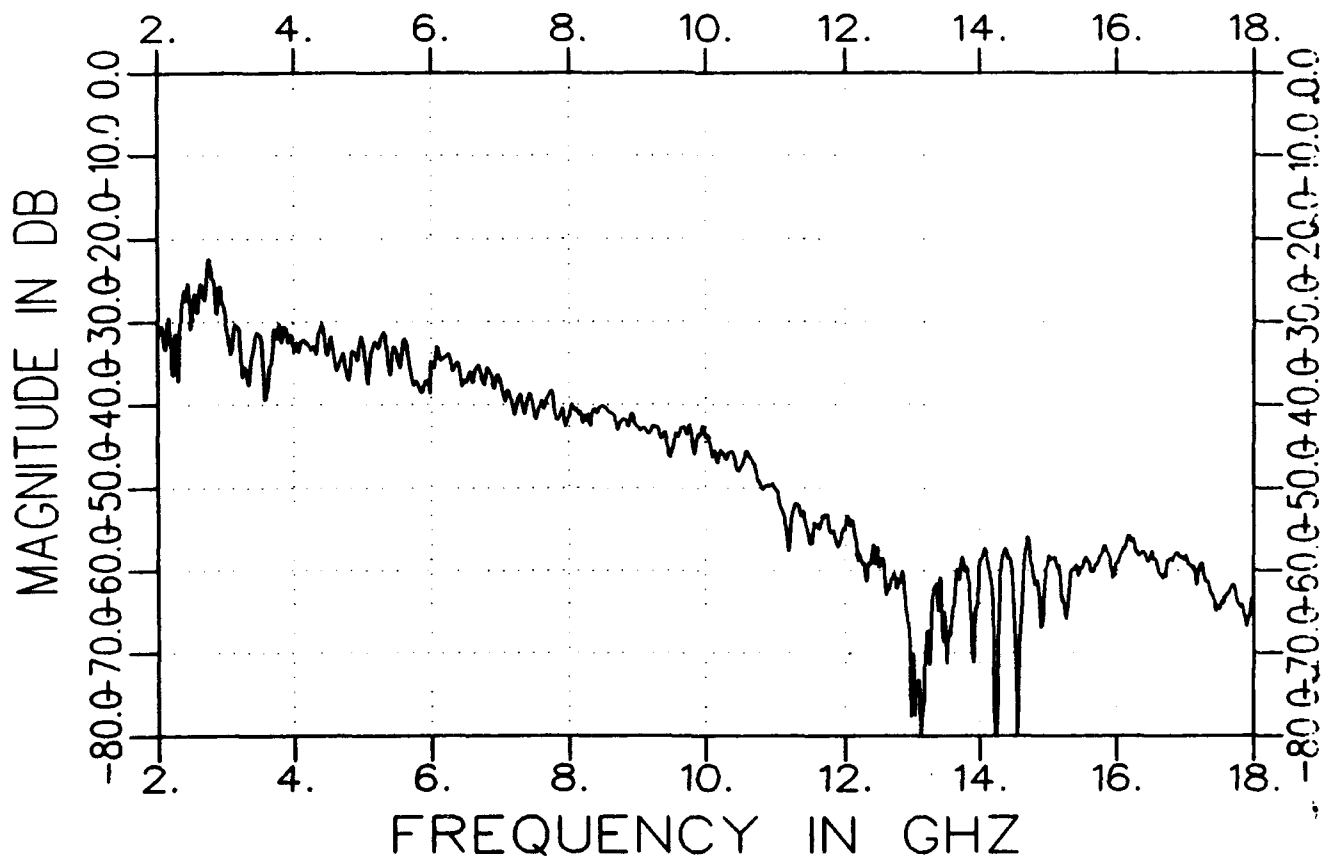
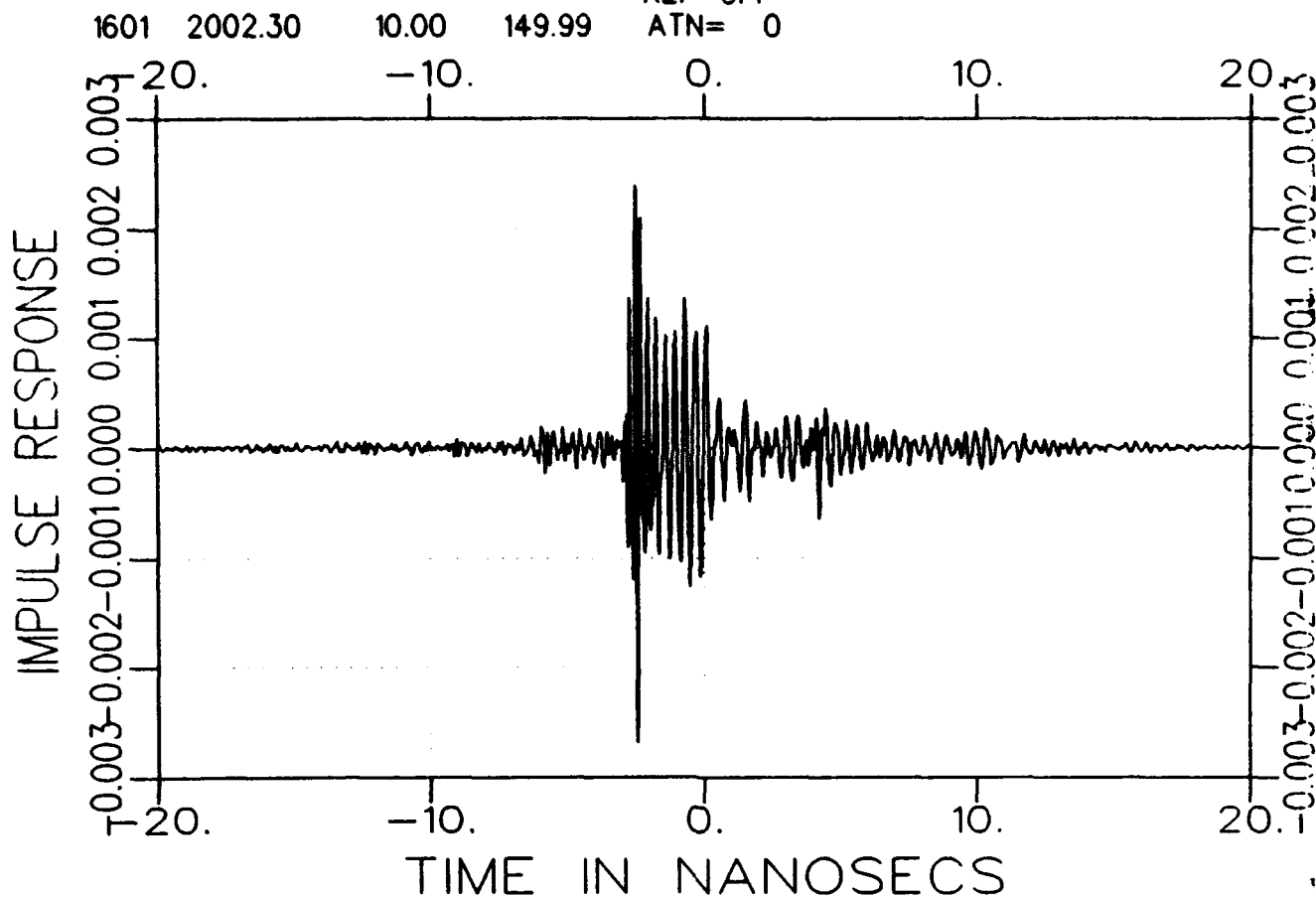
FREQUENCY IN GHZ



i3225fal500-a.tar  
TARGET

FREQ. 08/13/93 14:41  
freq naked v

AVE= 82  
REF=OFF  
ATN= 0



j3225fa0900-a.tar  
TARGET

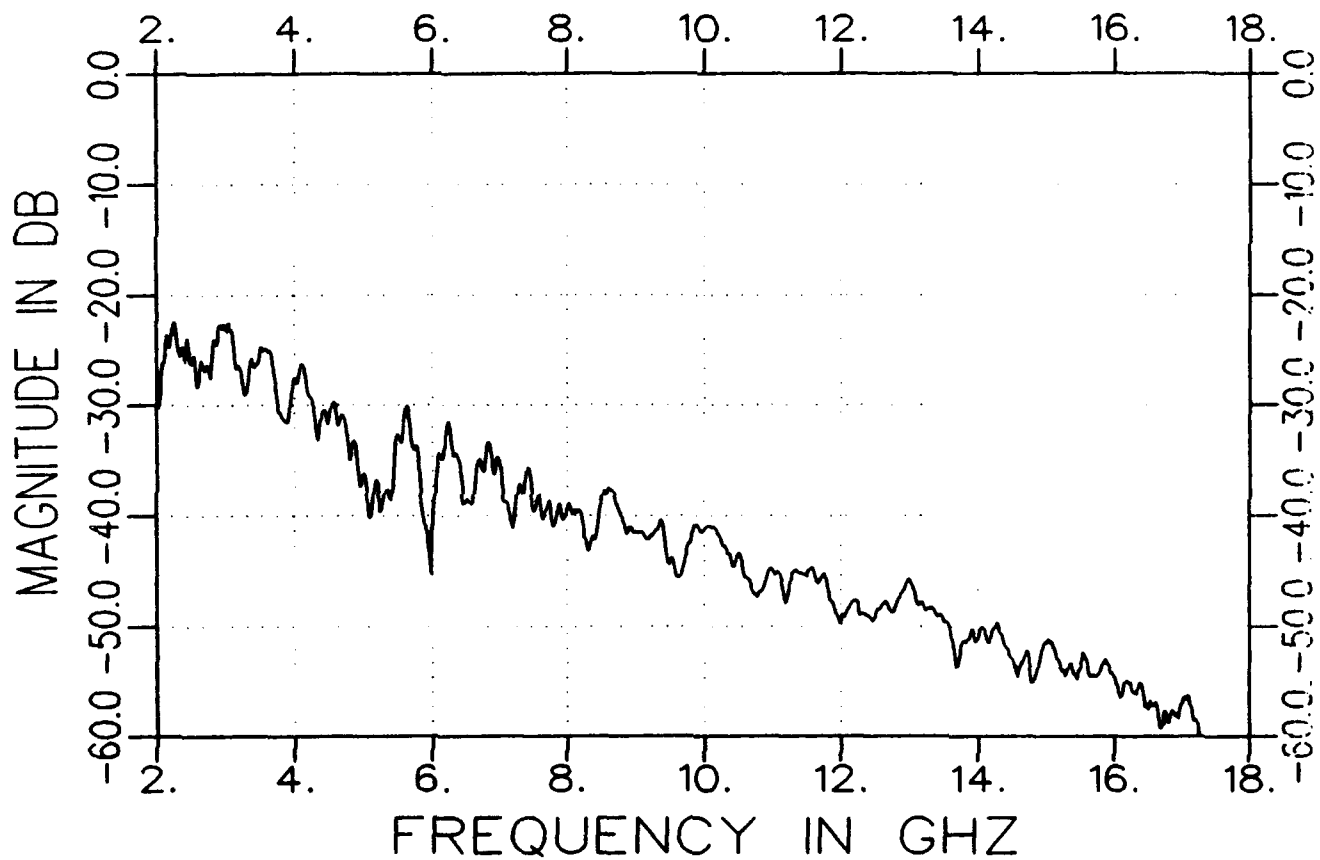
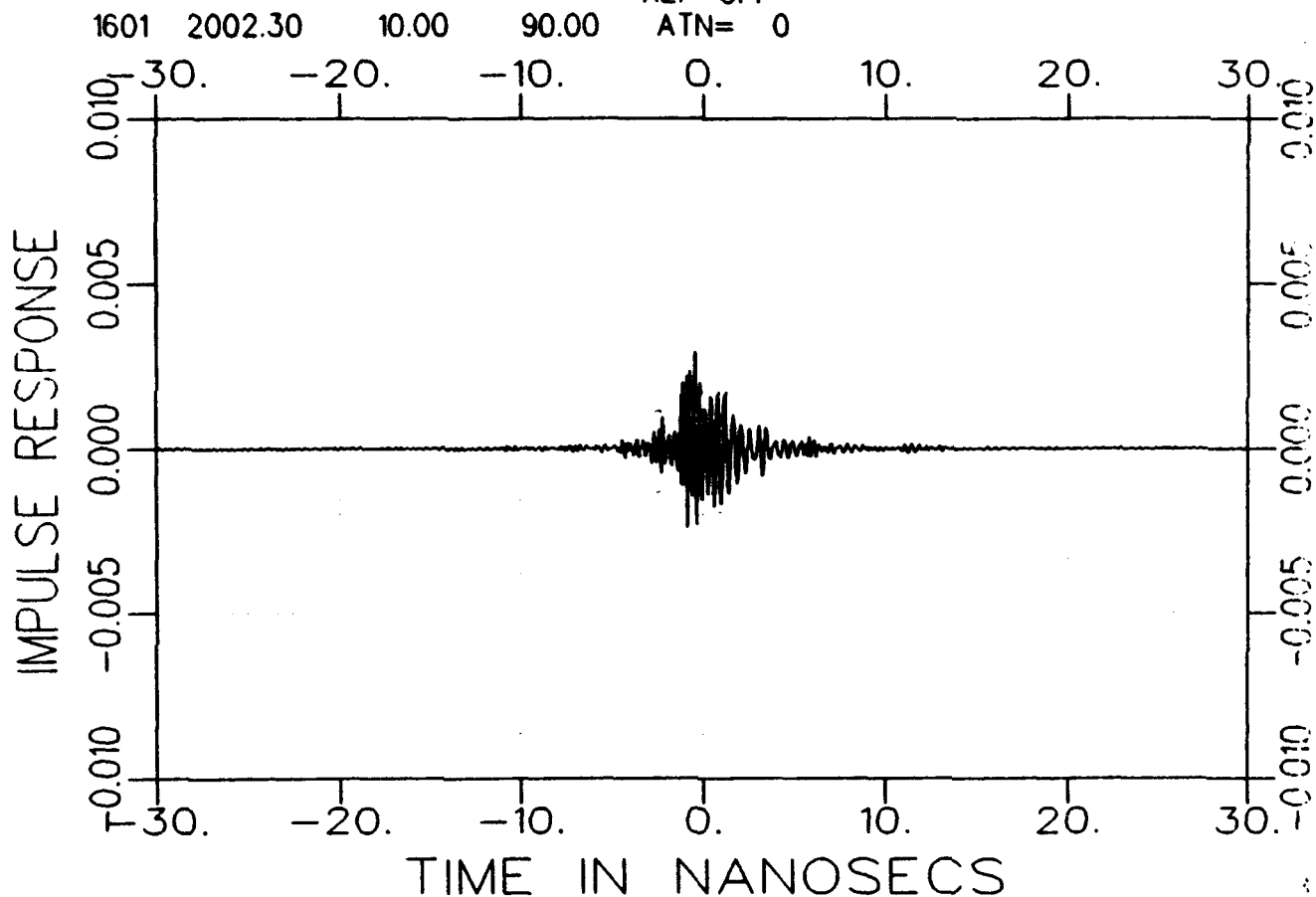
FREQ. 08/13/93 14:51

freq naked h

AVE= 82

REF=OFF

ATN= 0

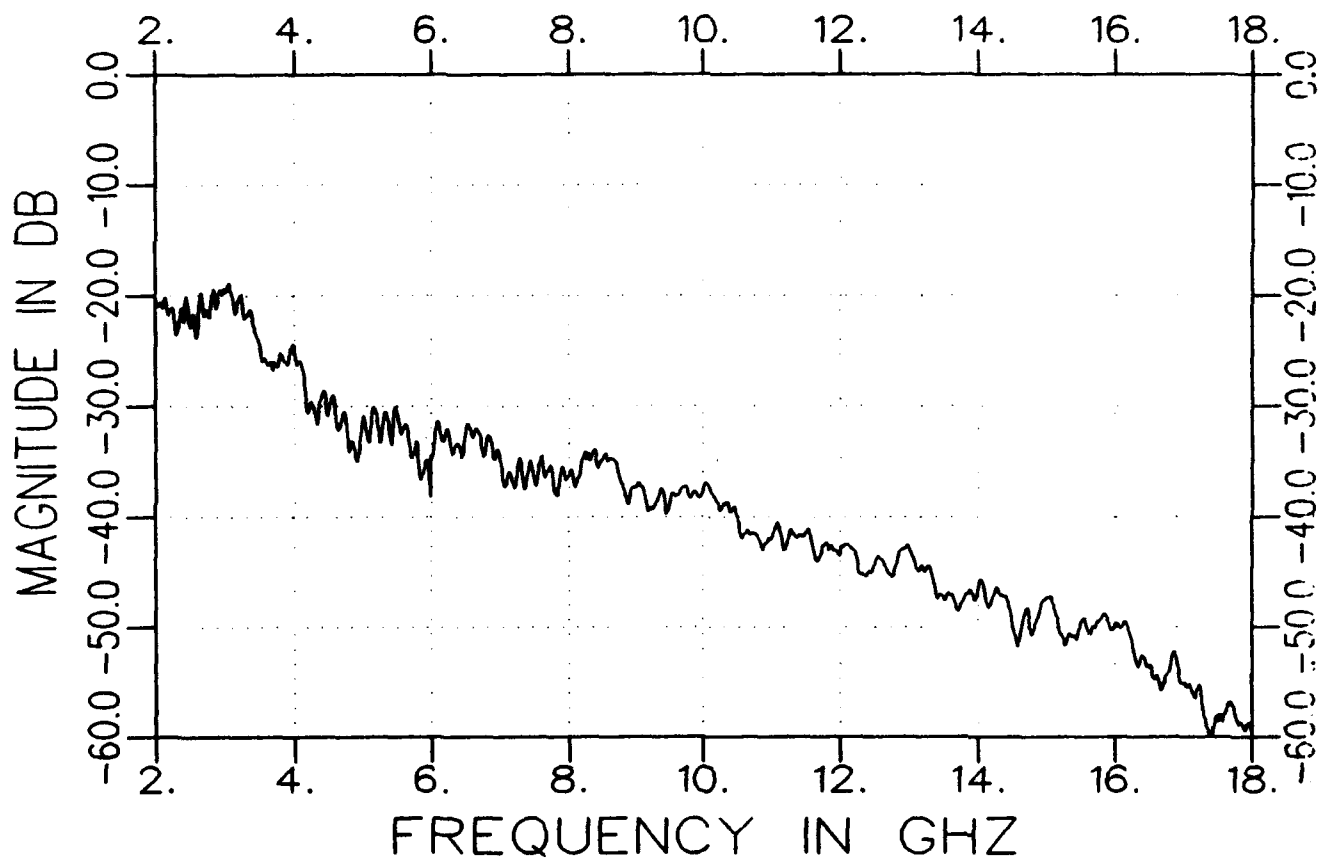
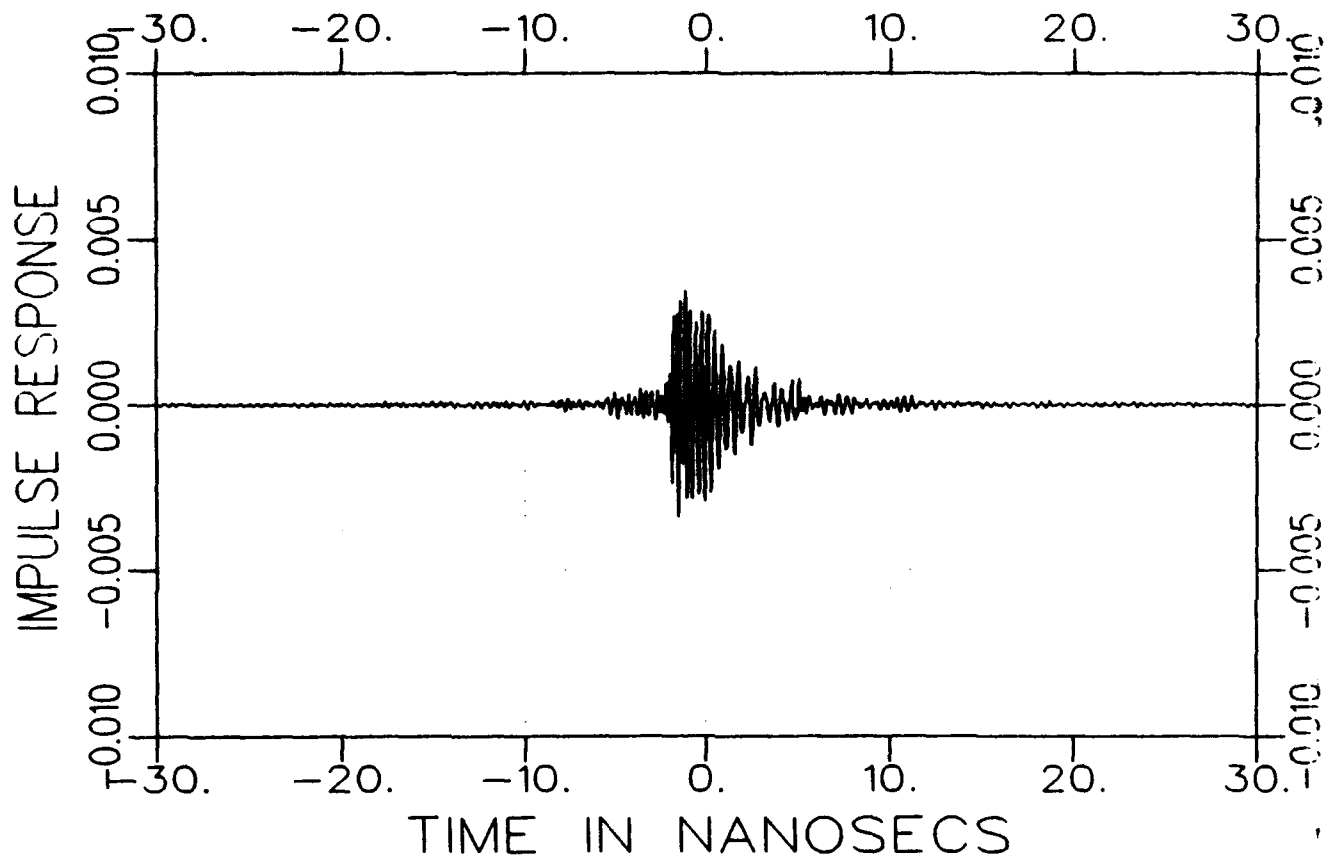


j3225fa1200-a.tar  
TARGET

FREQ. 08/13/93 14:52  
freq naked h

AVE= 82  
REF=OFF

1601 2002.30 10.00 120.00 ATN= 0



j3225fa1500-a.tar  
TARGET

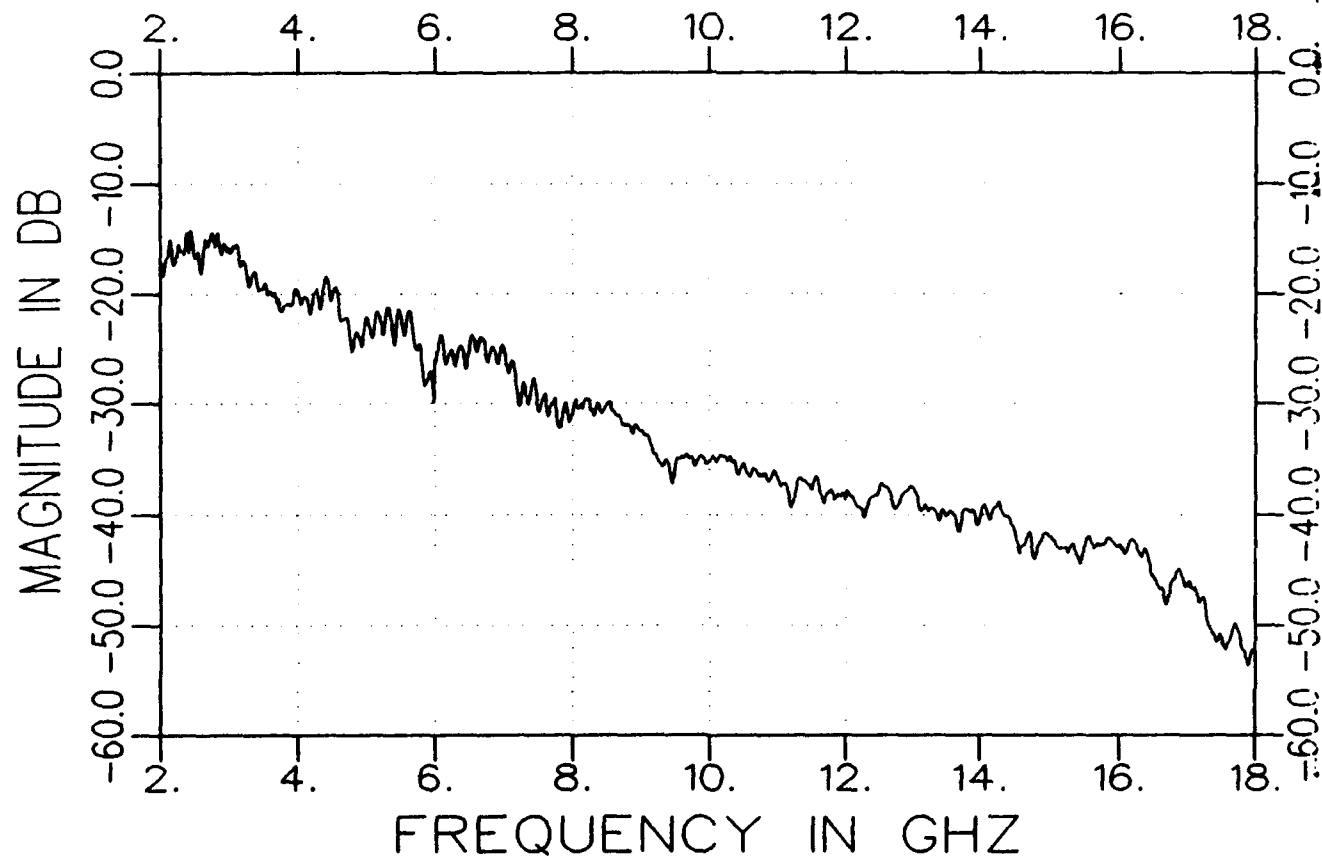
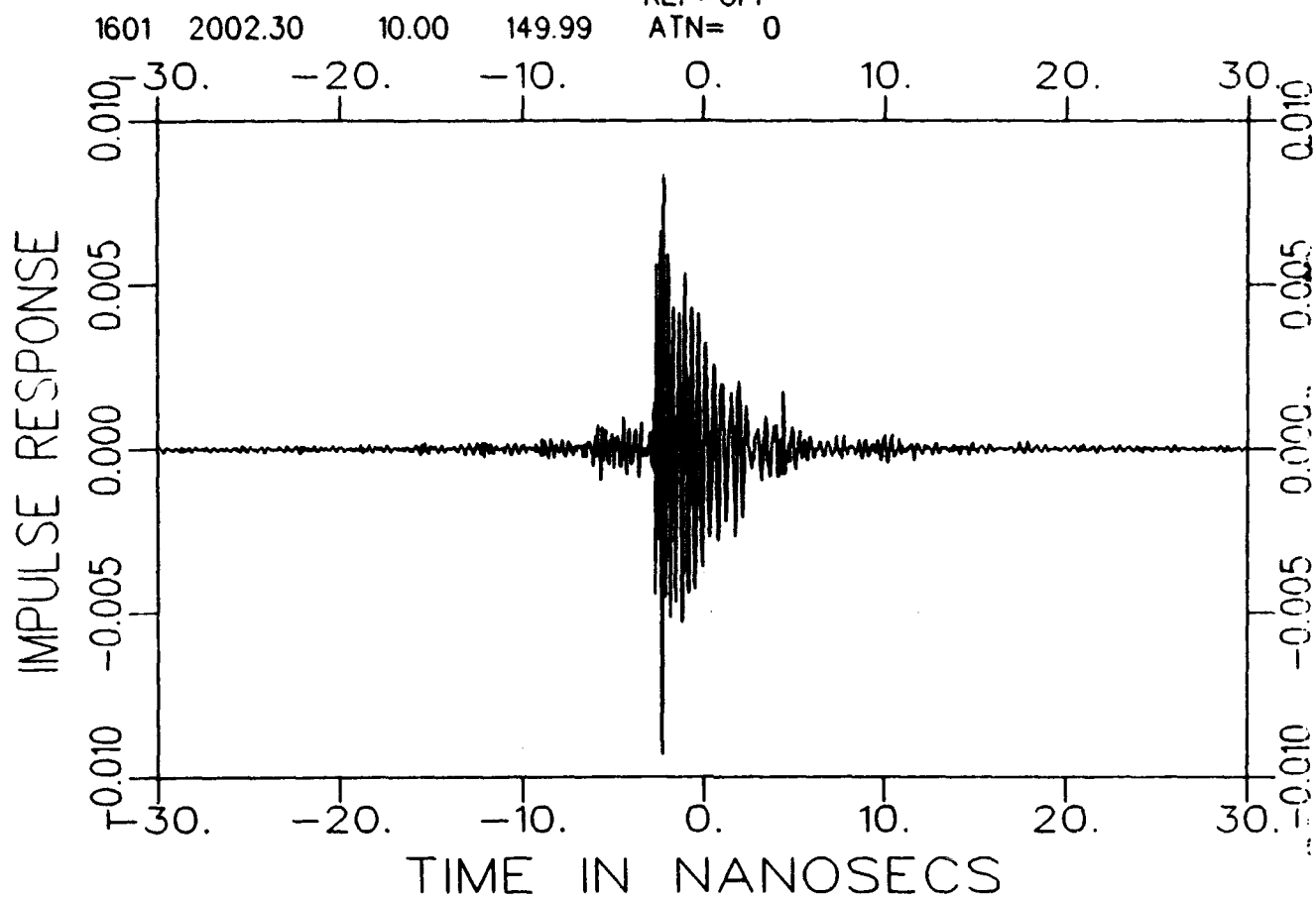
FREQ. 08/13/93 14:53

freq naked h

AVE= 82

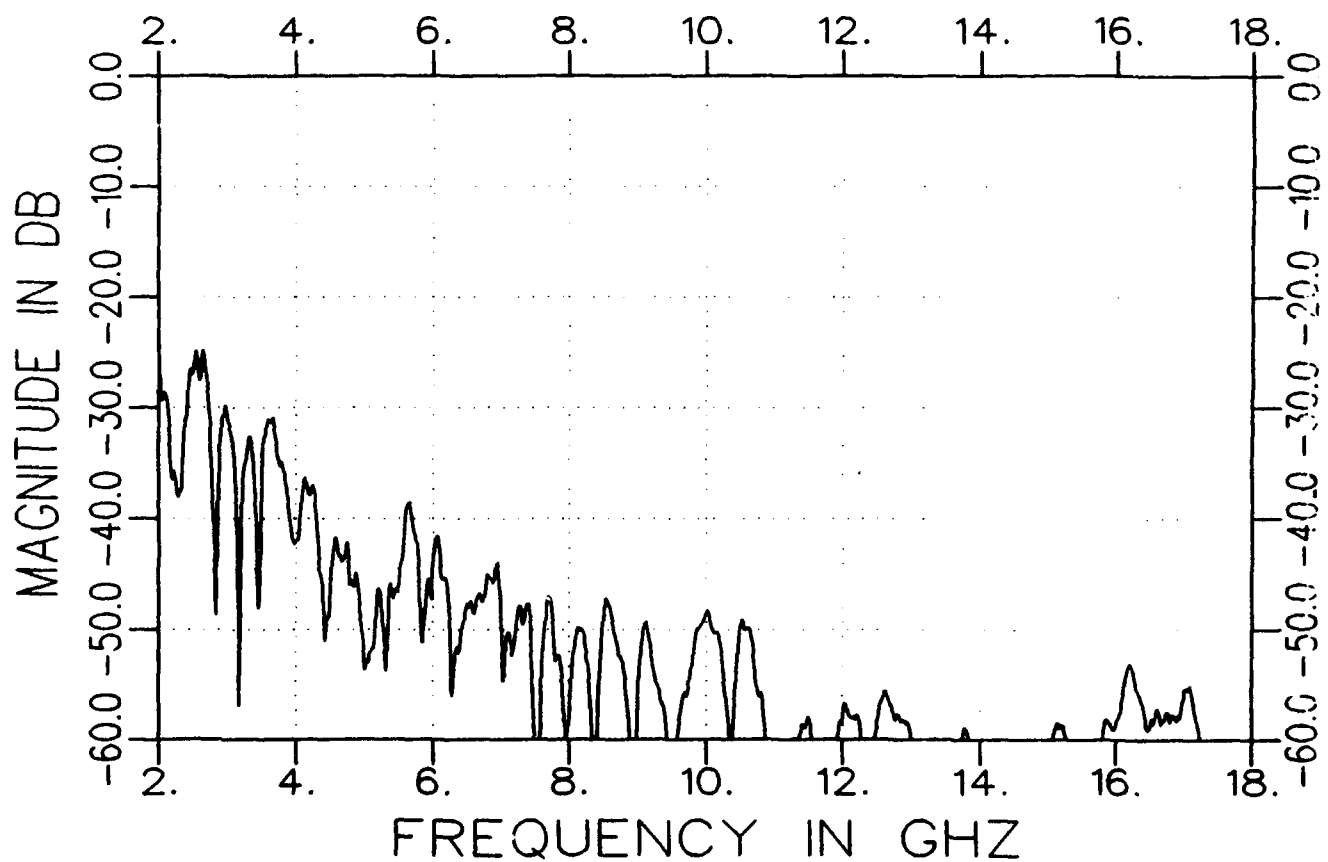
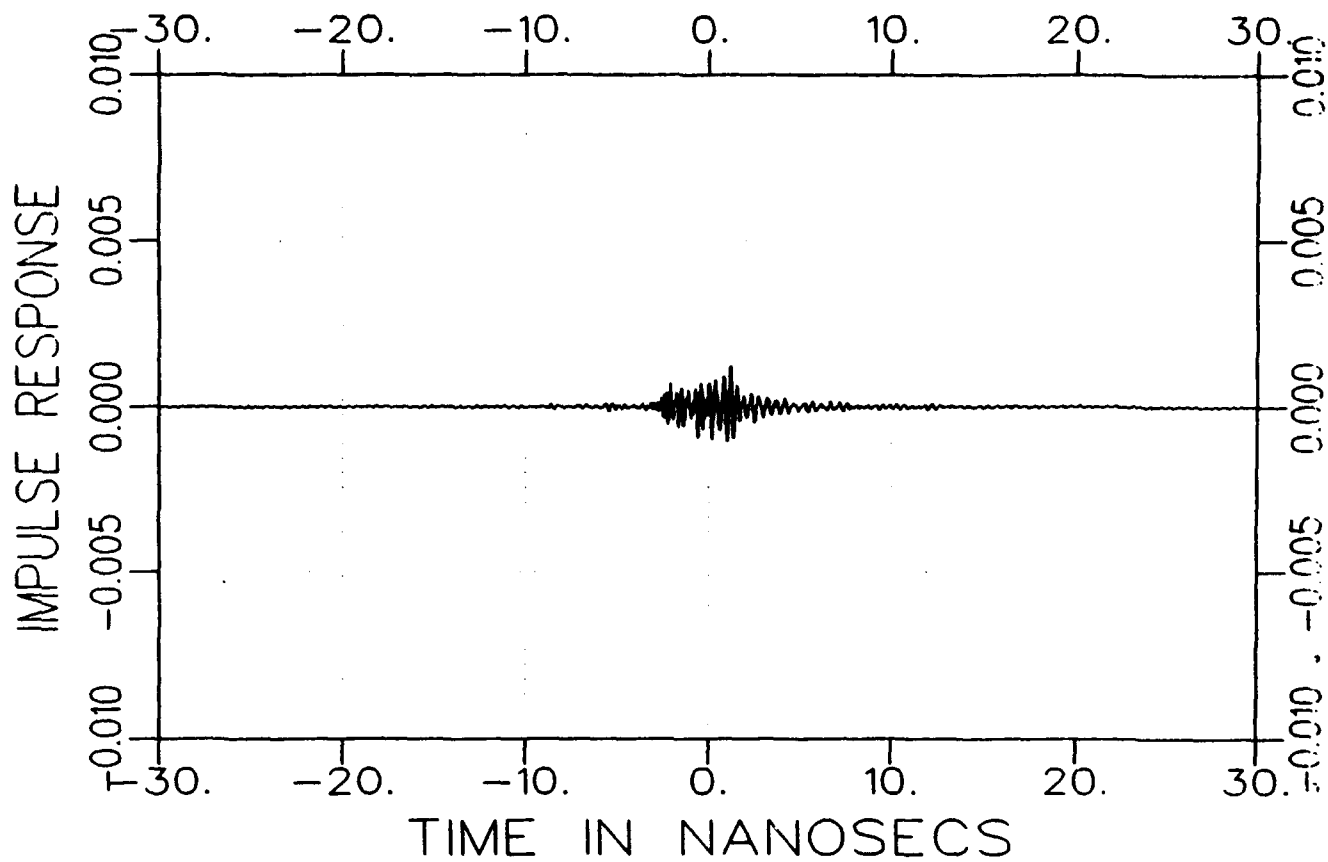
REF=OFF

ATN= 0



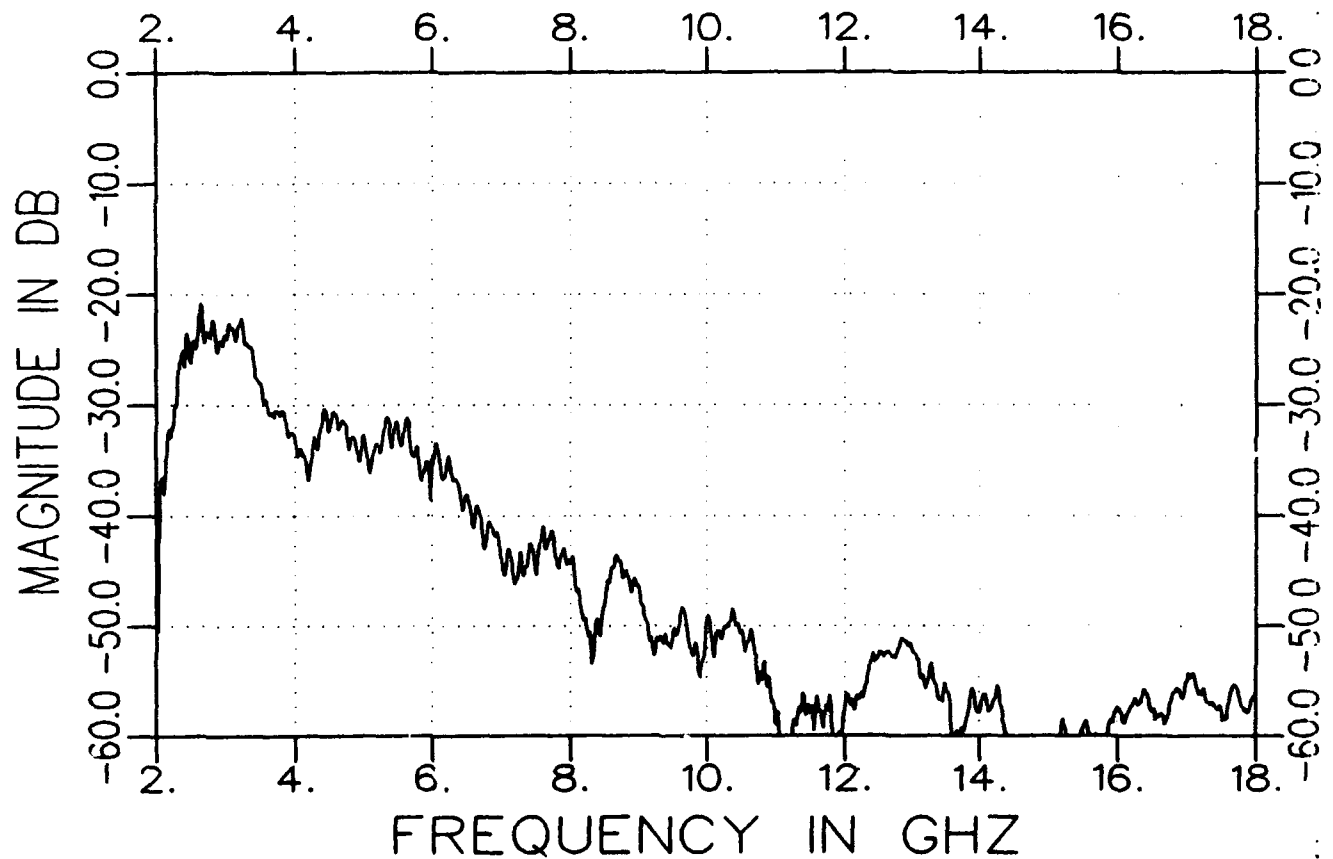
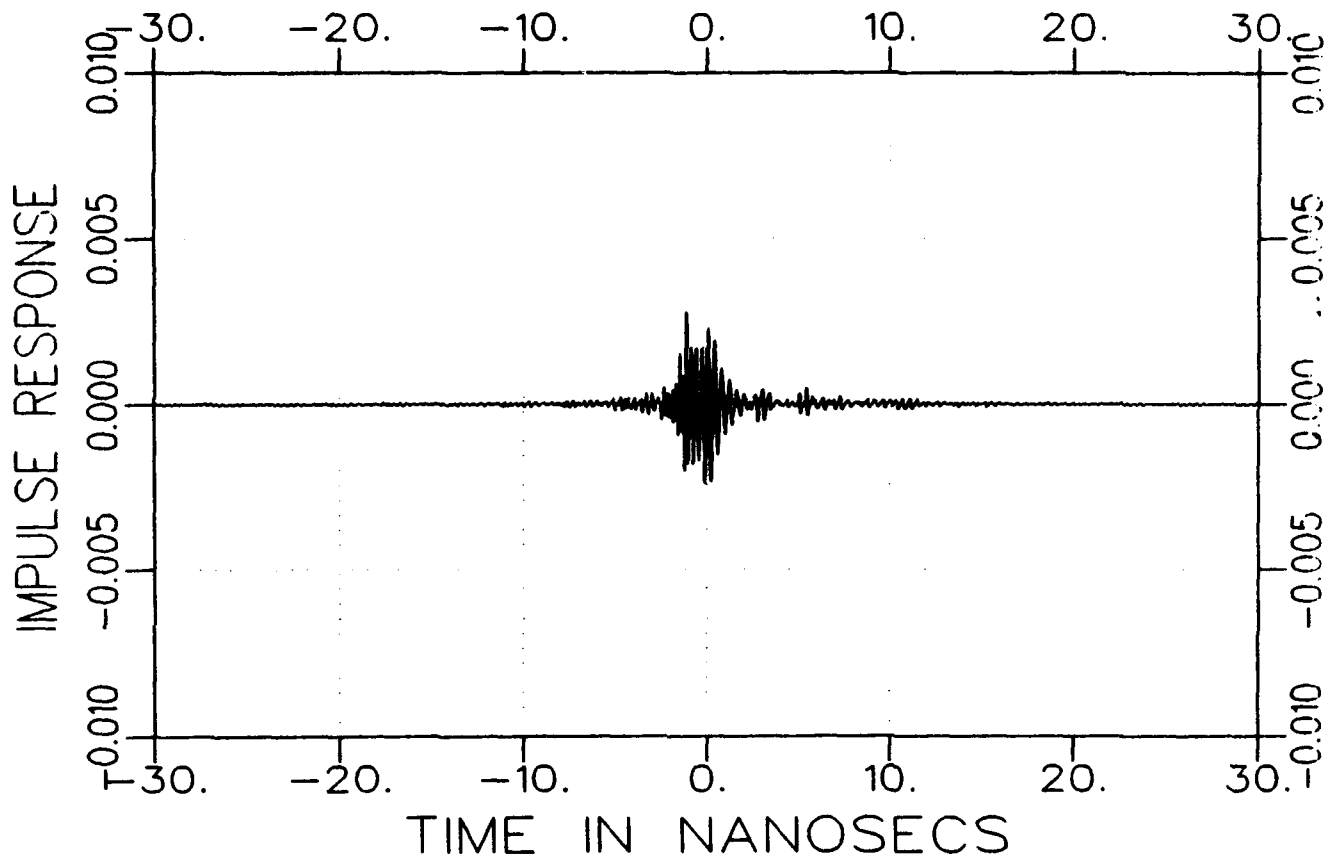
k3225fa0900-a.tar  
TARGET

FREQ. 08/13/93 14:57  
freq l cap grid AVE= 82  
REF=OFF  
ATN= 0



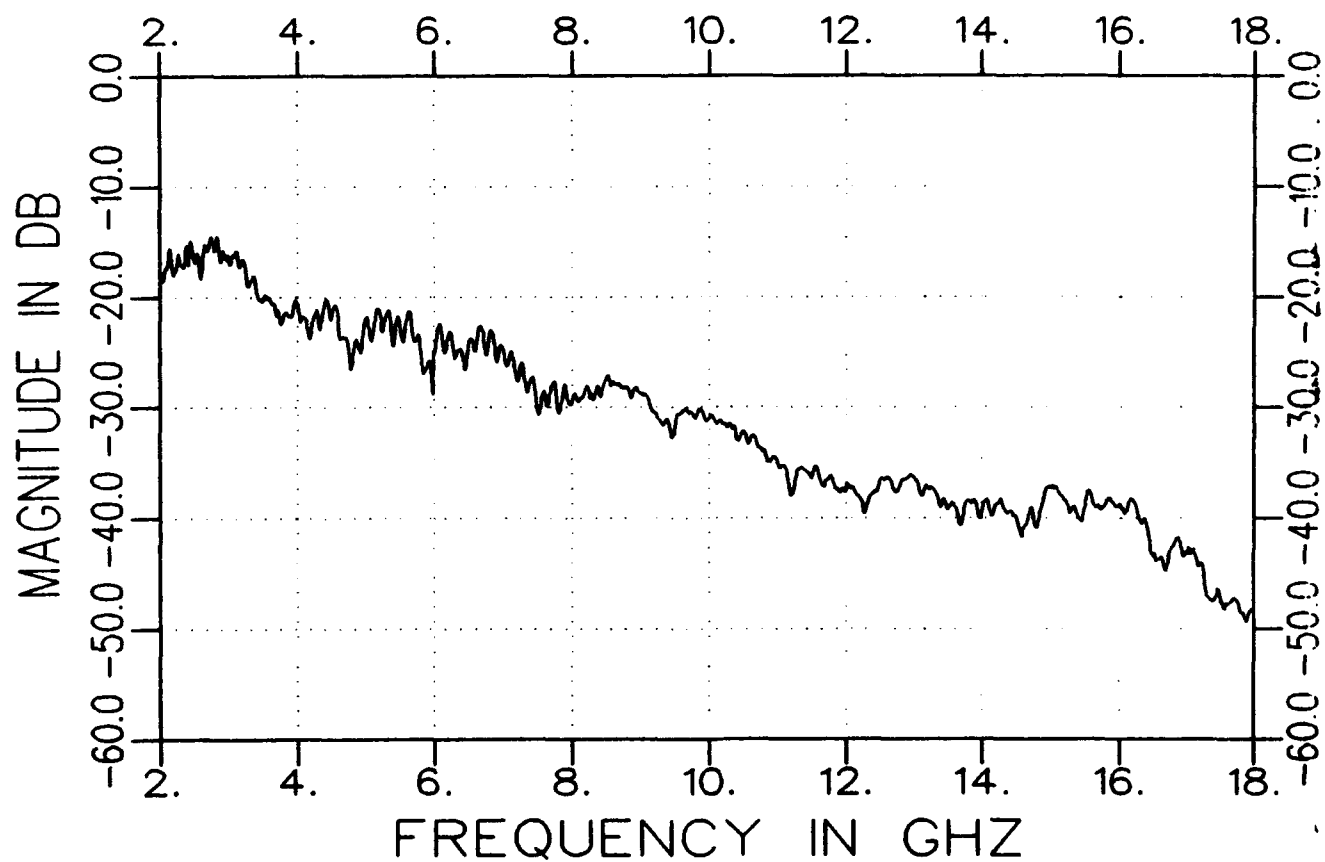
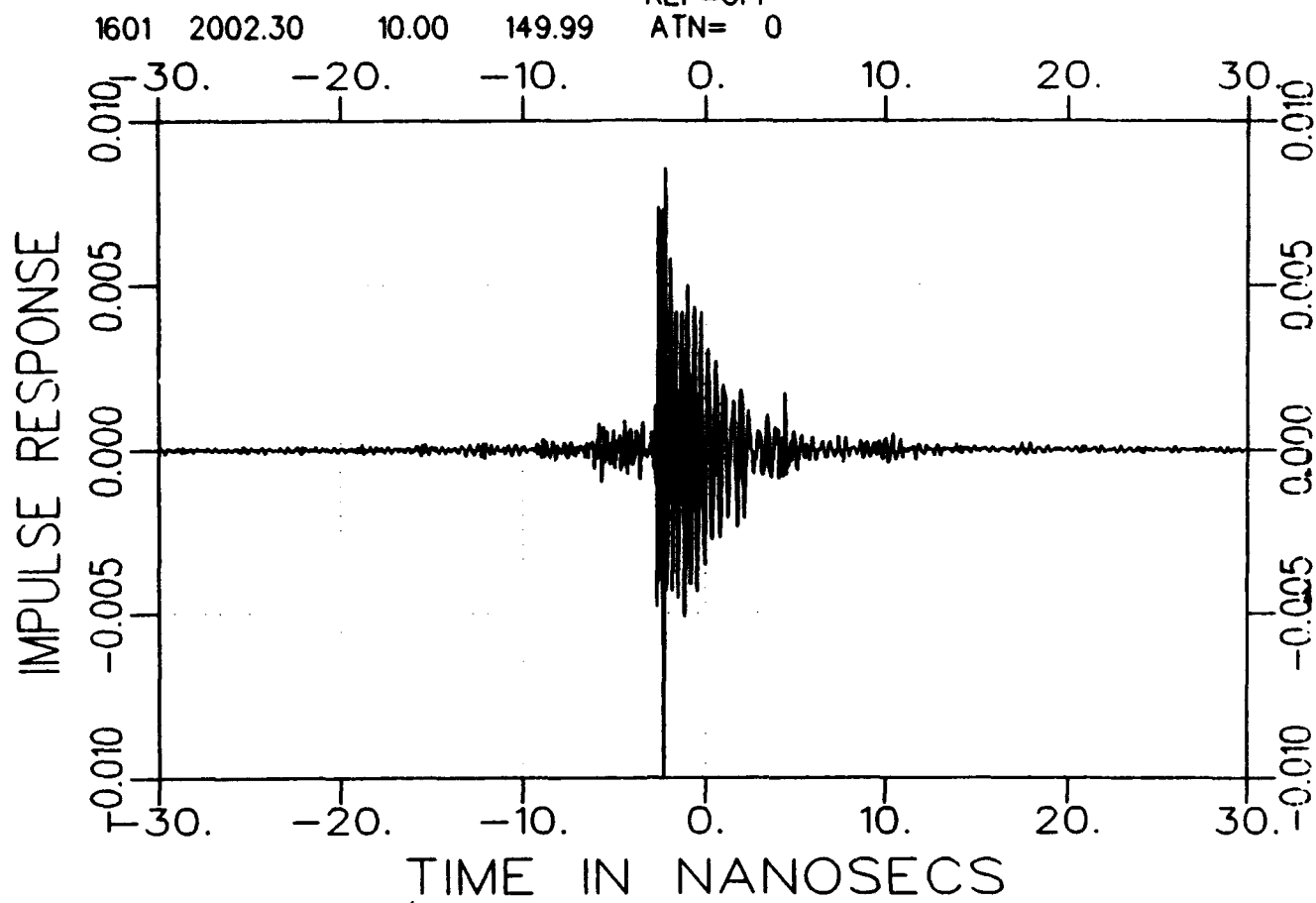
k3225fa1200-a.tim  
TARGET

FREQ. 08/13/93 15:00  
freq l cap grid AVE= 82  
REF=OFF  
ATN= 0



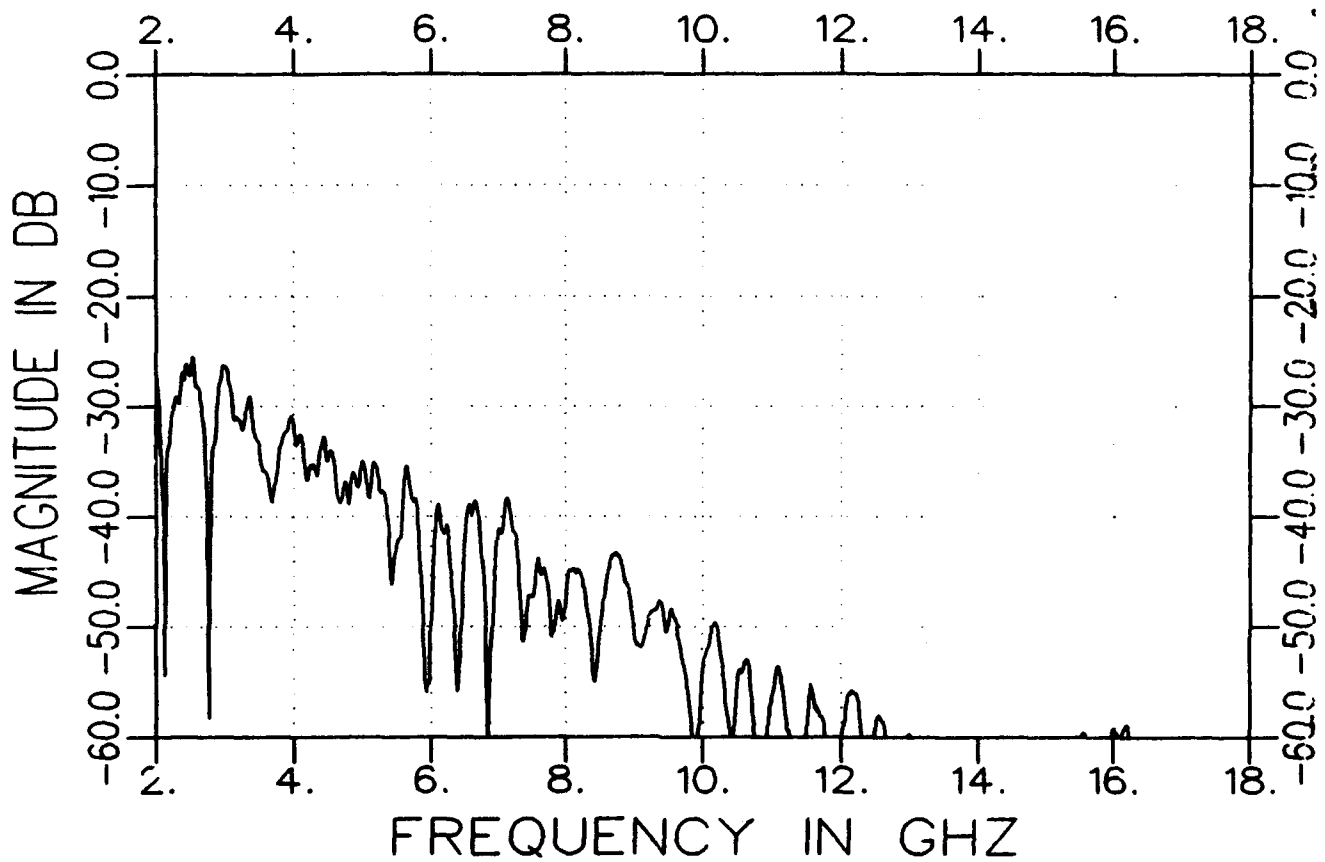
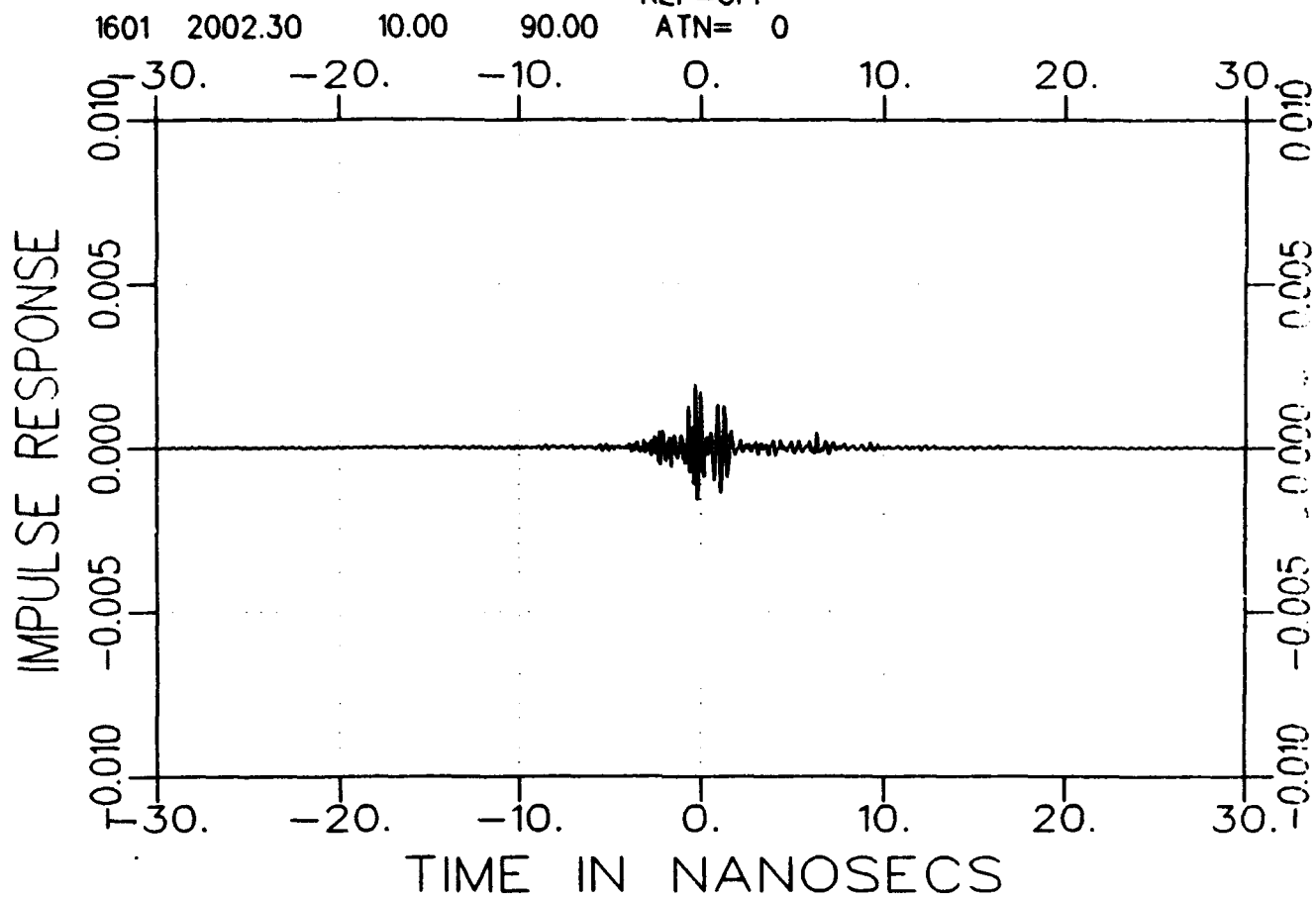
k3225fa1500-a.tar  
TARGET

FREQ. 08/13/93 14:59  
freq l cap grid AVE= 82  
REF=OFF  
ATN= 0



13225fa0900-a.tar  
TARGET

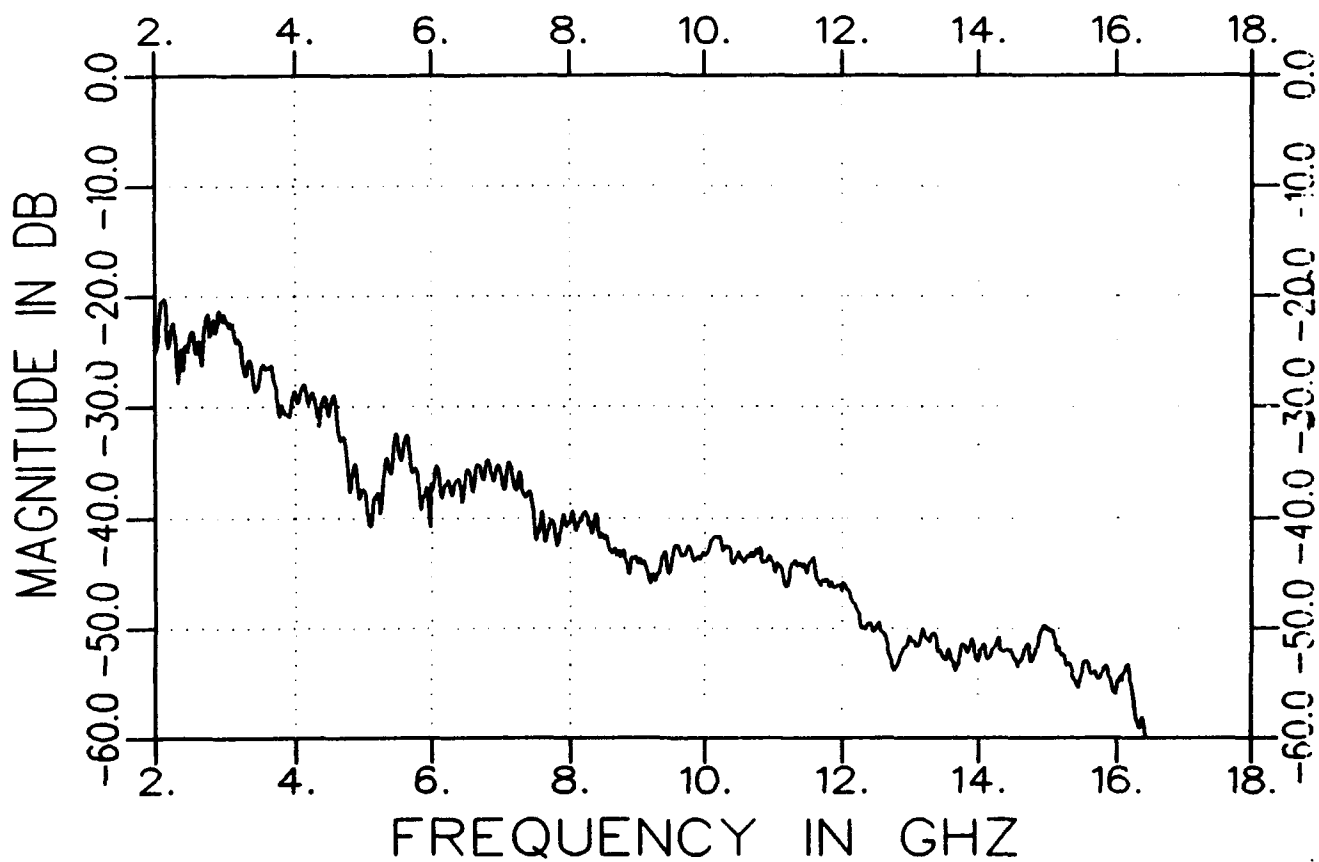
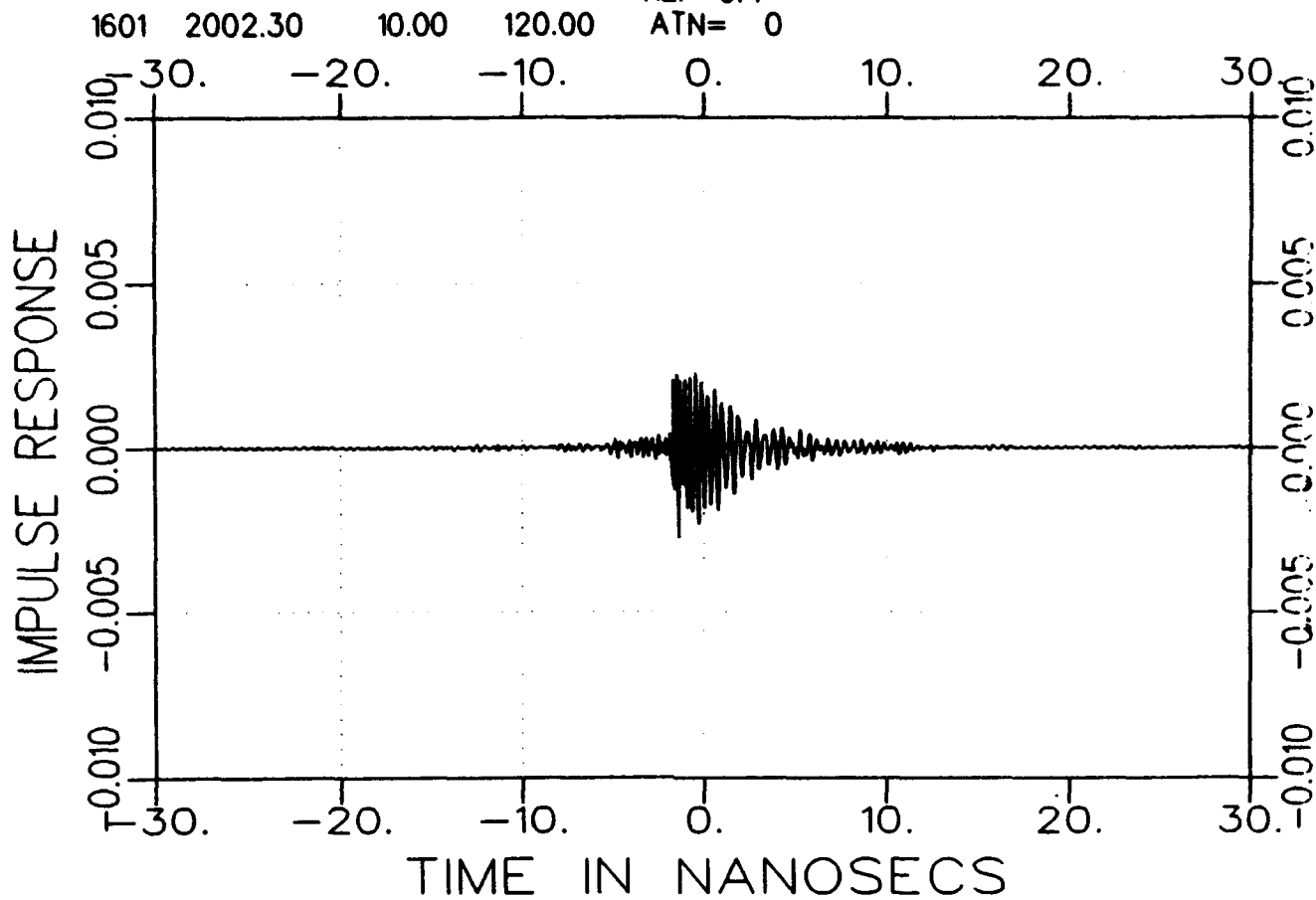
FREQ. 08/13/93 15:06  
freq s cap grid AVE= 82  
REF=OFF  
ATN= 0





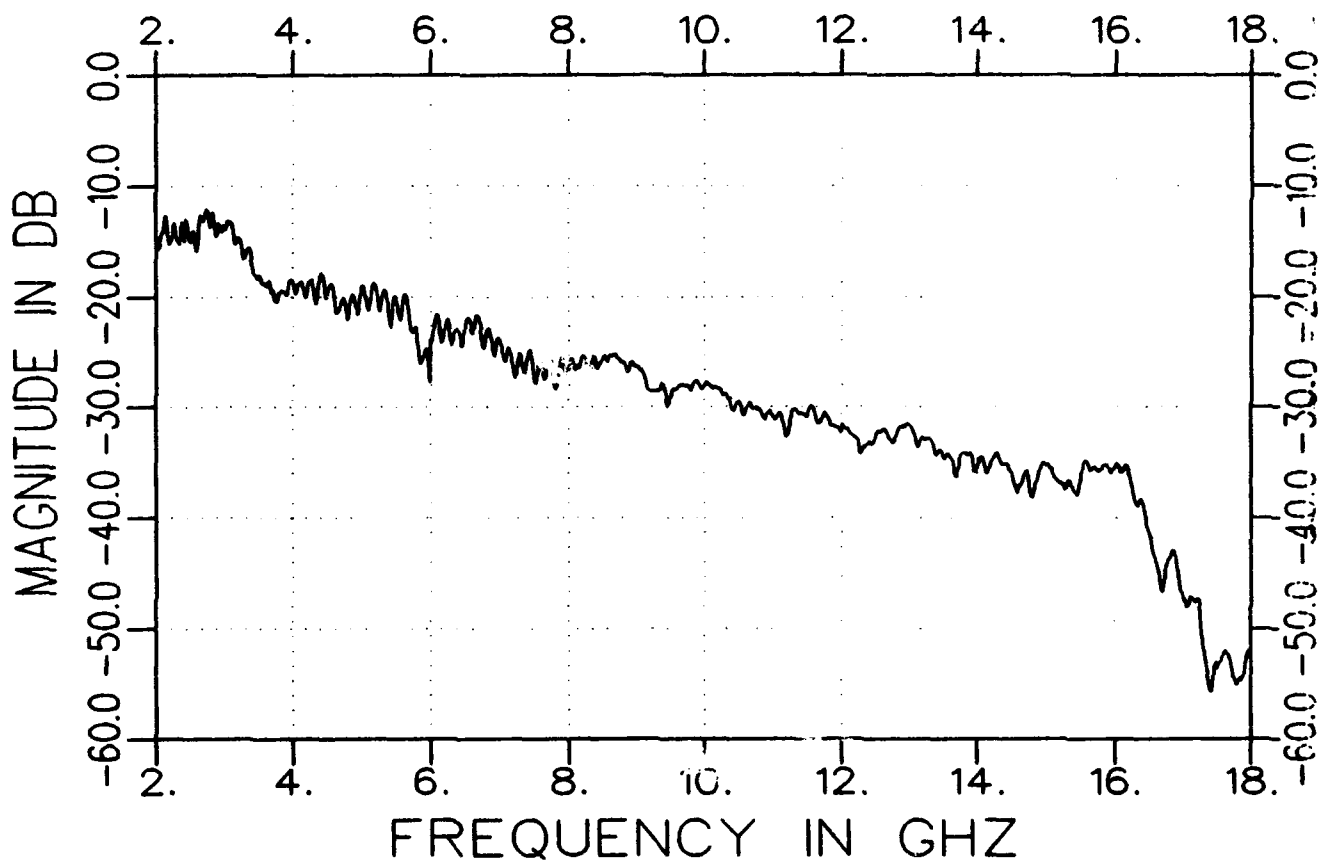
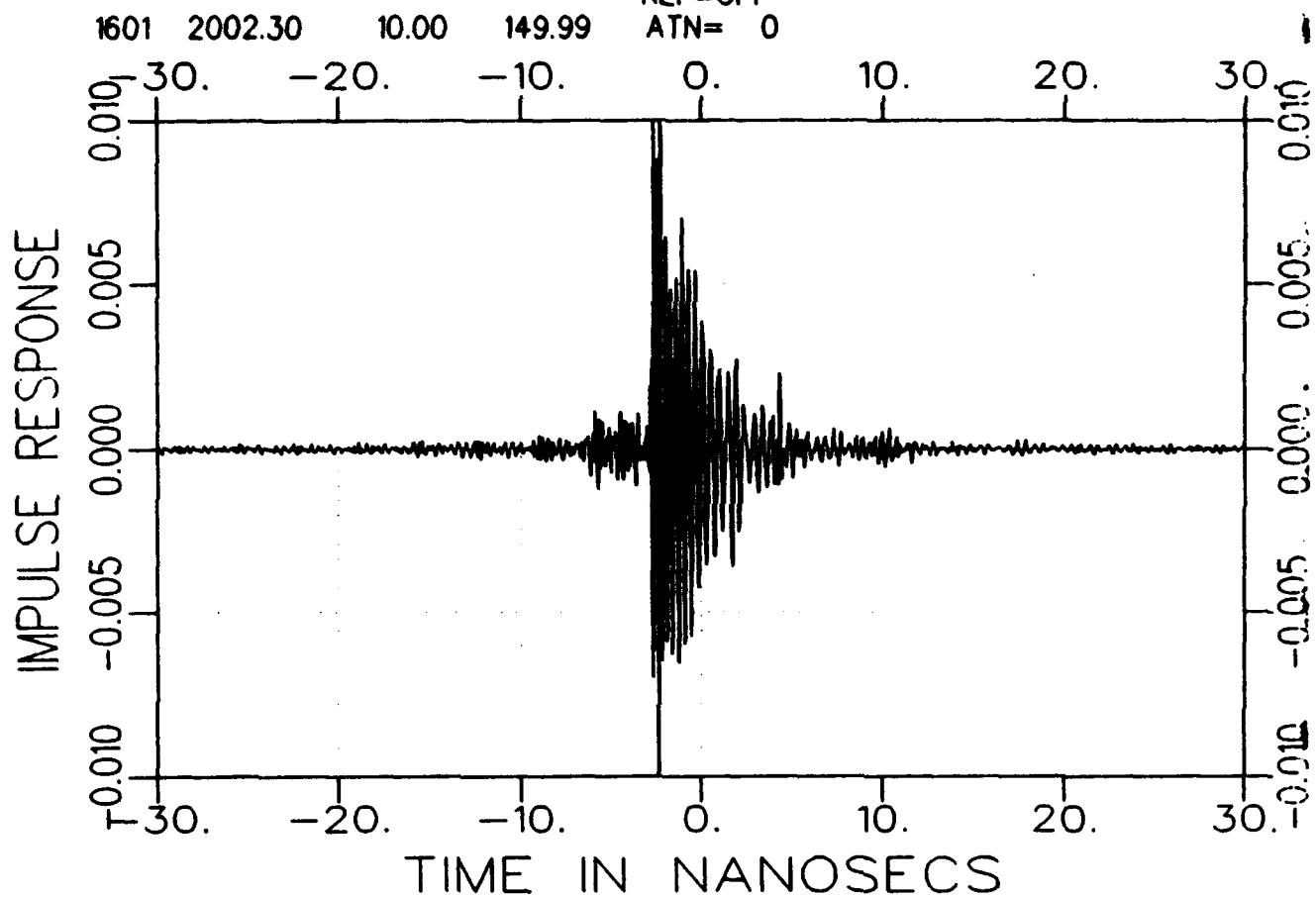
13225fa1200-a.tar  
TARGET

FREQ. 08/13/93 15:07  
freq s cap grid AVE= 82  
REF=OFF  
ATN= 0



13225fa1500-a.tar  
TARGET

FREQ. 08/13/93 15:08  
freq s cap grid AVE= 82  
REF=OFF  
ATN= 0



## APPENDIX D

### METHOD OF MOMENTS DATA

The Method of Moments data was calculated by two separate codes. The first code was a TEz code written by Captain J. P. Skinner [19]. This code was a singly-periodic PMM code which used piecewise sinusoid basis functions. The second code was a TMz code written by myself which used pulse basis functions. The following is a listing of the TMz code.

```
c
c  Lt. Russell A. Burleson TEz 2D scattering code
c
c  Moment Method Code for 2D geometries read from input file 'INPUT.DAT'
c  for TMz incident wave.
c  ida = the number of points allowed
c  w = frequency in rad/sec
c  zmat,imat,vmat=impedance,current and voltage matrix
c      which are sent out to zmat.dat imat.dat vmat.dat
c  zmat.dat can be readin by setting ireadz=1
c  freq = in Hz
c  all x,y coordinates in meters
c  o2d.dat = is the scattered echo width in dB (not dBm like before)
c  output.dat = is the scattered field in V/m
c  input.dat = made from another program
c
c
c      parameter (ida=615)
c
c      real w,uo,pi,phi,phip,phase,degstart,degstop
c      real x(ida),y(ida),deg,o2d,o2dlog,wavelength
c
c      complex ef(ida),es,sum
c      complex za(ida),zb(ida),zmat(ida,ida),vmat(ida),imat(ida),j
c
c      integer nm,irdz,ngo,isc,p,check,iwz,iwi,iwv
c      integer ia(ida),ib(ida)
c
c      open(unit=26,file='o2d.dat',status='unknown')
c      open(unit=27,file='output.dat',status='unknown')
c
c      pi=3.141592654
c      uo=1.256637061e-6
```

```

      j=(0.,1.)
      check=1
5     format(3x,1f15.3)
c
c
*****
**
c
*****
**
c   THIS IS THE MAIN PROGRAM
c
c   THIS GETS THE INPUT DATA FROM 'INPUT.DAT'
C
C
      call getinput(w,isc,deg,ngo,irdz,p,phip,nm,x,y,ia,ib,za,zb,
      lida,iwz,iwi,iwv,degstart,degstop)
      close (unit=21)
C
      write(*,*)'This is set up to run for ',nm,' number of modes'
      if ((nm+1).gt.ida) then
        write(6,78)
78     format(2x,'This will not work--too many modes--reset IDA')
        goto 998
      endif
C
C   THIS FILLS IN THE IMPEDANCE MATRIX OR READS IT IN FROM A FILE
C
C
      if (irdz.eq.0) then
        call ztot(nm,x,y,ia,ib,p,w,zmat,ida)
        write(6,71)
71     format(2x,'The impedance matrix has been filled')
      if (iwz.eq.1) open(unit=23,file='zmat.dat',status='unknown')
        do 10 m=1,nm
          do 20 n=1,nm
            if (iwz.eq.1) write(23,*)zmat(m,n)
20         continue
10        continue
          close(unit=23)
        endif
c
      if (irdz.eq.1) then
        if (iwz.eq.1) open(unit=23,file='zmat.dat',status='unknown')
          do 30 m=1,nm
            do 40 l=1,nm
c          read(23,*)zmat(m,l)
40         continue
30        continue
          write(6,72)
72     format(2x,'The impedance matrix has been read in')

```

```

        close(unit=23)
    endif
C
C
c   THIS CORRECTS THE DIAGONAL OF THE IMPEDANCE MATRIX FOR NON
PEC SURFACE
C
C
    call zimped(zmat,x,y,ia,ib,za,zb,nm,ida)
c
    write(6,73)
73    format(2x,'The impedance diagonal has been adjusted')
c
c
c   THIS PART ENDS THE PROGRAM IF YOU JUST WANT THE IMPEDANCE
MATRIX
C
    if (ngo.eq.0) goto 998
c
c
c
c   THIS PART DETERMINES THE BISTATIC RADAR ECHO WIDTH
c
    if (isc.eq.1) then
c
    call volt(vmat,x,y,ia,ib,nm,phip,w,ida,iwv)
    write(6,74)
74    format(2x,'The voltage matrix has been computed for incident angle')
    write(6,5)phip
c
    call amp(zmat,imat,vmat,nm,check,ida,iwi)
    write(6,75)
75    format(2x,'The current matrix has been computed')
C
    do 50 i=(degstart/deg),(degstop/deg)
    phi=i*deg
    call scat(ef,phi,x,y,ia,ib,w,nm,ida)
    sum=(0.,0.)
c
    do 60 n=1,nm
    sum=sum+(imat(n)*ef(n))
60    continue
c
    es=sum
    o2d=2*pi*((cabs(es))**2)
    wavelength=2*3.141592654*3.0e8/w

    o2dlog=10*log10(o2d/wavelength)
c
    phase=atand(imag(es)/real(es))
c
    if (real(es).lt.0) phase=phase+180

```

```

        if (phase.gt.180) phase=phase-360
        write(26,*)phi,o2dlog
        write(27,*)phi,o2d,o2dlog,cabs(es),phase
        write(6,76)
76      format(2x,'The bistatic field has been determined for angle')
        write(6,5)phi
50    continue
c
      endif
c
c    THIS PART DETERMINES THE MONOSTATIC RADAR ECHO WIDTH
c
      if (isc.eq.0) then

        do 55 i=(degstart/deg),(degstop/deg)
        phi=i*deg
        phip=phi
        call volt(vmat,x,y,ia,ib,nm,phip,w,ida,iwz)
c
        call amp(zmat,imat,vmat,nm,check,ida)
        check=2
c
c
        call scat(ef,phi,x,y,ia,ib,w,nm,ida,iwi)
        sum=(0.,0.)
c
          do 65 n=1,nm
          sum=sum+(imat(n)*ef(n))
65      continue
c
        es=sum
        o2d=2*pi*((cabs(es))**2)
        o2dlog=10*log10(o2d)
c
        phase=atand(imag(es)/real(es))
c

        if (real(es).lt.0) phase=phase+180
        if (phase.gt.180) phase=phase-360
        write(26,*)phi,o2dlog
        write(27,*)phi,o2d,o2dlog,cabs(es),phase
        write(6,77)
77      format(2x,'The monostatic field has been calculated for angle')
        write(6,5)phi
55    continue
c
      endif
c
c
c
c
998  stop
      end

```

```

C
C   END OF THE MAIN PROGRAM
C
C
C *****
C ***
C
C *****
C ***
C
C *****
C ***
C
C
C
C
C
C *****
C ***
C
C
C
C
C   subroutine getinput(w,isc,deg,ngo,ireadz,p,phip,nm,x,y,ia,ib,za,zb
1,ida,iwz,iwi,iwv,degstart,degstop)
C
C
C   This subroutine inputs the following data
C   f = frequency in hertz
C   isc = 0,1 for monostatic or bistatic radar
C   deg = real number increment of degrees to span over
C   degstart,stop=start and stop angles to be seen in degrees
C   ireadz = 0,1 tell whether to compute/read impedance matrix for PEC body
C   iwz,iwi,iwv=0,1 tell wheter to not write/write imp, volt, amp matrixes
C   p = EVEN number of divisions to be used in Simpson's rule integration
C   phip = incident plane wave angle in degrees
C   np = number of node points
C   x(i),y(i) = rectangular coordinates of node points (meters)
C   nm = number of modes
C   ia(i),ib(i) = integer values of endpoint node points for each mode
C   za(i),zb(i) = complex impedance at each node point (ohms)
C
C
C   integer isc,np,nm,ia(ida),ib(ida),ireadz,ngo,p
C   real w,f,x(ida),y(ida),deg,degstart,degstop
C   complex za(ida),zb(ida)
C
C   open(unit=21,file='input.dat',status='old')
C   read(21,*)f
C   w=2*3.141592654*f
C   read(21,*)isc

```

```

    read(21,*)deg
    read(21,*)degstart
    read(21,*)degstop
    read(21,*)ngo
    read(21,*)ireadz
    read(21,*)iwz
    read(21,*)iwi
    read(21,*)iwv
    read(21,*)p
    read(21,*)phip
    read(21,*)np

    if (np.gt.ida) then
    write(*,*)'There are too many points, reset ida'
    write(*,*)'ida = ',ida
    write(*,*)'np = ',np
    stop
    end if

c
    do 100 i=1,np
    read(21,*)x(i),y(i)
100 continue
c
    read(21,*)nm
    open(unit=22,file='graph.dat',status='unknown')
    do 110 i=1,nm
    read(21,*)ia(i),ib(i)

c
c   This part writes to the graph file for a gnuplot of our geometry
c
c
c
    write(22,*)x(ia(i)),y(ia(i))
    write(22,*)x(ib(i)),y(ib(i))
    if (i.eq.nm) write(22,*)x(ib(i)),y(ib(i))

c
110 continue
    close (unit=22)

c
    do 120 i=1,nm
    read(21,*)za(i),zb(i)
120 continue
c
    close (unit=21)
    return
    end

c
c
*****
***   c

c
    subroutine ztot(nm,x,y,ia,ib,p,w,zmat,ida)
c

```



```

c
c   This subroutine determines the PEC impedance matrix using ZSELF and ZMUT
c   uo = is the permability of free space
c   dn,dm = length of each mode (must be less than .1 wavelengths)
c
c
c       integer ia(ida),ib(ida),p,nm
c       real uo,w,x(ida),y(ida),h,dn,dm
c       complex zmat(ida,ida)
c
c       uo=1.256637061e-6
c       do 210 m=1,nm
c       do 200 n=1,nm
c       dn=sqrt((x(ia(n))-x(ib(n)))**2+(y(ia(n))-y(ib(n)))**2)
c       dm=sqrt((x(ia(m))-x(ib(m)))**2+(y(ia(m))-y(ib(m)))**2)
c       h=dn/p
c
c       if (n.eq.m) call zself(zmat,m,w,p,h,ida)
c       if (n.ne.m) call zmut(zmat,x,y,m,n,p,dn,dm,ia,ib,w,ida)
200  continue
210  continue
c
c       return
c       end
c
c
c *****
c ***
cc
c
c       subroutine zself(zmat,m,w,p,h,ida)
c
c
c   This subroutine determines the self impedance terms of the PEC matrix
c   using equivalent endpoint technique. It also uses 10 times the number
c   of divisions used in the mutual impedance subroutine for better
c   accuracy. It needs the subroutine HANK to run.
c
c   feo = is the equivalent endpoint
c
c
c       integer p
c       real k,h,si,xx,uo,c
c       complex sum,feo,h0,h1,h2,hextra,zmat(ida,ida)
c
c       p=p*10
c       h=h/10
c       uo=1.256637061e-6
c       k=w/(3e8)
c       c=(w*uo)/(6*p)
c       sum=(0.,0.)
c       xx=k*h

```

```

call hank(xx,h0,hextra,0)
xx=2*k*h
call hank(xx,h1,hextra,0)
feo=(4.656*h0)-(3.656*h1)
c
sum=fco*c
do 250 i=2,((p/2)+1)
si=3+(-1)**i
if (i.eq.((p/2)+1)) si=1
xx=(i-1)*k*h
call hank(xx,h2,hextra,0)
sum=sum+(c*si*h2)
250 continue
c
h=h*10
p=p/10
zmat(m,m)=sum
return
end

c
c
*****
***
c
c
subroutine zmut(zmat,x,y,m,n,p,dn,dm,ia,ib,w,ida)
c
c
c This subroutine determines the mutual impedance terms of the PEC matrix
c pmn = distance between center points of the modes
c pmi = distance from the ith portion of the nth mode to the mth mode
c
c This subroutine needs the subroutine HANK to run
c
c
integer ia(ida),ib(ida),p
real x(ida),y(ida),pmn,pmi,dn,dm,deltx,dely,si,c,w,uo,xm,ym,k,xx
complex sum,h2,hextra,zmat(ida,ida)
c
k=w/(3e8)
uo=1.256637061e-6
c=(w*uo)/(12*p)
sum=(0.,0.)
xm=(x(ia(m))+x(ib(m)))/2
ym=(y(ia(m))+y(ib(m)))/2
xn=(x(ia(n))+x(ib(n)))/2
yn=(y(ia(n))+y(ib(n)))/2
pmn=sqrt((xm-xn)**2+(ym-yn)**2)
c
if (pmn.lt.(100*dn)) goto 230
if (pmn.lt.(100*dm)) goto 230
xx=k*pmn

```

```

      call hank(xx,h2,hextra,0)
      zmat(m,n)=((w*uo)/4)*h2
      goto 240
c
230  do 220 i=1,(p+1)
      si=3.+(-1)**i
      if (i.eq.1) si=1.
      if (i.eq.(p+1)) si=1.
      deltx=(x(ib(n))-x(ia(n)))/p
      delty=(y(ib(n))-y(ia(n)))/p
      xi=x(ia(n))+(i-1)*deltx
      yi=y(ia(n))+(i-1)*delty
      pmi=sqrt((xm-xi)**2+(ym-yi)**2)
      xx=k*pmi
      call hank(xx,h2,hextra,0)
      sum=sum+(si*h2)
220  continue
      zmat(m,n)=c*sum
c
240  return
      end
c
c
*****
*
c
c
      subroutine zimped(zmat,x,y,ia,ib,za,zb,nm,ida)
c
c
c      This subroutine determines the diagonal impdeance matrix terms used to
c      correct our impedance matrix for non PEC surfaces. Assuming piecewise
c      linear impedances.
c
c
c      integer ia(ida),ib(ida),nm
c      real x(ida),y(ida),dn
c      complex zmat(ida,ida),za(ida),zb(ida),zmn,j
c
c      j=(0.,1.)
c      do 50 i=1,nm
c      zmn=(za(i)+zb(i))/2
c      dn=sqrt((x(ia(i))-x(ib(i)))**2+(y(ia(i))-y(ib(i)))**2)
c      zmn=zmn/dn
c      zmat(i,i)=zmat(i,i)+zmn
50  continue
c
      return
      end
c
*****
***

```

```

c
c
c
c
*****
***
      subroutine volt(vmat,x,y,ia,ib,nm,phip,w,ida,iwv)
c
c
c      This subroutine determines the voltage matrix from a plane wave.
c      phip = incident plane wave angle in degress
c
c      integer ia(ida),ib(ida),l,nm,c
c      real xl,yl,phip,w,x(ida),y(ida)
c      complex vmat(ida),j
c
c      j=(0.,1.)
c      c=3e8
c
c      if (iwv.eq.1) open(unit=24,file='vmat.dat',status='unknown')
c      do 300 l=1,nm
c      xl=(x(ia(l))+x(ib(l)))/2
c      yl=(y(ia(l))+y(ib(l)))/2
c      vmat(l)=exp(j*(w/c)*((xl*cosd(phip))+(yl*sind(phip))))
c      if (iwv.eq.1) write(24,*)l,vmat(l)
300 continue
c      close (unit=24)
c      return
c      end
c
c
c
c
*****
***
C
      subroutine amp(zmat,imat,vmat,nm,check,ida,iwi)
c
c
c
c      This subroutine determines the current matrix from the impedance and
c      voltage matrices. It also destroys the impedance matrix in the process
c      This subroutine needs the CROUT subroutine
c      imat = current matrix
c      iwi=0,1 to not or write the current matrix
c
c      integer nm,check
c      complex zmat(ida,ida),vmat(ida),imat(ida)
c
c
c      if (iwi.eq.1) open(unit=25,file='imat.dat',status='unknown')
c      do 43 l=1,nm
c      imat(l)=vmat(l)
43 continue
c      call crout(zmat,imat,ida,1,0,check,nm)

```

```

        do 45 l=1,nm
            if (iwi.eq.1) write(25,*)l,imat(l)
45    continue
c
        close (unit=25)
        return
        end
c
c
*****
***
        subroutine scat(ef,phi,x,y,ia,ib,w,nm,ida)
c
c
c    This subroutine determines the scattered field from a point
c
        integer ia(ida),ib(ida)
        real phi,x(ida),y(ida),alpha,dn,k,deltx,dely,uo,pi,psi,a
        complex ef(ida),j,lambda,c
c
        uo=1.256637061e-6
        pi=3.141592654
        lambda=(0.,0.)
        j=(0.,1.)
        k=w/(3e8)
        c=-((w*uo)/4)*sqrt(2/(pi*k))*exp(j*(pi/4))
c
        do 400 n=1,nm
            deltx=x(ib(n))-x(ia(n))
            dely=y(ib(n))-y(ia(n))
            dn=sqrt(deltx**2+dely**2)
c
            if (deltx.eq.0) then
                if (dely.gt.0) alpha=90
                if (dely.lt.0) alpha=270
            endif
c
            if (deltx.ne.0) then
                alpha=atand(dely/deltx)
                if (deltx.lt.0) alpha=alpha+180.
            endif
c
c
            a=cosd(phi-alpha)
            if (a.ne.0) lambda=((exp(j*k*a*dn))-1)/(j*k*a)
c
            if (a.eq.0) lambda=dn
c
            psi=k*((x(ia(n))*cosd(phi))+(y(ia(n))*sind(phi)))
            ef(n)=(c/dn)*exp(j*psi)*lambda
c
400    continue

```

```

      return
      end
C
C
*****
***
C
C
C
SUBROUTINE HANK(XX,H,H1,ID)
C
C   HANKEL FUNCTION OF THE SECOND KIND
C
C   XX = REAL ARGUMENT
C   H = H OF ORDER 0
C   H1 = H OF ORDER 1
C   ID = 0 IMPLIES COMPUTE H ONLY
C        1 IMPLIES COMPUTE H1 ONLY
C        2 IMPLIES COMPUTE BOTH
C
C   COMPLEX H,H1
C   DOUBLE PRECISION D,DX,C,EA,EB,FA,FB
C   X=ABS(XX)
C   DX=X
C   IF(X.GE.3.)GO TO 10
C   C=DX*DX/9.
C   D=(DLOG(DX)-.69314718056)*.63661977237
C   IF(ID.EQ.1)GO TO 8
C   B =(((((.21E-3*C-.39444E-2)*C+.444479E-1)*C-.3163866)*C+.1265
16208E+1)*C-2.2499997)*C+1.
C   Y = D*B +.36746691+((((-.24846E-3*C+.427916E-2)*C-.4261214E-1)
2*C+.25300117)*C-.74350384)*C+.60559366)*C
C   H=CMPLX(B,-Y)
C   IF(ID.EQ.0)RETURN
8   B1 =(((((.1109E-4*C-.31761E-3)*C+.443319E-2)*C-.3954289E-1)*C+
3.21093573)*C-.56249985)*C+.5)*DX
C   Y1 = D*B1 +(((((.27873E-2*C-.400976E-1)*C+.3123951)*C-1.3164827)
4*C+.2.1682709)*C+.2212091)*C-.6366197724)/DX
C   H1=CMPLX(B1,-Y1)
C   RETURN
10 D=3.0D0/DX
C   C=1/DSQRT(DX)
C   IF(ID.EQ.1)GO TO 18
C   EA=C*(((((.14476E-3*D-.72805E-3)*D+.137237E-2)*D-.9512E-4)*D-
5.552740E-2)*D-.77E-6)*D+.797884560803)
C   FA=(((((.13558E-3*D-.29333E-3)*D-.54125E-3)*D+.262573E-2)*D-
6.3954E-4)*D-.4166397E-1)*D-.785398163397+DX
C   B=EA*DCOS(FA)
C   Y=EA*DSIN(FA)
C   H=CMPLX(B,-Y)
C   IF(ID.EQ.0)RETURN
18 EB=C*(((((-.20033E-3*D+.113653E-2)*D-.249511E-2)*D+.17105E-3)*D+

```



```

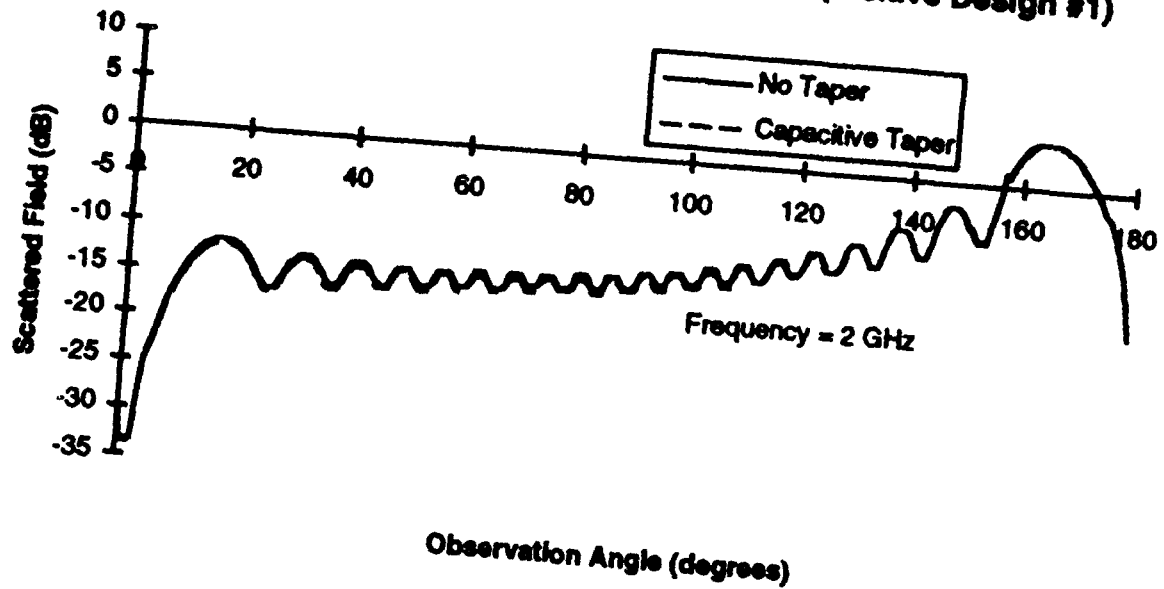
      DO 11 K=1,LLL
11  F=F-C(I,K)*C(K,L)
      C(I,L)=F
      IF(L.EQ.I)GO TO 20
      P=C(L,L)
      IF(ISYM.EQ.0)GO TO 15
      F=C(L,I)
      DO 12 K=1,LLL
12  F=F-C(L,K)*C(K,I)
      C(L,I)=F/P
      GO TO 20
15  F=C(I,L)
      C(L,I)=F/P
20  CONTINUE
22  DO 30 L=1,N
      P=C(L,L)
      T=S(L)
      IF(L.EQ.1)GO TO 30
      LLL=L-1
      DO 25 K=1,LLL
25  T=T-C(L,K)*S(K)
30  S(L)=T/P
      DO 38 L=2,N
      I=N-L+1
      II=I+1
      T=S(I)
      DO 35 K=II,N
35  T=T-C(I,K)*S(K)
38  S(II)=T
      IF(TWR.LE.0) GO TO 100
      WRITE(6,5)
      CNOR=.0
      DO 40 I=1,N
      SA=CABS(S(I))
40  IF(SA.GT.CNOR)CNOR=SA
      IF(CNOR.LE.0.)CNOR=1.
      DO 44 I=1,N
      SS=S(I)
      SA=CABS(SS)
      SNOR=SA/CNOR
      PH=.0
      IF(SA.GT.0.)PH=57.29578*ATAN2(AIMAG(SS),REAL(SS))
44  WRITE(6,2)I,SNOR,SA,PH
      WRITE(6,5)
100 RETURN
      END

```

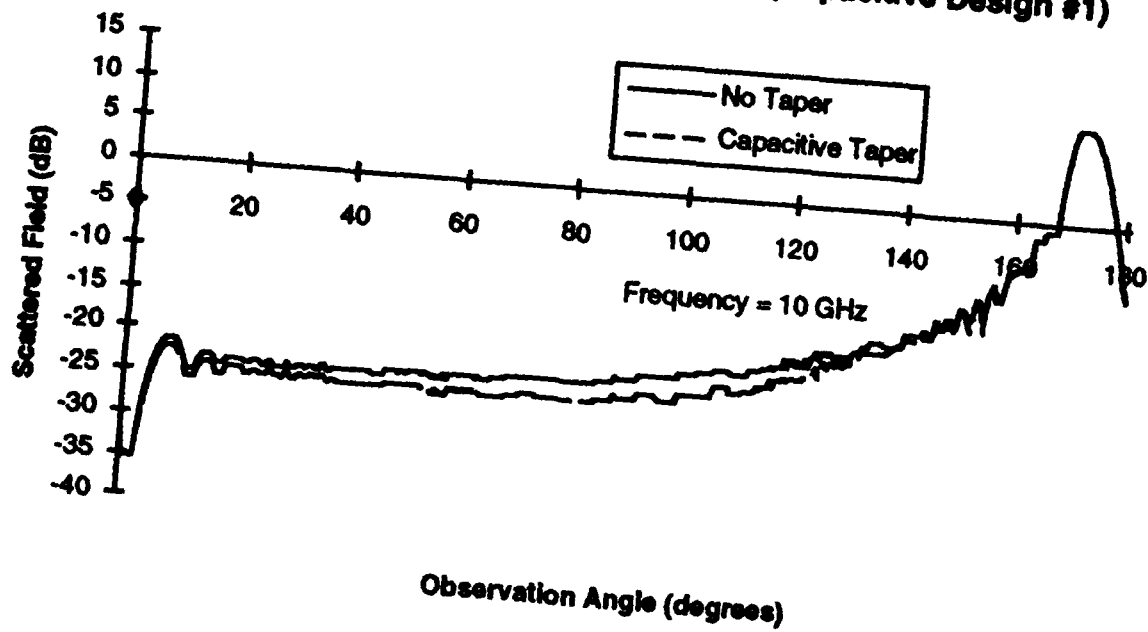


The following are the graphs from the MoM results from both codes.

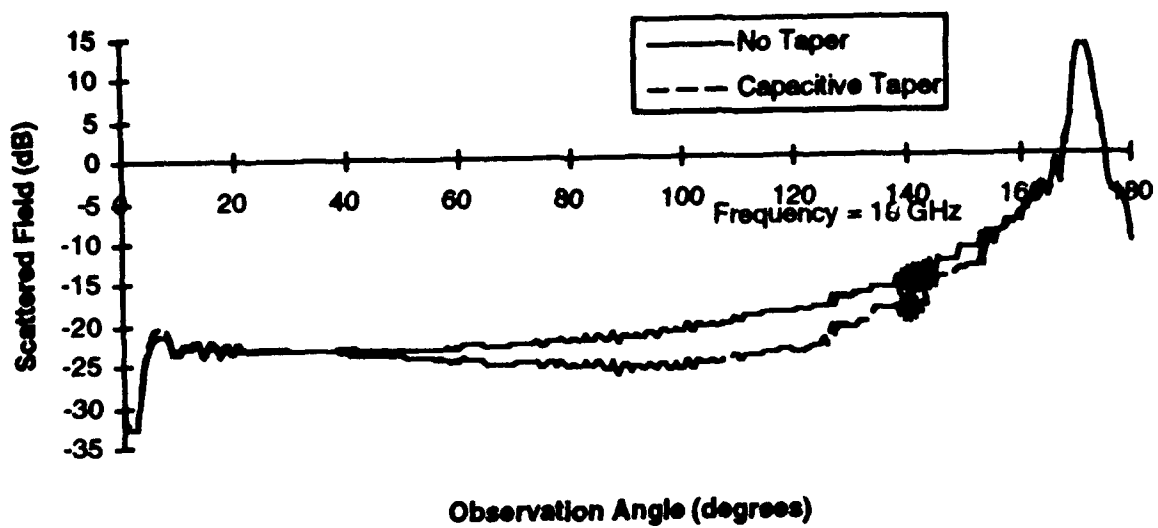
**Scattered Field vs Observation Angle (Capacitive Design #1)**



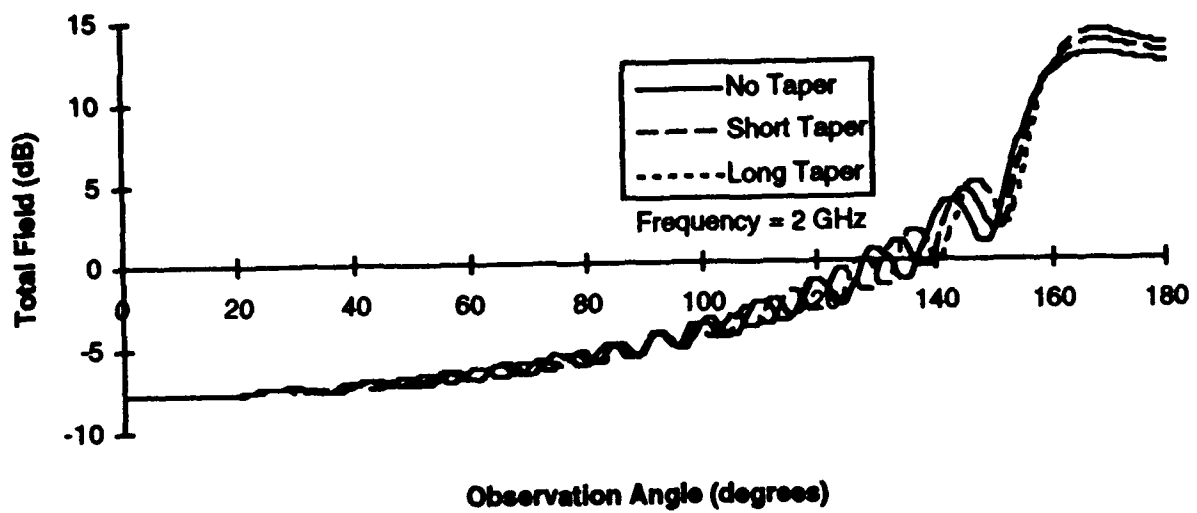
**Scattered Field vs Observation Angle (Capacitive Design #1)**



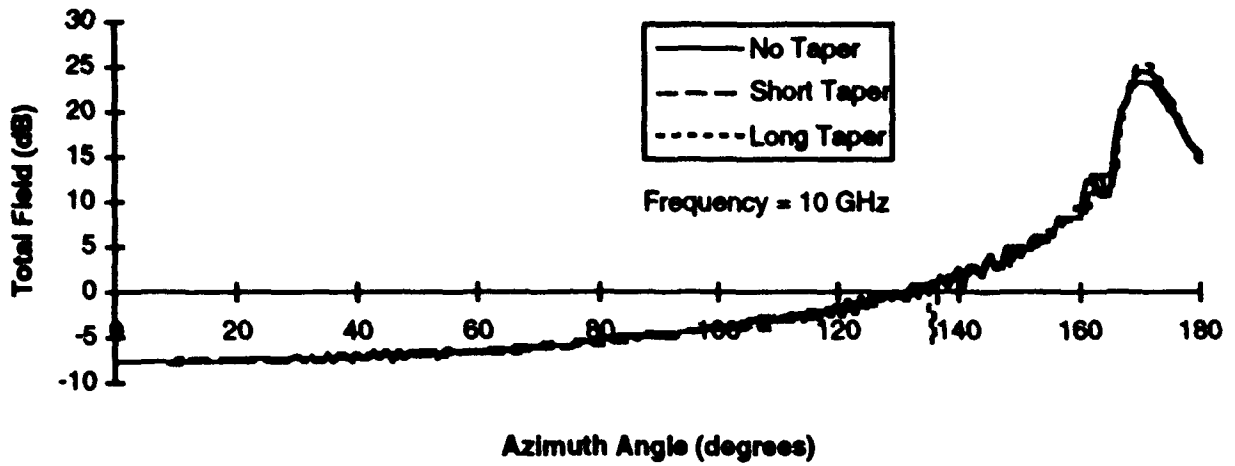
**Scattered Field vs Observation Angle (Capacitive Design #1)**



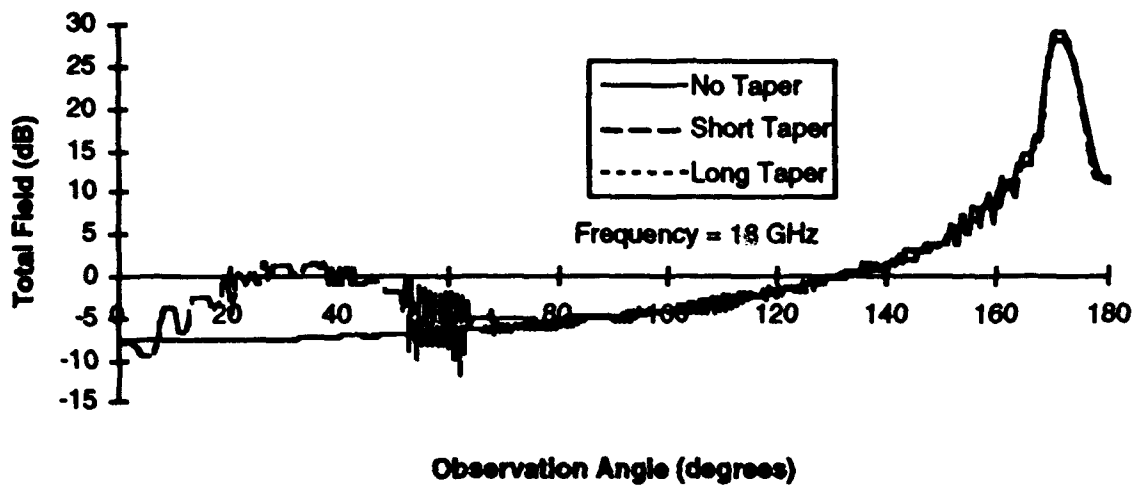
**Total Field vs Observation Angle (Inductive Design #1)**



**Total Field vs Azimuth Angle (Inductive Design #1)**



**Total Field vs Observation Angle (Inductive Design #1)**

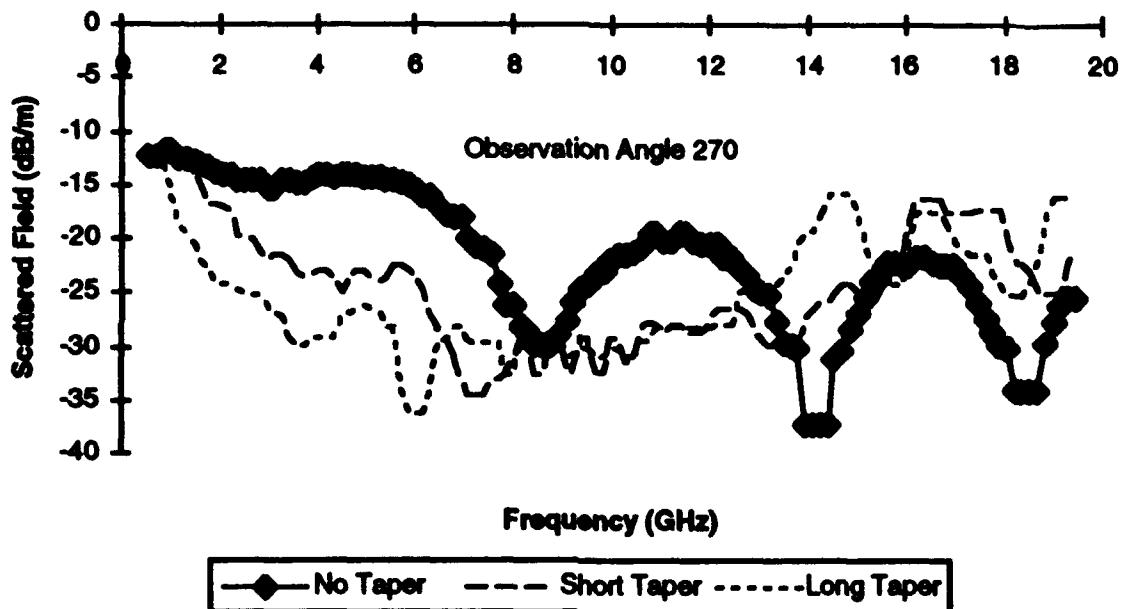


## APPENDIX E

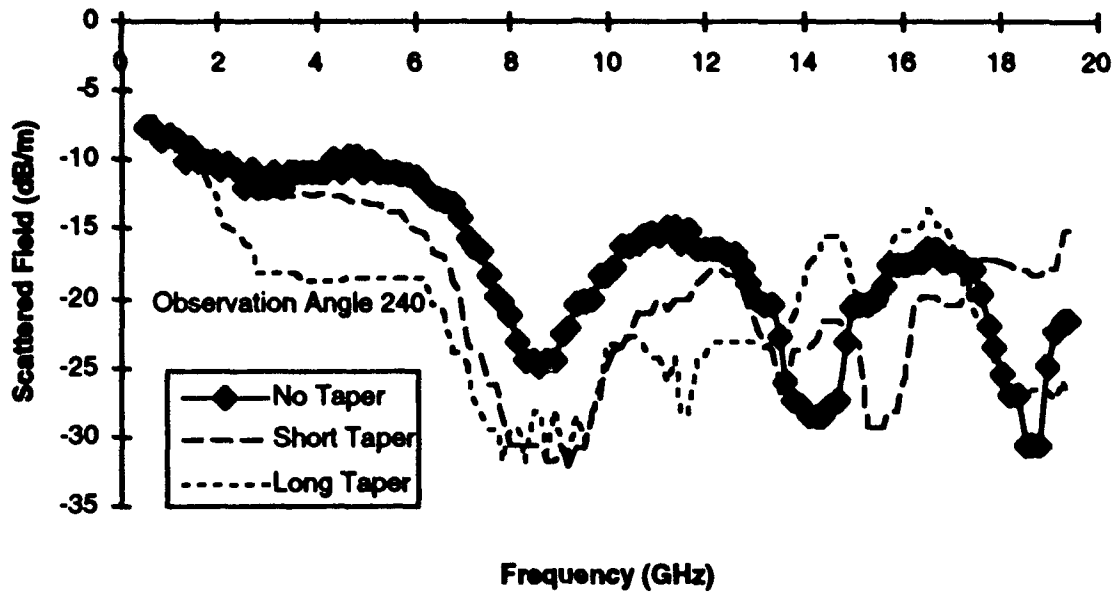
### FDTD RESULTS

This appendix contains all the FDTD results on the modeling of the second capacitive taper. The results are shown as scattered field vs frequency for different angles.

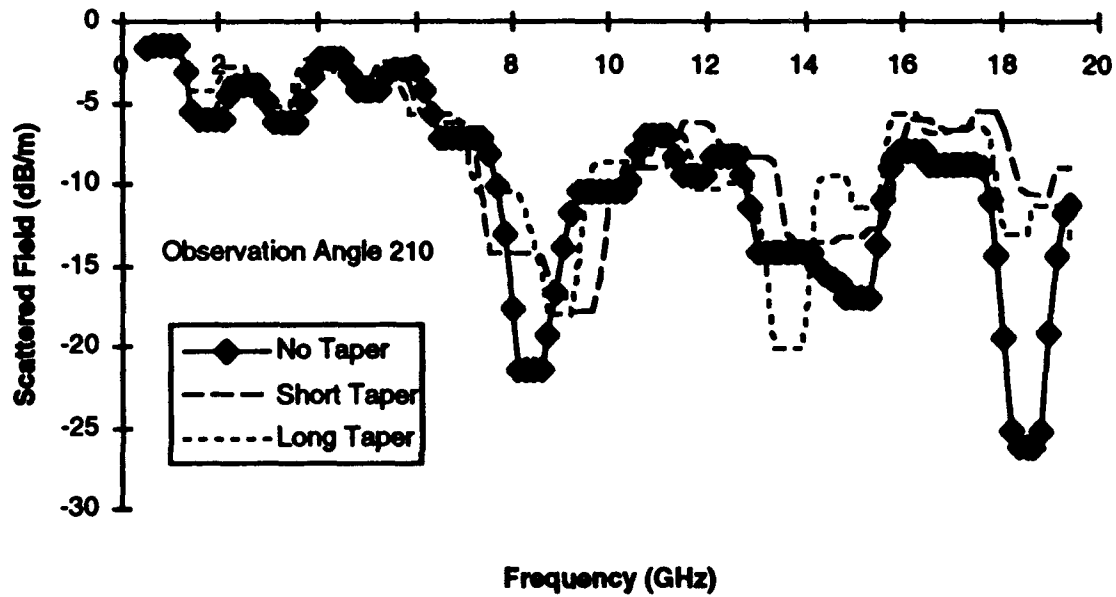
**FDTD Scattered Field vs Frequency**



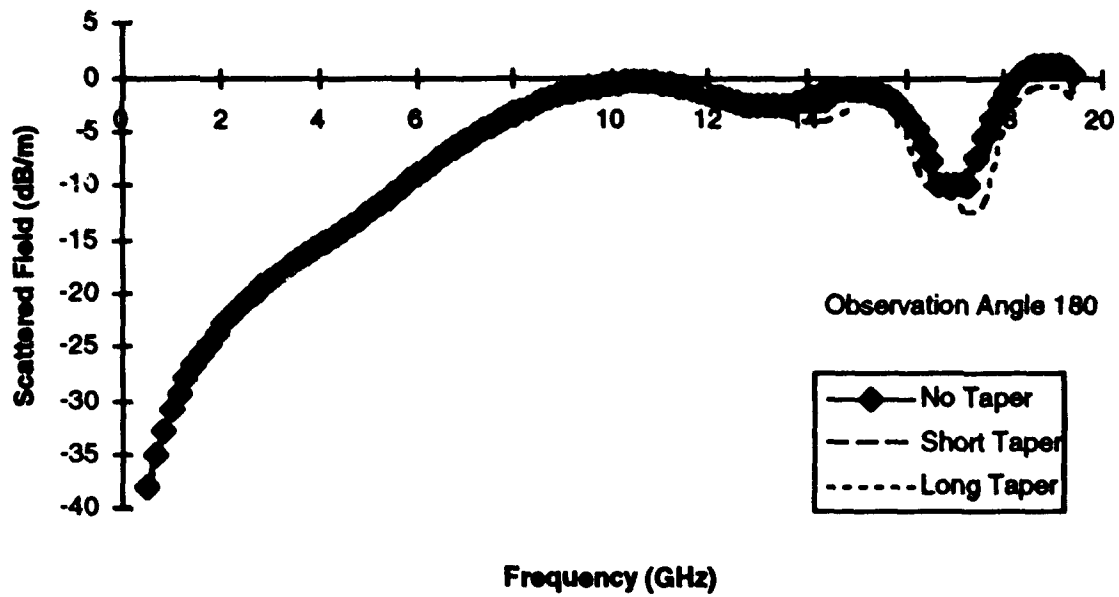
**FDTD Scattered Field vs Frequency**



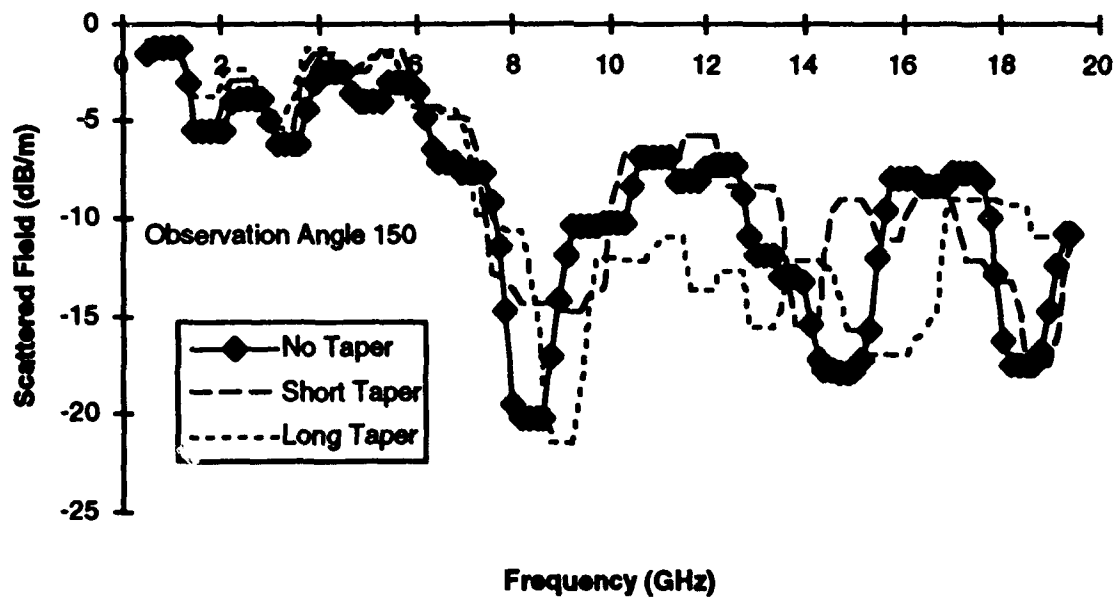
**FDTD Scattered Field vs Frequency**



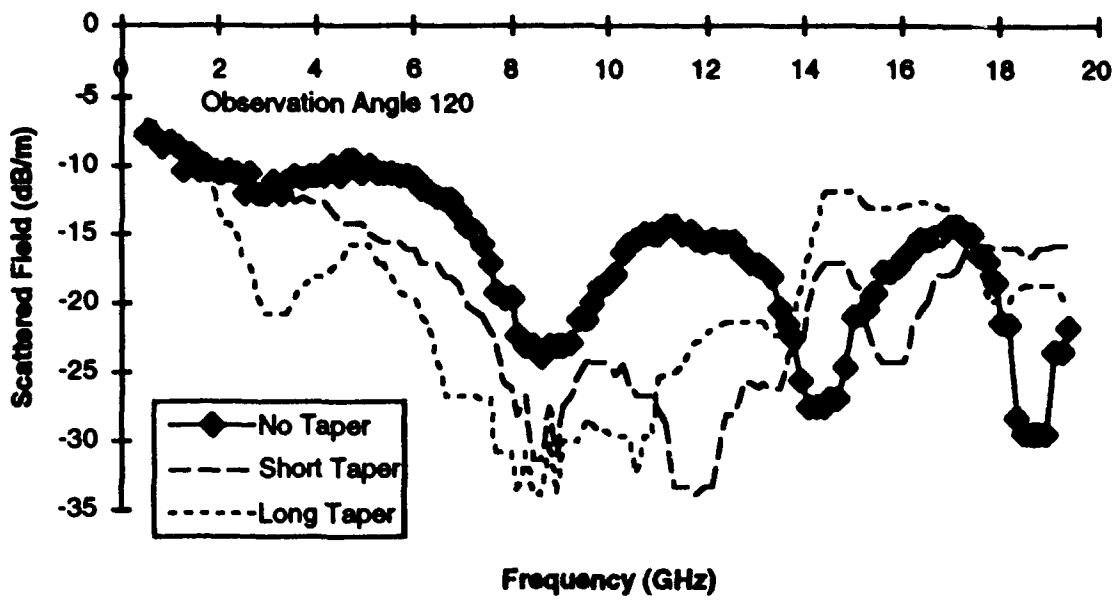
**FTD Scattered Field vs Frequency**



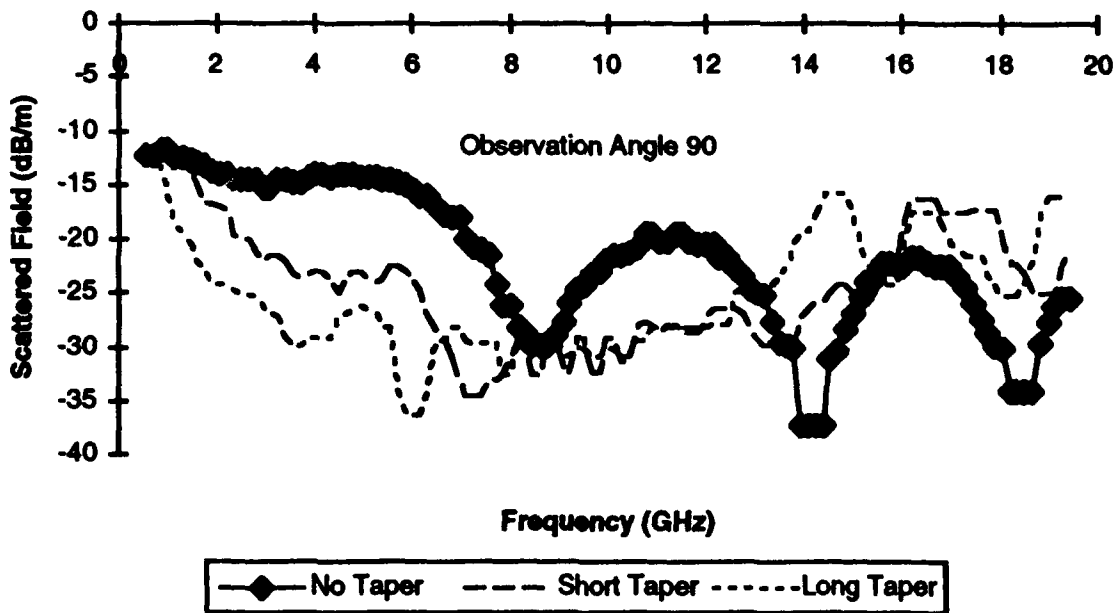
**FTD Scattered Field vs Frequency**



**FDTD Scattered Field vs Frequency**



**FDTD Scattered Field vs Frequency**



## Bibliography

1. C. A. Balanis, *Antenna Theory, Analysis and Design*. New York: John Wiley & Sons, 1982.
2. L. W. Henderson, *Introduction to PMM*, Technical Report 715582-5, The Ohio State University Electroscience Laboratory, Department of Electrical Engineering; prepared under Contract F33615-83-C-1013 for Avionics Laboratory (AFWAL/AAWP-3) Air Force Wright Aeronautical Systems Command, Wright-Patterson Air Force Base, OH, Feb. 1986.
3. J. Beggs, R. Luebbers, and H. Langdon, *User's Manual for TEC: PSU FDTD Code Version C for Two-Dimensional Transverse Electric (TE) Transient Scattering from Frequency-Independent Dielectric and Magnetic Materials*. University Park PA, June 1993.
4. J. G. Maloney, G. S. Smith and W. R. Scott, "Accurate Computation of the Radiation from Simple Antennas Using the Finite Difference Time Domain Method," *IEEE Transactions on Antennas and Propagation*, vol. 38-7, pp. 1059-1068, Jul. 1990.
5. J. R. Wait, "Reflection at Arbitrary Incidence from a Parallel Wire Grid," *Applied Scientific Research*, vol. B-4, pp 393-400, 1955.
6. S. W. Yoder. *Analysis of Strip Gratings and Meanderlines Using Doubly Infinite Planar Arrays*. MS thesis. The Ohio State University, Columbus OH, 1992.
7. L. Carin, L. B. Felsen, and M. R. McClure, "Time-Domain Design-Oriented Parametrization of Truncated Periodic Strip Gratings," *IEEE Microwave and Guided Wave Letters*, vol. 3, no. 4, April 1993.
8. L. Carin and L. Felsen, "Efficient Analytical-Numerical Modelling of Ultra-Wideband Pulsed Plane Wave Scattering from a Large Strip Grating," *International Journal of Numerical Modelling: Electronic Networks, Devices and Fields*, vol. 6, 3-17, pp. 3-17, 1993.
9. L. Carin and L. B. Felsen, "Time harmonic and Transient Scattering by Finite Periodic Flat Wire Arrays: Hybrid (Ray)-(Floquet mode)-(MoM) Algorithm and Its GTD Interpretation", *IEEE Transactions on Antennas and Propagation*, vol. AP 41-3, Apr. 1993, pp. 412-421.
10. R. I. Primich, "Some Electromagnetic Transmission and Reflection Properties of a Strip Grating," *IRE Transactions on Antennas and Propagation*, vol. AP-5, pp. 176-182, April 1957.
11. C. C. Chen, "Transmission Through a Conducting Screen Perforated Periodically with Apertures," *IEEE Transactions Microwave Theory and Technology*, vol. MTT-18, pp. 627-632, Sept. 1970.



12. S. W. Lee, "Scattering by a Dielectric-Loaded Screen," *IEEE Transactions on Antennas and Propagation*, vol. AP-19, pp. 656-665, Sept. 1971.
13. J. P. Montgomery, "Scattering by an Infinite Periodic Array of Thin Conductors on a Dielectric Sheet," *IEEE Transactions on Antennas and Propagation*, vol. AP-23, no. 1, pp. 70-75, Jan. 1975.
14. D. S. Lerner, "A Wave Polarization Converter for Circular Polarization," *IEEE Transactions on Antennas and Propagation*, vol AP-13, pp. 3-7, Jan. 1965.
15. C. Terret, J. R. Levrel, and K. Mahdjoubi, "Susceptance Computation of a Meander-Line Polarizer Layer," *IEEE Transactions on Antennas and Propagation*, vol. AP-32, pp. 1007-1011, Sept. 1984.
16. L. Young, L. A. Robinson, and C. A. Hacking, "Meander-Line Polarizer," *IEEE Transactions on Antennas and Propagation*, vol. AP-21, pp. 376-378, May 1973.
17. R. S. Chu and K. M. Lee, "Analytical Model of a Multi-Layered Meander-Line Polarizer Plate with Normal and Oblique Plane-Wave Incidence," *IEEE Transactions on Antennas and Propagation*, vol. AP-35, pp. 652-661, June 1987.
18. R. G. Kouyoumjian and P. H. Pathak, "A Uniform Geometrical Theory of Diffraction for an Edge in a Perfectly conducting Surface," *Proceedings of the IEEE*, vol. 62-11, pp. 1448-1461, Nov. 1974.
19. J. P. Skinner. *Scattering Form a Finite Collection of Transverse Dipole and Axial Slot Arrays with Edge Effects*. Ph.D. dissertation. The Ohio State University, Columbus OH, 1991.
20. K. S. Yee, "Numerical Solution of Initial Boundary Value Problems Involving Maxwell's Equations in Isotropic Media," *IEEE Transactions on Antennas and Propagation*, vol. AP-14, pp. 302-307, May 1966.
21. K. S. Kunz and Raymond J. Luebbers, *The Finite Difference Time Domain for electromagnetics*. Boca Raton: CRC Press Inc., 1993.
22. Z. P. Liao, H. L. Wong, Y. Baipo, and Y. Yifan, "A Transmitting Boundary for Transient Wave Analyses," *Scientia Sinica*, vol. A-27, no. 10, Oct. 1984, pp. 1063-1076.

### ***Vita***

Lieutenant Russell A. Burleson was born on 15 Dec 1968 in Lake City, Florida. He graduated from Leesville Senior High School in Leesville, Louisiana in 1986. Lieutenant Burleson then attended Louisiana State University and A & M at Baton Rouge, Louisiana, graduating with a B. S. E. E. in 1991. Upon graduation, he was nominated for a regular commission as a distinguished R. O. T. C. graduate. While awaiting active duty, Lieutenant Burleson was a plant quality engineer for the Procter & Gamble Manufacturing Company in Alexandria, Louisiana. His first tour of active duty was at the Air Force Institute of Technology at WPAFB, Ohio to receive a M. S. E. E. degree with emphasis in electromagnetics in December 1993. Lieutenant Burleson is a member of Eta Kappa Nu and Tau Beta Pi and is presently a certified Engineer-In-Training in the state of Louisiana.

Permanent Address: 1029 Middy Dr.  
WPAFB, OH 45433  
(513)259-1231

REPORT DOCUMENTATION PAGE			Form Approved OMB No. 0704-0188	
<small>Public reporting burden for this document estimate is 1 hour per response, including the time for reviewing instructions, searching existing data sources, gathering and maintaining the data needed, and completing and reviewing the collection of information. Send comments regarding this burden estimate or any aspect of this collection of information, including suggestions for reducing the burden, to Washington Headquarters Services, Directorate for Information Operations and Reports, 1215 Jefferson Davis Highway, Suite 1204, Arlington, VA 22202-4302, and to the Office of Management and Budget, Paperwork Reduction Project (0704-0188), Washington, DC 20503.</small>				
1. AGENCY USE ONLY (Leave blank)	2. REPORT DATE December 1993	3. REPORT TYPE AND DATES COVERED Master's Thesis		
4. TITLE AND SUBTITLE A Study of Two Dimensional Tapered Periodic Edge Treatments to Reduce Wideband Edge Diffraction			5. FUNDING NUMBERS	
6. AUTHOR(S) Russell A. Burleson				
7. PERFORMING ORGANIZATION NAME(S) AND ADDRESS(ES) Air Force Institute of Technology, WPAFB OH 45433-7765			8. PERFORMING ORGANIZATION REPORT NUMBER AFIT/GE/ENG/93D-02	
9. SPONSORING/MONITORING AGENCY NAME(S) AND ADDRESS(ES) Captain Raley Merek Phillips Laboratory (PL/WSR) Kirtland AFB, NM 87117-6008			10. SPONSORING/MONITORING AGENCY REPORT NUMBER	
11. SUPPLEMENTARY NOTES				
12a. DISTRIBUTION/AVAILABILITY STATEMENT Approved for public release; distribution unlimited			12b. DISTRIBUTION CODE	
13. ABSTRACT (Maximum 200 words)  This is a brief summary of a study to reduce diffraction from an infinite two dimensional edge using tapered periodic surfaces. The concept is to use the impedance characteristics of a periodic surface to create a tapered impedance, much like a tapered resistance commonly used for diffraction reduction. This approach has several advantages over tapered resistive treatments to include ease of fabrication, better engineering control of the impedance and negligible loss absorbed by the taper. In this study, four periodic tapers were design, built and tested. These tapers were also modeled using a variety of numerical techniques. The results from this study were quite promising.				
14. SUBJECT TERMS Edge Treatments, FSS, TPS, Wideband, Diffraction			15. NUMBER OF PAGES 236	
			16. PRICE CODE	
17. SECURITY CLASSIFICATION OF REPORT UNCLASSIFIED	18. SECURITY CLASSIFICATION OF THIS PAGE UNCLASSIFIED	19. SECURITY CLASSIFICATION OF ABSTRACT UNCLASSIFIED	20. LIMITATION OF ABSTRACT UL	